IFMBE Proceedings

Simona Vlad · Nicolae Marius Roman (Eds.)

Volume 71

6th International Conference on Advancements of Medicine and Health Care through Technology; 17–20 October 2018, Cluj-Napoca, Romania

MEDITECH 2018

Springer

IFMBE Proceedings

Volume 71

The International Federation for Medical and Biological Engineering, IFMBE, is a federation of national and transnational organizations representing internationally the interests of medical and biological engineering and sciences. The IFMBE is a non-profit organization fostering the creation, dissemination and application of medical and biological engineering knowledge and the management of technology for improved health and quality of life. Its activities include participation in the formulation of public policy and the dissemination of information through publications and forums. Within the field of medical, clinical, and biological engineering, IFMBE's aims are to encourage research and the application of knowledge, and to disseminate information and promote collaboration. The objectives of the IFMBE are scientific, technological, literary, and educational.

The IFMBE is a WHO accredited NGO covering the full range of biomedical and clinical engineering, healthcare, healthcare technology and management. It is representing through its 60 member societies some 120.000 professionals involved in the various issues of improved health and health care delivery.

Simona Vlad • Nicolae Marius Roman
Editors

6th International Conference on Advancements of Medicine and Health Care through Technology; 17–20 October 2018, Cluj-Napoca, Romania

MEDITECH 2018

Springer

Editors
Simona Vlad
Faculty of Electrical Engineering
Technical University of Cluj-Napoca
Cluj-Napoca, Romania

Nicolae Marius Roman
Faculty of Electrical Engineering
Technical University of Cluj-Napoca
Cluj-Napoca, Romania

ISSN 1680-0737 ISSN 1433-9277 (electronic)
IFMBE Proceedings
ISBN 978-981-13-6206-4 ISBN 978-981-13-6207-1 (eBook)
https://doi.org/10.1007/978-981-13-6207-1

Library of Congress Control Number: 2019930365

This Springer imprint is published by the registered company Springer Nature Singapore Pte Ltd.
The registered company address is: 152 Beach Road, #21-01/04 Gateway East, Singapore 189721, Singapore

Organization

Organizer

Romanian National Society for Medical Engineering and Biological Technology
Technical University of Cluj-Napoca, Romania
"Iuliu Haţieganu" University of Medicine and Pharmacy, Cluj-Napoca, Romania

Partners

Medical University of Vienna, Austria
The University of Sheffield, UK
"Dr. Constantin Papilian" Military Emergency Hospital, Cluj-Napoca, Romania

Conference Chair

Nicolae Marius Roman—*Technical University of Cluj-Napoca, Romania*

Honorary Chair

Radu Vasile Ciupa—*Technical University of Cluj-Napoca, Romania*

Scientific Advisory Committee

Laura Bacali (RO)
Doina Baltaru (RO)
Maria Beudean (RO)
Lelia Ciontea (RO)
Radu Ciorap (RO)
Radu V. Ciupa (RO)
Mariana Constantiniuc (RO)
Cecilia Cristea (RO)
Paul Farago (RO)
Anca Galaction (RO)
Monica Gavris (RO)
Stefan Gergely (RO)
Zoltan German-Sallo (RO)

Laura Grindei (RO)
Sorin Hintea (RO)
Rodica Holonec (RO)
Rod Hose (UK)
Ioan Jivet (RO)
Mircea Leabu (RO)
Patricia Lawford (UK)
Kang-Ping Lin (TW)
Angela Lungu (RO)
Eugen Lupu (RO)
Dan S. Mandru (RO)
Alma Maniu (RO)
Winfried Mayr (A)
Amalia Mesaros (RO)
Bogdan Micu (RO)
Dan D. Micu (RO)
Dan Milici (RO)
Alexandru Morega (RO)
Mihaela Morega (RO)
Marius Muji (RO)
Calin Munteanu (RO)
Mihai S. Munteanu (RO)
Radu A. Munteanu (RO)
Anca I. Nicu (RO)
Maria Olt (RO)
Sever Pasca (RO)
Alessandro Pepino (IT)
Traian Petrisor (RO)
Petre G. Pop (RO)
Dan V. Rafiroiu (RO)
Corneliu Rusu (RO)
Radu Sestras (RO)
Dan I. Stoia (RO)
Mihai Tarata (RO)
Marina Topa (RO)
Vasile Topa (RO)
Mircea Vaida (RO)
Doru Ursutiu (RO)
Liliana Verestiuc (RO)
Radu C. Vlad (RO)
Simona Vlad (RO)
Dan Zaharia (RO)

Local Organizing Committee

Alexandru Avram
Radu V. Ciupa
Levente Czumbil
Rodica Holonec
Angela Lungu
Calin Munteanu

Mihai S. Munteanu
Anca I. Nicu
Maria Olt
Sever Pasca
Dan V. Rafiroiu
Nicolae Marius Roman
Marina Topa
Simona Vlad

Invited Speakers

Kang-Ping Lin, IFMBE Secretary-General, Chung-Yuan Christian University, Taiwan
Asia-Pacific Outlook of Medical Device Developments & Opportunities

Helmut Hutten, Institute of Medical Engineering, Graz University of Technology, Austria
Does MBES need an Ethical Code?

Ramon Pallàs Areny, Universitat Politècnica de Catalunya (BarcelonaTech), Spain
Cardiovascular Tracking with Four Electrodes

Winfried Mayr, Medical University of Vienna, Austria
Functional Electrical Stimulation in Movement Rehabilitation

Thordur Helgason, Inst. f. Biomed and Neural Engineering, TVD Landspitali-University Hospital/Reykjavik University, Iceland
Transcutaneous Spinal Cord Stimulation for the Abbreviation of Spasticity: Methods and Results

Alessandro Pepino, University of Naples "Federico II", Italy
University Support Services for Inclusion of Student with Disabilities and Learning Disabilities could be an Opportunity of Improvement for all the Students

Lucio Tommaso De Paolis, University of Salento, Italy
Augmented Visualization in Medicine and Surgery

Sanjay Padhiar, INAS S.A. Craiova, Romania
Towards High Fidelity "in silico" Computer Modelling and Simulation in Surgery

Alma Maniu, University of Medicine and Pharmacy "Iuliu Haţieganu", Cluj-Napoca, Romania
Nanotechnology and Based Targeted Drug Delivery in Cochlear Implantation

Harry Solomon, American Medical Informatics Association, USA
Healthcare Interoperability and Standards By the Numbers—A Framework for Answering "Why…"

Leonard Cezar Păstrăv, Katholieke Universiteit Leuven, Belgium
Monitoring the Stability of Bone-implant Structures by Vibration Analysis Structural Health Monitoring Techniques Applied in Orthopaedics

Dan L. Dumitraşcu, University of Medicine and Pharmacy "Iuliu Haţieganu", Cluj-Napoca, Romania
Application of the High-resolution Manometry in the Investigation of the Esophageal Motility

Doru Ursuţiu, "*Transilvania*" *University of Braşov, Romania*
Affective Education in Medicine Through the new Technologies

Dan Zaharia, University of Medicine and Pharmacy "Grigore T. Popa", Iaşi, Romania
Electrodiagnostic Evaluation of Peripheral Nerve Injuries and Compressions

Liliana Verestiuc, University of Medicine and Pharmacy "Grigore T. Popa", Iaşi, Romania
Bioinspired Multi-Sensitive Materials for Tissue Engineering and Regenerative Medicine

Doina Baltaru, "Dr. Constantin Papilian" Emergency Military Hospital of Cluj-Napoca, Romania
Technical Issues Specific to Military Medical Assistance
Mircea Gelu Buta, "Babeş-Bolyai" University of Cluj-Napoca, Romania
Genetics and Vaccines
Monica Gavriş, "Dr. Constantin Papilian" Emergency Military Hospital of Cluj-Napoca, Romania
The Advantages of Femtosecond Laser in Corneal Refractive Surgery and Cataract Surgery
Mihai Tarata, University of Medicine and Pharmacy of Craiova, Romania
Potential of the Mechanomyogram
Mihai-Alexandru Mărginean, "Dr. Constantin Papilian" Emergency Military Hospital of Cluj-Napoca, Romania
The Modern Therapy of Pain; Technical News
Ciprian Roman, "Dr. Constantin Papilian" Emergency Military Hospital of Cluj-Napoca, Romania
VR Advantages and Disadvantages in Kinetotherapy
Anton Naiba, "Dr. Constantin Papilian" Emergency Military Hospital of Cluj-Napoca, Romania
Simulation—Applications in Emergency Medicine Training

Sponsors

Laitek Medical Software—Romania HQ
Medical Technologies Infinity SRL
Tehno Industrial SA
Farmec SA
INAS SA
Cefmur SA
Constelatia Construct SRL

Media Partners

Radio Romania Cluj
TVR Cluj

Preface

The 6th "Conference on Advancements of Medicine and Health Care Through Technology"—MediTech 2018 took place in Cluj-Napoca on October 17–20, 2018.

The MediTech Conference has become an international academic forum for clinical engineers and doctors alike for researchers in medicine, medical physics, and biomedical engineering.

The lectures of the conference highlighted many concerns in the field of medical engineering. The authors, Romanians and foreigners, presented the latest research results in universities, clinics, medical devices domain, hospitals, etc.

It was a good opportunity for all participants to exchange their know-how and build up an academic collaboration in one of the most important fields of science and technology—medical engineering.

We were honored for the second consecutive attendance of Prof. Kang-Ping Lin, IFMBE Secretary General, from Chung-Yuan Christian University, at the official opening of the conference. He said:

> I am greatly honored to be invited at this international conference (MediTech-2018). On behalf of IFMBE, I am delighted to show all participants that the mission of IFMBE is to encourage, support and assist BME activities all over the world. At the same time, we promote exchange and cooperation of Science and Technology, integrate industrial technology and clinical application through advancement of research, development, application, management of technology and education training. MediTech Conference becomes a brand well known and respected in Romania and surrounding countries. It is important to point out that this conference was organized by Romanian National Society for Medical Engineering and Biological Technology with Technical University and University of Medicine and Pharmacy from Cluj-Napoca which should be an example for conferences in biomedical engineering and also for research in that area.

All papers submitted for presentation went through a review process and were evaluated by two reviewers. The papers chosen to be presented at the conference were accompanied by manuscripts to be published in these *Proceedings*.

We would like to kindly thank all participants, speakers, academics, researchers, doctors, members of the Technical University, "Iuliu Hatieganu" University of Medicine and Pharmacy, Military Emergency Hospital Cluj-Napoca, the members of the Scientific and Organizing Committees for their hard work and dedication and we hope that they will continue supporting MediTech Conference.

Cluj-Napoca, Romania

Prof. Nicolae Marius Roman
MediTech 2018 Conference Chair

Contents

Part I Clinical Engineering Assessment

Spectrofluorimetric Characterization of Serum Pentosidine and Retinol Binding Protein in Healthy Rats and Rats with Streptozotocin-Induced Diabetes 3
D. M. Ciobanu, L. E. Olar, R. Ştefan, G. Roman, and I. Papuc

Eye Examination for Early Detection of Diabetic Neuropathy-Role of Corneal Confocal Microscopy 9
Georgeta Victoria Inceu, C. L. Vonica, and G. Roman

Doppler Ultrasonography, a Rapid Evaluation Method of the Major Risk in the Vascular Pathology 17
Elena Gligor, A. I. Roman, V. Ossian, D. Gligor, M. Beudean, and M. Olt

Part II Medical Devices, Measurements and Instrumentation

A Side-Polished Fluorescent Fiber Sensor for the Detection of Blood in the Saliva 23
P. Farago, Anida-Maria Băbțan, R. Galatus, R. Groza, N. M. Roman, C. N. Feurdean, and A. Ilea

Analysis of Postural Imbalance Due to Handling Weights During Physical Activities 29
D. Cotoros, C. Druga, I. Serban, and A. Stanciu

The Use of Thermal Imaging Techniques as a Method of Monitoring the New Born 35
Catalina Luca, C. Corciovă, D. Andriţoi, and R. Ciorap

Smart Wearable SpO_2 Monitor for Newborns 41
M. Datcu, C. Luca, and C. Corciova

Applied Measurements and Instrumentation for Improving Diagnostic Devices and Systems in Metropolitan Polluted Environments with Nitric and Carbon Oxides 45
Lavinia Andrei, Doru Băldean, and Adela Ioana Borzan

Three Way Automated Blood-Sampling Device Mixer for Blood Gas Analysis 51
Manole-Stefan Niculescu

Techniques for Sorting Components from Dismembered Medical PCBs 59
R. Holonec, L. Grindei, M. Purcar, R. Copîndean, and F. Dragan

Intelligent Medical Distance Assistance Device 65
Robert Fuior, Andrei Gheorghiță, and Călin Corciovă

The Use of Thermography as a Prediction Element in the Maintenance of Medical Equipment 73
D. Andritoi, C. Luca, C. Corciova, and R. Ciorap

Method for Body Impedance Measurement 79
R. Copîndean, R. Holonec, F. Dragan, and C. Muresan

Monitoring of Obstructive Sleep Apnea Using Virtual Instrumentation Techniques 85
R. Holonec, S. Vlad, A. I. Roman, and L. Rápolti

Application for Detection of Epileptic Seizures 91
R. Holonec, S. Vlad, and L. Rapolti

Exposure to UHF Electromagnetic Radiation in Urban Areas 97
A. Pastrav, P. Dolea, E. Puschita, C. Codau, T. Palade, and I. Palade

Monitoring of Cardiovascular Parameters During Rehabilitation After Stroke Event 103
Radu Ciorap, Doru Andritoi, Catalina Luca, and Calin Corciova

Modelling of Piezoelectric MEMS in Biomedical Applications 109
A. Avram, R. C. Bogdan, A. Bojiță, and M. Purcar

Comparative Effect of Ethyl Urethane and Cycloheximide in *Lepidium sativum* L. Seed Germination and Radicle Growth 115
O. Viman, K. Balla, L. Holonec, M. Tămaș, D. L. Dumitrașcu, V. Șandor, and L. Nedelcu

Numerical Simulation of the Temperature Propagation in Superposed Biological Media, with Applications in Dental Treatment 123
V. Mureşan, N. M. Roman, T. Coloşi, M. Abrudean, O. P. Stan, and O. Bunta

Part III Biomedical Signal and Image Processing

Identification of Animal Species from Their Sounds 133
Gavril-Petre Pop

Evaluating a Method of Offline Detection of P_3 Waves 139
Dorina Ancău, Nicolae-Marius Roman, and Mircea Ancău

An ECG Morphological Analysis Algorithm for Hybrid Patient Monitoring 145
A. Raza, Paul Farago, M. Cirlugea, and S. Hintea

Empirical Mode Decomposition in ECG Signal De-noising 151
Zoltán Germán-Salló, Márta Germán-Salló, and Horaţiu-Ştefan Grif

Emotion Recognition from Speech Signal in Multilingual Experiments 157
Corina Albu, Eugen Lupu, and Radu Arsinte

Automated Collagen Segmentation from Masson's Trichrome Stained Images—Preliminary Results 163
M. S. Şerbănescu, R. V. Teică, M. Tărâță, D. Georgescu, D. O. Alexandru, N. C. Manea, W. Wolf, R. M. Pleşea, and I. E. Pleşea

The Role of Convolutional Neural Networks in the Automatic Recognition of the Hepatocellular Carcinoma, Based on Ultrasound Images 169
D. Mitrea, R. Brehar, P. Mitrea, S. Nedevschi, M. Platon(Lupşor), and R. Badea

An Augmented Reality Platform for Preoperative Surgical Planning 177
S. Teodoro Vite, C. F. Domínguez Velasco, S. Muscatello, M. Á. Padilla Castañeda, and L. T. De Paolis

Part IV Telemedicine and Health Care Information Systems

Multi-agent Healthcare Information System on Hadoop 185
Gabriel Cristian Dragomir-Loga, A. Lacatus, L. Loga, and L. Dican

PAC Bayesian Classifier with Finite Mixture Model for Oral Cancer Classification 195
S. K. Prabhakar and H. Rajaguru

Health Information Exchange for Management of Disaster Victims Using FANET 201
Adrian Crețu, Camelia Avram, Dan Radu, Benoît Parrein, Adina Aştilean, and Claudiu Domuța

Random Forest and Sequential Model for Anomalies Detection in the Activities of the People with Dementia 207
D. Moldovan, A. Visovan, M. Bologa, C. Pop, V. R. Chifu, I. Anghel, T. Cioara, and I. Salomie

Sequence Labeling for Extracting Relevant Pieces of Information from Raw Text Medicine Descriptions 215
Radu Razvan Slavescu, Constantin Masca, and Kinga Cristina Slavescu

Development of Bluetooth Enabled Pediatric Temperature Monitoring Device 221
Ciprian Mugurel Fort, N. M. Roman, and S. Gergely

Part V Biomechanics, Robotics and Rehabilitation

The Analysis of Bio-Signals and Sensors for Robotic Assisted Rehabilitation 229
Nicoleta Pop, Calin Vaida, Giuseppe Carbone, Florin Craciun, Kinga Major, Cristian Abrudan, Ferenc Puskas, and Doina Pisla

Experimental Study Regarding the Performance of a Motor-Imagery Brain-Computer Interface Across Different Electrodes Placement 237
A. Ianoşi-Andreeva-Dimitrova and Dan S. Mândru

A New Proposal for Solving Equations of Angular Contact Ball Bearing Using Evolutionary Techniques 241
A. Gheorghita, M. Turnea, M. Ilea, M. Rotariu, G. Constantin, and D. Arotaritei

Modeling of the Complex Walk Assist Equipment 247
Adrian Abrudean and Dan S. Mândru

Voice Controlled Wheelchair for People with Disabilities 255
P. Pop-Coman, N. M. Roman, M. Steopan, V. Ispas, S. Bugnar, and M. Olea

Rehabilitation of Orthopedic and Neuropsychological Complications After Hip Arthroplasty 261
A. M. Culai, P. Mihancea, and I. Onac

Robotics in Minimally Invasive Procedures: History, Current Trends and Future Challenges 267
C. Vaida, N. Al Hajjar, V. Lazar, F. Graur, A. Burz, R. Elisei, E. Mois, and D. Pisla

Part VI Health Technology Assessment

The Influence of Socio-Demographic, Psychological and Medical Variables on Patient Satisfaction with Diabetes Care in the Hospital Setting in Romania 277
Anca Constantinescu-Dobra, A. Sabou, and M. C. Coțiu

Is Internet Marketing a Useful Tool for GPs Communicating with Students? A Focus Group Exploratory Study 283
Anca Constantinescu-Dobra and M. C. Coțiu

Utility of 3D Reconstructions for Preoperative Planning in Functional Endoscopic Sinus Surgery (FESS) 287
D. Radeanu, Constantin Stan, and A. A. Maniu

Quantifiable Risk Factors in Medical Equipment Management Program 291
Călin Corciovă, D. Andriţoi, C. Luca, and R. Ciorap

Oncological Outcome After Robotic Surgery for Rectal Cancer 297
Bogdan Vasile Micu, C. M. Micu, D. Chirila, H. Silaghi, R. A. Iusan, M. S. Muresan, T. R. Pop, C. Ionescu, and N. Constantea

Prognostic Implications of Sentinel Lymph Node Mapping in Stage I and II Colorectal Cancer Patients 301
Bogdan Vasile Micu, C. M. Micu, D. Chirila, H. Silaghi, D. R. Miclaus, M. S. Muresan, T. R. Pop, N. Constantea, and C. Ionescu

Metallic Nanoparticles in Otology 305
A. A. Maniu, M. Perde-Schrepler, E. Fischer-Fodor, A. Florea, George Sebastian Chis, and A. I. Roman

New Era for Technology in Healthcare Powered by GDPR and Blockchain 311
O. P. Stan and L. Miclea

Part VII Miscellaneous Topics

Temperature Effect on Tribo-Mechanical Properties of Dental Materials 321
C. Birleanu, M. Pustan, V. Merie, and M. S. Pop

Magnetic Submicron Systems Loaded with Chemotherapeutic Agent (Paclitaxel) for Breast Cancer Therapy 329
V. Balan, S. Malihin, and L. Verestiuc

Identifying Relevant Research Directions for Graduation Projects in Medical Engineering 335
D. Cotoros, C. Druga, I. Serban, and A. Stanciu

Improvement of the Fluidized Bed Tribocharging Device for Electrostatic Separation of Plastics from Electronic Medical Waste 341
L. Călin, M. Bilici, and A. Samuilă

Complex Influence of Intense Electric Fields upon Ozone and Free Radicals from Aqueous Solutions 347
R. E. Suărăşan, S. R. Budu, I. Suărăşan, Dumitriţa Moldovan, and Radu Fechete

Author Index 351

Part I
Clinical Engineering Assessment

Spectrofluorimetric Characterization of Serum Pentosidine and Retinol Binding Protein in Healthy Rats and Rats with Streptozotocin-Induced Diabetes

D. M. Ciobanu, L. E. Olar, R. Ştefan, G. Roman, and I. Papuc

Abstract

Recently, the fluorescence techniques have become increasingly important in medical diagnostics. Moreover, there is a growing need to introduce cost-effective and no time-consuming techniques for the investigation of various fluorophores in humans and animals with diabetes mellitus. In the studied literature, the newly diagnosis of diabetes mellitus and, subsequently, the risk of developing diabetes complications are reported to be correlated with the production of serum fluorophores pentosidine and retinol binding protein. As far as we are aware, there has been no study on the simultaneous fluorescence evaluation of pentosidine and retinol binding protein in biological fluids obtained from animals. In the present study, the emission intensity and levels of serum pentosidine and retinol binding protein were monitored in both healthy rats and rats with streptozotocin-induced diabetes. The results showed that the height of the peak at ~382 nm attributed to the presence of pentosidine in the serum, and the height of the peak at ~465 nm attributed to retinol binding protein in the serum were significantly higher in rats with streptozotocin-induced diabetes compared to healthy control rats. Also, their contributions to the total fluorescence of serum were significantly higher in rats with streptozotocin-induced diabetes compared to healthy control rats. Thus, fluorescence spectroscopy might be a reliable and useful technique that can be successfully applied in the evaluation and monitoring of serum pentosidine and retinol binding protein in both healthy rats and rats with streptozotocin-induced diabetes.

Keywords

Pentosidine • Retinol binding protein • Diabetes mellitus • Rats • Fluorescence spectroscopy

1 Introduction

Due to the increased number of animals and humans diagnosed with diabetes mellitus worldwide [1, 2], finding new methods and protocols for diabetes' biomarkers evaluation is mandatory. Pentosidine and retinol binding protein represent two of the recent studied compounds in diabetes mellitus [3–6]. Their increased levels in different body fluids and tissues were associated with the newly diagnosis of diabetes mellitus and, subsequently, with a higher risk of developing diabetes complications [3, 5, 7, 8]. However, as far as we are aware, there are no studies that have described the simultaneous fluorescence of both serum pentosidine and serum retinol binding protein in animals with diabetes mellitus compared to healthy controls. Thus, we decided to conduct a study in order to evaluate the levels of both pentosidine and retinol binding protein using spectrofluorimetry in the serum samples obtained from healthy rats and rats with streptozotocin-induced diabetes.

Pentosidine is formed through the reaction of glucose with lysine, arginine and ribose in the serum [9]. Increased pentosidine formation was described in various diseases associated with oxidative stress, including diabetes mellitus [10]. The evaluation of pentosidine in patients with diabetes may give us a valuable marker of long-term glycemic control which could seriously impact glycated hemoglobin levels [11]. Pentosidine is a fluorescent product which has been quantified and evaluated through various techniques such as: spectrofluorimetry, enzyme-linked immunosorbent assay, high-performance liquid chromatography and mass spectrometry [12]. However, there are limited data regarding the serum measurement of pentosidine in rats with streptozotocin-induced diabetes compared to controls using

D. M. Ciobanu · G. Roman
Iuliu Haţieganu University of Medicine and Pharmacy, Cluj-Napoca, Romania

L. E. Olar (✉) · R. Ştefan · I. Papuc
University of Agricultural Sciences and Veterinary Medicine, 3-5 Manastur, Cluj-Napoca, Romania
e-mail: loredana.olar@usamvcluj.ro

S. Vlad and N. M. Roman (eds.), *6th International Conference on Advancements of Medicine and Health Care through Technology; 17–20 October 2018, Cluj-Napoca, Romania*, IFMBE Proceedings 71,
https://doi.org/10.1007/978-981-13-6207-1_1

a simple and rapid method for quantitative determination such as the fluorescence technique followed by the Gaussian deconvolution of the obtained spectra.

Retinol is one on the most used parameters for the evaluation of serum vitamin A concentration in living organisms [13]. In the systemic circulation, there are three classes of specific transport proteins for vitamin A and its metabolites, called retinol binding proteins [14, 15]. The cellular retinol binding protein is the most abundant retinol binding protein in most tissues, such as: the liver, kidney and lung [15]. In fact, in order to prevent the disappearance of this retinol binding protein from blood by filtrating in the renal glomeruli, in the systemic circulation appears another protein called transthyretin [16, 17]. It was suggested that the complex formed between retinol and retinol binding protein is more fluorescent than free retinol [16, 18, 19]. The results of several investigations suggest an association of retinol binding protein with the newly diagnosis and presence of insulin resistance, diabetes mellitus and metabolic syndrome [5, 7, 20, 21].

In this paper, we wanted to simultaneously investigate the serum levels of pentosidine and retinol binding protein using fluorescence spectroscopy followed by the deconvolution method of the obtained spectra in an animal model of diabetes mellitus disease.

Therefore, we assessed the heights of the peaks attributed to these serum constituents and their contributions to the total serum fluorescence in rats with streptozotocin-induced diabetes compared to healthy control rats. Thus, eventual changes in the condition of these fluorophores could help the monitoring of animals' physiological response to diabetes mellitus diagnosis and to specific diabetes therapies.

2 Materials and Methods

2.1 Animals

The experiment was conducted in accordance with Romanian laws regarding correct manipulation of laboratory animals and was approved by the local Ethical Committee of University of Agricultural Sciences and Veterinary Medicine in Cluj-Napoca, Romania.

A number of 10 Wistar rats with the age of 6–7 weeks old, weighing between 250 and 300 g were used in this experiment. They were housed in two stainless steel cages with free access to food and water and under standard environmental conditions: temperature 24 ± 5 °C, relative humidity 60 ± 4%, light/dark cycle (12 h/12 h). The same rats were used in the first and second part of the study (after the administration of streptozotocin and, consequently, the induction of experimental diabetes mellitus).

2.2 Induction of Diabetes

Diabetes mellitus was induced with a single intraperitoneal dose of 60 mg/kg streptozotocin (Sigma, Aldrich). The experimental diabetes was induced in a number of 1–4 days after streptozotocin administration. Rats with blood glucose levels >300 mg/dl were considered as having diabetes mellitus [22].

2.3 Blood Sampling

The venous blood (0.2 ml) was collected from the orbital sinus of healthy rats and rats with streptozotocin-induced diabetes in 0.5 ml Eppendorf tubes. Further, the blood was centrifuged at 1000 g for 10 min. The levels of glycemia were measured using commercially available methods (Hitachi, Roche Diagnostics).

For the spectrofluorimetric analyses, further dilutions of serum (4 µl) were performed (1:500) using physiological serum (NaCl 0.9%).

2.4 Spectrofluorimetric Determination of Pentosidine and Retinol Binding Protein

The spectrofluorimetric analysis was made using a FP-8200 spectrofluorometer (Jasco, Japan) (Fig. 1). The measurements were performed at room temperature using a 1 cm quartz cell. The serum spectra were recorded in a region from 360 to 600 nm using an excitation of 335 nm [23, 24] at a medium sensitivity.

The fluorescence intensity was recorded at the emission maximum of ~380 nm for pentosidine [24] and at ~465 nm [19] for the retinol binding protein, with a wavelength accuracy of ±2 nm.

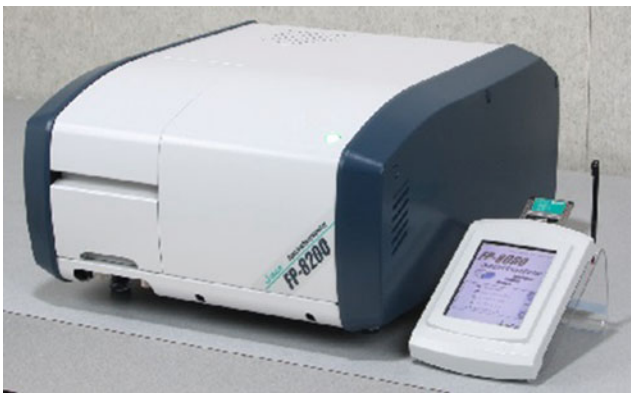

Fig. 1 Spectrofluorometer FP-8200 (Jasco, Japan)

The interpretation of obtained data was done using Origin Pro 8.1 software. Further, we performed the deconvolution of the obtained spectra using the peak analyzer option of Origin Pro 8.1 software in order to have a better quantification of the serum levels of pentosidine and retinol binding protein in rats with and without diabetes [24, 25]. Therefore, utilizing a combination of six Gaussian bands, we established the peaks position and full width at half maximum while the intensity was allowed to vary in order to match the line shape of the experimental spectra (Fig. 2).

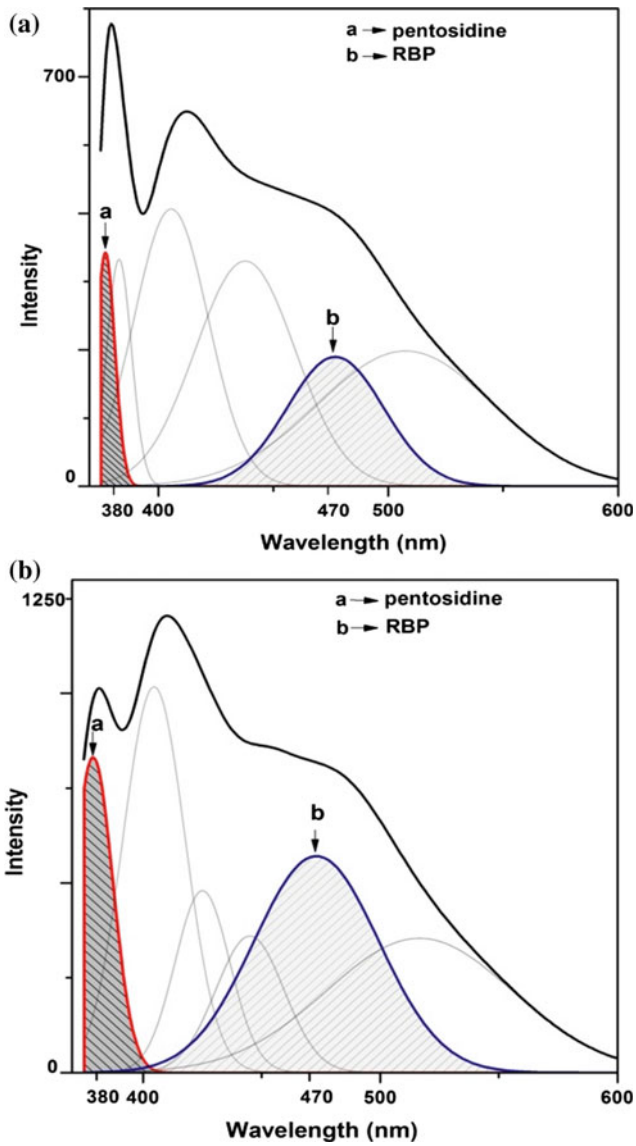

Fig. 2 The deconvolution of fluorescence spectrum of serum collected from rats before (**a**) and after the administration of streptozotocin (**b**) (excitation wavelength of 335 nm)

2.5 Statistical Analysis

Data analyses were performed using R commander version 3.0.1 for Windows. Peak heights and areas under the peak were normally distributed when evaluated using Kolmogorov–Smirnov test, and were expressed as means ±standard deviation. Group comparisons of the mentioned variables were performed using t-test. A p value <0.05 was considered statistically significant.

3 Results

Figure 3 shows the emission intensities of pentosidine and retinol binding protein in the serum of healthy rats and rats with streptozotocin-induced diabetes.

The height of the peak from ~380 nm attributed to the presence of pentosidine in the serum was significantly higher in rats with streptozotocin-induced diabetes compared to healthy rats ($p < 0.001$). Also, significant differences between the rats with streptozotocin-induced diabetes and healthy controls were noticed for the height of the peak near 470 nm attributed to the presence of retinol binding protein in the serum ($p < 0.001$). Moreover, when comparing the average contribution (area under the peak) of pentosidine and retinol binding protein to the total fluorescence of serum in rats with streptozotocin induced diabetes and healthy rats, the results showed that a statistically significant difference exists between the two study groups ($p < 0.001$) (Table 1).

4 Discussions

We evaluated the heights of the fluorescence signals attributed to pentosidine and retinol binding protein and their contributions to the total fluorescence of serum in order to study these biochemical compounds in the serum of healthy rats and how they change with the induction of diabetes mellitus. Concerning the existing connection between an increased pentosidine formation and the presence of diabetes mellitus, it was declared that hyperglycemia promotes the accumulation of pentosidine [10]. In our study, the fluorescence evaluation of pentosidine in rats with streptozotocin-induced diabetes revealed significantly higher peaks and contributions to the total fluorescence of serum compared to healthy control rats.

Therefore, we can declare that the levels of pentosidine in rats with diabetes mellitus were statistically significant higher compared to healthy controls. Similarly, previous studies reported significant difference in pentosidine formation between the patients with diabetes and controls [26]. In the same study, it was mentioned that the presence of complications of diabetes such as retinopathy and chronic

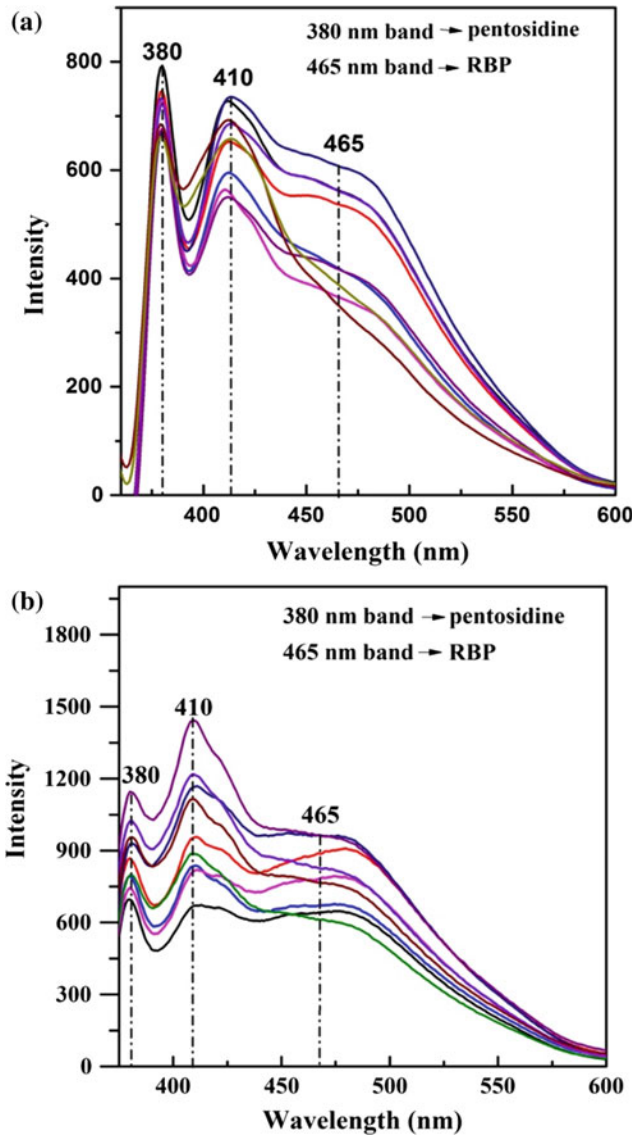

Fig. 3 The emission spectrum of serum pentosidine and retinol binding protein (RBP) in healthy controls (**a**) and rats with streptozotocin-induced diabetes (**b**)

Table 1 The characterization parameters of pentosidine and retinol binding protein that significantly ($p < 0.001$) differentiate between healthy rats and rats with streptozotocin-induced diabetes

	Characterization parameters		
	Peak center (nm)	Peak height (a.u)	Average of the area under the peak (cm^{-1})
Control rats	~380	708.6 ± 44.5	2.3 ± 0.4
	~470	465 ± 95.3	13.3 ± 0.9
Rats with streptozotocin induced diabetes	~380	877.1 ± 135.7	8.0 ± 1.2
	~470	789.4 ± 126.3	24.2 ± 2.7

nm, nanometers; a.u., arbitrary units

kidney disease leaded to significantly higher pentosidine levels [26]. It has been reported that an increased concentration of pentosidine measured by reverse-phase high performance liquid chromatography might be an independent predictor of all-cause and cardiovascular mortality and that it may represent a useful biomarker for monitoring clinical outcome in patients with end-stage renal disease [27]. In our article, we used a cost-efficient and no time-consuming fluorescence spectroscopic method with a high sensitivity and selectivity of detection for the investigation of pentosidine in the serum of rats with streptozotocin-induced diabetes.

We compared the contributions and the heights of the serum peak near 465 nm, attributed to retinol binding protein in healthy control rats and rats with streptozotocin-induced diabetes. Our results showed that both the heights of the peak attributed to retinol binding protein and its contribution to the total fluorescence of the serum were significantly higher in rats with streptozotocin-induced diabetes compared to controls, suggesting higher levels of this product in the presence of diabetes. Our results are somewhat in concordance with a study that reported higher serum and urine concentrations of retinol binding protein in type 2 diabetes mellitus patients compared to healthy controls [28]. Our study showing increased serum levels of retinol binding protein in rats with streptozotocin-induced diabetes highlights the similarities between these two species concerning the retinol metabolism in diabetes mellitus, and therefore, the possibility of using these animals as models in studying the pathogenesis of human diabetes mellitus. According to other studies, the levels of retinol in insulin treated diabetes mellitus patients and in streptozotocin induced diabetes mellitus rats were significantly lower than the levels of control subjects [29]. This finding was supported by numerous observations, such as: lower transthyretin levels or the presence of some problems in the synthesis of retinol binding protein due to altered renal function [30]. As can be observed, at this time, in the literature isn't established whether or not the levels of retinol binding protein are actually increased in patients with diabetes mellitus. Our study brings an improvement to the existing literature and claims an increased level of retinol binding protein in rats with streptozotocin induced diabetes mellitus when compared to healthy control rats. Also, we describe an increased serum retinol level in rats with streptozotocin induced diabetes.

5 Conclusions

In conclusion, the contributions of both pentosidine and retinol binding protein to the total serum fluorescence and also the heights of these peaks attributed to the presence of these biochemical compounds in serum are significantly

higher in rats with streptozotocin-induced diabetes mellitus compared to healthy control rats. On the basis of these data, we could claim the fact that the levels of pentosidine and retinol binding protein are significantly higher in the serum of rats with streptozotocin-induced diabetes compared to controls.

In addition, fluorescence spectroscopy represents a reliable and no time-consuming technique that can be applied successfully in the evaluation and monitoring of both serum pentosidine and retinol binding protein in animals diagnosed with diabetes mellitus.

Future studies should better investigate the correlation of pentosidine and retinol binding protein as determined by fluorescence spectroscopy with others biochemical compounds such as hyperglycemia and glycated hemoglobin and with the presence of diabetic complications in order to better understand the pathophysiology of these compounds in diabetes mellitus in both humans and animals.

Acknowledgements The work was supported by an internal grant (4994/3/08.03.2016) financed by the Iuliu Haţieganu University of Medicine and Pharmacy Cluj-Napoca.

Conflict of Interest The authors declare that they have no potential conflict of interest relevant to this article.

References

1. O'Neill, D.G., Gostelow, R., Orme, C., et al.: Epidemiology of Diabetes Mellitus among 193,435 cats attending primary care veterinary practices in England. J. Vet. Int. Med. **30**(4), 964–972 (2016). https://doi.org/10.1111/jvim.14365
2. Cho, N.H., Shaw, J.E., Karuranga, S., et al.: IDF Diabetes Atlas: global estimates of diabetes prevalence for 2017 and projections for 2045. Diabetes Res. Clin. Pract. **138**, 271–281 (2018). https://doi.org/10.1016/j.diabres.2018.02.023
3. Kerkeni, M., Saïdi, A., Bouzidi, H., et al.: Pentosidine as a biomarker for microvascular complications in type 2 diabetic patients. Diab. Vasc. Dis. Res. **10**(3), 239–245 (2013). https://doi.org/10.1177/1479164112460253
4. Ram, J., Snehalatha, C., Selvam, S., et al.: Retinol binding protein-4 predicts incident diabetes in Asian Indian men with prediabetes. BioFactors **41**(3), 160–165 (2015). https://doi.org/10.1002/biof.1209
5. Rhee, E.J., Plutzky, J.: Retinoid Metabolism and Diabetes Mellitus. Diabetes Metab. J. **36**(3), 167–180 (2012). https://doi.org/10.4093/dmj.2012.36.3.167
6. Tanaka, M.: Relationship between urinary pentosidine concentration and vascular complications in type 2 diabetic patients. J Diabetes Metab. **7**, 640 (2016). https://doi.org/10.4172/2155-6156.1000640
7. Cabré, A., Lázaro, I., Girona, J., et al.: Retinol-binding protein 4 as a plasma biomarker of renal dysfunction and cardiovascular disease in type 2 diabetes. J. Intern. Med. **262**(4), 496–503 (2007)
8. Novery, E., Susanah, S., Rachmadi, D.: The Correlation of urine retinol binding protein-4 and serum HbA1c with glomerular filtration rate in type 1 (insulin-dependent) diabetic children: a perspective on the duration of diabetes. Open J. Pediatrics **05**(2), 134–140 (2015). https://doi.org/10.4236/ojped.2015.52020
9. Grandhee, S.K., Monnier, V.M.: Mechanism of formation of the Maillard protein cross-link pentosidine. Glucose, fructose, and ascorbate as pentosidine precursors. J. Biol. Chem. **266**(18), 11649–11653 (1991)
10. Sternberg, M., M'bemba, J., Urios, P., et al.: Skin collagen pentosidine and fluorescence in diabetes were predictors of retinopathy progression and creatininemia increase already 6 years after punch-biopsy. Clin. Biochem. **49**(3), 225–231 (2016). https://doi.org/10.1016/j.clinbiochem.2015.10.011
11. Rabbani, N., Thornalley, P.J.: Hidden complexities in the measurement of fructosyl-lysine and advanced glycation end products for risk prediction of vascular complications of diabetes. Diabetes **64**(1), 9–11 (2015). https://doi.org/10.2337/db14-1516
12. Requena, J.R., Price, D.L., Thorpe, S.R., Baynes, J.W.: Measurement of pentosidine in biological samples. Aging Methods Protoc. **38**, 209–217 (2000). https://doi.org/10.1385/1-59259-070-5:209
13. Tanumihardjo, S.A.: Assessing vitamin A status: past, present and future. J. Nutr. **134**(1), 290S–293S (2004)
14. Raghu, P., Sivakumar, B.: Interactions amongst plasma retinol-binding protein, transthyretin and their ligands: implications in vitamin A homeostasis and transthyretin amyloidosis. Biochimica et Biophysica Acta (BBA)—Proteins Proteomics **1703**(1), 1–9 (2004). https://doi.org/10.1016/j.bbapap.2004.09.023
15. Silvaroli, J.A., Arne, J.M., Chelstowska, S., et al.: Ligand binding induces conformational changes in human cellular Retinol-binding Protein 1 (RETINOL BINDING PROTEIN 1) revealed by atomic resolution crystal structures. J. Biol. Chem. **29**(16), 8528–8540 (2016). https://doi.org/10.1074/jbc.M116.714535
16. Berry, D.C., Croniger, C.M., Ghyselinck, N.B., et al.: Transthyretin blocks retinol uptake and cell signaling by the holo-retinol-binding protein receptor STRA6. Mol. Cell. Biol. **32**(19), 3851–3859 (2012). https://doi.org/10.1128/MCB.00775-12
17. Monaco, H.L.: The transthyretin-retinol-binding protein complex. Biochimica et Biophysica Acta (BBA)—Protein Struct. Mol. Enzymol. **1482**(1–2), 65–72 (2000). https://doi.org/10.1016/s0167-4838(00)00140-0
18. Futterman, S., Swanson, D., Kalina, R.E.: A new, rapid fluorometric determination of retinol in serum. Invest Ophthalmol. **14**(2), 125–130 (1975)
19. Kawaguchi, R., Zhong, M., Sun, H.: Real-time analyses of retinol transport by the membrane receptor of plasma retinol binding protein. J. Visualized Exp. JoVE **71**, e50169 (2013). https://doi.org/10.3791/50169
20. Kraft, R., Herndon, D.N., Kulp, G.A. et al.: Retinol binding protein: marker for insulin resistance and inflammation postburn? JPEN. J. Parenteral Enteral Nutr. **35**(6) (2011). https://doi.org/10.1177/0148607111413901
21. Klisić, A., Kavarić, N., Bjelaković, B., et al.: The association between retinol-binding protein 4 and cardiovascular risk score is mediated by waist circumference in overweight/obese adolescent girls. Acta Clin. Croat. **56**(1), 92–98 (2017). https://doi.org/10.20471/acc.2017.56.01.14

22. Kim, Y.S., Kim, N.H., Lee, S.W., et al.: Effect of protocatechualdehyde on receptor for advanced glycation end products and TGF-beta1 expression in human lens epithelial cells cultured under diabetic conditions and on lens opacity in streptozotocin-diabetic rats. Eur. J. Pharmacol. **569**(3), 171–179 (2007)
23. Séro, L., Sanguinet, L., Blanchard, P., et al.: Tuning a 96-well microtiter plate fluorescence-based assay to identify AGE inhibitors in crude plant extracts. Molecules **18**(11), 14320–14339 (2013). https://doi.org/10.3390/molecules181114320
24. Takahashi, M., Oikawa, M., Nagano, A.: Effect of age and menopause on serum concentrations of pentosidine, an advanced glycation end product. J Gerontol A **55**(3), M137–M140 (2000). https://doi.org/10.1093/gerona/55.3.M137
25. Olar, L.E., Ciobanu, D.M., Matei, F., Papuc, I.: The assessment of fluorophores advanced glycation end products-to-kynurenine ratio in healthy and diabetic rats and humans. Studia. UBB Chemia. **63** (1), 37–53 (2018). https://doi.org/10.24193/subbchem.2018.1.03
26. Sugiyama, S., Miyata, T., Ueda, Y., et al.: Plasma levels of pentosidine in diabetic patients: an advanced glycation end product. J. Am. Soc. Nephrol. **9**(9), 1681–1688 (1998)
27. Machowska, A., Sun, J., Qureshi, A.R et al. Plasma pentosidine and its association with mortality in patients with chronic kidney disease. PLoS one 4; **11**(10): e0163826 (2016). https://doi.org/10.1371/journal.pone.0163826
28. Chang, Y.H., Lin, K.D., Wang, C.L., et al.: Elevated serum retinol-binding protein 4 concentrations are associated with renal dysfunction and uric acid in type 2 diabetic patients. Diabetes Metab. Res. Rev. **24**(8), 629–634 (2008). https://doi.org/10.1002/dmrr.894
29. Abahusain, M.A., Wright, J., Dickerson, J.W.: Retinol, alpha-tocopherol and carotenoids in diabetes. Eur. J. Clin. Nutr. **53**(8), 630–635 (1999)
30. Tuitoek, P.J., Ziari, S., Tsin, A.T., et al.: Streptozotocin-induced diabetes in rats is associated with impaired metabolic availability of vitamin A (retinol). Br. J. Nutr. **75**(4), 615–622 (1996)

Eye Examination for Early Detection of Diabetic Neuropathy-Role of Corneal Confocal Microscopy

Georgeta Victoria Inceu, C. L. Vonica, and G. Roman

Abstract

Diabetes mellitus registers an alarming increase globally, taking epidemic proportions. Diabetic neuropathies are considered the most prevalent chronic complications of diabetes, affecting up to 50% of subjects with diabetes during lifetime. Distal symmetric polyneuropathy (DSPN), a length-dependent injury of peripheral nerves is the most frequent type among diabetic patients. Small nerve fibers are the first affected in the natural progression of the disease and their early damage can be assessed using corneal confocal microscopy (CCM). We applied CCM to the study group of 90 patients with type 2 diabetes, to identify early signs of diabetic neuropathy, to stratify patients into classes of severity of diabetic neuropathy and to find potential correlation between clinical, metabolic parameters and diabetic neuropathy severity. In our study, 88.89% of the patients were diagnosed as having DSPN, 37.77% of them with mild form, 38.88% with moderate neuropathy and 12.22% with severe neuropathy. Patients with diabetic neuropathy had a significantly higher BMI ($p = 0.04$) and abdominal circumference, higher HbA1c ($p = 0.36$) and a higher total cholesterol ($p = 0.43$) compared with patients without DSPN. Also, the Toronto Clinical Neuropathy Score was significantly higher in patients with pathological changes of the sub-basal corneal plexus ($p = 0.04$). Patients with DSPN had a significantly longer duration of diabetes ($p = 0.04$) and a worse glycemic control, compared with patients without DSPN. The result of our study proved that CCM can be used as a reliable diagnosis tool for early detection of small nerve fiber damage, considering that corneal sub-basal plexus changes precede clinically detected peripheral nerve changes.

Keywords

Distal symmetric polyneuropathy • Corneal confocal microscopy • Small nerve fibers

1 Introduction

Worldwide, we are witnessing to an impressive dynamic of the increase in the prevalence of diabetes, a chronic, progressive disease that requires continued medical care based on multifactorial risk reduction strategies [1]. Diabetes induced complications represent a major health burden, with an important impact on the quality of life of diabetic patients [2]. Type 2 diabetes is a significant cause of blindness, foot ulcerations and amputation and end-stage renal failure [3]. The economic cost of diabetes is also very high and it's continually rising [4, 5].

Diabetic neuropathies are considered the most prevalent chronic complications of diabetes, affecting up to 50% of subjects with diabetes during lifetime [6]. Diabetes can affect different components of the nervous system, and diabetic neuropathies can manifest in various forms with different clinical manifestations, but the most frequent type of diabetic neuropathy is distal symmetric polyneuropathy (DSPN), a diffuse and length-dependent damage of peripheral nerves [7]. Diabetic peripheral neuropathy is the most important risk factor for foot ulcerations [8–10], which may lead to lower extremity amputation among people with diabetes [11, 12] and drive significant economic cost of diabetic neuropathy. An early diagnosis and proper staging of diabetic neuropathy is essential for therapeutic decisions and early interventions.

In the natural history of diabetic neuropathy, the involvement of different nerves fibers is selective, small nerve fiber being affected earliest in the disease progression, prior to the development of the large fiber injury [13, 14].

G. V. Inceu (✉) · C. L. Vonica · G. Roman
"Iuliu Hatieganu" University of Medicine and Pharmacy, 2-4 Clinicilor Street, Cluj-Napoca, Romania
e-mail: georgetainceu@yahoo.com

G. Roman
Clinical Center of Diabetes, Nutrition, Metabolic Diseases, Cluj-Napoca, Romania

S. Vlad and N. M. Roman (eds.), *6th International Conference on Advancements of Medicine and Health Care through Technology; 17–20 October 2018, Cluj-Napoca, Romania*, IFMBE Proceedings 71,
https://doi.org/10.1007/978-981-13-6207-1_2

Small Aδ and C nerve fibers of the sensory and autonomic nervous system represents 70–90% of the peripheral nerve fibers. Small nerve fiber loss usually presents with pain, dysesthesia and autonomic dysfunction [13]. The involvement of large fiber may cause loss of protective sensations, numbness, impaired balance and walking. All this increase the risk of falls, foot trauma, ulceration and amputation [15].

The screening and diagnosis of diabetic neuropathy is mainly based on symptoms questionnaires, clinical examination, reflex tests and quantitative sensory tests [16]. Nerve conductions study are used to confirm the diagnosis, even though these electrophysiologic studies can assess only the large-diameter nerve fiber status [17]. To assess small nerve fiber loss, the golden diagnosis test is considered the quantification of intra-epidermal nerve fiber density (IENFD) in skin biopsies [18, 19]. Lately, there is a growing body of evidence that corneal confocal microscopy (CCM) can be used as a reliable screening tool and diagnosis method in diabetic sensorimotor polyneuropathy [20–22]. More than that, CCM can also be used in patients with other types of neuropathy such as Human Immunodeficiency Virus-associated sensory neuropathy [23], chemotherapy-induced neuropathy [24], as well as chronic inflammatory demyelinating polyneuropathy [25].

In people with diabetes have been described several abnormalities in corneal morphology including reduction in corneal nerve bundles, reduced thickness, thinner epithelium [26, 27], and a strong correlation have been demonstrated between injuries of peripheral nerves due to diabetes and damages in corneal sub-basal nerve plexus detected with CCM [28]. So, in the light of these strong evidence, CCM can be considered a surrogate marker of small fiber neuropathy [29].

2 Objectives

A. *To quantify small unmyelinated nerve fiber loss in patients with type 2 diabetes using CCM*
B. *To stratify patients into classes of severity of diabetic neuropathy*
C. *To assess potential correlation between clinical, metabolic parameters and DSPN severity*

3 Materials and Methods

90 patients with type 2 diabetes from Cluj-Napoca Diabetes Clinical Center were included in the study, between September 2012-November 2012. Inform consent was obtained from all the participants All the patients were assessed for anthropometric parameters: weight, height, waist circumference and body mass index (BMI), and laboratory measurements. The presence of DSPN was assessed using Semmes-Weinstein Monofilament Testing (SWMT), vibration perception with the 128-Hz tuning fork, Rapid-Current Perception Threshold (R-CPT) measurements using the Neurometer®, and CCM. The Neurological Symptom Score (NSS) [30] and the Toronto Clinical Neuropathy Score (TCNS) [31] which includes an assessment of symptoms (present or absent), sensory loss (normal or abnormal), and reflexes (normal, reduced, or absent), were used. For the TCNS, based on the outcome, a score of 6–8 denotes mild neuropathy, 9–11 moderate, and ≥ 12 severe neuropathy.

CCM was performed using a Heidelberg Retina Tomograph. This is a confocal retinal microscope with a Rostock module attached that allows it to shrink focal length and so, can make cornea and no retinal section. The images were analyzed manually by an ophthalmologist and four parameters were quantified: the total number of nerves per image (TNN); the number of main branches (NMN), the number of branches connections (NBC), and the branches/connections ratios (BCR) [21]. According to these parameters, DSNP was stratified into three severity classes as presented in Table 1.

Statistical analysis was performed using SPSS 15.0 (SPSS Inc, Chicago, USA). The normality of variables distribution was evaluated using Kolmogorov–Smirnov test. Continuous data were expressed as means ±standard deviation when normally distributed or as median for non-parametric data. Qualitative data were expressed as numbers and percentages. Group comparisons of all variables were performed using t-test for groups with normally distributed data, and Mann–Whitney test for groups with not normally distributed data. A ***p*** values less than 0.05 was considered statistically significant.

Table 1 DSPN severity classes according to the CCM parameters

Parameters	Without DSPN	Mild	Moderate	Severe
TNN	>25	20	15	10
NMB	>8	5–7	2–4	≤ 1
NBC	>20	<15	<10	<5
BCR	<1.25	1.3	1.5	>2

DSPN-distal symmetric polyneuropathy, TNN-the total number of nerves per image, NMB-the number of main branches, NBC-the number of branches connections, BCR-the branches/connections ratios

4 Results

The study group included 90 patients with type 2 diabetes who met the inclusion criteria. Of these, 56.7% (51) were female, and 4.3% (39) were males. The characteristics of the study group are presented in Table 2.

According to the protocol described in Materials and methods, after performing CCM, we assigned the patients according to the presence of diabetic neuropathy and further on the severity classes of diabetic neuropathy: 11.11% (10) without DSPN, 37.7% (34) mild DSPN, 38.8% (35) moderate DSPN, 12.2% (11) severe DSPN. Figure 1 shows the images of patients with and without DSPN.

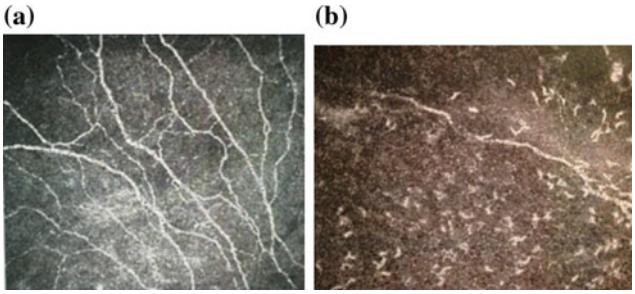

Fig. 1 Sub-basal nerve plexus of a subject without DPN (**a**) and with severe DPN (B)

Table 2 Baseline characteristics of the study group

Parameter	Mean ±SD
No. of patients	90
Mean age (years)	61.58 ± 10.092
Sex (male)	43.3% (n = 39)
Mean diabetes duration (years)	8.31 ± 6.61
Smoking	16.7% (n = 15)
Alcohol	28.9% (n = 26)
Hypertension	82.2% (n = 74)
Total cholesterol (mg/dl)	179.3 ± 40.6
HDL-cholesterol (mg/dl)	45.3 ± 13.3
LDL-cholesterol (mg/dl)	101.3 ± 35.7
Triglycerides (mg/dl)	163.4 ± 69.1
Mean HbA1c (%)	7.5 ± 1.1
BMI (kg/m^2)	31.6 ± 5.14
Retinopathy	23.3% (n = 21)

BMI-body mass index, HDL-high density lipoprotein, LDL-low density lipoprotein, HbA1c-glycated hemoglobin. Data are presented as means ±SD (standard deviation)

Were further analyzed the differences between patients without DSPN and those with DSPN (regardless of severity) (Table 3). Patients with diabetic neuropathy had a significantly higher BMI (p = 0.04) and abdominal circumference, higher HbA1c (p = 0.36) and a higher total cholesterol (p = 0.43) compared with patients without DSPN. Also, the Toronto Clinical Neuropathy Score was significantly higher in patients with pathological changes of the sub-basal corneal plexus (p = 0.04).

Patients with morphological changes of the sub-basal corneal plexus had a significantly longer duration of diabetes (p = 0.04) compared to patients without diabetic neuropathy and additionally, the duration of diabetes correlated positively with the severity of diabetic neuropathy (5.6 ± 3.44 years in patients without DSPN, 8.01 ± 5.86 years in patients with mild DSPN, 9.4 ± 6.53 years in patients with severe DSPN) (Fig. 2).

Table 3 Clinical and biochemical parameters in patients with and without DSPN, assessed by CCM

Parameter	No DSPN	Established DSPN	p-value
Age (years)	60.9 ± 12.67	61.66 ± 9.82	0.87
Diabetes duration (years)	5.6 ± 3.44	8.65 ± 6.85	0.04
Weight (kg)	85.2 ± 15.88	87.96 ± 15.39	0.52
BMI (kg/m^2)	29.57 ± 0.43	31.9 ± 5.28	0.04
WC (cm)	102.7 ± 9.7	110.69 ± 12.37	0.04
HbA1c (%)	6.8(6.7–8.1)	7.59 ± 1.17	0.36
Total cholesterol (mg/dl)	168.7 ± 32.32	180.72 ± 41.52	0.43
HDL cholesterol (mg/dl)	41 ± 14.54	45.9 ± 1.22	0.24
Triglycerides (mg/dl)	169.7 ± 57.56	162.64 ± 70.79	0.41
LDL cholesterol (mg/dl)	93.76 ± 15.46	102.29 ± 37.5	0.39
NSS	7.1 ± 5.92	7.63 ± 4.97	0.7
TCNS	2.1 ± 2.23	3.49 ± 2.71	0.04

BMI-body mass index, WC-waist circumference, HbA1c-glycated hemoglobin, HDL-high density lipoprotein, LDL-low density lipoprotein, NSS- The Neurological Symptom Score, TCNS-The Toronto Clinical Neuropathy Score. Data are presented as mean or median ± SD

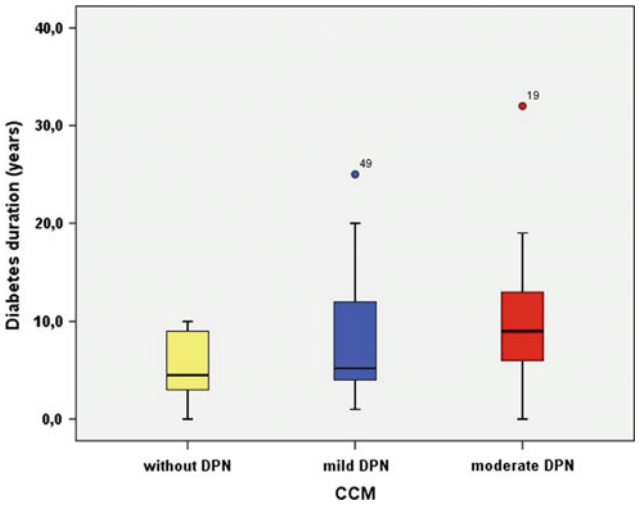

Fig. 2 Significantly higher diabetes duration in patients with higher classes of diabetic neuropathy. CCM-Corneal Confocal Microscopy, DPN-Diabetic peripheral neuropathy

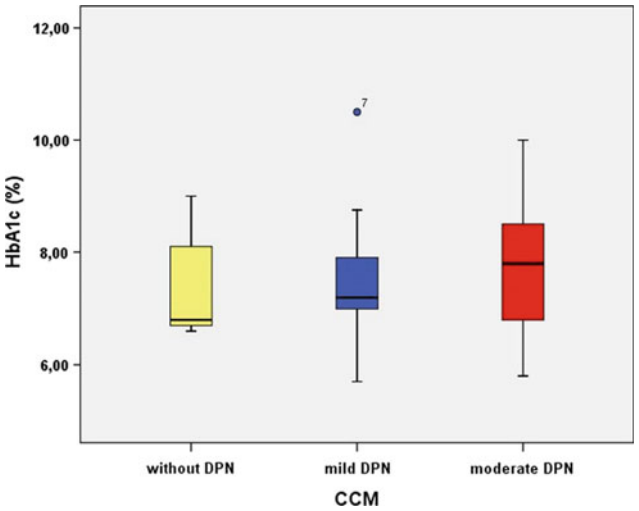

Fig. 3 Correlation between HbA1c and diabetic neuropathy severity

The patients were divided according to HbA1c value in two categories: with good glycemic control (HbA1c < 7%) and suboptimal glycemic control (HbA1c $\geq$ 7%), and the results showed that patients with good glycemic control had a shorter duration of diabetes, better anthropometric indices and better lipid profile compared to patients with unsatisfactory glycemic control (Table 4).

We noticed an increasing trend in glycated hemoglobin value with the increase in the severity of diabetic neuropathy, by analyzing this parameter in the study patients (without DSPN, with mild, moderate and severe DSPN) (Fig. 3).

Patients in the study group were assessed for protective sensation (using the Semmes-Weinstein Monofilament Testing), and the results were compared with those obtained from the sub-basal corneal plexus imaging through CCM. Although a significant percentage of patients with preserved protective sensation were diagnosed with diabetic neuropathy (64 patients), statistical significance was not reached in this case (p = 0.29) (Table 5).

Following the calculation of the Kendall correlation coefficient, there was a tendency for patients with abnormal protective sensitivity to associate with lower severity classes of neuropathy (according to CCM parameters) (Table 6).

Table 4 Characteristics of patients in the studied group according to the HbA1c value

Parameter	HbA1c < 7	HbA1c $\geq$ 7	p-value
Age (years)	63.1 ± 8.47	60.78 ± 10.83	0.17
Diabetes duration (years)	8.26 ± 7.38	8.34 ± 6.25	0.01
BMI (kg/m^2)	30.51 ± 4.65	32.23 ± 5.33	0.27
WC (cm)	108.16 ± 11.22	110.66 ± 12.87	0.18
Total cholesterol (mg/dl)	177.23 ± 36.92	180.52 ± 42.7	0.48
HDL cholesterol (mg/dl)	46.55 ± 14.77	44.72 ± 12.68	0.51
Triglycerides (mg/dl)	158.32 ± 63.12	166.11 ± 72.56	0.04
LDL cholesterol (mg/dl)	99.01 ± 34.27	102.57 ± 36.77	0.24
NSS	7.81 ± 4.78	7.44 ± 5.22	0.04
TCNS	3.1 ± 2.29	3.46 ± 2.88	0.17

BMI-body mass index, WC-waist circumference, HbA1c-glycated hemoglobin, HDL-high density lipoprotein, LDL-low density lipoprotein, NSS-The neurological symptom score, TCNS-The Toronto clinical neuropathy score. Data are presented as mean or median ± SD

Table 5 DSPN diagnosed by using protective sensation testing and CCM

	CCM				
Protective sensation	No DSPN	Mild DSPN	Moderate DSPN	Severe DSPN	Total
Lost	0	5	8	3	16
Normal	10	29	27	8	74
Total	10	34	35	11	90

Data are presented as number of patients. CCM-corneal confocal microscopy, DSPN-distal symmetric polyneuropathy

Table 6 Correlation between CCM and protective sensation

	Protective sensation
Kendall correlation coefficient	−0,24
	0,04

CCM-corneal confocal microscopy

5 Discussions

Corneal confocal microscopy is a method with over 20 years of experience in the evaluation of diabetic neuropathy [32, 33]. This study included 90 patients with type 2 diabetes who were assessed for the presence of diabetic neuropathy using CCM and were then classified on severity classes of diabetic neuropathy according to an original protocol [21]. 88.89% of the patients were diagnosed as having DSPN, 37.77% of them with mild form, 38.88% with moderate neuropathy and 12.22% with severe neuropathy. In the literature, several studies have confirmed and validated the use of CCM in both diagnosis and risk stratification of the disease [28, 34, 35]. Tavakoli et al. [36] assessed 101 diabetic patients (type 1 and 2) for the presence of diabetic neuropathy using CCM. In their study, 66.33% of patients is classified as having diabetic neuropathy (36.63% mild neuropathy, 12.84% moderate and 13.86% severe diabetic neuropathy).

Analyzing patients with and without DSPN, we noticed significant differences between BMI (31.9 ± 5.28 vs. 29.57 ± 3.43 kg/m^2, $p = 0.04$) and abdominal circumference (110.69 ± 12.37 vs. 102.7 ± 9.7 cm, $p = 0.04$) between the two groups. Edwards and colleagues [37] also found statistically significant differences in BMI and abdominal circumference between patients with and without diabetic neuropathy ($p < 0.05$).

We found a statistically significant difference ($p = 0.04$) between duration of diabetes in patients without DSPN (5.6 ± 3.44 years) compared to patients with DSPN (8.65 ± 6.85 years). Additionally, the duration of diabetes had an ascending trend within the severity classes of diabetic neuropathy, more obvious for patients with moderate neuropathy (22.5% of the subjects had diabetes duration less than 5 years, 44.1% between 5 and 10 years, and 52% had a history of diabetes over 10 years). Our results are consistent with those reported in other studies using CCM to assess diabetic neuropathy [36, 38]. In a study involving 231 patients with diabetes [37], the length of small unmyelinated nerve fibers of the sub-basal corneal plexus correlated inversely and statistically significantly with the duration of diabetes mellitus ($r = -0.20$).

HbA1c showed an increase trend with the severity classes of diabetic neuropathy, finding consistent with those reported by Petropoulos and co [39] in their study on 111 diabetic patients and 47 healthy volunteers, assessed by CCM. HbA1c was statistically significantly higher in patients with diabetes and highest values of HbA1c were recorded in patients with severe diabetic neuropathy.

In our studied group, an important number of patients with preserved protective ($n = 64$) and vibratory ($n = 66$) sensation, were actually identified as having pathological changes of the sub-basal corneal plexus, an essential finding that supports the hypothesis that small unmyelinated nerve fiber loss precede the large myelinated nerve fibers damage, which highlights one of the limitations of the conventional methods of diabetic neuropathy assessment, applied in everyday practice, the ability to quantify only the large myelinated nerve fibers. An important percentage of patients with diabetes who had no clinical signs of neuropathy was shown to have abnormal corneal sub-basal nerve plexus changes, demonstrating that corneal changes precede clinically detected peripheral nerve changes.

6 Conclusions

Screening and diagnosis of peripheral diabetic neuropathy remain a challenge for the clinician, as there is no consensus on how to do it. On the other hand, the importance of early detection and adequate management of diabetic neuropathy results from the fact that up to 50% of patients is asymptomatic, with a high risk of painless injuries. Neuropathic symptoms and deficits affect the quality of life and life expectancy of patients with diabetes, inducing a significant rate of morbidity and mortality.

Corneal confocal microscopy is a noninvasive technique to analyze corneal structure and anatomy allowing the study

of the different layers of cornea, the most innervated organ of human body [6].

The results of this study demonstrated the accuracy of confocal corneal microscopy in the diagnosis of peripheral diabetic neuropathy compared to classical advocated methods used to assess diabetic neuropathy. CCM can be considered an important diagnosis instrument for the detection of small fiber neuropathy, the earliest manifestation of DSPN, having the potential to identify patients with minimal signs of neuropathy.

Conflict of Interest The authors declare that they have no conflict of interest.

Statement of Human and Animal Rights

The procedures involving human subjects conducted in this study were in accordance with the ethical standards of the responsible committee on human experimentation (institutional and national) and with the Helsinki Declaration of 1975, as revised in 2000 and 2008.

References

1. American Diabetes Association: Standards of medical care in diabetes-2018. Diab. Care **41**(1(Suppl)), S1–S1582 (2018)
2. International Diabetes Federation: IDF Diabetes Atlas 8th Edition. International Diabetes Federation. Available at http://www.diabetesatlas.org/ (2017)
3. Fowler, M.J.: Microvascular and macrovascular complications of diabetes. Clin. Diab. **26**(2), 77–82 (2008). https://doi.org/10.2337/diaclin.26.2.77
4. Seuring, T., Archangelidi, O., Suhrcke, M.: The economic costs of type 2 diabetes: a global systematic review. Pharmacoeconomics **33**(8), 811–831 (2015)
5. American Diabetes Association: Economic costs of diabetes in the U.S. in 2012. Diab. Care **36**(4), 1033–1046 (2013)
6. Tesfaye, S., Boulton, A.J.M., Dyck, P.J., et al.: Diabetic neuropathies: Update on definitions, diagnostic criteria, estimation of severity, and treatments. Diab. Care **33**(10), 2285–2293 (2010)
7. Pop-Busui, R., Boulton, A.J., Feldman, E.L., et al.: Diabetic neuropathy: a position statement by the American diabetes association. Diab. Care **40**, 136–154 (2017)
8. Frykberg, R.G., Zgonis, T., Armstrong, D.G., Driver, V.R., et al.: Diabetic foot disorders. A clinical practice guideline (2006 revision). J. Foot Ankle Surg. **45**(5), S1–S66 (2006)
9. Boulton, A.J.M., Kirsner, R.S., Vileikyte, L.: Neuropathic diabetic foot ulcers. N. Engl. J. Med. **351**, 48–55 (2004)
10. Abbott, C.A., Carrington, A.L., Ashe, H., et al.: The North-West diabetes foot care study: incidence of, and risk factors for, new diabetic foot ulceration in a community-based patient cohort. Diabet. Med. **19**(5), 377–384 (2002)
11. Lavery, L.A., Armstrong, D.G., Harkless, L.B.: Classification of diabetic foot wounds. J. Foot Ankle Surg. **35**(6), 528–531 (1996)
12. American Diabetes Association: Consensus Development Conference on Diabetic Foot Wound Care: 7–8 April 1999, Boston, Massachusetts. American Diabetes Association. Diabetes Care **22**(8), 354–60 (1999)
13. Brines M., Culver D.A., Ferdousi, M. et al.: Corneal nerve fiber size adds utility to the diagnosis and assessment of therapeutic response in patients with small fiber neuropathy **8**, 4734 (2018)
14. Lewis, I.J.H., Perkins, B.A., Lovblom, L.E., et al.: Using in vivo corneal confocal microscopy to identify diabetic sensorimotor polyneuropathy risk profiles in patients with type 1 diabetes. BMJ Open Diab. Res. Care **5**, e000251 (2017). https://doi.org/10.1136/bmjdrc-2016-000251
15. Bril, V.: Treatments for diabetic neuropathy Journal of the Peripheral nervous. System **17**, 22–27 (2012)
16. Boulton, A.J., Malik, R.A., Arezzo, J.C., et al.: Diabetic somatic neuropathies. Diab. Care **27**, 1458–1486 (2004)
17. Callaghan, B.C., Kerber, K.A., Lisabeth, L.L., et al.: The role of neurologists and diagnostic tests in the management of distal symmetric polyneuropathy. JAMA Neurol. **71**(9), 1143–1149 (2014)
18. Lauria, G., Bakkers, M., Schmitz, C., et al.: Intraepidermal nerve fiber density at the distal leg: a worldwide normative reference study. J. peripheral nerv. syst. **15**(3), 202–207 (2010)
19. Engelstad, J.K., Taylor, S.W., Witt, L.V., et al.: Epidermal nerve fibers Confidence intervals and continuous measures with nerve Conduction. Neurology **79**, 2187–2193 (2012)
20. Tavakoli, M., Petropoulos, I.N., Malik, R.A.: Corneal confocal microscopy to assess diabetic neuropathy: an eye on the foot. J. Diab. Sci. Technol. **7**(5), 1179–1189 (2013)
21. Inceu, G., Demea, H., Veresiu, I.A.: Corneal confocal microscopy—a novel, noninvasive method to assess diabetic peripheral neuropathy. Rom. J. Diab. Nutr. Metab. Dis **21**(4), 319–326 (2014)
22. Tavakoli, M., Marshall, A., Pitceathly, R., et al.: Corneal confocal microscopy: a novel means to detect nerve fibre damage in idiopathic small fibre neuropathy. Exp. Neurol. **223**(1), 245–250 (2010)
23. Kemp, H.I., Petropoulos, I.N., Rice, A.S.C., et al.: Use of Corneal Confocal Microscopy to Evaluate Small Nerve Fibers in Patients With Human Immunodeficiency Virus. JAMA Ophthalmol **135**(7), 795–800 (2017)
24. Ferdousi, M., Azmi, S., Petropoulos, I.N., et al.: Corneal confocal microscopy detects small fibre neuropathy in patients with upper gastrointestinal cancer and nerve regeneration in chemotherapy induced peripheral neuropathy. PLoS ONE **10**(10), e0139394 (2015)
25. Stettner, M., Hinrichs, L., Guthoff, R. et al.: Corneal confocal microscopy in chronic inflammatory demyelinating polyneuropathy. Ann. Clin. Transl. Neurol. 3(2), 88–100 (2015)
26. Maddaloni, E., Sabatino, F.: In vivo corneal confocal microscopy in diabetes: Where we are and where we can get. World J Diabetes **7**(17), 406–411 (2016)
27. Wang, E.F., Misram, S.L., Patel, D.V.: In: Vivo Confocal Microscopy of the Human Cornea in the Assessment of Peripheral Neuropathy and Systemic Diseases. BioMed Research International. http://dx.doi.org/10.1155/2015/951081
28. Malik, R.A., Kallinikos, P., Abbott, C.A., et al.: Corneal confocal microscopy: a non-invasive surrogate of nerve fibre damage and repair in diabetic patients. Diabetologia **46**, 683–688 (2003)
29. Quattrini, C., Tavakoli, M., Jeziorska, M., et al.: Surrogate markers of small fiber damage in human diabetic neuropathy. Diabetes **56**, 2148–2154 (2007)
30. Meijer, J., Smit, A., Sonderen, E., et al.: Symptom scoring systems to diagnose distal polyneuropathy in diabetes: The diabetic neuropathy symptom score. Diab. Med. **19**(11), 962–965 (2002)
31. Perkins, B.A., Olaleye, D., Zinman, B., Bril, V.: Simple screening tests for peripheral neuropathy in the diabetes clinic. Diab. Care **24**(2), 250–256 (2001)

32. Papanas, N., Ziegler, D.: Corneal confocal microscopy: a new technique for early detection of diabetic neuropathy. Curr. Diab Rep. **13**(4), 488–499 (2013)
33. Jiang, M.-S., Yuan, Y., Gu, Z.-X., Zhuang, S.-L.: Corneal confocal microscopy for assessment of diabetic peripheral neuropathy: a meta-analysis. Br. J. Ophthalmol. **100**(1), 9–14 (2016)
34. Ahmed, A., Bril, V., Orszag, A., et al.: Detection of diabetic sensorimotor polyneuropathy by corneal confocal microscopy in type 1 diabetes: a concurrent validity study. Diabetes Care **35**(4), 821–828 (2012)
35. Ishibashi, F., Okino, M., Ishibashi, M., et al.: Corneal nerve fiber pathology in Japanese type 1 diabetic patients and its correlation with antecedent glycemic control and blood pressure. J. Diab. Invest. **3**(2), 191–198 (2012)
36. Tavakoli, M., Quattrini, C., Abbott, C., et al.: Corneal confocal microscopy: a novel noninvasive test to diagnose and stratify the severity of human diabetic neuropathy. Diab. Care **33**(8), 1792–1797 (2010)
37. Edwards, K., Pritchard, N., Vagenas, D., et al.: Utility of corneal confocal microscopy for assessing mild diabetic neuropathy: baseline findings of the LANDMark study. Clin. Exp. Optom. **95**(3), 348–354 (2012)
38. Tavakoli, M., Kallinikos, P.A., Efron, N., et al.: Corneal sensitivity is reduced and relates to the severity of neuropathy in patients with diabetes. Diab. Care **30**(7), 1895–1897 (2007)
39. Petropoulos, I.N., Alam, U., Fadavi, H., et al.: Corneal nerve loss detected with corneal confocal microscopy is symmetrical and related to the severity of diabetic polyneuropathy. Diab. Care **36** (11), 3646–3651 (2013)

Doppler Ultrasonography, a Rapid Evaluation Method of the Major Risk in the Vascular Pathology

Elena Gligor, A. I. Roman, V. Ossian, D. Gligor, M. Beudean, and M. Olt

Abstract

The benefit ultrasonography brings in medical practice when dubbed by a competent user is unquestionable. The following considerations support the assertion that the technique is non-invasive for the patient and the user, inexpensive, offering real-time relations as compared to other imaging and high performance techniques such as CT and MRI. In our clinical study, the four patients selected were representative for the above mentioned conclusions, being hospitalized and diagnosed sonographically with: tissue hematoma, pseudoaneurysm, arteriovenous fistula and venous thrombosis. After discharge, patients were clinically and sonographically monitored after 1, 3 and 6 months. The technique has also imposed a choice of treatment appropriate to each individual case, namely a conservative treatment for the patients with hematoma, pseudoaneurysm and arteriovenous fistula. For the patient with venous thrombosis, the prescribed treatment was medical. A surgical treatment (excision and ligation) for the pseudoaneurysm was also discussed. After a 6-month surveillance and delay, thrombosis was performed. We mention that the prognosis is also favorable after a surgical treatment when the evaluation and timing are correctly chosen.

Keywords

Pseudoaneurysm • Arteriovenous fistula • Venous thrombosis • Hematoma

1 Introduction

The Doppler ultrasound is a way of exploring the cardiovascular apparatus based on the Doppler Effect (described in 1842 by Hristian Doppler), which consists in modifying the frequency of the received signal when the emission source and/or the receiver are moving away from one another. At the level of the cardiovascular device, the color Doppler codifies the blood flow through the color providing exceptional user relationships.

Increasing the number of invasive (catheterization) or non-invasive procedures in medical practice as well as a traumatology that is more and more common in daily work has led to an increase in the number of vascular complications, including the following: hematoma with extensive skin blood swellings, pseudoaneurysms, arteriovenous fistulas and venous thrombosis. Post-catheterization, the frequency of complications depends on the nature of the intervention (performed for diagnostic or therapeutic purposes).

In the medical literature, the frequency of reported complications is considered to be below 1% for diagnostic catheterization, up to 9% for coronary angioplasty and over 16% for intracoronary stenting [1–3].

2 Material and Method

This study included a limited number of adult patients aged 42–76 years, namely 2 men and 2 women with severe vascular disease (pseudoaneurysm, arteriovenous fistula and venous thrombosis) admitted to the Recovery Hospital over

E. Gligor (✉) · M. Beudean
Rehabilitation Hospital, 46-50 Viilor, Cluj-Napoca, Romania
e-mail: elenagligor2006@yahoo.com

A. I. Roman
Regional Gastroenterology Institute, Cluj-Napoca, Romania

V. Ossian
Bendis Clinic, Cluj Napoca, Romania

D. Gligor
Cluj Municipal Clinical Hospital, Cluj-Napoca, Romania

M. Olt
Technical University of Cluj Napoca, Cluj-Napoca, Romania

S. Vlad and N. M. Roman (eds.), *6th International Conference on Advancements of Medicine and Health Care through Technology; 17–20 October 2018, Cluj-Napoca, Romania*, IFMBE Proceedings 71,
https://doi.org/10.1007/978-981-13-6207-1_3

the past five years. Post-discharge, patients were periodically monitored after 1, 3 and 6 months, respectively.

The exploration technique used was Doppler ultrasound, using the eSAOTE MyLAB 50 device with 3.5; 5; 7.5 and 10 MHz transducers.

Taking into account the patient's nutritional status (obesity), the presence of skin lesions (ulceration) or the existence of possible hematomas, the high frequency linear transducer of 10 MHz has been used frequently.

2.1 Clinical Occurence

The existence of a vascular pathology (hematoma, pseudoaneurysm or thrombosis) was suspected in the patient after a trauma history (concussion or penetrating trauma with vascular wall damage) at one of the extremities. Extensive ecchymosis was clinically diagnosed with non-painful and non-pulsatile palpable mass as in the presence of a hematoma, pseudoaneurysm, abscess, or a thrombotic process.

2.2 Paraclinic Diagnosis

The use of US Doppler ultrasound has led to rapidly and accurately determine the pathology involved. Thus, hematoma or thrombosed pseudoaneurysm are avascular pathological processes with the absence of the characteristic signal or without blood flow signal (Fig. 1).

If the hematoma is difficult to address through the US Doppler technique, the CT technique can be used to accurately assess the presence and extent of it.

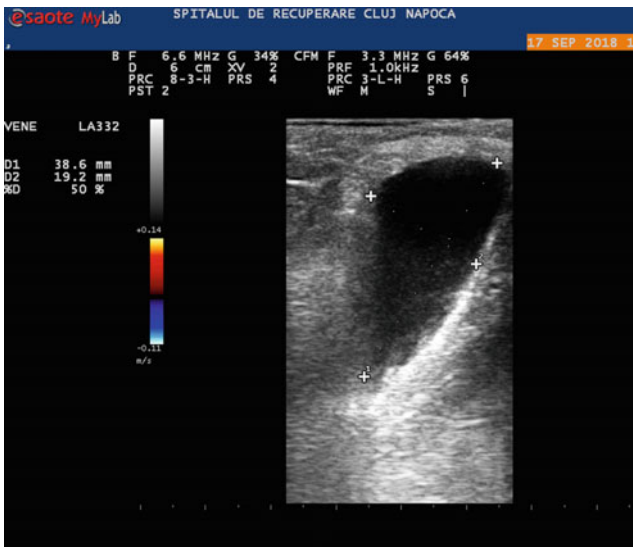

Fig. 1 The sonographic image of a hematoma in a patient after an arterial puncture

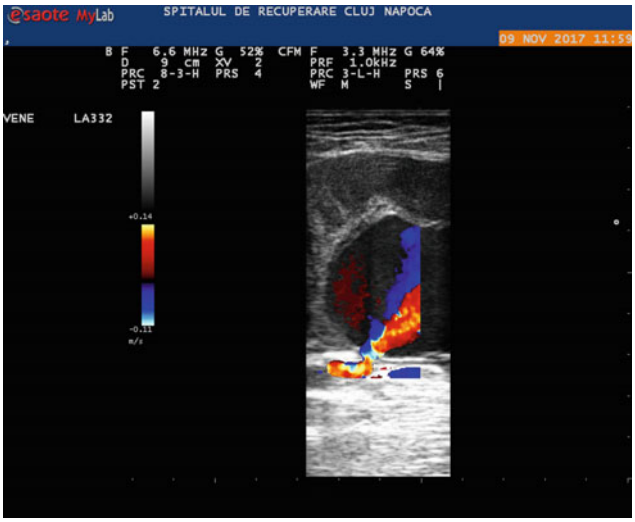

Fig. 2 The image of an arterial pseudoaneurysm emerged post-catheterization at the inguinal level obtained at color Doppler

Another entity encountered in clinical practice is the Pseudoaneurysm (PSA). Recent communications from the medical literature [4–6] show an increase in its incidence taking into account the increased number of arterial catheterizations for diagnostic or therapeutic purposes. Sonographically, PSA is a spectacular visible vascular mass connected to the artery from which it derives through a narrow portion called "neck" or tract (Fig. 2).

Concerning the hemodynamic aspect, during the systole the blood flow present in the tract and within the dilated area of the PSA is anterograde; in diastole, after increasing pressure in the dilated area, at exit the blood flow becomes retrograde and "returns" to the artery.

Complications in PSA could be: local pain, infection, compression neuropathy or rupture as a surgical emergency. However, many of the small size PSAs have a good evolution to spontaneous thrombosis while others go to surgical treatment. In the case of a post-procedural pulsating mass, it is mandatory to perform a sonographic examination to avoid a diagnostic error (including lymph nodes located inguinal and very well vascularized; sonographically, the lymph nodes are hypoechogenic on the gray scale and rich internal vasculature to Color Doppler). Confusion with a PSA also occurs when we limit ourselves to a clinical exam. Other sources of error may be venous dilatations with or without thrombotic mass positioned on the large saphenous vein, but which can be correctly diagnosed using the color and pulsed Doppler, using in this case a high-frequency linear transducer [7, 8].

Another complication that may be relatively common after an inguinal vascular approach is the arteriovenous fistula encountered in a patient for hemodialysis (Fig. 3) [9].

In addition to the above mentioned, arterial trauma, when a peripheral atherosclerotic disease is present, may lead to an

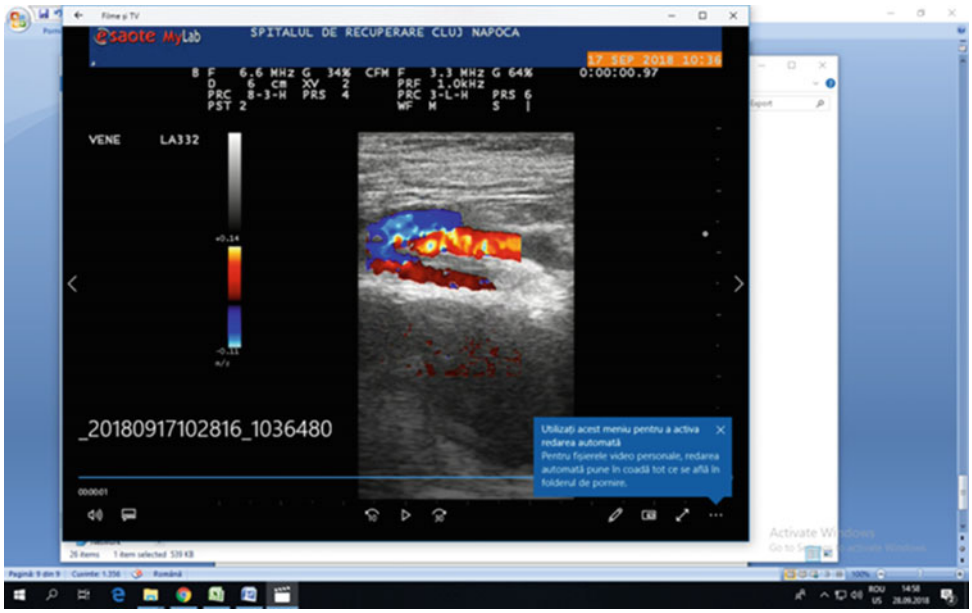

Fig. 3 The post-interventional image of an arteriovenous fistula at femoral level in a hemodialysis patient

artery dissection, which may be difficult-to-diagnose and may represent a surgical emergency being secondary to acute arterial occlusion. Hemorrhage and bleeding at the catheterization site may also lead to vein compression.

Another common pathology, whether as a primary or secondary complication in another pathology, is deep vein thrombosis (DVT) that is already a public health problem [10, 11] that already affects millions of subjects worldwide. There are varied predisposing factors (pelvic or lower limb surgery, pregnancy, physical inactivity, coagulopathy, etc.). In certain studies [3–5] it is stated that 40% of patients diagnosed with cancer (pancreas, ovary, liver, brain etc.) in the first year of illness develop distance metastases and thrombotic processes (Fig. 4). As a major complication arising from a DVT, the pulmonary embolism is present in about 90% of the patients with DVT in the lower limbs.

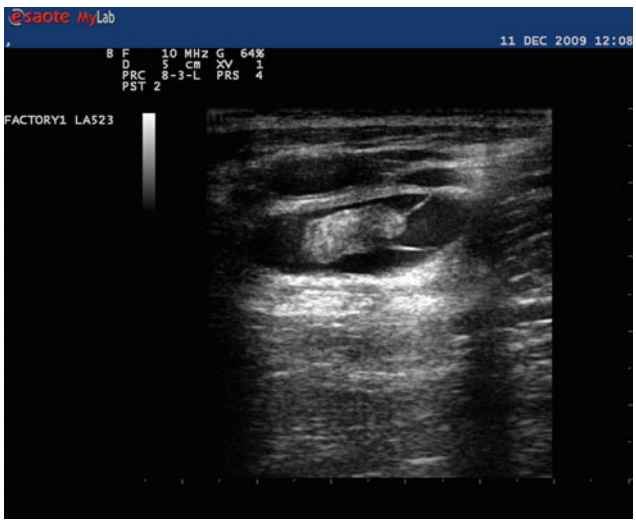

Fig. 4 Sonographic image of a thrombus fixed on the left large saphenous veins in a young patient with metastases at distance

B-mode sonography offers a good resolution for venous thrombosis. Sonographically, a healthy vein, is compressible with unidirectional flow and no internal echoes. Another complication of venous thrombosis is the occurrence of chronic venous insufficiency syndrome involving destruction of venous valves. Johnson and Col. argue that 41% of patients develop chronic venous insufficiency after a DVT episode.

3 Conclusions

The benefit that ultrasound exploration brings to the medical field is undeniable when doubled by a correct interpretation of the acquired images.

Ultrasonography is a non-invasive and sensitive method for rapidly establishing the diagnosis of vascular pathology (pseudoaneurysm, arteriovenous fistula, hematoma, thrombosis);

Ultrasonography can also be used as a screening test for the bedside patient (neurology service);

Ultrasound is also useful in evaluating therapeutic success in emergency patients treated with percutaneous thrombolysis or for viewing the closure of a pseudoaneurysm or of an arteriovenous fistula by external compression or by other therapeutic methods.

Acknowledgements The authors would like to thank the Recovery Hospital of Cluj-Napoca for letting them use the eSAOTE MyLAB 50 device for the Doppler Ultrasound technique.Conflict of InterestThe authors declare that they have no conflict of interest.

References

1. Gligor, E.: Fiziopatologie. Ed. Casa Cartii de Stiinta, Cluj-Napoca (2007)
2. Gligor, E., Ciupa, R., Roman, M., Gligor, D.: Fiziologie si explorare functionala—Notiuni fundamentale. Ed. Casa Cartii de Stiinta, Cluj-Napoca (2012)
3. Bluth, I.E., Arger, H.P., Benson, B.C., et al.: Ultrasonography in Vascular Diseases: A Practical Approach To Clinical Problems. Thieme Medical Publishers, New York (2001)
4. Luther, A., Kuman, A. et al.: Pseudoaneurysme arteriale periferice. Indian J. Surg. **77**(suppl.2): 603–607 Dec (2015)
5. Perler, B.A.: Tratamentul chirurgical al pseudoaneurismului femural dupa cateterizare cardiaca. Cardiovascular Surg. **1**, 118–121 (1993)
6. Darbari, A., Tandon, S., Chandra, G. et al.: Pseudoaneurismul arterial periferic post-traumatic. Ind. J. Thorac. Cardiovasc. Surg **22**: 182–197 [Pub Med] (2006)
7. Helvie, M.A., Rubin, J.M., Silver, T.M., et al.: The distinction between femoral artery pseudoaneurysms and other causes of groin masses: value od duplex Doppler sonography. AJR **150**, 1177–1180 (1988)
8. Middleton, M.A., Middelton, W.D.: Femoran hernia simulating pseudoaneurysm on colour Doppler sonography **160**, 1291–1292 (1993)
9. Igidbashian, V.N., Mitchell, D.G., Middleton, W.D. et al.: Iatrogenic femoral arteriovenous fistula: diagnosis with colour Doppler. Radiology **170**(3 pt. 1), 749–752 (1989)
10. Haire, V.D.: Arm Vein Thrombosis. Clin. Chest Med. **16**(2), 341–351 (1955)
11. Knudson, G.J., Wiedmeyer, D.A., Erickson, S.J., et al.: Colour Doppler Sonographic Imaging in the assessment of upper-extremity deep venous trombosis. AJR **154**, 399–403 (1990)

Part II

Medical Devices, Measurements and Instrumentation

A Side-Polished Fluorescent Fiber Sensor for the Detection of Blood in the Saliva

P. Farago, Anida-Maria Băbțan, R. Galatus, R. Groza, N. M. Roman, C. N. Feurdean, and A. Ilea

Abstract

Laboratory analyses of body fluids for the determination of disease-signaling biomarkers is an important stage of the diagnostics procedure. Although blood is recognized to provide the most reliable diagnostics data, blood collection is an invasive procedure and is perceived with reluctance by many patients. Therefore, the presence of disease-signaling biomarkers in other body fluids is investigated. This paper proposes the block diagram of a hybrid salivary sensor which correlates optoelectronic sensing with electrochemical sensing. Saliva is indeed a preferred body fluid for sampling, however it may also contain other compounds, as for example oropharyngeal mucosae, blood, etc. In the context of the hybrid salivary sensor, this paper investigates two solutions for the implementation of an optical salivary sensor for the identification of blood in the saliva. In the proposed solutions, blood is identified by color, rather than by chemistry. Therefore, pure optical means can be used, making the implementation in the shape of a side polished fiber straightforward. The novelty of this work consists in the employment of a fluorescent optical fiber for the construction of the fiber optic sensor. A laboratory proof of principle validates the proposed solutions.

Keywords

Salivary sensor • Blood identification • Fluorescent optical fiber • Side-polished optical fiber sensor

1 Introduction

The analysis of body fluids for the determination of disease-signaling biomarkers is an important stage of the diagnostic procedure [1].

Although blood analyses are recognized by the medical society to provide the most reliable data for diagnosis and disease management, the collection of blood is an invasive procedure and is perceived with considerable reluctance by many patients. Therefore, researchers aim towards investigating the presence of disease-signaling biomarkers in other body fluids, e.g. blood, saliva, sweat, tears, etc. [1–4].

There is some preference for saliva versus other body fluids, motivated by the simplicity of collection, as well as a reduced risk of infection spread and cross-contamination [5]. Saliva however may also contain fluids from different origins, e.g. oropharyngeal mucosae, blood, etc. [1], which may also be an indicator for specific pathologies.

This paper proposes the implementation of an optical salivary sensor for the detection of blood in the saliva. The optical salivary sensor is proposed in the context of hybrid optical end electrochemical salivary sensing.

The concept envisioned for the implementation of the salivary sensor with hybrid optical and electrochemical sensing is illustrated in the block diagram from Fig. 1, and is explained as follows.

The block diagram from Fig. 1 consists of the following functional modules. The optical salivary sensor performs salivary sensing following optoelectronic means. Simultaneously, the electrochemical salivary sensor performs salivary sensing following voltammetry procedures. A digital signal processor (DSP) module correlates the measurements

P. Farago (✉) · R. Galatus · R. Groza
Bases of Electronics Department, Technical University of Cluj-Napoca, Cluj-Napoca, Romania
e-mail: paul.farago@bel.utcluj.ro

A.-M. Băbțan · C. N. Feurdean · A. Ilea
Faculty of Dentistry, Department of Oral Rehabilitation, Oral Health and Dental Office Management, "Iuliu Haţieganu" University of Medicine and Pharmacy, 15 Babes Street, 400012 Cluj-Napoca, Romania
e-mail: anida.baezamica@yahoo.ro

N. M. Roman
Electrotechnics and Measurements Department, Technical University of Cluj-Napoca, Cluj-Napoca, Romania

S. Vlad and N. M. Roman (eds.), *6th International Conference on Advancements of Medicine and Health Care through Technology; 17–20 October 2018, Cluj-Napoca, Romania*, IFMBE Proceedings 71,
https://doi.org/10.1007/978-981-13-6207-1_4

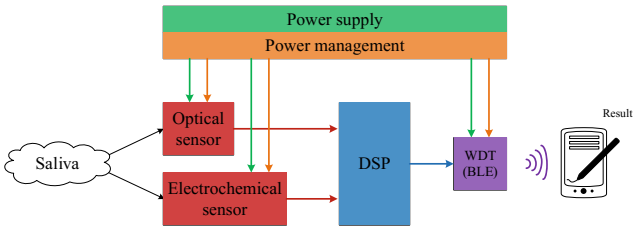

Fig. 1 Block diagram of the proposed salivary sensor with hybrid optical and electrochemical sensing

from both optical and electrochemical sensing modules in order to assess and interpret the acquired salivary data and to formulate some conclusions. The measurement and interpretation results are then transmitted to a handheld mobile device, e.g. smartphone, tablet, etc., via the wireless data transmission (WDT) module. Considering the intra-oral nature of the sensing application, Bluetooth low-energy (BLE) communication is envisioned for the WDT module. Finally, power supply of the hybrid salivary sensor is performed within the power supply and power management modules.

Blood in the saliva is identified by the proposed optical sensor by color, rather than by chemistry. Therefore, the proposed optical salivary sensor is based on the side-polished optical fiber technique. The novelty of the proposed solution is the employment of a fluorescent optical fiber for the implementation of the salivary sensor.

Fluorescent fibers are optical fibers doped with some fluorophores in order to emit fluorescent radiation in response to an incident UV or visible light [6–8]. The dependency of the fluorophore operation on environmental factors is extended to fiber operation. Accordingly, fluorescent fiber operation, i.e. generation and propagation of fluorescent radiation, depends on a series of factors, e.g. geometry, illumination intensity, temperature, chemical environment, etc. Consequently, the employment of fluorescent fibers for the design and development of sensing applications is straightforward, and it is sensible to investigate its employment for salivary sensing.

This paper is organized as follows. Section 2 presents some theoretical fundamentals regarding the operation of fluorescent fibers. Next, Sect. 3 proposes two solutions for the implementation of the optical salivary sensor, developed around the side-polished fiber. Section 4 presents some experimental results obtained with the laboratory proof of concept, which validate the proposed solutions for salivary sensing in order to detect blood in the saliva. Some conclusions are finally drawn.

2 The Fuorescent Optical Fiber

The aim of this paper is to propose an implementation of the optical sensor for the detection of blood in the saliva. In the proposed implementation, the optical salivary sensor employs a fluorescent fiber as the sensing element. For this purpose, some theoretical fundamentals regarding fluorescent fibers are first presented.

Fluorescent fibers are PMMA fibers which employ fluorescent dyes for doping the fiber core [9]. As a result, fluorescent fibers are optical fibers which emit fluorescent radiation in response to an incident phenomenon, most commonly UV or visible light, but also molecular oxygen, high energy particles, etc. [6–8].

Operation of the fluorescent fiber is depicted in the energy level system in Fig. 2 and is extrapolated from fluorophore behavior. Energy of the photons of an incident light source of wavelength λ_a, namely the absorption wavelength, is absorbed by the fluorophore molecules, which brings the electrons into the excited state. Electron relaxation occurs then in two stages. First, non-radiative relaxation occurs in-between energy levels of the excited state. Second, relaxation occurs from the excited state to the ground state, which is either non-radiative, i.e. quenching, or radiative, i.e. fluorescent radiation of wavelength λ_e [9–11].

Fluorescent emission naturally occurs at a longer wavelength than the excitation wavelength, namely

$$\lambda_a < \lambda_e \tag{1}$$

Additionally, the emission spectrum is usually sharper in comparison to the absorption spectrum. These phenomena translate to having a lower emission power in comparison to the excitation power.

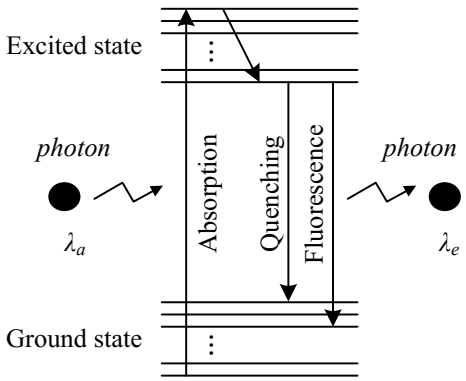

Fig. 2 Fluorophore energy level system

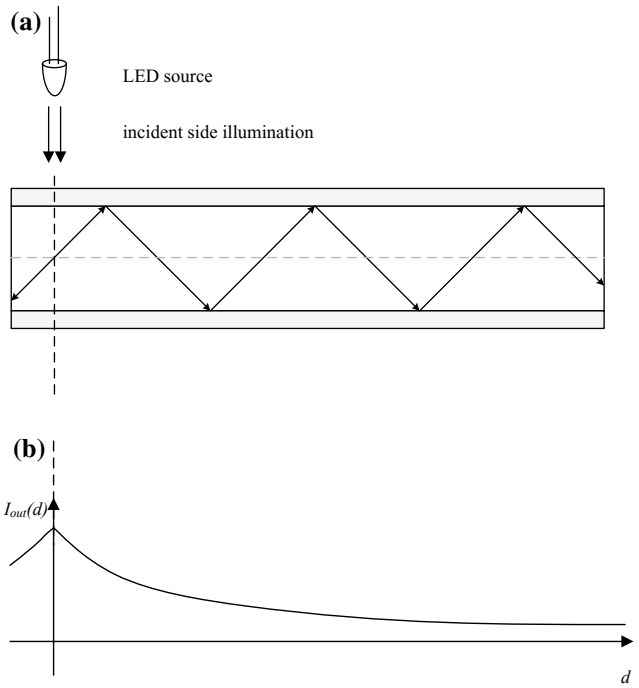

Fig. 3 **a** Propagation of fluorescent radiation along the optical fiber via TIR, **b** plot of the Beer Lambert law [13]

Fluorescent radiation generated within the core of a fluorescent fiber as a response to incident illumination with intensity I_{in} is propagated along the fiber via total internal reflection (TIR) [12, 13], as illustrated in Fig. 3a. The radiation intensity I_{out} follows an exponential attenuation vs. the fiber length d, as illustrated in Fig. 3b and prescribed by the Lambert-Beer law:

$$I_{out}(d, \lambda_e) = \eta \cdot I_{in} \cdot \exp(-\alpha(\lambda_e)d) \tag{2}$$

where η is a measure proportional to the total fiber illumination energy and $\alpha(\lambda_e)$ is the fiber attenuation coefficient [6, 7]. The latter is also wavelength-selective as expressed in

$$\alpha(\lambda) = \rho \cdot \mu(\lambda) \tag{3}$$

where the parameters account for the dye concentration ρ and the dye absorption coefficient μ [12–15].

3 Implementation of the Optical Salivary Sensor

The most straightforward implementation of an optical fiber sensor is the side-polished optical fiber [16, 17], as illustrated in Fig. 4, and explained as follows.

Under normal propagating conditions, as shown in Fig. 3, total internal reflection assumes that the core and cladding refractive indices n_{co} and n_{cl} follow [10, 12]

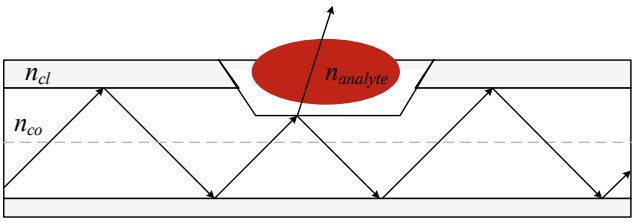

Fig. 4 The side-polished fiber optic sensor

$$n_{co} > n_{cl} \tag{4}$$

which, according to Snell's law

$$\frac{\sin\theta_i}{\sin\theta_r} = \frac{n_{cl}}{n_{co}} \tag{5}$$

determines a critical angle of the optical fiber given by

$$\theta_c = 90^\circ - \arcsin\left(\frac{n_{cl}}{n_{co}}\right) = \arccos\left(\frac{n_{cl}}{c_{co}}\right) \tag{6}$$

To be noticed is that the 90° term in Eq. (6) stands for the fact that the critical angle in optical fibers is defined with respect to the longitudinal axis, rather than to the normal which is the case in physics.

Next, the fiber is polished in order to locally expose the fiber core, as illustrated in Fig. 4. This area of the optical fiber becomes the sensing region. An analyte, in this case saliva, placed on the optical fiber sensing region will produce a local change of the fiber cladding to $n_{analyte}$, which will change the fiber critical angle and consequently the fiber emission intensity.

The solution proposed in this paper for the implementation of the optical salivary sensor is developed around the 81 0084 Blue fluorescent fiber from Industrial Fiberoptics. A KMAC SV2100L spectrometer is deployed on the fiber end to analyze the radiation spectrum, i.e. wavelength and intensity.

The first proposed solution is based on filtering the evanescent radiation in the optical fiber sensing region. The diagram of the proposed sensor is illustrated in Fig. 5.

We have applied side illumination of the fluorescent fiber in order to produce fluorescence. The advantages of side illumination consist in the removal of the requirement for

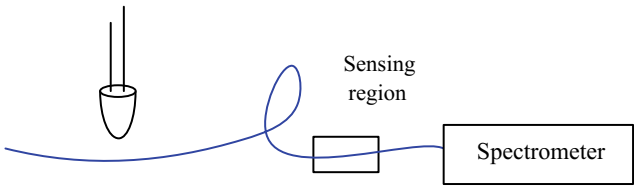

Fig. 5 Conceptual diagram of the side-polished fiber optic salivary sensor, based on filtering the evanescent radiation

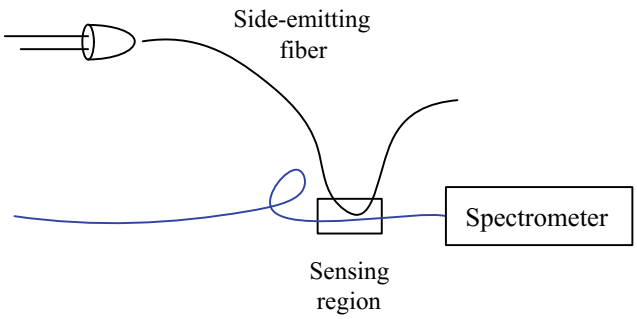

Fig. 6 Conceptual diagram of the side-polished fiber optic salivary sensor, based on filtering the incident light coming from a side-emitting fiber

coupling optics [12], which also leads to a reduction of size and costs. Fluorescent radiation is generated in the illumination region and is propagated along the fiber. Provided that the analyte is clear, i.e. no blood in the saliva, some propagated fluorescent radiation will leave the fiber in the sensing region.

In the proposed solution, sensing of blood in the saliva is based on the color of the analyte. Blood in the saliva performs a filtering of the evanescent radiation, such that blue florescence would expectedly be confined in the optical fiber.

The second proposed solution is based on the application of light into the fluorescent fiber through the sensing region, i.e. the exposed core. A side-emitting fiber is used for this purpose, deployed as illustrated in the block diagram from Fig. 6.

The setup from Fig. 6, with the side-emitting fiber deployed along the fluorescent fiber in the sensing region, is depicted in Fig. 7.

White light is applied axially to the side-emitting fiber, which is then fed into the fluorescent fiber core via the analyte. Provided that the analyte is clear, i.e. no blood in the saliva, the white light fed into the fluorescent fiber will generate and propagate fluorescence. Blood in the saliva however will filter the broadband white light and only red spectrum will be applied into the fiber core. Red incident light however falls outside the blue fluorophore absorption spectrum, and therefore, it will not generate any fluorescence. The red light will however propagate along the fiber core, adding a red peak to the fluorescence spectrum.

4 Experimental Results

The laboratory proof of principle of the proposed salivary sensor was implemented using the 81 0084 blue fluorescent fiber from Industrial Fiber optics, a 3 V coin battery and a Chibitronix SMD LED. The challenge of integrating the

Fig. 7 Photograph of the side-polished fiber optic salivary sensor, based on filtering the incident light coming from a side-emitting fiber

optical sensor into the mouth tray consists in the physical size of the electronic components. The laboratory proof of principle of the optical salivary sensor is described as follows.

The wirings were traced directly into the mouth tray. For this purpose, canals were drilled into the mouth tray which were filled afterwards with conductive paint. Locations were also drilled for the battery pins, the LED and two connectors with a jumper to act as a switch. Next, a canal was drilled in order to fit the blue fluorescent fiber. Particular care was paid to having the fiber end overlap the LED in order to have side-illumination of the fluorescent fiber.

The mouth tray with the integrated optical sensor is depicted in Fig. 8.

The fluorescent fiber far end was connected to the KMAC SV2100L spectrometer to analyze the fiber emission spectrum and intensity.

In our tests, we have used Ringer solution in place of saliva and burgundy red dye to replicate blood. The employment of the red dye instead of biological or artificial blood is motivated by the fact that the proposed salivary sensor detects the presence of blood through color, and not through chemistry.

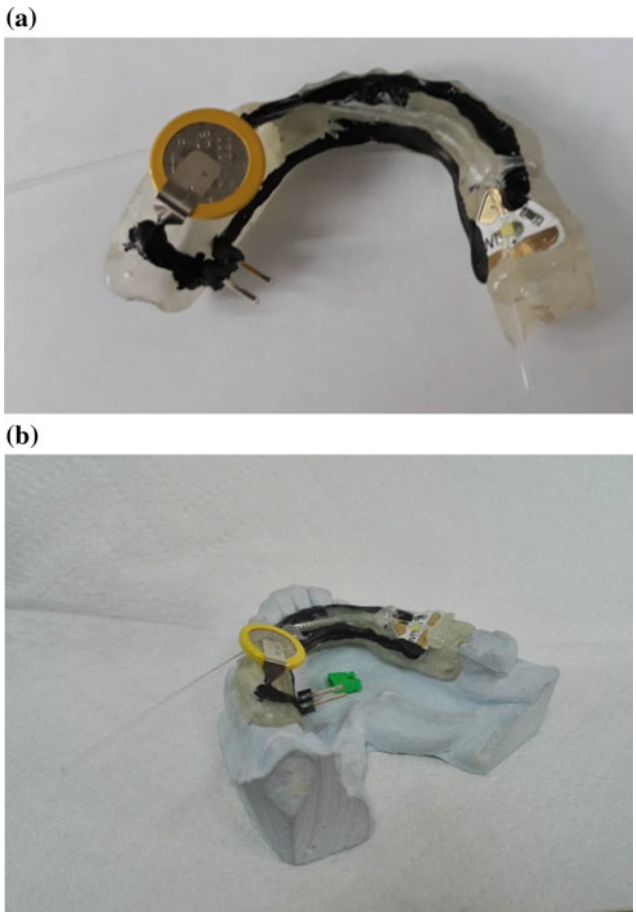

Fig. 8 The side-polished fiber optic salivary sensor integrated on a mouth tray: **a** top view and **b** lateral view

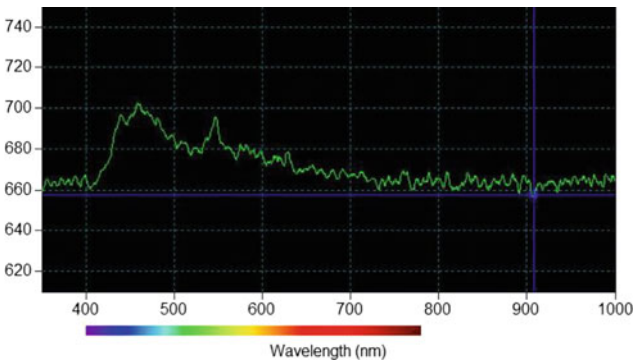

Fig. 9 The blue fluorescent fiber emission spectrum with the application of Ringer solution to the sensing region

The blue fluorescent fiber emission spectrum with the application of Ringer solution onto the sensing region is illustrated in Fig. 9.

The spectrum illustrated in Fig. 9 highlights three spectral peaks: the main blue peak at 460 nm, the second green peak at 545 nm and the third orange peak at 613 nm. This spectrum was raised under normal illumination conditions and constitutes the reference spectrum for further experiments.

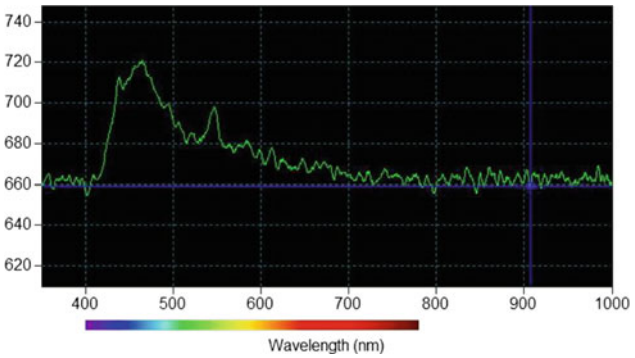

Fig. 10 The blue fluorescent fiber emission spectrum of the sensor setup in Fig. 5, with the application of Ringer solution and red dye to the sensing region

The first experiment tests the applicability of the salivary sensor setup from Fig. 5 to detect blood in the saliva. The test scenario assumes the application of Ringer solution with burgundy dye onto the sensing region. The resulting fiber emission spectrum illustrated in Fig. 10.

As illustrated in Fig. 10, the main blue peak exhibits an increase in amplitude of about 20 counts. This increase is consequent with our assumptions. Nevertheless, the magnitude of the increase is smaller than we have expected.

To be noticed is the fact that salivary sensing on a mouth tray isn't performed in a completely dark environment. Therefore, the 20 count variation of the peak amplitude may very well be the result of variations in the ambient illumination conditions.

The second experiment tests the applicability of the salivary sensor setup from Fig. 6 to detect blood in the saliva. Addition of the burgundy red dye to the Ringer solution, and application of the colored solution onto the fiber sensing region determines a red spike of the fiber emission spectrum around 620 nm, as illustrated in Fig. 11.

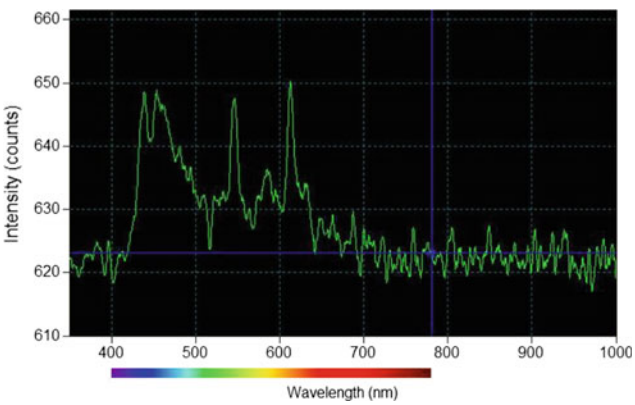

Fig. 11 The blue fluorescent fiber emission spectrum of the sensor setup in Fig. 6, with the application of Ringer solution and red dye to the sensing region

5 Conclusions

This paper proposed and investigated two solutions for the implementation of a fiber optic salivary sensor for the determination of blood in the saliva. The proposed optical sensor is aimed for implementation in a hybrid salivary sensor, which correlates optoelectronic sensing with electrochemical sensing. The novelty of this work consists in the employment of a fluorescent optical fiber in order to build a side-polished fiber optic sensor.

The first optical sensing setup assumes the selective filtering of the evanescent fluorescent radiation in the sensing region. Accordingly, clear saliva, i.e. absence of blood in the saliva, would allow a larger amount of fluorescent radiation to evanesce from the fiber, in comparison to "red" saliva, i.e. presence of blood, which would filter the evanescent radiation. According to laboratory measurements, the difference in the spectral magnitudes of the fiber emission spectra in the presence and absence of blood can very well be attributed to variations of ambient illumination conditions. Therefore, at this stage of the development process, measurement results with this setup cannot be considered conclusive for the identification of blood in the saliva.

The second optical sensing setup assumes the selective filtering of incident light, applied directly into the sensing region. Accordingly, clear saliva, i.e. absence of blood in the saliva, would allow the application of white light which will generate and propagate fluorescence, whereas "red" saliva, i.e. presence of blood, would produce an additional red peak in the fluorescence spectrum. Laboratory measurements validate this setup for the identification of blood in the saliva.

Acknowledgements This study was supported by "Iuliu Haţieganu" University of Medicine and Pharmacy Cluj-Napoca, Ph.D. Grant no 3999/01.10.2016, and partially by the COFUND-ERA-HDHL ERA-NET Project, European and International Cooperation—Subprogram 3.2—Horizon 2020, PNCDI III Program—Biomarkers for Nutrition and Health—"Innovative technological approaches for validation of salivary AGEs as novel biomarkers in evaluation of risk factors in diet-related diseases", no 25/1.09.2017.

Conflict of Interest The authors declare that they have no conflict of interest.

References

1. Malon, R.S.P., Sadir, S., Balakrishnan, M., Córcoles, E.P.: Saliva-based biosensors: noninvasive monitoring tool for clinical diagnostics. Biomed. Res. Int. **2014**, 962903 (2014). https://doi.org/10.1155/2014/962903
2. Chiappin, S., Antonelli, G., Gatti, R., de Palo, E.F.: Saliva specimen: a new laboratory tool for diagnostic and basic investigation. Clin. Chim. Acta **383**(1–2), 30–40 (2007)
3. Kaufman, E., Lamster, I.B.: The diagnostic applications of saliva—a review. Crit. Rev. Oral Biol. Med. **13**(2), 197–212 (2002)
4. Lee, Y.H., Wong, D.T.: Saliva: an emerging biofluid for early detection of diseases. Am. J. Dentistry **22**(4), 241–248 (2009)
5. Jung, D.G., Jung, D., Kong, S.H.: A lab-on-a-chip-based non-invasive optical sensor for measuring glucose in saliva. Sensors (Basel, Switzerland) **17**(11): 2607 (2017). https://doi.org/10.3390/s17112607
6. Laguesse, M.F.: Optical potentiometer using fluorescent optical fiber for position measurement. Appl. Opt. **28**(23), 5144–5148 (1989)
7. Aiestaran, P., Dominguez, V., et al.: A fluorescent linear optical fiber position sensor. Opt. Mater. **31**(7), 1101–1104 (2009)
8. Egalon, C.O.: Axial versus side illumination of a fluorescent cladding optical fiberlink (2017). https://oceanoptics.com/wp-content/uploads/Claudio-Egalon-Axial-VS-Side-Illumination-of-a-Fluorescent-Cladding-Optical-Fiber.pdf
9. Miluski, P., Kochanowicz, M., et al.: Emission properties and energy transfer in Perylene-Rhodamine 6 G co-doped polymeric fiber. Chinese Optics Letters **14**(12), 121602 (2016)
10. Farago, P., Galatus, R. et al.: Fluorescent fiber implementation of an angle sensor, ICTON, Bucharest, Romania (2018)
11. Farago, P., Galatus, R. et al.: Fluorescent fiber implementation of a high-resolution distributed position sensor. In: Proceedings SPIE 10680, Optical Sensing and Detection V, 106801E (9 May 2018). https://doi.org/10.1117/12.2307494
12. Galatua, R., Farago, P., et al.: Distributed fluorescent optical fiber proximity sensor: towards a proof of concept. Spectrochim. Acta Part A Mol. Biomol. Spectrosc. **198**, 7–18 (2018)
13. Farago, P., Galatus, R., et al.: Low-cost Quasi-distributed position sensing platform based on blue fluorescent optical fiber, in Prof. of 2017 IEEE 23rd International Symposium for Design and Technology in Electronic Packaging (SIITME), Constanta, Romania (2017)
14. Laguesse, M.F., Bourdinaud, M.J.: Characterization of fluorescent plastic optical fibers for x-ray beam detection. In: Proceedings of SPIE—Plastic Optical Fibers, vol. **1592** (1991)
15. Ray, J.A.: (2010) An overview of macrobending and microbending of optical fibers, Corning
16. Khan, M., Kang, B., et al.: Fiber-optic multi-sensor array for detection of low concentration volatile organic compounds. Opt. Express **21**, 20119–20130 (2013)
17. Ahn, J., Seong, T., et al.: Fiber-optic waveguide coupled surface plasmon resonance sensor. Opt. Express **20**, 21729–21738 (2012)

Analysis of Postural Imbalance Due to Handling Weights During Physical Activities

D. Cotoros, C. Druga, I. Serban, and A. Stanciu

Abstract

Present paper is based upon a thorough analysis using specific devices in the Medical Engineering Laboratory meant to study the influence of handling various weights on the postural balance and implicitly on the health conditions. The weight was handled in different positions of the weight and it was lifted either by bending the body and keeping the legs straight or by bending the knees. The imbalance was determined by analyzing the aspect of the stability area using a Kistler force platform.

Keywords

Weight handling • Stability area • Imbalance • Force platform

1 Introduction

Handling weights can be a basic daily activity or an important part of training for improving sportive performance or rehabilitating weakened muscles. According to some prestigious sports associations, physical activities requiring weight lifting can be beneficial for reducing cardiovascular diseases risk by improving blood pressure and also glucose metabolism [1, 2].

Some studies found that isometric efforts of lower intensity and dynamic resistive exercises are not a negative influence upon symptoms of cardiovascular diseases, being even more beneficial than treadmill exercising [3].

Muscle weakening and poor balance can also be the main causes in accidental falls, especially for elderly people or people recovering from various locomotion impairing events [4].

Other studies concluded that imbalance may occur due to the difference of strength between the dominant and non dominant limb as a result of previous injuries or specific sports demands [5, 6].

On the other hand, skilled and high performance weight-lifters present a limited range of motion (ROM) in the shoulders area and display less possibilities of learning new types of motor skill according to [7].

The problem to be addressed is regarding the imbalance occurred due to the inclusion of an additional weight in different positions of the body and limbs. It is a well known fact that for a human body standing, the center of mass is located at approx. 55% of the height (around the belly button), while for a bent over body it will shift outside it.

Adding weight lifting to the body posture will lead to a certain imbalance because the center of mass will shift accordingly and the human body will adjust its position in order to maintain balance.

2 Experimental Setup

Experimental tests were performed upon a sample of 22 persons (7 males, 15 females) aged 21–23, students in Medical Engineering and Optometry who agreed to perform the weight lifting in various positions.

All subjects are healthy and do not suffer of any neurological or physiological disease.

The equipment used for determining the degree of imbalance of the body during weight lifting is a Kistler force platform and the weight is a standard 5 kg dumbbell.

The subjects were instructed for the first stage of the experiment to maintain equilibrium in a neutral anatomic position on the force platform for 30 s in order to have a reference term for comparing the stability area after performing the weight handling. Neutral position with an intermediate base of support usually means that body weight is equally distributed upon the two feet. The measurements

D. Cotoros (✉) · C. Druga · I. Serban · A. Stanciu
Department of Product Design, Mechatronics and Environment, University Transilvania, 29 Eroilor Av, Brasov, Romania
e-mail: dcotoros@unitbv.ro

S. Vlad and N. M. Roman (eds.), *6th International Conference on Advancements of Medicine and Health Care through Technology; 17–20 October 2018, Cluj-Napoca, Romania*, IFMBE Proceedings 71,
https://doi.org/10.1007/978-981-13-6207-1_5

Fig. 1 Subject in neutral position

were made 3 times for each subject for the neutral position, as shown in Fig. 1.

For the second stage the subjects were instructed to pick up the weight in front of them keeping the legs straight, as shown in Fig. 2.

Then the subjects had to pick up the weight in front of them and bend their knees while they were doing this, as shown in Fig. 3.

Next stage required picking up the weight laterally and use whatever position they want for their knees. All subjects

Fig. 2 Subject bending keeping straight knees, weight in front

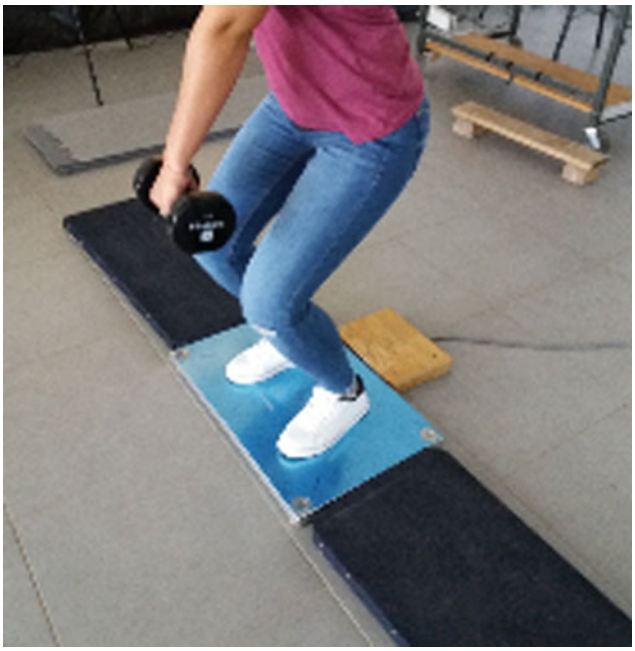

Fig. 3 Subject bending knees, weight in front

considered the motion possible only by bending the knees, as shown in Fig. 4.

Next the subjects were instructed to bend their body, keep the legs straight and lift the weight using their right hand (dominant) first to the front of the body keeping a straight elbow, then laterally and up keeping the elbow straight again. Measurements were also made for the situation when the upwards lift was made with a bent elbow.

Finally the subjects had to bend their knees to pick up the weight and perform the same motions as in the previous stage, then set it back again.

Fig. 4 Subject taking the weight laterally with bent knees

Measurements results acquired by help of the Kistler force platform and a connected laptop were processed using Bioware software. The information provided by each measurement concern the variation of forces on 3 perpendicular axes, variation of moments and also the stability area which shows the projections of the center of mass on the supporting surface during the entire recording.

As the problem we approached was regarding the balance, the most expressive information was provided by the stability area and the changes occurring due to weight support variation, changes that may indicate which positions are producing less imbalance upon the human body and implicitly less possibilities of producing accidents or fall over.

3 Results and Discussions

According to the statistics provided by the software, the range of the center of mass deviation in the stability area was between 0.025 and 0.07 m on Ox and 0.02 and 0.027 m on Oy, during maintaining the neutral position (static), some examples of the obtained diagrams are shown in Figs. 5 and 6.

Obviously not all subjects have the same sense of balance although their ages are similar and they are all in good health conditions. Interviewing the subjects it came out that some of them were performing sportive activities in their free time and as a result their balance was considerably better.

In Fig. 7, there is an example of diagram for the case when the weight was picked up with straight legs from the front of the subject.

The diagram shows clearly the occurrence of imbalance not only on the Oy direction where the weight is but also on lateral direction Ox, due to the adjustment efforts made by the body to maintain balance. The variation of the center of mass position on Oy increases to 0.045–0.055 m on Oy and to 0.07–0.095 m on Ox.

The variation of the reaction force between the feet and the ground is also interesting to watch, as the weight lifting is clearly visible on the diagram, see Fig. 8. The reaction force will increase suddenly after 5 s with roughly 40 N, with an obvious oscillation at the picking up moment (immediately after second 5).

Figure 9 is an example for the situation when the weight was picked up with bent knees from the front of the subject.

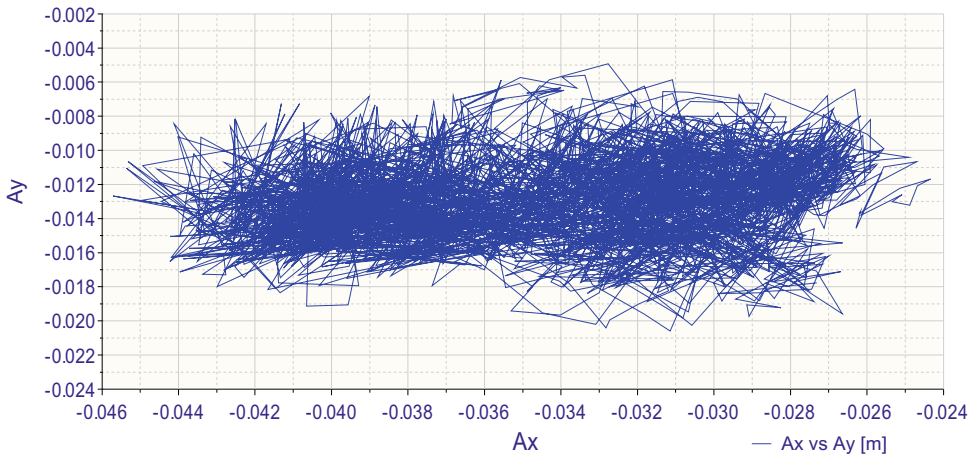

Fig. 5 Stability area in neutral position for a well balanced subject

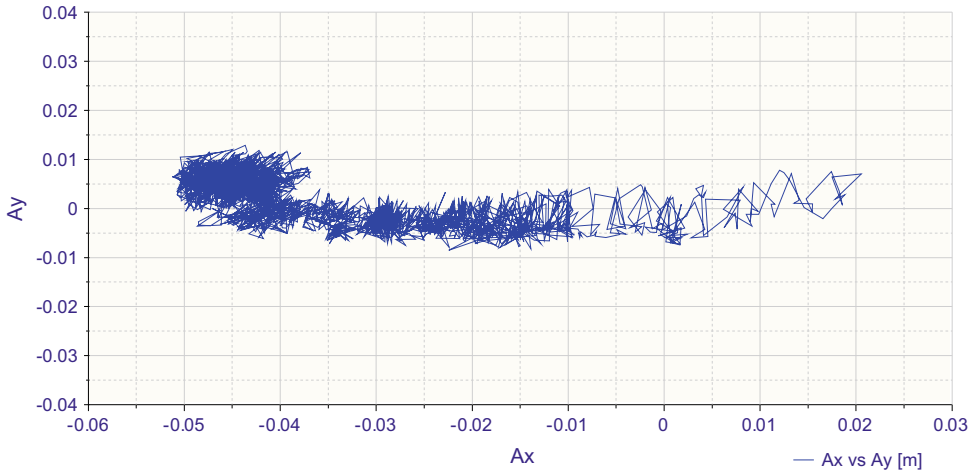

Fig. 6 Stability area for a poor balanced subject

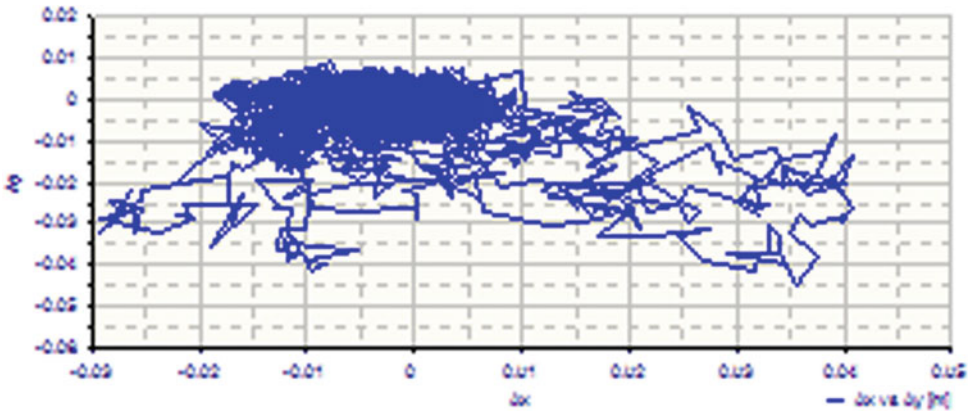

Fig. 7 Stability area for subject picking up weight with straight knees, weight in front

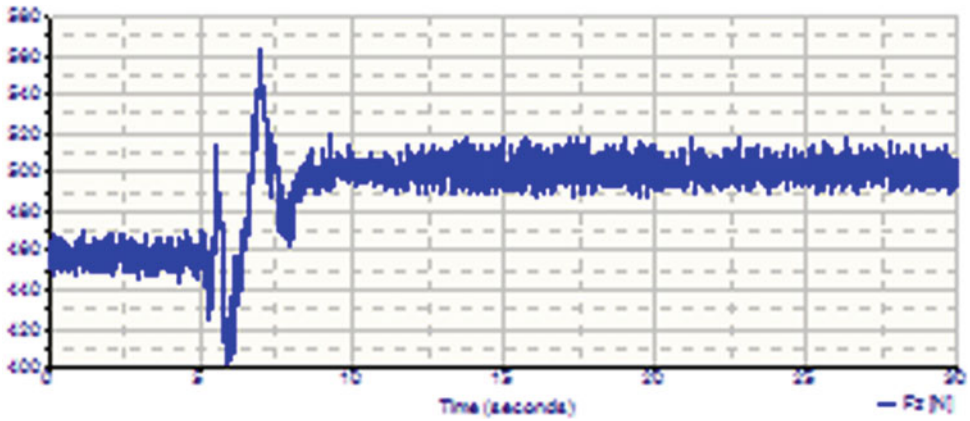

Fig. 8 Reaction force variation during weight lifting

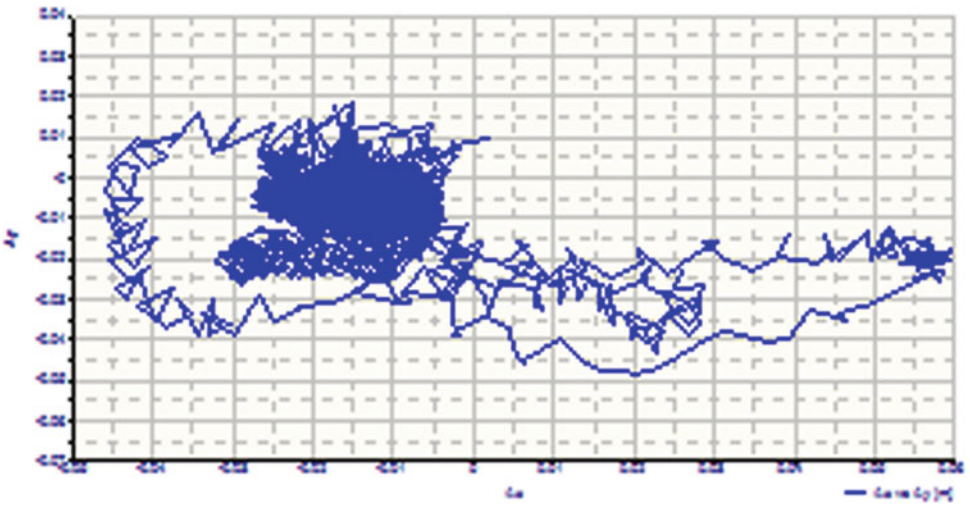

Fig. 9 Stability area for subject picking up weight with bent knees, weight in front

The imbalance on Oy direction reaches between 0.04 m and 0.066 m, while along the axis Ox it goes somewhere between 0.08 and even 0.11 m, which is much higher than the situation with straight knees.

Figure 10 shows the variation of the reaction force for the bent knees situation. Obviously the force will increase after picking up the weight with roughly 50N and presents a strong variation while picking up the weight.

When the subjects were asked to pick up the weight which was placed laterally, they found it was possible to take it only by bending their knees. An example for the stability area in this particular situation is shown in Fig. 11.

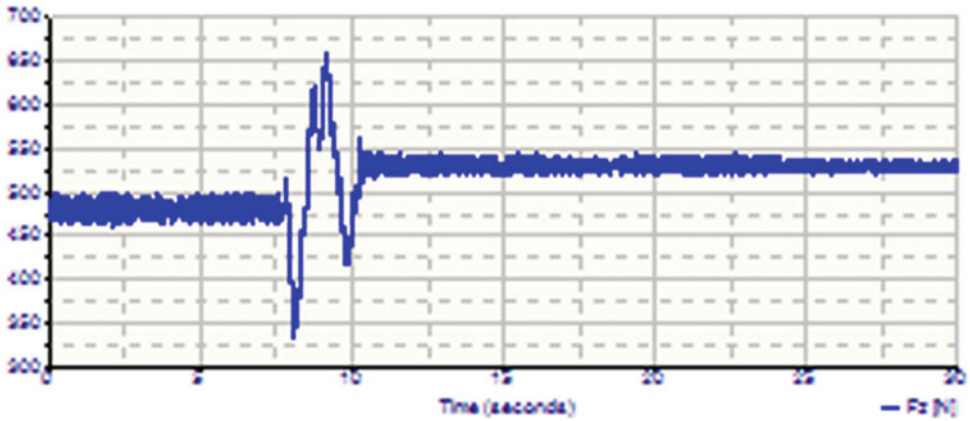

Fig. 10 Variation of reaction force with bent knees lifting

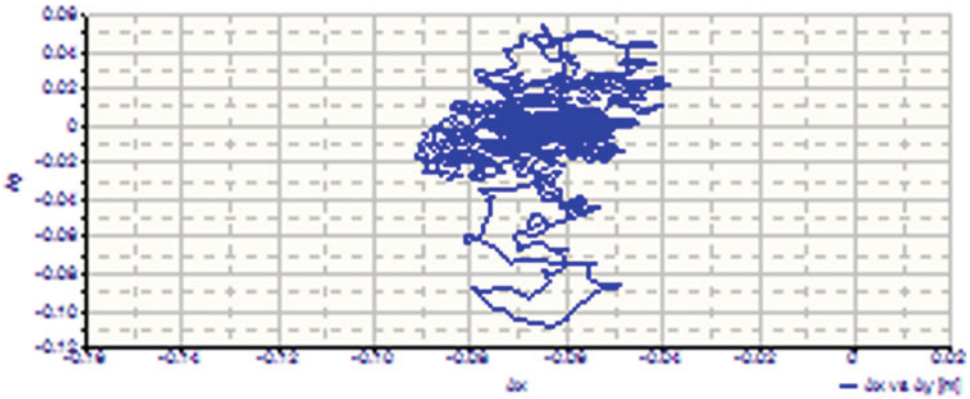

Fig. 11 Stability area for subject picking up weight laterally

The display of the stability area shows an interesting spreading, imbalance was higher on the axis Oy (perpendicular to the direction of weight lifting) and lower on the axis Ox, demonstrating that the subject is trying to adjust by increasing the displacement along an axis perpendicular to the one where the load is acting.

The next phase of the experiment required the subjects to pick up the weight and move the arm forwards, laterally and upwards, first with a straight elbow and then upwards with the bent elbow. Some examples for the stability areas in these situations are shown in Figs. 12 and 13.

The imbalance is higher on the axis Ox (lateral direction) going up to 0.14 m and not too high on the axis Oy, reaching a maximum of 0.05 m. Both areas show striking similarities proving the fact that the position of the elbow does not influence the degree of imbalance.

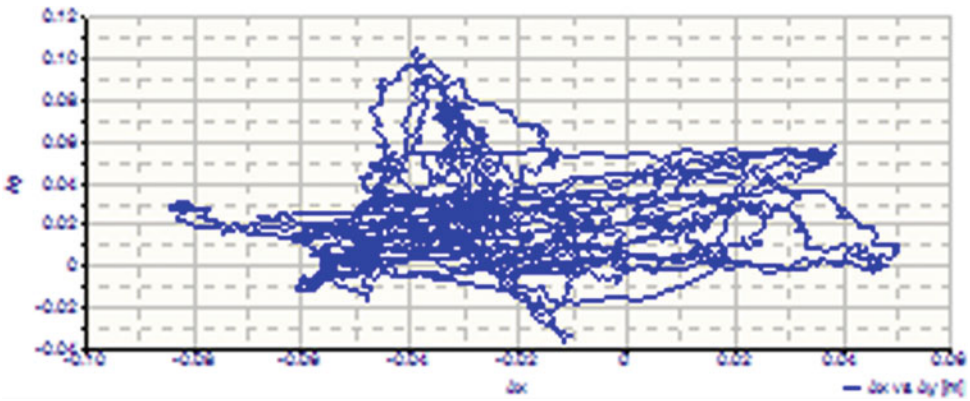

Fig. 12 Stability area when moving the weight and keeping the arm straight

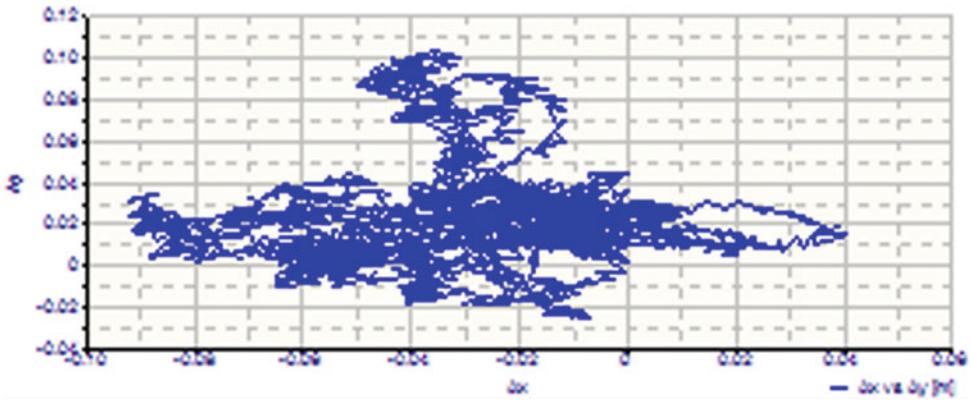

Fig. 13 Stability area when moving weight and bending elbow

4 Conclusions

The necessity of lifting various weights may occur not only in sportive activities but also during daily jobs or housework. Even if the weight is moderate a certain imbalance of the body center of mass will occur, leading to additional strain on muscles for adjustment or even upon the joints. If the imbalance reaches higher values the body strain for adjustment will also be higher, besides accidental trips or falls may endanger the subject.

The experiments proved that the loss of balance is higher on a perpendicular direction to the one where the weight is placed. Also the imbalance is higher when the knees are bent during the lifting because an additional motion of the body intervenes. Also the position of the elbow during the displacement of the arm holding the weight does not influence the balance in a significant manner.

Acknowledgements All experiments were performed within the Advanced Mechatronic Systems Research Centre from Transilvania University of Brasov.

Conflict of Interest The authors declare that they have no conflict of interest.

References

1. Velloso, E., Bulling, A., Gellersen, H., Ugulino, W., Fuks, H.: Qualitative activity recognition of weight lifting exercises. In: Proceedings of 4th International Conference in Cooperation with SIGHCHI, Stuttgart, Germany (2013)
2. O'Donovan, G., Blazevich, A.J., Boreham, C., Cooper, A.R., Crank, H., Ekelund, U., Fox, K.R., Gately, P., Giles-Corti, B., Gill, J.M., Hamer, M.: The ABC of physical activity for health: a consensus statement from the British association of sport and exercise sciences. J. Sports Sci. **28**(6), 573–591 (2010)
3. Featherstone, J.F., Holly, R.G., Ezra, A.: Physiologic responses to weight lifting in coronary artery disease. Am. J. Cardio. **71**, 257–292 (1993)
4. Gardner, M.M., Buchner, D.M., Robertson, M.C., Campbell, A.J.: Practical implementation of an exercise-based falls prevention programme. Age Ageing **30**, 77–83 (2001)
5. Newton, R.U., Gerber, A., et al.: Determination of functional strength imbalance of the lower extremities. J. Strength Conditioning Res. **20**(4), 971–977 (2006)
6. Host, H.H., Sinacore, D.R., Bohnert, K.L., Steger-May, K., Brown, M., Binder, E.F.: Training induced strength and functional adaptation after hip fracture. Phys. Ther. **87**(3), 292–303 (2007)
7. Kordi, H., Mohamadi, J., Ghotbi, M.: Teaching a new sport skill to weightlifters: problem in performance and motor learning. J. Human Sport Exerc. **8**(4), 996–1007 (2013). https://doi.org/10.4100/jhse.2013.84.10

The Use of Thermal Imaging Techniques as a Method of Monitoring the New Born

Catalina Luca, C. Corciovă, D. Andriţoi, and R. Ciorap

Abstract

In this paper we present a report on the use of thermographic imaging techniques as a monitoring tool in newborn respiratory rate. The basis of this type of monitoring is the processing of real-time thermographic images. This contactless monitoring method it is absolute necessary because it is designed to monitor a very fragile category of patients: premature new born babies. Our biomedical signal of interests it is represented by the spontaneous breaths of the newborn. In the present study we demonstrate that the respiratory rate of the preterm newborn can be monitored based on the analysis of temperature changes that occurs in the anterior nasal area (nostrils).

Keywords

Image analysis • Infrared thermography • Signature detection • Wavelet analysis

1 Introduction

Respiratory Rate is one of the few signs that rely on clinical observation and not electronic conformation. In new born babies it can be particularly challenging to measure it because the new born it is unsettled or crying, meaning it is harder to observe their breathing movements and make an accurate count [1, 2].

Apnea (sudden breathing discontinuation for more than 20 s) and bradycardia (decrease in heart rhythm) are the main problems faced by the premature newborn [3].

Thermography is a method of non-invasive imaging, without side-effects and without contraindications to the patient [4].

Infrared thermography can be used to monitor fluctuations in facial skin surface temperature using an infrared detection device [5].

2 Materials and Method

In this project, we conducted a study on the possibility of using the thermographic technique in Infra-Red as a method of monitoring the respiratory frequency of premature newborns.

Real-time Infra-Red thermograms (RTIRT) were collected using OPTRIS PI160 IR camera, having a measurable temperature range of −20 to 900 °C, Spectrum 7.5–13 µm, Image Recording Rate from 120 Hz and optical resolution: 160 × 120 Pixels. This device allows the transfer of images using an O6 lens, 6° × 5° lens, f = 35.5.

The thermographic camera was positioned distant from the subject, the distance varies between 50 and 100 cm, and we recorded the thermographic images. In real-time, the images were sent to a laptop for post-processing. Post-processing includes filtering and color conversion [6, 7].

The acquisition protocol for IR thermographic images consists of three distinct phases. Each phase has a 2 min duration. There are 2 recording phase, and between them there is a 2 min interval for recalibration of IR thermographic camera. We established this recalibration phase to correct any non-uniformity. In the first 2 min of recording we do a localization of the nasal region of the neonate, so we can establish the ROI (region of interest) for post-processing process.

Were examined 20 newborn babies with gestational age averaging 31 weeks. All patients were admitted directly after birth at the Regional Center for Neonatal Intensive Care Unit "Cuza Voda" Iasi. Were excluded children with additional risk factors, other than prematurity, for example with

C. Luca (✉) · C. Corciovă · D. Andriţoi · R. Ciorap
Department Biomedical Sciences, University of Medicine and Pharmacy "Grigore T. Popa", 9–13 Kogalniceanu Street, 700454 Iasi, Romania
e-mail: luca.katalina@yahoo.com; catalina.luca@bioinginerie.ro

S. Vlad and N. M. Roman (eds.), *6th International Conference on Advancements of Medicine and Health Care through Technology; 17–20 October 2018, Cluj-Napoca, Romania*, IFMBE Proceedings 71,
https://doi.org/10.1007/978-981-13-6207-1_6

chromosomal abnormalities or cerebral hemorrhage. The study project and the protocol were approved by the Ethics Committee of the "Cuza Voda" Hospital of Obstetrics and Gynecology Iasi and the consent of the parents was obtained before enrolling in the study. None of the children were ventilated mechanically.

3 Results and Discussions

After a primary processing of the obtained images with the software of OPTRIS PI60 camera, we exported the images to Matlab for a supplementary post-processing and pre-filtering. With the help of Matlab Systems Identification Toolbox, we removed the average temperature value and we analysed the motion of the obtained images. The distance between the camera and the newborn was kept less than 100 cm, to eliminate background IR radiation from surrounding objects.

The first post-processing step was building time-varing signals for each thermographic pixel in ROI. We tried to build the temperature time profile for each picture.

The obtained images have been examined at different times in time.

After the Matlab post-processing and pre-filtering step, we were able to correlate the thermographic images with the breathing signal. The thermographic images obtained is called "pulsed thermography" because the recorded process is repetitive in nature.

To realize a better correlation of the obtained thermographic images, we have made a mathematical approximation for IR images, that depends on the five main parameters shown in Fig. 1. We could define Q_t as total heat flow rate as following:

$$Q_t = Q_{rd}(t) + Q_c(t) + Q_e(t) + Q_p(t) (1)$$

The global equation for the heat transfer inside the nasal cavity at the nostrils level will be the sum of the following components of the heat flux:

- Q_{rd}: the rate of dissipated heat by radiation between the air flow and the nasal surface
- Q_c: the heat dissipated by convection between the skin and mucosa
- Q_e: the rate of heat dissipated by evaporation at the nasal surface
- Q_p: the rate of heat dissipated by the blood infusion.

In the temperature signal derived from IR thermography, a change in temperature from 0.5–0.70 °C was seen in relation to the thermal rate signal of the breath. In addition, healthcare actions (e.g. incubator door opening, child manipulation) also influenced the temperature profile (Fig. 2).

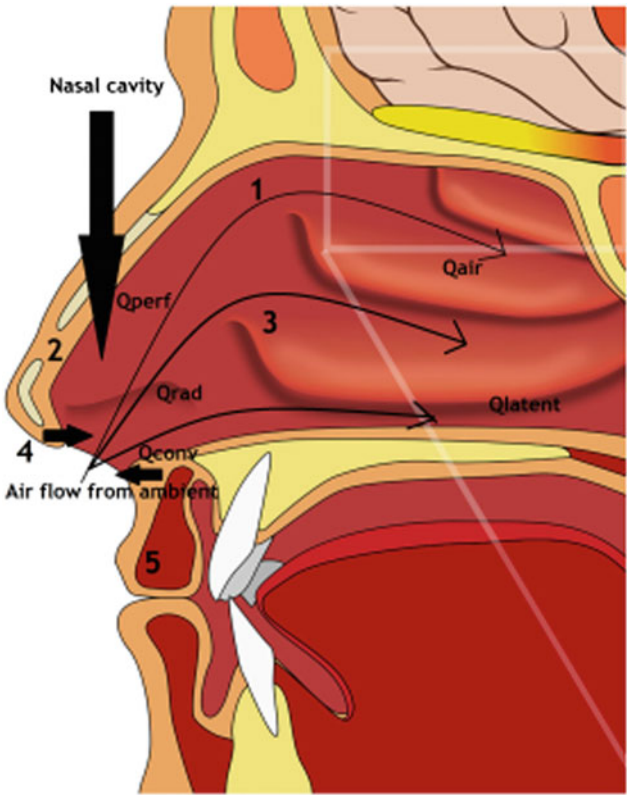

Fig. 1 Anatomical section through the nasal cavity, showing physiology of heat transfer processes [8]

ROI defined over the neonate nostrils, where the analysis performed over two minute interval.

A first step in processing the newborn's thermographic images is the edge detection technique. This technique has been used in our case to process IR thermographic images, as it is necessary to locate and define the area of interest. Applied contour drawing techniques aimed at eliminating areas with a constant temperature of the image, leaving only the areas where temperature variations occur, so that it can extract the newborn's respiratory rate.

Image Enhancement Techniques are used to highlight and clarify image characteristics in display and analysis. The role of improvement techniques is to process the image so that the resulting image contains more information than the original image. In our case, the Improvement technique was performed as a post-processing step.

Smooth Spatial Filters (LPF) have also been used to reduce noise. With their help, we succeeded in selecting low-frequency components and reduced or in some cases eliminating high frequencies.

The noise reduction in Matlab can be achieved by using linear or nonlinear filters. Examples of LPFs are; average filters, statistical commands, and Gauss filters. Examples of statistical filters include maximum, minimum, median, and mod filters. For our imagery, because we want a biomedical

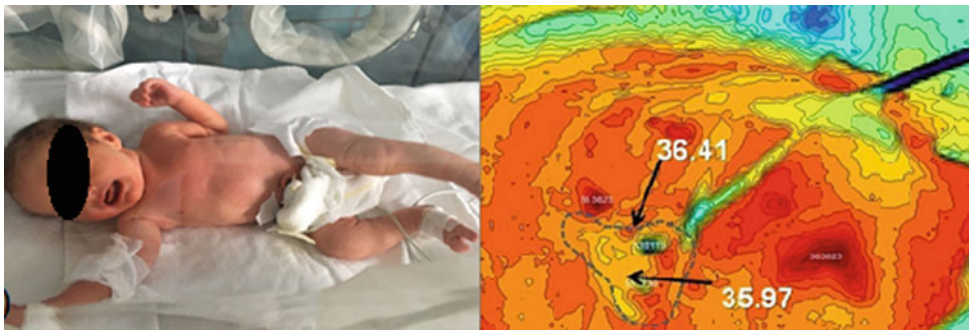

Fig. 2 A newborn placed in a closed Isolette C 2000 type incubator, with ROI defined on the nostrils with a well-detected IRT signature that shows a change in temperature to 0.7 °C

signal to be recorded, we used the Median filters, the average filters, and the Gaussian filters.

Was used the Medium Filter to reduce noise rather than to delimit the edges. With it was also eliminated the impulse noise. As it is known, applying the median filter involves replacing each pixel in the image with the median of the neighbor pixels.

This is not the first time that IR thermography signal analysis has been applied to monitor neonates respiratory rate, but is the first time when the signal obtained it is correlated with the respiration rate signal obtained from a respiration rate monitor.

Because the measurements took place in NICU section, and we talk about the biggest Neonatal Care Center from Romania, we had some clinical challenges. We have been monitoring the most fragile category of patients, premature new born babies, that are highly vulnerable and physiologically unstable.

We have tried to elaborate working protocols and to configure the measurements setup so that we do not interfere with any routine care procedures for the neonates (Fig. 3).

Because we recorded other vital signs such as ECG, heart beat and respiratory rate, we were able to compare the respiration rate signal derived from IR thermography images with the recorded vital signal, as shown in Fig. 4.

The results presented in this study indicate that IR thermography can be included in future ways of monitoring newborns in NICU. At this point, the results obtained during the measurements using the thermography technique are not fully categorized and require more reliable measurement protocols.

The results from this experiment showed clear changes in temperature in the nasal region and also a difference during inspiration and expiration. Following results from IR image processing, it was possible to extract the newborn's respiratory rate, as can be seen in Figs. 4 and 5. The disadvantage is that at this point there is no information on the quality of breathing.

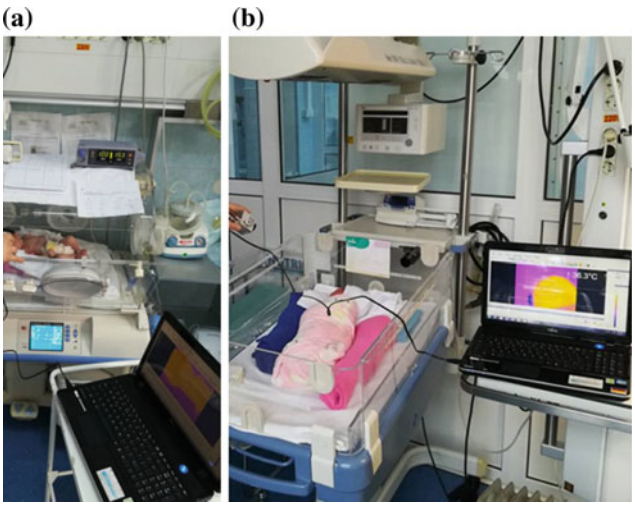

Fig. 3 Measurements setup, the exact location of the thermographic and laptop system exemplified in two different types of measurements: **a** newborn on a radiant body temperature maintenance system, and **b** newborn in a closed incubator for maintenance of body temperature

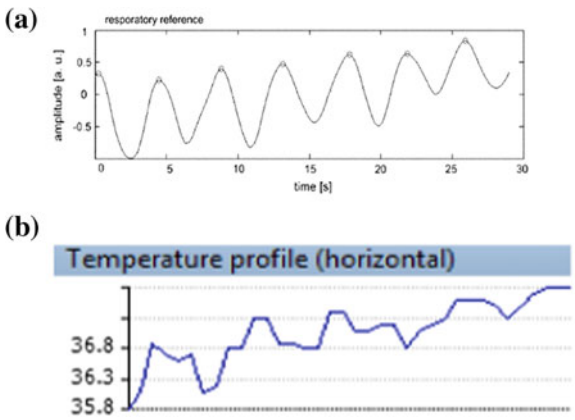

Fig. 4 **a** The graphical representation of respiration rate, derived from the bedside intensive care monitoring module on patient no. 5, **b** the graphical representation of respiration rate, derived from RTIRT

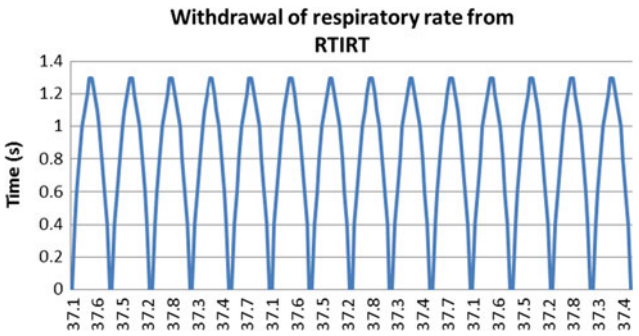

Fig. 5 The graphic that shows the withdrawal of respiratory rate from Real-time Infra Red Thermograms on patient no. 10

While changes in convective heat transfer due to breathing in adults are easily observed using an IR camera, breathing monitoring of premature babies remains a challenge due to a much lower respiration temperature variation.

Extracting the signal from the IR thermal imaging depends also on the viewing angle set for the IR camera. Therefore, an optimal viewing angle will result in better image quality and greater usability to set ROI. Following the comparative analysis of the respiratory signal we obtained and the respiratory rate recorded with a monitor, there seems to be a slight delay. We also found a slight low temperature difference between inspiration and expiration in the nasal fossa region shown in Fig. 6, where it can be seen that the maximum temperature difference is about 0.70 °C.

Although at this time respiratory rate monitoring using IR thermography in adults is used, this work has shown that IR thermography allows respiratory monitoring without direct contact to neonates in NICU. The basis of the study is the convective heat transfer at the level of breathing-induced nasal fossa region in dedicated ROIs. So far, the method seems more effective in adults than in newborns due to large volumes of lungs in adults.

The method proposed by us requires improvements in image processing and the detection of nasal region limits. Moreover, the results presented are preliminary and require additional studies in a larger number of newborns and under different care sets. At this point we can say thermographic monitoring can help estimate possible loss of temperature as part of thermoregulation and can also be considered as a first step in assessing non-invasive respiratory behavior of premature babies.

4 Conclusions

Although not a large number of measurements have been carried out, we believe that the preliminary results obtained provide a good basis for the subsequent study of early nasal breathing with the help of thermography.

The presented method can be an effective quantitative technique to measure the nasal symmetric flow pattern in premature infants. This can provide information on the depth and frequency of each breath cycle in order to get an early sign of changes in child behavior and to be able to use this technique in assessing the apathy of prematurity. Also, the temperature difference up to 0.70 °C can be interpreted as part of the baby's thermoregulation.

This study will continue with the inclusion of 100 cases studied, and in parallel we began developing a miniaturized system that uses the thermographic technique to continuously monitor newborn respiration.

After the authors' knowledge, this is the first time the IR thermographic technique has been applied to monitor preterm infants with low gestation age. there were also special clinical challenges because the measurements took place in NICU.

In the signal derived from IR thermal imaging, a change in temperature of 0.5–0.7 °C was seen due to the newborn's

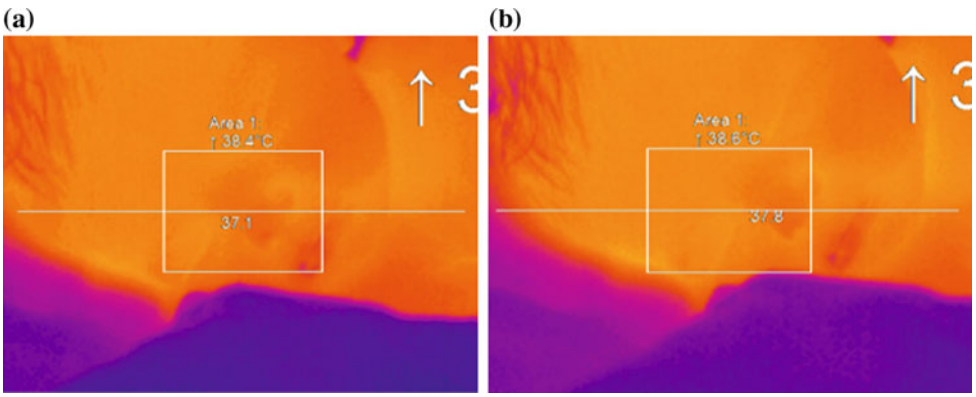

Fig. 6 Difference seen with the thermographic camera between inspiration and expiration. In figure **a** we observe a temperature of 37.1 °C in the area of the nasal fossils corresponding to the inspiration and in figure **b** we observe the temperature of 37.8 °C corresponding to the expiration

breathing processes. It has also been observed that healthcare actions (e.g. incubator door opening, child manipulation) have influenced the temperature profile. Despite the remaining problems, the authors believe that the presented technique is a promising and effective step to establish contactless monitoring of newborns in NICU.

Acknowledgements Scientific research funded by the "Grigore T. Popa" University of Medicine and Pharmacy Iasi, based on the contract no. 29027/28.12.2016

Conflict of Interest The authors declare that they have no conflict of interest.

References

1. Daw, W., Kingshott, R., Saatchi, R., Burke, D., Holloway, A., Travis, J., Evans, R., Jones, A., Hughes, B., Elphick, H.: Medical devices for measuring respiratory rate in children. J. Adv. Biomed. Eng. Technol. **3**(1), 23 (2016)
2. Hsu, C.H., Chow, J.C.: Design and clinic monitoring of monitoring of a newly developed non-attached infant apnea monitor. Biomed. Eng. Appl. Basis Commun. **17**, 126–133 (2005)
3. Dharmendra, J., Nimavat, M.D.: Apnea of prematurity. In: Ted Rosenkrantz, M.D. (ed.) FAAP more. https://emedicine.medscape.com/article/974971-overview. Accessed 06 Nov 2016
4. Szentkuti, A., Skala Kavanagh, H.A., Grazio, S.: Infrared thermography and image analysis for biomedical use. Periodicum Biologorum **113**(4), 385–392 (2011)
5. Poblano, A, Haro, R.: Sleep development and apnea in newborns. In: Clinic of Sleep Disorders, School of Medicine, National University of Mexico and Laboratory of Cognitive Neurophysiology, National Institute of Rehabilitation, Mexico City, Mexico; World's largest Science, Technology and Medicine Open Access book publishe, pp. 115–122
6. Darnall, R.A., Ariagno, R.L., Kinney, H.C.: The late preterm infant and the control of breathing, sleep, and brainstem development: a review. Clin. Perinatol. **33**, 883–914 (2006)
7. Tkáčová, M., Hudák, R., Foffová, P., Živčák, J.: An importance of camera—subject distance and angle in musculoskeletal applications of medical thermography. Acta Electrotechnica et Informatica **10** (2), 57–60 (2010)
8. Abbas, A.K., Heimann, K., Jergus, K., Orlikowsky, T., Leonhardt, S.: Neonatal non-contact respiratory monitoring based on real-time infrared thermography. BioMed. Eng. Online **10**, 93 (2011). https://doi.org/10.1186/1475-925X-10-93

Smart Wearable SpO_2 Monitor for Newborns

M. Datcu, C. Luca, and C. Corciova

Abstract

Monitoring vital signs is a must in Neonatal Intensive Care Units. The objective of this work is to design and implement a neonatal pulse oximeter in an innovative form, easy to use in NICU (Neonatal Intensive Care Unit) or by parents at home, at an affordable price. Pulse oximetry is a method to measure oxygen saturation of blood (SaO_2) and heart rate (HR); these parameters indicate the assessment of acid-base balance, if breathing is performed in an efficient manner, and if cellular metabolism is effective. For premature newborns or newborns on term the oxygen saturation decreases in case of intracranial hemorrhage, which is the major complication of a newborn, respiratory insufficiency due to insufficient development of the lungs, associated with respiratory pathology and heart failure. This is the reason why we designed an innovative pulse oximeter- that we called P-SOCK.

Keywords

Oxygen saturation • Heart rate • Newborn • Pulse oximeter

1 Introduction

Pulse oximetry is a noninvasive method of measuring the oxygenation level in the blood which provides an estimate of blood saturation and oxyhemoglobin. The procedure is based on the difference in the absorption of red light by oxyhemoglobin and reduced hemoglobin, using a pulse oximeter which use a photoelectric system [1].

Pulse oximetry is very important in the case of newborn monitoring because they can desaturate very quickly with increased oxygen consumption, low functional residual capacity and increased closure volume.

Data provided by pulse oximetry is required when the patient's oxygenation level is unstable, including intensive care, critically patients, and any emergency department of any hospital. The need for oxygen is a priority case because no living being can survive without oxygen [2].

The ability of pulse oximetry to detect SpO2 of only arte-rial blood is based on the principle that the amount of red and IR light absorbed fluctuates with the cardiac cycle, as the arterial blood volume increases during systole and de-creases during diastole; in contrast, the blood volume in the veins and capillaries as well as the volumes of skin, fat, bone, remain relatively constant.

The pulse oximeter uses two light sources: a source in the infrared spectrum (905 nm) and a source in the visible—red spectrum (660 nm). Light sources and sensors are mounted in a couple that attaches to the finger pulp or ear lobe. As the background absorption of radiation by venous blood, sub-cutaneous tissue and skin are virtually constant, the only variable is the amount of Hb (pulsating wave) [3].

Pulse oximetry measures the oxygen saturation of the blood on the basis of the absorption properties of the blood. When combined with oxygen, hemoglobin (Hb) changes its light absorption characteristics. Pulse Oximeter exploits the difference in light absorption between Hb and the amount of oxygenated hemoglobin (HbO_2). HbO_2 absorbs more infra-red light (wavelength 660 nm) and less red light (wave-length 940 nm) than Hb [4].

2 Materials and Method

This smart wearable monitor for infants represents a new biomedical application, and absolutely necessary because it is designed to monitor the most fragile patients: premature infants and newborn babies. The main purpose of this project

M. Datcu (✉) · C. Luca · C. Corciova
Department of Biomedical Sciences, University of Medicine and Pharmacy Grigore T. Popa, Iasi, Romania
e-mail: madalina.dtc@gmail.com

S. Vlad and N. M. Roman (eds.), *6th International Conference on Advancements of Medicine and Health Care through Technology; 17–20 October 2018, Cluj-Napoca, Romania*, IFMBE Proceedings 71,
https://doi.org/10.1007/978-981-13-6207-1_7

is to develop a monitoring system using the latest technologies and medical bio signal collecting their unification in a unique, wearable, inexpensive and accessible. Our signals of interest are the Heart Beat and the SpO2 of the newborn/infant.

A special quality of this wearable monitor is that it can be cleaned and sterilized due to the technologies used in its construction. Aseptic compliance is very important due to the types of patients who addresses the monitoring system.

We know that apnea of prematurity is the most common problem that affects premature infants due to insufficient development occurred following the respiratory system and the congenital heart disease is the most common congenital disorder in newborns, so we propose a wearable system for monitoring this type of fragile patients, applicable in the NICU section, Pediatric Intensive Care Units and at home, being very easy to use also by parents.

In addition, with more and more sufficient consideration of infant needs and clinical requirements, the application of integrated sensing and consumer electronics technology is improving the reliability and comfort of monitoring systems, which ensure the quality of life and longterm health prospects of the infants. The use of wearable electronics and intelligent textiles effectively avoid the disturbance to infants caused by conventional sensor techniques which may include skin irritation, hampering due to wires, interruption of sleep, and lack of communication with parents.

The proposed system is the redesign of the classic pulse oximeter in an innovative sockshaped system. This device is made of a special elastic material, inside is placed the transmits them to the microcontroller.

The microcontroller processes the bio signals and transmit them wireless through Bluetooth technology to another module which contain an LCD where the oxygen saturation value is displayed. If this value is within the normal range, the LED will be green, and if the measured parameter is below the normal value, the LED will turn red and a sound alert will be issued to alert the NICU staff, or the parent if it is used at home.

The microcontroller is represented by Arduino, an easy-to-use open source hardware platform and software.

Our system consists of two modules.

The first module consists of an external component made of Arduino Nano to which a Bluetooth module was connected and the sock that we named P-SOCK inside is placed the MAX3100 sensor that measures the oxygen saturation in the blood and the heart rate.

Arduino Nano is a small, complete board, based on ATmega328; to this we have connected the MAX30100 sensor which is an integrated circuit (IC), pulse oximetry sensor and heart rate ideal for monitoring medical devices that can be worn.

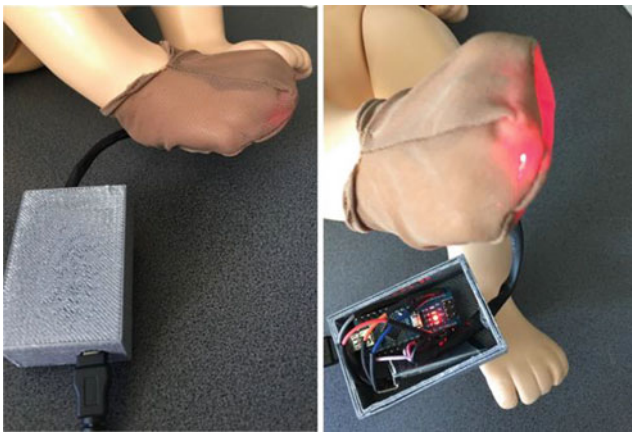

Fig. 1 Module I placed on the foot of baby simulator BabySim

This sensor will be located inside the sock to have a perfect contact with the newborn baby's leg (Fig. 1).

For transmitting data, a Bluetooth Module HC-05 was used because it can be both "master" and "slave", it can receive and transmit information.

System innovation is also represented by its form. To get the perfect contact between the MAX30100 sensor and the newborn foot we made a sock of special material that we took from compression stockings. They are elastic and rigid at the same time, to avoid sensor movement on the foot. This material do not produce irritation and let the skin breathe. Material composition: 25% elastane (EL) and 75% polyamide (PA).

The clamping and fastening system is made of polyamide and consists of two components: hook and loop (Fig. 2). The woven "hook" band is composed of tiny, flexible hooks that assemble with the loop of very small loops. By press-ing the two components an adjustable and very safe closing is achieved [6].

The second module is designed to display measured values (oxygen saturation and heart rate) on a large LCD screen and also this contain an alarm with optical and visual signals if the values exceed the normal limits set by us.

The alarm system is composed of optical and acoustic signals. These are intended to alert NICU staff or parents if it is used at home.

The optical system is a RGB LED that is green when the oxygen saturation value and heart rate are within normal or red when these values are not within the normal range, and also the LCD that constantly displays the SpO_2 and pulse value. The acoustic system is an acoustic piezoelectric alarm represented by a buzzer (Fig. 3).

Fig. 2 Textile material and fastening system

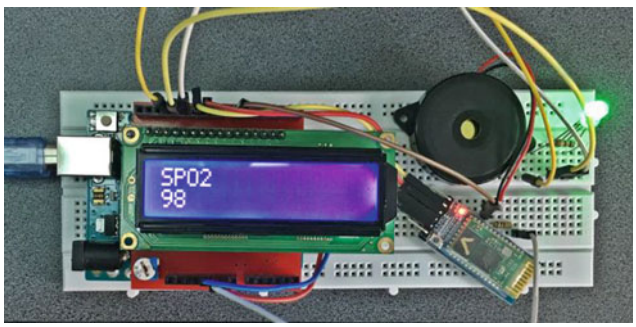

Fig. 3 Module II

3 Results

After the codes have been run, then reset both Arduino cards and remove the power from HC-05 and HC-06. HC-06 starts first. The LED must flash rapidly 5 times per second. This indicates that it is waiting for a connection or associated. Subsequently, HC-05 starts. The LED will blink several times when it is switched on first and then change the usual flashing pattern every few seconds.

The LED on the HC-06 will be active for the entire duration of the operation (it does not blink). So the modules are connected [8].

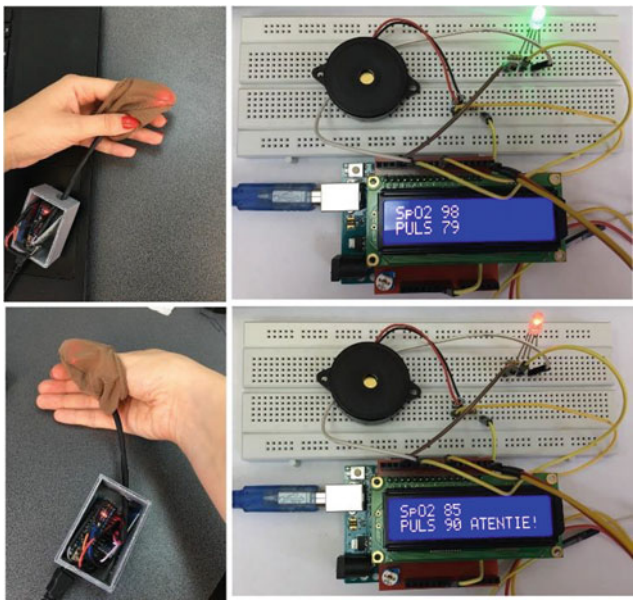

Fig. 4 Testing the device

To test the device, we placed the finger tip on the MAX30100 sensor, and to obtain a negative value we made ischemia by pressing on finger (Fig. 4).

This wearable system contain a wide variety of components: sensor—MAX30100, wearable materials, smart textiles, power supplies, wireless communication modules, processing and control units, an interface for the user, software, and advanced algorithms for data extraction and decision making. To achieve reliable, comfortable and user-friendly neonatal monitoring, wearable sensor systems proposed by us satisfies the following requirements:

- It includes a monitoring of fundamental vital functions, it is safe to be used in NICU or at home because it monitors and warns;
- Even if the device is in incubator or in a Kangaroo system it is able to provide continuous monitoring (Kangaroo is a form of developmental care that involves contact on the largest surface of the newborn's skin with the mother's (or father's) skin.);
- It is non-invasive;
- It is capable of allowing the inclusion of several monitoring functions—exporting data to a family doctor, for example;
- It provides viable data to be interpreted by hospital staff/parents;
- It is easy to wear and to remove the non-washable parts.

For continuous monitoring of newborns, the traditional method involves direct supervision of patients. This method involves specialized staff and it is very difficult for hospital staff and parents to identify pathological conditions. The main function of the P-SOCK device is to provide continuous monitoring with a gentle observation of the monitored values, and if complications occur, appropriate treatments, appropriate therapies can be applied.

4 Conclusions

Continuous monitoring of partial oxygen saturation in the blood and pulse especially in premature newborns case with various associated pathologies is absolutely necessary.

The P-SOCK Pulse Oximeter has proven to be an ideal device for Neonatal Intensive Unit Care, but especially for parents at home, because it is very easy to use, requires no medical knowledge, and performs continuous monitoring. It is important to know that it has optical and acoustic signals for alarming when the values fall below normal limits.

The results obtained from the P-SOCK pulse oximetry test have shown that this method complies with all medical standards on patient safety and may be a convenient alternative for continuous monitoring of SpO_2 and heart rate.

This monitoring system, by using the MAX30100 sensor and all the components included, has proven that this new-born monitoring device can be made at a very low cost. If the system proposed by us were to scale up, production costs would fall further. Starting from the fact that a disposable pulse oximetry sensor used in the newborn cost between 25 and 100$, depending on the producer, the entire value of the system reaches a production cost of 50$.

This is a huge benefit for hospitals as well as accessibility to new techniques for premature newborns monitoring.

Future Research Directions:

- Develop the proposed system so that it can be patented in the two variants: P-SOCK Home Using and P-SOCK NICU Using.
- Development of a phone application that communicates directly with the system and monitors in real time proposed parameters - partial oxygen saturation in the blood and pulse;
- Graphical display of parameters on the device screen;
- Attachment of an oxygen therapy device, with automatic control of the oxygen fraction FiO2, which works automatically if values fall below normal limits.

Conflict of Interest The authors declare that they have no conflict of interest.

References

1. Ahrens, T.S., Ott, K.: Comparison of three new generation pulse oximeters in a medical intensive care unit. Crit. Care Med. **34**(12), A85 (2006)
2. Tin, Win, Lal, Mithilesh: Principles of pulse oximetry and its clinical application in neonatal medicine. Semin. Fetal Neonatal Med. **20**, 192–197 (2015)
3. Costin, H., Rotariu, C.: Electronică medicală—o abordare practică, p. 95. Editura U.M.F. Gr. T. Popa, Iaşi (2007)
4. Dănăilă, C.: Angela Dăscălescu şi Ion Antohe. Hematologie clinică. Editura U.M.F. Gr. T. Popa, Iaşi (2017)
5. https://datasheets.maximintegrated.com/en/ds/MAX30100.pdf. Accessed in March 2018
6. http://donis.ro/content/html/detalii_produs.php?a=0&id_produs=1451&id_categorie=29. Accessed in May 2018
7. https://www.teachmemicro.com/arduino-bluetooth/. Accessed June 2018
8. HC-05 Bluetooth Module User's Manual V1.0

Applied Measurements and Instrumentation for Improving Diagnostic Devices and Systems in Metropolitan Polluted Environments with Nitric and Carbon Oxides

Lavinia Andrei, Doru Băldean, and Adela Ioana Borzan

Abstract

The problem of pollution in transportation and road traffic, especially in metropolitan areas, rise a significant concern regarding the health of the inhabitants and the rapid diagnostic procedures on site. It is important to know exactly what the problem is when it comes to toxicity in highly traffic areas. The present paper shows an applied solution for monitoring and control of pollutants, such as nitric oxides and carbon oxide in automotive and transportation sector in order to increase the potential of health security in road traffic activity. There were some measurements done in laboratory. Also the sensors were calibrated and tested. A hardware in the loop system was also used in order to test the validity of the hypotheses for monitoring and for giving the signal of hazard condition regarding pollution with nitric and carbon oxides.

Keywords

Nitrogen • Carbon • Pollutant • Sensor • Instrument

1 Introduction

In the recent decades, the development of new types of automotive security and medical systems has increased in order to contribute to the life protection and pollution reduction in transport and traffic sectors [1–6].

The present paper studies the opportunity and the technical possibilities to implement and test a system for monitoring and alerting the vehicle occupants (driver and passengers) for hazardous and risk conditions in road traffic and transport security, combining medical expertise with automotive engineering experience (as the authors are in their field of activity) for a final achievement and proper results in accordance with a meditech scientific event. Some of the most important conditions for controlling the nitric oxides and other important pollutant emissions (such as carbon oxide) and some of their environmental effects is to have proper instruments for measurement, to integrate sensors and transducers to monitor compounds which are risk for health and environment. In this work there are highlighted some precise achievements in controlling nitric oxides (NO_x) and other pollutants, with their respect to the potential influence on human health. Nitric oxides generate important health problems for humans and animals, showing a risk level in class A1 toxicity. Sickness affecting the respiratory system, including both upper tract and lungs, is influenced by pollutants from combustion. The smoke and residual pollutants from combustion processes are also important risk factors regarding pulmonary health problems and they are a source for acid rains. Programing the process definition of the multiple sources of air pollution and of instruments for control (and monitor) by optimizing step by step technical and medical infrastructure, changing thus air structure composition and reducing the ambient risk hazards are imperative sequences to control the evolution of health condition. There are some articles that present the real data concerning nitric oxides and their influence. Pollutants such as nitric oxides, carbon oxide and ozone in gaseous form are problematic due to the fact of their high risk toxicity and contribution to particle matter (PM) and smog formation. The combined hazard increases the health problems.

Nitric oxides are a group of reactive gases formed by oxygen and nitrogen. Density of nitrogen oxide is 1,25 kg/m^3 and it melting point is −164 °C. Its boiling point is −152 °C and the solubility is 60 mg/L. Nitrogen dioxide is four times more polluting then nitrogen oxide. For the plant protection the limit value of NO_x must be under 30 μg/m^3. Both plants and animals are strongly affected by the pollution with

L. Andrei
Health Department, Clinical Hospital of Infectious Diseases, Cluj-Napoca, Romania

D. Băldean (✉) · A. I. Borzan
Ministry of Education, Technical University of Cluj-Napoca/Automotive and Transportation Department, Muncii, 103-105 Cluj-Napoca, Romania
e-mail: doru.baldean@auto.utcluj.ro

S. Vlad and N. M. Roman (eds.), *6th International Conference on Advancements of Medicine and Health Care through Technology; 17–20 October 2018, Cluj-Napoca, Romania*, IFMBE Proceedings 71,
https://doi.org/10.1007/978-981-13-6207-1_8

nitrogen and carbon oxides. There are some sicknesses which are determined by these pollutants such as pulmonary diseases and immune disturbances. After a threshold exposure even death occur. Some of these pollutants are significantly impactful on the health and life of the human and animals thus being important a degree of control and a thoroughly study applied on their influence [7–15].

The present paper brings a innovative idea into testing scheme to improve the bulk of know-how and information regarding nitric and carbon oxide gases level monitor and control, by instrumenting and applying latest equipment in combustion pollutant research and reduction. There have to be a general approach based on interdisciplinary and trans-disciplinary studies. Control measures are an imperative as long as these emissions are hazardous to life and health in general. Thus through conducted research the authors have targeted the identification of a solution for measuring the nitric and carbon oxides levels, and the signaling on board when the hazardous value is recorded in order to successfully implement a safety feature on urban or metropolitan vehicles.

2 Experimental Setup Materials and Methods

The materials applicable in the practical tests and essential for validating the hypothesis are presented in Table 1. The type of the internal combustion engine was chosen to provide the emissions of nitric and carbon oxides for measurement and testing. In order to gain real values and some differences between measurements according to each specific regime, there must be coupled to engine's crank shaft a dynamometer. The later one increases the torque on the crank shaft to develop resistance to rotation. The resistant torque determines the increases on the fuel injection duty, thus the time of opening injector needle is a little longer leading to an increased fuel amount into the engine. This surplus of fuel sprayed in the intake or compression stroke of the engine cycle increases the temperature of the gases influencing the combustion sequence. A better combustion, more oxidation reaction increases the temperature and the reaction speeds. There is a limit for optimal operation, because there is a temperature and a speed value over which oxidation reactions take place between oxygen and nitrogen (instead of oxygen and carbon, as it is expected). Also, due to the high speeds of combustion the incomplete burning of carbon atoms occur meaning that some energy is lost and a certain degree of toxicity is generated.

The experimental bench scheme is depicted in Fig. 1. The test chamber 1 is filled with necessary equipment specified in Table 1. An internal combustion engine (ICE) 4 is installed on a testing bench 5. The ICE is coupled with a transmission 6 and dynamometer 7 placed on the damping supports 8. A crank angle encoder 3 and its wire connection 2 is linked by transducer 24 to a central automation unit 20 for data acquisition from al the sensors, regarding intake air parameters (temperature, pressure)—in the intake air manifold 30—with the air control sensor 29 that communicate with the corresponding transducer 23. The exhaust parameters in the exhaust pipe line 27 are monitored with the sensor unit 25 and transducer 22 by the central unit 20. Dynamometer speed and torque are determined and recorded via connection between sensor 26 and transducer 21 with the boombox. Energy supply for dynamometer power unit is done through power cable 10, from socket 11 with the electric interface 9. A USB cable with terminal A 14 connected to the dashboard 13, and with terminal B 19 linked to central unit 20, for fast user control and emergency stop button 15. The dashboard features the red color signal 16 for hazard call which lights up a led indicator when the nitric and carbon oxides are reaching the risk value. The control room 18 has the automation system and processing power unit 12. The setup equipment is configured as a complete testing laboratory which facilitates the experimental testing.

Table 1 Practical test materials

Component	Size	Importance
Internal combustion engine	4 cylinder	High
Dynamometer	Up to 500 kW	High
Transmission	Rigid	High
Automation system	>3 Ghz	High
Exhaust control	manifold	High
Intake control	Airflow meter	High
Fuel measurement	5 L tank	High
Control room	>10 m^3	High
Safety button	Standard	High
Emergency signal	Standard red	High
Nitrogen sensor	Standard	High
Carbon oxide sensor	Standard	High
Colorful spectrum code for signal	User adapted	Medium
Alternative solutions suggestion	–	Medium/optional
Docs/info availability	User defined	Medium/optional
Wireless connectivity	–	Medium/optional
Storage unit	User adapted	Medium/optional
USB communication interface	Standard	Medium/optional

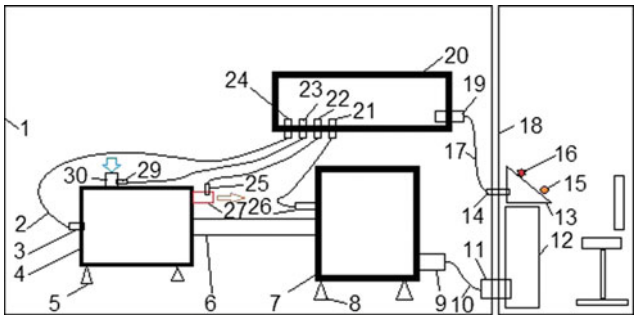

Fig. 1 Schematic of the laboratory equipment

Table 2 Power units specs

Internal combustion engine	4 stroke-4 inline cylinders	Direct injection
Dynamometer	Electric driven	>200 kW
Transmission	Cardanic shaft	Angle of 35°
Coupling	Removable Flywheel	Mass of 10 kg

The internal combustion engine which is assigned for the present research is a compression ignited unit with 4 cylinders and 1900 cm^3 displacement. The unit of injection is a direct system with 4 jets. Higher loads are determined via torque increase from dynamometer unit. Specific sensors are receiving signals from testing assembly line.

Details regarding the power units, ICE and dynamometer, are presented in Table 2.

A schematic of the configuration for in-vehicle control system application is given in Fig. 2. Vehicle 1 signals the hazard problem (high levels of nitrogen and carbon oxides), via dash panel indicator 2, to the driver and occupants after determining the cumulated values in the cockpit with the specific sensor unit 3 and from road traffic area with outside sensory unit 4. The processing unit 5 is placed near the driver zone with a higher degree of accessibility.

Total pollutant combined T_{PC} in the first assembly of the monitor and control system is determined with relation (1).

$$T_{PC}^{1} = NO_x + CO \quad (1)$$

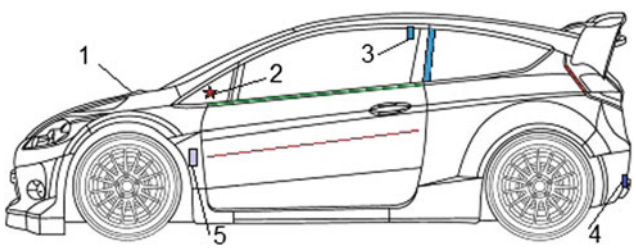

Fig. 2 Schematic of the mobile in-vehicle equipment

Nitrogen oxides combine are determined with the relation 2 in order to calculate the total pollutants for each scenario in real time.

$$NO_x = NO + NO_2 + N_2O \quad (2)$$

The sensors are set to long exposure to pollutants during which the nitric and carbon oxides are released through exhaust system and with an adjustable delay the ambient sensor triggers the signal toward the central processing unit. Thus the system will record the values instantaneously. Through repeated experiments and tests with different engine loads there are studied and recorded the nitric and carbon oxides levels.

3 Results

The values recorded in laboratory environment for three different regimes are shown in Fig. 3, in which the low charge (a) of air-fuel mixture given to the ICE is processed and captured in the range of 50–60 ppm vol of NO_x. In this case the CO is 5 ppm vol. The medium (b) loading regime is 300–400 ppm vol of NO_x and 10 ppm vol of CO. The peak (c) value determined during the practical tests was higher then 900 ppm vol of NO_x and 15 ppm vol for CO.

In order to evaluate the nitric and carbon oxides there were measured in real time all the values and recorded as a graph for pointing out the peaks and hazard scenarios.

Continued measurements during test are shown in Fig. 4 and the procedures followed were in accordance with the ethical standards of the responsible committee on human

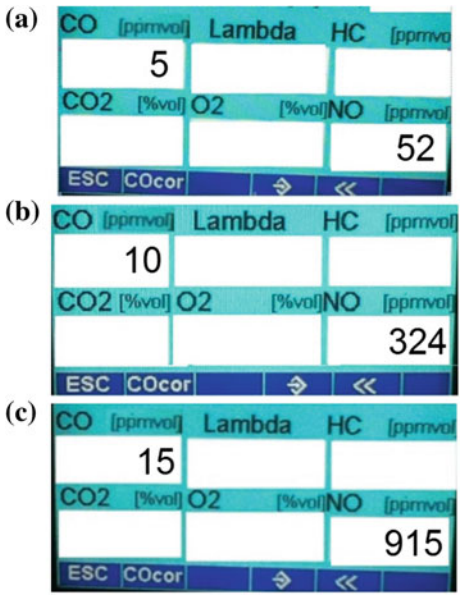

Fig. 3 Measurements of carbon and nitric oxides (CO and NO_x)

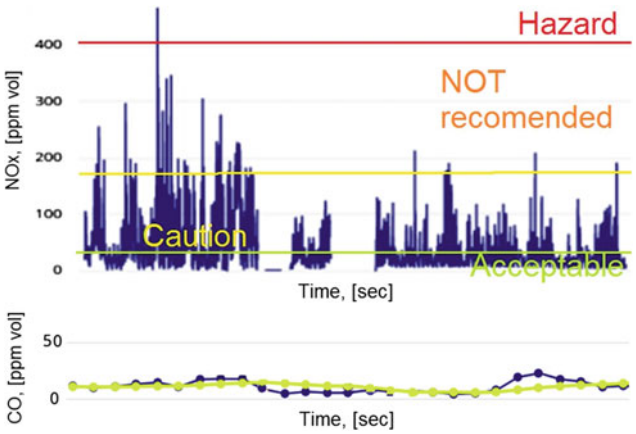

Fig. 4 Measurements of carbon and nitric oxides (CO and NO_x)

experimentation (institutional and national) and with the Helsinki Declaration of 1975, as revised in 2000 and 2008. The laboratory instruments and benches are certified and UN approved for specific tests. Higher values lead to an hazard or risk for health condition and medical care and proper measures are to be taken. The results are only concerning the potential of testing, value recording and caution.

4 Discussion

It may be observed that the peak values over 400 ppm vol of NO_x are very few in number, but it may pose a concern anyway to what extent should be dealt with such scenarios. The "not recommended" and "caution" scenarios are the important regimes of operation and they are very common in modern traffic and transportation in metropolitan and highway areas. For such cases there is defined a strategy of alerting the driver and the occupant with signals and/or with a color coded display signal on dash board for preventive measures. For risk cases in which there is a hazard and fresh air is needed an alternative strategy must provide a oxygen reserve and a mask available on board. A schematic for placing the oxygen mask 2 for in-vehicle control system application is given in Fig. 5. Vehicle 1 is provided with protecting equipment and oxygen distribution system for the cases of hazard condition with overpassing the threshold limits of nitric and carbon oxides.

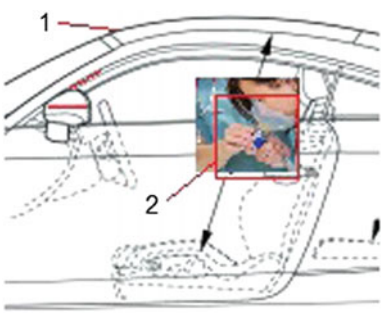

Fig. 5 Schematic of the mobile in-vehicle protecting equipment

5 Conclusions

On the basis of obtained results and tests the system for measuring nitrogen and carbon oxides and alerting the driver about hazard situations may be tested in real time traffic. For complete system testing additional research are needed.

Acknowledgements The paper has been realized on the basis of the research contract "PN-III-P2-2.1-CI-2018-1227" (VINEFUEL).

Conflict of Interest "The authors declare that they have no conflict of interest". The authors of this work have no financial or ownership profits in any equipment or elements described. The article's authors declare that all of them have no inherent economic, professional or personal benefits which could have determined the outputs or trend-lines of the analyze presented in this paper.

References

1. Berge, E., Bartnicki, J., Olendrzynski, K., Tsyro, S.G.: Long-term trends in emissions and transboundary transport of acidifying air pollution in Europe. J. Environ. Manage. **57**(1), 31–50 (1984). https://doi.org/10.1006/jema.1999.0275
2. Brodzinsky, R., Cantrell, B.K., Endlich, R.M., Bhumralkar, C.M.: (1984) A long-range air pollution transport model for eastern north America—II, nitrogen oxides. Atmos. Environ. **18**(11), 2361–2366 (1967). https://doi.org/10.1016/0004-6981(84)90006-4
3. Butland, B.K., et al.: Air pollution and the incidence of ischaemic and haemorrhagic stroke in the South London Stroke Register: a case–cross-over analysis. J. Epidemiol. Commun. Health. **71**(7), 707–712 (2017). https://doi.org/10.1136/jech-2016-208025
4. Camuffo D (2014) Parameters to describe air masses and vertical motions. Microclimate for Cultural Heritage, https://www.sciencedirect.com/topics/earth-and-planetary-sciences/pollution-transport
5. Cepeda, M., Schoufour, J., et al.: Levels of ambient air pollution according to mode of transport: a systematic review. Lancet Public Health **2**(1), e23–e34 (2017). https://doi.org/10.1016/S2468-2667(16)30021-4
6. Dadvand, P., et al.: Traffic-related air pollution and spectacles use in school children. PLoS One **12**(4), e0167046 (2017). https://doi.org/10.1371/journal.pone.0167046
7. Endlich, R.M., Nitz, K.C., Brodzinsky, R., Bhumralkar, C.M.: A long-range air pollution transport model for eastern North America—I, sulfur oxides. Atmos. Environ. **18**(11), 2345–2360 (1984). https://doi.org/10.1016/0004-6981(84)90005-2
8. Hagenbjörk, A., et al.: The spatial variation of O_3, NO, NO_2 and NO_x and the relation between them in two Swedish cities. Envir. Monit Assess. **189**(4), 161 (2017). https://doi.org/10.1007/s10661-017-5872-z
9. Harrison, R.M., et al.: Efficacy of recent emissions controls on road vehicles in Europe and implications for public health. Sci. Rep. **7**, 1152 (2017). https://doi.org/10.1038/s41598-017-01135-2
10. Khreis, H., et al.: Traffic-related air pollution and childhood asthma: recent advances and remaining gaps in the exposure

assessment methods. Int. J. Environ. Res. Public Health. **14**(3), 312 (2017). https://doi.org/10.3390/ijerph14030312

11. Kim, Y.M., et al.: Short-term effects of weather and air pollution on atopic dermatitis symptoms in children: a panel study in Korea. PLoS One **12**(4), e0175229 (2017). https://doi.org/10.1371/journal.pone.0175229
12. Lee, H., et al.: Short-term air pollution exposure aggravates Parkinson's disease in a population-based cohort. Sci. Rep. **7**, 44741 (2017). https://doi.org/10.1038/srep44741
13. Johansson, B.: Strategies for reducing emissions of air pollutants from the Swedish transportation sector. Transp. Res. Part A: Policy Pract. **29**(5), 371–385 (1995). https://doi.org/10.1016/0965-8564(95)00003-7
14. Nishioka, S.: Traffic pollution: control policy and research trend. Transp. Res. Part A: Gen. **23**(1), 73–81 (1989). https://doi.org/10.1016/0191-2607(89)90142-8
15. Qu, Y., An, J., He, Y., Zheng, J.: An overview of emissions of SO_2 and NO_x and the long-range transport of oxidized sulfur and nitrogen pollutants in East Asia. J. Environ. Sci. **44**, 13–25 (2016). https://doi.org/10.1016/j.jes.2015.08.028

Three Way Automated Blood-Sampling Device Mixer for Blood Gas Analysis

Manole-Stefan Niculescu

Abstract

The blood gas assay is one of the most important procedures that need to be performed in case of an emergency. In the intensive care, emergency, pediatrics, nephrology, neonatal it is mandatory for the results of the arterial blood gas assay to be precise and accurate. A proper mixing procedure is required before analyzing the sample in order to prevent blood coagulation and to harmonize the content. An automated mixing system can be the solution for assuring the correct analysis procedures which implies providing the correct results and the proper functionality of the blood gas analyzer. An original prototype of this kind of system will be presented in this paper.

Keywords

Arterial blood gas • Blood gas analysis • Hemoglobin • Heparin • Automated mixer • Blood gas analyzer • Prototype

1 Introduction

Point-of-care (POC) is a new domain in the healthcare market that is currently under development and helps the medical professionals to decide fast in their act taking into consideration the clinical results of a series of blood investigations.

The difference between the laboratory and the point-of-care domain is the size and the speed of the equipment. The turnaround time for the laboratory equipment is greater than the one from the point-of-care due to the elaborated assay technique that implies reagent preparation, incubation, pre-calibration of the system and the sample measurement. The laboratory analyzers are bulky and it is needed clinical trained professionals to operate and to perform the maintenance of the equipment.

Point-of-care is a field where small and precise instruments are used to perform a quick assay with low sample preparation and maintenance. Some of those products do not require clinically trained personnel because either they are Clinical Laboratory Improvement Amendments (CLIA)—waived or they are very easy to use. CLIA is a certified clinical amendment that was established in order to ensure the correct assay procedures in case of sample measurement on a healthcare instrument. Most point-of-care instruments are CLIA-waived, which means that can be operated also by users with no medical experience.

The point-of-care equipment is mainly portable and it is installed in the unit where the clinical tests are performed, not like in the case of the laboratory unit where all the samples are centralized and analyzed based on priority. Being always at the disposal of the clinician, point-of-care devices are the flexible solution for monitoring the clinical state of a patient and can be transported to the site where it is needed for the investigations to be performed. POC analyzers are not used for certified patient result, being used for screening the patient's health state and to observe if the treatment is efficient.

2 Blood Gas Testing and the Acid-Base Balance

The blood gas testing is the primary procedure that needs to be done when the evaluation of the overhaul health state of a patient is mandatory in case of an emergency.

The basic parameters for this clinical investigation are the arterial gases (pO_2, pCO_2) and the pH. Those gas exchange indexes represent the fastest way of estimating the clinical relationship between pulmonary dysfunction and the pulmonary shunt fraction [1].

M.-S. Niculescu (✉)
S.C. Ana Concept S.R.L., Dorneasca, Bucharest, Romania
e-mail: niculescu.manolestefan@yahoo.com

S. Vlad and N. M. Roman (eds.), *6th International Conference on Advancements of Medicine and Health Care through Technology; 17–20 October 2018, Cluj-Napoca, Romania*, IFMBE Proceedings 71,
https://doi.org/10.1007/978-981-13-6207-1_9

2.1 The Partial Pressure of Oxygen

The oxygen is essential for the cell and tissue metabolism. The cardiopulmonary system is responsible for oxygen transportation to the cells and it involves the following processes: convection, O_2 linkage to the hemoglobin, transportation and cell oxygenation. The oxygen partial pressure (pO_2) has become a standard metric for the respiratory system and for the acid-base relationship. It reflects the ability of the lungs to provide oxygen to the body.

Hypoxia is a case of abnormal respiratory function due to parenchymal pulmonary diseases (pneumonia, asthma, pulmonary edema or fibrosis) caused by pulmonary blood shunt. The abnormal functions of the respiratory system needs to be compensated with mechanical ventilation.

2.2 The Partial Pressure of Carbon Dioxide

The carbon dioxide is the product of the normal cell metabolism and it is transported by the blood to the lungs and kidneys for liberation [2]. The CO_2 is transported in the blood stream as bicarbonate (HCO_3^-), as it follows:

$$CO_2 + H_2O \leftrightarrow H_2CO_3 \leftrightarrow HCO_3^- \quad (1)$$

The H_2CO_3, HCO_3^- and CO_2 levels from the blood have an important role in modifying the pH:

$$pH = pK + \log\frac{base}{acid} = pK + \log\frac{HCO_3^-}{CO_2 + H_2CO_3} \quad (2)$$

Analyzing (2), it can be evaluated further the respiratory state of the patient in a direct proportional manner between the pH and acid-base balance (HCO_3^-/H_2CO_3). When the pCO_2 is elevated, the patient will suffer hypercapnia and similar, low pCO_2 levels will lead to hyperventilation resulted from hypoxia, fever, cerebral disease and cirrhosis.

2.3 The Quantified Activity of the H^+ Ions

The normal cellular metabolism requires a controlled and exact ecosystem in which the concentration of H^+ ions must be balanced and maintained at a low level. This activity reflects the acid-base balance from the blood, where the acids are donor H^+ ions and the bases are substances located in the lungs, kidneys and blood that will accept H^+ ions in order to maintain the acid-base ratio at a controlled level for normal cellular activity.

The concentration of H^+ ions are very low numbers, thus a more simplified equation was described by Sorenson [2]:

$$pH = -\log_{10} c\,H^+ \quad (3)$$

From (3) it can be stated that the value of the pH is inversely proportional with the actual concentration of H^+ ions from the sample.

2.4 The Hemoglobin

The arterial gases quantify the functionality of the respiratory system, which is the vital biological structure of the body. Along with the arterial gases, the hemoglobin is an important parameter that is involved in the respiration process. It is the element that ensures the oxygen transportation, being a ferroprotein with tetrameric structure and representing 80–90% of the dry waste of the erythrocyte [3].

It is composed of the heme and the globin, the first one being composed of a tetrapyrrolic nucleus which contains iron ions and the second one representing 96% of the weight of the total hemoglobin with a structure of a pair of alpha chains with 141 amino-acids and a pair of beta chains with 146 amino-acids. The hemoglobin is dependent of the pH, pO_2, pCO_2 and the patient's temperature and it is the sum of all its fractions, the oxyhemoglobin (FO_2Hb), deoxyhemoglobin (FHHb), carboxyhemoglobin (FCOHb) and methemoglobin (FMetHb):

$$tHb = FO_2Hb + FHHb + FMetHb + FCOHb \quad (4)$$

The fractions of the hemoglobin are measured optically using a co-oximetry module.

2.5 Blood Gas Quick Result Interpretation

As a first diagnostic for the patient, there are three factors that will provide sufficient information about the vital functions: pH, HCO_3^- and pCO_2. Comparing those three parameters, a first quick diagnostic can be stated (Fig. 1):

The normal pH for the arterial human blood is between 7.35 and 7.45. If the value of the pH is below 7.35, it occurs acidosis and if the value of pH is above 7.45, there will be a case of alkalosis. The metabolism generates acids which need to be balanced in order to maintain the pH at a normal level. The acids are balanced with the help of the lungs which perform CO_2 exhaling and the kidneys which excrete

Respiratory acidosis	pH ↓	pCO_2 ↑
Respiratory alkalosis	pH ↑	pCO_2 ↓
Metabolic acidosis	pH ↓	HCO_3^- ↓
Metabolic alkalosis	pH ↑	HCO_3^- ↑

Fig. 1 The respiratory and metabolic acidosis and alkalosis

the acids through urine, regulating the concentration of bicarbonate (HCO_3^-) in the blood [4].

The clinical investigations of those specific parameters are performed on a blood gas analyzer. Along with the arterial gases, pH and hemoglobin, a blood gas analyzer can also measure the level of the metabolites glucose/lactate and the ions of Na^+, K^+, Ca^{++} and Cl^-.

3 The Measurement Principle of a Blood Gas Instrument

The active block of a blood gas analyzer is the sensor panel, which can be composed of electrochemical electrodes or planar sensors. The sensors acquire and transform the amount of recognized ions in electric signal in two ways: the potentiometry and the amperometry [5].

Potentiometry represents the measurement of the potential generated by two electrodes from an electrochemical cell when no external current is applied and the cell is in a state of equilibrium. The electrodes are immersed in an electrolyte solution and the concentration of an analyte is measured by a voltmeter. Every electrode acts like a semicell and contains an internal reference element which ensures the constant potential for the cell. The generated potential between the two electrodes is correlated with the concentration of the specific analyte. With no current applied, the generated potential of the cell is the difference between the measurement and reference electrode (Fig. 2).

The measured potential for the electrochemical cell (E_{cell}) is influenced by the potential of the liquid junction (E_{lj}) and the membrane potential (E_{memb}):

$$E_{cell} = \left(E_{ref} + E_{memb}\right) - \left(E_{ext} + E_{lj}\right) \tag{4}$$

The blood gas analyzer is measuring the potential of the cell (E_{cell}) when the analyte solution represents the blood. The selective membrane filters only one type of ion for which the concentration needs to be measured from the sample.

The blood gas parameters measured with potentiometry are mainly electrolytes (Na^+, K^+, Ca^{++} and Cl^-.), pH and the arterial gases.

Amperometry is the procedure that is used for measuring the concentration of a substance by applying to the electrochemical cell a voltage between two electrodes and measuring the generated current that results from the oxidation or the reduction reaction of the target molecule. When the sample reaches the two electrodes, a known voltage is applied between the anode and cathode. The parameter that needs to be measured is either oxidizable or reductible. In both cases, the electrochemical reaction produces a current flux between the anode and the cathode and it is directly proportional with the concentration of the substance. The metabolites glucose and lactate are measured with amperometry.

Hemoglobin has two different measurement technologies: potentiometry for determining the concentration of haematocrit and calculating the hemoglobin or measuring the total hemoglobin along with its fractions by co-oximetry [6].

The co-oximetry is an optical procedure that involves a source lamp that will transmit light through the blood sample to the polychromator. The diode array measures the absorbance of the resulted light at different wavelengths. This will allow the concentrations of the hemoglobin and its fractions to be quantified and calculated (Fig. 3).

The absorbance (A) at different wavelengths is calculated using the Beer-Lambert law, where I_1 is the intensity of the light measured by the diode array and I_0 is the intensity of the light emitted by the source light:

$$A = -\log_{10} I_1/I_0 \tag{5}$$

The blood gas instrument has parameter specific reference sensors that are disposed in series forming a continuous path for the sample and measuring simultaneously every specific analyte. Some blood gas analyzers have attached to the sample path a sliding optical cell that is used by the co-oximeter module to measure the hemoglobin and its fractions directly.

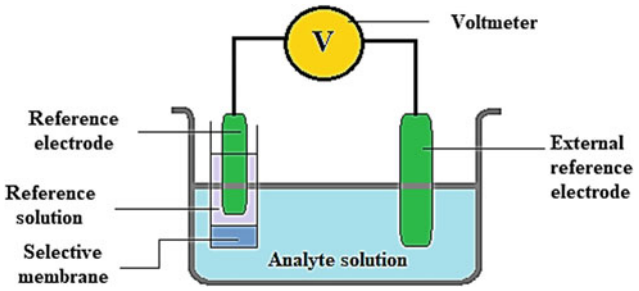

Fig. 2 Electrochemical cell for potentiometric measurement

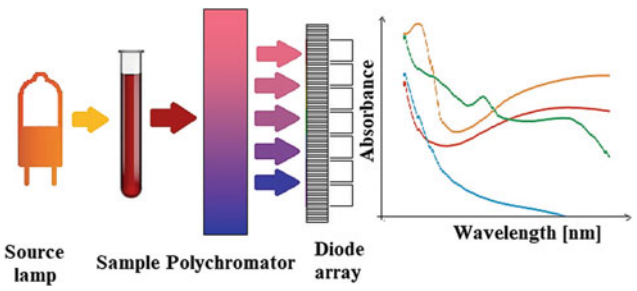

Fig. 3 The co-oximeter assembly

4 The Three WAY Automated Blood-Sampling Device Mixer

The results of a blood gas assay must be precise in order not to prescribe a false diagnostic and sample preprocessing measures should be taken prior to analyze the sample on the blood gas instrument.

The blood gas syringe contains solid or liquid heparin to prevent blood coagulation and blocking the instrument's functionality due to a clot aspiration from the blood-sampling devices. Mixing is mandatory before analysis because the sample should be homogenized not only for anticoagulation purposes, but also it is a demanding requirement to maintain the same assay conditions in order to provide high accuracy and precision for the results [7].

False reporting patient results are a known issues in the laboratory and point-of-care area and often the results of healthy patients are shifting from the normal patient ranges to pathological ranges due to operation errors.

In order to prevent those errors in the blood gas domain, an automated blood-sampling device mixer must be implemented. The mixing procedure is done by the operator before analyzing the sample, but this requirement sometimes lacks.

It will be presented an automated mixing system that helps the operator to ensure proper accuracy and precision of the results and also to save time with the mixing process because it will be done automatically.

The only existing automated mixer available on the market is the one that mixes the blood sample inclined in one position in a magnetic field that is applied to a miniature golden ball that is situated in the sample syringe. The novelty of the three way mixer is that it can be used for different type of syringes and also for capillary tubes, where the coagulation may occur faster.

Mixing the sample on three ways will ensure that all the particles inside the blood will be disposed homogeneous and no sedimentation or particle concentration will occur at the edge of the blood-sampling device. When the blood will travel the sensor path, the same homogeneous sample will be analyzed by the specific analyte sensor. The same situation is for the hemoglobin, which is more sensitive because of its optical measurement. A non-mixed sample will lead to erythrocyte sedimentation immediately after the sample collection and absorbance modification will occur.

The costs for the blood-sampling devices will be reduced because this mixer is compatible with all types of blood gas syringes and additionally, can be used also capillary tubes.

The experimental setting is composed of three motors, one servo and two stepper motors that will act simultaneously when the blood-sampling device is inserted. The device can be either syringe or capillary tube because the port where is inserted is flexible, being made of silicone rubber in the interior and plastic on the exterior. This fixation port is linked to the roller motor, which is responsible for the rotation of the blood-sampling device on its own axis.

To trigger the mixing process, a reflective optical sensor is located on the common rod with the roller motor. When an object is detected, the mixing process will start in 5 s. This way it will ensure that the operator will have enough time to fix the device in the port.

The common rod is linked to the servo motor for the pitch movement, which will have a constant left-right rotation of 270°, that will allow for the blood-sampling device to flip to the left and to the right in the same time as it spins on its own axis.

The servo motor is connected to the third stepper motor on a slider with screw and nut that will move forward and backward the whole mixer assembly. The forward-backward movement is controller by a flag that will slide between the two optical sensor F and R. Those two sensors have the role to detect the end of the forward-backward sliding process in order to change the rotation sense of the screw.

After 12 s, the mixing process is finished and the user can take the blood-sampling device.

The three way movement will ensure that the sample is homogeneous and the results will be more accurate and precise. It must be mentioned that for the blood gas analysis, the sample must be analyzed within 10 min because air will influence the arterial gases and will modify the sample's pH (Fig. 4).

There are some blood gas analyzers which have automated scheduled calibrations that will take from 3 to 6 min to finish. If the operator has already collected the blood in the device, he can put it in the mixer during the calibration. If the sample is not removed in 30 s after the mixing process is finished, the loop will start again in order to prevent erythrocyte sedimentation and clotting.

The three way mixer is designed to be standalone, having no connectivity to the blood gas analyzer because this may influence its performance since are measured μA and μV

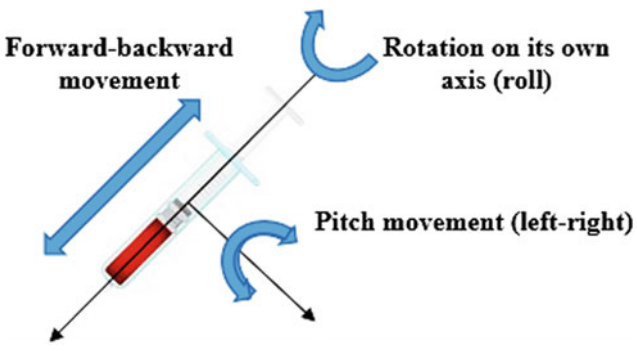

Fig. 4 The three way movement of the blood-sampling device during the mixing process

from the blood sample. Any unauthorized extension that is made to the instrument is forbidden.

The samples were analyzed on an Opti CCA-TS2 blood gas analyzer. They were collected by authorized medical personnel and no patient names or other confidential data was collected in order to respect the privacy. The scope of this project was to evaluate the performance of the prototype of the three way automated mixer (Figs. 5 and 6).

For this experiment, samples were collected from three different patients. One of them was intubated, having a FiO_2 of 70%. The sample collection was done by authorized medical personnel and the testing procedure was done in accordance with the ethical standards. Inform consent was obtained from the three participants where the samples were collected from.

Three samples from every patient were collected at a 5 min interval one from the other. The collected and unmixed samples were analyzed first and immediately after aspiration, they were put in the mixer. After the non-mixed (NM) sample was analyzed, the automated mixed sample (AM) was submitted for analysis.

The second sample from the same patient was collected and analyzed in the same manner in order not to let the clinical condition to modify and to maintain the same analysis conditions after each rerun. Similar, the third

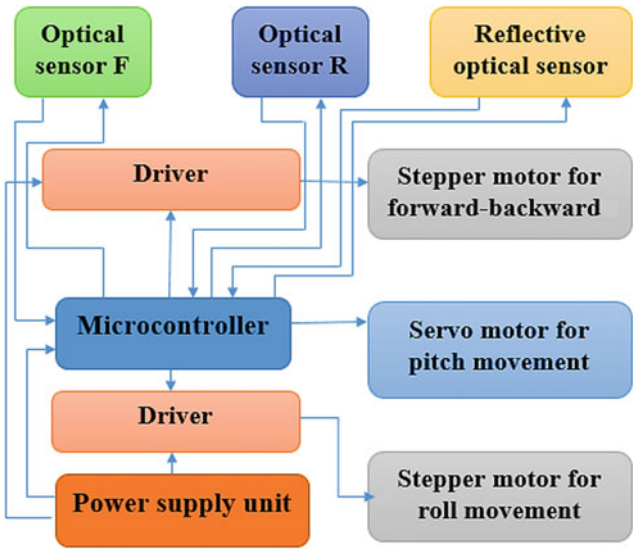

Fig. 5 The block schematic of the three way automated blood-sampling device mixer

Fig. 6 The main menu of the blood gas analyzer (left) and a patient result (right)

sample was analyzed and were calculated the standard deviation and the variation coefficient for every parameter to observe the results' repeatability. As lower the SD and the CV are, the closer the results are one to each other and the more precise and accurate the system is [7].

All the collected blood samples were arterial because only for the arterial samples a normal patient reference interval can be established.

The arterial blood is oxygenated and comes directly from the alveoli, where the gas exchange process takes place. The lungs exchange the venous non-oxygenated blood with oxygenated blood through the alveoli. The oxygenated blood is pumped by the heart in the whole body to provide the tissues and the organs oxygen from the arterial blood. After the tissue respiration takes place, the venous blood is transported to the lungs. Since deoxygenation process varies from person to person depending on several factors, the normal patient ranges were established only for arterial blood.

The experimental results are listed in Table 1.

To have a better interpretation of the experimental results and to certify the performance of the automated blood-sampling mixing system, the results for sample 001 were plotted for every parameter, with two curves representing the results of the assay with no mix and the results with the automated mix.

In the same manner, the plots for the other samples can be done, but it can be stated that from the results, the standard deviation and the coefficient of variation are lower for the automated mixed samples (Fig. 7).

Table 1 Experimental results

Sample ID	Run	pH	pCO_2 (mmHg)	HCO_3^- (mmol/L)	tHb (g/dL)
001	1—NM	7.385	41.8	24.2	15.8
001	2—NM	7.432	40.4	26.0	15.1
001	3—NM	7.310	42.7	20.8	16.3
SD		0.062	1.159	2.665	0.603
CV (%)		0.83	2.78	11.27	3.83
001	1—AM	7.405	42.0	25.4	15.6
001	2—AM	7.411	41.7	25.6	15.8
001	3—AM	7.398	42.9	25.6	15.8
SD		0.007	0.624	0.089	0.115
CV (%)		0.09	1.48	0.35	0.73
002	1—NM	7.464	37.4	25.9	11.2
002	2—NM	7.521	36.1	28.6	10.9
002	3—NM	7.422	38.2	24.1	11.4
SD		0.050	1.060	2.258	0.252
CV (%)		0.67	2.85	8.63	2.25
002	1—AM	7.455	36.3	24.7	11.3
002	2—AM	7.407	35.7	21.7	10.9
002	3—AM	7.413	35.4	21.8	11.3
SD		0.026	0.458	1.668	0.231
CV (%)		0.35	1.28	7.34	2.07
003	1—NM	7.253	43.2	18.4	12.4
003	2—NM	7.338	41.5	21.5	12.3
003	3—NM	7.289	42.4	19.7	12.8
SD		0.043	0.850	1.563	0.265
CV (%)		0.58	2.01	7.86	2.12
003	1—AM	7.311	44.0	21.5	12.4
003	2—AM	7.373	43.6	24.5	12.6
003	3—AM	7.357	43.8	23.7	12.3
SD		0.032	0.200	1.595	0.153
CV (%)		0.44	0.46	6.86	1.23

5 Conclusions

The arterial blood gas analysis in one of the most important assay that is performed in case of an emergency or to monitor the evolution of the clinical health of a treated patient.

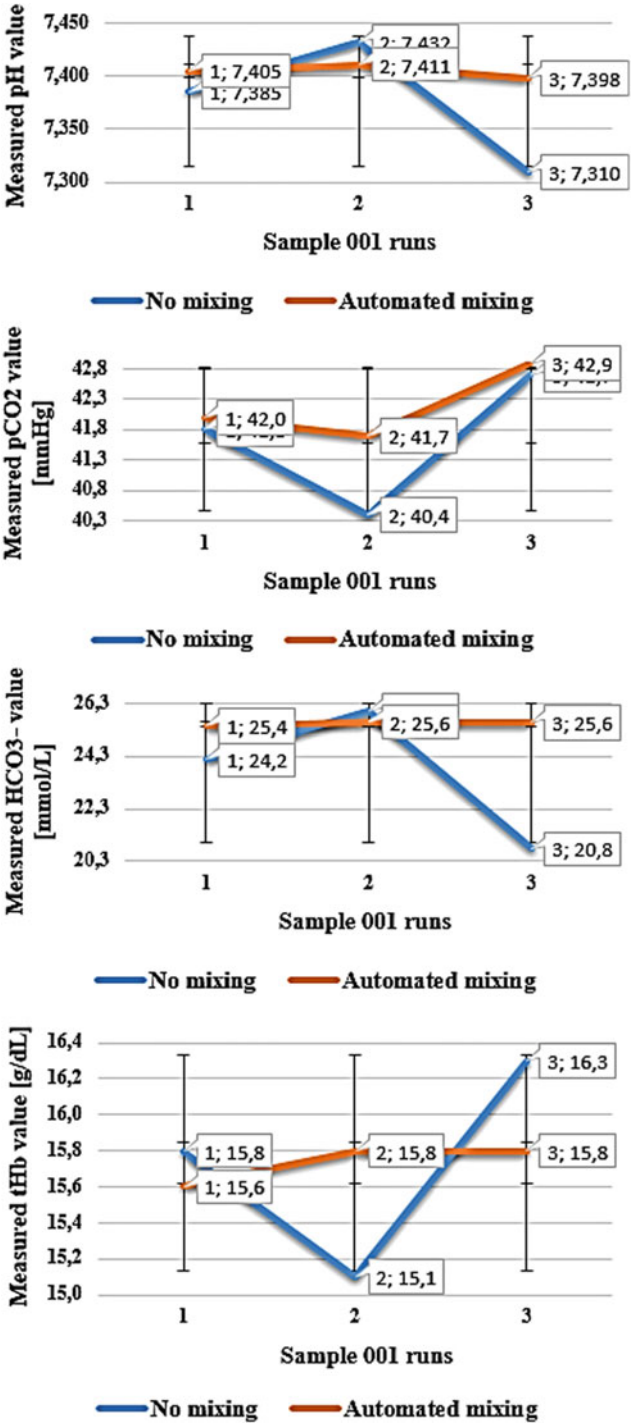

Fig. 7 The variation plots for the results with no mixing of the blood sample compared with the automated mixing process

The results obtained after the arterial blood sample analysis is performed can contain a quick information about the clinical state of the patient only by observing the relationship between pH, HCO_3^- and pCO_2.

The sample results can be influenced by the preanalytical procedure. Before analysis, the sample must be mixed in order to ensure the homogeneity.

The automated three way mixer eliminated the probability of appearing operating errors during a blood gas assay. It saves time and it ensures the precision and accuracy of the results, increasing the quality of the medical act.

Conflict of Interest The author declares that he has no conflict of interest.

References

1. National Committee for Clinical Laboratory Standards: Blood gas and pH analysis and related measurements, C46-A, Vol. 21, pp 22 (2001)
2. Emancipator, K.: Critical values: ASCP practice parameter. Am. J. Clin. Pathol. **108**, 247–251 (1997)
3. Biale, J.B.: Laboratory medicine hematology, St. Louis, CV Mosby, p. 18 (1982)
4. Levinsky NG (1994) Acidosis and alkalosis, Harrison's principles of internal medicine, pp. 260–262. New York
5. Kirchhoff, J.R., Lunte, C.E., Heineman, W.R., Kaplna, L.A.: Electrochemistry: principles and measurements, 2nd edn, pp. 213–217. CV Mosby, St. Louis (1989)
6. Benesch RE, Yung S (1973) Equations for the spectrophotometric analysis of hemoglobin mixtures, pp. 245–248
7. Niculescu MS (2017) Optical method for improving the accuracy of biochemical assays. In: The 6th IEEE International Conference on E-Health and Bioengineering, Sinaia, pp. 1–2

Techniques for Sorting Components from Dismembered Medical PCBs

R. Holonec, L. Grindei, M. Purcar, R. Copîndean, and F. Dragan

Abstract

A printed circuit board, or PCB, is a piece of hardware that acts as a base and provide electrical connections to the mounted components. PCBs are present in almost all types of electronic waste including cell phones, computers, printers, and medical devices. Waste of electrical and electronic equipment (WEEE) is one the fastest growing waste streams in the EU and is expected to grow to more than 12 million tons by 2020 [1]. The waste PCBs contain metals and major hazardous components and this make them the most difficult parts of WEEE to be recycled. Waste PCBs recycling is a preoccupation not only to their rich content, but also due to their potential risk for environment and human health. E-waste causes damage the nervous system, circulatory system, kidneys, lungs or skin [2]. The paper aims to develop a smart sorting system for components resulted from dismembered medical PCBs. The proposed application is based on image processing and it was tested at a laboratory scale. The application can be included in a complex e-waste sorting system.

Keywords

Printed circuit board (PCB) • E-waste • Recycling • Intelligent sorting system

1 Introduction

Printed circuit boards (PCBs) have become extremely important in the medical field. In recent years, technology has experienced an explosive development in the medical field ranging from medical diagnosis, treatment to medical research. This involves computerization and consequently the use of reliable, high-performance and high quality medical PCBs. These requirements have led to a continuous process of renewal of medical equipment and to the early renunciation of so-called "old" equipment. The consequence of this process is the accumulation of a large amount of electronic waste or "Waste Electrical and Electronic Equipment" (WEEE).

Regarding the WEEE management, two main aims of it can be specified. [3]. The first one is referring to the rational and conservative usage of natural resources by recovery of the materials and energy included in waste and the second one concerns the protection of natural environment by reducing the quantity of unsorted waste.

The medical PCBs, and so the resulting e-waste can be found in a large variety of devices and applications like: pacemakers, defibrillators, heart monitors, electrocardiogram (ECG) equipment, magnetic resonance imaging (MRI) or computer tomography (CT) scanners, ultrasonic equipment, body temperature monitors, blood glucose monitors, electrical muscle stimulation equipment but also computers and their peripherals, computer monitors, telephones, wireless devices, televisions, printers so on [2]. As a remark, medical devices often do not have typical standards of PCBs shape and size. The reason is that medical printed circuit boards must fit into as small of an area as possible while still remaining resistant to damage.

Recycling e-waste is now a priority for humanity. The state of the art in PCB recycling depends on the quality of the board, which is defined by the consistency of noble metals and the number of recyclable components. For instance, researchers indicate that the PCB from active implantable medical devices, like pacemakers or implantable cardioverter defibrillators, present quantities of gold, superiors of PCB of other electronic devices [4]. It has been demonstrated that these implantable medical devices have the conditions to be valorized, since they were disinfected after their explantation.

R. Holonec (✉) · L. Grindei · M. Purcar · R. Copîndean · F. Dragan
Electrical Engineering Faculty, Technical University, Cluj-Napoca, Romania
e-mail: rodica.holonec@ethm.utcluj.ro

S. Vlad and N. M. Roman (eds.), *6th International Conference on Advancements of Medicine and Health Care through Technology; 17–20 October 2018, Cluj-Napoca, Romania*, IFMBE Proceedings 71,
https://doi.org/10.1007/978-981-13-6207-1_10

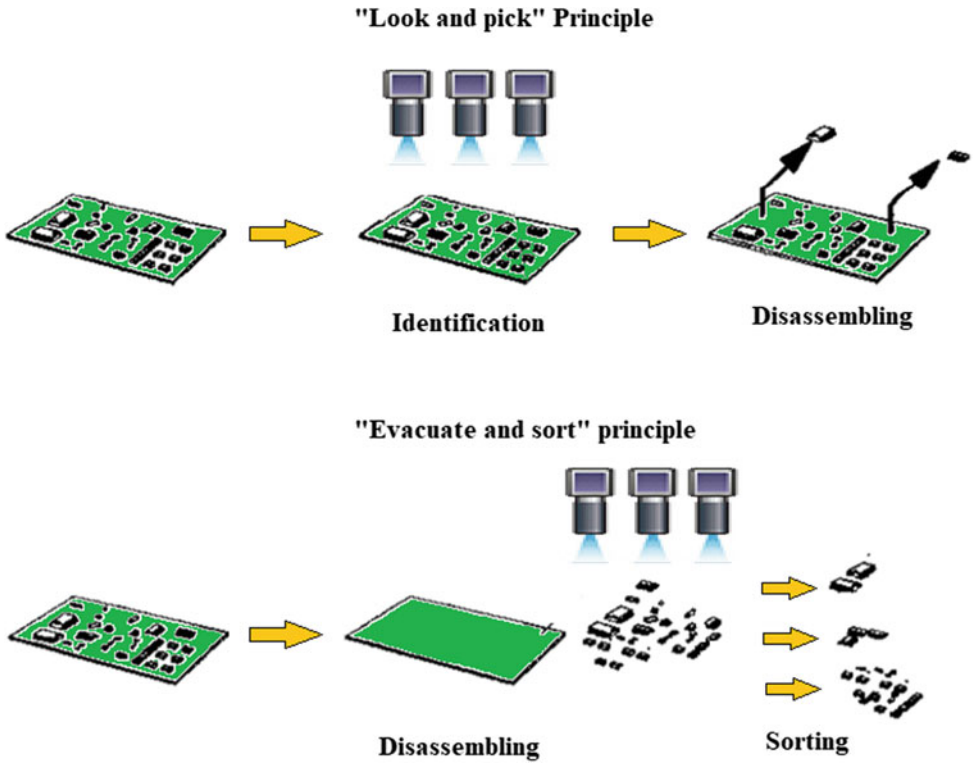

Fig. 1 Disassembly principles

In the e-waste recycling perspective [5], the separation or sorting process is of great importance. There are many sorting methods but those of based on dissembling have the advantage of hazardous components (polychlorinated byphenyls, mercury) isolation. In PCBs recycling systems there are used selective disassembly based on "look and pick" principle and simultaneous disassembly based on "evacuate and sort" principle like in Fig. 1 [6, 7].

Regarding the second method, the PCB components can be sort using intelligent systems based on specific sensors and computerized visual inspection. Thus, systems use real-time "machine vision" principles combined with artificial intelligence. The purpose of smart sorting is to preserve the shape and structure of the PCBs components, without crushing them, for the easy and economical separation and recycling of secondary waste [8].

Applying the proposed technologies would result in a high rate of recovery of the various materials (gold, silver, copper, aluminum, tin, platinum, palladium, gallium, tantalum, tellurium, germanium, selenium, iron, glass, plastic) contained in electronic waste.

2 Sorting Criteria and System Principle

The printed circuit boards in general, and the medical types in particular, consist of three basic parts: the non-conducting substrate or laminate, the conductive circuits printed on or inside the substrate and mounted components. The components mounted on PCBs generally include transistors, chips, connectors, capacitors, etc. each of them having different material composition [9, 10]. The waste resulted from dismembering of printed circuit boards can be classified as in Table 1.

Presuming a PCB recycling process, where the disassembly stage has already been completed, the next stage that of separation is very important. There are various sorting methods for the PCB scraps like those based on size, material properties (density, magnetic characteristics, conductivity) color, shape etc. The separating process can be made in steps according to the flowchart illustrated in Fig. 2.

Regarding the large size components, a smart separation that is based on their image recognition can be made by using a machine vision system (Fig. 3). The most of sorting machine vision systems are made on belt conveyors and they include a lighting system, an image acquisition system, a PC platform, an inspection software and a process controller [11, 12]. The software in such systems is often a multifunctional one, so that it fulfils functions such as image processing, calibration, conveyor belt control, robotic arm guiding, object presence checking, object counting, and more.

In the classification process, a characteristic vector will comprise the extracted features of the input image. Extracting features reduces the amount of information in the image by measuring certain properties that fit these images into

Table 1 Waste resulting from dismantling printed circuit boards

Components types	Components aspect	Components types	Components aspect
Capacitors	 9	Plastic components	
Radiators	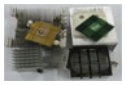	Screws	
Chips and SMD microchips	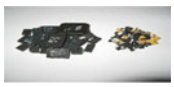	Batteries	
Magnetic components		Undissolved components	 124.29 124.29
Dismantled PCBs		Transistors	

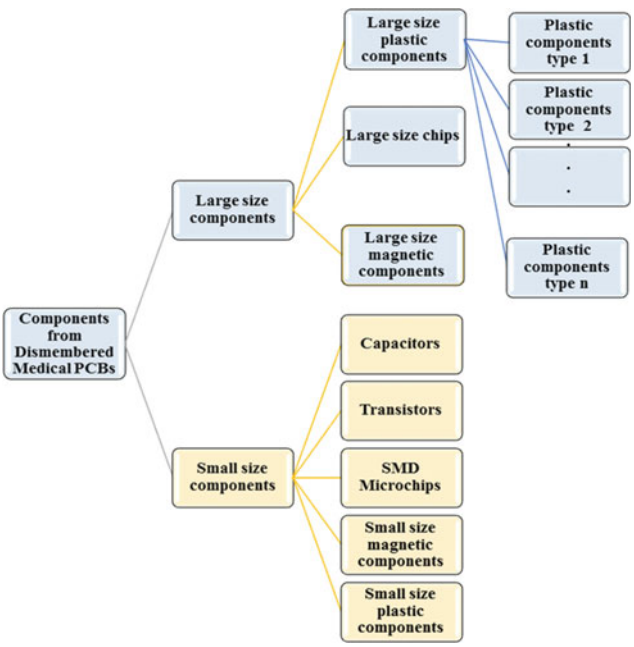

Fig. 2 Sorting criteria for PCBs components

different classes. For sorting applications, it is necessary to select as efficiently as possible the characteristics that preserve class separation. A form descriptor is a characteristic vector based on the analysis of particle measurements. Each type of descriptor contains one or more form measurements from a sample.

3 System Implementation

An experimental smart sorting system, for large size PCBs disassembled components from a typical PCB computer motherboard, was implemented (Fig. 4). The system is a low cost one and its principles can be used in a complex material recycling process that uses components resulted from dismembered PCBs.

The PCB components come one by one on the conveyor belts, first on the black conveyor belt (1) and then on white conveyor belt (9). The two servomotors that controls the conveyors are controlled by MID 7604 controller (2) from National Instruments. Images are acquired by three

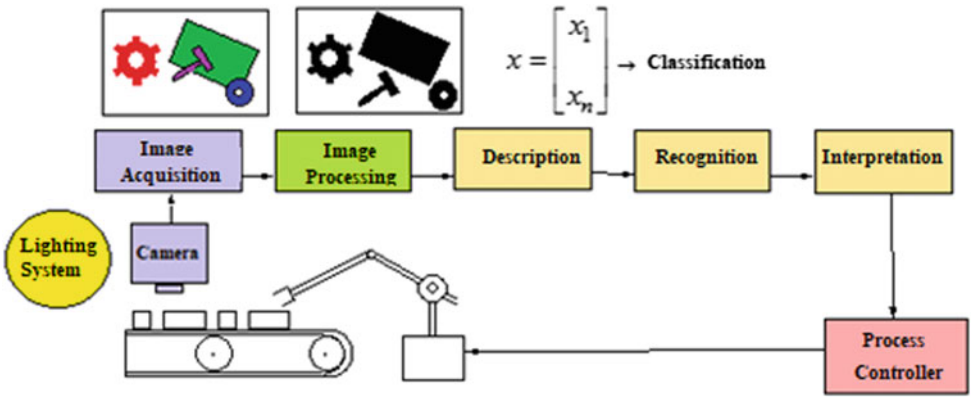

Fig. 3 Sorting machine vision system

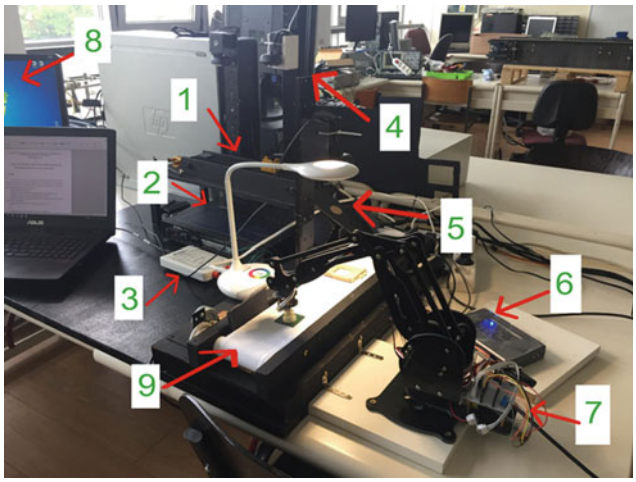

Fig. 4 The smart sorting system

Microsoft LifeCam HD-3000 web cameras (4). The components are classified and sorted. For the class of large size chips the sorting process is made by using a robotic arm (7). These objects will be placed in a separate container.

The software system components use the LabVIEW programming environment from National Instruments, along with NI Vision Development Module, LabVIEW Motion Control Tools and LabVIEW for MyRIO board [13].

The application runs on two computers (8), the first one is used for the conveyors control and for objects classification, and the second one for controlling the robotic arm through the MyRIO device (6). For sensing the presence of metallic composition or metallic inclusions in the plastic components, a proximity sensor (5) and a MyDAQ board (3) were used. The block diagram in Fig. 5 shows the interaction mode between the hardware components.

3.1 Conveyor Belt System

The mechanical part of the proposed system consists of two conveyor belts that are designed to carry the sorted components from one strip to another (Fig. 6). The conveyor belts are driven by two stepper motors and they are disposed at a level difference from one another to facilitate the passage of the components. The passage of the objects between the two conveyers is made on a smooth surface on which a proximity sensor has been placed to notify the presence of the metal elements in the sorted objects. The significant difference between these two conveyor belts is their size and material color (black and white). This is justified by the color of the PCBs components. Because the image acquisition is made with a CCD camera, the lighter (colored) objects have images with high contrast on black surfaces and the dark ones have high contrast on white surfaces.

3.2 Sorting Algorithm

The front panel of the LabVIEW application contains information about the steps taken in the classification process (Fig. 7).

The application is made in a "State Machine" architecture and it contains the following states:

Image acquisition from camera 1 (camera 1, Default).

The first web camera senses the presence of an object on the strip and resets the state of the proximity sensor (False). If the object is present, the sorting process starts.

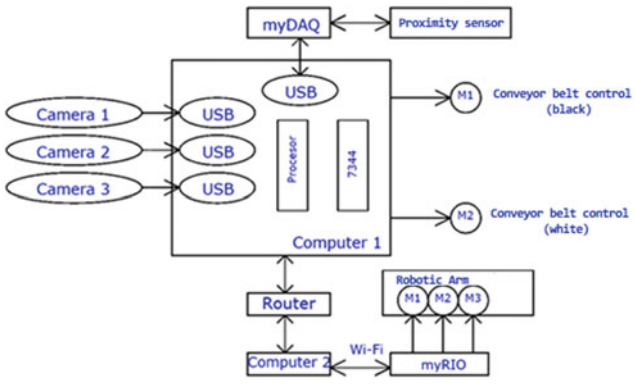

Fig. 5 Sorting system hardware configuration

Fig. 6 The conveyor belt 1(black surface)

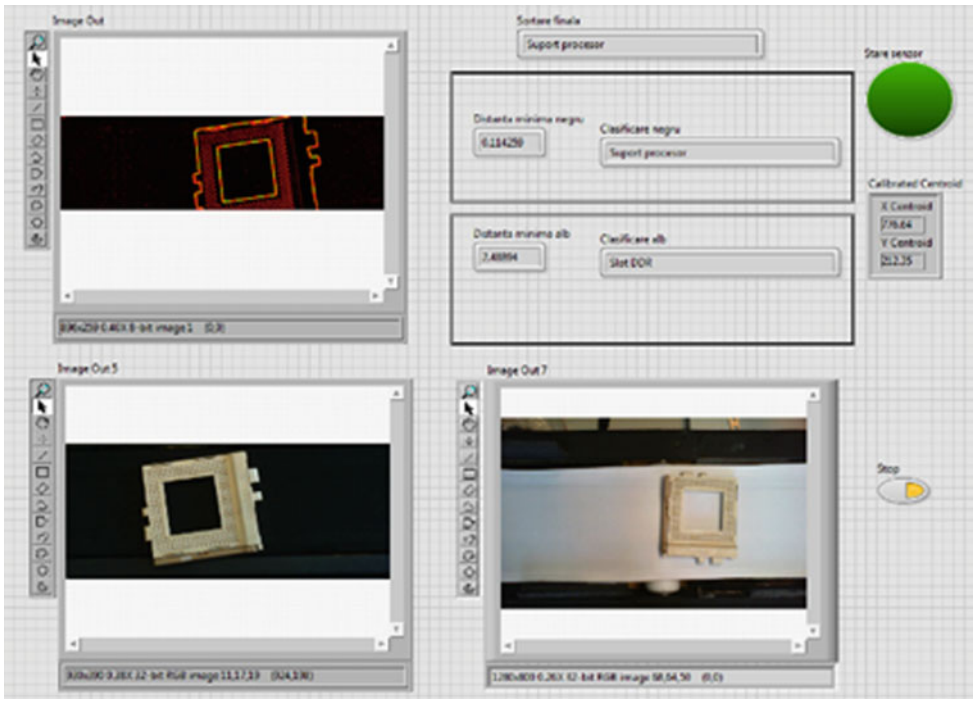

Fig. 7 Sorting LabVIEW application-front panel

Image acquisition from camera 2 (camera 2,).

The first conveyor belt (black) is moving until the object is right under camera 2. This moment is detected using the next image processing by extracting the color plan (green), applying a mask and drawing interest area (ROI), filtering with a Gaussian smoothing filter, applying a Sobel filter (Edge Detection) and respectively by applying a Edge Detector edge detector. These steps were established using the NI Vision Assistant.

Image acquisition from camera 2 and object classification on the black conveyor belt.

The image of the object is acquired with a minimal level of brightness (30) and then processed by application of a mask, a value plane extraction and finally a "Particle Classification" algorithm.

A "Particle Classifier" file has been created for the object having light colors. Each time in the classification process a training based on the images of objects taken in different positions was made. The final information refers to the object class and the minimum distance to this class. After classification, the conveyor will start again by passing the over the proximity sensor.

Image acquisition from camera 2 and object classification on the white conveyor belt.

In this step by applying a centroid operator on the pre-processed image, the coordinates x, y of the object center is obtained. Then a new object classification on the white conveyor belt is made. The algorithms are similar to the object classification on the black conveyor belt, but with a different "Particle Classifier" file.

Sorting objects on the conveyor belt.

The stepper motor will move the object in the sorting area. Here, based on the classification results and on minimum distances, the class of the objects are decided. According to that the components will get out of the conveyor belt in the proper container. For the large size chips the robotic arm will place the component in a separate container (Fig. 8).

Resuming sorting steps.

The sorting system can work continuously with the restriction that the feeding of the objects on the strip is at the rate required by all the above steps.

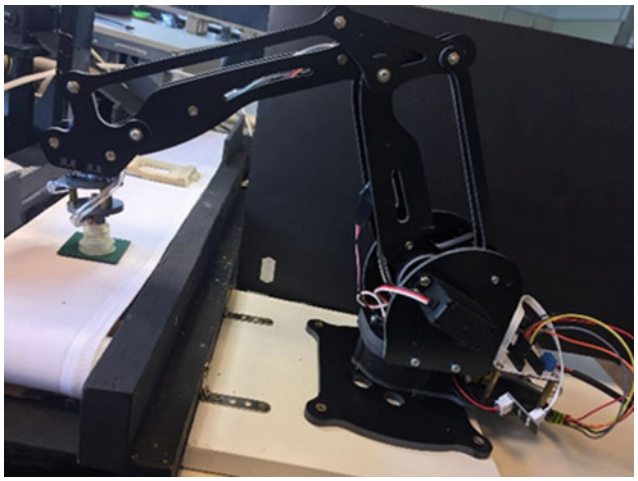

Fig. 8 Sorting robotic arm

The system was tested for different dismantled components resulted from the PCB. They were sorted into the following classes: power supply connectors, IDE cable connectors, analog audio connectors, processor sockets, VGA connectors, PCI connectors, LPT/RS232 connectors, LPT socket supports, integrated chipsets, integrated circuits, DIN power connectors/battery supports, DDR slots, ISA slots and IC sockets.

4 Conclusions

Regarding waste electrical and electronic equipment (WEEE), large quantities of waste printed circuit boards (PCBs) are released into environment [5]. E-waste recycling consists of three main steps: collection, pre-processing and end-processing [14]. Each step is critical for the recovery of metals and recycling economy. In the pre-processing stage, the component sorting of dismembered PCBs can be made in an intelligent way in order to reduce at minimum the mechanical processing (crashing) of the e-waste scrap.

In the proposed intelligent sorting application, large size components, commonly met on a PCB motherboard, are transported on two strips, one black for the classification of the light objects and the other for the classification of the dark ones. The system ensures the visualization and classification of the components and the presence of the metal in their composition. Objects are classified according to their shape and dimension in several categories.

The proposed algorithms have the advantage of being efficient and relatively easy to implement which makes it possible to use them on a waste medical PCBs sorting specific system. In this case, a careful knowledge about components regarding their dimensions, shapes or materials is needed. Thus the classifier will be adapted to the specific application.

Acknowledgements This work was supported by a grant of the Romanian Ministry of Research and Innovation, CCCDI-UEFISCDI, project number PN-III-P1-1.2-PCCDI-2017-0652/84PCCDI/2018, within PNCDI III

Conflict of Interest The authors declare that they have no conflict of interest.

References

1. Akkucuk, U.: Handbook of Research on Waste Management Techniques for Sustainability, 1 edn. IGI Global (2015)
2. Shantaram, M., Shafy, S., Fatimah, R.: A concern of e-waste in the hospital setting and its ways of disposal. Int. J. Appl. Biol. Pharm. Technol. **5**(2) (2014)
3. Matkowski, P., Friedel, K.: Management of waste electrical and electronic equipment in Poland—ecological, organizing and economical aspects. In: 2008 International Students and Young Scientists Workshop—Photonics and Microsystems, Wroclaw, Poland, 20–22 June 2008
4. Guimarães, R., Carvalho, J., Leal, V., Guerner Dias, A.J.: Characterization, treatment proposal and metal recovery in waste of active implantable medical devices. Comunicações Geológicas **101**, Especial II, 1011–1014 (2014)
5. Zeng, X., Zheng, L., Xie, H., Lu, B., Xia, K., Chao, K., Li, W., Yang, J., Lin, S., Li, J.: Current status and future perspective of waste printed circuit boards recycling. In: The Seventh International Conference on Waste Management and Technology. Procedia Environ. Sci. **16**, 590–597 (2012)
6. Feldmann, K., Scheller, H.: The printed circuit board—a challenge for automated disassembly and for the design of recyclable interconnect devices. In: International Conference on Clean Electronics Products and Technology, Edinburgh (1995)
7. Feldmann, K., Scheller, H.: Partially automated conceptions for separation of used electronic devices. In: VDIWDE-Gesellschaft Mikro- und Feinwerktechnik, Seminar 'Praxis of electronic scrap recycling'. Duisburg (1993)
8. Dorneanu, S.A.: Electrochemical recycling of waste printed circuit boards in bromide media. Part I: preliminary leaching and dismantling tests. Studia UBB Chemia, LXII 3, 177–186 (2017)
9. Li, J., Shrivastava, P., Gao, Z., Zhang, H.-C.: Printed circuit board recycling: a state-of-the-art survey. IEEE Trans. Electron. Packing Manufac. **27**(1) (2004)
10. Kopacek, B.: Intelligent disassembly of components from printed circuit boards to enable re-use and more efficient recovery of critical metals. In: Electronics Goes Green 2016+, Berlin, 7–9 September (2016)
11. Cojocaru, D.: Aplicaţii industriale ale vederii artificiale. Scientific Seminar of Computer Engineering Dept., Automation, Computer and Electronics Faculty, ELSE Software, pp 141–156, nr. 7-8, Craiova, Romania (1996)
12. Borang, T.: s.a.,—Vedere artificiala in robotica, Editura Universitatea Tehinca Bucureşti, Bucureşti (1993)
13. Kwon, K.-S.: Steven Read, „Practical Guide to Machine Vision Software—An Introduction with LabVIEW, Wiley"-VCH (2014)
14. Meskers, C.E.M., Hagelüken, C., Salhofer, S., Spitzbart, M.: Impact of pre-processing routes on precious metal recovery from PCs. In: Proceedings of the European Metallurgical Conference (EMC), Innsbruck, Austria, 28 June–1 July 2009

Intelligent Medical Distance Assistance Device

Robert Fuior, Andrei Gheorghiță, and Călin Corciovă

Abstract

The objective of this project is to realize and implement a complex system for remote monitoring of vital functions. The IOT-based health care system for the elderly is the cheapest medical device based on the IOT platform for patients and physicians. It provides a solution for measuring body parameters such as ECG, temperature, humidity and pulse. It also detects the location of patients to be sent to a doctor and in case of emergency it is possible to automatically call the emergency number accompanied by the GPS data.

Keywords

Microcontroller • ECG • Temperature • Humidity • Pulse • GPS • GSM • IOT

1 Introduction

According to the latest research it has been found that about 2,000 people die on a monthly basis due to neglect of health. This is due to time constraint and ignorance of health through the increased volume of daily activity.

The objective of this work was to realize and implement a complex system of remote monitoring of vital functions.

As technology is in continuous development, portable medical devices have a great contribution to regular monitoring and checking of health, which is recommended to be done monthly or quarterly for people with chronic pathologies. It is also obvious that the evolution of technology improves the quality of life. The current project wants to provide healthcare over the internet, providing vital cell information on the mobile phone and recording their history. The advantage of this project is that it can be used independently of user technical education and makes it easier to monitor health than available systems. Android apps allow a person to access the information directly on their mobile phone in various contexts, making it easy to handle [1].

The IOT-based health care system for the elderly is the cheapest medical device based on the IOT platform for patients and physicians. Provides a solution for measuring body parameters such as ECG, temperature, humidity and pulse. It also detects the condition of the body and the location of the patients.

The mobile application for the patient and physicians contains a very simple graphical interface for reading all parameters in the mobile phone or anywhere in the world by using Internet connectivity and in case of emergency it can automatically be called emergency number 112 accompanied by patient's GPS coordinates and of his state at that time.

2 Materials and Method

The proposed system is a real-time vital parameter monitor designed to alert/alert deviations from the physiological values of the patient. It also detects the condition of the body and the location of the patients. The mobile application for patients and physicians contains a very simple graphical interface for reading all the parameters in the mobile phone or anywhere in the world by using the internet connectivity made through the GSM module. The basic components of the system are: Arduino Mega control unit, which takes the signals from the ECG module, pulse, temperature, humidity, light, SD module, GSM module, GPS module and Bluetooth module, the display (Fig. 1).

The ATmega2560 microcontroller on the Arduino Mega design plate has a 5 V operating voltage, but with a voltage stabilizer it can power up to 12 V. It has 54 input and output

R. Fuior (✉) · A. Gheorghiță · C. Corciovă
University of Medicine and Pharmacy "Grigore T. Popa", Str. Universității nr. 16, Iasi, Romania
e-mail: fuior.robert@gmail.com

A. Gheorghiță
Politehnica University of Bucharest, Bucharest, Romania

S. Vlad and N. M. Roman (eds.), *6th International Conference on Advancements of Medicine and Health Care through Technology; 17–20 October 2018, Cluj-Napoca, Romania*, IFMBE Proceedings 71,
https://doi.org/10.1007/978-981-13-6207-1_11

Fig. 1 Device block diagram

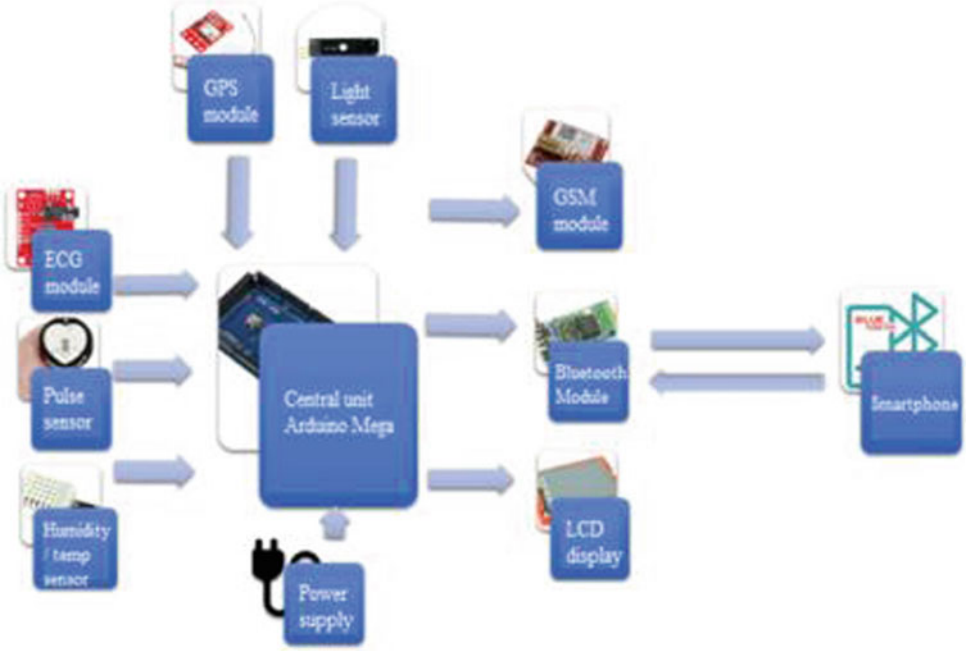

pins (external connections), 15 pins of PWM (Pulse-Width Modulation), which we can buy/transfer, but also 16 analog pins. It also has 4 UART pins that are generally used to display information on the display. The flash memory is 256 KB, of which 8 KB occupy the bootloader with a 16 MHz operating frequency (Fig. 2) [2].

The ECG signal acquisition and amplification part is made by SparkFun's AD8232. It functions as an operational amplifier that measures the electrical activity of the heart and produces an analog signal at the output. It also contains filters for smoothing and attenuating noise that may appear during the measure. AD8232 is designed to extract and amplify low-value biopotentors [3, 4].

AD8232 I used pins: LO+, LO−, OUTPUT, 3.3 V and GND, the SDN pin will be used to further optimize the device. The exits to the electrodes will be through the ports RL, LA, RA. In the right hand the electrode will be connected to the RA port, the electrode at the LA port is connected to the left hand, and at the RA the left electrode's electrode (Fig. 3).

In the next step I made the application displaying the ECG signal through MIT App Inventor 2. App Inventor 2 is an open source and cloud-based software, which means it works directly on the browser. We chose this program because it is free and easy to learn, being very intuitive. This makes it easier for the patient to monitor and view the history at any time (Fig. 4).

The XD-58C pulse sensor, a plug-and-play sensor, is designed to work with a development board equipped with at least one analogue pin. This product is useful for collecting heartbeat data in different situations, such as during exercise because it is powered at a 3.3 V low-power voltage. Receiving the signal from the sensor will connect to port A0

Fig. 2 Arduino Mega 2560

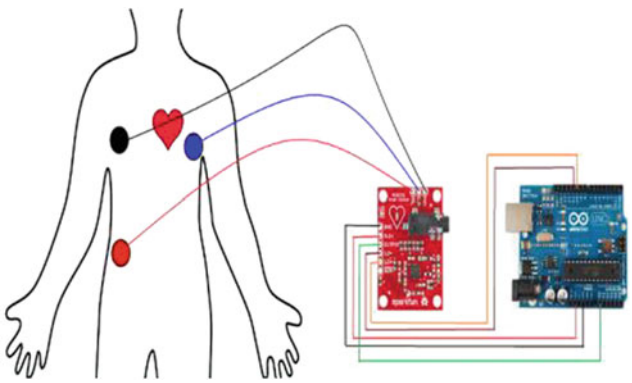

Fig. 3 Operational amplifier AD8232

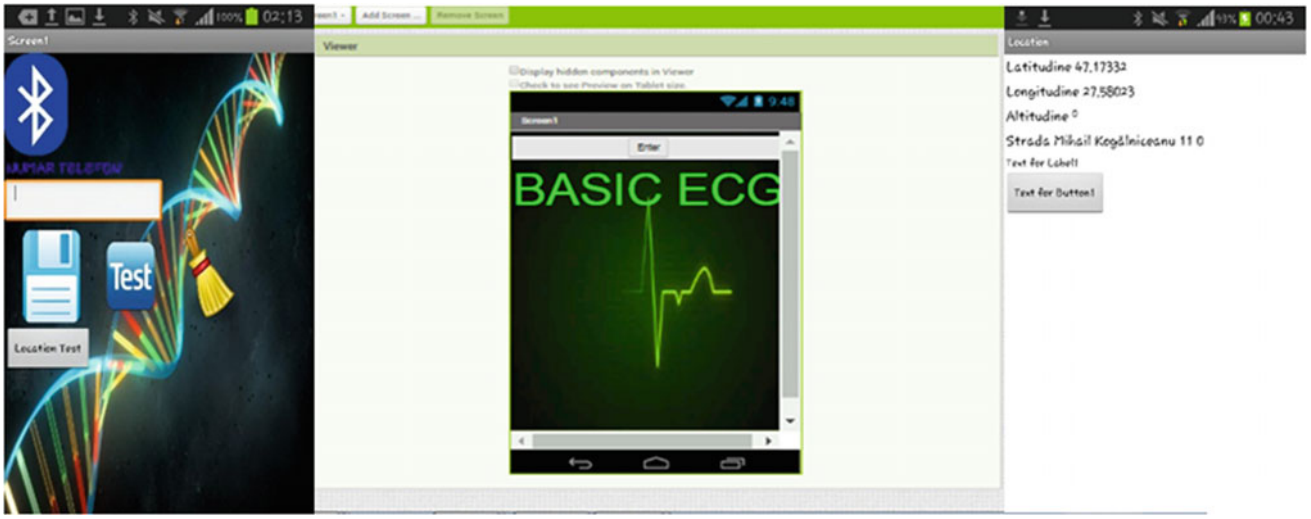

Fig. 4 MIT App Invertor 2

Fig. 5 The pulse sensor XD-58C

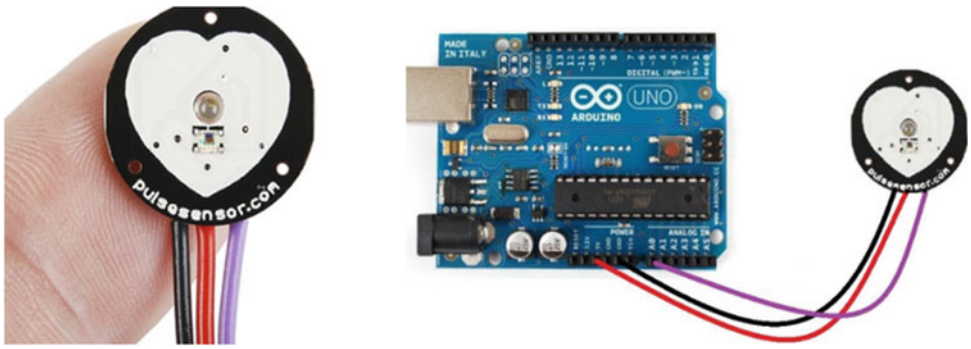

of the Arduino development platform. At the same time, it can also be placed on the ear lobe or on the finger without damaging the patient's activity. Pulse monitoring is done in real time (Fig. 5).

The DHT22 sensor is a small, inexpensive and handy humidity and temperature sensor. Use a capacitive moisture sensor and a thermistor to measure ambient air and body surface. It can be placed in the upper limbs, but also in the heart area. It provides a digital signal on the D2 data pin (no analogue pin is needed). It is easy to use, but it takes care of reading the data, but also interpreting it because it returns two types of values read by the sensor, namely temperature and moisture from the body [2] (Fig. 6).

The Master Slave HC-05 Bluetooth Module with a 5 V supply voltage and a 30 mA consumption and to make a connection between the device and a smartphone. It has 4 control pins out of which 2 are power supply and 2 communication. Communication with the Arduino development platform is a serial UART based on the SDA and SCL ports. It has a 10-m range and automatic reconnection. For the display itself, an application was developed in MIT App Inventor 2 [3] (Fig. 7).

Fig. 6 Humidity and temperature sensor DHT22

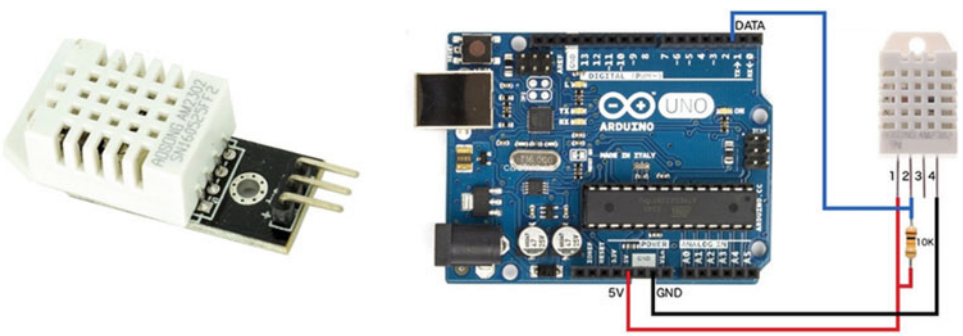

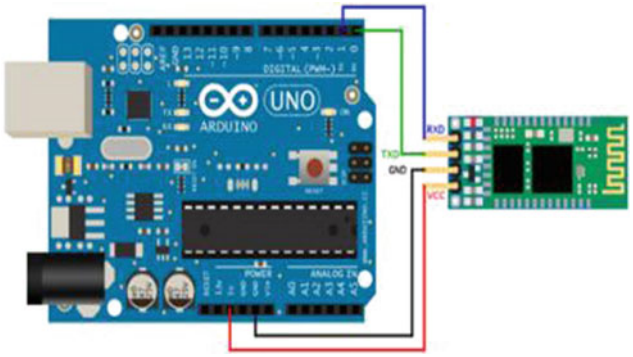

Fig. 7 Bluetooth module HC-05

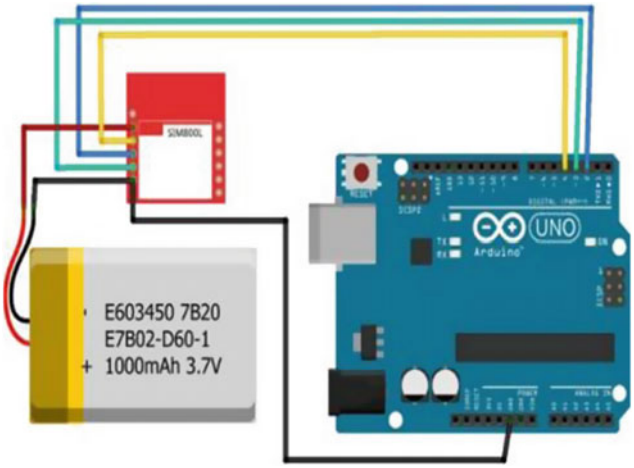

Fig. 9 The GSM module and connection configuration

The GPS module used uses radio waves and satellite navigation to determine the position. It emits satellite signals. The position (latitude, longitude, altitude) is calculated by knowing the position of at least four satellites receiving the GPS signal at different times. Normally, three satellites are sufficient to determine the three coordinates (space position), and the fourth satellite is used to minimize errors. It communicates via serial transmission of RX and TX ports from the microcontroller, and feeds at a voltage of 5 V [5, 6] (Fig. 8).

The SIM800L GSM module is powered at a voltage of 3.4–4.4 V and communicates with the Arduino development platform via the serial UART interface. It has the role of having a continuous internet connection of the entire device via the 3G or 4G network, but also sending an emergency message to the emergency service. In the urgent message there is information about the patient's condition and the location provided by the GPS module.

The connection of the mode is as follows: The VCC pin on the module can be connected to 3.3 V on Arduino either on an external battery and on the GND at the table. The RST port will be linked to D2 to be able to reset the mode according to the written program. The RX and TX pin connected to D3 and D4 are data communication between the Arduino development board and the whole module. The commands for initializing and verifying the function of the mode are made immediately when the whole device is switched on so that if signal connection errors or invalidation of the SIM card are transmitted as a warning message to the patient [4] (Fig. 9).

The LCD display has 2.8 inches and a resolution of 320 × 240 pixels. It works at 3.3 and 5 V. The shield contains a resistive touchscreen and also has an SD card slot on which txt data can be saved, but uploads bmp-sized images to display on the display. These data saved on the SD card can be interpreted later by a specialist. It is compatible with several Arduino development platforms, by default with Arduino Mega. The screen has a background light control pin, which helps save energy, so it can automatically turn off the lighting side to reduce power consumption [2] (Fig. 10) [7, 8].

Fig. 8 The GPS module

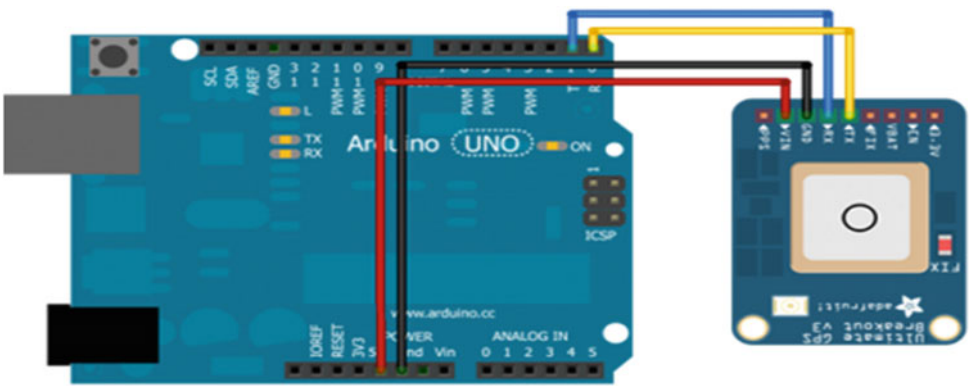

Fig. 10 LCD display

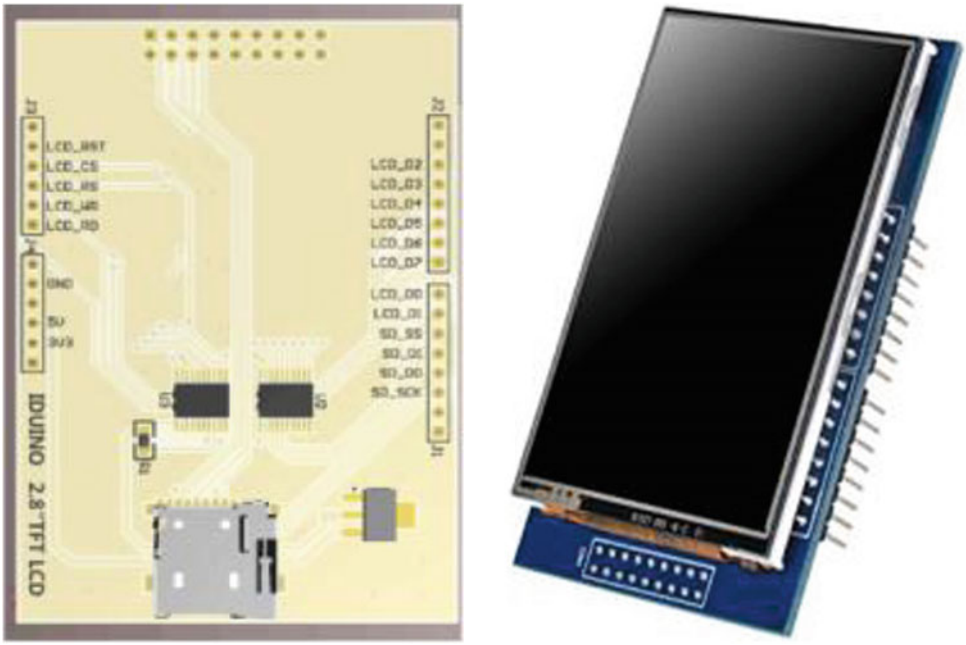

To be able to schedule it, you must attach the manufacturer's libraries where all the connection ports are defined for both the display side and the data save side of the SD card. These libraries access different ports of the way communication between the LCD and the Arduino plate is made. Supports memory cards with up to 16 GB capability to create folders for txt and bmp files. In order to be easier then interpreting them.

The light sensor aims to save the energy and battery of the device by putting the screen on stand by after a 5 min inactivity, but also when the device is covered. The sensor works at a 5 V voltage with extremely low power consumption and is based on the reflection between an IR led and a phototransistor. The IR light will emit a light that the phototransistor will receive when it reflects at a distance of 0–4 cm. With a small signal, the sensor also has an operational amplifier and a filter to amplify and filter the input signal for better signal capture accuracy (Fig. 11).

The power supply side of the device was powered by a 5 V voltage charging module, consisting of a Li-Ion battery with a capacity of 2200 mA. The complete system has an autonomy of 8–10 h. The percentage of the battery is displayed on the display, but also by warning lights when the battery is discharged or in the charging process. The device can be charged to any type of charger with a USB plug as it has a Micro-USB connection (Fig. 12) [9, 10].

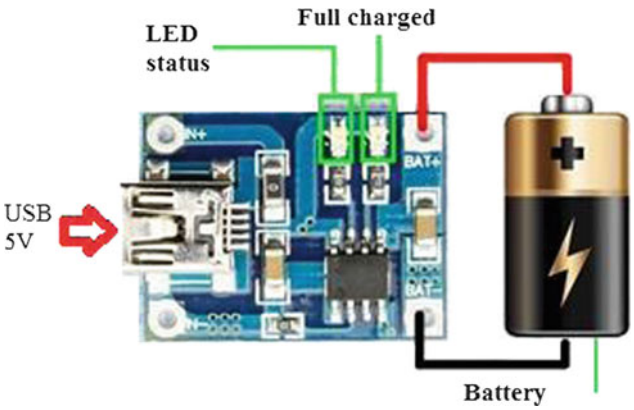

Fig. 12 Power supply

Fig. 11 The light sensor

3 Results

The source code of the system, in addition to the functions related to the acquisition and processing of biosensors, contains a series of code lines dedicated to the user interface. It has been desired to obtain a device which does not require complex technical knowledge in use. The graphical interface has been entirely created and includes several submenus.

Once the device is powered on, it will show if we want to start or put it on standby. This is done by pressing the two buttons on the side, one for validating the startup and moving to the next step and the other for the invalidation to put the whole system in the standby mode (Fig. 13).

Using the ECG module, we obtained a series of signals that correspond to the physiological route in a trunk that were first displayed on the computer through the Processing software to get a better picture and then be displayed on the display. This software contains libraries that can process signal processing as it can implement signal processing functions such as Fourier Transform or Sampling [11] (Fig. 14).

Calibration of the signal was done using the Metron PS420 heart simulator to highlight the symptoms and illnesses of some cardiac pathologies (ventricular fibrillation, myocardial infarction).

The values recorded by the pulse sensor were taken over by the microcontroller and processed with the aid of some algorithms to be displayed. The temperature at which determinations were made ranging between 36.96 and 37.01 °C, with a humidity of approximately 33.4%.

The system designed and built works according to the established requirements. So we've also built a 3D design and print carcass. 3D realization was done in Autodesk Fusion 360. It is a discreet, portable device that can be used at home, in the office or on a walk (Figs. 15 and 16).

Licenta_ECG_FINAL_NOI_TESTE_2_butoane_testeU.ino §

```
tft.println("IoT DEVICE");
tft.setTextColor(ILI9341_RED);
//tft.setCursor(0,100);
 V1= analogRead(1);
 tft.drawRect(1, 40, tft.width()-1, 82, ILI9341_BLUE);
 tft.drawRect(1, 150, tft.width()-1, 170,ILI9341_BLUE);
 tft.setTextColor(ILI9341_YELLOW, ILI9341_BLACK);
 tft.setTextSize(2);
 tft.setCursor(35, 45);
 tft.println("PULS");
 tft.setCursor(150, 45);
 tft.println("TEMP");
 tft.fillRect(2, 62, tft.width()-5, 37, ILI9341_BLACK);
 tft.setTextSize(3);
 tft.setTextColor(ILI9341_GREEN,ILI9341_BLACK );
 tft.setCursor(30, 72);
 tft.print(BPM);
 tft.setTextColor(ILI9341_YELLOW,ILI9341_BLACK);
 tft.setTextSize(2);
 tft.print("BPM");
 float temperatura = readTempInCelsius(10,A5);
 tft.setTextSize(3);
```

Fig. 13 Source code

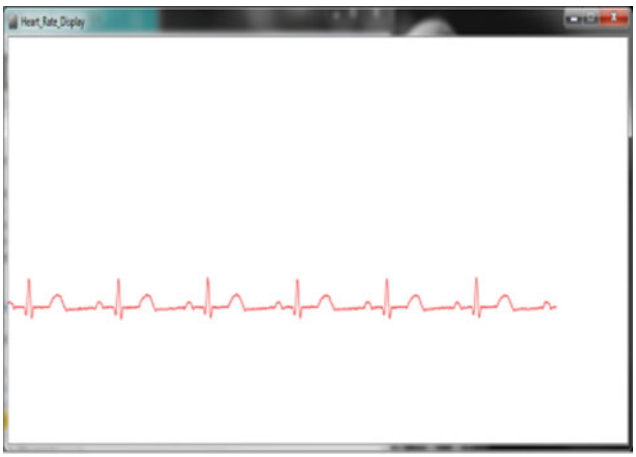

Fig. 14 ECG signal

Fig. 15 3D device design

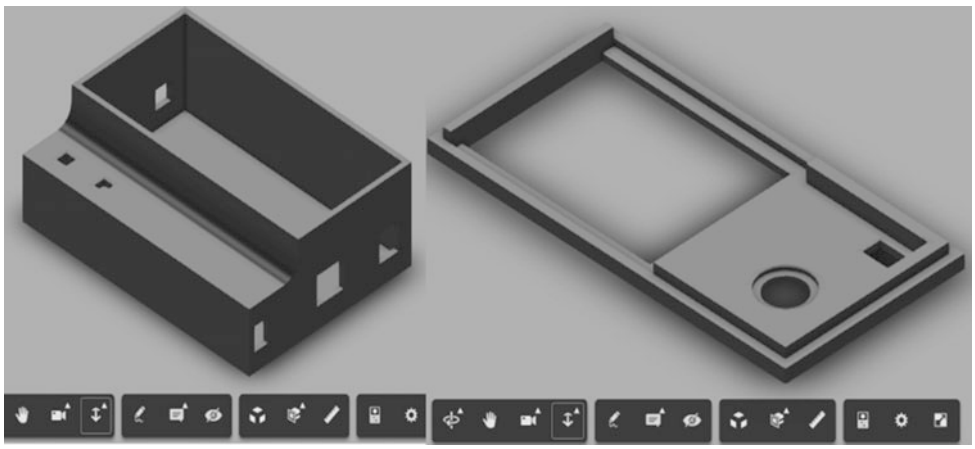

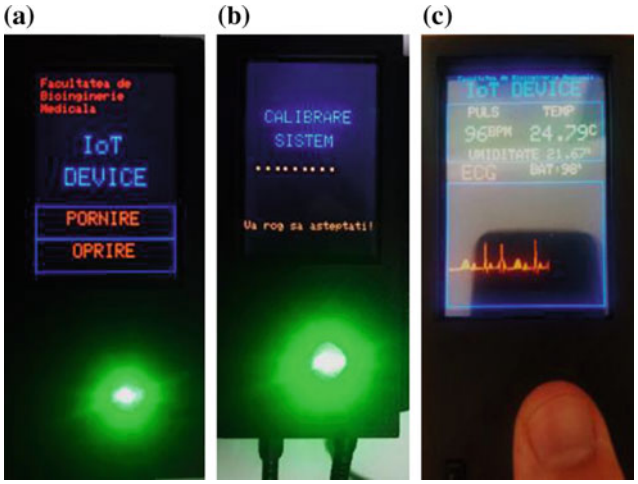

Fig. 16 **a** Device startup menu, **b** calibration menu, **c** monitoring menu

4 Conclusions

Preliminary results have shown that the device is capable of taking the signals obtained from the attached modules so that we finally have a complete set of data for the functional evaluation of the patient.

Optimization of the device is to achieve accuracy of real-time data but also a patient's safety that can be medically supervised remotely, any alteration of its status being immediately signaled to allow a rapid medical response.

In the future, we want to associate the equipment with an accelerometer in order to have a clearer picture of the positioning of the assisted subject in space.

The system is easy to use, without discomfort, being a discreet, portable device that can be used at home, in the office or on a walk with an autonomy of up to 8–10 h.

The development of such a system is a field of research involving medical and engineering knowledge, medical bioengineering being the basis of research in this area of knowledge.

Future Research Directions:

- On the hardware side, by optimizing the components used, you could make a miniaturization of the entire system so that it is more reliable. In this respect, the current modules can be replaced with some SMD-type more efficient, thus minimizing the energy consumption.
- Addition of additional sensors in order to increase the parameters.
- On the software side, develop additional functions for more elaborate analysis and processing for ECG analysis.
- The development of electrodes from a material with low resistivity, with the shape and size appropriate for these types of recordings.

Increase system fidelity using approved components to capture the signal.

Conflict of Interest The authors declare that they have no conflict of interest.

References

1. Ashton, K.: That 'Internet of Things' Thing. Retrieved 9 May 2017 (22 June 2009)
2. Display LCD are 2.4″. https://www.optimusdigital.ro/ro/ (2018)
3. Bluetooth Master Slave HC-05. https://www.optimusdigital.ro/ro/ (2018)
4. GSM SIM800L. https://www.optimusdigital.ro/ro/gsm-i-gprs/
5. Gao, H.Q., Duan, X.H., Guo, X.Q., Huang, A.P., Jiao, B.L.: Design and tests of a smartphones-based multi-lead ECG monitoring system. In: 35th Annual International Conference of the IEEE Engineering in Medical and Biology Society (EMBC), 2013 (In Press)
6. Bove, K.E., Rowlands, D.T., Scott, R.C.: Observations on the assessment of cardiac hypertrophy utilizing a chamber partition technique. Circulation (2015)
7. Chan, C.-C., Chen, C.-W., Chou, W.-C., Ho, Y.-L., Lin, Y.-H., Ma, H.-P.: Live demonstration: a mobile ECG healthcare platform. In: 2012 IEEE Biomedical Circuits and Systems Conference (BioCAS), p. 87 (2012)
8. Internet of medical things: a review of recent contributions dealing with cyber-physical systems in medicine. IEEE J. Mag. ieeexplore.ieee.org. Retrieved 23 June 2018
9. Karlgren, J., Fahlén, L., Wallberg, A., Hansson, P., Ståhl, O., Söderberg, J., Åkesson, K.-P.: Socially intelligent interfaces for increased energy awareness in the home. The internet of things. Lecture Notes in Computer Science, pp. 263–275. Springer, 4952 (2008)
10. Lau, D.T., Liu, J., Majumdar, S., Nandy, B., St-Hilaire, M., Yang, C.S.: A cloud-based approach for smart facilities management. In: Proceedings of the 2013 IEEE Conference on Prognostics and Health Management (PHM). Gaithersburg, USA (2013)
11. Tan, L., Wang, N.: Future internet: the internet of things. In: 3rd International Conference on Advanced Computer Theory and Engineering (ICACTE), vol. 5, pp. 376–380 (20–22 August 2010)

The Use of Thermography as a Prediction Element in the Maintenance of Medical Equipment

D. Andritoi, C. Luca, C. Corciova, and R. Ciorap

Abstract

Currently, the complexity of the equipment involves a problem in the training of maintenance professionals, maintenance predictive techniques being similar to medical diagnostic techniques, whenever a symptom that requires tests to diagnose the problem occurs. Total Preventive Maintenance or TPM is a type of maintenance plan used in production and various industrial fields. Overall, this is a theory about how the tools, parts and machinery used for production services are maintained so that life is as increased without incident and as safe. This concept is used to reduce maintenance costs, dead times with the aim of improving and rationalizing production and customer service. The most effective tools for preventive maintenance applications, Infrared Cameras provide the amazing ability to see what other diagnostic tools cannot. Using these cameras to discover hidden issues before they turn into serious situations, help keep your equipment in peak performance, avoiding expensive equipment damage and improving safety. Infrared thermal imaging has been used as a non-destructive and non-direct technique to examine progressive deterioration processes and failure mechanisms of different medical equipment. After the study, we can conclude that thermal imaging has major advantages over other diagnostic techniques because measuring equipment does not emit harmful radiation, thermal scanning does not require direct contact with the object to be analyzed, malfunctions are detected quickly and this procedure can be repeated whenever or needed, allowing real-time analysis.

Keywords

Medical equipment • Predictive maintenance • Thermal radiation • Thermography • Transmittance

D. Andritoi (✉) · C. Luca · C. Corciova · R. Ciorap
University of Medicine and Pharmacy "Grigore T Popa" Iasi, Iasi, Romania
e-mail: doru.andritoi@gmail.com

1 Introduction

As the medical devices market is global and the number of devices imported by the European Union increases, it is indispensable to coordinate the activities of national authorities when they concern issues that concern different member states. The guarantee of increased reliability is done through good maintenance. Currently, the complexity of the equipment involves a problem in the training of maintenance professionals, maintenance predictive techniques being similar to medical diagnostic techniques, whenever a symptom that requires tests to diagnose the problem occurs.

In accordance with European Standard EN13306, maintenance refers to: "the combination of all technical, administrative and managerial actions during the lifecycle of a piece of equipment to maintain or restore it to a state in which it can perform the desired function".

Maintenance is a general term for a wide range of operations in all sectors of activity and across all types of work environments [1]. Analysis of the efficiency issues of various equipment, over 30 years, has shown that maintenance policy is responsible for approximately 17% of production disruptions or quality problems.

The other 83% is due mostly to inappropriate operating practices, defective design, etc. (Fig. 1).

Developing a maintenance strategy at a company level does not reduce to one type of maintenance [2]. There will always be a reactive, corrective, preventive and predictive maintenance mix. Also, an important factor in choosing a type of maintenance is the consequences of a possible defect in the equipment/system. The appearance of a defect can pose problems of work or production security, or can lead to environmental problems. There are defects that cause high costs related to production losses, or defects that can make equipment unrecoverable.

Whether it is called "planned maintenance" or if the more traditional term "preventive maintenance" is used, it is

S. Vlad and N. M. Roman (eds.), *6th International Conference on Advancements of Medicine and Health Care through Technology; 17–20 October 2018, Cluj-Napoca, Romania*, IFMBE Proceedings 71,
https://doi.org/10.1007/978-981-13-6207-1_12

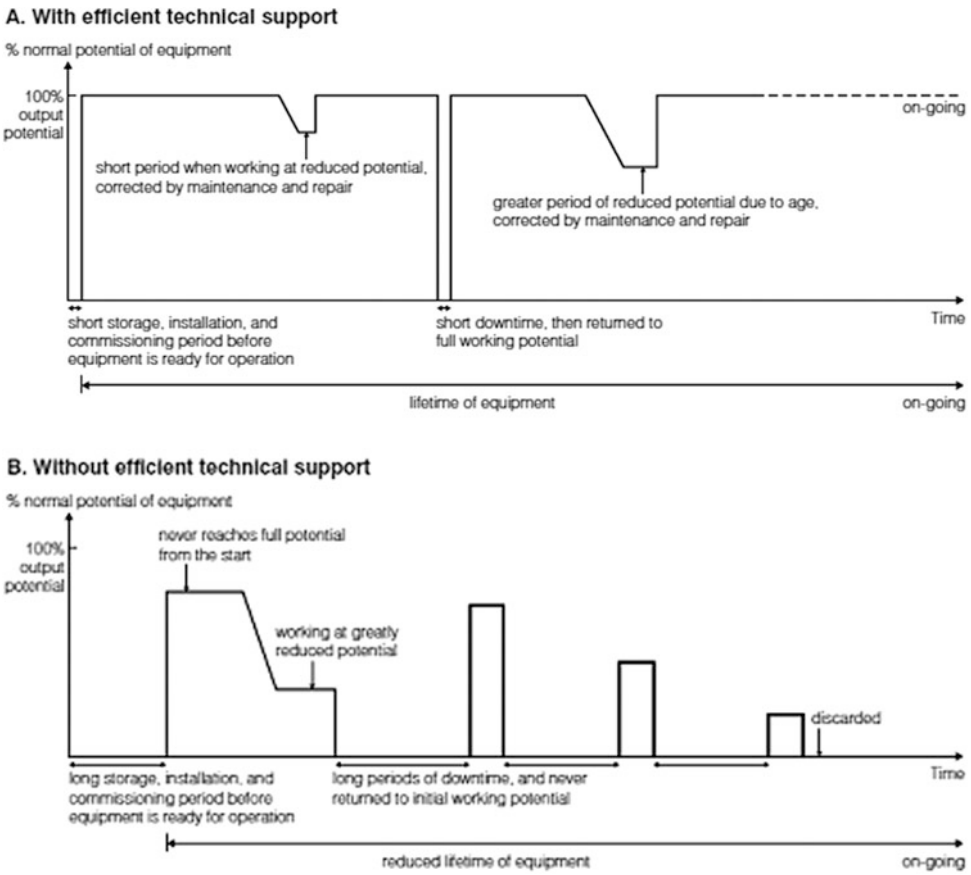

Fig. 1 Adapted from: Mallouppass A. 1986, "Background document for the WHO programmer on maintenance and repair of hospital and medical equipment", WHO, Geneva, Switzerland

certainly the focus that preventative maintenance is done on time.

In the development of an effective predictive maintenance policy it is necessary to involve management teams who need to understand the need to implement it with additional costs but which will prove their effectiveness over time [3].

When predictive maintenance works effectively as a maintenance strategy, this brings more cost savings:

- Minimize maintenance time for the equipment;
- Reducing lost production hours on maintenance;
- Minimizing the cost of spare parts and consumables.

2 Maintenance of Equipment in Medical Institutions

In choosing the strategy to implement a certain type of maintenance, it must first be taken into account that maintenance does not require the execution of repairs in the shortest time but is mainly a means of preventing losses caused by equipment problems [4, 5]. Currently, most hospitals follow these policies only the manufacturer's specifications, recommended for devices ignoring other provisions of national or European level. For example, the intervals for a periodic check vary from 6 to 12 months, depending on the type of device and the degree of risk. Class III (high risk) devices such as defibrillators should be inspected every 6 months and Class II (average risk) devices such as electrocardiographs should be inspected annually.

However, the need for these recommended intervals is questionable. It is essential to establish an evidence-based inspection or maintenance treatment derived from the field data analysis.

As in health care, prevention of failures is more effective than focusing on fixing them. Repairs are always costly because they require specialized staff and often costly replacement parts. Regular inspection and maintenance, using service manuals and checklists, makes the maintenance impact maximized and costs minimized [6].

The common premise from which predictive maintenance starts is that periodic or continuous monitoring of mechanical, electrical or other system or process performance indicators can provide the data necessary to ensure the maximum interval between repair and maintenance work, respectively to minimize the cost of interruptions unplanned production due to possible malfunctions. However, predictive maintenance is more than that. It is in fact the means of improving and increasing productivity, product quality and total efficiency of manufacturing and production systems.

Components of a system, such as pumps, electric motors or hydraulic transmission systems, etc. as integral parts of the system must operate at the optimum parameters to ensure that the projected performance of the system as a whole is attained.

During maintenance problems, in addition to the known techniques for monitoring and diagnostics (vibration monitoring, tribology), must be considered and other system parameters such as flow rates, voltages, currents, temperatures, etc.

Thermography is a modern, non-irradiating and non-invasive method, developed over four decades, used in various fields of activity.

Infrared scanning is recommended as a regular maintenance procedure in many situations, extracting so solid results as quickly as possible and without interrupting process flow, a key benefit to the industry, regardless of the age of the equipment [7].

3 Measurements

Experimental measurements were performed within the "Medical Device Security Testing" laboratory of the Faculty of Bioengineering for several types of infusion equipment.

For the experiment, we used the IAGU system to which the infusion pump was connected, and the thermography measurements were made using the Optris PI60 thermo graphic camera. The fluid used during the experiments was a salt water solution. We have chosen to use this type of fluid to facilitate the experiment, knowing that the viscosity of the infusion solutions varies a lot.

Equipment connection in the experiment was performed according to the scheme in Fig. 2.

An insulating material (polystyrene with a thickness of 5 cm) was also used in the experiment to thermally separate the surrounding environment and the ambient temperature at the time of testing was 24 °C, an air conditioner located inside the test lab. The experiment setup can be seen in Fig. 3.

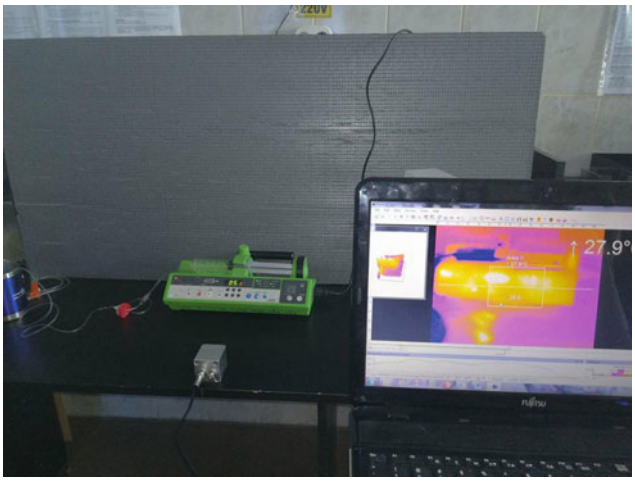

Fig. 3 Experiment setup

In order to measure "thermal radiation", infrared thermometer uses a wavelength of between 1 and 20 μm. The intensity of the radiation emitted depends on the material. This constant material contingency is described by emissivity which is a known value for most materials.

Measurement of IR thermal radiation is the basis for measuring non-contact temperature and thermography. In principle, the IR (W) thermal radiation leaving the surface (A) is called "output" or "radiosity".

This energy W can be emitted from the surface, reflected from the surface or transmitted through the surface. It is important that the total radiance is equal to the sum of the emitted component, the reflected component and the transmitted component.

Summing up these three components, the result should normally be equal to the unit:

$$\alpha + \rho + \tau = 1 \tag{1}$$

α absorption;
ρ reflectivity;
τ transmittance.

Fig. 2 Connection schematic

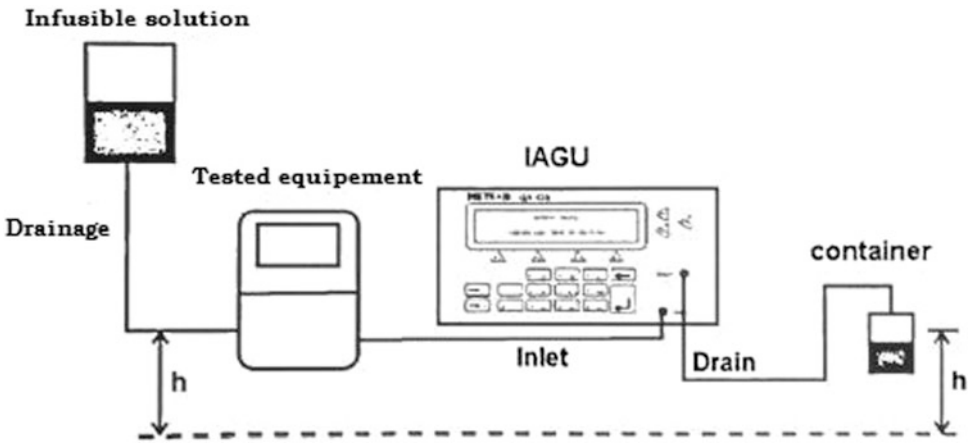

For further simplification, if the IR thermal detector is positioned in front of the target surface, then the net radiation (Wnet) to be detected is equal to the transmittance of the IR thermal radiation:

$$W(net) = W\tau = \tau * W(t) \quad (2)$$

The temperature of a body depends on the balance between heat production and heat loss.

4 Results and Discussions

It was desired to establish a correlation between the temperature reached by some components of the equipment and the degree of wear of the equipment. Measurements were performed under controlled humidity and temperature conditions.

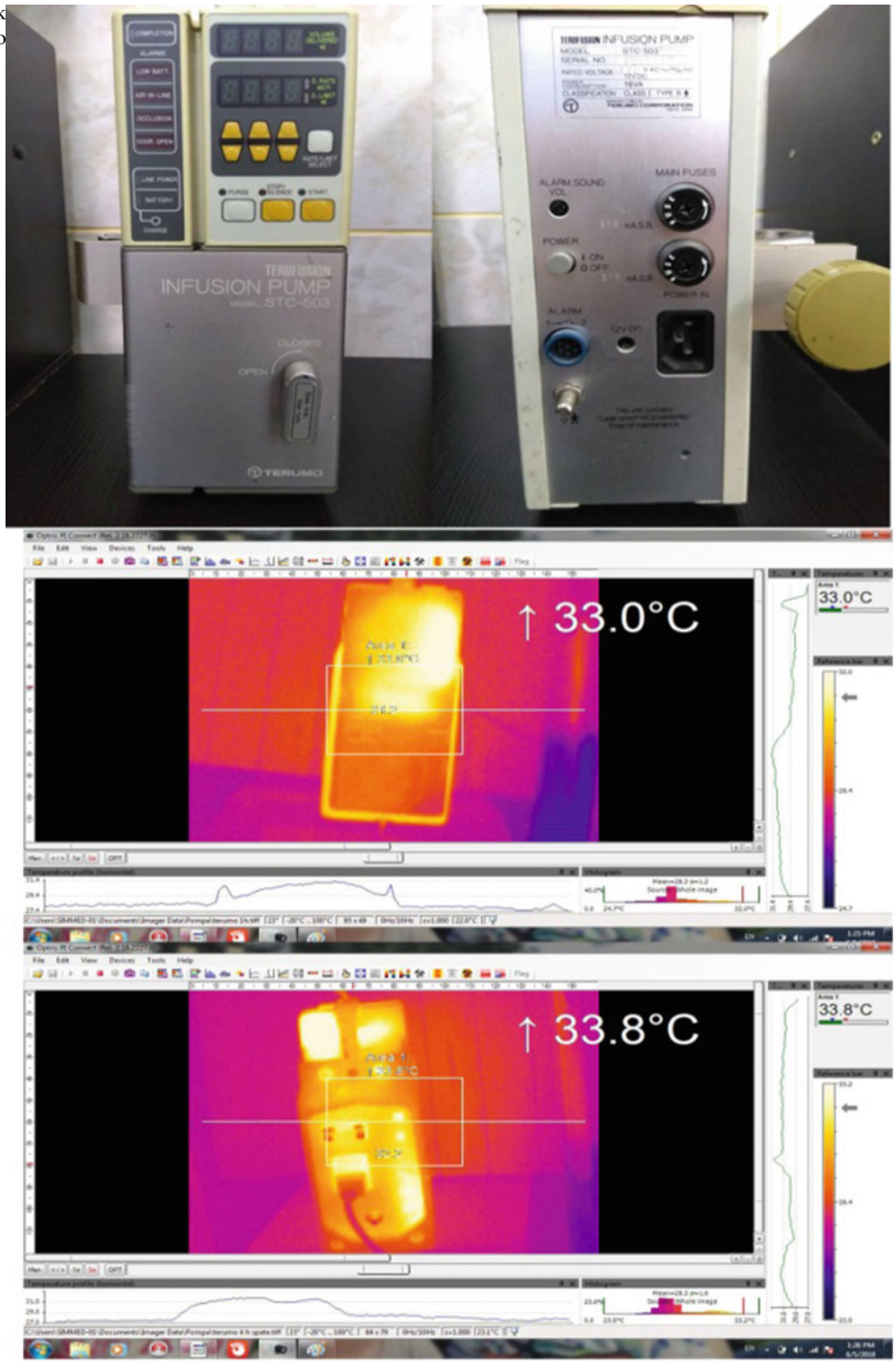

Fig. 4 Normal view, front and back (on top); thermo graphic image also front and back

On equipment without defects, the heating of a zone occurs gradually, over time, from an initial value to one of the "balance", corresponding to normal operation. This equilibrium value is believed to be reached within 1–2 h of starting the machine and will remain relatively constant throughout the test period, in the case of defective equipment, a much faster and continuous increase was observed.

A number of 9 equipment (3 different models) were tested. During the thermo graphic camera measurements several areas of overheating were found as can be seen in Fig. 4.

The retrieval of the thermo graphic images was made in different planes for as many areas of interest at different times of operation. The recording time was 12 h for each piece of equipment.

After the acquisition, the data was processed for analysis using the dedicated OPTRIS PI60 Thermal Camera software, with the changes being highlighted by the numeric values recorded in the areas of interest.

Although the equipment can record continuously (video format), we chose to use only the measured values considered important moments (initial 30 min of operation and then every hour).

Increasing the temperature, as we expected, occurred over time for several areas of interest. In Fig. 5, a temperature increase of 30 min, one hour and two after commissioning is observed in the Terufusion TE-172.

Thermal analysis allows measurement of the temperature of the target surface and the rate of variation.

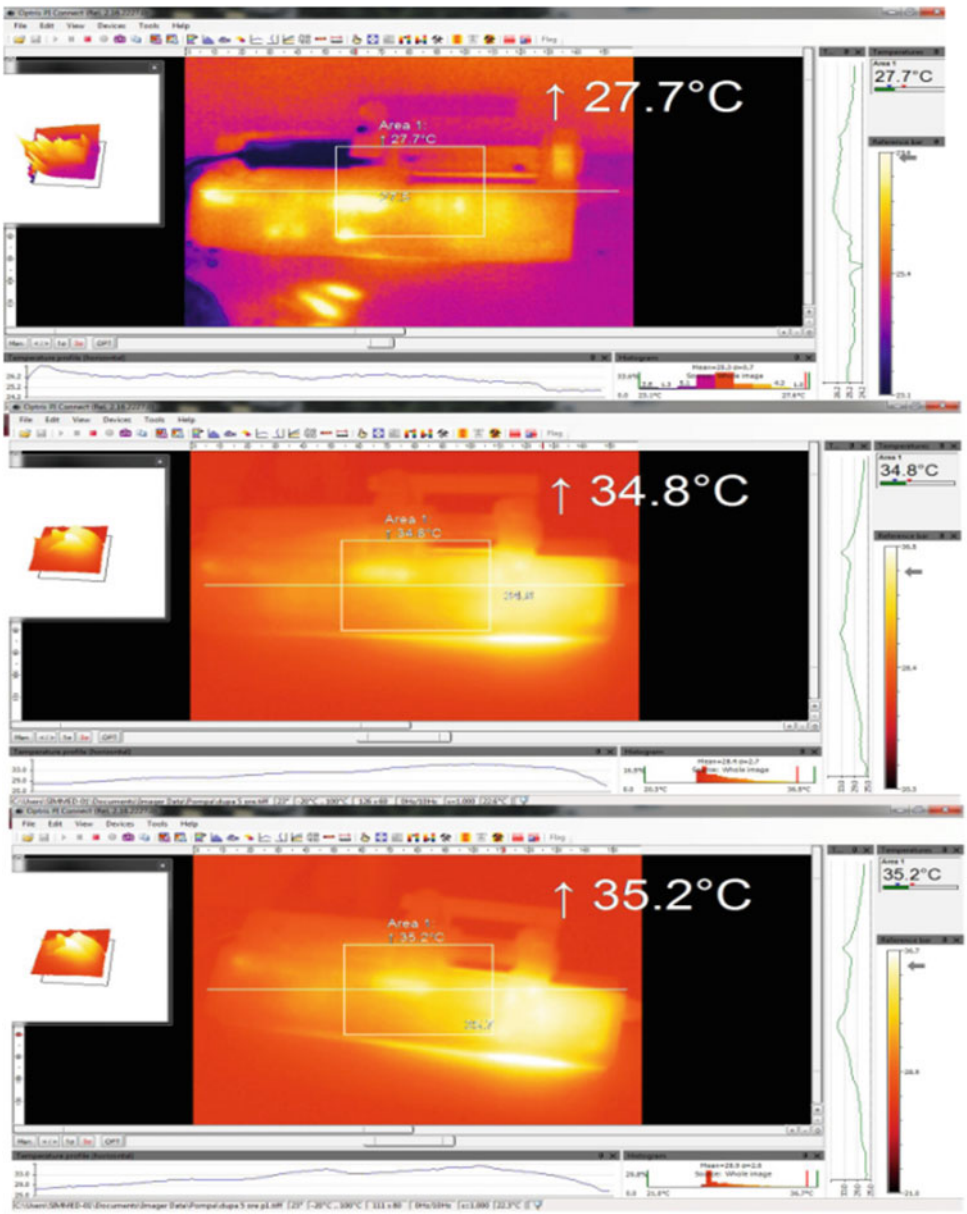

Fig. 5 Temperature value after 30 min, after one hour and after two hour

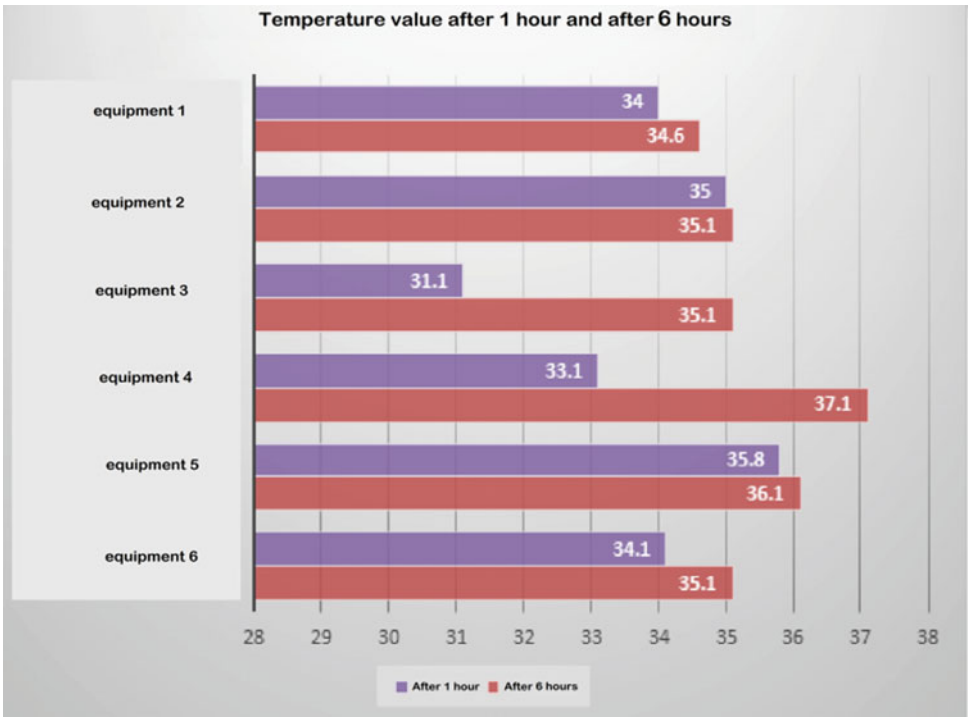

Fig. 6 Temperature value after 1 and 6 h

The graph in Fig. 6 reflects heat that occurs after 1 and 6 h for a total of six equipment analyzed. The study may be a starting point for a far more detailed research direction to develop protocols to be used in predictive maintenance processes for medical equipment.

5 Conclusions

Predictive maintenance is in fact a philosophy or an attitude that, based on operating conditions, allows the optimization of an entire system. A comprehensive predictive maintenance management uses the best methods (vibration monitoring, thermography, tribology, etc.) to obtain the operating parameters of the industrial subsystems under which they will schedule maintenance and repair. The originality of the proposed solution is the use of thermography in this type of study. Through the results we have demonstrated the applicability and effectiveness of this type of approach.

Conflict of Interest The authors declare that they have no conflict of interest.

References

1. Baker, T., et al.: Debating the medical device preventive maintenance dilemma and what is the safest and most cost-effective remedy. J. Clin. Eng. Roundtable, July/September (2003)
2. Mallouppass, A.: Background document for the WHO programmer on maintenance and repair of hospital and medical equipment. WHO, Geneva, Switzerland (1986)
3. Bevilacqua, M., Braglia, M.: The analytic hierarchy process applied to maintenance strategy selection. Reliab. Eng. Syst. Saf. **70**(1), 71–83, October 2000. https://doi.org/10.1016/s0951-8320(00)00047-8 (2000)
4. Corciovă, C., Andritoi, D., Ciorap, R.: Elements of risk assessment in medical equipment. Advanced Topics in Electrical Engineering (ATEE), 2013 https://doi.org/10.1109/atee.2013.6563427 (2013)
5. Andriţoi, D., Luca, C., Corciovă, C., Ciorap, R.: Predictive maintenance application for health technology management. Advanced Topics in Electrical Engineering (ATEE), 2013 https://doi.org/10.1109/atee.2013.6563431 (2013)
6. Corciovă, C., Andriţoi D., Luca C., Ciorap R.: Prioritization of medical devices for maintenance decisions. In: Vlad, S., Roman, N. (eds.) International Conference on Advancements of Medicine and Health Care Through Technology, 12–15th October 2016, Cluj-Napoca, Romania. IFMBE Proceedings, vol. 59. Springer, Cham (2017)
7. Huda, A.S.N., Taib, S.: Application of infrared thermography for predictive/preventive maintenance of thermal defect in electrical equipment. Appl. Thermal Eng. **61**(2, 3), 220–227 November (2013)

Method for Body Impedance Measurement

R. Copîndean, R. Holonec, F. Dragan, and C. Muresan

Abstract

The paper proposes a method for body or bioelectrical impedance (BI) measurement based on voltage measurement and analysis at different frequencies with a four-electrodes configuration and the principles of virtual instrumentation. The measured values are used to calculate: the effective (root mean square) values of voltages and currents, the apparent power, the active power, the phase shift, the resistance and the electrical capacity of the body. For the experiment, an NI PCI-6110 data acquisition board and the LabVIEW programming environment from National Instruments were used.

Keywords

Bioelectrical impedance • Series/parallel resistance • Series/parallel capacity • Data acquisition • Virtual instrumentation • LabVIEW

1 Introduction

When the human body is coupled to a voltage supply, its electrical resistance is an important factor in determining the amount of the current flowing through it.

The magnitude of the bioelectrical resistance is essentially determined by the structure of the tissues on where the electric current flows. Other factors that influence the value of human body resistance are [1–3]:

- the value of applied voltage;
- duration of the current going through the tissues;
- temperature;
- the place of touch;
- surface and contact pressure;
- humidity;
- mental condition etc.

The resistance of the human body has a nonlinear behavior and it decreases considerably as the electric current flows, which determines the increase of damage caused by the electrocution. Because there are diverse human body tissue structures, there are different resistances and consequently different values for measured current. Considering these aspects, it's very difficult to reproduce an equivalent electrical circuit of the human body. Thus, by simplification, the resistance of the human body is believed to have two components: skin resistance and the resistance of the internal tissues. The resistance of the skin has the largest weight in the total of the human body resistance. The electrical resistance of the skin can be expressed by R_{skin} as:

$$R_{skin} = \frac{\rho \cdot d}{S}. \quad (1)$$

In relation (1) "ρ" is the electrical resistance of the skin that corresponds to the contact surface; "d" is the thickness of the skin and "S" is the contact surface area.

The electrical resistance of the skin R_{skin} also depends on body part that is touching the voltage supply. All these elements are to be considered to determine the dielectric strength of the protective electro-insulating equipment. The values ρ and d can be extremely different, not only for different people but also for the same person and they may vary widely in relation with the contact point.

The impedance of the human body, which is considered a non-homogeneous electric conductor, is called the bioelectrical impedance (Z) and it represents a combination of the electrical resistance R and capacitive reactance $1/\omega C$, in the form of [4]:

$$Z = \sqrt{R^2 + \frac{1}{\omega^2 \cdot C^2}}. \quad (2)$$

R. Copîndean · R. Holonec (✉) · F. Dragan · C. Muresan
Electrical Engineering Faculty, Technical University, Cluj-Napoca, Romania
e-mail: rodica.holonec@ethm.utcluj.ro

S. Vlad and N. M. Roman (eds.), *6th International Conference on Advancements of Medicine and Health Care through Technology; 17–20 October 2018, Cluj-Napoca, Romania*, IFMBE Proceedings 71,
https://doi.org/10.1007/978-981-13-6207-1_13

In relation (2), C represents the total electrical capacity of the human body. It consists of an electrostatic capacity that occurs due to the voltage applied on the outer skin surface and a polarization capacity due to the phenomenon of polarization when the electrical current passes through the human body. In practical applications the influence of the electrical capacity is neglected, so that, finally, the biological impedance is considered as an equivalent electrical resistance.

In connection to the greater or lesser predisposition to electrocution, it has been tried the characterization of the electrical properties of the human body by the so-called "impedance angle". Thus, considering the impedance of the human body as being formed by its resistance and capacitive reactance, the value of the impedance angle, denoted by δ, can be determined as in Fig. 1.

In the specialized literature, results are given related to the complementary angle and the tangent of this angle:

$$\tan \varphi = \frac{1}{R\omega C}. \tag{3}$$

The impedance as a complex size [5, 6] can be determined under:

- Cartesian form, as:

$$Z = R + jX. \tag{4}$$

where R, the resistance, is the real part and X, the reactance, the imaginary part.

- Polar form, as:

$$Z = |Z|e^{j\varphi} = |Z|(\cos \varphi + j \sin \varphi). \tag{5}$$

In (5), the impedance module and phase shift are expressed through the next relations:

$$|Z| = \sqrt{R^2 + X^2} \tag{6}$$

$$\varphi = \arctan \frac{X}{R}. \tag{7}$$

The nature of the impedance of the human body is given by the sign of the imaginary component:

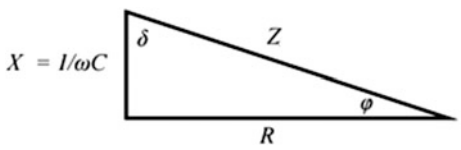

Fig. 1 The triangle of the human body impedance [4]

- X > 0 inductive nature,
- X < 0 capacitive nature,
- X = 0 resistive nature.

In this paper, the capacitive nature of the skin, and the capacitive reactance X_C are discussed:

$$X_C = \frac{1}{\omega C}. \tag{8}$$

Circuit parameters for the impedance are defined by models of associated electric circuits. Equivalent series circuits or parallel circuits are used as simplified models to represent the impedance in most of the situations. These simplifications, where the parasite circuit elements are neglected, can be made by respecting some severe measurement conditions.

Classical series and parallel circuit models for the human body impedance comprise resistance and capacity connected as in Fig. 2.

In case of the series circuit, Z is preferred to be represented as:

$$Z = R_s + jX_s. \tag{9}$$

In case of the parallel circuit, Y being the admittance, is preferred to be represented as:

$$Y = \frac{1}{z} = G + jB. \tag{10}$$

In (10), the conductance and susceptibility are determined as:

$$G = \frac{1}{R_P} \tag{11}$$

$$B = \frac{1}{X_P}. \tag{12}$$

Both models (series and parallel) describe the susceptibility B and the impedance Z as

$$B = \frac{1}{R_P} + j\frac{1}{X_P} = \frac{1}{R_S + jX_S} = \frac{1}{Z}. \tag{13}$$

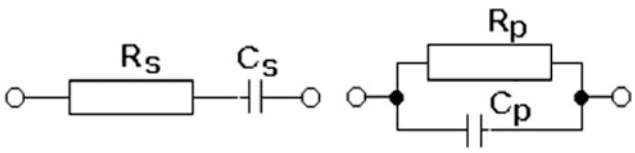

Fig. 2 Series and parallel circuit models for the equivalent impedance of the human body

Thus, the equivalence relations are obtained:

$$R_P = \frac{R_S^2 + X_S^2}{R_s} \tag{14}$$

$$X_P = \frac{R_S^2 + X_S^2}{X_s}. \tag{15}$$

In conclusion, by knowing the elements of a series/parallel model of the human body, the elements of the other parallel/series model can be determined.

2 The Principle of the Method

In Fig. 3, the four-electrode bioelectrical impedance measurement configuration is represented. Here the voltage measuring circuit is separated from the current injection circuit.

The effective value of the voltage with a high impedance $Z_{voltmeter} > 10$ MΩ can be measured. Because the current delivered through voltage measuring circuit is considerably smaller than the one delivered by the sinusoidal signal generator I = 1 ÷ 100 μA, the measured voltage will be not affected by the resistance of the electrodes which is smaller than the voltmeter impedance.

The value, in module, of the impedance is:

$$|Z| = \frac{V_{RMS}}{I_{RMS}}. \tag{16}$$

If the measurements are realized by a data acquisition system then the samples of the voltage v_k and the current i_k, taken over several periods of the signal provided by the generator, can be calculated [7, 8] as:

$$V_{RMS} = \sqrt{\frac{1}{n}\sum_{k=1}^{n} (v_k)^2} \tag{17}$$

$$I_{RMS} = \sqrt{\frac{1}{n}\sum_{k=1}^{n} (i_k)^2}. \tag{18}$$

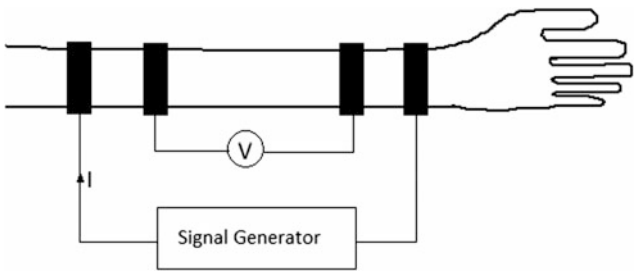

Fig. 3 The principle of impedance measurement and electrodes placing

It is possible to obtain the active power P, the apparent power S and the cosφ power factor according to the relations:

$$P = \sqrt{\frac{1}{n}\sum_{k=1}^{n} u_k * i_k} \tag{19}$$

$$S = V_{RMS} * I_{RMs} \tag{20}$$

$$cos\varphi = \frac{P}{S}. \tag{21}$$

For the series circuit model of the impedance, from the Eqs. (5), (9), (16), (21), the series resistance is obtained:

$$R_S = |Z| \cos\varphi = \frac{V_{RMS}}{I_{RMS}} \cdot \frac{P}{S} = \frac{P}{I_{RMS}^2} = \frac{\sqrt{\frac{1}{n}\sum_{k=1}^{n} u_k * i_k}}{\frac{1}{n}\sum_{k=1}^{n} (i_k)^2}. \tag{22}$$

The series reactance X_S will be:

$$X_S = |Z| \sin\varphi = \frac{V_{RMS}}{I_{RMS}} \sqrt{1 - \left(\frac{P}{S}\right)^2} = \frac{1}{2\pi f C_S}. \tag{23}$$

In relation (23) f represents the signal generators frequency.

The series capacitance will be:

$$C_S = \frac{1}{2\pi f \frac{V_{RMS}}{I_{RMS}} \sqrt{1 - \left(\frac{P}{S}\right)^2}}. \tag{24}$$

3 Experimental Implementation

3.1 Hardware

The measurement method is implemented by using the hardware configuration illustrated in Fig. 4 where the bioelectric impedance Z is connected to the data acquisition (DAQ) unit using a four electrodes configuration.

The practical application was realized with the help of the following components:

- NI PCI-6110 data acquisition board (National Instruments) [9], where an analog output AO0 was used to generate the signal and two analog differential inputs AI1, AI2, for the reading of the voltage and the current;
- 1 kΩ resistance for the conversion of voltage to current;
- Body impedance (represented by the analyzed subject);
- Conductive textile tape electrodes.

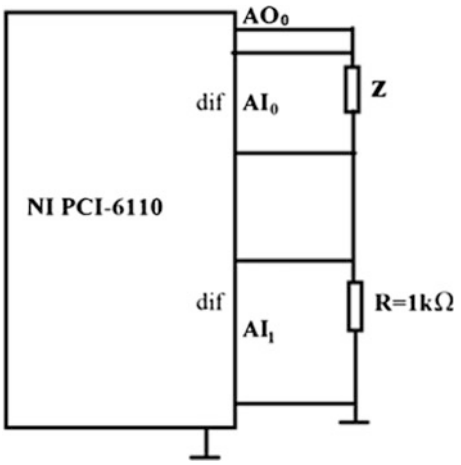

Fig. 4 Scheme for the impedance connections to the DAQ board

3.2 Software

For the application control and also for data processing, LabVIEW graphical programming software from National Instruments [10] was used. The algorithm (Fig. 5) uses the function called Signal-Sine for the signals generation and sends the signals to the analog output AO0.

Two differential analog inputs, AI0 and AI1, where used to read the voltage and electrical current. The voltage on the body impedance is read directly. The voltage dropping on the resistance will be divided by 1000 in order to obtain the value of the electrical current. Therefore, the current will have low values (μA) reaching maximum 1 mA.

The effective value of the voltage and electrical current will be calculated. There is also calculated the value of the instantaneous power which, mediated, will give the value of the active power P. The apparent power S is computed by multiplying the effective voltage with the effective current.

The voltage-to-current phase shift is calculated by dividing the active power to apparent power, and finally the values of cosφ and sinφ are obtained. Having both values, cosφ and sinφ, and multiplying them with the Z impedance module, the real and the imaginary parts are obtained.

3.3 Experimental Data

In order to validate the proposed method, measurements were made on a set of resistors and capacitors connected in series and then in parallel.

Measurements were made on the same subject, with four and two electrodes. Results can be observed in Table 1.

In the case of the four-wire measurements, the voltage measuring electrodes were placed at 9 cm one to another. The current electrodes were placed as in Fig. 3, the with a distance of 15 cm between them.

For the case of the two-wire measurements, only the voltage electrodes were used, he current electrodes where attached to them.

It can be observed that in the case of two-wires measurements, at the same frequency, the resistance values are higher than in the case of four-wires measurements.

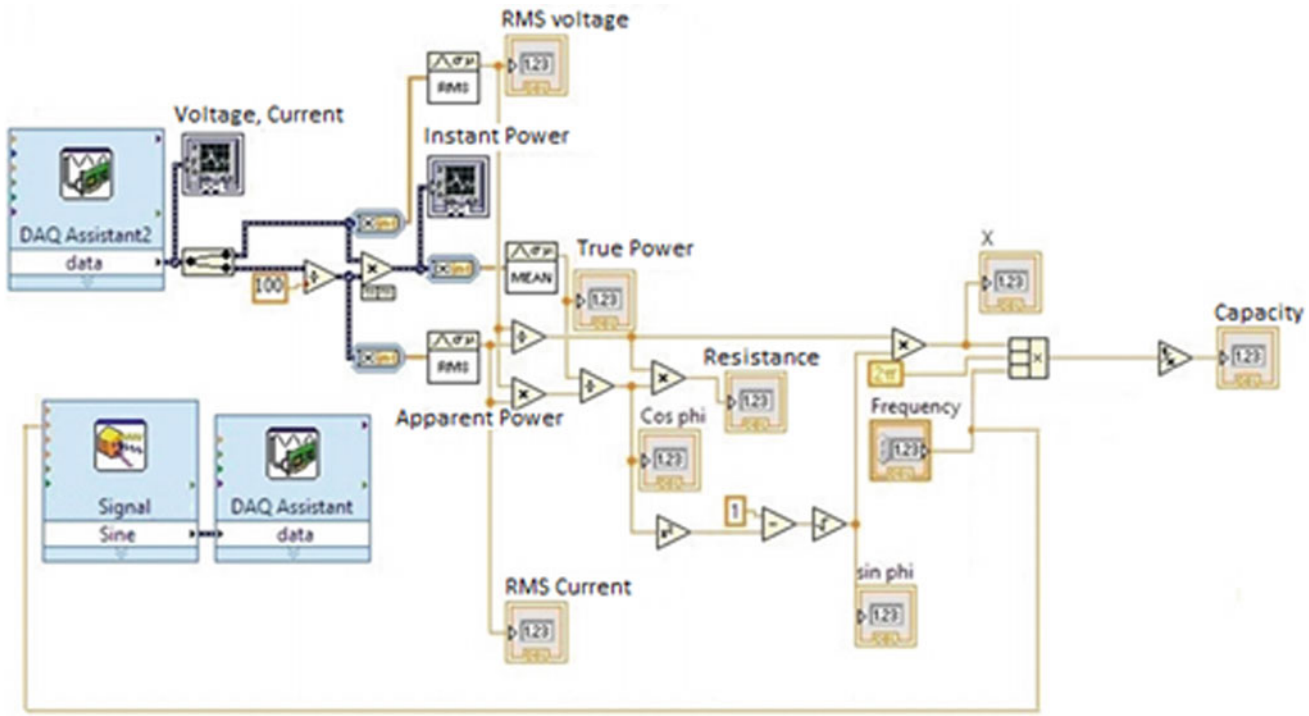

Fig. 5 Block diagram of the application

Table 1 Measurements performed on a subject with four and two electrodes

Electrode numbers	Frequency (Hz)	R_S (KΩ)	C_S (nF)	R_P (kΩ)	C_P (nF)
4 wire	100	46	24	130	16
	1000	6	9	47	9
2 wire	100	58	24	135	12
	1000	7	10	50	8

4 Conclusions

In Fig. 3, a four-wires impedance measurement method was proposed in order to eliminate the influence of the contact electrode resistance.

Impedance measurement gives information about the resistance and capacity of a human body. Using clinical tests, one can determine what information are significant regarding the measured capacity.

The LabVIEW programming environment offers many features that greatly facilitate numerical processing. The equations presented in the paper can be implemented on a microcontroller, and in consequence portable and low cost devices can be developed.

Conflict of Interest The authors declare that they have no conflict of interest.

References

1. Dawson, M.E., Schell, A.M., Filion, D.L.: The electrodermal system. In: Handbook of Psychophysiology, Cambridge University Press (2007)
2. Taji, B., Chan, A.D.C., Shirmohammadi, S.: Effect of pressure on skin-electrode impedance in wearable biomedical measurement devices. IEEE Trans. Instrum. Meas. **67**(8), August (2018)
3. Tebrean, B., Silaghi-Dumitrescu, R., Crişan, T.E.: Modelling of the coplanar capacitors for dermal or transdermal drug delivery system monitoring. In: Proceedings of the Romanian Academy, Series A, vol. 14, nr. 2/2013, pp. 134–143. ISSN: 1454-9069
4. David, V., Sălceanu, A., Creţu, E.: Măsurări în biomedicină şi ecologie. Aplicaţii,. Editura Setis, Iaşi. ISBN 973-86764-3-6 (2005)
5. Todoran, G., Munteanu, R.A., Holonec, R., Copindean, R.: Measurement of series circuit parameters Z, R, L, C by multiple synchronous detection method. Acta Electronica **48**(1), 64–70 (2007), Cluj-Napoca, Romania. ISSN 2344-5637, ISSN-L 1841-3323
6. Miron, M., Miron, L.: Masurari Electrice si Electronice, Editura Academiei Forfelor Aeriene "Henri Coanda" Brasov (2003). ISBN 973-8415-13-6
7. Antoniu, M., Antoniu, E., Poli, Ş.: Măsurări electronice, vol. 2. In: Satya (ed.) Aparate şi sisteme de măsură numerice, Iaşi. ISBN: 9739794548 (2001)
8. Copindean, R., Munteanu, R.A., Maier, M., Iudean, D.: Considerations regarding the determination of active and reactive power in three-phase circuits using Hilbert dephasing operator. In: Conference: 2017 International Conference on Modern Power Systems (MPS), Cluj-Napoca, Romania Publisher: IEEE. https://doi.org/10.1109/mps.2017.7974452
9. NI PCI-6110/6111 Specifications, User Manual Mulitfunction I/O Devices for PCI Bus Computers, National Instruments Corporation, http://www.ni.com/pdf/manuals/370980a.pdf
10. National Instruments—LabVIEW, Getting Started with LabVIEW, June 2013, 373427 J-01

Monitoring of Obstructive Sleep Apnea Using Virtual Instrumentation Techniques

R. Holonec, S. Vlad, A. I. Roman, and L. Rápolti

Abstract

People spend a third of their life sleeping. It is essential for a good health and indispensable for the good functioning of the human body to maximize its physical and mental capacity. In the last years there was a significant increase in sleep disorders that have a big impact on people's life quality. One of these disorders is sleep apnea, which is often not diagnosed and is common between children and adults too. Apnea is characterized by periods of breathing interruption. The most common form of sleep apnea, called obstructive sleep apnea (OSA), is caused by partial or complete obstruction of the patient's upper airways. Normally, at each inspiration, the pressure in the upper airways decreases under atmospheric pressure, creating a tendency for collapse of the upper airways. The main aim of this paper is to design a LabVIEW based system for monitoring and detecting an episode of sleep apnea based on biomedical signals taken from different sensors.

Keywords

Obstructive sleep apnea • ECG • SpO_2 • Respiratory rate • Signal processing • Virtual instrumentation • LabVIEW

1 Introduction

Sleep is a normal recurring and reversing physiological state, characterized by the temporary suspension of consciousness, by relatively inhibited sensory activity, by slowing down the vital organ functions like respiratory rhythm and heart rate, by muscle relaxation and dropping of the body temperature (about 0.5 °C). During the sleep, the relationship with the environment is suppressed but the vegetative functions remain intact. Sleep allows the restoration of the body's energetic and functional potential in order to resume its normal activity as it's waking [1].

One of the reasons for which sleeping hours are important for a person is that in this period, the brain is cleansed of toxins accumulated during daytime. Sleeping is also essential for regeneration of heart muscles, blood vessels, tissues and cells. The duration of sleep has a big influence on the immune system.

A restful sleep should have an optimal duration that varies with the age and respects a structure represented on average by five cycles of 90 min. Each cycle is structured in several stages, according to the criteria of Rechtschaffen and Kales [2].

From the ventilation point of view, sleeping, as a whole, is usually accompanied by hypoventilation regardless of its stages. During normal sleep up to five respiratory events may occur without any pathological significance. Respiratory dysfunctions refer to a wide variety of abnormal respiratory cycles. Although these dysfunctions mainly appear only when the patient is sleeping, it could also appear when the patient is awake. If the number of these respiratory breaks increase it will increase the number of repeated sudden awakes, sleep fragmentation and other symptoms and complications [2].

Sleep apnea syndrome could appear at any age and affects 4% of the male population, 2% of female population and 0.7% of children. Besides apnea, there are other types of breathing disorders including hypopnea, tachypnea, hyperpnoea and dyspnea. For example, hypopnea, that is very similar with apnea, means low or shallow breathing. Hyperpnoea on the other hand is characterized by heavy and rapid breathing.

R. Holonec (✉) · S. Vlad · L. Rápolti
Electrical Engineering Faculty, Technical University, Cluj-Napoca, Romania
e-mail: rodica.holonec@ethm.utcluj.ro

A. I. Roman
Regional Gastroenterology Institute, Cluj-Napoca, Romania

S. Vlad and N. M. Roman (eds.), *6th International Conference on Advancements of Medicine and Health Care through Technology; 17–20 October 2018, Cluj-Napoca, Romania*, IFMBE Proceedings 71,
https://doi.org/10.1007/978-981-13-6207-1_14

There are different levels of sleep testing [3]. The standard test is the polysomnograph, that is very important to doctors for the treatment of patients with obstructive sleep apnea.

The detection and monitoring of OSA require, especially for portable devices, the measurement of at least three cardiorespiratory parameters [4, 5]. In this paper, a virtual instrumentation system is proposed in order to monitor a patient with OSA, by putting on the same front panel information about heart and lung activities: electrocardiogram (ECG), blood oxygen saturation (SpO_2) and breath rate. The advantage of the proposed system is that it can be anytime improved and optimized by adding other monitoring physiological parameters like electroencephalogram (EEG), electrooculogram (EOG) or other breathing characteristics.

2 System Description

For the implementation of the proposed system (Fig. 1), the following biomedical signals are considered relevant: the pulse, the ECG signal, the respiratory rate and the blood oxygen saturation (SpO_2). The signals are acquired and processed with the help of the LabVIEW programming environment from National Instruments.

2.1 The Hardware Structure

The system is implemented on the NI ELVIS II platform (National Instruments) and it comprises three main modules, each dedicated to the specific physiological parameters:

- The ECG module for monitoring the heart activity
- The breathing monitor module for breath rate measurement. A piezoelectric sensor was used for this purpose.
- The SpO_2 measuring module. The measurement of oxygen saturation in peripheral blood was made by using a two LEDs based system (with red and infrared light).

The connections of the main modules to the NI ELVIS II platform are illustrated in Fig. 2.

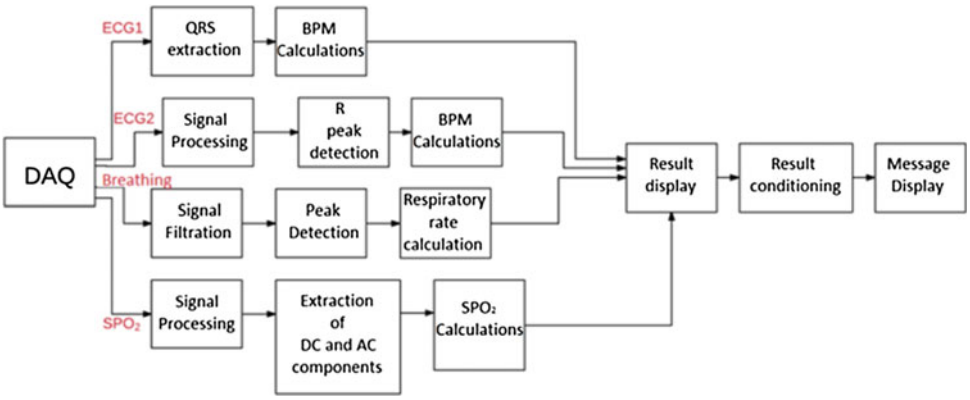

Fig. 1 System block diagram

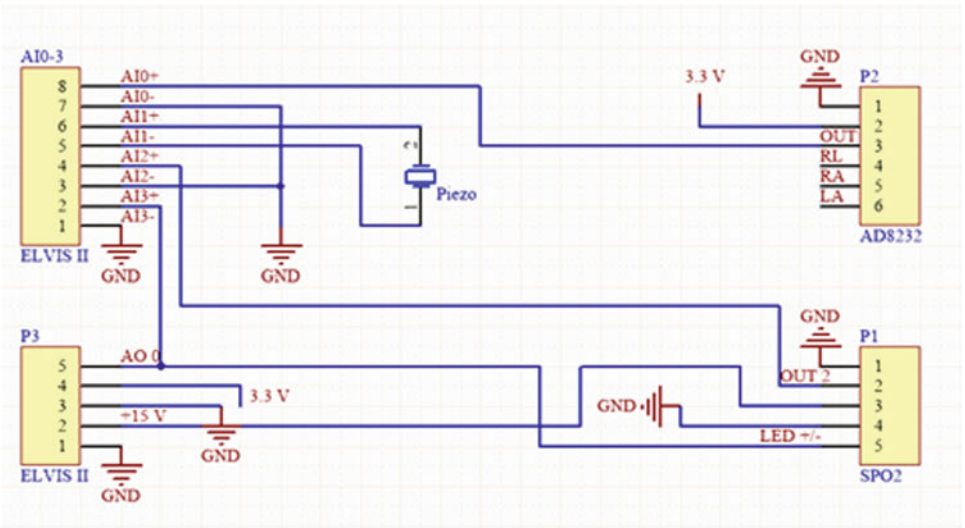

Fig. 2 The hardware configuration for OSA monitoring

2.2 The Heart Activity Monitoring

The AD8232 integrated module signal analyzer is used for the acquisition of the ECG signal. This module is designed to collect, amplify, and filter out low noisy biopotential signals.

For the acquisition of the ECG signal, in this application, the cardiac monitor configuration is used. The standard derivative system with three electrodes [6] is used by placing them as follows (Fig. 3):

- on the left side of the thorax between the ribs 2 and 3 representing the left arm (LA) (active electrode)
- on the right side of the thorax between the ribs 2 and 3 representing the right arm (RA) (active electrode)
- on the left side of the last pair of ribs (reference electrode).

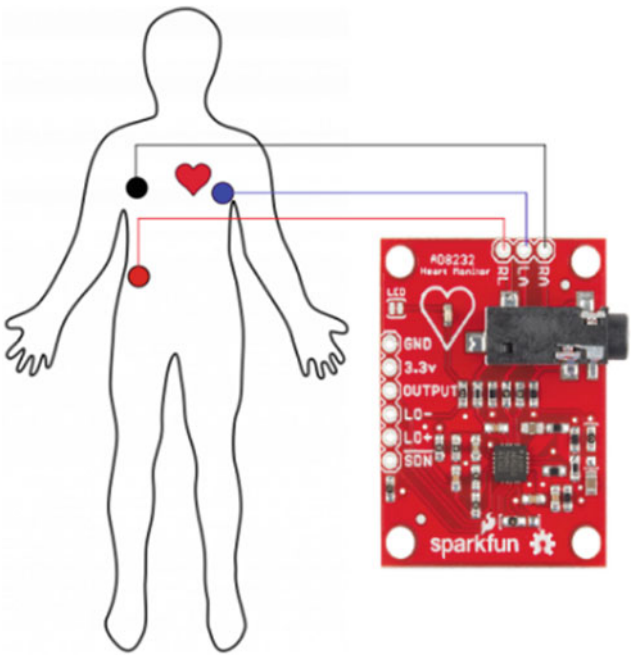

Fig. 3 The AD8232 sensor pads placements

2.2.1 The Respiratory Monitoring

For the respiratory rate monitoring, a piezoelectric sensor attached to an elastic strap (Fig. 4) is used [7].

By placing the sensor on the thorax, the respiration movements can be recorded (Fig. 5) and so the respiratory rate can be computed.

A supplementary method of breath monitoring is to use a simple microphone placed near the vocal cords, on the subject neck. The breath sounds associated with the inhalation and exhalation are also detected and recorded (Fig. 6).

2.2.2 The SpO_2 Monitoring

The purpose of pulse oximetry is to measure the percentage of oxygenated hemoglobin (HbO_2) to the total hemoglobin (Hb) (oxygenated plus deoxygenated) in the arterial blood [8]. The measurement method is an optical having the advantages of non-invasive techniques [9]. For monitoring the pulse oximetry, a light emitter-receiver sensor, placed on the subject finger, was implemented.

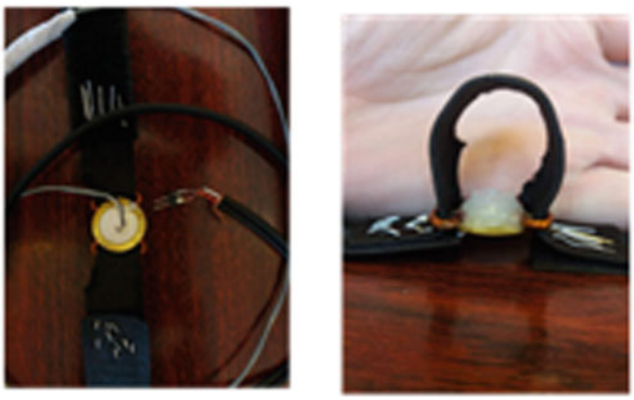

Fig. 4 Respiratory rate sensor

Fig. 5 The respiratory signal

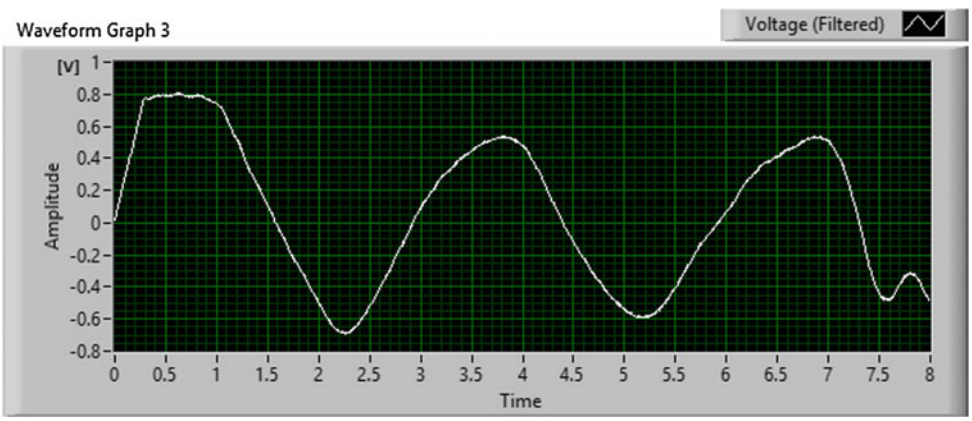

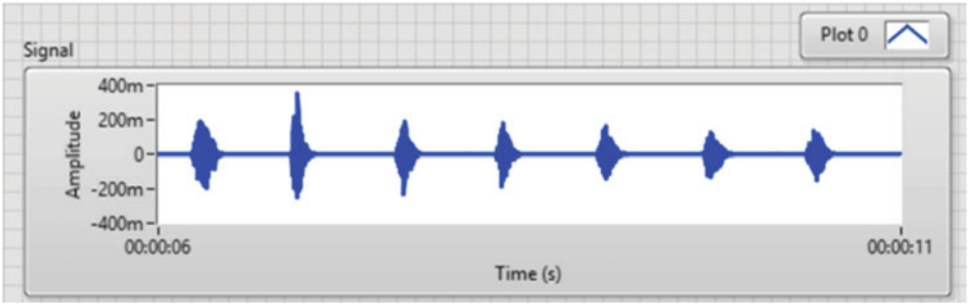

Fig. 6 The recorded breath sound

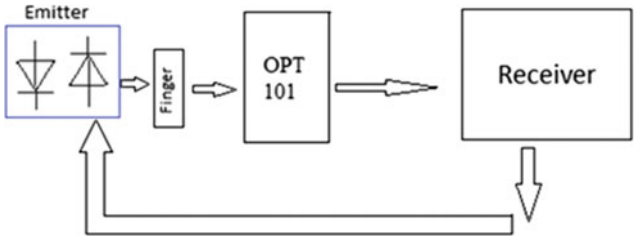

Fig. 7 Block diagram of the SpO_2 monitoring module

The emitter uses one red LED and one infrared LED that transmit the light to the photodetector by using the transmission method. The receiver is an OPT 101 integrated circuit (Fig. 7).

The LEDs from the SpO_2 sensor are placed in a single capsule and they are controlled by NI Elvis II acquisition platform on analog output AO0. The control signals are pulse width modulated (PWM) waveforms and they have a duty cycle of 25%.

The signals acquired by the receiver are known as the photoplethysmogram (PPG) signals (Fig. 8). PPG signals (red and infrared) can give information about the periodicity of the pulse rate and about the value of SpO_2.

The value of SpO_2 is computed with relation (1):

$$SpO_2 = A - B * R \tag{1}$$

The A and B coefficients are computed using multiple calibrations and the ratio R is computed with:

$$R = \frac{\frac{AC_R}{DC_R}}{\frac{AC_{IR}}{DC_{IR}}} \tag{2}$$

where:

AC_R and AC_{IR} is the pulsatile component (AC) of the Red and Infrared PPG signal

DC_R and DC_{IR} is the non-pulsatile (DC) component of the Red and Infrared PPG signal.

2.3 Software Implementation

For monitoring the obstructive sleep apnea, an application has been developed in the LabVIEW environment. The biosignals acquired from the ECG, breath and SpO_2 sensors are processed and displayed on the front panel of the program (Fig. 9). The signals are processed by using specialized virtual instruments from the "Biomedical Toolkit".

The ECG signal is passed through the "Feature Extractor.vi" and "Calculate ECG Features Stats.vi" in order extract the QRS complex and the heart rate.

To determine the respiratory rate, the acquired signal from the piezoelectric sensor was first filtered with a low pass filter and then it has been normalized (−1 and 1). The "Peak Detector.vi" is used to detect the peaks that represent the moments of inhalation. Calculation of the breathing rate is achieved by counting the inhalations over a 10 s period.

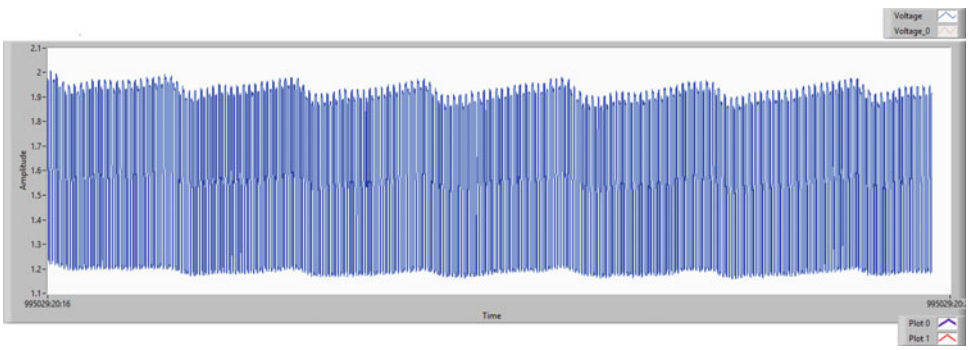

Fig. 8 PPG measured signal

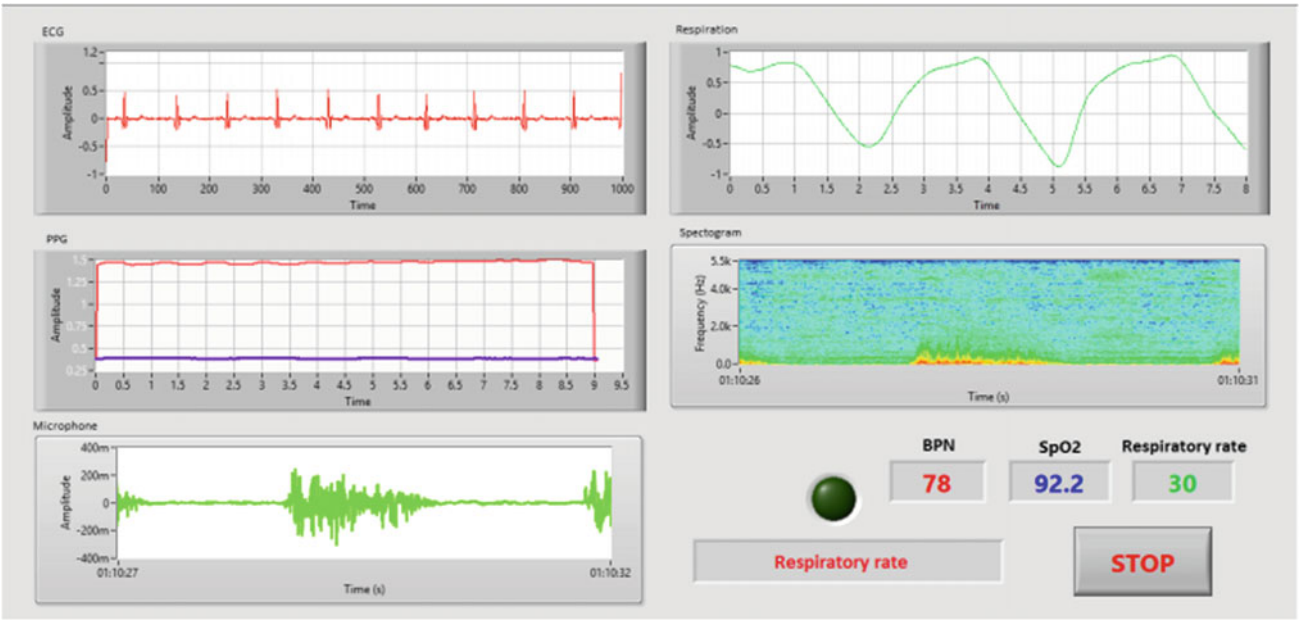

Fig. 9 Front panel of the virtual instrument

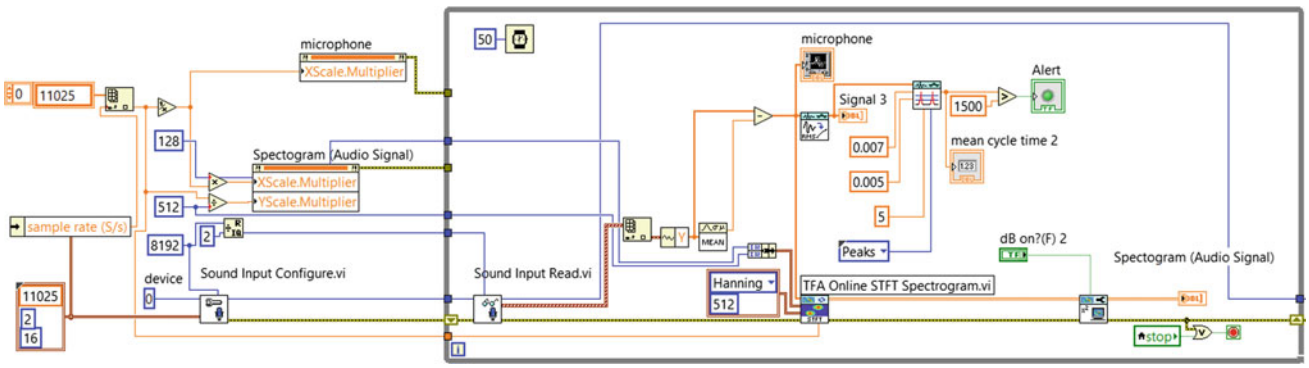

Fig. 10 Respiratory rate computation using the microphone signal

A supplementary method for determining the respiratory rate was implemented by using a microphone placed next to the piezoelectric sensors on the same elastic strap. The acquired signal is displayed in a waveform graph and on a spectrogram. The last was obtained by using the "TFA Online STFT Spectrogram.vi". The computation of short-time Fourier transform (STFT) uses a 512 Hanning window length, 128 time steps and a 512 FFT block size as indicated in Fig. 10. The alarm level for respiratory rate was established first by eliminating the DC component and then by applying the "Biosignal Rate Extractor.vi" that computes the cycle of the spiky-type signal.

The PPG signals and the computed SpO_2 values are also displayed on the front panel.

The application was tested on 20 healthy people in order to optimize the signals acquisitions and proceedings. These people simulated the behavior of patients having OSA. Inform consent was obtained from all the participants. By processing these signals experimental sleep apnea alerts were established. Therefore, the user of this application can monitor obstructive sleep apnea having visual and quantitative information about the patient sleep quality.

3 Conclusions

The proposed paper aimed to study and implement a system for monitoring obstructive sleep apnea (OSA) by developing an experimental device that uses virtual instrumentation principles. Three type of sensors were used: ECG, breathing and SpO_2. A user-friendly interface was implemented in such a manner that the supervising staff could read and

determine accurately the state of a patient. In the future a classifier including significant features from all acquired signals can be developed. The proposed system can be improved for a portable solution. The sensors can be also miniaturized and integrated into textiles.

Conflict of Interest The authors declare that they have no conflict of interest.

References

1. Rechtschaffen, A., Kales, A. (eds.): A Manual of Standardized Terminology, Techniques and Scoring System of Sleep Stages in Human Subjects. Brain Information Service/Brain Research Institute, University of California, Los Angeles (1968)
2. Goodday, R.H.B.: Obstructive sleep apnea syndrome: diagnosis and management. J.-Can. Dental Assoc. **67**(11), 652–658 (2001)
3. Canadian Sleep Society, Blackman, A., McGregor, C., Dales, R., Driver, H.S., Dumov, I., et al.: Canadian sleep society/canadian thoracic society position paper on the use of portable monitoring for the diagnosis of obstructive sleep apnea/hypopnea in adults. Can. Respir. J. **17**(5), 229–232 (2010)
4. Crupi, R., Faetti, T., Paradiso, R.: Preliminary evaluation of wearable wellness system for obstructive sleep apnea detection. In: The 37th Annual International Conference of the IEEE Engineering in Medicine and Biology Society (EMBC) (2015)
5. Kushida, C., Littner, M., Morgenthaler, T., Alessi, C., Bailey, D., Coleman, J.J., Friedman, L., Hirshkowitz, M., Kapen, S., Kramer, M., LeeChiong, T., Loube, D., Owens, J., Pancer, J., Wise, M.: Practice parameters for the indications for polysomnography and related procedures: an update for 2005. Sleep **28**(4), 499–521 (2005)
6. Chowdhury, M.H., Hossain, Q.D., Saha, P., Rahaman, M.M.: Design, Fabrication and Performance Evaluation of a Three Electrode ECG Recorder
7. Bhaskar, A., Subramani, S., Ojha, R.: Respiratory belt transducer constructed using a singing greeting card beeper. Adv. Physiol. Educ. **37**(1), 117–118 (2013)
8. Crisan, S., Tebrean, B.: Low cost, high quality vein pattern recognition device with liveness detection. Workflow and implementations. Measurement **108**, 207–216 (2017). Elsevier
9. Iudean, D., Munteanu, R., Jr., Bindea, E.M., Muresanu, D.F., Selejan, O.: Low cost prototype for viewing a map of vascularization. In: IFMBE Conference, 5th International Conference on Advancements of Medicine and Health Care through Technology—(MediTech2016), pp. 89–94, Cluj-Napoca, Romania, July 26–29, 2016

Application for Detection of Epileptic Seizures

R. Holonec, S. Vlad, and L. Rapolti

Abstract

Epilepsy is a neurological disease characterized by the presence of one or more seizures. The patient has different symptoms but the worst of them are the convulsions. This disease is marked by a variety of disorders that reflect brain dysfunction having different causes [1, 2]. In young children, epilepsy is often attributed to birth trauma, congenital abnormalities or genetic disorders and in adults to cerebral vascular accidents, tumors and cerebrovascular diseases. Epilepsy imposes on individuals and their families a tremendous physical, psychological and social effort. Early detection of this disorder is very helpful. The aim of this application was to design a low cost-system for monitoring an epileptic episode based on measured bio-parameters like temperature and wrist motion. The proposed system is implemented using a bracelet equipped with sensors connected to an Arduino board that transmits the signals to a smartphone where an Android application runs.

Keywords

Epileptic seizure • Accelerometer • Signal processing • Android

1 Introduction

Epileptic convulsions are defined by paroxysmal events of transient alteration of consciousness or by other signs or symptoms that may be given by brain dysfunction. Epileptic seizures are convulsive events accompanied by excessive and abnormally synchronized neuronal electrical changes that can be seen on the electroencephalogram (EEG). When the affected brain area is limited, they are called partial or local seizures. When both brain hemispheres are affected simultaneously, on wide surface, with the loss of consciousness, they are called generalized seizures.

There are situations when with no electrical changes in the brain but people have all the symptoms common with epilepsy seizures. Non-epileptic seizures have no identifiable physical cause, but they are believed to be physical reactions to psychological stresses.

Epileptic seizure detection systems are generally based on physiological and inertial changes that occur during the crisis. These changes can be detected in electrocardiogram (ECG), heart rate, pulse, respiration, electrodermal activity, pulse oximetry (SpO2), blood pressure, skin temperature, electromyogram (EMG), accelerometer, gyroscope or magnetometer sensors [3, 4]. There are several types of generalized seizures like clonic, tonic, tonic-clonic, myoclonia, absence, and atonic. Tonic-clonic seizures are characterized by strong involuntary muscle contractions when arms become almost rigid or by uncontrolled jerking movement. At the same time heart beats are accelerated, breathing can stop because of the diaphragm that is contracted. The seizures can evolve in the clonic phase with rhythmic muscle contractions. Intense incontinence and perspiration can occur. Generalized tonic-clonic seizure can also cause a change in body temperature [5]. All these external manifestations take place in addition to the internal ones at the cerebral level.

Acute symptomatic crises are generally tonic-clonic seizures that occur in the absence of epilepsy in response to a wide range of symptoms such as hyponatremia and other disorders like fever in infants and young children.

In order to minimize the consequences of the epileptic seizures, there are devices capable to detect ongoing crises and to provide notifications to the patient relatives or clinicians. The existing detection systems use the inertial signals

R. Holonec (✉) · S. Vlad · L. Rapolti
Electrical Engineering Faculty, Technical University, Cluj-Napoca, Romania
e-mail: rodica.holonec@ethm.utcluj.ro

S. Vlad and N. M. Roman (eds.), *6th International Conference on Advancements of Medicine and Health Care through Technology; 17–20 October 2018, Cluj-Napoca, Romania*, IFMBE Proceedings 71,
https://doi.org/10.1007/978-981-13-6207-1_15

and muscular activities. But there are systems that combines information from multiples sensors like: electromyogram type, 3D accelerometer or 3D gyroscopes [3]. There also combinations of the responses of these sensors with electroencephalogram (EEG) recordings [6, 7].

Closed loop systems built around epileptic seizures are also able to provide rapid therapies in response to early onset clinical crises, thus limiting complications or potentially stopping their spread [8]. A seizure/convulsion detection system must be able to determine the presence or absence of ongoing seizures [9]. The development of a system for detection and prediction algorithms involves three phases:

- preprocessing and filtering of sensors output signals
- processing and analyzing of acquired and conditioned signals
- alerting and convulsions reduction actions.

Each of these phases represents a challenge researching and implementation of a performant epileptic seizure detection system.

2 System Description

The electronic system presented in the paper is a low cost portable device that detects early the epileptic seizures (Fig. 1). The device uses human body movements and temperature changes to detect the onset of an epileptic seizure. As soon as the device detects change in sensors output, it sends a coded signal to the user's phone. This signal is decoded, analyzed and, when is necessarily, a sound alarm is activated and notifications are sent.

2.1 The System Hardware Structure

The hardware structure of the designed system (Fig. 2) consists of the following components:

- Arduino Nano with ATmega328
- Bluetooth module HC-06 type
- Three-axis accelerometer ADXL335 type,
- Temperature sensor LM35 type
- Buzzer device.

The Arduino module was programed so it can read all the data provided by the sensors (accelerometer and temperature sensor) and to transmit all the data via Bluetooth to the user's mobile device. To fit all the sensors on a wrist, a Velcro tape was used (Fig. 3). The components where positioned in such a manner so they would have the maximum efficiency possible. The temperature sensor was placed as close as possible to the wrist, so it could read a more accurate temperature. Next to the temperature sensor the accelerometer was placed so it could detect the wrist actigraphy.

2.2 The Software Implementation on Arduino Nano Device

The programming of the Arduino Nano was made by using the Arduino IDE software. The program implemented has the capabilities to read all the sensors and to transmit data through the Bluetooth unit, but also it has a debugging function for analyzing the data that is read from the sensors. The debugging function is necessary for sensors calibration

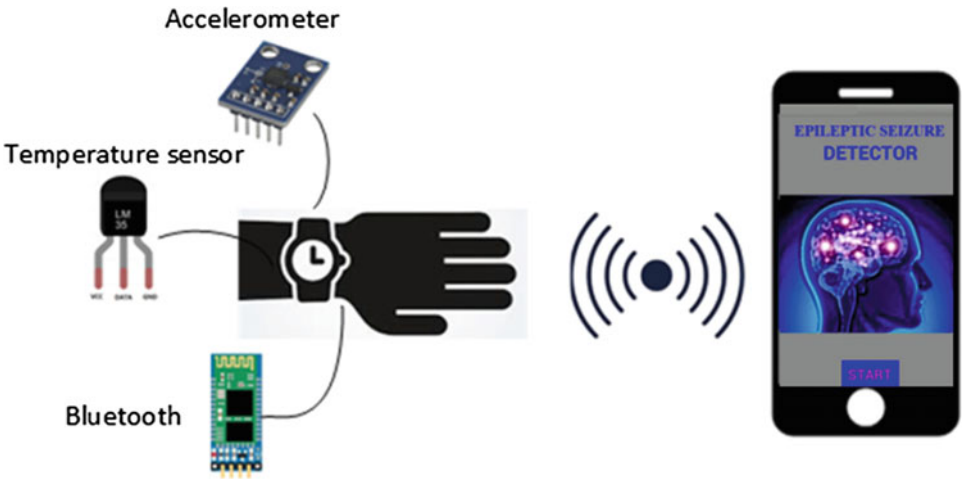

Fig. 1 Portable low-cost epileptic seizure detection system

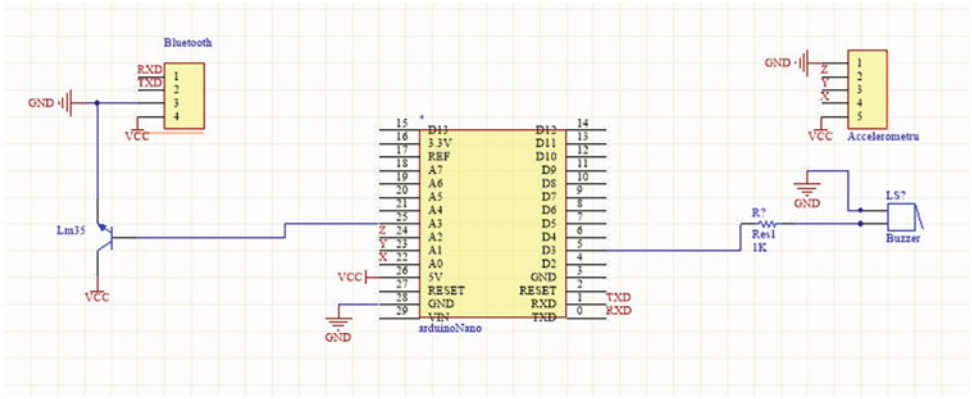

Fig. 2 The system hardware configuration

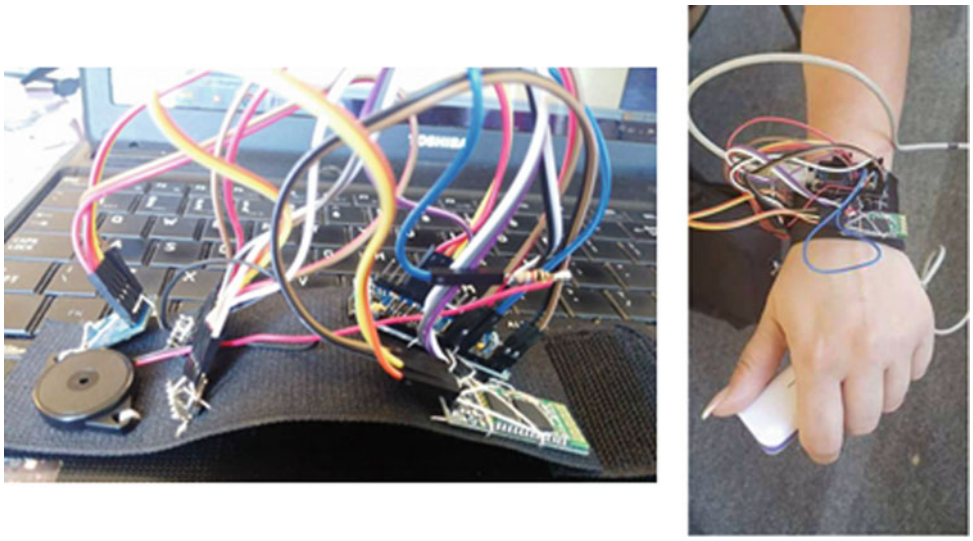

Fig. 3 The sensors placement on the bracelet

and positioning. The data that is transmitted by the Bluetooth module works with a baud rate of 9600. All the data is transmitted serial from the Arduino board to the Bluetooth module, which will encode the data and transmit it to the Android application. The software helps to detect the motion of the person that wears the bracelet. When this user falls down or any convulsions take place, the software sends a warning signal to the Android application and sounds a buzzer present on the bracelet. The threshold conditions for accelerometer output signals where found by simulating seizure body movements. The data collected from temperature sensor was used to implement a separate algorithm for detecting a threshold where the sudden variations of temperature must be taken into account.

2.3 The Software Implementation on Android Platform

The software implementation of the proposed system on android platform was made by using AppInventor, an open source web application originally provided by Google and now updated by the Massachusetts Institute of Technology (MIT). The application, allows newcomers to create software for the Android operating system (OS). It uses a graphical interface very similar to the Scratch which allows the user to drag and drop visual objects to create an application that can work on Android devices.

The first screen of "Epileptic Seizure Detector" App is illustrated in Fig. 4.

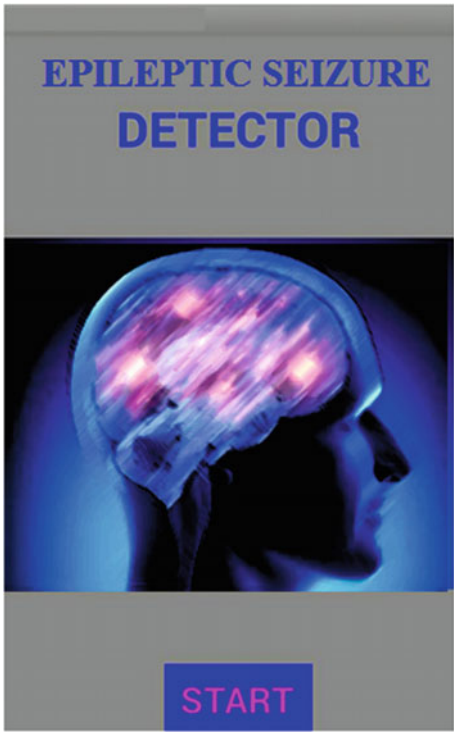

Fig. 4 Epileptic Seizure Detector application

The application needs an initial condition for working properly: the user's phone must have its Bluetooth connectivity activated, otherwise it could not connect to the Arduino Nano. By checking for the existing connections, it prompts the user to select the available Bluetooth adapter from the Arduino. When passing to the second screen of the application (Fig. 5, left), the user can see the time and date and the sensors outputs values that are transmitted by the Arduino device.

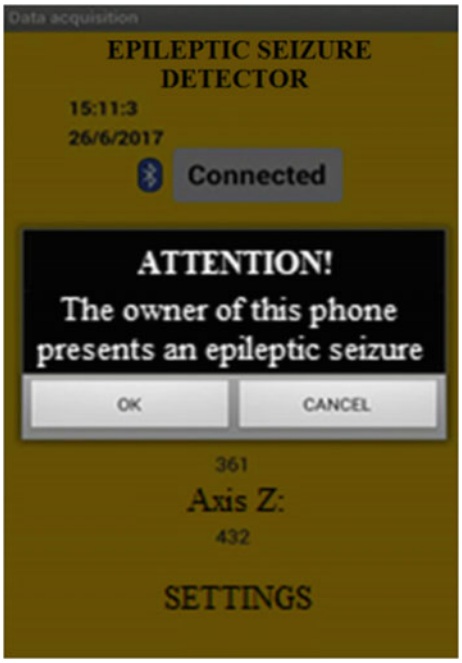

Fig. 6 Alert on the "Epileptic Seizure Detector" App

The application also has an implemented function, which sends an alarm message to any of selected contacts (Fig. 5, middle). This message can be personalized (Fig. 5, right). All of these can be set from the Settings button which is positioned on the second screen. The advantage of this feature is that any person knowing about your condition or even doctor could be notified to take the right precautions. In the case of an epileptic seizure the alarm signal transmitted from the Arduino via Bluetooth to the phone will show a pop-up massage with the message "Attention! The owner of this phone presents an epileptic seizure" (Fig. 6). The

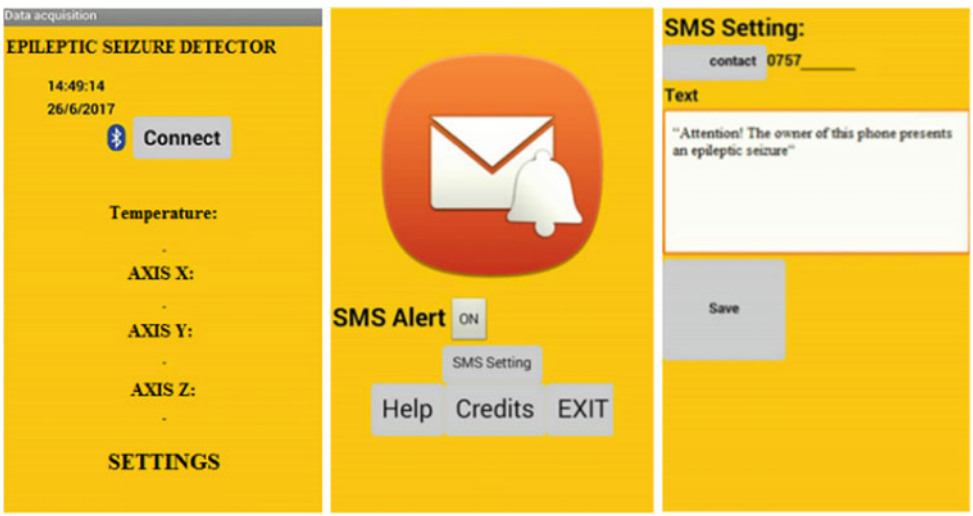

Fig. 5 The application screens and settings

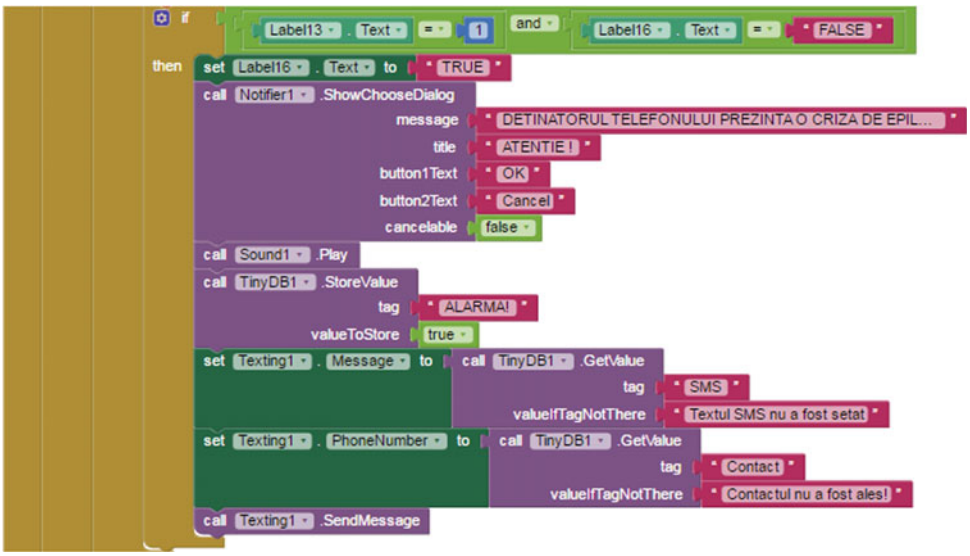

Fig. 7 App Inventor for "Seizure Epilepsy Detector" implementation

witnesses at the epileptic seizure will be also notified by a warning sound. When anybody presses the "OK" button, a list with instructions will be displayed. These instructions contain the minimum procedures that must be done for helping the person in need.

All the functions of the "Epileptic Seizure Detector" application where implemented with the help of App Inventor for Android (Fig. 7). This has several built-in features, easily accessible to the programmer, including the SMS transmitting, Bluetooth communication, database building or contact list accessing.

3 Conclusions

This paper describes a portable low cost system for detecting epileptic seizures. The detection circuit uses an Arduino board and it is designed to be placed on a bracelet and to communicate with an Android-based mobile phone. The Bluetooth module transmits the information to the application named "Epileptic Seizure Detector", which has been created for this purpose. The application is developed for data acquisition and alert messages. The epileptic seizure is detected by sensing the wrist movements with the help of a three-axis accelerometer (x, y, z) and a temperature sensor that detects the changes in body temperature.

The proposed system is a simple one having the advantage that the person that is wearing perceives it more as a clothing accessory than a medical device.

The bracelet can also be used without a smartphone, because the buzzer device is mounted on it and sends an alarm sound anytime when an epileptic seizure take place.

In the future, the application could be developed by adding on the same bracelet a gyroscope or a patient GPS location system and consequently a classifier including the significant features representing an epileptic seizure.

Conflict of Interest The authors declare that they have no conflict of interest.

References

1. Conradsen, I.: Detection of Epileptic Seizures with Multi-Modal Signal Processing. Dissertation DTU Elektro (2013)
2. Poh, M.-Z.: Continuous Assessment of Epileptic Seizures With Wrist-Worn Biosensors. Dissertation Massachusetts Institute of Technology (2011)
3. Gheryani, M., Salem, O., Mehaoua, A.: Detection of nocturnal epileptic seizures from wireless inertial measurements and muscular activity. In: IEEE Global Communications Conference, GLOBECOM, Singapore, 2017
4. Ulate-Campos, A., Coughlin, F., Gaínza-Lein, M., Sánchez Fernández, I., Pearl, P.L., Loddenkemper, T.: Automated Seizure Detection Systems and Their Effectiveness for Each Type of Seizure, Seizure, Elsevier, vol. 40, pp. 88–101, August 2016
5. Sharvon, S., Guerrini, R., Cook, M., Hatoo, S.L.: Oxford Textbook of Epilepsy and Epileptic Seizures. Oxford University Press (2012)

6. Nijsen, T.M., Arends, J.B., Griep, P.A., Cluitmans, P.J.: The potential value of three-dimensional accelerometry for detection of motor seizures in severe epilepsy. Epilepsy Behav. **7**, 74–84 (2005)
7. Teohari, V.-M., et al.: Epilepsy seizure detection app for wearable technologies. In: Conference Proceedings AmI (2014)
8. Ramgopal, S., et al.: Seizure detection, seizure prediction, and closed-loop warning systems in epilepsy. Epilepsy Behav. **37,** 291–307 (2014)
9. Ramirex-Alaminos, J.-M., Sendra, S., Lloret, J., Navarro-Ortiz, J.: Low-cost wearable bluetooth sensor for epileptic episodes detection. In: IEEE ICC 2017—SAC Symposium E-Health Track

Exposure to UHF Electromagnetic Radiation in Urban Areas

A. Pastrav, P. Dolea, E. Puschita, C. Codau, T. Palade, and I. Palade

Abstract

Employing various wireless technologies in everyday activities has increased the quality of life, exposing us to an increasing amount of electromagnetic radiation. In urban areas the electromagnetic pollution is more significant for the common mobile communication frequency bands because of the multitude of base stations deployed to serve a large amount of users. As such, when deploying new telecommunication sites, the operators must comply with the regulations and be aware of the existing EM background. This paper presents an overview of health risks for these frequency bands and focuses on the evaluation of the electromagnetic radiation while performing a measurement campaign in the central area of Cluj-Napoca for the 700–1000 MHz frequency range.

Keywords

Electromagnetic pollution • Electromagnetic radiation • Spectrum analyzer

1 Introduction

From low frequencies (1 Hz–100 kHz) used in power lines, electric appliances and electronic devices, to high frequencies (100 kHz–300 GHz) in telecommunications, to infrared radiation (780 nm–1000 μm) in heating devices, to ultra violet radiation (100–400 nm) in sunbeds, or X-rays (0.01–10 nm) in medical imaging and gamma rays in irradiation, we make use of the electromagnetic (EM) radiation to improve the quality of life. As such, their effect on health and environment has been vastly studied in order to limit the damage they may cause and ensure the safe usage in every-day activities.

Given the amount of energy they carry, X and gamma rays are included in the ionizing part of the EM spectrum, being able to remove electrons from atoms and posing the bigger health risk. The lower frequency bands (e.g. radiowaves, microwaves, infrared, visible light) are included in the non-ionizing radiation (NIR) category as the EM waves cannot ionize (except for part of the UV). However, NIR may still damage the body if used improperly.

International agencies and organizations published guidelines regarding exposure to NIR, including basic restrictions and maximum permissible exposure levels to minimize the impact on our health.

The technological boom in wireless communications increased the EM pollution in the Ultra High Frequency (UHF) band (300 MHz, 3 GHz), especially in the urban areas where the number of users is high and more base stations have to be deployed.

As such, this paper aims at briefly presenting the exposure risk assessed by the scientific community and some limitations indicated by international standards for the common mobile communications band. Moreover, to provide a more realistic view on the EM pollution and the exposure level in central area of Cluj-Napoca, Romania, a measurement campaign is conducted to determine the strength of the electromagnetic field (EMF) in the 700–1000 MHz frequency range.

The remainder of this paper is organized as follows. Section 2 presents the health risks of exposure to NIR, emphasizing on radiofrequency (RF) and the UHF band and indicates the most widely used standards regarding NIR exposure. Section 3 describes the measurement campaign employing the Rohde & Schwarz FSH Spectrum analyzer while Sect. 4 presents the measurement results. Section 5 concludes the paper.

A. Pastrav (✉) · P. Dolea · E. Puschita · C. Codau · T. Palade
Communications Department, Technical University of Cluj-Napoca, Cluj-Napoca, Romania
e-mail: Andra.PASTRAV@com.utcluj.ro

I. Palade
"Iuliu Hatieganu" University of Medicine and Pharmacy, Cluj-Napoca, Romania

S. Vlad and N. M. Roman (eds.), *6th International Conference on Advancements of Medicine and Health Care through Technology; 17–20 October 2018, Cluj-Napoca, Romania*, IFMBE Proceedings 71,
https://doi.org/10.1007/978-981-13-6207-1_16

2 Health Effects of Non-ionizing Radiation

Given the amount of EM sources that surround us, it is logical to be concerned and assess their effect on our health and on the environment.

Although not as harmful as the ionizing ones, the non-ionizing radiation can still have thermal effects on the biological tissue. Moreover, there is a general agreement that NIR may also cause non-thermal effects and studies have been conducted to evaluate the impact of NIR exposure.

While some studies do not provide compelling evidence of any effect [1], other studies present the danger of living in a highly EM polluted area, showing an increase in the cancer rate [2] or neurobehavioral malfunction [3].

Since NIR comprises a very large frequency range, the International Commission on Non-Ionizing Radiation Protection (ICNIRP) defines a number of sub-bands and identifies their specific effects on health, as follows [4].

Exposure to the low frequency (LF) fields leads to the generation of electric fields and currents inside the organism which may cause a range of effects from phosphenes, electric charging of the skin and tingling, to tissue burns [4]. Although some studies suggest a correlation between childhood leukemia and long-term exposure to 50–60 Hz magnetic field, the scientific evidence is not compelling and low-level LF exposure is not harmful [4].

Higher on the spectrum, exposure to High Frequency (HF) electromagnetic fields mainly causes heating of the tissue and may cause heatstrokes and burns if the thermal threshold is exceeded. Studies have been conducted to determine the effect of exposure below this threshold, evaluating the connection with health problems like headaches, concentration problems, sleep quality, cognitive function, or cardiovascular effects with no conclusive results other than a small effect on brain activity [4].

Depending on the duration and intensity, exposure to infrared radiation (IR) may result in thermal injuries. The damage to the skin may vary from mottling caused by long-term exposure to low intensity IR to burns caused by high intensity IR. Moreover, periodic exposure to extreme heat may damage the eyes considerably, as the heat causes aggregation of lens proteins, resulting in cataracts [4].

The visible radiation becomes harmful when exposing ourselves to extremely bright sources which may cause retinal burns and leading to vision loss.

Exposing the whole body to high doses of visible and infrared radiation may cause heat stress.

Exposure to UV radiation in small doses is healthy as it helps with Vitamin D synthesis. However, high levels of UV radiation damage the skin, from sunburns and skin wrinkling to several types of cancer (e.g. malignant melanoma) [4]. Eye cancer, cataract and retinal damage are also among the effects of long-term exposure to UV radiation.

Among these sub-bands, a particular interest has been shown for the HF range as the number of mobile phones and other wireless devices increased, raising awareness on the possible health risks. As such, more and more research focused on the exposure to UHF which includes most of the bands employed in cellular communications. An extensive number of experiments was conducted to evaluate the cancer occurrences in lab rats from exposure to RF and microwave radiation. The overview in [5] presents the methodology and the obtained results for more than 15 studies regarding rats exposed to lifelong RF and microwave radiation. While some results suggest a correlation between RF exposure and cancer, most of the findings showed no carcinogenic effect. Because of the flaws, inconsistencies and biases in the experiments, a decisive conclusion cannot be drawn [5].

Studies on humans had a similar outcome. Epidemiological studies looked into the risk of brain tumors and some of them reported a statistical increase for long-term heavy mobile phone users [4]. Groups like the Independent Expert Group on Mobile Phones (IEGMP) and Scientific Committee on Emerging and Newly Identified Health Risks (SCENIHR) [6] recommended more research and reviewed the existing scientific literature in order to determine if the use of mobile phones increases the cancer risk, without conclusive results.

The Interphone study [7, 8], the largest of this kind, coordinated by the International Agency for Research on Cancer (IARC) [9], started in 2000 and for a 5-year period analyzed the correlation between mobile phone usage and brain tumors in over 5000 patients. The results regarding acoustic neuroma [10], glioma and meningioma [11] suggest a reduced risk of brain tumor for phone users compared with non-users, but still leave room for debate.

However, that data referred to people who had been using mobile phones for up to 10 years and for far less applications than today's users. Not to mention that the devices have been improved since then to efficiently use the available resources (e.g. battery, bandwidth, frequency, power), making the task of monitoring the effects of RF exposure more difficult.

Whether or not long-term RF and microwave exposure causes cancer (especially brain tumors) remains controversial. However, IARC considered the evidence strong enough to take precocious measures and classify, in 2011, RF radiation as a possible carcinogen to humans.

To limit the possible adverse effects of NIR, and RF in particular, several protection guidelines and standards have been developed. The most popular [12] are the ICNIRP guidelines published in 1998 [13] and the IEEE standard for safety levels with respect to human exposure to radio

Table 1 ICNIRP SAR basic restrictions below 1 GHz

Service (Band)	Whole body average SAR (W/kg)	Localized SAR (head and trunk) (W/kg)	Localized SAR (limbs) (W/kg)	E-field strength (V/m)
FM broadcast (88–108 MHz)	0.08	N/A	N/A	28.0
Trunking (806–869 MHz)	0.08	2	4	40.0
Mobile telephony (824–894 MHz)	0.08	2	4	40.6
Mobile telephony (890–960 MHz)	0.08	2	4	41.0

frequency electromagnetic fields published in 2005 [14]. In the US, the limits proposed by the Federal Communications Commission (FCC) in 2006 [15] have the power of law.

ICNIRP closely monitors the effects of RF radiation on health and environment and periodically revises the exposure guidelines, the newest version (i.e. 2018) being available for public consultation. Table 1 shows the specific absorption rate (SAR) basic restrictions and Electric (E) field strength reference level for general public exposure to main communications frequency bands below 1 GHz [16].

3 Measurement Campaign in Cluj-Napoca

While most of the studies focused on the health effects of mobile phone usage, another aspect that needs to be considered is the exposure to RF radiation generated by the base stations that serve the users. The output power of a base station is small (i.e. 10–50 W [4]) compared to radio or TV broadcasting (i.e. kW to MW [4]) and the field strength decreases rapidly with the distance, however, the exposure to this radiation is continuous (unlike the exposure to mobile phone radiation which is limited) [4]. As such, to assess the level of radiation in urban areas, a measurement campaign was launched for the central region of Cluj Napoca.

The upper part of the sub-1 GHz band (>700 MHz) was considered because it is used in the deployment of most mobile cellular networks (2G, 3G, 4G).

3.1 Measurement Scenario

The map of Cluj-Napoca, occupies roughly a 100 km^2 area which can be divided in nine regions: Central, South-East, East, North-East, North, North-West, West, South-West and South of approximately 11 km^2 each. The Central region, being most crowded, contains a larger number of mobile communications cells served by a large number of base stations. As such, for a proper EMF evaluation, strategic measurement points have to be considered.

Dividing the Central Region into 16 equivalent rectangles results in smaller regions (i.e. approximately 0.69 km^2) which are comparable with typical cell dimensions (1–30 km for macro-cells, 200–2000 m for micro-cells, and 4–200 m for pico-cells). Performing EMF measurements in the centers of these 16 regions (in the locations marked in Fig. 1) should provide a realistic view on the EM pollution in the area.

Table 2 indicates the exact locations of the measurement points and the relevant characteristics of the area.

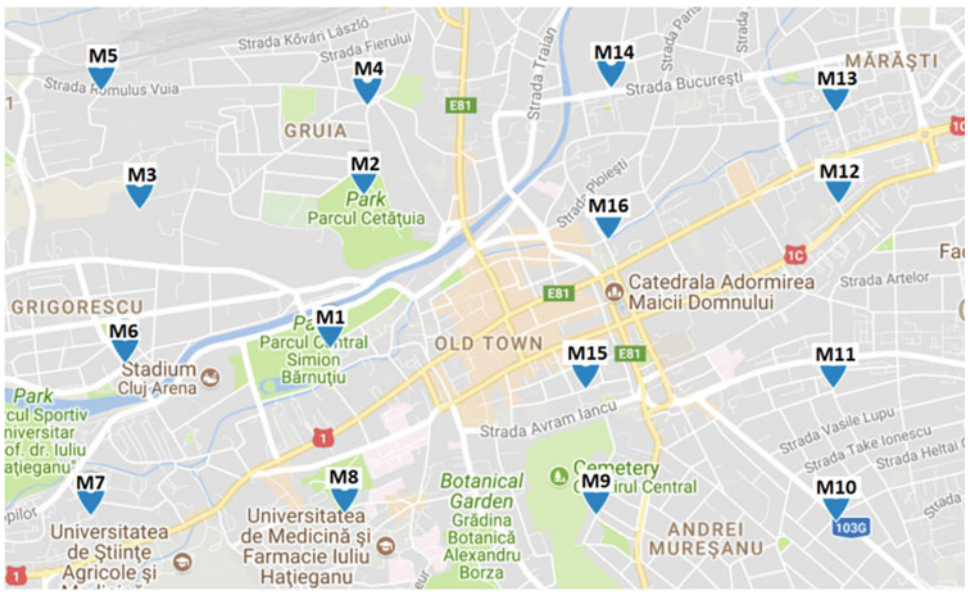

Fig. 1 Marked locations for the measurement points

Table 2 Locations of the 16 measurement points

Marker	Area properties	Latitude N	Longitude E	Altitude (m)
M01	Central Park	46.76966	23.57942	347
M02	panoramic view—touristic attraction	46.77586	23.58142	397
M03	Residential area	46.77527	23.56816	388
M04	Crowded intersection close to CFR Stadium	46.77948	23.58161	369
M05	Residential area	46.78007	23.56590	349
M06	Cluj Arena stadium and sports complex	46.76903	23.56731	340
M07	High rise buildings	46.76287	23.56528	364
M08	Student campus	46.76298	23.58027	376
M09	Residential area	46.76289	23.59516	390
M10	Residential area	46.76265	23.60933	364
M11	Residential area	46.76804	23.60915	359
M12	High-rise buildings	46.77550	23.60945	333
M13	Medium-rise buildings	46.77919	23.60931	332
M14	Oil station, medium- and high-rise office buildings	46.78019	23.59604	334
M15	University	46.76800	23.59454	349
M16	Hospital, school	46.77404	23.59588	339

4 The EMF Measurement System

For this measurement campaign, the R&S TS-EMF measurement system (illustrated in Fig. 2) which employs three main elements: the R&S FSH Spectrum analyzer, the isotropic antenna and the dedicated software specifically designed for EMF measurements [17] was used.

We focused on the 700–1000 MHz frequency range, defining a testing routine with 10 frequency sweeps within that band.

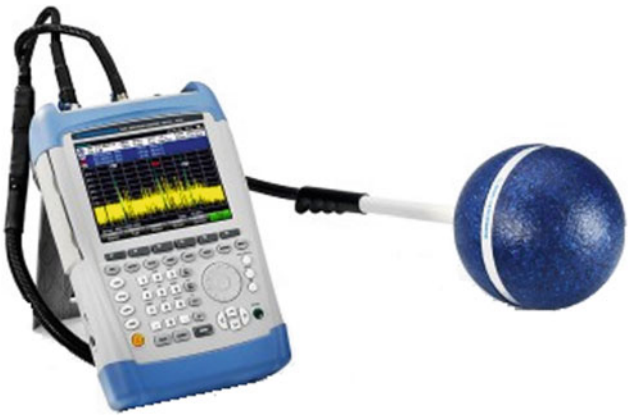

Fig. 2 R&S FSH Spectrum analyzer and 30 MHz–3 GHz isotropic antenna

5 Measurement Results

Figure 3 plots the frequency spectrum for the 16 locations presented above.

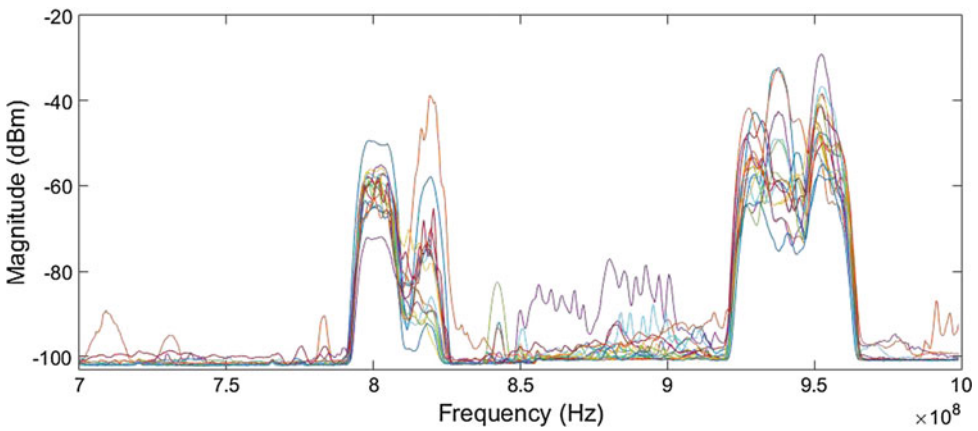

Fig. 3 Frequency spectrum for all 16 locations

According to these results the frequency bands 790–820 MHz (with the highest peak at −40 dBm) and 920–960 MHz (with the highest peak at −30 dBm in the student campus) present high EM activity, but within the ICNIRP limits. These bands correspond to mobile cellular networks providing voice/data services in the area, with LTE in the lower band and UMTS and GSM downlink in the higher band.

6 Conclusions

Exposure to EM radiation is inevitable and it must be closely monitored. This paper aimed at presenting the health risk of exposure to NIR and assess the level of EM radiation in Cluj-Napoca in the 700 MHz–1 GHz band (used for cellular mobile communications). The results show that in areas with a large number of users, the level is higher than in less crowded areas. However, the level is below the ICNIRP limit and it shouldn't be harmful to humans.

Acknowledgements This paper was partially supported by a grant of the Ministry of Innovation and Research, UEFISCDI, project number 6 Sol/2017 within PNCDI III, and by a grant of the Ministry of National Education and Scientific Research, RDI Programme for Space Technology and Advanced Research—STAR, project number 116/2016.

Conflict of Interest The authors declare that they have no conflict of interest.

References

1. Wolf, R., Wolf, D.: Increased incidence of cancer near a cell-phone transmitter station. Int. J. Cancer Prev. **1**(2), 123–128 (2004)
2. Vecchia, P., Matthes, R., Ziegelberger, G., Lin, J., Saunders, R., Swerdlow, A.: Exposure to high frequency electromagnetic fields, biological effects and health consequences (100KHz–300 GHz). Int. Comm. Non-Ionizing Radiat. Protect. (2009)
3. Abdel-Rassoul, G., Abou El-Fateh, O., Abou Salem, M., Michael, A., Farahat, F., El-Batanouny, M., Salem, E.: Neurobehavioral effects among inhabitants around mobile phone base stations. NeuroToxicology **28**(2), 434–440 (2007)
4. ICNIRP—The International Commission on Non-Ionizing Radiation Protection at https://www.icnirp.org/
5. Lin, J.C.: Cancer occurrences in laboratory rats from exposure to RF and microwave radiation. IEEE J. Electromag. RF Microwaves Med. Biol. **1**(1), 2–13 (2017)
6. Scientific Committee on Emerging and Newly Identified Health Risks (SCENTHR) at https://ec.europa.eu/health/scientific_committees/emerging_en
7. Interphone Study Group: Brain tumour risk in relation to mobile telephone use: results of the INTERPHONE international case-control study. Int. J. Epidemiol. **39**(3), 675–694 (2010)
8. Interphone Study Group: Acoustic neuroma risk in relation to mobile telephone use: results of the INTERPHONE international case–control study. Cancer Epidemiol. **35**, 453–464 (2011)
9. IARC at https://www.iarc.fr/
10. International Commission on Non-Ionizing Radiation Protection (ICNIRP): Guidelines for limiting exposure to time-varying electric, magnetic and electromagnetic fields (100 kHz to 300 GHz) Appendix B: Health Risk Assessment Literature ICNIRP at https://www.icnirp.org/en/activities/public-consultation/consultation-1.html (2018)
11. Swerdlow, A., Feychting, M., Green, A.C., Kheifets, L., Savitz, D. A.: ICNIRP SCI review: mobile phones, brain tumours and the interphone study: where are we now? Environ. Health Perspect. **119**(11), 1534–1538 (2011)
12. Lin, J.C.: Radio-frequency radiation safety and health: recent activities on radio-frequency exposure guidelines. URSI Radio Sci. Bull. **2014**(351), 73–74 (2014)
13. International Commission on Non-Ionizing Radiation Protection (ICNIRP): Guidelines for limiting exposure to time-varying electric, magnetic, and electromagnetic fields (Up to 300 GHz). Health Phys. **74**, 494–522 (1998)
14. Institute of Electrical and Electronic Engineers (IEEE): IEEE C95. l-2005—Standard for Safety Levels with Respect to Human Exposure to Radio Frequency Electromagnetic Fields, 3 kHz to 300 GHz. New York, IEEE Press (2005)
15. US Federal Communications Commission, Office of Engineering and Technology: Evaluating Compliance with FCC Specified Guidelines for Human Exposure to Radiofrequency Radiation. OET Bulletin 65, Washington, DC (1997)
16. Non-Ionizing Radiation Protection Standards and Policies at http://www.wireless-health.org.br/downloads/LASR2010-Protection Standards-Policies.pdf
17. User Manual for TS-EMF, Portable EMF Measurement System, Version 6.1.50, Rohde & Schwarz Test and Measurement Division, Munich (2010)

Monitoring of Cardiovascular Parameters During Rehabilitation After Stroke Event

Radu Ciorap, Doru Andritoi, Catalina Luca, and Calin Corciova

Abstract

The paper proposes a solution for monitoring of cardiovascular parameters during rehabilitation after stroke. Stroke is the most important cause of long-term disability in Europe. The effects of stroke can vanish after a short period or can remain for the rest of the life depending on therapeutic program. The system developed for this study is not only therapeutically devices that use virtual reality for rehabilitation exercises but also record one or more biomedical parameters such as: electromyogram (EMG), electrocardiogram (ECG), pulse wave, heart rate (HR), respiration rate or oxygen concentration in the blood (SpO_2). These physiological parameters are selected according to the physician's prescription and the patient needs. It was observed the cardiovascular system status, analyzing the heart rate variability. During therapeutic procedure it was recorded ECG (1 lead) and heart rate variability (HRV) was calculated. The results were used to determine the stress level induced by the rehabilitation program.

Keywords

Stroke • Rehabilitation • Biomedical parameters • Medical devices for home use • Virtual reality

1 Introduction

Cardiovascular disease (CVD) is the primary cause of death in many countries. Early detection of risk factors is important to establish preventive measures which may lead to reduced hospitalization costs [1].

R. Ciorap (✉) · D. Andritoi · C. Luca · C. Corciova
Faculty of Medical Bioengineering, "Grigore T. Popa" University of Medicine and Pharmacy, Universitatii 16, Iași, Romania
e-mail: radu.ciorap@bioinginerie.ro

According to the American Heart Association (AHA) the rate of death attributable to CVD is approximately 1 death every 39 s [2]. Cerebral vascular accident (CVA) or stroke is main complication of chronic cardiovascular diseases and it is one of the leading causes of morbidity and mortality worldwide. On average, every 40 s, someone in the United States has a stroke [2].

In Europe rates of deaths from stroke vary from 30 to 170 per 100,000 of the population. It observed higher rates of stroke in eastern and lower rates in southern European countries [3]. Also the risk of stroke varied more than 2-fold in men and women [3]. In Romania even if the prevalence of CVD is higher in men the prevalence of stroke is higher in women [4].

The stroke can be classified in 2 main types: haemorrhagic and ischaemic. The haemorrhagic stroke is the most seriously event and it is provoked by a burst brain blood vessel. Represents approximately 15% of all strokes and it is the main causes of death. The ischaemic stroke represents around 85% of all strokes (including transient ischaemic attacks or TIAs) [4]. It occurs when blood flow to the brain is blocked and causes different types of disability.

After stroke less than one third of the patients recover completely. Rehabilitation program after stroke event consists of all processes that help mental and physical recovery of patients and have the potential to promote motor recovery [5]. Methods of rehabilitation after a stroke vary from person to person, but they have the same goals, acquisition of functional status and independence to provide minimal help from other people [6] (Fig. 1).

Hand dysfunction strongly influence on the independence with everyday tasks and affect around 77% of people after a stroke event [7]. In a top 10 research priority, the people with stroke experience place hand recovery on first [8].

The rehabilitation of a person implies the existence of a concordance between person and environment in which they live.

S. Vlad and N. M. Roman (eds.), *6th International Conference on Advancements of Medicine and Health Care through Technology; 17–20 October 2018, Cluj-Napoca, Romania*, IFMBE Proceedings 71,
https://doi.org/10.1007/978-981-13-6207-1_17

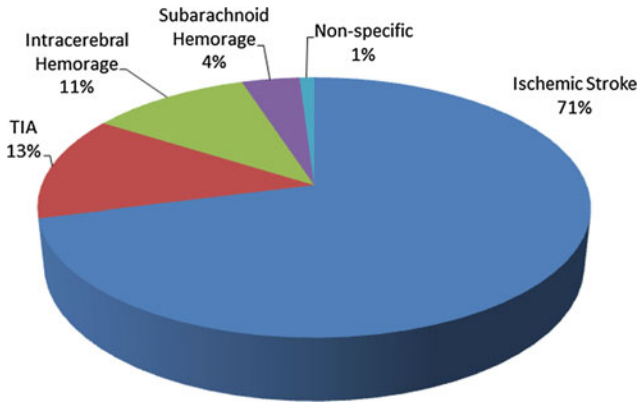

Fig. 1 Types of stroke according to Georgia Department of Public Health 2016

In our days, the use of virtual reality environments allow patients to perform tasks that mimic real life in rehabilitation clinics [9], but it tends increasingly more in the future these tasks can be done at home, sending data and receiving feedback from doctors from hundreds of miles distant. Virtual environments should not only be used to augment current ability but to find tools that enable transfer of the skills and abilities achieved during rehabilitation to function in the "real" world [10].

There are many solutions for arm rehabilitation, some of them use virtual reality methods or EMG control of movement for encourage self-administrated training in patients' home environment [11–13].

2 Material an Methods

Our system is not only a rehabilitation device that use virtual reality for recovery of upper limb function but also provide the possibility to record a full set of physiological parameters. These parameters that can be recorded are customized for each patient, making possible a complete monitoring of the disease [14, 15]. The target group is represented by persons with upper limb disability after a stroke event and all of these people have also other disease like diabetes, hypertension or another cardio-vascular disorder. The possibilities to have a wide area of physiological parameters give to the doctors and therapists a real chance to optimise the treatment [16, 17].

For developing the monitoring device it was used custom developed hardware and software. Low power amplifiers and transducers were connected to the device for physiological parameters acquisition.

The logical structure of the monitoring system is composed of a network of Parameters Monitoring Device (PMD) that is connected to a Coordinator Device (CD) [18].

For this paper it was chosen to record surface EMG and 1 canal ECG. Was used the MyoWare Muscle Sensor, produced by SparkFun, for acquiring electromyography (EMG) and AD8232 SparkFun Single Lead Heart Rate Monitor for acquiring electrocardiographic signal (ECG) (Fig. 2).

It was recorded ECG in 3 situations: before rehabilitation session, during rehabilitation session and after rehabilitation session. R-R intervals extracted from ECG were used for heart rate variability analysis [19, 20]. EMG signal was used for detecting the muscle fatigue.

Fig. 2 Rehabilitation session using VR

In some cases, the patients have also other diseases like cardiovascular abnormalities associated with endocrine diseases that produce a lot of electrocardiographic changes [21, 22]. This solution is an important tool for the physician in taking the therapeutically decision and for the optimization of the treatment.

3 Results

It was performed an analysis of heart rate variability (HRV) in frequency domain using ECG signal [23].

The frequency domain analysis of heart rate involves analyzing the spectrum of signal strength representing the R-R interval.

Power spectral density (PSD) was calculated [24] and analyzed in 3 spectral components (Fig. 3): very low power spectra (VLF) (from 0.003 to 0.04 Hz), low frequencies (LF) (from 0.04 to 0.15 Hz) and high frequencies (HF) (range 0.15–0.4 Hz). Distribution by frequency domains reflect the shift between sympatic and parasympatic.

Simpato-vagal index (calculated as the ratio between the LF component and the HF component) before, during and after exercises in the recovery program for three subjects is represented in Figs. 4, 5 and 6. A ratio greater than one reflects an predominantly sympathetic influence, while a subunit report reveals a predominantly parasympathetic influence of the nervous system on the body.

4 Conclusions

In this paper it was presented a solution for monitoring cardiovascular parameters during rehabilitation after stroke.

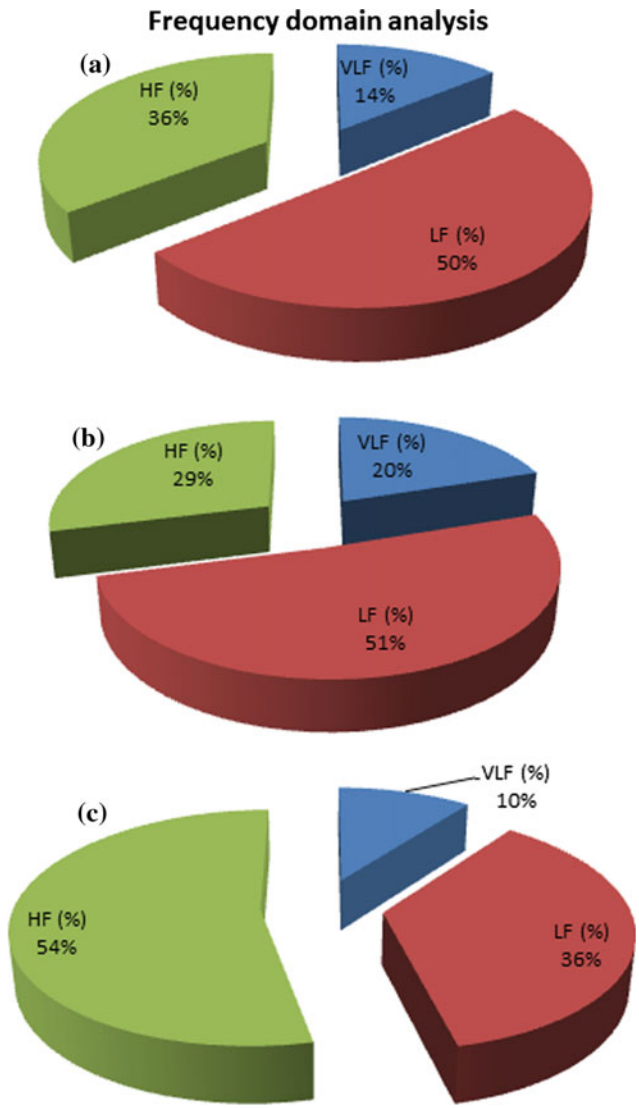

Fig. 3 Frequency domain analysis

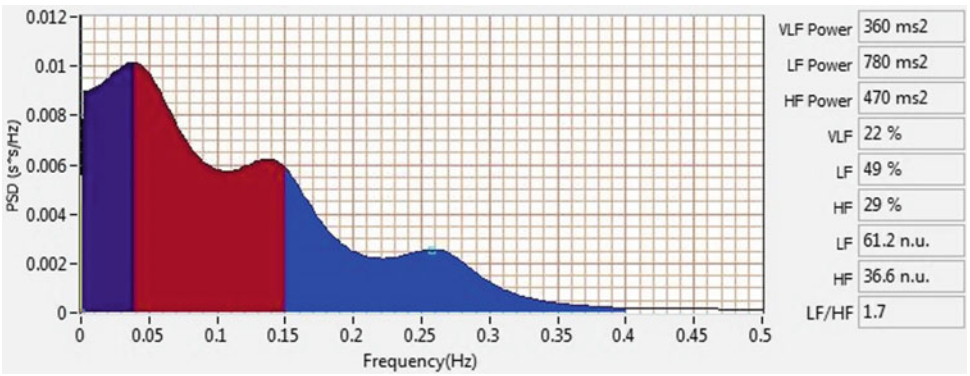

Fig. 4 Representation of spectral power distribution in case of HRV analysis before recovery session

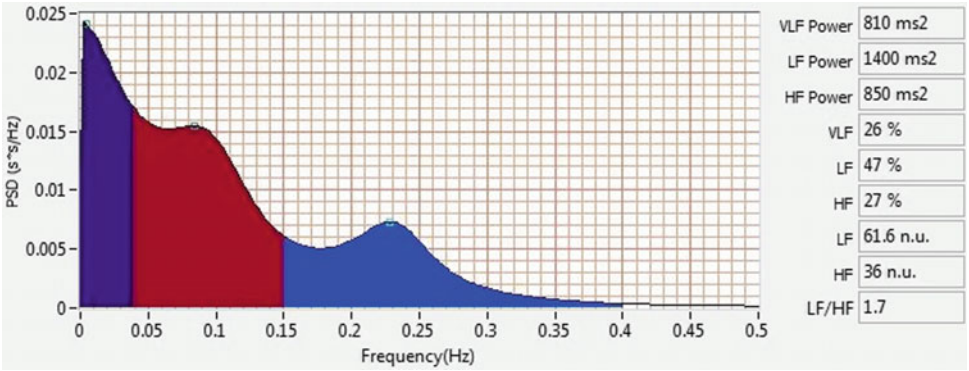

Fig. 5 Representation of spectral power distribution in case of HRV analysis during recovery session

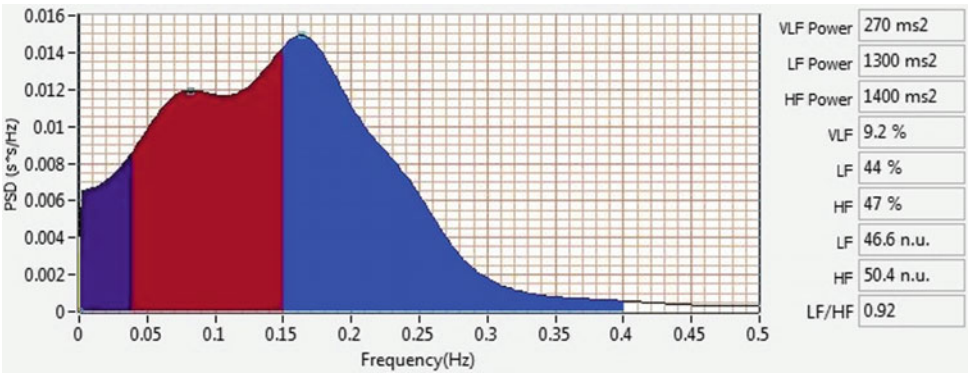

Fig. 6 Representation of spectral power distribution in case of HRV analysis after recovery session

It was performed an analysis of heart rate variability (HRV) in frequency domain and power spectral density (PSD) was calculated and analyzed in 3 spectral components.

In the case that in the therapy it is used a virtual reality or an augmented reality system the LF/HF ratio can estimate patient adaptability to the virtual environment.

This information can be used for the development of customized training program for each patient.

Conflict of Interest The authors declare that they have no conflict of interest.

References

1. Costache, I.I., Miftode, E., Petriş, O., Popa, A.D., Iliescu, D., Botnariu, E.G.: Associations between area of residence and cardiovascular risk. Rev. Cercet. Interv. Soc. **49**, 68–79 (2015)
2. Roger, V.L., Go, A.S., Lloyd-Jones, D.M., et al.: Heart disease and stroke statistics–2012 update: a report from the American Heart Association. Circulation **125**, e2–e220 (2012)
3. Heuschmann, P.U., Di Carlo, A., Bejot, Y. et al.: Incidence of stroke in Europe at the beginning of the 21st century. Stroke **40**, 1557–1563 (2009)
4. Costache, I.I., Miftode, E., Mitu, O., Aursulesei, V.: Sex differences in cardiovascular risk factors in a rural community from North Romania region. Rev. Cercet. Interv. Soc. **55**, 204–214 (2016)
5. Chen, J., Nichols, D., Brokaw, E.B., Lum, P.S.: Home-based therapy after stroke using the hand spring operated movement enhancer (HandSOME). IEEE Trans. Neural Syst. Rehabil. Eng. **25**, 2305–2312 (2017). https://doi.org/10.1109/TNSRE.2017.2695379
6. Ciorap, M., Munteanu, M., Andritoi, D., Ciorap, R.: Low cost device for "at home" rehabilitation after a stroke event. Int. Conf. Knowl.-Based Organ. **24**(3), 26–31. https://doi.org/10.1515/kbo-2018-0132 (2018)
7. Basteris, A., Nijenhuis, S.M., Stienen, A.H.A., Buurke, J.H., Prange, G.B., Amirabdollahian, F.: Training modalities in robot-mediated upper limb rehabilitation in stroke: a framework for classification based on a systematic review. J. NeuroEng. Rehab. **11**, 111 (2014). https://doi.org/10.1186/1743-0003-11-111
8. Pollock, A., St George, B., Fenton, M., Firkins, L.: Top ten research priorities relating to life after stroke. Lancet Neurol. **11**(3), 209 (2012). https://doi.org/10.1016/S14744422(12)700297
9. Schultheis, M.T., Rizzo, A.A.: The application of virtual reality technology in rehabilitation. Rehabil. Psychol. **46**(3), 296–311 (2001)
10. Sveistrup, H.: Motor rehabilitation using virtual reality. J. NeuroEng. Rehab. **1**(10). https://doi.org/10.1186/1743-0003-1-10 (2004)
11. Ciorap, R., Arotariţei, D., Topoliceanu, F., Lupu, R., Corciovă, C., Ungureanu, M.: E-health application for home monitoring of neuro-muscular rehabilitation (Aplicaţie e-Health pentru monitorizarea la domiciliu a recuperării neuro-musculare). Med.-Surg. J.-Rev. Med.-Chir. **109**(2), 440–444 (2005)

12. Wittmann, F., Held, J.P., Lambercy, O., Starkey, M.L., Curt, A., Hover. R., Gassert, R., Luft, A.R., Gonzenbach, R.R.: Self-directed arm therapy at home after stroke with a sensor-based virtual reality training system. J Neuroeng Rehab 13. https://doi.org/10.1186/s12984-016-0182-1 (2016)
13. Muri, F., Carbajal, C., Echenique, A.M., Fernandez, H., Lopez, N. M. Virtual reality upper limb model controlled by EMG signals. In: Journal of Physics Conference Series X, 19th Argentinean Bioengineering Society Congress (SABI 2013), p. 477. https://doi.org/10.1088/1742-6596/477/1/012041 (2013)
14. Ciorap, R., Hritcu-Luca, C., Corciova, C., Stan, A., Zaharia, D.: Home monitoring device for cardiovascular diseases. In: IFMBE Proceedings, vol. 26, International Conference on Advancements of Medicine and Health Care through Technology, Cluj-Napoca, Romania, pp. 49–52. https://doi.org/10.1007/978-3-642-04292-8_11 (2009)
15. Ciorap, R., Andritoi, D., Pomazan, V., Petcu, L., Ungureanu, F., Zaharia, D.: E-health system for monitoring of chronic diseases. IFMBE Proceedings, vol. 25(5), World Congress on Medical Physics and Biomedical Engineering, Munich, Germany, pp. 259–262. https://doi.org/10.1007/978-3-642-03904-1-72 (2009)
16. David, V., Salceanu, A., Ciorap, R.: Acquisition and analysis of biomedical signals in case of peoples exposed to electromagnetic fields. In: Mukhopadhyay S.C., Postolache, O.A. (eds.) Pervasive and Mobile Sensing and Computing for Healthcare, pp 269–295. Springer (2012)
17. Ciorap, R., Corciova, C., Ciorap, M., Zaharia, D.: Optimization of the treatment for chronic disease using an e-health system. In: 7th International Symposium on Advanced Topics in Electrical Engineering 2011, Bucureşti, Romania, pp. 143–146 (2011)
18. Pomazan, V.M., Petcu, L.C., Sintea, S.R., Ciorap, R.: Active data transportation and processing for chronic diseases remote monitoring. In: International Conference on Signal Processing Systems (ICSPS 2009), Singapore, pp. 853–857 (2009)
19. Andriţoi, D., David, V., Ciorap, R.: An portable device for ECG and photoplethysmographic signal acquisition. In: 2014 International Conference and Exposition on Electrical and Power Engineering (EPE 2014), Iasi, Romania. https://doi.org/10.1109/icepe.2014.6969967 (2014)
20. Ciorap, M., Munteanu, M., Andritoi, D., Ciorap, R.: Low cost device for at home rehabilitation after a stroke event. Int. Conf. Knowl-Based Organ. **24**(3), 26–31 (2018). https://doi.org/10.1515/kbo-2018-0132
21. Costache, I.I., Ungureanu, M.C., Iliescu, D., Petriş, A., Botnariu, G. (2015) Electrocardiographic changes in the most frequent endocrine disorders associated with cardiovascular diseases. Review of the literature. Revista Medico-Chirurgicală a Societăţii de Medici şi Naturalişti din Iaşi. **119**(1), 9–13 (2015)
22. Costache, I.I., Al Namat, R., Mitu, F., Ciocoiu, M., Aursulesei, V., Mitu, O., Costache, A.D., Marcu, D., Buburuz, A.M.: The prognostic value of left bundle branch block and biochemical parameters in alcoholic dilated cardiomyopathy. Rev. Chim. **68** (12), 2967–2969 (2017)
23. Andriţoi D, Corciovă C, Luca C, Matei D, Ciorap R.: Heart rate dynamics study on the impact of "mirror therapy" in patients with stroke. In: International Conference Advancements of Medicine and Health Care Through Technology MEDITECH 2016, Cluj-Napoca, Romania, 2016. https://doi.org/10.1007/978-3-319-52875-5_5 (2016)
24. Andritoi, D., David, V., Ciorap, R., Branzila, M.: Recording and processing electrocardiography signals during magneto therapy procedures. Environ. Eng. Manage. J. **12**(6), 1231–1238 (2013)

Modelling of Piezoelectric MEMS in Biomedical Applications

A. Avram, R. C. Bogdan, A. Bojiță, and M. Purcar

Abstract

The article provides to the reader a brief of the piezoelectric materials characteristics and their possibilities in biomedical microdevices development. The first section of this article presents the basics of piezoelectric MEMS. The research is focused on microgrippers since this technology is widely used in biomedical applications. The second section of this article present a review of both the direct and inverse piezoelectric effects and the piezoelectric coupling formulation used for modelling biomedical microgrippers. An analysis of piezoelectric gripper based on finite-element calculations is presented in which the fundamental electroelastic equations governing piezoelectric media are solved numerically. A study on how different geometries, different piezoelectric materials and even different mesh densities influences the performances of the microgripper are described in the last section of this article. The experimental results confirm their efficiency and demonstrate that the piezoelectric microgrippers are well suited in biomedical applications.

Keywords

MEMS • Piezoelectric devices • Micro grippers • Biomedical applications

1 Introduction in Mems

Over the past several decades, the researchers in the field of Micro-Electro-Mechanical Systems (MEMS) have developed an extremely large number of microdevices [1, 2] for a wide range of industry applications [6, 7] including: electronics industry, automotive industry, aerospatiale industry even medical and biology industry. Many of these micromachined devices have demonstrated performances exceeding those of their macroscale equivalent devices, in a remarkably way. For example, the micromachined version of a temperature sensor usually outperforms a temperature sensor made using the most precise macroscale machining techniques [1].

The formulation that a reduced scale device can provide significant progress in performances was first stated by Nathansen (1967). This, together with Bean (1978) and Peterson (1982) works, provided a framework for expansion of MEMS studies. Not only the exceptional performances of MEMS devices, but their fabrication method—similar with the same fabrication techniques used in the integrated circuit industry—which can translate into device low production costs, as well as other benefits.

Biomedical engineers have also developed many piezoelectric MEMS for biomedical applications. Some of the piezoelectric devices are used by doctors in diagnostic other are used by surgeons in medical operations [2]. Medical applications of piezoelectric MEMS are such as drug delivery, blood flow and blood pressure monitoring, robotic operating tools, etc. The microgripper is widely used in biology and medical applications. Considering that gripping of micro structural parts in biomedical field is very complex procedure [1, 2], its necessary to discuss the issue in detail.

A microgripper dedicated to micromanipulation and microassembly tasks is presented in this paper. Based on a piezoelectric actuator, the microgripper presents both a high range and a high positioning resolution. In order to improve the performances of the microgripper, different geometries and materials are modeled in this work [5–7].

A. Avram (✉) · R. C. Bogdan · A. Bojiță · M. Purcar
Department of Electrotechnics and Measurements, Technical University of Cluj-Napoca, Cluj-Napoca, Romania
e-mail: alex.avram@ethm.utcluj.ro

S. Vlad and N. M. Roman (eds.), *6th International Conference on Advancements of Medicine and Health Care through Technology; 17–20 October 2018, Cluj-Napoca, Romania*, IFMBE Proceedings 71,
https://doi.org/10.1007/978-981-13-6207-1_18

2 Piezoelectric Actuated Microgrippers

Micro-scale technologies growth in the last years leads to a branched development in areas such as electronics, mechanical and information technology. Extremely useful in medicine and biology are piezoelectric actuated microgrippers, with their key properties; stability, control, precision and manufacturing costs. Further more, are present in medicine and biology covering areas like dermatology, diagnostics, minimally invasive surgery and micro scale drug delivery [2–5].

Recently used also in micro assembly, parts and micro technologies, microgrippers use the piezoelectric actuation for their characteristic properties. Various prototypes of microgrippers with different actuation methods, such as electrothermal, electrostatic [6, 7], electromagnetic, piezoelectric actuators [5] and memory shape alloy are widely open on international market. The handling and the manufacturing are made with high care because of micro gripper's small dimensions (less than 800 μm). The dimensions of the microgripper were designed in such a way that micro-manufacturing technologies could be used, leading to low-cost and an easy adaptation to different needs.

The tools of making such small devices are uncommon; micro-positioning and micro-manipulation are a must in medical industry. The use of microgrippers requires some special conditions like low vibration facilities, stable environment and qualified personnel.

3 Modelling Piezoelectric Devices

When modelling a piezoelectric actuated microdevice the constitutive relationships of piezoelectrics have to be considered. Both the direct and inverse piezoelectric effects can be approached, while the coupling between these two phenomena's can be formulated using either the strain-charge or stress-charge formulations.

One particularity of piezoelectric materials is that ma-terials become electrically polarized when a mechanical force is applied. Looking from the microscale perspective, when mechanical displacement occurs, the atoms within the studied domain converts into electric dipoles. In certain crystal structures, these dipoles combines in order to give an electric polarization. This phenomena is known as the direct piezoelectric effect, and this is always accompanied by the converse piezoelectric effect. Looking at the opposite phenomenon, here a solid deformation occurs when piezoelectric material is placed in an electric field.

When studying these phenomena, one has to consider the coupling between the mechanical strain and the electric field, which is determined by the equations:

$$\begin{aligned} \boldsymbol{S} &= s_E \boldsymbol{T} - d^T \boldsymbol{E} \\ \boldsymbol{D} &= \boldsymbol{d}\boldsymbol{T} - \varepsilon_T \boldsymbol{E} \end{aligned} \tag{1}$$

where, **S** is the mechanical strain, **T** is the mechanical stress, **E** is the electric field, and **D** is the electric displacement field. The parameters $\boldsymbol{s_E}$, $\boldsymbol{d}$, and $\boldsymbol{\varepsilon_T}$, correspond to the material properties, the coupling and the permittivity.

Equation (1) can be formulated into the stress-charge form, which relates the material stresses to the electric field:

$$\begin{aligned} \boldsymbol{T} &= c_E \boldsymbol{S} - e^T \boldsymbol{E} \\ \boldsymbol{D} &= \boldsymbol{e}\boldsymbol{S} - \varepsilon_S \boldsymbol{E} \end{aligned} \tag{2}$$

The material properties, $\boldsymbol{c_E}$, e, and $\boldsymbol{\varepsilon_S}$ are related to $\boldsymbol{s_E}$, $\boldsymbol{d}$, and $\boldsymbol{\varepsilon_T}$ from (1). It is mentioned that one can use either form of these relations when modelling piezoelectric [5].

4 Numerical Result and Discussions

In this work, three microgrippers with different designs are studied in order to determine how geometry and material influences the gripping performances. The 2D CAD models (Model 1, 2 and 3) of the proposed microgrippers are presented in Fig. 1. These piezoelectric actuated MEMS are based the same working principle. Each micromechanical system has two clamps (the mobile components) which are fixed at the bottom surface (connected on fixed components) and actuated by two side piezoelectric blocks (see Fig. 1).

When piezoelectric actuators are connected to an electric potential, their expansion (dotted arrow direction) determine the movement of the clamp with maximum displacement at the tip (double arrow direction). Considering that, piezoelectric actuators in all three models have the same dimensions, and they are connected to same electric potential, different clamp designs and especially the side actuators position, should influence the maximum displacement at tip.

The 3D CAD designs of the piezoelectric microgrippers and their dimensions are described in Fig. 2. The height of the MEMS structure is 700 μm for all three designs. The width of these structures footprint is 130 μm for Model 1, 2 and 160 μm for Model 3, when considering the same depth of 100 μm for all three designs.

The thickness of the clamps is 10 μm in all three cases with a constant distance of 20 μm at the tip. The side piezoelectric blocks have same dimensions of 160 μm

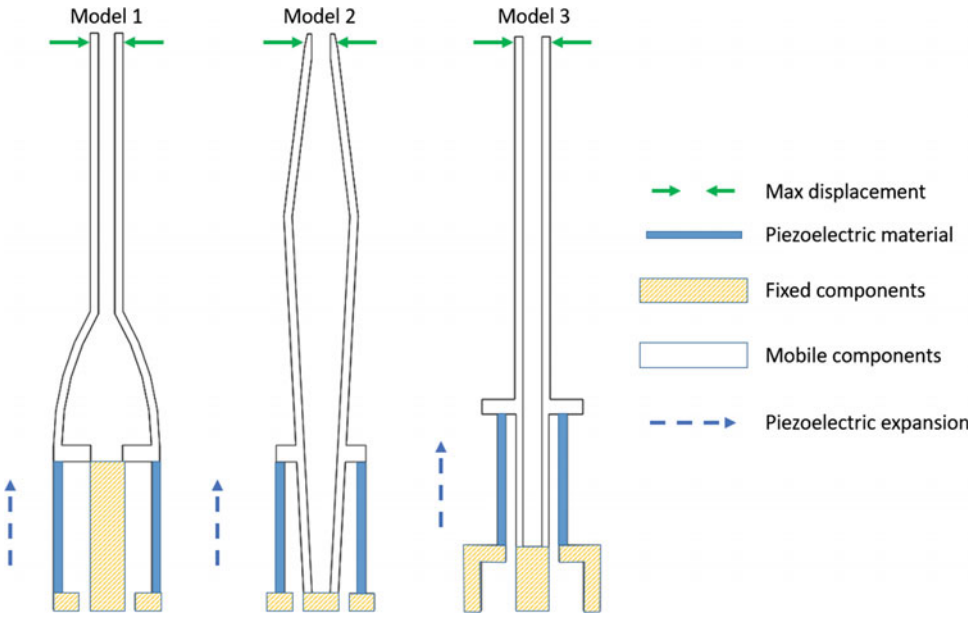

Fig. 1 The 2D CAD designs of the three microgripper models with fixed and mobile components and side piezoelectric material actuators

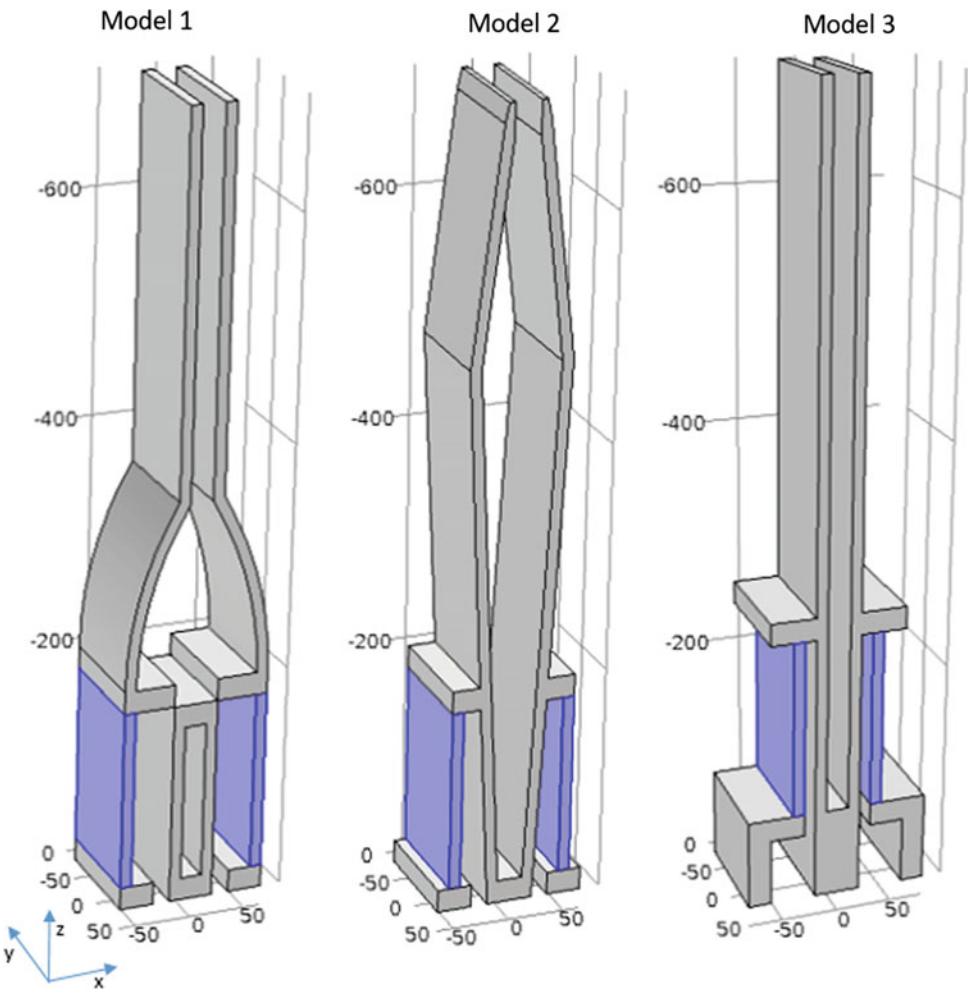

Fig. 2 The 3D CAD designs of the three microgripper models with side piezoelectric actuators at the bottom

height, 10 μm widths and 100 μm depth, for all three models. The actuators blocks have the same placement height of 20 μm for Models 1, 2 with in-between distance of 100 μm for Model 1 and 80 μm for Model 2. In Model 3 the height of actuators blocks is 80 μm while the in-between distance is 60 μm.

The three models were implemented using SolidWorks 2014 design software and exported to simulation tool in ACIS (*.sat) file format. The numerical analysis of these models was performed with COMSOL Multiphysics simulation tool using the Piezoelectric Devices module. This module activates the Solid Mechanics (*solid*) study for strain and the Electrostatics (*es*) study for the electric field computation. The coupling between the strain and the electric field is determined by the constitutive relation in (1).

The material used in simulations is Lead Zirconate Titanate (PZT-5H) for all solid bodies. This piezoceramic material is the most commonly used engineering piezoceramic.

In the Solid Mechanics (*solid*) study a Fixed Constraint boundary condition is applied on the surfaces of the fixed components marked in Fig. 1.

In the Electrostatics (*es*) study a Ground boundary condition is applied on the bottom surfaces of piezoelectric actuators in Figs. 1 and 2, while an Electric Potential boundary condition is applied on the top surfaces. The value of the Electric potential is varied 40–200 V, with 40 V increment, in order to study the maximum displacement at the tip of the clamp for all three models.

The electrical potential distribution (in Volts) is studied in the middle cross plane of the piezoelectric actuators and presented in Fig. 3.

As mentioned in Chapter "Eye Examination for Early Detection of Diabetic Neuropathy-Role of Corneal Confocal Microscopy", the result of applying a given driving voltage in the piezoelectric actuators is translated to displacement in all structures of the same stiffness. Thus, the total displacement of piezoelectric actuated MEMS (in μm) is studied in order to extract the maximum displacement [5] at the tip of the clamp for all three cases. A comparation is sowed in Fig. 4, showing that different geometries can influence the clamping of a microgripper.

It is easy to see that, the highest displacement value at comparative MEMS dimensions, same piezoelectric actuator

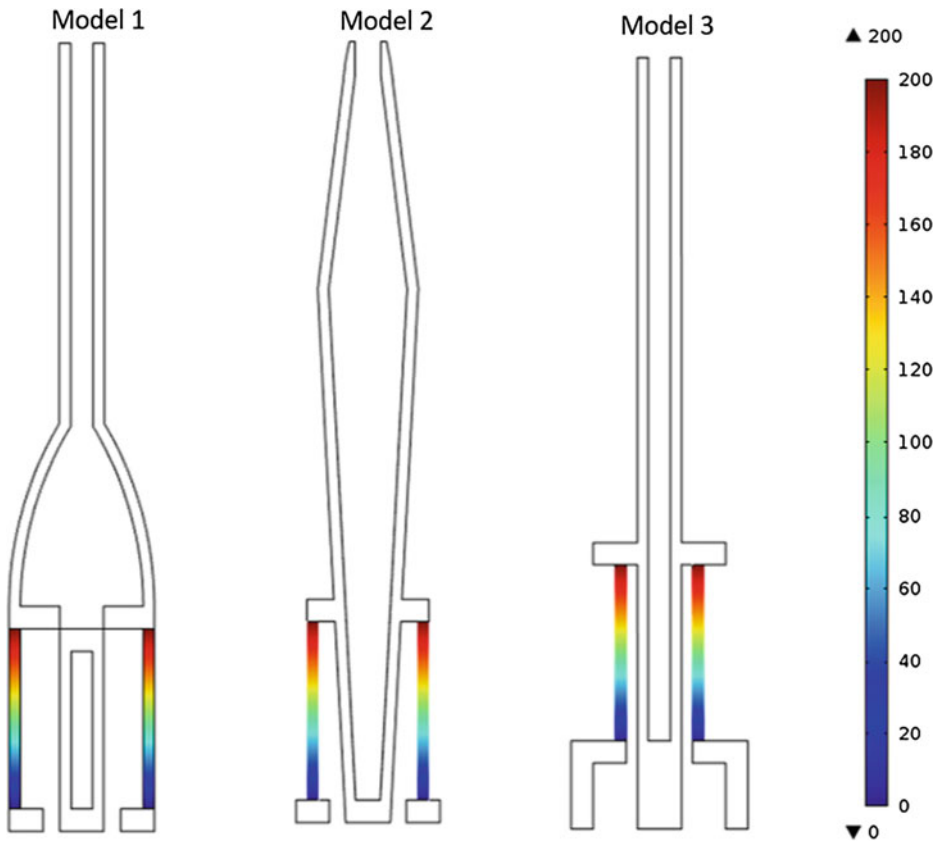

Fig. 3 The surface electrical potential distribution (V) in the piezoelectric material actuators of the three designs

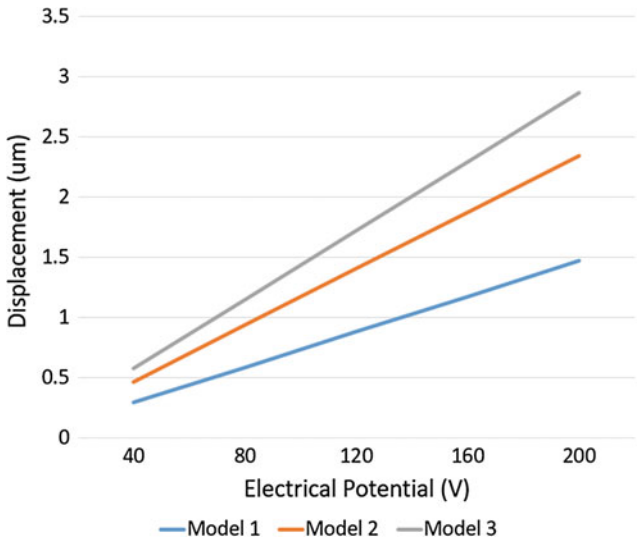

Fig. 4 The maximum displacement (μm) at the clamp tip for the three geometry designs of piezoelectric actuated MEMS

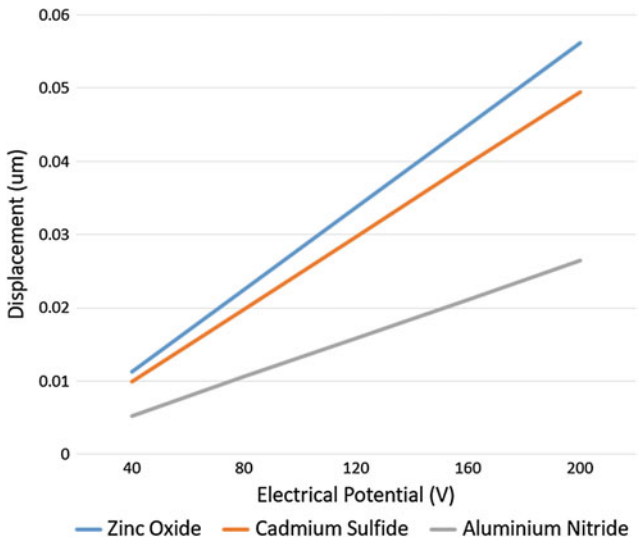

Fig. 5 The maximum displacement (μm) at the clamp tip of Model 3 for the three piezoelectric materials considered

volumes and same driving potential is obtained with the design of Model 3, while the smallest displacement is obtained with design of Model 1. The maximum displacement range of 1.5–3 μm for the PZT studied structures at 40–200 V loads was also studied in research works [2–5].

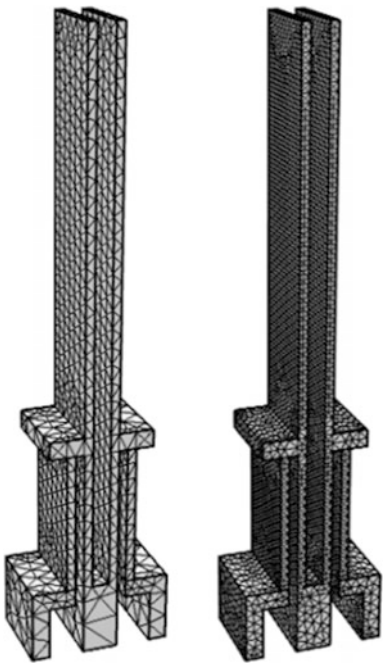

Fig. 6 The normal and extremely fine mesh densities of Model 3

In order to study how different piezoelectric materials influence the maximum displacement of a microgripper [5], the Model 3 gripper is simulated with three different materials. In this study, the Zinc Oxide (ZnO), Cadmium Sulfide (CdS) and Aluminium Nitride (AlN) were considered. Same boundary conditions as in Geometry study were applied on the Model 3 and the maximum displacement at the camp tip was extracted for all three cases. The results comparison is s are presented in Fig. 5.

It is easy to conclude from this study that the highest displacement value on same MEMS structure, given the same boundary conditions but different material properties is obtained with the Zinc Oxide material, while the smallest displacement is obtained with Aluminium Nitride.

Last but not least, a study for the influence of the mesh network density was carried out in order to find how the discretization influences the maximum displacement of the piezoelectric actuated MEMS.

In this case, the Model 3 with the same given boundary conditions and the PZT-5H material was considered. Five types of mesh densities were selected from the Mesh study in COMSOL. The numerical analysis was performed for Normal (see Fig. 6, left), Fine, Finer, Extra fine and Extremely fine (see Fig. 6, right) mesh densities. The number of Domain elements increases with the mesh density type, as plotted in Fig. 7.

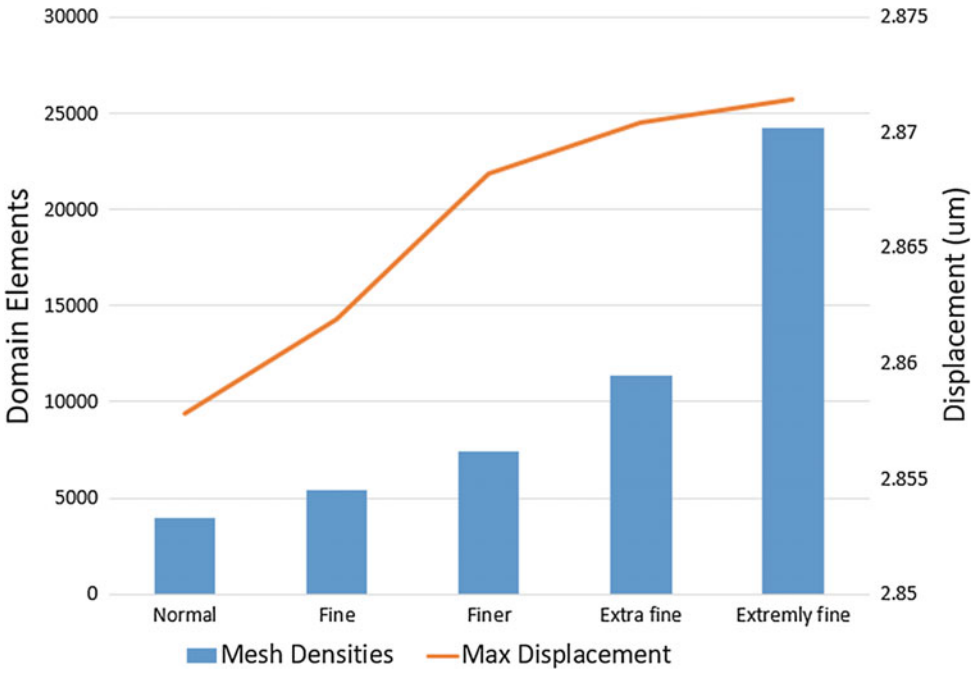

Fig. 7 The maximum displacement (μm) at the clamp tip of Model 3 for five different mesh densities

5 Conclusions

Micro-scale technologies development in the last years leads to a branched expansion in biomedical field. Furthermore, piezoelectric actuated MEMS are present in microgrippers systems. In order to improve the performances of a micro-gripper structure, different geometries and materials are modeled in this work.

The results presented in Chapgter "A Side-Polished Fluorescent Fiber Sensor for the Detection of Blood in the Saliva" reveal that, different displacement values in the structure are obtained when varying the structural design of the microgripper. Withal, when using same simulation conditions but different material properties for piezoelectric actuators, the total displacement at the clamp tip is changing. This study underlines that geometry and material parameters can be tuned for high range and a high positioning resolution.

Acknowledgements The research activities were supported through an UTCN internal grant CI2017, Nr. 1989/12.07.2017.

Conflict of Interest The authors declare that they have no conflict of interest.

References

1. Vijaya, M.S.: Piezoelectric Materials and Devices, Applications in Engineering and Medical Sciences, CRC Press, Taylor & Francis Group, LLC (2013)
2. Ye, X., Zhang Z.-J., Sun, Y. Wang, Q.: A Bi-morph Piezoelectric Ceramic Microgripper Integrating Micro-force Detecting and Feed-back. School of Mechanical Engineering, Beijing Institute of Technology, Beijing, China
3. Lakin, K.M., Kline, G.R., McCarron, K.T.: High-Q microwave acoustic resonators and filters. IEEE Trans. Microw. Theor. Tech. **41**(12), 2135–2139 (1993)
4. von Buren, T., Mitcheson, P.D., Green, T.C., Yeatman, E.M., Holmes, A.S., Troster, G.: Optimization of inertial micropower generators for human walking motion. IEEE Sens. J. **6**, 28–38 (2006)
5. Popovici, D., Constantinescu, F., Maricaru, M. et al.: Modeling and Simulation of Piezoelectric Devices, Modelling and Simulation. InTech (2008)
6. Tebrean, B., Crisan, S., Muresan, C., Crisan, T.E.: Low cost command and control system for automated infusion devices. In: International Conference on Advancements of Medicine and Health Care Through Technology, October 2016, Cluj-Napoca, Romania (2016)
7. Crisan, S., Tarnovan, I.G., Tebrean, B., Crisan, T.E.: Optical multi-touch system for patient monitoring and medical data analysis. In: International Conference on Advancements of Medicine and Health Care Through Technology, vol. 26, pp. 279–282 (2009)

Comparative Effect of Ethyl Urethane and Cycloheximide in *Lepidium sativum* L. Seed Germination and Radicle Growth

O. Viman, K. Balla, L. Holonec, M. Tămaş, D. L. Dumitrașcu, V. Șandor, and L. Nedelcu

Abstract

The seed germination test of *Lepidium sativum* L. offers intrinsic data obtained within this complex process and details on the mechanisms of action of two pharmacologically distinct substances, ethyl urethane, a general anesthetic and cycloheximide, an inhibitor of protein biosynthesis in eukaryotes. The rate of germination of the species gives the test efficiency and the possibility of multiple experimental versions at identical time periods. Testing was carried out in aqueous media consisting of filter paper soaked with water or aqueous solutions of the two substances. It was evaluated the frequency of seed germination and the length of the radicle at 24 and 48 h after exposure. Comparison of results was made by nonparametric and parametric statistical tests to reject the null hypothesis at $p < 0.05$. Germination in the control group was over 90% and the length of rootlets was over 8 mm at 48 h. Ethyl urethane 1% delayed the germination, but it reached in 48 h at values close to those of the control group. The length of the radicle was significantly reduced, less than 3 mm. At this concentration, ethyl urethane clearly, but reversibly, inhibits germination. The germination is almost blocked at concentrations of 10% ethyl urethane, the effect being irreversible and the length of rootlets is at the limit of measurement. Cycloheximide 0.01% reduces to a greater extent than ethyl urethane 1% the germination frequency and length of rootlets; the action is irreversible. Inhibitory effects on germination of ethyl urethane and cycloheximide, substances with different pharmacological targets, show the importance of the general processes of cell excitability and the participation of specific proteins in the cascade phenomenon of germination in plants.

Keywords

Germination • *Lepidium sativum* L. • Ethyl urethane • Cycloheximide

1 Introduction

Seed germination in plants is a very complex process, influenced by external factors and numerous endogenous molecules [1–3]. By testing the effects of some substances on germination, one can obtain useful data regarding the physiology of this phenomenon and the possibility to influence it. In the process of seed germination several modulators can occur with general effects on plant cells [4–6].

Observations on germination can be further adapted to more complex tests on other plant and animal systems [7]. This issue is important because germination tests are relatively easy to be made, inexpensive and most of them are reproducible.

The further described experiences have followed the effects of ethyl urethane, a nonvolatile, hydrosoluble general anesthetic [8] and of cycloheximide, an inhibitor of protein biosynthesis in eukaryotes [9] in the seed germination test of *Lepidium sativum* L. This plant was chosen for the experiment due to its outstanding germinative characteristics, having a fast development of radicle formation and showing a convenient choice through efficiency.

O. Viman · L. Holonec (✉)
University of Agricultural Sciences and Veterinary Medicine, Cluj-Napoca, Romania
e-mail: lholonec@usamvcluj.ro

K. Balla · M. Tămaş · D. L. Dumitrașcu · V. Șandor
"Iuliu Haţieganu" University of Medicine and Pharmacy, Cluj-Napoca, Romania

L. Nedelcu
University "Transilvania", Braşov, Romania

S. Vlad and N. M. Roman (eds.), *6th International Conference on Advancements of Medicine and Health Care through Technology; 17–20 October 2018, Cluj-Napoca, Romania*, IFMBE Proceedings 71,
https://doi.org/10.1007/978-981-13-6207-1_19

2 Materials and Methods

2.1 Biological Material

The experiment was based on seeds of *Lepidium sativum* L. of Brassicaceae family [10], harvested one year before testing. Through a preliminary examination, the seeds with apparent morphological defects were removed.

2.2 Testing Device of Germination

The test of Botany Department of the Faculty of Pharmacy of UMF "Iuliu Haţieganu" Cluj-Napoca [7] was applied. There were used Petri plates of adequate size, wallpapered with filter paper of circular shape soaked with the aqueous solutions. The seeds were placed on the wet paper at proper distances. The plates have been maintained at room temperature (16–18 °C) under natural light-darkness regime. The filter paper was resoaked with water and with the medical solutions at intervals of 12 h [11].

Evaluation of germination was made on a total period of 48 h with measurements at 24 and 48 h (see Table 1—experimental protocol). It was determined the proportion of sprouted seeds and measured the length of the radicle with the aid of an adapted device, graded in mm.

In advance, it was appreciated the influence of seed imbibition with water for 12 h previous to their placing on Petri plates.

2.3 Indicators of Germination and Statistical Tests Used

The frequency of germination, nonparametric index, was expressed in percentages. The comparison of results between the formed groups was made through 2 × 2 tables which took into consideration the chi-square distribution. The length of the radicles was calculated in mm and the values have been expressed through average mean and standard error ($s_{\bar{x}} \pm$ e.s.). For the comparison of results we appealed to the parametric unpaired bilateral "t"-Student test. In both tests, the null hypothesis was rejected at values of $p < 0.05$.

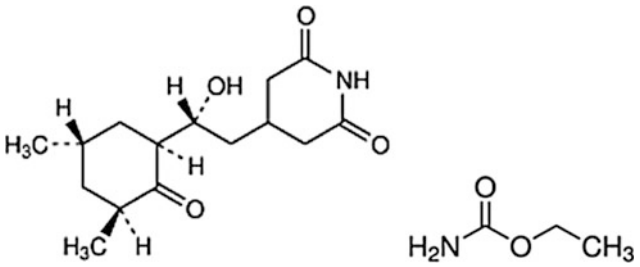

Fig. 1 Left: cycloheximide (CAS 66-81-9); right: ethyl-carbamate (Ethyl urethane) (CAS 51-79-6)

2.4 Pharmacological Agents Used

I. For the control groups, tap water was used at room temperature.
II. Ethyl urethane (ethyl-carbamate, Carlo Erba—Milano). We used aqueous solutions of ethyl urethane 1 and 10%.
III. Cycloheximide (Actidione®—Sigma), aqueous solution 0.01% (Fig. 1).

Both ethyl urethane and cycloheximide are being used in vitro. They present significant risks, especially potentially cancerous [12]. Because of this reason the preparation and the handling of substances was made in accordance with the indications of the producer using protection materials (gloves) and avoiding direct contact with these solutions. Unused solutions as well as the biological material and the consumables have been treated according to the international regulations in force for avoid environmental contamination.

Table 1 Experimental protocol

Group	Time (h)			
	−12	0	24	48
I	–	Water	Effect evaluation	Effect evaluation
II	–	Urethane 1%		
III	–	Cycloheximide 0.01%		
IV	Water	Water		
V	Urethane 1%	Water		
VI	Cycloheximide 0.01%	Water		
VII	Water	Urethane 10%		

2.5 Experimental Protocol

There were made more experimental versions constituting groups of 100 seeds each. The two indicators of germination, the frequency of germination and the length of radicles were determined at 24 and 48 h (Table 1).

I. In order to follow the influence of the imbibition pre-treatment in water, we placed 100 seeds on each of the two Petri plates. One group of seeds was placed directly on the filter paper soaked with water, while the other group was put to germination after 12 h of the previous imbibition with water (Tables 1 and 2).
II. Three groups of seeds were placed from the beginning on the soaked filter papers and evaluated as in the previous version after 24 and 48 h. The seeds from the first group were placed on filter paper soaked with water. The second group was submitted to the effects of a solution of ethyl urethane 1%, while for the third group it was used a solution of cycloheximide 0.01% (Table 3).
III. In this variant there were used three groups of seeds pre-treated differentiated through soaking for 12 h, with water for the first group, with ethyl urethane for the second group and with cycloheximide 0.01% for the third group. After an interval of 12 h all the seeds from the three groups have been placed on filter paper soaked with water. The evaluation was made as in the previous versions at 24 and 48 h (Table 4).
IV. In the fourth version, the control group was placed regularly on filter paper soaked with water. The other group was pre-treated through imbibition for 12 h with ethyl urethane 10% and then passed on to the paper in aqueous environment (Table 5).

Table 2 Effects of previous soaking with water on germination

Group	Germination (%)/h			Radicle length (mm) ($s_{\bar{x}} \pm$ e.s.)/h		
	24 h	48 h	$p_{24–48}$	24 h	48 h	$p_{24–48}$
I Water	93	93	1	0.81 ± 0.06	8.27 ± 0.45	<0.0001
IV Water pretreatment	85	89	>0.5	1.13 ± 0.1	8.84 ± 0.66	<0.0001
P: I versus IV	>0.1	>0.45		< 0.006	> 0.476	

Table 3 Effects of ethyl urethane 1% and cycloheximide 0.01% on germination

Group	Germination (%)/h			Radicle length (mm) ($s_{\bar{x}} \pm$ e.s.)/h		
	24 h	48 h	$p_{24–48}$	24 h	48 h	$p_{24–48}$
Water	93	93	1	0.81 ± 0.06	8.27 ± 0.45	<0.0001
Urethane 1%	70	90	<0.001	0.17 ± 0.02	2.74 ± 0.16	<0.0001
Cycloheximide 0.01%	33	54	<0.005	0.05 ± 0.01	0.16 ± 0.04	<0.001
P: I versus II	<0.014	>0.6		<0.0001	<0.0001	
P: I versus III	<0.0001	<0.0001		<0.0001	<0.0001	
P: II versus III	<0.0001	<0.0001		<0.0001	<0.0001	

Table 4 Germination under conditions of pretreatment with water, ethyl urethane 1% and cycloheximide 0.01%

Group	Germination (%)/h			Radicle length (mm) ($s_{\bar{x}} \pm$ e.s.)/h		
	24 h	48 h	$p_{24–48}$	24 h	48 h	$p_{24–48}$
Water	85	89	1	1.13 ± 0.1	8.84 ± 0.66	<0.0001
Urethane 1%	55	81	<0.001	0.19 ± 0.03	3.39 ± 0.32	<0.0001
Cycloheximide 0.01%	26	32	<0.005	0.04 ± 0.01	0.07 ± 0.02	<0.001
P: I versus II	<0.0001	>0.16		<0.0001	<0.0001	
P: I versus III	<0.0001	<0.0001		<0.0001	<0.0001	
P: II versus III	<0.0001	<0.0001		<0.0001	<0.0001	

Table 5 Effects of ethyl urethane 10% on germination

Group	Germination (%)/h			Radicle length (mm) ($s_{\bar{x}} \pm$ e.s.)/h		
	24 h	48 h	$p_{24–48}$	24 h	48 h	$p_{24–48}$
I Water	85	89	>0.5	1.13 ± 0.1	8.84 ± 0.66	<0.0001
IV Water pretreatment	17	17	1	0.03 ± 0.01	0.03 ± 0.01	1
P: I versus IV	<0.0001	<0.0001		<0.0001	<0.0001	

3 Results

I. The sprouting of seeds of *Lepidium sativum* L. was noticed after a few hours and was significant at 24 h. Previous imbibition with water increased insignificantly the proportion of germinated seeds, but increased the length of radicle after 12 h. At 48 h there were no significant differences between the pre-treated group and the one placed directly on to filter paper. After 24 h in aqueous environment, most seeds germinated, while only a small number of seeds germinated between 24 and 48 h. In regard with the length of the radicle at 24 h, this one was approximately of 1 mm and increased above 8 mm at 48 h (Table 2).

II. Ethyl urethane in solution of 1% lowered the proportion of germination at 24 h, but did not change it at 48 h. The length of radicles was significantly reduced in regard with the group treated with water at 24 h and as well at 48 h.
Cycloheximide 0.01% diminished the frequency of germination at 24 and 48 h. At 24 h the length of the radicle was tiny and increased very little at 48 h (Table 3).

III. The results of the pretreatment with water are included in the first version (Table 2).
The pre-treatment with ethyl urethane 1% and cycloheximide 0.01% with 12 h previous to placing on Petri plates influenced characteristically the indicators of germination. It is worth mentioning that seeds pre-treated with the two substances were placed on filter paper soaked with water, interrupting their action this way. Pre-treatment of seeds with ethyl urethane reduced the sprouting percentage at 24 h, with minimal influence on this parameter at 48 h. The growing of radicles was further inhibited also after the removal of ethyl urethane from the environment of seeds (Table 4).
Pre-treatment with cycloheximide reduced significantly the frequency of germination at 24 and 48 h. The growth of the radicles was basically stopped through the pre-treatment with cycloheximide. The inhibitory effect on radicular growth was highly pronounced with values at the limit of measurement. The irreversible character of action of cycloheximide 0.01% was obvious on *Lepidium sativum* L. seed germination.

IV. Ethyl urethane 10% blocks almost completely both sprouting and implicitly radicular growth, having an obvious effect at 24 h and constant even after the removal of the substance from contact with seeds. As in the case of cycloheximide, the antigerminative effect was obviously irreversible (Table 5).

4 Discussion

Used for intrinsic observations of the process, germination tests are also useful for the evaluation of some substances and drugs with presuming modulatory effects on germination [2]. Among these tests, *Lepidium sativum* L. seeds sprouting distinguishes through efficiency and reproducibility [7, 11]. In the present paper we used two substances with well-defined pharmacological effects frequently intended for the study of animal physiology and pathology. Ethyl urethane is a non-volatile hydrosoluble general anesthetic with blocking action on neuronal cell excitability and at a less extent on other cell types [13]. Cycloheximide is an inhibitor of protein biosynthesis in eukaryotes, extensively used in animal experiments [12, 14], on cellular cultures [9] and also, on plants and vegetal tissues [15]. Even though the pharmacological spectrum of both substances is relatively wide, the two types of effects previously mentioned are essentially involved in their mechanism of action.

The germination study in *Lepidium sativum* L. seeds shows the inhibitory character of ethyl urethane and cycloheximide on the germination frequency and on initial growth of the *Lepidium* radicle. At low concentrations, ethyl urethane has reversible inhibitory effects. Increasing these concentrations, the two indicators of germination are irreversibly inhibited.

Cycloheximide under the concentrations used has also an antagonistic effect on germination parameters, an effect of irreversible nature (Tables 2, 3, 4 and 5). Taking into consideration the characteristic pharmacological mark, it may be stated the importance of general excitability processes, as

well as of the specific protein biosynthesis in the process of seed germination of plants.

In fact, 140 years ago Claude Bernard revealed the net inhibitory effect of ethyl ether on seed germination of various species [16]. Afterwards, other generally volatile anesthetics from the vegetal area have been experimented, observing also actions on plant motility and photosynthesis besides the inhibitory effects on seed germination [17]. It was also noticed another interesting phenomenon, namely the production by plants, under stress conditions, of ethylene and ethyl ether, gaseous, respectively volatile substances with general anesthetic effects. Based on these observations, Claude Bernard generalized the phenomenon of narcosis in animals and plants [16, 17]. Another remarkable figure of the 19th century biology, Charles Darwin, studied thoroughly in another context the germination phenomenon of plants and the influence of some chemical substances on germination [18, 19].

In regard to ethyl urethane there is the possibility of influencing some physiological processes proper to germination. As other general anesthetics, and firstly the volatile ones, ethyl urethane inhibits sprouting of seeds. This inhibitory effect can be attributed to general cellular excitability [17]. As far as cycloheximide is concerned, the pharmacological analysis yet imposes caution in attributing the inhibitory effect of protein synthesis at blocking seed germination [20]. The substance inhibits the protein biosynthesis in animals and in most plants including fungi [12]. Cycloheximide affects the protein cytosolic biosynthesis and does not intervene on mitochondrial protein biosynthesis. Because mitochondria in animals and chloroplasts in plants have prokaryotic origin, this particularity of cycloheximide brings another argument on the specificity of protein inhibition in eukaryotes [21].

At this moment, there are enough data in order to outline the mechanism of protein biosynthesis in eukaryotes. Cycloheximide intervenes on translation in the elongation stage; the substance is fixed on place E (exit) of the ribosomal subunit 60S and restrains at this level translocation (Fig. 2). Cycloheximide binds to mRNA and ribosomal proteins. It is proper to cycloheximide the stabilization of the ribosome after the first cycle of translocation, so that the elongation at tripeptides is blocked [9, 12].

Depending on the cell type, cycloheximide intervenes on apoptosis and in most cases induces the accomplishment of this type of programmed death. The antiapoptotic protein biosynthesis is blocked and the proapoptotic protein biosynthesis is favoured [22].

Apparently surprising, cycloheximide can induce the biosynthesis of some proteins [23] like hepatic uridinekinase. Cycloheximide also influences the half-life of template RNA [24].

Besides the inhibitory effect on protein synthesis, cycloheximide influences other cellular processes, the uptake of oxygen, absorption of some inorganic and organic ions, amino acid uptake. Also, in *Chlamydomonas reinhardi*, cycloheximide stimulates the breakdown of nucleic acids [25].

The blocking of protein biosynthesis is being constantly observed in intact plants. On cellular cultures, the effects of cycloheximide are much more heterogeneous; thus, the protein biosynthesis is inhibited in beet, pea and peanut cells, but is not influenced in the ricin ribosomes, leaves of tobacco and wheat germs [15].

The effect on fungi is extremely varied. The growth of most saprophytic fungi is blocked in culture environments, whereas most pathogenic fungi develop in the presence of cycloheximide. Also, through mutations of ribosomal proteins, it may appear the resistance of cycloheximide in *Sacharomyces* and *Kluyveromyces* genus [9].

Concerning germination, this process is influenced by a multitude of external factors and also by endogenous molecules with hormonal role [26–28]. The complexity of germination phenomena concerns multiple stages conducted

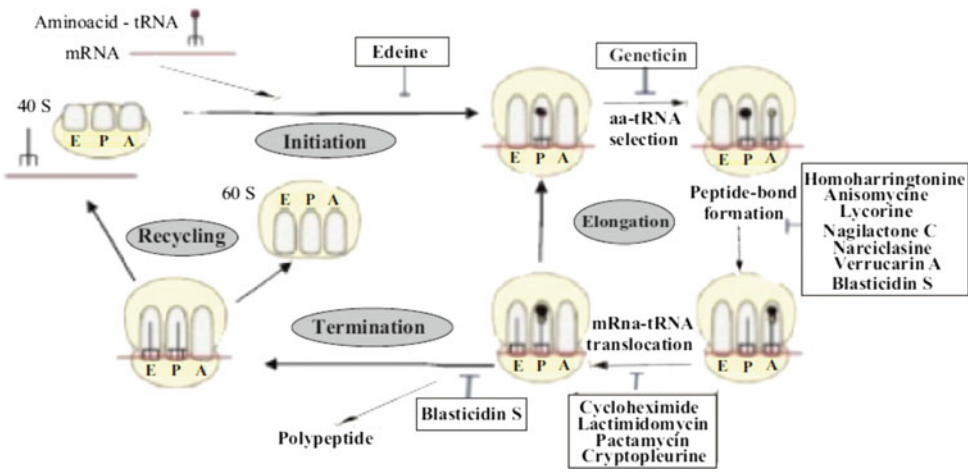

Fig. 2 Protein biosynthesis in eukaryotes

in short periods of time and the effects of various modulators of germination [5, 6, 29, 30].

The most important hormones for seed germination are the abscisic acid with inhibitory role [31–33] and the gibberellins with stimulating role [34–37]. There also intervene ethylene [26, 28, 33, 38] and brassinosteroids [39] and at a lower extent, cytokinins [4] through stimulation of the germination process. Auxin does not influence germination significantly, but it can interfere with the path of abscisic acid [5].

There are some data on seed germination through use of cycloheximide (*Arabidopsis thaliana* L. Heynh.). The effects depend on the proportion between stored proteins in seeds and the ones newly synthesized during germination [40].

Also, there has been followed the effects on granules germination and pollen tube formation. The effects depend on the vegetal species and on the stages surprised in the study [41].

The obvious inhibitory effects of ethyl urethane and cycloheximide observed in the experiences performed may be attributed to the two important cellular processes: general excitability and protein biosynthesis. The reproducibility of the germination process offers quality to testing other substances and drugs, obtaining a preliminary profile of pharmacological actions.

5 Conclusions

1. The results obtained on *Lepidium sativum* L. seeds germination confirm the reproducible character and the remarkable efficiency of this test.
2. The evaluation of *Lepidium sativum* L. germination was made through the determination of sprouting frequency of seeds (nonparametric test) and through the measurement of radicle length (parametric test).
3. Germination was almost complete at 24 h after the triggering of the process and radicle growth was highly pronounced in the interval of 24–48 h.
4. Ethyl urethane 1% delays the process of germination, but the proportion of sprouted seeds reaches similar values as those from the control group at 48 h. In this respect, at this concentration the effect of ethyl urethane is reversible.
5. Ethyl urethane 1% slows significantly the growth in length of the radicle at 24 and 48 h.
6. Ethyl urethane 10% has a pronounced blocking effect on germination, effect that stays constant on the entire period of exposure, proving the irreversible character of the action of the substance. Radicle growth was almost completely inhibited.
7. Cycloheximide 0.01% has a significantly continuous inhibitory effect on germination frequency on the entire period of exposure.
8. Cycloheximide at this concentration has a significant effect of stopping radicle growth. The effect of cycloheximide is much more pronounced comparatively with the one of ethyl urethane 1% and is irreversible.
9. Ethyl urethane and cycloheximide have different biophysical and biochemical mechanisms of action, but both substances inhibit *Lepidium sativum* L. seed germination. The data obtained puts into evidence both the importance of general excitability of vegetative cells and the protein biosynthesis in the cascade of germination process in plants.

Acknowledgements This research received no specific grant from any funding agency in the public, commercial, or not-for-profit sectors.

Conflict of Interest The authors declare that they have no conflict of interest.

References

1. Angelovici, R., Galili, G., Fernie, A.R., Fait, A.: Seed desiccation: a bridge between maturation and germination. Trends Plant Sci. **15**, 211–218 (2010)
2. Miernyk, J.A., Hajduch, M.: Seed proteomics. J Proteomics. **74**, 389–400 (2011)
3. Miransari, M., Smith, D.L.: Plant hormones and seed germination. Environ. Exp. Bot. **99**, 110–121 (2014)
4. Khan, A.A.: Cytokinins: permissive role in seed germination. Science **171**, 853–859 (1971)
5. Rajjou, L., Duval, M., Gallardo, K., et al.: Seed germination and vigor. Annu. Rev. Plant Biol. **63**, 507–533 (2012)
6. Tan, L., Chen, S., Wang, T., Dai, S.: Proteomic insights into seed germination in response to environmental factors. Proteomics **13** (12–13), 1850–1870 (2013)
7. Pitea, M., Mărie, A., Cristea, R., Tămaș, M., Arieșan, V.: Untersuchungen über sulfamido–urethane. Arch. Pharm. (Weinheim) **306**, 702–706 (1973)
8. Chavan, B.G., Bhide, S.V.: Binding of urethane with macromolecules from all organelles. J. Natl. Cancer Inst. **50**, 1459–1461 (1973)
9. Schneider-Poetsch, T., Ju, J., Eyler, D.E., et al.: Inhibition of eukaryotic translation elongation by cycloheximide and lactimidomycin. Nat. Chem. Biol. **6**, 209–217 (2010)
10. Sîrbu, C., Oprea, A., Patriche, C.V., Samuil, C., Vîntu, V.: Alien species of *Lepidium* in the flora of Romania: invasion history and habitat preference. Not. Bot. Horti. Agrobo. **42**, 239–247 (2014)
11. Șandor, V.L., Katalin, B., Cuparencu, B., Tămaș, M., Kory, M., Gavriș, A.D. (1994) The inhibition of germination by ethyl urethane. In: Al X-lea Congres Național de Farmacie, Cluj-Napoca. Rezumatele Lucrărilor Științifice, pp. 414–415 (1994)
12. Garreau de Loubresse, N., Prokhorova, I., Holtkamp, W., Rodnina, M.V., Yusupova, G., Yusupov, M.: Structural basis of the

inhibition of the eukaryotic ribosome. Nature **513**(7519), 517–522 (2014)
13. Griswold, D.E., Alessi, E.F.: Inhibition of carrageenin induced inflammation by urethane anesthesis in adrenalectomized and sham operated rats. J. Pharmacol. Methods **8**, 161–164 (1982)
14. Oksvold, M.P., Pederson, N.M., Forfang, L., Smeland, E.B.: Effect of cycloheximide on epidermal growth factor receptor trafficking and signaling. FEBS Lett. **586**, 3575–3581 (2012)
15. Ellis, R.J., MacDonald, I.R.: Specificity of cycloheximide in higher plant systems. Plant Physiol. **170**(46), 227–232 (1970)
16. Bernard, C.: Nouvelles expériences dans le but de montrer que l'anesthésie peut être produite chez tous les êtres vivants. C. Rend. S. Soc. Biol., 1877, 6e série, t3, p. 312. Exemplaire numérisé: BIU Santé (Paris) Adresse permanente: http://www.biusante.parisdescartes.fr/histmed/medica/cote?clber065 (1876)
17. Grémiaux, A., Yokawa, K., Mancuso, S., Baluška, F.: Plant anesthesia supports similarities between animals and plants: Claude Bernard's forgotten studies. Plant. Signal. Behav. **9**(1), e27886 (2014). Epub 2014 Jan 29. PMID: 24476640, PMCID: PMC4091246
18. Darwin, C.R.: Effect of salt-water on the germination of seeds. Gardeners' Chron. Agric. Gaz. **47**, 773 (1855)
19. Weitbrecht, K., Müller, K., Leubner-Metzger, G.: First off the mark: early seed germination. J. Exp. Bot. **62**, 3289–3309 (2011)
20. Fitter, S.S., Hunt, L.D., Fletcher, J.S.: Resistance of plant cells to cycloheximide. Proc. Okla. Acad. Sci. **55**, 49–50 (1975)
21. Chakrabarti, S., Dube, D.K., Roy, S.C.: Effects of emetine and cycloheximide on mitochondrial protein synthesis in different systems. Biochem. J. **128**, 461–462 (1972)
22. Alessenko, A.V., Boikov, PYa., Filippova, G.N., Khrenov, A.V., Loginov, A.S., Makarieva, E.D.: Mechanisms of cycloheximide-induced apoptosis in liver cells. FEBS Lett. **416**, 113–116 (1997)
23. Susorov, D., Mikhailova, T., Ivanov, A., Sokolova, E., Alkalaeva, E.: Stabilization of eukaryotic ribosomal termination complexes by deacylated tRNA. Nucl. Acids Res. **43**(6), 3332–3343 (2015). https://www.ncbi.nlm.nih.gov/pubmed/25753665. Epub 2015 Mar 9. PMID: 25753665, PMCID: PMC4381076. https://doi.org/10.1093/nar/gkv171
24. Cihák, A., Cerná, J.: Stimulatory effect of cycloheximide and related glutarimide antibiotics on liver uridine kinase. FEBS Lett. **23**, 271–274 (1972)
25. McMahon, D.: Cycloheximide is not a specific inhibitor of protein synthesis in vivo. Plant Physiol. **55**, 815–821 (1975)
26. Arc, E., Sechet, J., Corbineau, F., Rajjou, L., Marion-Poll, A.: ABA crosstalk withethylene and nitric oxide in seed dormancy and germination. Front Plant Sci. **4**, 63 (2013). https://www.ncbi.nlm.nih.gov/pubmed/23531630. eCollection 2013. PMID: 23531630, PMCID: PMC3607800. https://doi.org/10.3389/fpls.2013.00063
27. Klose, C., Arendt, E.K.: Proteins in oats; their synthesis and changes during germination: a review. Crit. Rev. Food Sci. Nutr. **52**, 629–639 (2012)
28. Lin, Z., Zhong, S., Grierson, D.: Recent advances in ethylene research. J. Exp. Bot. **60**, 3311–3336 (2009)
29. Tan-Wilson, A.L., Wilson, K.A.: Mobilization of seed protein reserves. Physiol. Plant. **145**, 140–153 (2012)
30. Thomas, T.L.: Gene expression during plant embryogenesis and germination: an overview. Plant Cell **5**, 1401–1410 (2012)
31. Finkelstein, R.R., Gampala, S.S., Rock, C.D.: Abscisic acid signaling in seeds and seedlings. Plant Cell **14**(Suppl), S15–S45 (2002)
32. Kitahata, N., Asami, T.: Chemical biology of abscisic acid. J. Plant. Res. **124**, 549–557 (2011)
33. Linkies, A., Leubner-Metzger, G.: Beyond gibberellins and abscisic acid: how ethylene and jasmonates control seed germination. Plant Cell Rep. **31**, 253–270 (2012)
34. García-Martinez, J.L., Gil, J.: Light regulation of gibberellin biosynthesis and mode of action. J. Plant Growth Regul. **20**, 354–368 (2001)
35. Gupta, R., Chakrabarty, S.K.: Gibberellic acid in plant: still a mystery unresolved. Plant Signal Behav. **8**, e25504 (2013)
36. Hauvermale, A.L., Ariizumi, T., Steber, C.M.: Gibberellin signaling: a theme and variations on DELLA repression. Plant Physiol. **160**, 83–92 (2012)
37. Schwechheimer, C., Willige, B.C.: Shedding light on gibberellic acid signalling. Curr. Opin. Plant Biol. **12**, 57–62 (2009)
38. Bleecker, A.B., Kende, H.: Ethylene: a gaseous signal molecule in plants. Annu. Rev. Cell Dev. Biol. **10**, 2330–2347 (2000)
39. Jiang, W.B., Lin, W.H.: Brassinosteroid functions in Arabidopsis seed development. Plant Signal Behav. **8**, e25928 (2013)
40. Kimura, M., Nambara, E.: Stored and neosynthesis mRNA in Arabidopsis seeds: effects of cycloheximide and controlled deterioration treatment on the resumption of transcription during imbibition. Plant Mol. Biol. **73**, 119–129 (2010)
41. Hao, H., Li, Y., Hu, Y., Lin, J.: Inhibition of RNA and protein synthesis in pollen tube development of Pinus bungeana by actinomycin D and cycloheximide. New Phytol. **165**, 721–730 (2005)

Numerical Simulation of the Temperature Propagation in Superposed Biological Media, with Applications in Dental Treatment

V. Mureşan, N. M. Roman, T. Coloşi, M. Abrudean, O. P. Stan, and O. Bunta

Abstract

In this paper, an example of numerical simulation of the temperature propagation in five biological media is presented. For the five spaces, successively disposed, respectively: tissue (A), tooth (B), steel (C), tooth (D) and again tissue (E), the structure parameters, respectively the time constants (T_1; T_2) and the space constants (S_1; S_2) are obtained using the dedicated program CTISP01(02) which implements equations which are presented in the paper. It is of great interest the temperature propagation in time and space, both in the interior of these spaces and at the separation limits between them. The dedicated program ZPROP03(04), that assures much flexibility and a large diversification for the similar studied applications was elaborated on the purpose of simulating the mathematical model of the propagation process, proposed in the paper. Direct applications of the presented simulations can be used in dental treatment domain.

Keywords

Thermal propagation in biological media • Analogical modeling partial differential equation (PDE) • Numerical simulation • Structure parameters

1 Introduction

The example of numerical simulation is referring to the transfer of an over-temperature $u_0 = 50$ °C (in relation to the temperature of 37 °C considered for the biological medium) [1] applied at the input of the medium (A). The heat transfer, implicitly the over-temperature transfer, is made from the input of medium (A), until at the output from the medium (E), point in which the temperature is notated with $y_{00E}(t, s_f)$, as is it shown (much simplified) in Fig. 1. The notations correlation, in Fig. 1, is: mediums (A) and (E) represent biological tissues (more exactly gum); mediums (B) and (D) represent different parts of the same tooth; medium (C) represents a metal introduced in the tooth as consequence of a dental treatment.

The study of the propagation of the over-temperature $u_0 = y_{00A}(t, s_0)$, in the five zones, respectively Z = A; Z = B; Z = C; Z = D and Z = E, in relation to time (t) and space (s), is limited in relation to the axes ($0r_A$); ($0r_B$); ($0r_C$); ($0r_D$) and ($0r_E$). Hence, limiting the study of the propagation phenomenon to only one axis, we avoid, in a first stage, the study of the temperatures evolutions in the three-dimensional space, in relation to the axes ($0p_Z$), ($0q_Z$) and ($0r_Z$), for Z = A, B, C, D and E. This aspect is due to the fact that the study of the propagation phenomena in three-dimensional space becomes unnecessarily complex. Consequently, the axial propagation distances ($0r_{...}$), exemplified in Fig. 2, are considered $s_A = 1$ mm; $s_B = 2$ mm; $s_C = 3$ mm; $s_D = 2$ mm; $s_E = 1$ mm.

For each from these five zones (Z), over-temperatures [2] will be notated with $y_{00Z}(t, s)$, with the remark that at the input (s_0) and at the output (s_f) of these zones, the notations become $y_{00Z}(t, s_0)$, respectively $y_{00Z}(t, s_f)$. Consequently, at the input of the zone (A) it results $y_{00A}(t, s_0) = u_0(t)$, and at the output of the zone (E) it results $y_{00E}(t, s_f)$.

V. Mureşan (✉) · T. Coloşi · M. Abrudean · O. P. Stan
Automation Department, Technical University of Cluj-Napoca, Cluj-Napoca, Romania
e-mail: vlad.muresan@aut.utcluj.ro

N. M. Roman
Electrotechnics and Measurements Department, Technical University of Cluj-Napoca, Cluj-Napoca, Romania

O. Bunta
Orthodontics Department, Iuliu Hatieganu University of Medicine and Pharmacy, Cluj-Napoca, Romania

S. Vlad and N. M. Roman (eds.), *6th International Conference on Advancements of Medicine and Health Care through Technology; 17–20 October 2018, Cluj-Napoca, Romania*, IFMBE Proceedings 71,
https://doi.org/10.1007/978-981-13-6207-1_20

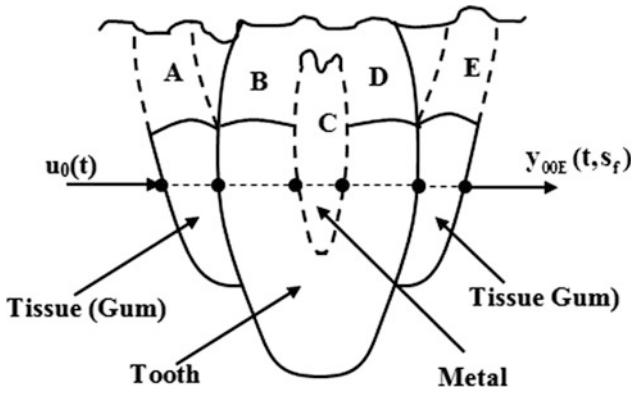

Fig. 1 The five media

2 Analogical Model of Propagation for $y_{00Z}(t, s)$

For each zone (Z) of the over-temperature propagation $y_{00Z}(t, s)$, an analogical model is considered, defined through a partial differential equation of II (second) order, with the two independent variables (t) and (s) [3–6], (respectively PDE II·2), of the form:

$$a_{00Z} \cdot y_{00Z} + a_{10Z} \cdot y_{10Z} + a_{01Z} \cdot y_{01Z} + a_{20Z} \cdot y_{20Z} + a_{11Z} \cdot y_{11Z} + a_{02Z} \cdot y_{02Z} = K_{yZ} \cdot [\varphi_{0.00Z} * u_0(t)]. \quad (1)$$

It is considered: $y_{ij} = \frac{\partial^{i+j} y}{\partial t^i \cdot \partial s^j}$, i = 0, 1, …, j = 0, 1, …; $a_{...Z}$ = constants; (K_{yZ}) is a proportionality constant, and the over-temperature step u_0 = const. Also, the operation "*" represents the convolution product between the $\varphi_{0.00Z}(t, s)$ and $u_0(t)$ signals (obviously in relation to time (t)). For $y_{...Z}(t, s)$ non-periodically damped evolutions in relation to time, the following approximating solutions are determined [7]:

$$y_{00Z}(t,s) = K_{yZ} \cdot F_{0SZ}(s) \cdot [F_{0TZ}(t) * y_{00(Z-1)}(t,s_{Zf})], \quad (2)$$

where $y_{00(Z-1)}(t, s_{Zf})$ corresponds to the over-temperature in relation to the edge (s_f), of the zone from upstream (Z − 1).

It is also considered:

$$F_{0TZ}(t) = \frac{1}{T_{1Z} - T_{2Z}} \cdot e^{-\frac{t}{T_{1Z}}} + \frac{1}{T_{2Z} - T_{1Z}} \cdot e^{-\frac{t}{T_{2Z}}}, \quad (3)$$

respectively

$$F_{0SZ}(s) = \frac{S_{1Z}}{S_{1Z} - S_{2Z}} \cdot e^{-\frac{s}{S_{1Z}}} + \frac{S_{2Z}}{S_{2Z} - S_{1Z}} \cdot e^{-\frac{s}{S_{2Z}}}, \quad (4)$$

where, for the final values (t_f) and (s_f) from Fig. 3, the following approximations are considered:

$$F_{0TZ}(t_f) \to 1, \quad (5)$$

$$F_{0SZ}(s_f) \to 0. \quad (6)$$

The (F…) functions from (3) and (4) are selected in order to approximate the temperature dynamics, in relation to both independent variables, with second order evolutions (the second order evolutions can be used for approximating evolutions with the order higher than two, in order to simplify, as much as it is possible, the mathematical models).

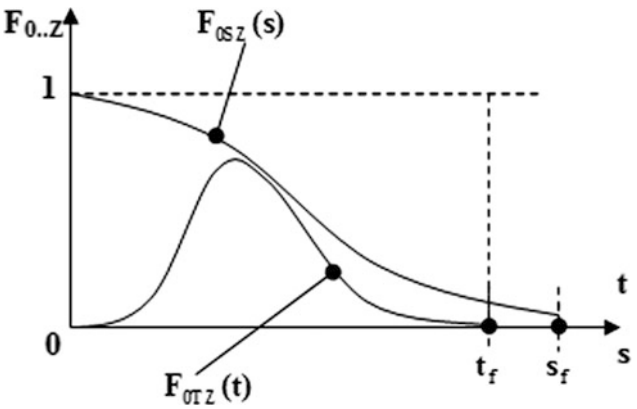

Fig. 3 The evolution of F_{0}…. functions

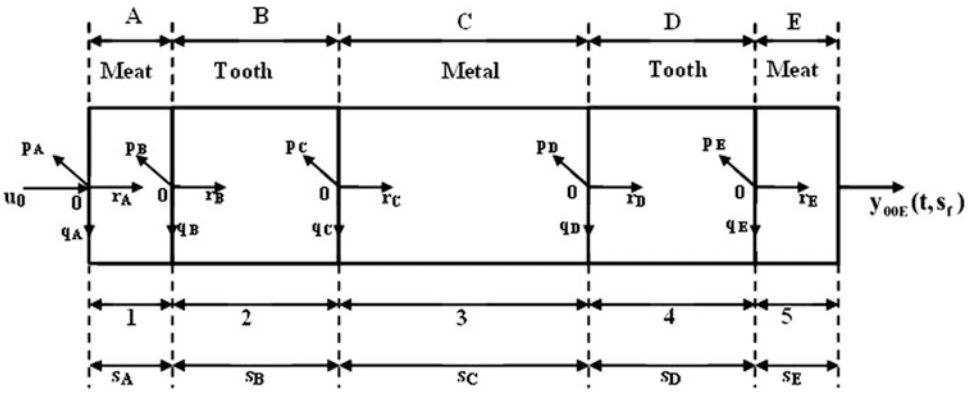

Fig. 2 The propagation distances

Table 1 Examples of time and space constants

Zone (Z)	T_{1Z} (s)	T_{2Z} (s)	S_{1Z} (mm)	S_{2Z} (mm)
A	0.470	0.705	2.2156	3.3234
B	0.940	1.410	2.4049	3.6074
C	0.3525	0.5287	6.1189	9.1784
D	0.940	1.410	2.4049	3.6074
E	0.470	0.705	2.2156	3.3234

Examples of time constants (T_{1Z}, T_{2Z}) and of space constants (S_{1Z}, S_{2Z}), resulted from the dedicated program CTISP01(02) used to compute the propagation process structure parameters, are presented in Table 1.

In an intuitive form, the processed data in CTISP01(02) are based on (t_{fZ}), (s_{fZ}), ($y_{\alpha Z}$) and ($y_{\beta Z}$) values, highlighted in Fig. 4, and used in the following equations [8]:

$$T_{1Z} = \frac{t_{fZ}}{\mu_{TZ} \cdot (1 + \lambda_{TZ})}; \tag{7}$$

$$T_{2Z} = \lambda_{TZ} \cdot T_{1Z}; \tag{8}$$

$$S_{1Z} = \frac{s_{fZ}}{\mu_{SZ} \cdot (1 + \lambda_{SZ})}; \tag{9}$$

$$S_{2Z} = \lambda_{SZ} \cdot S_{1Z}, \tag{10}$$

where

$$\mu_{TZ} = \frac{t_{fZ}}{(T_{1Z} + T_{2Z})} = (4, \ldots, 5) \tag{11}$$

and

$$\mu_{SZ} = \frac{s_{fZ}}{(S_{1Z} + S_{2Z})} = (4, \ldots, 5). \tag{12}$$

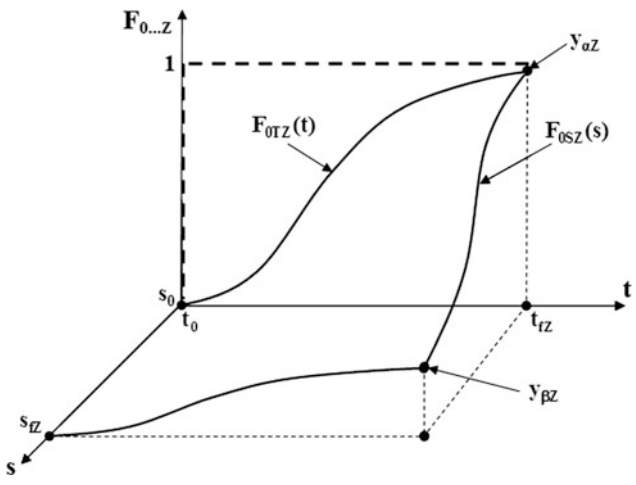

Fig. 4 The evolution of F…. functions in an intuitive form

The definition of (λ_{TZ}) and (λ_{SZ}) is usually associated with the localization of the inflexion abscissae, respectively

$$t_{iZ} = \frac{T_{1Z} \cdot T_{2Z}}{T_{2Z} - T_{1Z}} \cdot \ln\left(\frac{T_{2Z}}{T_{1Z}}\right) = \frac{\lambda_{TZ} \cdot T_{1Z}}{\lambda_{TZ} - 1} \cdot \ln(\lambda_{TZ}) \tag{13}$$

and

$$s_{iZ} = \frac{S_{1Z} \cdot S_{2Z}}{S_{2Z} - S_{1Z}} \cdot \ln\left(\frac{S_{2Z}}{S_{1Z}}\right) = \frac{\lambda_{SZ} \cdot S_{1Z}}{\lambda_{SZ} - 1} \cdot \ln(\lambda_{SZ}). \tag{14}$$

In general $1.1 \leq \lambda_{TZ} \leq 10$ and $1.1 \leq \lambda_{SZ} \leq 10$, with usual values $\lambda_{TZ} = 1.5 \div 3$, respectively $\lambda_{SZ} = 1.5 \div 3$.

For the ($a_{\ldots Z}$) coefficients from the five PDEs II·2 from (1) is recommended to present the following formulae: $a_{00Z} = 1$; $a_{10Z} = T_{1Z} + T_{2Z}$; $a_{01Z} = S_{1Z} + S_{2Z}$; $a_{20Z} = T_{1Z} \cdot T_{2Z}$; $a_{02Z} = S_{1Z} \cdot S_{2Z}$; $a_{11Z} = (T_{1Z} + T_{2Z}) \cdot (S_{1Z} + S_{2Z})$, with the remark that sometimes the modification of these relations is justified.

3 Numerical Simulation of the Propagation Process

The numerical simulation of the propagation process is based on the dedicated program ZPROP03(04) which implements the mathematical model presented in Sect. 2.

Basically, the following stages are passed through [8]:

(a) There are declared: the structure parameters, the initial conditions, the steps of the numerical integration (Δt) and of the results extraction (Δy) and details associated to the equivalent system formed by the zones (A), …, (E).

(b) The iterative logistics follows the determination of the matrix of partial derivatives of the state vector (**Mpdx**), associated with Taylor series [8], up to derivatives of six order inclusively.

(c) The final solution—numerically simulated—contains the state vector (transposed) $\mathbf{x}_{\mathbf{kZ}}^{(\mathbf{T})} = (y_{00Z}; y_{10Z}; y_{20Z}; y_{30Z}; y_{40Z}; y_{50Z})_k$ for each iteration (k), respectively for each moment $t_k = k \cdot \Delta t$. For each zone (Z), the over-temperatures are represented in $(t_k,s)_Z$ coordinates, where the distances (the propagation depths) (s_Z), were arbitrary chosen on ($\frac{S_{fZ}}{10}$) intervals. The final time of iterative computation did not increase over 8 (eight)

seconds and the resulted cumulated relative errors in percentage [9–11] have values $CREPy_{00kZ} \leq 10^{-2}$ (values which prove the high accuracy of the simulations).

(d) In Tables 2, 3, 4, 5 and 6, the zones A, B, C, D and E present the evolutions of the over-temperature $y_{00}(t, s)$, for the same time intervals (t), respectively [0.01; 0.2; 0.5; 1; 2; 3; 5; 8] s. The propagation depths (s) were considered $(\frac{S_f - S_0}{10})_Z$ for each zone (Z), hence assuring a good interpolation for $y_{00}(t, s)$, too, at t = const. and (s) variable, in the interior of each zone. The passing from a zone to the next superposed zone is made with a step $\Delta s = 0.01$ mm, so: (1 to 1.01) mm from the zone A to B, then (3 to 3.01) mm from the zone B to C, then (6 to 6.01) mm from the zone C to D and finally (8 to 8.01) mm from the zone D to E.

Passing through the Tables 2, 3, 4, 5 and 6, for different zones, either for $y_{00}(t = \text{var.}; s = \text{const.})$ and for $y_{00}(t = \text{const.}; s = \text{var.})$, the propagation of the over-temperature $y_{00}(t, s)$ can be followed with sufficient details.

An interesting interpretation of this phenomenon, successively on all these zones, could highlight the discontinuities of the over-temperature from the separation limit between the zones, too, as example following the evolutions: $y_{00}(0.2; s)$; $y_{00}(0.5; s)$; $y_{00}(1; s)$; $y_{00}(2; s)$; $y_{00}(3; s)$; $y_{00}(5; s)$ and $y_{00}(8; s)$, for $(0 \leq s \leq 9)$. There are remarked the following discontinuities for $y_{00}(t, s)$ (in transitory regime): the decreasing one from (A) to (B), then the increasing one from (B) to (C), then the decreasing one from (C) to (D) and finally the increasing one from (D) to (E). In steady state regime, at t = 8 s, it is remarked a slow damping of these discontinuities or even values direction changes. In general,

Table 2 Zone A (meat) ZPROP03(04)

Z	s\t	0.01	0.2	0.5	1	2	3	5	8
	0	7×10^{-3}	2.39	11.02	25.86	42.72	48.07	49.86	49.99
	0.1	7×10^{-3}	2.39	11.01	25.84	42.69	48.03	49.82	49.96
	0.2	7×10^{-3}	2.38	10.99	25.79	42.60	47.94	49.73	49.86
	0.3	7×10^{-3}	2.37	10.95	25.71	42.47	47.79	49.58	49.71
A	0.4	7×10^{-3}	2.36	10.91	25.60	42.30	47.59	49.37	49.50
	0.5	7×10^{-3}	2.35	10.85	25.47	42.08	47.35	49.12	49.24
	0.6	7×10^{-3}	2.34	10.78	25.31	41.82	47.05	48.82	48.93
	0.7	7×10^{-3}	2.32	10.71	25.13	41.52	46.72	48.48	48.59
	0.8	7×10^{-3}	2.30	10.62	24.93	41.19	46.35	48.09	48.21
	0.9	7×10^{-3}	2.28	10.53	24.71	40.84	45.95	47.68	47.79
	1	7×10^{-3}	2.26	10.43	24.48	40.45	45.52	47.22	47.34

Table 3 Zone B (tooth) ZPROP03(04)

Z	s\t	0.01	0.2	0.5	1	2	3	5	8
	1.01	1.8×10^{-3}	0.64	3.48	10.35	24.52	34.63	44	47.20
	1.2	1.75×10^{-3}	0.62	3.42	10.18	24.10	34.03	43.25	46.37
	1.4	1.7×10^{-3}	0.61	3.35	9.97	23.60	33.33	42.36	45.42
	1.6	1.68×10^{-3}	0.60	3.27	9.74	23.08	32.58	41.41	44.40
B	1.8	1.64×10^{-3}	0.58	3.19	9.51	22.52	31.79	40.41	43.32
	2	1.6×10^{-3}	0.57	3.11	9.26	21.93	30.97	39.36	42.20
	2.2	1.55×10^{-3}	0.55	3.03	9.00	21.33	30.11	38.27	41.04
	2.4	1.50×10^{-3}	0.54	2.94	8.74	20.71	29.94	37.17	39.85
	2.6	1.46×10^{-3}	0.52	2.85	8.48	20.08	28.36	36.04	38.64
	2.8	1.42×10^{-3}	0.50	2.76	8.21	19.45	27.47	34.91	37.43
	3	1.41×10^{-3}	0.49	2.67	7.95	18.82	26.57	33.77	36.21

Table 4 Zone C (metal) ZPROP03(04)

Z	s\t	0.01	0.2	0.5	1	2	3	5	8
	3.01	1.2×10^{-2}	3.70	15.34	31.42	44.08	46.46	46.90	46.92
	3.3	0.012	3.65	15.17	31.06	43.59	45.93	46.36	46.39
	3.6	0.012	3.61	14.98	30.68	43.04	45.36	45.79	45.81
	3.9	0.019	3.56	14.79	30.28	42.48	44.76	45.19	45.21
C	4.2	0.011	3.51	14.58	29.86	41.89	44.14	44.56	44.58
	4.5	0.011	3.46	14.37	29.43	41.29	43.51	43.92	43.94
	4.8	0.011	3.41	14.16	28.98	40.66	42.85	43.26	43.28
	5.1	0.011	3.59	13.93	28.53	40.03	42.18	42.58	42.60
	5.4	0.011	3.30	13.71	28.07	39.38	41.50	41.89	41.91
	5.7	0.010	3.25	13.48	27.60	38.73	40.81	41.20	41.22
	6	0.010	3.19	13.25	27.13	38.06	40.11	40.49	40.51

Table 5 Zone D (tooth) ZPROP03(04)

Z	s\t	0.01	0.2	0.5	1	2	3	5	8
	6.01	7.5×10^{-4}	0.27	1.47	4.37	10.36	14.63	18.59	19.93
	6.2	7.2×10^{-4}	0.26	1.41	4.19	9.93	14.02	17.82	19.11
	6.4	7×10^{-4}	0.24	1.34	4.01	9.49	13.41	17.04	18.27
	6.6	6.6×10^{-4}	0.23	1.29	3.83	9.07	12.81	16.28	17.46
D	6.8	6.3×10^{-4}	0.22	1.23	3.66	8.67	12.24	15.56	16.69
	7	6×10^{-4}	0.21	1.17	3.50	8.28	11.70	14.86	15.94
	7.2	5.8×10^{-4}	0.20	1.12	3.34	7.91	11.16	14.19	15.22
	7.4	5.5×10^{-4}	0.19	1.07	3.18	7.55	10.66	13.54	14.52
	7.6	5.2×10^{-4}	0.18	1.02	3.04	7.20	10.17	12.92	13.86
	7.8	5×10^{-4}	0.17	0.97	2.90	6.87	9.70	12.33	13.22
	8	4.7×10^{-4}	0.17	0.93	2.76	6.55	9.25	11.76	12.61

Table 6 Zone E (meat) ZPROP03(04)

Z	s\t	0.01	0.2	0.5	1	2	3	5	8
	8.01	1.6×10^{-3}	0.51	2.37	5.57	9.21	10.36	10.75	10.77
	8.1	1.56×10^{-3}	0.50	2.32	5.44	8.99	10.11	10.50	10.52
	8.2	1.52×10^{-3}	0.49	2.25	5.30	8.76	9.85	10.22	10.25
	8.3	1.50×10^{-3}	0.47	2.20	5.16	8.53	9.59	9.95	9.983
E	8.4	1.45×10^{-3}	0.46	2.19	5.02	8.30	9.34	9.69	9.721
	8.5	1.4×10^{-3}	0.45	2.08	4.89	8.09	9.10	9.44	9.466
	8.6	1.37×10^{-3}	0.44	2.03	4.76	7.87	8.86	9.19	9.216
	8.7	1.33×10^{-3}	0.43	1.98	4.64	7.66	8.62	8.95	8.973
	8.8	1.30×10^{-3}	0.41	1.92	4.51	7.46	8.39	8.71	8.736
	8.9	1.26×10^{-3}	0.40	1.87	4.39	7.26	8.17	8.48	8.504
	9	1.2×10^{-3}	0.39	1.82	4.28	7.07	7.96	8.25	8.278

a significant "overheating" of the metallic zone (C) in comparison with all the others zones, is remarked. Globally, due to the thermal propagation phenomenon through absorption, the over-temperature $y_{00}(t, s)$ decreases progressively with the increasing of the depth (s).

In Figs. 5, 6. 7, 8 and 9, the curves associated to the data from Tables 2, 3, 4, 5 and 6 are graphically presented (running the simulation program in MATLAB [12]). In Fig. 5, the evolution of the temperature in the zone A, in relation to time (t), is presented, for the propagation depths: s = 0 mm; s = 0.5 mm; s = 0.7 mm; s = 1 mm.

In Fig. 6, the evolution of the temperature in the zone B, in relation to time (t), is presented, for the propagation depths: s = 1.01 mm; s = 1.6 mm; s = 2.4 mm; s = 3 mm.

In Fig. 7, the evolution of the temperature in the zone C, in relation to time (t), is presented, for the propagation depths: s = 3.01 mm; s = 4.2 mm; s = 5.1 mm; s = 6 mm.

In Fig. 8, the evolution of the temperature in the zone D, in relation to time (t), is presented, for the propagation depths: s = 6.01 mm; s = 6.8 mm; s = 7.4 mm; s = 8 mm.

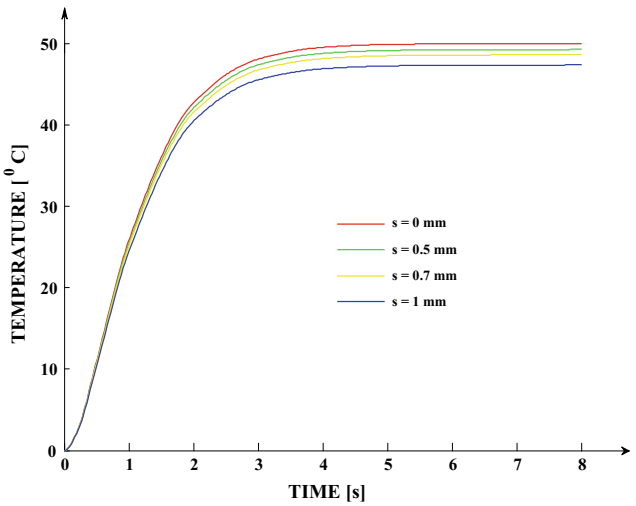

Fig. 5 The temperature evolution for different propagation depths in zone A

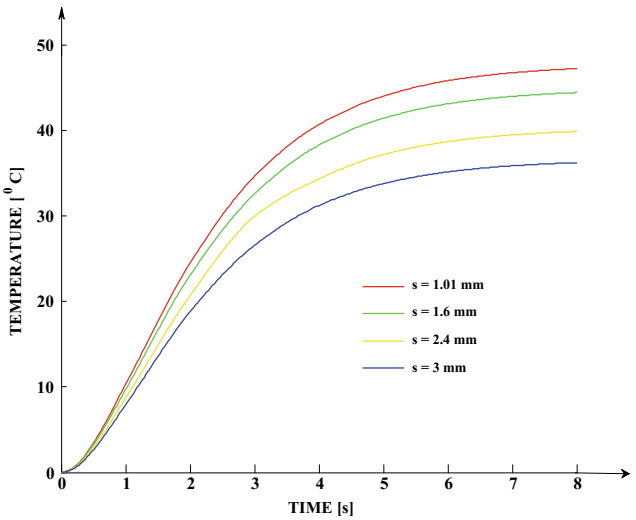

Fig. 6 The temperature evolution for different propagation depths in zone B

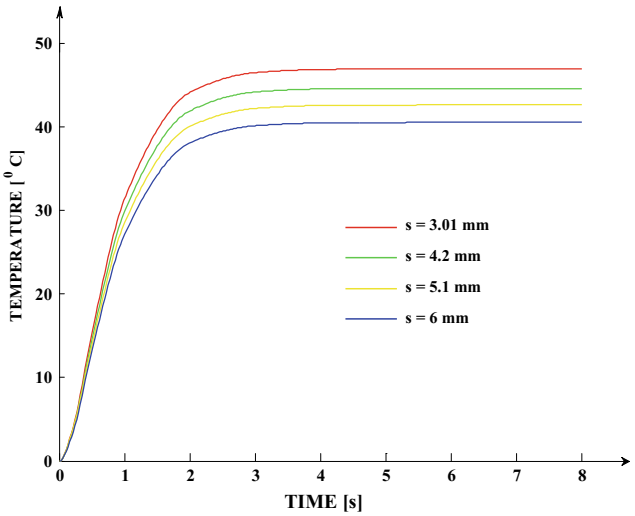

Fig. 7 The temperature evolution for different propagation depths in zone C

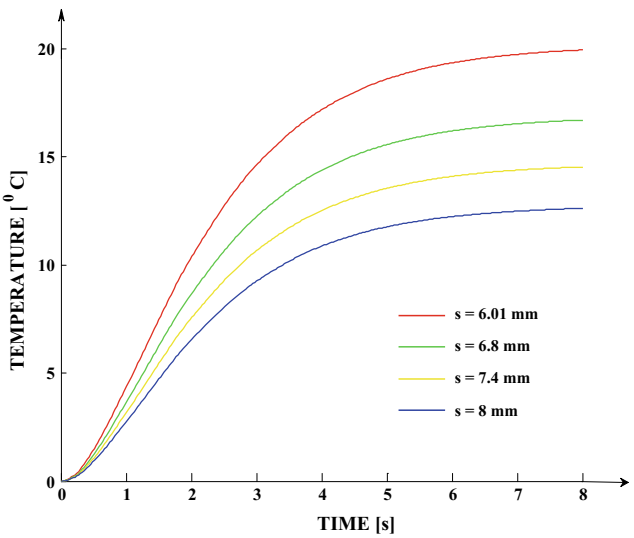

Fig. 8 The temperature evolution for different propagation depths in zone D

In Fig. 9, the evolution of the temperature in the zone E, in relation to time (t), is presented, for the propagation depths: s = 8.01 mm; s = 8.3 mm; s = 8.7 mm; s = 9 mm.

In Fig. 10, the evolution of the temperature, in relation to propagation depth (s), in all the five zones is presented, for the following propagation moments: t = 1 s; t = 2 s; t = 3 s; t = 8 s.

The discontinuities in the temperature propagation occur at the separation limit between the consecutive zones, at the propagation depths: s = 1 mm; s = 3 mm; s = 6 mm, respectively s = 8 mm. This phenomenon occurs due to the fact that the zones are of different biological types. Also, the zone C is of inorganic type. Consequently, the considered zones have different physical properties.

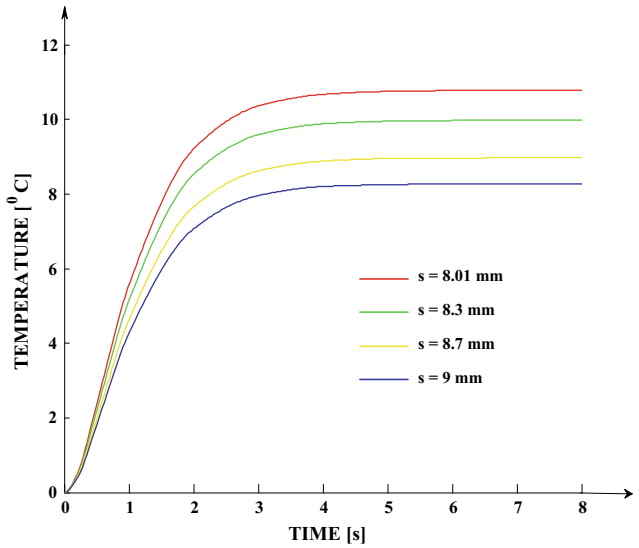

Fig. 9 The temperature evolution for different propagation depths in zone E

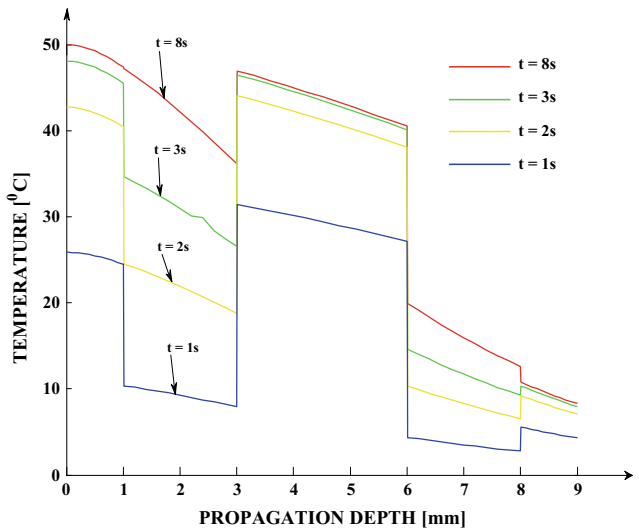

Fig. 10 The temperature evolution, in relation to the propagation depth, for different propagation moments in all the five zones

4 Conclusions

1. The analogical modeling presented in the paper is based on the partial differential equations PDE II·2 from (1), different for each zone (A), (B), (C), (D) and (E).
2. The analytical solutions that verify each of these five PDEs (associated to the five zones), corresponds to the exponential functions, non-periodically damped in relation both to time (t) and to the propagation depth (s), presented in (2).
3. The structure parameters (T_1, T_2, S_1, S_2) are approximated through an experimental-numerical method, for each zone, using the program CTISP01(2), that solves transcendental equations in relation with (T_1 and $\lambda_T)_Z$, respectively (S_1 and $\lambda_S)_Z$, where the zone (Z) corresponds with (A), (B), (C), (D) and (E). The numerical integration, in relation to time, of the five PDEs II·2 (with the different $(a_{\ldots Z})$ coefficients, function of the zone (Z)), was operated through the dedicated program ZPROP03(04), based on an iterative logic. This program solves the algorithm associated to the matrix of the partial derivatives of the state vector (**Mpdx**) method, associated with Taylor series, up to the partial derivatives of six order inclusively. The over-temperature $y_{00A}(t, s_0) = u_0 = 50^0$C, can be generated with a dental drill, too, for the adjustment of the dental surface. Certainly its value can be easily changed in the ZPROP03(04) program initialization stage. Consequently, the presented study has many applications in dental treatment domain.
4. The interpretation of the over-temperatures $y_{00}(t, s)$ obtained for each of the zones (A), (B), (C), (D) and (E), can imply interesting conclusions concerning the propagation in the interior of these zones, especially the discontinuities in quantity and direction, at the separation limit between these zones. The presence of the metallic medium from the zone (C) can imply a significant discontinuity and "over-increasing" for $y_{00C}(t, s)$.
5. Due to the two dedicated programs, respectively CTISP01(02) and ZPROP03(04), this study can be easily diversified and adapted for numerous specific phenomena of propagation in biological media.

Conflict of Interest The authors declare that they have no conflict of interest.

References

1. Colosi, H., Achimaş, A., Roman, N.M.: Evaluarea Biomecanicii Ortodontice prin Modelare şi Simulare. Galaxia Gutenberg, Cluj-Napoca (2011)

2. Abrudean, M.: Systems theory and automatic regulation. Mediamira Publishing house, Cluj-Napoca (1998)
3. Li, H.-X., Qi, C.: Spatio-Temporal Modeling of Nonlinear Distributed Parameter Systems: A Time/Space Separation Based Approach. Springer (2011)
4. Krstic, M.: Systematization of approaches to adaptive boundary control of PDEs. Int. J. Robust Nonlinear Control **16**, 801–818 (2006)
5. Morris, K.A.: In: Levine, W.S. (ed.) The Control Theory Handbook, Control of Systems Governed by Partial Differential Equations. CRC Press (2010)
6. Curtain, R.F., Morris, K.A.: Transfer functions of distributed parameter systems. Automatica **45**(5), 1101–1116 (2009)
7. Coloşi, T., Abrudean, M., Ungureşan, M.-L., Mureşan, V.: Examples of numerical Simulation for systems with distributed and lumped parameters through the Mpdx method with approximating solutions. UTPRESS Publishing House, Cluj-Napoca (2013)
8. Coloşi, T., Abrudean, M., Ungureşan, M.-L., Mureşan, V.: Numerical Simulation of Distributed Parameter Processes. Springer (2013)
9. Sita, I.-V.: Building control, monitoring, safety and security using collaborative systems. In: 4th International Conference on Intelligent Networking and Collaborative Systems, Bucharest, Romania, pp. 662–667 (2012)
10. Inoan, I.: Movement control of an unloading machine from a rotary furnace. In: Proceeding of AQTR 2010, THETA 17th edition, Cluj-Napoca, Romania, pp. 131–134 (2010)
11. Ungureşan, M.-L., Niac, G.: Pre-equilibrium kinetics. modeling and simulation. Russian J. Phys. Chem. **85**(4), 549–556 (2011)
12. User Guide, Matlab 7.5.0 (R2007b)

Part III
Biomedical Signal and Image Processing

Identification of Animal Species from Their Sounds

Gavril-Petre Pop

Abstract

Identification of animal species based on their sounds has already proven to be useful in biodiversity assessment. In this paper we explore the use of a combined Teager—cepstral—TESPAR (Time Encoded Signal Processing And Recognition) analysis to discriminate between different animal species. Our experiments using this approach together with classification techniques shows that TESPAR S-matrices of Teager cepstral coefficients along with some additional features can be successfully used to discriminate between different animal species, even in the conditions of small training sets.

Keywords

Animal species identification • Cepstral coefficients • TESPAR analysis • Teager energy operator • Machine learning

1 Introduction

Identification of animals by their sounds is important for biodiversity assessment, especially in detecting and locating animals [1]. Many animals generate sounds either for communication or to accompany their living activities.

One of the important tasks when analyzing animal sounds is to measure the acoustically relevant features. Majority of bioacoustics signals processing systems use time-frequency techniques such as the Fourier analysis, wavelets and energy distributions [2]. Most authors use cepstral coefficients (especially Mel frequency cepstral coefficients—MFCC) as acoustic characteristics for training and then testing under different classification systems.

Previously we have approached the possibility of using the TESPAR S-matrix applied to individual cepstral coefficients to visual differentiate sounds from different animal species. In this paper we investigate the use of Teager-MFCC coefficients (alone or along with other features) with TESPAR analysis to differentiate the sounds of different animal species. To test our idea we implemented a dedicated application for cepstral and TESPAR analysis (to generate final features) and a classification system using the machine learning Random Forest algorithm.

2 Features

Spectral features are frequently used to process acoustic signals. One of the most used spectral feature is represented by the MFCC coefficients (Mel Frequency Cepstral Coefficients). This is justified by the fact that some of the MFCC coefficients contain specific information about the emitter of sound, while other MFCC coefficients contain information about the message contained in the acoustic signal.

Another type of MFCC coefficients are obtained if, first, apply the Teager (or Teager-Kaiser) energy operator (TEO) on initial acoustic signal and then repeat the processing necessary to obtain the MFCC coefficients. In this way, we obtain so-called Teager-MFCC coefficients (T-MFCC) [3]. The TEO, is capable under appropriate signal constraints of accurately tracking the instantaneous amplitude and instantaneous frequency of the signal [4]. For discrete signals, the Teager operator is defined as:

$$\Psi[x_n] = x_n^2 - x_{n-1}x_{n+1} \tag{1}$$

In addition to the T-MFCC coefficients we also used other features, of which the best results we obtained with the following:

G.-P. Pop (✉)
Communications Department, Technical University of Cluj-Napoca, G. Baritiu, 26-28, Cluj-Napoca, Romania
e-mail: petre.pop@com.utcluj.ro

S. Vlad and N. M. Roman (eds.), *6th International Conference on Advancements of Medicine and Health Care through Technology; 17–20 October 2018, Cluj-Napoca, Romania*, IFMBE Proceedings 71,
https://doi.org/10.1007/978-981-13-6207-1_21

– Kurtosis:

$$K = \frac{\frac{1}{N}\sum_{i=1}^{N}(X_i - \mu)^4}{\sigma^4} \quad (2)$$

Where μ is the mean and σ is the standard deviation.

– Spectral Flux:

$$SP = \sqrt{\sum_{i=1}^{N-1}(X_{i+1} - X_i)} \quad (3)$$

3 Tespar Analysis

TESPAR algorithm is intended to classify time domain signals using some specific signal shape parameters. This algorithm is based on the position estimations of the signal real and complex zeroes. The first category of zeroes (real) correspond to the zero crossings of the initial signal while the complex zeroes are associated with local extremes (minima or maxima), points of inflexion etc. The detection of all complex zeroes is a difficult task but most of them can be simply estimated by combining [5] two descriptors (attributes) associated with each epoch of the time domain signal waveform (Fig. 1):

- the duration (D) between two successive real zeroes expressed as the number of samples between two zero crossings;
- the shape (S) between two successive real zeroes approximated by the number of minima (or maxima).

In this way, a signal in the time domain can be described as a succession of value pairs for these descriptors. Since many identical epochs with same duration and number of minima are likely to occur, it was born the idea of using an alphabet that associates a symbol for each value pair (D, S)

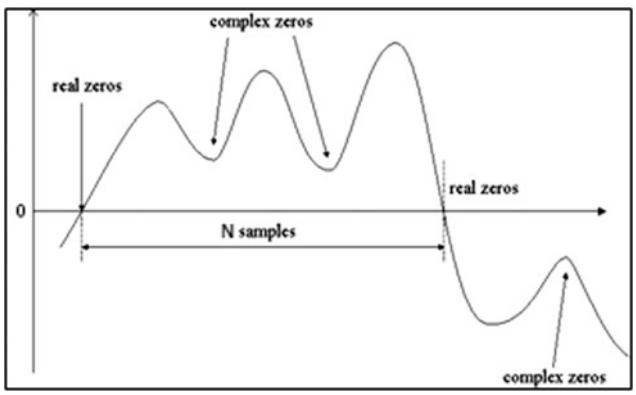

Fig. 1 TESPAR analysis for a time domain signal

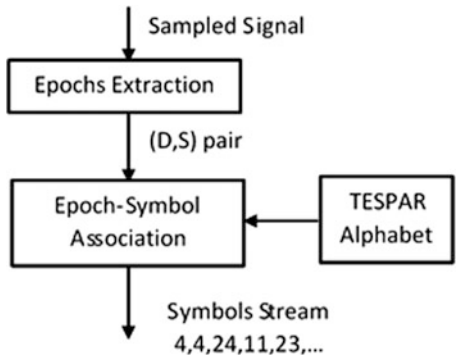

Fig. 2 TESPAR coding process

so that the initial signal can be described as a sequence of symbols in that alphabet (Fig. 2).

Another approach use an additionally signal descriptor A, for each epoch, such as epoch maximum amplitude, epoch energy, etc. In this case, the coding is based on a comparison of two successive epochs (for each descriptor D, S, A), as shown in Fig. 3. This is TESPAR DZ alphabet [6] with fixed number of symbols (in this case 27), regardless of the duration or complexity of an epoch. It should be mentioned

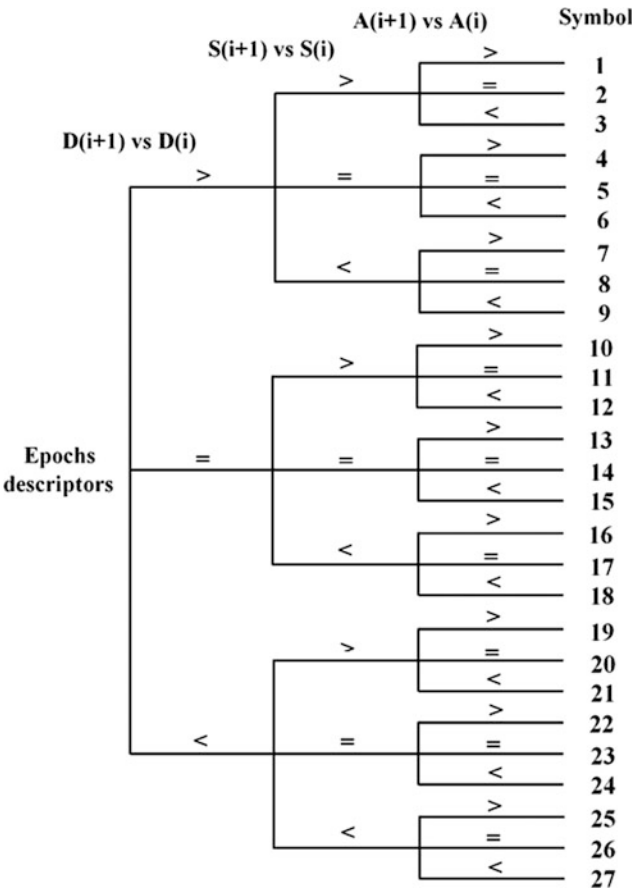

Fig. 3 TESPAR DZ alphabet with 27 symbols

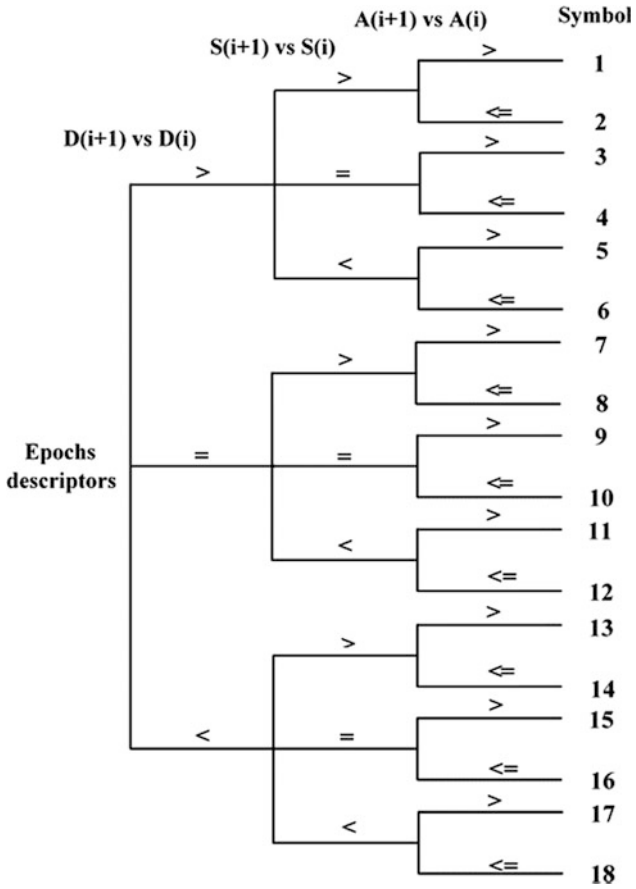

Fig. 4 TESPAR DZ alphabet with 18 symbols

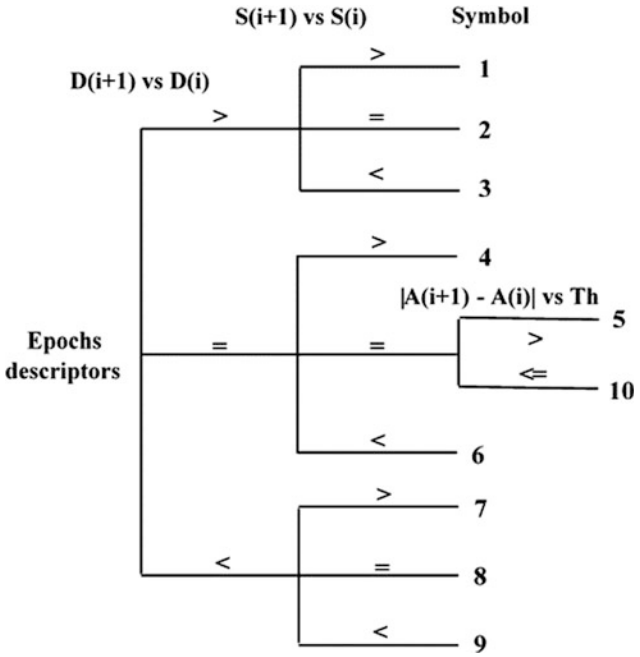

Fig. 5 TESPAR DZ alphabet with 10 symbols

that, in this case, the succession of epochs (duration, form, auxiliary descriptor value) is very important during the evolution of the signal over time.

Wanting to use a classifier, with a small amount of training data, it is desirable to have as few symbols as possible. For descriptors types A taken into account there are few situations where the values of the descriptor A are equal or very close for two successive epochs. For this reason we have designed two other TESPAR alphabets with 18 (Fig. 4) and 10 symbols respectively (Fig. 5).

Regardless of the alphabet used, the resulting TESPAR symbols string may be converted into fixed-dimension matrices [7]. The S-matrix is the histogram of TESPAR symbols. Given a symbol stream $s(i)$ of length M (resulting from the coding process using a specific alphabet with symbols 1,…, N), the elements of S matrix can be expressed as:

$$S_n = \frac{1}{M}\sum_{i=0}^{M-1} T_i, \quad 1 \le n \le N \tag{4}$$

where:

$$T_i = \begin{cases} 1, & \text{if } s(i) = n \\ 0, & \text{otherwise} \end{cases} \tag{5}$$

The contribution of each symbol to the S-matrix values can be weighted by the value of the associated A descriptor.

4 Experiments, Results and Discussions

To extract the attributes required for classification we realized a dedicated application that allows:

- pre-processing the acoustic signal (determine and eliminate silence zones, preemphazis, frame blocking, windowing) for a certain window length;
- computing a user specified number of T-MFCC coefficients for each frame;
- select and compute additional features (kurtosis/spectral flux) for each frame;
- TESPAR analysis (zero crossings, epochs, minima number for each epoch) for the selected feature values, with the possibility to visualize the epochs;
- generating symbol stream (coding) specifying the alphabet used (18 or 10 symbols) and the type of

additional epoch descriptor (epoch energy-En/epoch maximum amplitude-MaxA/maximum epoch Teager energy-MaxTE and threshold value-Th);
- generate and visualize TESPAR *S* matrix with the possibility of weighing symbols contribution;
- saving the TESPAR S matrix previously generated in the *arff* format (Attribute-Relation File Format) specific to the Weka application [8].

In our experiments we used sounds from different animal species (domestic and wild: bear, birds, cat, cow, elephant, lion, pig and sheep), taken from free sources [9, 7] and with great diversity in the quality of recordings and the acoustic parameters used. We used the TESPAR-DZ alphabet because it is invariable at the sampling frequency used to record the sounds (alphabet symbols are determined based on the ratio between two successive epochs).

Finally, we used a total of 25 audio recordings for each animal, of which 20 were used to train the classification algorithm (a total of 160 recordings for training) and the remaining 5 records were used for predictions (a total of 40 recordings for predictions).

We chose the Random Forest (RF) [10] algorithm for classification and conducted a series of experiments to find the combination of algorithm-specific model parameters (number of attributes to randomly investigate—K; number of iterations or the number of trees–I) that give the best results.

In our training-prediction experiments we used an instance (a set of attribute values together with associated class) for each animal sound recording, which means a total number of attributes equal to the product of the number of symbols in the TESPAR alphabet (in our case 18 or 10) and the number of features (T-MFCC coefficients and additional features).

Evaluation of predictive model in the training phase was done with the 10 folds cross-validation. For predictions, the confusion matrix and the TP Rate accuracy parameter were retained.

The following figures show the best results from the classification experiments for the two types of alphabet DZ with 18 symbols (Figs. 6 and 7) and 10 symbols (Figs. 8 and 9) respectively. In these figures N is the number of T-MFCC coefficients, K is the Kurtosis and SF is the spectral flux.

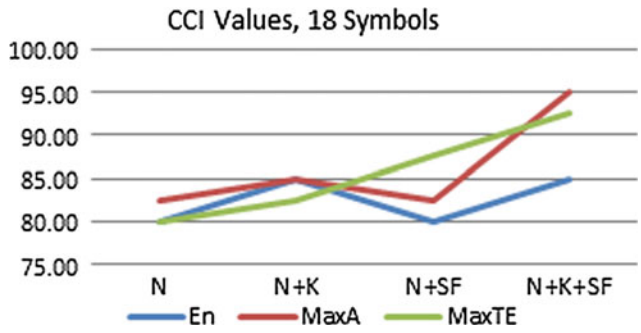

Fig. 6 Correctly classified instances (CCI; %) for 18 symbols alphabet

Good results obtained even for a small number of symbols and features can be explained by TEO ability to obtain representative time-frequency information for each animal species even on the basis of a small number of training records.

As can be seen, T-MFCC coefficients alone do not provide good classification rates (max 82.5%). Adding features provides much better results (95%). We conducted experiments with several types of additional features, both in the time domain and in the frequency domain. The best results were obtained with Kurtosis and spectral flow.

```
 a b c d e f g h  <-- classified as
 4 0 0 0 1 0 0 0 | a = bear
 0 5 0 0 0 0 0 0 | b = birds
 0 0 5 0 0 0 0 0 | c = cat
 0 0 0 5 0 0 0 0 | d = cow
 0 0 0 0 5 0 0 0 | e = elephant
 0 0 0 0 0 5 0 0 | f = lion
 0 0 0 0 0 1 4 0 | g = pig
 0 0 0 0 0 0 0 5 | h = sheep
```

Fig. 7 Confusion matrix for 18 symbols alphabet, N = 8, 10 ms, T-MFCC + Kurtosis + Spectral Flux, MaxA

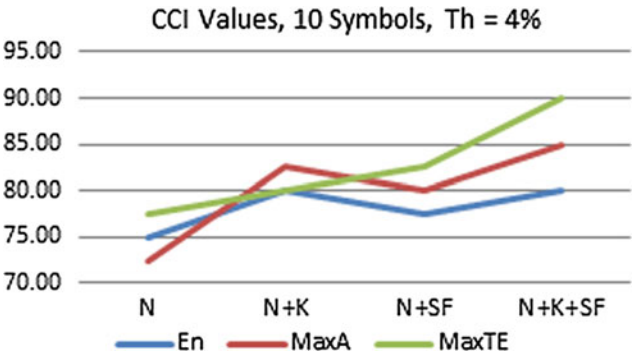

Fig. 8 Correctly classified instances (CCI; %) for 10 symbols alphabet

```
 a b c d e f g h  <-- classified as
 5 0 0 0 0 0 0 0 | a = bear
 0 5 0 0 0 0 0 0 | b = birds
 0 0 5 0 0 0 0 0 | c = cat
 0 0 0 5 0 0 0 0 | d = cow
 0 0 0 0 5 0 0 0 | e = elephant
 0 0 0 0 0 4 0 1 | f = lion
 0 0 1 0 0 0 3 1 | g = pig
 0 0 1 0 0 0 0 4 | h = sheep
```

Fig. 9 Confusion matrix for 10 symbols alphabet, N = 8, 10 ms, T-MFCC + Kurtosis + Spectral Flux, MaxTE, Th = 4%

As for the descriptor A, the best results were obtained with the epoch maximum amplitude and with the epoch maximum instantaneous Teager energy.

5 Conclusion

In this work, we investigated the use of TESPAR S-matrices of Teager cepstral coefficients along with some additional features and Random Forest classification algorithm to discriminate between animal species based on their sounds. First results show that the TESPAR S-matrices could be successfully used for this purpose. T-MFCC coefficients allow good results even in the conditions of small sets of training data with small length and, perhaps most important, with different sampling frequencies.

Conflict of Interest The authors declare that they have no conflict of interest.

References

1. Lee, C.-H., Lee, Y.-K., Huang, R.-Z.: Automatic recognition of bird songs using cepstral coefficients. J. Inf. Technol. Appl **1**(1), 17–23 (2006)
2. Chesmore, E.D.: Automated bioacoustic identification of species. An. Acad. Bras. Ciênc. **76**(2), 435–440 (2004)
3. Kaiser, J.F.: Some useful properties of Teager's energy operators. In: IEEE International Conference on Acoustics, Speech, and Signal Processing, pp 149–152 (1993)
4. Patil, H.A., Basu, T.K.: Identifying perceptually similar languages using teager energy based cepstrum. Eng. Lett. **16**(1), 151–159 (2008)
5. King, R.A., Phipps, T.C.: Shannon, TESPAR and approximation strategies. In: ICSPAT 98, vol. 2, pp. 1204–1212. Toronto, Canada, Sept. 1998 (1998)
6. Lupu, E., Emerich, S., Beaufort, F.: On-line signature recognition using a global features fusion approach. Acta Tech. Napoc., Electron. Telecommun. **50**, 13–20 (2009)
7. http://www.findsounds.com/types.html
8. http://www.cs.waikato.ac.nz/ml/weka/
9. http://soundbible.com/tags-animal.html
10. Breiman, L.: Random Forests. Mach. Learn. **45**(1), 5–32 (2001)

Evaluating a Method of Offline Detection of P_3 Waves

Dorina Ancău, Nicolae-Marius Roman, and Mircea Ancău

Abstract

Interest in using portable devices in neuroscience applications for people with serious motoric deficits has been growing in the last few years. The Emotiv EPOC$^+$ headset is one such device. This study aimed to assess the ability of this headset to determine event-related potentials and especially P_3. Four healthy subjects participated in this experiment during which the headset recorded potential evoked by auditory and visual stimuli. The method, the program of stimuli, the results of the measurements as well as the statistical approaches have already been established in previous studies. The measurements were performed with the headset and the software TestBench attached to the device. Data analysis was performed offline on electrodes FC_5, FC_6, F_3, F_4, P_7, P_8, O_1 and O_2. The Emotiv EPOC$^+$ headset was capable to distinguish the characteristic deflections of the P_3 component of event-related potentials. Even across a small number of subjects and trials the high signal-to-noise ratio of the device did not preclude a statistically significant result. The result obtained can be considered as a first step in determining P_3 or other ERP components using Emotiv EPOC$^+$.

Keywords

Emotiv EPOC$^+$ • Event-related potential (ERP) • P_3 • Brain-computer interface (BCI)

1 Introduction

A Brain-Computer Interface (BCI) is a communication and control system designed to decode brain bioelectric activity and then transform it into a control signal for a specific application, e.g., a clinical one. For people with neuromuscular disabilities or neurodegenerative diseases with serious motoric deficits, it is an alternative to natural communication or neuromuscular pathways, like an artificial bypass.

Control signals can be categorized into three categories [1]: event-related potentials (ERP), spontaneous signals and hybrid signals. Especially evoked potentials can be used to guide brain-computer interfaces. Evoked potentials are any stereotypical response of the brain to a stimulus, be it external or internal, sensory, cognitive or motoric. It can be measured at the level of the scalp by an electroencephalogram and is interpreted as a variation of the electrical field potential due to the extracellular summation of synchronous postsynaptic currents of many neurons from the surface of the cerebral cortex. The most well-known potentials are Steady State Visually Evoked Potentials (SSVEPs) and P_3. The most common ways to record these potentials are those that use high-resolution, professional EEG equipment, which, besides the large number of electrodes and therefore a cumbersome attachment to the scalp, requires a high acquisition cost. Incidentally, the P_3 speller is one of the most commonly used applications in BCI systems. The past few years have also witnessed remarkable performance in the development of low-cost and affordable portable devices. This latter point of view is relevant in measuring actual tasks by using a BCI in combination with existing assistive technologies. Emotiv EPOC$^+$ is a portable, multichannel interface designed, among other things, for research practice. Its potential for the acquisition and analysis of EEG signals has already been confirmed by numerous studies presented in the literature. Lievesley et al. [2], in 2011 have used the interface to test the control of a technical support system.

D. Ancău (✉) · N.-M. Roman
Faculty of Electrical Engineering, Technical University of Cluj-Napoca, Memorandumului 28, Cluj-Napoca, Romania
e-mail: dorina.ancau@yahoo.com

M. Ancău
Faculty of Machine Building, Technical University of Cluj-Napoca, Cluj-Napoca, Romania

S. Vlad and N. M. Roman (eds.), *6th International Conference on Advancements of Medicine and Health Care through Technology; 17–20 October 2018, Cluj-Napoca, Romania*, IFMBE Proceedings 71,
https://doi.org/10.1007/978-981-13-6207-1_22

With the exception of low transfer rates and poor accuracy, the results were encouraging. More than that, it was the use of Emotiv EPOC headset in a P_3 detection algorithm based on response to certain auditory stimuli [3, 4] or visuals [5]. The results indicated a high accuracy for ERP peaks, e.g., P_1, N_1, P_2, N_2 and P_3, but not for MMN (mismatch negativity) component. In 2013, Badcock et al. [6], adapt the Emotiv EPOC interface to the recording of evoked potentials elicited by auditive stimuli in adults and later, in 2014, in children.

A particular case of evoked potential is the error-related potential that arises from the awareness of a discrepancy between the expected result and the recorded outcome of an action or other subject (man or machine).

Theoretically, one can conceive a method of deciphering a complex intention by decomposing it with an algorithm in multiple successive binary decisions, which a subject with disabilities can address by issuing an error-related potential or not. A first step in achieving such an interface, providing portability and versatility, is testing the Emotiv EPOC$^+$ on recording well-known evoked potentials.

The approach of this study is based on the determination of the P_3 potential with the Emotiv EPOC$^+$ headset and the subsequent analysis of the recorded signal. Section 2 of this paper describes the methods and equipment used to conduct the experiments, and the third presents the results obtained.

The following sections mark the offline analysis of the signals, the conclusions and finally the perspectives of the research in this direction.

2 Experimental Setup

P_3 reflects, probably, the result of a process of distinguishing between an irrelevant (frequent or standard) and a relevant (rare or non-standard) stimulus. P_3 can be measured from an EEG signal in relation to the aperiodic appearance of some stimuli [7] at ca. 300–500 ms from the stimulus onset.

The recording of the evoked potentials was made using the Emotiv EPOC$^+$ headset with 14 (+2) channels corresponding to 14 electrodes that are placed directly on the scalp: AF_3, F_7, F_3, FC_5, T_7, P_7, O_1, F_4, F_8, AF_4 (locations P_3 and P_4 are CMS and DRL, ground and reference electrodes).

The study comprised two experimental protocols, one for training and one for data acquisition.

The analysis of the results was carried out only on the values obtained in the data acquisition session. The stimuli, in the form of images or sounds, were repeatedly presented on a computer using a program set in Psychtoolbox. Subjects were seated 1 m in front of a computer screen and monitored the succession of images and sounds.

Visual stimuli consisted of two squares, one red and one green, which appeared randomly in the middle of the screen for 200 ms. The probability of the stimulus occurence was set at 85% for blocks 1 and 4, and 75% for blocks 2 and 3 for standard ones (red square) and 15% and 25% for non-standard ones (green square). The interval between these stimuli was 500 ms. The duration of a block was approximately 2 min in visual stimulus sessions and about 4 min in auditory stimuli.

Auditory stimuli were composed of 85% standard tones of 150 ms and 1200 Hz and 15% deviant tones (nonstandard) of 150 ms and 1500 Hz. To avoid habituation, the interval between these stimuli was randomly chosen between 0.980 and 1.100 s. Rare tones were also presented randomly after 4–8 standard tones. The structure of the blocks and the number of stimuli of the two recording sessions is presented in Fig. 1. The two experimental sessions made it possible to check the frequency of occurrence of P_3 potentials in the records and also to control the results by comparing the signals from different tests and paradigms. The software attached to Emotiv EPOC$^+$ provides a working interface that displays real-time data stream (EEG) and monitors the quality of contact areas between electrodes and scalp through an impedance correlation index. Unlike most EEG systems designed for research purposes, EPOC Emotiv$^+$ is

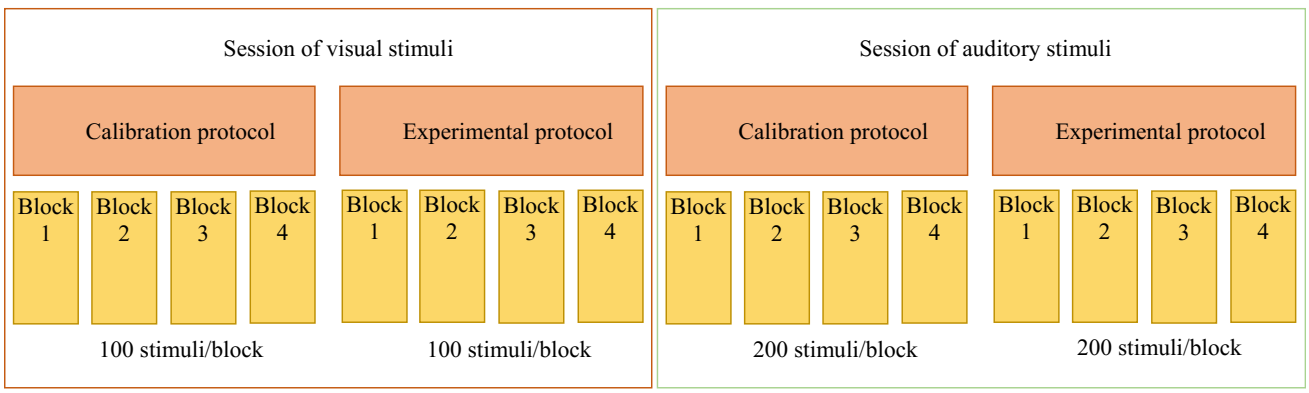

Fig. 1 Stimuli setup

not provided with hardware to integrate event trigger data into the EEG data stream.

Although the original TestBench software offers an event marking option through the serial port of the computer, this can lead to a substantial temporary inaccuracy of more than 20 ms. Some studies have addressed this challenge through hardware changes to the equipment for the purpose of providing accurately time-lock the EEG signal to the onset of each stimulus sacrificing EEG channels and using them for time markers [6].

In this experiment, the synchronization between the stimulus programs and EEG signal recording, was performed using an NTP protocol and the time markers were inserted into the electroencephalograms before the offline analysis. Synchronization between computers was of the order of 10–20 ms, an acceptable difference in record evoked potentials acquiring. The EEG signals were recorded at a sampling frequency of 128 Hz. The EEGLAB Matlab toolbox was used to visualize, process and analyze the obtained signals.

A preprocessing before the analysis consisted of eliminating the timebase, filtering the signal between 2 and 20 Hz, and then applying independent component analysis and manual filtering to remove artifacts. Epochs were set at 650 ms for visual stimuli and 750 ms for the auditory stimuli.

3 Experimental Results

To export the recorded data in EEGLab, a Matlab script was created.

Consistent with previous studies, P_3 appeared on the recorded signal as a positive voltage deviation with values generally ranging from 2 to 5 μV from 300 to 600 ms from the onset of the stimulus.

The peak amplitude of the P_3 component was, as expected, larger in non-standard stimulus trials (for auditory stimuli, mean ± S.D. [μV], std.: FC_5 −0.301 ± 0.642, FC_6 −0.105 ± 0.879, n = 2528 epochs; target: FC_5 0.711 ± 1.499, FC_6 0.596 ± 1.668, n = 414 epochs; Student's t-Test, H = 1, P = 2.2e-3; for visual stimuli: mean ± S.D. [μV], std.: FC_5 0.027 ± 0.750, FC_6 0.328 ± 1.06, n = 1062 epochs; target: FC_5 0.905 ± 0.1887, FC_6 0.851 ± 1.713, n = 286 epochs; Student's t-Test, H = 1, P = 4e-3), Table 1.

In line with this, high amplitudes of the signals around a latency of 300 ms could be visually noted in non-standard stimulus trials.

A representative grand average from the electrode FC_5 of subject S_4 from a visual stimulus session can be seen in Fig. 2.

Table 2 shows the number of valid epochs from the 320 standard and 80 nonstandard trials in the visual and, correspondingly, 680 and 120 trials from the auditory paradigm.

Table 1 Peak amplitudes and latencies of the P_3 component for visual and auditory trials

Session/subject	Session of visual stimuli							
	S_1		S_2		S_3		S_4	
Electrode	V (μV)	Latency (ms)	V (μV)	Latency (ms)	V (μV)	Latency (ms)	V (μV)	Latency (ms)
FC_5	3.364	460.937	4.181	351.562	4.105	453.125	4.990	304.687
FC_6	3.599	453.125	2.494	437.500	5.160	500.000	1.416	312.500
F_3	1.675	445.312	1.611	351.562	3.103	445.312	3.569	382.812
F_4	3.882	453.125	4.102	351.562	4.336	500.000	3.839	304.687
P_7	1.700	343.801	2.266	370.554	4.110	312.500	3.842	304.700
P_8	0.758	375.011	0.933	343.800	1.924	351.612	1.662	367.200
O_1	2.932	328.125	2.002	343.800	5.263	312.500	3.275	492.187
O_2	1.785	460.900	5.933	445.312	4.501	453.125	3.700	375.000
Session/subject	Session of auditory stimuli							
	S_1		S_2		S_3		S_4	
Electrode	V (μV)	Latency (ms)	V (μV)	Latency (ms)	V (μV)	Latency (ms)	V (μV)	Latency (ms)
FC_5	2.453	468.750	3.302	414.062	3.961	406.250	4.811	414.062
FC_6	2.798	429.687	3.484	406.300	3.679	320.312	5.821	406.250
F_3	0.292	328.100	1.065	367.200	4.686	359.375	2.290	351.562
F_4	1.676	421.875	5.508	367.200	2.227	359.375	3.881	421.875
P_7	2.752	320.300	3.522	382.800	3.838	312.500	4.471	359.400
P_8	1.029	398.414	0.685	367.200	0.381	310.655	0.569	351.600
O_1	4.099	359.375	4.160	351.600	2.493	406.250	2.313	398.400
O_2	4.129	367.187	4.572	359.400	1.124	304.687	5.189	468.800

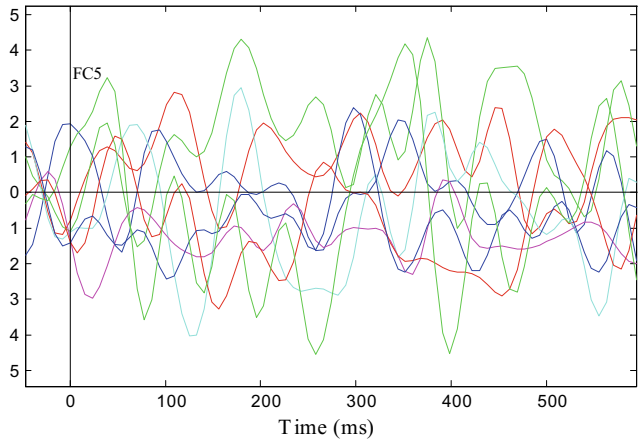

Fig. 2 Grand averages of the visually evoked potential on electrode FC_5 in subject S_4. Green lines correspond to target epochs (non-standard stimulus) and red and blue lines correspond to standard epochs

Table 2 Total number of valid epochs

Stimulus type		Visual stimuli	Auditory stimuli
Subject			
Sub. 1	Standard	222	666
	Target	62	108
Sub. 2	Standard	246	594
	Target	73	101
Sub. 3	Standard	284	605
	Target	72	93
Sub. 4	Standard	310	663
	Target	79	112

The validity of each measurement was confirmed by visual inspection of the records and then calculation of the distribution of the signals, which corresponded, as expected, to a normal distribution, Table 3.

4 Discussion

It is known that the maximum amplitude of P_3 is recorded especially in the median region of the brain, which corresponds to the electrodes Fz, Cz and Pz. However, because of the small number of available electrodes of Emotiv EPOC$^+$, the FC_5, FC_6, F_3, F_4, P_7, P_8, O_1 and O_2 electrodes were used for analysis. Recorded data showed high amplitudes on the FC_5, FC_6 and O_1 and O_2 electrodes. This confirmed the results of a study by Ekanayake [8].

For S_1, for example, the maximum amplitude of P_3 decreased from the FC_5 and FC_6 electrodes to those in the parietal and occipital zones in the visual stimulus session. An explanation could be the attenuation of signal propagated from the frontal-central area. This was not the case with auditory stimuli, where there was a large amplitude in O_1 and O_2. A more subtle data analysis of the P_3 component would consist in separating the temporal axis of an epoch into equal size samples and analyzing them individually.

Table 3 Mean and standard deviation of peak amplitudes of P_3 on electrodes FC_5 and FC_6

Mean and standard deviation		μ (μV)		σ (μV)	
Stimuli		FC_5	FC_6	FC_5	FC_6
Visual	Standard	0.0027	0.3278	0.7503	1.0606
	Target	0.9050	0.8509	1.8869	1.7125
Auditory	Standard	−0.301	−0.105	0.6415	0.8794
	Target	0.7109	0.5961	1.4988	1.6677

Another alternative would be to increase the number of data points by performing multi-block experiments on multiple subjects. This would be particularly relevant to compensate the low signal-to-noise ratio for Emotiv EPOC$^+$.

Small values recorded on F_3 and F_4 electrodes may be caused by blinking artifacts or imperfect contacts between electrodes and scalp. For example, P_7 and P_8 electrodes have been influenced by heart rate and many of the epochs have been eliminated on this criterion.

The result of the current study may be a first step in establishing Emotiv EPOC$^+$ as a tool for measuring evoked potentials.

5 Conclusion

This study investigated the P_3 detectability without the use of a classifier using Emotiv EPOC$^+$ in four subjects. The obvious biological and technical artifacts in the EEG signal have been eliminated by filtering and analyzing the independent components or by changing the reference potential.

From the data obtained, the quality of the recorded signals was quantified. The resulting P_3 wave was not particularly clear using the above procedures, but given the possibility of more detailed statistical analysis, introducing an ERP component classifier and expanding the number of experiments, the result obtained can be considered as a first step in determining P_3 or other ERP components using Emotiv EPOC$^+$. It has also been noted that the lack of a reliable tool to insert time-markers during recording may be a weak point of this headset. More effort is needed to improve the performance of the device in determining such low amplitude signals and time-locked.

Conflict of Interest The authors declare no conflict of interest.

Reference

1. Ramadan, Rabie A., Vasilakos, Athanasios V.: Brain computer interface: control signals review. Neurocomputing **223**, 26–44 (2017)
2. Lievesley, R., Wozencroft, M., David Ewins, D.: The Emotiv EPOC neuroheadset: an inexpensive method of controlling assistive technologies using facial expressions and thoughts? J. Assist. Technol. **5**, 67–82 (2011)
3. Debener, S., Minow, F., et al.: How about taking a low-cost, small, and wireless EEG for a walk? Psychophysiology **49**, 1617–1621 (2012)
4. De Vos, et al.: P300 speller BCI with a mobile EEG system: comparison to a traditional amplifier. J. Neural Eng. vol. **11**, (2014). https://doi.org/10.1088/1741-2560/11/3/036008
5. Duvinage, M., et al.: Performance of the Emotiv EPOC headset for P300-based applications. BioMed. Eng. OnLine **12**, 56 (2013)
6. Badcock, N.A. et al. Validation of the Emotiv EPOC EEG system for research quality auditory event-related potentials in children (2015). https://doi.org/10.7717/peerj.907
7. Luck, S.J.: An Introduction to the event-related potential technique, 2nd edn, pp. 95–102, MIT Press (2014). ISBN 978-0-262-52585-5
8. Ekanayake, H.: P300 and Emotiv EPOC: Does Emotiv EPOC capture real EEG? (2010). http://neurofeedback.visaduma.info

An ECG Morphological Analysis Algorithm for Hybrid Patient Monitoring

A. Raza, Paul Farago, M. Cirlugea, and S. Hintea

Abstract

Screening and diagnosis in ubiquitous healthcare environments is performed by the medical staff in the presence of a variety of medical data originating from continuous in vivo patient monitoring. This assumes the correlation of data, such as vital signs, biopotentials, activity tracking, bio-markers, etc., in the context of hybrid clinical monitoring. The hybrid patient monitoring setup envisioned in this work targets the simultaneous assessment of body fluids via electro-optical means and of electrophysiological data, i.e. electrocardiogram, via biopotential monitoring. Accordingly, the aim of this paper is to propose an electrocardiogram morphological analysis algorithm applicable in the framework of the envisioned hybrid monitoring setup. Electrocardiogram morphological analysis is performed in time domain in two stages. The R, S and Q waves are first identified via comparison to a threshold value. Then, the P and T waves are identified via cross-correlation to a reference signal. The novelty of this work is that cross-correlation is performed after the QRS complex was eliminated from the electrocardiogram. Expectedly, this leads to improved results in wave identification and to a reduction of false detections. Matlab simulation results validate the proposed procedure.

Keywords

Biomedical equipment • Biomedical monitoring • Biomedical signal processing • Signal processing algorithms

Introduction

In modern ubiquitous healthcare environments, a variety of medical data originating from continuous in vivo patient monitoring is available to the medical staff for screening towards the formulation of a diagnosis. The diagnostics procedure assumes that, in the context of hybrid clinical monitoring [1], medical data originating from vital signs, biopotentials, activity tracking, bio-markers, etc., must be correlated in order to sum up to a sustained conclusion with regard to the patient's state oh health. For exemplification, screening and diagnosis of myocardial necrosis can be performed by correlating the electrocardiogram (ECG) with measures of saliva-based serum biomarkers [2]. Another example, a skin-worn wearable hybrid sensor provides fitness monitoring via biochemical lactate sensing and ECG [1].

Biomedical monitoring creates the link between the biological part, i.e. functioning of the human body, and the electronic part, i.e. measurable electronic signals. Ubiquitous healthcare environment targets miniature, wearable, portable and even implantable hybrid monitoring devices. In this context, low-power, low-voltage and low-noise biomedical electronics answers the need for reliable measurements regarding the functioning of the human body [3].

One significant feature of wearable health monitors is the ability of patients to self-monitor their state of health [4]. This, on one hand, reduces hospital crowding. On the other hand, it allows patients to become more self-aware and to contribute to their state of health.

The hybrid monitoring setup envisioned for this work targets the simultaneous assessment of body fluid data via electro-optical biosensors and electrophysiological data via biopotential monitoring. Keeping in mind the variety of the biological stimuli, some aspects have to be taken into account with regard to the acquisition front-end. Ag/AgCl electrodes are used for ECG acquisition, whereas specific optoelectronic transducers are required for bio-sensing.

A. Raza · P. Farago (✉) · M. Cirlugea · S. Hintea
Bases of Electronics Department, Faculty of Electronics, Telecommunications and Information Technology, Technical University of Cluj-Napoca, George Barițiu, 26-28, 400027 Cluj-Napoca, Romania
e-mail: paul.farago@bel.utcluj.ro

S. Vlad and N. M. Roman (eds.), *6th International Conference on Advancements of Medicine and Health Care through Technology; 17–20 October 2018, Cluj-Napoca, Romania*, IFMBE Proceedings 71,
https://doi.org/10.1007/978-981-13-6207-1_23

Further on, ECG processing targets the assessment of the ECG morphology, whereas optoelectronic bio-sensing targets the measurement of the sensed parameters.

The aim of this paper is to propose an ECG morphological analysis algorithm for applicability in the context of hybrid patient monitoring. The morphological analysis is performed in two stages. The R wave and the QRS complex are identified by comparison to a threshold level. Next, identification of the P and T waves is performed by cross-correlation to a reference ECG signal after the QRS complex has been eliminated and replaced with isoelectric line, which constitutes the novelty of this work. Elimination of the QRS complex before the cross-correlation will expectedly reduce the number of false identifications.

This article is organized as follows. Section 2 presents a description of the hybrid monitoring setup. Next, Sect. 3 presents the ECG morphological analysis algorithm. Simulation results are presented in Sect. 4. Finally, some conclusions are drawn in Sect. 5.

The Hybrid Patient Monitoring Setup

The block diagram of the proposed hybrid monitoring setup is illustrated in Fig. 1 and is explained as follows. The patient monitoring setup consists of two modules. An optical sensor performs sensing of body fluids, e.g. saliva, blood, sweat, etc., using optical means. For exemplification, Djuric et al. uses reflective photoplethysmography (PPG) as an optical means for the long-term measurement of arterial blood flow waveform [5]. Kwon et al. develops a reflection type optical sensor for the non-invasive measurement of blood oxygen saturation [6]. With regard to optical salivary sensing, Tan et al. describes a surface immobilized optical protein sensor for the detection of cancer markers in the saliva [7]. Optical perspiration sensing can be exemplified by the employment of 2-hydroxy-1,4-naphthoquinone as sensing material to detect hydration levels [8], as described by Alomari et al. Next, after the optical sensing module, specific signal processing procedures are performed in the signal analysis and interpretation section in order to compute some (vital) signs and possibly indicate a diagnosis.

The proposed hybrid monitoring setup aims to correlate medical information gathered by the optical sensor with electrophysiological data. For this purpose, the second module in the patient monitoring setup is an ECG acquisition module which uses Ag/AgCl electrodes to sense the electrical activity of the heart, followed by specific ECG acquisition preprocessing in terms of $\times 100$ gain, 0.05–100 Hz bandpass filtering and 50 Hz reject filtering [9]. A Mikroelektronika EMG click bundle was used for this purpose. Next, after analog to digital conversion (ADC), a digital signal processing (DSP) section operates towards extracting morphological parameters from the ECG signal.

ECG Morphological Analysis Algorithm

The implementation of the proposed ECG morphological analysis algorithm, illustrated in the block diagram in Fig. 2 is explained as follows. Acquisition of the lead-I ECG signal is performed with the Mikroelektronika EMG click bundle and the Analog Discovery acquisition board from Digilent. Using the Scope tool from the Digilent Waveforms environment, the ECG signal is saved to a. csv format which is then imported to Matlab for some pre-processing and morphological analysis. Pre-processing of the ECG signal consists of de-noising, which is performed in this work by application of a mean filter with an 18 sample window length. At this stage, it is sensible to assume a “clean” ECG signal available for further analysis and wave identification.

Morphological analysis is performed in the time domain in two stages. First, the R wave and the QRS complex are identified by comparison to a threshold value. Afterwards, the P and T waves are identified by means of cross-correlation with a reference ECG signal. The novelty of the proposed solution consist in having the QRS complex eliminated from both the reference and acquired ECG signals before the identification of the P and T waves respectively. This approach will presumably reduce the false detections of the P and T waves.

Each step in the proposed ECC wave identification algorithm is detailed as follows. First, identification of the R wave is straightforward. The R peak has the largest amplitude in the ECG signal. Accordingly, it is considerably

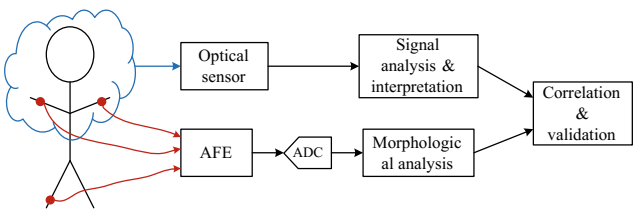

Fig. 1 Block diagram of the proposed hybrid patient monitoring setup

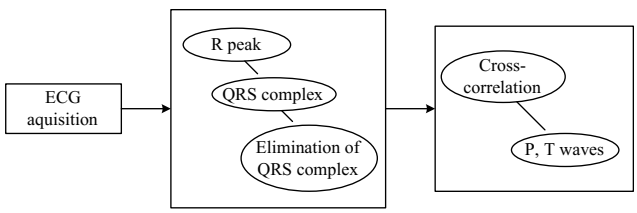

Fig. 2 Block diagram of the proposed ECG analysis algorithm

larger than every other wave of the ECG signal and its amplitude can easily be determined using a *maximum* function. The R wave is then easily identified by comparison with a threshold value, which is considered to be a relative 50% of the R peak rather than an absolute comparison threshold value. Indeed, the 50% threshold level ensures that the threshold level is above both the P and the T wave amplitudes respectively.

The proper identification of the R wave must also consider the segments situated under the threshold level. Accordingly, a number of samples situated in-between the zero-crossing and the threshold level on the R-wave rising edge, as well as in-between the threshold level and the zero-crossing on the R-wave falling edge, must also be added to the R wave. For this purpose, we have empirically determined that the number of samples which must be added to the R wave before and after the threshold crossings correspond to 1.85 and 0.15% of the R-R interval respectively. For exemplification, a 0.68 s R-R interval with a 2.6 kHz sampling rate gives an additional 33 samples before and 3 samples after the threshold crossings on the rising and falling edges respectively.

The Q and the S waves are next identified as the *local minima* before and after the R peak respectively. Since the S peak has the largest negative value of the ECG signal, its amplitude is again easily determined using a *minimum* function. The S waves are then identified and isolated similarly to the R waves, namely comparison to a 50% threshold of the maximum negative value, followed by the addition of samples before and after the threshold crossings on the rising and falling edges respectively.

On the other hand, isolation of the Q wave following the same procedure imposing a comparison threshold is limited by local minima due to noise. To handle this limitation, the ECG wave was filtered with a 4th order 2 Hz cutoff frequency Butterworth highpass filter and a 4th order 20 Hz cutoff frequency Butterworth lowpass filter. This enables the determination of the Q wave indices as the local minima before the R peak indices in the filtered signal.

In the second stage, the ECG wave identification algorithm operates towards identifying the P and the T waves respectively by means of cross-correlation to a reference signal [10, 11]. Although effective, this approach is limited in the presence of artifacts and noise. Indeed, similarities between the P and the T waves, also highlighted in terms of power spectral density, spectrogram analysis and average power [12], may cause the false detection of the P and T waves respectively.

In our approach, we keep the idea of cross-correlating the ECG signal to a reference signal. However, prior to cross-correlation, we eliminate the QRS complex from both the reference signal and the ECG under analysis. Thus, we only cross-correlate two signals consisting of the P and the T waves respectively. The proposed approach would presumably reduce the number of false detections of the P and T waves.

The cross-correlation maxima resembles the maximum values for the segments where the QRS complex was deleted from both the reference signal and the ECG under analysis signal. This is due to the fact that the two signals exhibit the best resemblance in those segments. In contrast to cross-correlating the original ECG and reference signals however, the cross-correlation side-lobes are in the proposed approach more prominent for the P and the T waves respectively.

Some band limitation filtering was further applied to the cross-correlation signal in order to limit the maxima due to the segments where the QRS complex was deleted, and to enhance the side peaks due to the P and T waves respectively. This procedure enhanced the identification of the lag between the P and T waves of the reference signal and the ECG under analysis respectively.

Simulation Results

The reference lead-I ECG frame, acquired from a healthy subject with the Mikroelektronika ECG click bundle and imported to Matlab is plotted in the top window from Fig. 3. The lead-I ECG signal under analysis is plotted next in the bottom window from Fig. 3.

The first stage of the ECG morphological analysis algorithm operates towards identification of the QRS complex in time domain via comparison to a threshold value. Isolation of the R, the S and the Q waves is illustrated in the top, middle and bottom subplots from Fig. 4 respectively.

The second stage of the ECG morphological analysis algorithm operates towards cross-correlating the ECG signal to a reference ECG frame in order to identify the P and the T waves. The reference ECG frame and the ECG under

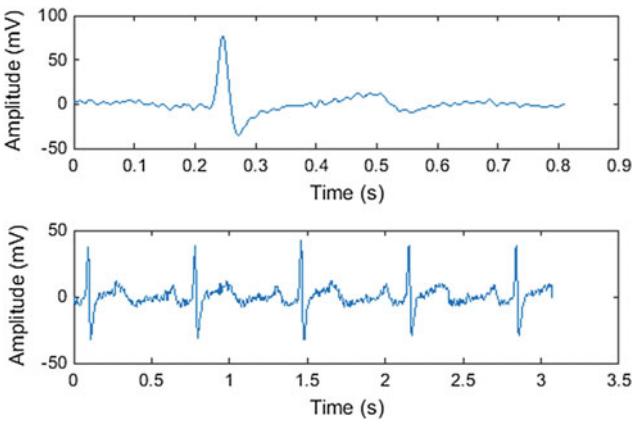

Fig. 3 The reference and the ECG under analysis signals

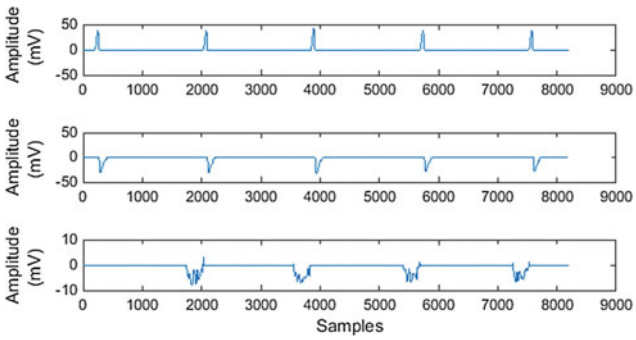

Fig. 4 The isolated R, S and T waves from the ECG signal

analysis signal, having the QRS complex eliminated, are illustrated in the top subplots from Fig. 5. The cross-correlation of the two signal is illustrated next in the third subplot from Fig. 5. Finally, the band-limited cross-correlation signal is illustrated in the bottom plot from Fig. 5. The blue and red ticks on the local maxima of the band-limited cross-correlation signal stand for the deviation of the P and T waves with respect to the reference ECG.

Finally, The ECG signal with the highlighted waves is plotted in Fig. 6.

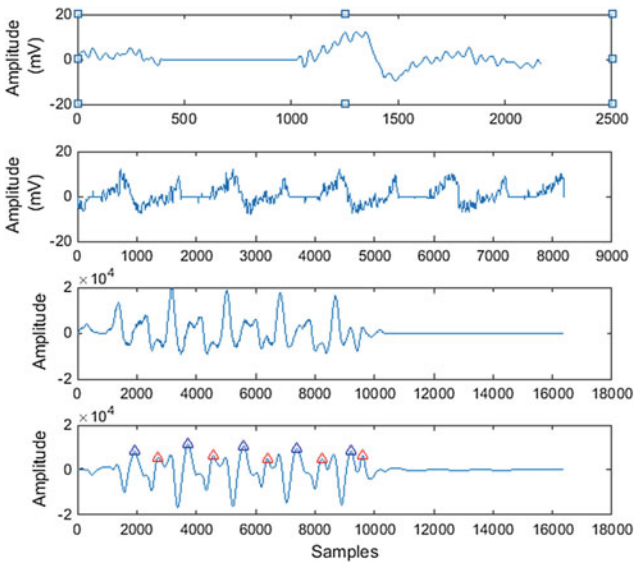

Fig. 5 Cross-correlation of the reference and under analysis ECG signals after the elimination of the QRS complex

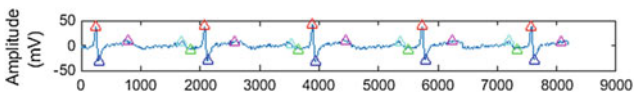

Fig. 6 The P, Q, R, S and T waves on the initial ECG signal

Conclusions

This paper presented a novel ECG morphological analysis algorithm for applicability in a hybrid patient monitoring setup for ubiquitous healthcare. The proposed algorithm employs traditional procedures for ECG time-domain analysis, namely comparison to some threshold values for the identification of the QRS complex and cross-correlation for the identification of the P and T waves. The novelty of this work consists in having the QRS complex removed from the ECG signal prior to cross-correlation. This operation was proven via simulation to lead to a reduction of false detections of the P and T waves.

At this stage of the development process, the proposed algorithm is validated with Matlab simulation. As future work, we target the implementation of the algorithm on a microcontroller and deploy it into an ECG monitoring setup for real-time estimation of the ECG morphology.

Acknowledgements This study was supported by the COFUND-ERA-HDHL ERANET Project, European and International Cooperation—Subprogram 3.2—Horizon 2020, PNCDI III Program—Biomarkers for Nutrition and Health—"Innovative technological approaches for validation of salivary AGEs as novel biomarkers in evaluation of risk factors in diet-related diseases", no 25/1.09.2017.

Conflict of Interest The authors declare that they have no conflict of interest.

References

1. Imani, S., Bandodkar, A.J., et al.: A wearable chemical–electrophysiological hybrid biosensing system for real-time health and fitness monitoring. Nature Commun. vol. **7** (2016)
2. Floriano, P.N., Christodoulides, N., et al.: Use of saliva-based nano-biochip tests for acute myocardial infarction at the point of care: a feasibility study. Clin. Chem. **55**(8), 1530–1538 (2009)
3. Sarpeshkar, R.: Ultra low power bioelectronics fundamentals, biomedical applications, and bio-inspired systems. Cambridge University Press (2010)
4. Odame, K., Du, D.: Towards a smart sensor interface for wearable cough monitoring, 2013. In: IEEE Global Conference on Signal and Information Processing (GlobalSIP) (2013)
5. Djurić, B., Suzić, S., et al.: An improved design of optical sensor for long-term measurement of arterial blood flow waveform. Biomed. Microdevices **19**(3), 48 (2017). https://doi.org/10.1007/s10544-017-0196-x
6. Kwon, K., Park, S.: An optical sensor for the non-invasive measurement of the blood oxygen saturation of an artificial heart according to the variation of hematocrit. Sens. Actuators A **43**(1–3), 49–54 (1994)
7. Tan, W., Sabet, L., et al.: Optical protein sensor for detecting cancer markers in saliva. Biosens. Bioelectron. **24**(2), 266–271 (2009)
8. Alomari, M., Liu, G., et al.: A portable optical human sweat sensor. J Appl Phys **116**, 18. https://doi.org/10.1063/1.4901332 (2014)

9. Thakor, N.V.: Biopotentials and electrophysiology measurement. CRC Press LLC (2000)
10. Ramli, A.B., Ahmad, P.A.: Correlation analysis for abnormal ECG signal features extraction, NCTT 2003. In: Proceedings of 4th National Conference of Telecommunication Technology. https://doi.org/10.1109/nctt.2003.1188342 (2003)
11. Last, T., Nugent, C.D., et al.: Multi-component based cross correlation beat detection in electrocardiogram analysis. Biomed. Eng. Online. https://doi.org/10.1186/1475-925x-3-26 (2004)
12. Joshi, S.L., Vatti, R.A., et al.: A survey on ECG signal denoising techniques, 2013. In: International Conference on Communication Systems and Network Technologies (CSNT), pp. 60–64 (2013)

Empirical Mode Decomposition in ECG Signal De-noising

Zoltán Germán-Salló, Márta Germán-Salló, and Horaţiu-Ştefan Grif

Abstract

Empirical Mode Decomposition (EMD) is an acknowledged procedure which has been widely used for non-stationary and nonlinear signal processing. The main idea of the EMD method is to decompose the processed signal into components without using any basis functions. This is a data driven representation and provides intrinsic mode functions (IMFs) as components. These are obtained through a so-called sifting process. This study presents an EMD decomposition-based filtering procedure applied to ECG signals (from specific databases), the results are evaluated through signal to noise ratio (SNR) and mean square error (MSE). The obtained results are compared with discrete wavelet transform based filtering results.

Keywords

Empirical mode decomposition • Signal processing • Denoising

1 Introduction

Signal processing involves procedures that ameliorate the understanding of information contained in various way received data. The most common processing method in the time or frequency domain is filtering in order to obtain an enhancement of the initial signal. Through filtering it is possible to remove unwanted components keeping or enhancing others. Usually, the most recognized procedures (frequency, time-frequency analysis) use different transforms in filtering and feature extraction. These transforms use basis function expansions which suppose priori knowledge about the signals.

For practical purposes, it is better to use an adaptive transform as the Empirical Mode Decomposition (EMD) which is strongly dependent on the original signal. The EMD as procedure was first proposed as the essential part of the Hilbert–Huang transform (HHT) [1]. EMD decomposes a signal in the time domain through an iterative sifting process. Shortly, this algorithm detects local maxima and minima in a signal, interpolates these values in upper and lower envelopes and removes theirs instantaneous mean value [2, 3]. This is made repetitively separating the high pass components in Intrinsic Mode Functions (IMFs) on the remaining centerline. The process of decomposition should be ended before loss of information appears, so a stop criterion is applied. In the specific literature several stoppage criteria are proposed [4], the most usual one is the Cauchy-type criteria which is based on the standard deviation of two consecutive IMFs. Via such procedure any signal can be decomposed into a series of prototype IMFs [5].

In this paper, EMD based filtering procedure is presented. This is fully data-driven and as iterative process explores sequentially the natural component scales of a signal.

The paper is formed as follows. Section 2 introduces the theoretical knowledge about EMD algorithm based on sifting process. Section 3 describes the de-noising algorithm based on IMFs thresholding and selective and partially reconstruction from them. The experimental results of the proposed method are presented in Sect. 4. Finally, the last section presents the conclusions which can be obtained after applying the proposed procedure and tries to find valuable new directions for further work.

Z. Germán-Salló (✉) · Horaţiu-Ştefan Grif
Faculty of Engineering, University of Medicine, Pharmacy, Sciences and Technology of Targu-Mures, 1, Nicolae Iorga, Tirgu-Mures, Romania
e-mail: zoltan.german-sallo@ing.upm.ro

M. Germán-Salló
Faculty of Medicine, University of Medicine, Pharmacy, Sciences and Technology of Targu-Mures, Tirgu-Mures, Romania

S. Vlad and N. M. Roman (eds.), *6th International Conference on Advancements of Medicine and Health Care through Technology; 17–20 October 2018, Cluj-Napoca, Romania*, IFMBE Proceedings 71,
https://doi.org/10.1007/978-981-13-6207-1_24

2 Empirical Mode Decomposition

The EMD decomposes a multi-component signal into its mono-component constituents. The algorithm is based on obtaining interpolated envelope curves defined by local maxima and minima of a discrete signal and iterative subtraction of the mean of these curves from the initial signal. For these is needed to identify all local minima and maxima in the signal. The upper and lower envelope curves are then obtained by interpolating these extrema through cubic spline functions. Sequentially removing the instantaneous mean value of these two envelopes leads to obtain IMFs. These at any time have zero instantaneous mean and the number of zero crossings is equal or greater with maximum one then the number of local extrema. These are the requirements which must be satisfied by IMFs [6].

The EMD decomposes the signal into IMFs following these procedural steps, named sifting process:

For a given discrete signal $s(t)$, m_1 is the mean value of its upper and lower envelope curves of local maxima and minima. The first prototype component c_1 is computed:

$$\mathrm{c_1 = s(t) - m_1} \tag{1}$$

In the second sifting process, c_1 is treated as the data, and m_{11} is the mean of c_1's upper and lower envelopes:

$$\mathrm{c_{11} = c_1 - m_{11}} \tag{2}$$

This sifting procedure is repeated k times, until c_{1k} is signal IMF, that is:

$$c_{1(k-1)} - m_{1k} = c_{1k} \rightarrow c_1 \tag{3}$$

If this component satisfies the stop criteria for IMF sifting, c_1 this will be the first IMF. The residual signal will be constructed as follows:

$$\mathrm{r(t) = s(t) - c_1} \tag{4}$$

If $r(t)$ satisfies the stop criterion for EMD then it will be the final residual signal and the EMD process will be finished. The IMF sifting method makes prototype IMFs more symmetric according to zero. The sifting process ends when a mathematical defined stoppage criterion is satisfied. This criterion serves to obtain an equitable decomposition without loss of information. The most common stoppage criterion was defined by Cauchy and acts when the standard deviation between two consecutive IMFs reaches a predefined value [7, 8]. The number of obtained IMFs depends on the original signal and on the threshold value used by the stoppage criterion. Practically the EMD procedure offers a projection of the analyzed signal onto a time-frequency space, preserving the time-varying behavior of each component. The result can be seen as a family of frequency ordered constituents, each of them contains lower frequency variations than the preceding one [9]. The procedure of plotting the envelope curves from local maxima and minima in the case of an ECG signal is shown in Fig. 1.

3 The Proposed Procedure

The proposed algorithm and the computational procedures are carried out in MATLAB. The used ECG signals are taken from MIT-BIH database. At first, the EMD procedure is applied to the signal in order to obtain the set of IMFs. Selective filtering of IMFs is the next step, after that the filtered (or smoothed) IMFs will be summed to obtain the reconstructed and filtered signal (Fig. 1). In this case filtering means a thresholding process for each IMF. These threshold values can be obtained experimentally or can be adapted from other types of denoising methods as discrete wavelet transform based procedures [10] (Fig. 2).

Usually the noisy signal x_n is assumed to be the superposition of a clean signal x and a Gaussian white noise n

$$\mathrm{x_n = x + n} \tag{5}$$

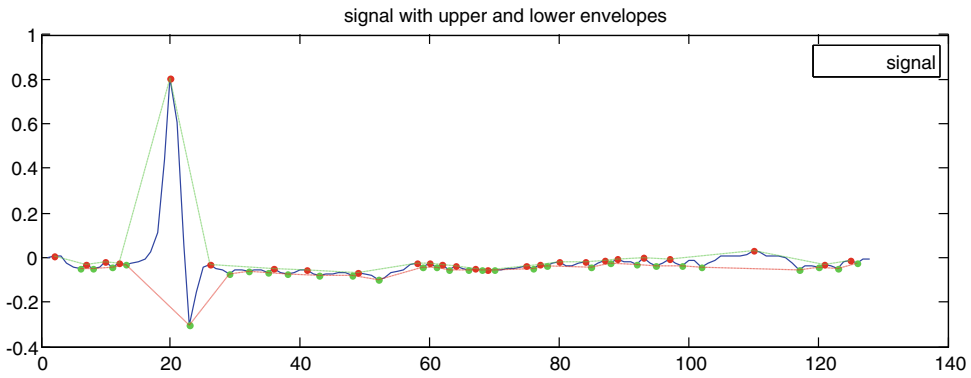

Fig. 1 The envelope settings on an ECG signal

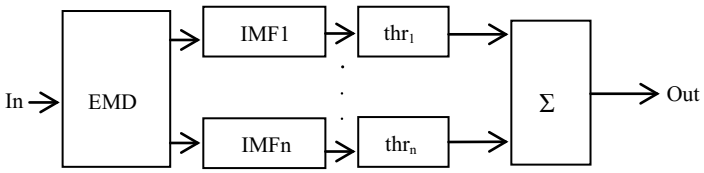

Fig. 2 The proposed procedure

This is a very simple approach, in real life the signal can be correlated with the noise and for a good analysis usually more sophisticated tools are needed. Also there are several types of noises (pink, blue, red) which can occur.

The filtering procedure should eliminate the noise and preserve the clear signal. The noisy signal x_n is first decomposed into noisy IMFs, these are processed by soft thresholding function in order to obtain an estimation of the noiseless IMFs [11]. In this study the threshold selection was performed using the rule based on Stein's Unbiased Estimate of Risk (quadratic loss function) which is used to determine the optimal shrinkage factor in a wavelet denoising [12]. Every IMF is filtered using the mentioned threshold and finally they are summed to obtain the denoised signal. In order to evaluate the filtering results added gaussian white noise, pink, was used. The level of added noise was varied. The followed parameters are the obtained signal to noise ratio (SNR) and the mean square error (MSE). The power of signal and noise are defined as

$$\mathrm{P_S} = \frac{1}{\mathrm{N}}\sum_{\mathrm{i}=1}^{\mathrm{N}} \mathrm{x_i^2}, \quad \mathrm{P_n} = \frac{1}{\mathrm{N}}\sum_{\mathrm{i}=1}^{\mathrm{N}} \mathrm{n_i^2} \tag{6}$$

The initial signal to noise ratio SNR_i (with known noise) and the obtained signal to noise ratio SNR (where x_f is the filtered signal) are

$$SNR_i = 10lg(P_S/P_n) \tag{7}$$

$$P_{Sf} = \frac{1}{N}\sum_{i=1}^{N}(x_{fi})^2, \quad P_{ne} = \frac{1}{N}\sum_{i=1}^{N}(x_{ni} - x_{fi})^2 \tag{8}$$

$$SNR = 10lg\left(\frac{P_{Sf}}{P_{ne}}\right) \tag{9}$$

where N is the length of the signal.

4 Experimental Results

This study uses signals of different lengths (1024 respectively 2048), added noise are of different types (Gaussian white, pink and blue) and values. The filtering procedures were performed under MATLAB the main results are presented below. The obtained IMFs for a 1024 length ECG signal are represented on Fig. 3.

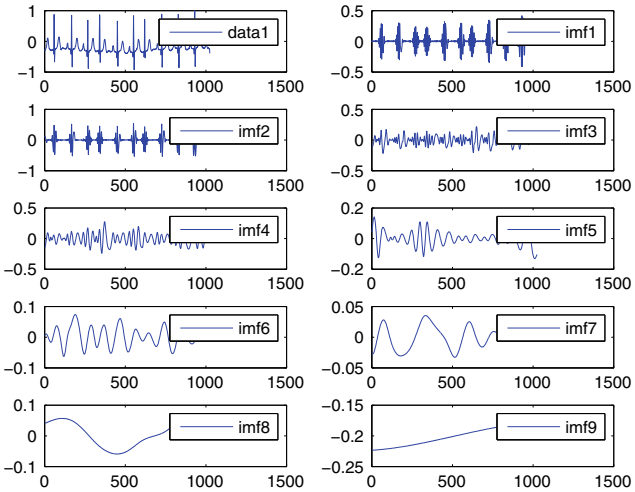

Fig. 3 The obtained IMFs for the signal corrupted by white noise

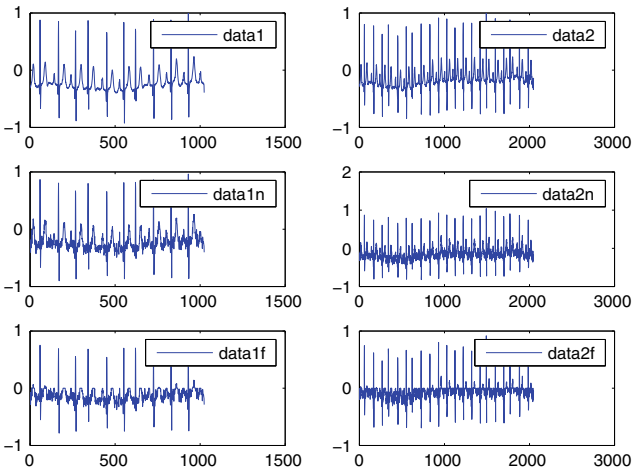

Fig. 4 The original, the noised and the EMD filtered signals

The thresholding procedure was performed taking account of the fact that the noise is located in lower order IMFs, so the threshold was applied linearly descendent with the ascending order of IMFs. The signals to noise ratio and the mean square error for a 1024 length ECG signal are presented on Fig. 4.

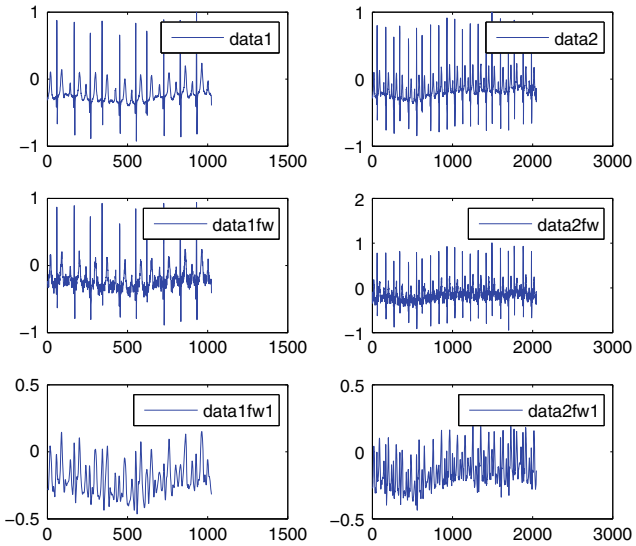

Fig. 5 The original, the noised and the DWT filtered signals

Table 1 Initial signal to noise ratio

k	0.01	0.025	0.05	0.075	0.1	0.125
SNR [dB]	40	32.04	26.02	22.49	20	18.068

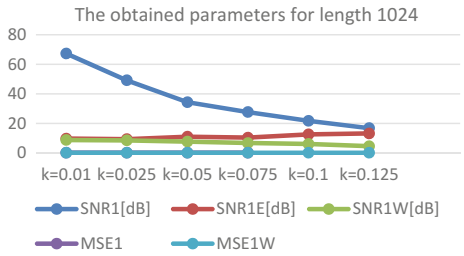

Fig. 6 SNR and MSE obtained for various noise levels

In order to evaluate the proposed method, a discrete wavelet transform (DWT) based denoising was performed, using a third level decomposition, a db4 type wavelet function and soft thresholding. The obtained results are presented on Fig. 5, the original, the noisy and DWT filtered signals (SNR1W, respectively MSE1W).

The initial SNRs between original and noisy signals are presented in Table 1. Different levels of Gaussian white noise were added. Parameter k indicates the percentile level of noise, which is presented also in form of initial signal to noise ratio, following the expression (9).

$$SNR_i = 10lg(P_S/P_n) = 10lg\left(\frac{1}{k}\right)^2 = -20lgk \qquad (10)$$

The main parameters, SNRs and MSEs for different lengths of signal are presented on Figs. 6 and 7.

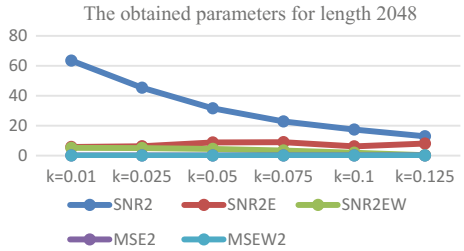

Fig. 7 SNR and MSE obtained for various noise levels

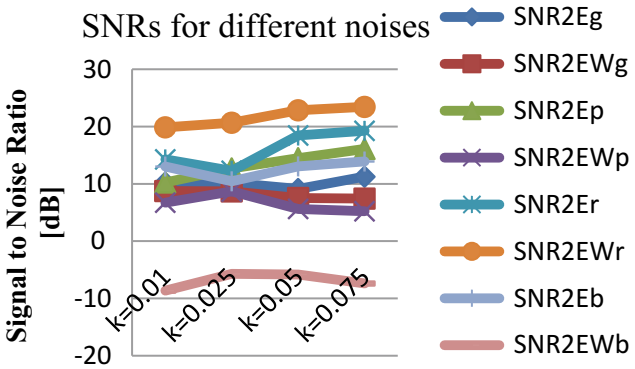

Fig. 8 SNR obtained for various noises with the same level

The same parameters obtained for length 2048 are presented on Fig. 7. The SNRs are computed in dBs.

Usually in real situations filtering procedures meet various types of noises. In order to evaluate the filtering procedure, this study used Gaussian white(g), pink(p), red(r) and blue(b) noises The SNR parameters obtained for different types of noise of the same level are presented in Fig. 8.

5 Conclusions

This study shows that EMD based filtering method can be used for denoising if the noise is supposed to be an additive signal. The process is fully signal driven, empirical and strongly dependent on the analyzed signal. The obtained simulation results show that EMD based denoising can offer in certain conditions good, even better results than discrete wavelet based procedures. A criterion for an efficient selection of a subset of relevant IMFs could improve the filtering results supposing that the noise is located in certain IMFs. The main disadvantage could be the lack of a rigorous mathematical modeling.

Conflict of Interest The authors declare that they have no conflict of interest.

References

1. Huang, N.E., et al.: The empirical mode decomposition and the Hilbert spectrum for non-linear and non stationary time series analysis. Proc. Roy. Soc. Lond. A **454**, 903–995 (1998)
2. Rilling, G., Flandrin, P., Gonalves, P.: On empirical mode decomposition and its algorithms. In: IEEE-EURASIP Workshop on Nonlinear Signal and Image Processing NSIP-03, Grado (I), June 2003
3. Rilling, G., Flandrin, P., Gonalves, P., Lilly, J.M.: Bivariate empirical mode decomposition. Sig. Proc. Lett. (submitted)
4. Huang, N.E., et al.: A confidence limit for the empirical mode decomposition and Hilbert spectral analysis. Proc. Roy. Soc. Lond. A **459**, 2317–2345 (2003)
5. Deering, R., Kaiser, J.F.: The use of a masking signal to improve empirical mode decomposition. In: ICASSP (2005). Smith, J., Jones, M. Jr., Houghton, L., et al.: Future of health insurance. N. Engl. J. Med. **965**, 325–329 (1999)
6. Wu, Z., Huang, N. E.: A study of the characteristics of white noise using the empirical mode decomposition method. Proc. R. Soc. Lond. A. **460**(2046), 1597–1611 (2003)
7. Flandrin, P., Goncalves, P., Rilling, G.: Detrending and denoising with empirical mode decomposition. In: Proceedings of XII EUSIPCO 2004, Vienna, Austria, Sept 2004
8. Tang, G., Qin, A.: ECG denoising based on empirical mode decomposition. In: 9th International Conference for Young Computer Scientists, pp. 903–906 (2008)
9. Kopsinis, Y., McLaughlin, S.: Development of EMD-based denoising methods inspired by wavelet thresholding. IEEE Trans. Sig. Process. **57**, 1351–1362 (2009)
10. Benitez, D., Gaydecki, P.A., Zaidi, A., Fitzpatrick, A.P.: The use of the Hilbert transform in ECG signal analysis. Comput. Biol. Med. **31**(5), 399–406 (2001)
11. Tang, G., Qin, A.: ECG de-noising based on empirical mode decomposition. In: 9th International Conference for Young Computer Scientists, pp. 903–906, Feb 2008
12. Boudraa, A.O., Cexus, J.C.: EMD-based signal filtering. IEEE Trans. Instrum. Meas. **56**(6), 2196–2202 (2007)

Emotion Recognition from Speech Signal in Multilingual Experiments

Corina Albu, Eugen Lupu, and Radu Arsinte

Abstract

Emotion recognition from speech signal has become more and more important in advanced human-machine applications. The detailed description of emotions and their detection play an important role in the psychiatric studies but also in other fields of medicine such as anamnesis, clinical studies or lie detection. In this paper some experiments using multilingual emotional databases are presented. For the features extracted from the speech material, the LPC (Linear predictive coding), LPCC (Linear Predictive Cepstral Coefficients) and MFCC (Mel Frequency Cepstral Coefficients) coefficients are employed. The Weka tool was used for the classification task, selecting the k-NN (k-nearest neighbors) and SVM (Support Vector Machine) classifiers. The results for the selected features vectors show that the emotion recognition rate is satisfactory when multilingual speech material is used for training and testing. When the training is made using emotional materials for a language and testing with materials in other language the results are poor. Therefore, this shows that the features extracted from speech display a closed dependency with the spoken language.

Keywords

Speech emotion recognition • Affective computing • Features extraction • Weka • Emotional databases

1 Introduction

Affective computing (AC) or emotion Artificial Intelligence is a field of research within cognitive computing and artificial intelligence that deal with collecting data from faces, voices and body language to recognize human emotion. An important feature of AC is to design human-computer interfaces able to detect and respond appropriately to the end-user's mood.

Speaking is a way of communicating thoughts through an articulated sound system, being the privileged communication between people, who are the only living creatures capable of using such a structured system. Speech is a complex signal which contains, besides the message to be transmitted, other information such as the identity of the speaker, the language, the state of health or the emotional state. All this information can become the aim of research having as input the speech signal. Emotions make speech more expressive and more effective.

Speech emotion recognition (SER) represents a field of research having as target the recognition of the emotional state of the speaker. Considering the different applications that emotion recognition can have from natural human-machine interaction, medical field to e-learning, monitoring, entertainment, and call-center, the voice can be analyzed, separately from body language, physiological parameters and facial expression, to identify the emotion.

Robert Plutchick, one of the most famous contemporary psychologists, created in 1980 the "emotion wheel" [1] and demonstrated how different emotions can integrate each other into creating new emotions. According to his theory, all emotions can be derived from eight primary emotions: trust, disgust, anticipation/expectancy, surprise, fear, anger, joy, sadness. They are placed in a 2D representation in opposite pairs. The intensity of emotion increases towards the center of the representation. Thus, terror at the center becomes afraid and then apprehension, ecstasy becomes joy and then serenity. Secondary emotions are represented as a combination of primary ones. We talk about love, obedience, creep, disapproval, remorse, contempt, aggression and optimism.

One of the most nuanced classifications of emotions is the theory of W. Gerrod Parrott who [2] identifies over 100 emotions, structured in a tree representation.

C. Albu · E. Lupu (✉) · R. Arsinte
Communications Department, Technical University of Cluj-Napoca, 26-28 Baritiu str., Cluj-Napoca, Romania
e-mail: eugen.lupu@com.utcluj.ro

S. Vlad and N. M. Roman (eds.), *6th International Conference on Advancements of Medicine and Health Care through Technology; 17–20 October 2018, Cluj-Napoca, Romania*, IFMBE Proceedings 71,
https://doi.org/10.1007/978-981-13-6207-1_25

The psychologist Paul Ekman, a pioneer in the study of emotions and his association with facial expression, defines six fundamental emotions: happiness, surprise, fear, disgust, anger, and sadness, in this work [3].

Klaus Scherer, one of the most important researcher studying voice and emotion, has shown through his works that the emotion expressed by voice, as in the case of the face, is universal. He sought to explain what changes produce the emotions in the voice signal [4].

2 Speech Emotion Recognition Background

Recognition of emotion in speech is practically achieved by processing the voice signal without linguistic information. Speech processing techniques provide many important information derived from prosodic and spectral features.

A SER system requires addressing several issues for making conclusive experiments, such as: choosing the right emotional speech database to evaluate system performance, choosing the right features for speech representation and selecting and designing an appropriate classifier.

2.1 Speech Features Correlated to Emotions

Emotion may influence speech in different ways: conscious and unconscious by the autonomic nervous system. A very good correlation between emotion and some speech attributes is presented in Table 1 [5].

Despite the difficulties in identifying the emotion in the vocal signal, the studies that are conducted highlight the most important features of the voice signal that can be extracted and can highlight different emotional states. Selecting and extracting the right features is one of the most important aspects of the recognition system.

The characteristics of the voice signal used to determine emotion are grouped into three categories:

- **Prosodic features**. Energy, duration, fundamental frequency (F0), formants are the most popular prosodic features. People make their mark on the duration, intonation and intensity of the voice signal. The prosodic features make human speech natural.
- **Spectral features** are obtained by analyzing the characteristics of the vocal tract, which is well reflected in the frequency domain analysis of the speech signal. Specific emotions may be responsible for producing different sound units in the vocal tract for different emotions.
  The advantage of using LPCCs is that fewer calculations are needed and vowels can be better described. MFCCs are commonly used in emotion recognition and provide good accuracy. Mel Coefficients (MFCC) and Cepstral Coefficients (LPCs) are some of the most used features that provide information about the voice signal. Bitouk et al. [6] have centralized some of the previous studies using the spectral characteristics for emotion recognition, the MFCC coefficients being identified to have been used in 21 papers, and one of the reasons for their use in the quoted study.
  Partila et al. [7] concludes that the best features for emotion classification are those extracted from MFCC.
- **Excitation source**. The excitation source feature is obtained from the speech signal after suppressing the vocal tract contributions. The functions of the excitation source are not popular in recognizing speech emotions. The reasons are that spectral characteristics are more popular and linear prediction characteristics can be confused with errors or noise [8].
  Recent trends in speech emotion recognition have highlighted the use of a combination of different features to achieve improved recognition performance. Kwon et al. [9] use for emotion classification the F0 related information, energy, formants, Mel-based energy, MFCC. Ververidis and Kotropoulos [10], through their study conclude that the formats, the pitch, the short-time signal energy, the MFCC coefficients, Teager energy operator cross section area are the most useful features that can be related to emotion.

Table 1 Summary of most general speech features correlated to emotions

	Anger	Joy	Sadness	Fear	Disgust
Speech rate	Slightly faster	Faster or slower	Slightly slower	Much faster	Very much slower
Pitch average	Very much higher	Much higher	Slightly slower	Very much higher	Very much lower
Pitch range	Much wider	Much wider	Slightly narrower	Much wider	Slightly wider
Intensity	Higher	Higher	Lower	Normal	Lower
Voice quality	Breathy, chest tone	Breathy, blaring	Resonant	Irregular voicing	Grumbled chest tone
Pitch change	Abrupt, on stressed syllables	Smooth, upward inflections	Downward inflections	Normal	Wide downward terminal inflections
Articulation	Tense	Normal	Slurring	Precise	Normal

2.2 Emotional Databases

Emotion speech database are collected for research purposes. Researchers developed databases for speech emotion recognition experiments but only few of them are public databases. There are some noticeable differences among these databases like: the number of the emotions recorded, the total size of the database, the source and the language of the speeches. Speech sequences used to develop emotional speech recognition systems can be divided into 3 types, namely [11]:

1. Databases with simulated (played) emotional sequences obtained with the actors that set forth a sentence in various emotional states. It's one of the easiest ways to collect emotional voice sequences.
2. Induced (elicit) emotional speech databases. It assumes getting a state through words, behavior, gestures or any other stimulus. Artificially simulates emotional situations without the interviewee's knowledge. He is involved in a conversation and according to the context created, he is placed in various emotional states. These databases are closer to natural ones than simulated but it is possible that subjects are not emotionally well involved.
3. Natural speech database. These can come from conversation sequences recorded at the call center, physician-patient dialogue, public places etc. It is, however, difficult to find a wide range of emotions in this way.

Some prominent examples of acted databases are the Berlin database of emotional speech (EMO-DB) and the Danish Emotional Speech corpus (DES). For 0induced emotional database may be considered for instance the SmartKom corpus and the German Aibo emotion corpus. A good synthesis of the emotional database is presented in the work of Anagnostopoulos et al. [12]. A small emotional database for Romanian language, SRoL, was developed by Teodorescu et al. [13], which we used in our experiments.

2.3 Classifiers

To perform SER there are different types of classifiers: Gaussian Mixtures Model (GMM), Support Vector Machine (SVM), Hidden Markov Model (HMM), Bayes classifier, k-nearest neighbors (K-NN), Artificial Neural Network (ANN) and Maximum Likelihood Bayesian classifier etc.

GMM are suitable for global features extracted from training utterances and achieves two levels of accuracy. ANN Classifiers have their own strength in identifying nonlinear boundaries separating the emotional states as well. SVM minimize empirical classification error and help in maximization of geometric-margin. Well, main thought behind the SVM model is use of kernel functions like linear, polynomial, radial basis function (RBF) for large extent [3, 6].

3 System Implementation and Experiments

For our experiments we chose emotional data from three databases: SRoL for Romanian, EMO-DB for German and RAVDESS for American English. In Table 2 the selected files for five different emotional states with a total of 755 files are presented.

From this database some features are extracted based on the references [7–9]. The chosen features are LPC coefficients (10), Mel cepstral coefficients (12), LPCC coefficients (10) and energy extracted from every frame of 20 ms of the speech signal. Then from all the frames of the file the average and the standard deviation for every extracted feature are computed, so resulting a feature vector of 66 coefficients for every speech file.

In the classification step the Weka tool was employed. For our experiments three different classifiers are used: K-NN (k = 3), SVM and Neural network. Several preliminary experiments were made to evaluate the classifiers for our database. First, we classified the database considering only the emotions (5 classes) and, second, considering the emotion in a certain language (15 classes). The 10-fold cross validation testing method was used (Table 3).

Based on these results and the time of training the models we decided to use the k-NN and SVM classifiers in our next experiments.

Another objective of the study was to establish the most well recognized types of emotions, regardless of spoken language. In this case, the scenario used in the previous experiment was employed, the data set was classified considering the 5 emotions, and ignoring the spoken language. According to the conclusions from the first analysis, to achieve this objective we used the first two classifiers k-NN

Table 2 Emotional data used in experiments

Language	Joy	Anger	Fear	Sadness	Neutral	Total
Romanian	36	30	27	30	30	153
German	70	126	66	61	79	402
English	40	40	40	40	40	200
Total	146	196	133	131	149	755

Table 3 Preliminary experiments results

	Experiment	5 classes	15 classes
Classifier	**10 fold cross validation**		
	K-NN (K=3)	72.71%	67.33%
	SVM (polykernel)	63.97%	73.43%
	SVM (RBFkernel)	69.00%	78.22%
	Neural networks	73.48%	77.29%

Table 4 Confusion matrix for the SER experiment using k-NN

Classified as	a (%)	b (%)	c (%)	d (%)	e (%)
a = joy	**67.12**	18.49	7.53	6.16	0.68
b = anger	16.84	**79.08**	1.53	2.04	0.51
c = neutral	10.07	4.70	**73.15**	5.37	6.71
d = fear	8.27	5.26	5.26	**75.19**	6.02
e = sadness	3.05	3.82	18.32	8.40	**66.41**

Table 5 Confusion matrix for the SER experiment using SVM(RBF-kernel)

Clasified as	a (%)	b (%)	c (%)	d (%)	e (%)
a = joy	**58.22**	28.77	4.11	6.16	2.74
b = anger	14.29	**79.08**	1.53	3.06	2.04
c = neutral	9.40	2.01	**64.43**	5.37	18.79
d = fear	10.53	1.50	3.76	**77.44**	6.77
e = sadness	3.05	6.87	31.30	4.58	**54.20**

and SVM (RBF kernel) to have the best results. The confusion matrix for speech emotion identification is shown in Table 4 for the k-NN classifier and in Table 5 for the SVM classifier (RBF kernel).

Analyzing the results, we can conclude that fear and anger can be identified with good accuracy ($\sim$80%), both physiologically determining the same changes, being part of the category of negative strong emotions, excitatory emotions.

It is harder to perceive sadness, this being a passive emotional state. Because there is an important confusion between the states of joy and anger, states that are otherwise in the opposite poles, the most suitable features must be sought to best define them, so that they can be identified with greater precision.

Another experiment had the goal to determine whether the same classifiers can be used to identify emotions of the same type but expressed in different languages. In this case, and considering other such studies [14], we analyzed how emotions in speech sequences are identified using classifiers trained in one language and tested in the other two languages.

Given the observations made so far in the case study, we chose to use the k-NN classifier for this experiment. This scenario leads to the existence of three situations that will be presented further. The averaged results for all emotions are presented in the Table 6. The results show that, if the training set is in one language and the testing sets are in different languages the emotion recognition rate is very poor. Hence, the information captured from the speech material for emotion recognition seem to be also language dependent.

Table 6 SER experiment for different languages using k-NN

Trained\Tested	English (%)	German (%)	Romanian (%)
English	96.5	26.5	20.3
German	29	92.48	21
Romanian	13.3	15.9	91.55

4 Conclusions

This article has been focused on emotion recognition experiments made on multilingual speech databases. The selected emotional databases are recorded for English (RAVDESS), German (EMO-DB) and Romanian (SRoL).

The extracted features target on spectral characteristic contained by the MFCC, LPCC and LPC coefficients and energy estimated over the whole utterance. The extracted vector contains the average and dispersion of every selected attribute. This choice was made because in the references, global statistics are generally found to be more suitable for this type of applications. As classifier for the experiments SVM and k-NN from the Weka tool were used.

The results provided by our experiments, using multilingual materials, show that for the chosen vector the recognition rates for the emotions are satisfactory for anger and fear close to 80%. For the other emotions, the results are less satisfactory and depend on the emotion and the classifier type.

Moreover, we may conclude that when for training a speech material is employed in a certain language and for testing speech data are used in other languages, the results are very poor. In conclusion, the extracted vector from the speech contains information connected to the language used for the utterances.

Further improvement in this line of work may be added to reduce the vector dimension and a feature selection may be considered. Adding new features to the acoustic vector may also be useful to improve performances such as those in [15].

Conflict of Interest The authors declare that they have no conflict of interest.

References

1. http://whatis.techtarget.com/definition/Plutchiks-Wheel-of-Emotions. Accessed 14.03.2018
2. http://www.theemotionmachine.com/classification-of-emotions/. Accessed 14.03.2018
3. Ekmon, P.: Emotions Revealed: Recognizing Faces and Feelings to Improve Communication and Emotional Life. Times Books, New York (2003)
4. Scherer, K.R.: Vocal communication of emotion: a review of research paradigms. Speech Commun. **40**, 227–256 (2003)
5. Murray, I., Arnott, J.: Toward the simulation of emotion in synthetic speech: A review of the literature on human vocal emotion. J. Acoust. Soc. Am. **93**, 1097–1108 (1993)
6. Bitouk, D., Verma, R., Nenkova, A.: Class-level spectral features for emotion recognition. Speech Commun. **52**(7–8), 613–625 (2010)
7. Partila, P., Voznak, M., Tovarek, J.: Pattern recognition methods and features selection for speech emotion recognition system. Sci. World J. **2015** (2015)
8. Koolagudi, S.G., Rao, K.S.: Emotion Recognition from Speech: A Review. Springer Science + Business Media, LLC, Berlin (2012)
9. Kwon, O., et al.: Emotion recognition by speech signals. In: Eurospeech, Geneva, pp. 125–128 (2003)
10. Ververidis, D., Kotropoulos, C.: Emotional speech recognition: resources, features, and method. Speech Commun. **48**, 162–1181 (2006)
11. Gadhe, R.P., et al.: Emotion recognition from speech: a survey. Int. J. Sci. Eng. Res. **6**(4), 632–635 (2015)
12. Anagnostopoulos, C.-N., et al.: Features and Classifiers for Emotion Recognition from Speech: A Survey from 2000 to 2011. Springer Science + Business Media, Dordrecht (2012). https://doi.org/10.1007/s10462-012-9368-5
13. Teodorescu, H.-N., et al.: Romanian Speech Database—SRoL, © 2014. http://www.etc.tuiasi.ro/sibm/romanian_spoken_language
14. Chicote, R.B.: Contribution to the analysis, design and evaluation of strategies for corpus-based emotional speech synthesis. Ph.D. thesis, Universidad Politecnica de Madrid (2011)
15. Emerich, S., Lupu, E.: Improving speech emotion recognition using frequency and time domain acoustic features. In: Proceedings of SPAMEC 2011, pp. 85–88

Automated Collagen Segmentation from Masson's Trichrome Stained Images—Preliminary Results

M. S. Şerbănescu, R. V. Teică, M. Tărâță, D. Georgescu, D. O. Alexandru, N. C. Manea, W. Wolf, R. M. Pleșea, and I. E. Pleșea

Abstract

We propose a new algorithm for automated collagen segmentation from Masson's trichrome stained images with two steps: color transfer from a known, optimum-stained image, followed by k-means clustering. The algorithm's output is scored by two proficient pathologists. Results show a good segmentation output (~60%) and strong agreement on pathologist's opinion on a good segmentation (Cohen's kappa = 0.8063).

Keywords

Collagen segmentation • Masson's trichrome • K-means clustering • Color transfer between images

1 Introduction

Prostate cancer is one of the most often oncological pathology in men with over 300,000 deaths annually [1]. The diagnosis in prostate cancer focuses on gland growth patterns, nuclei and cytoplasmic aspects, leaving behind the stromal component. With previous observations on stromal modification in prostate cancers [2–5] our team aims to automatically grading the prostate cancer using mainly the stromal component.

Computer aided diagnosis (CAD) in histopathologic diagnosis is a growing field having two main advantages: objectivity and speed. In the field of digital pathology, CAD software mimics the pathologist's diagnosis methods. Glass slides with histological stained tissue sections are digitalized (photographed or scanned with dedicated hardware—slide scanners) and exported as digital images files which can further be analyzed by computer algorithms.

Masson's trichrome procedure (TC) is a three-color staining protocol used in histology. The recipes evolved from Claude L. Pierre Masson's [6] for distinguishing cells from surrounding connective tissue.

TC produces:

- red—muscle, cytoplasm and erythrocytes,
- blue or green—collagen and mucus,
- black—nuclei.

Mainly used in muscular, cardiac, hepatic, kidney [7] fibrous pathologies, TC staining can be used whenever the highlight of collagen fibers is needed.

Though the theoretic description of the TC staining sets the collagen tint to green or blue, different staining conditions and image acquisition errors, make segmentation a difficult task.

The aim of current research is to develop a fully unsupervised segmentation algorithm, capable of isolating the collagen from TC stained digital images which will be later used for feature extraction algorithms. The algorithm is based on a color transfer from an optimum-stained image followed by k-means clustering based segmentation.

M. S. Şerbănescu (✉) · R. V. Teică · M. Tărâță · D. Georgescu · D. O. Alexandru · N. C. Manea
Medical Informatics & Biostatistics, University of Medicine and Pharmacy of Craiova, 2-4 Petru Rareș, Craiova, Romania
e-mail: mircea_serbanescu@yahoo.com

R. V. Teică
e-mail: tvrossy@gmail.com

W. Wolf
EIT 3 - Institut Für Informationstechnik, Universität der Bundeswehr, Munich, Germany

R. M. Pleșea
Medical Genetics, University of Medicine and Pharmacy of Craiova, Craiova, Romania

I. E. Pleșea
Pathology, University of Medicine and Pharmacy "Carol Davila", Bucharest, Romania

S. Vlad and N. M. Roman (eds.), *6th International Conference on Advancements of Medicine and Health Care through Technology; 17–20 October 2018, Cluj-Napoca, Romania*, IFMBE Proceedings 71,
https://doi.org/10.1007/978-981-13-6207-1_26

2 Materials and Methods

2.1 Color Spaces

A color space is a specific organization of colors, an abstract mathematical model which describes the range of colors as tuples of numbers.

Depending on their application color spaces can differ in tuple size and logical inter-connections properties.

The most often used color space in digital color representation is the RGB (red-green-blue) color model, an additive color model in which red, green and blue light are added together, to reproduce a broad array of colors. Most used color space in whole slide imaging (WSI) is 24-bit RGB color space, where each of the color components describing a pixel, is represented on 8 bits. The disadvantage of the RGB color space is that it is not perceptually uniform, which means that altering one of the three components will affect the perception of the other two.

The CIELAB color space (lαβ or Lab) is a color space defined by the International Commission on Illumination (CIE) in 1976 that expresses color as three numerical values: L for the lightness and a (α) and b (β) for the green–red and blue–yellow color components. It was designed to be perceptually uniform with respect to human color vision, meaning that the same amount of numerical change in these values corresponds to about the same amount of visually perceived change, but it turned out it can successfully be used in computer algorithms for controlled image alterations.

Conversion from RGB to lαβ color space is possible using intermediate color spaces (XYZ, LMS) and the following equations [8]:

$$\begin{bmatrix} X \\ Y \\ Z \end{bmatrix} = \begin{bmatrix} 0.5141 & 0.3239 & 0.1604 \\ 0.2651 & 0.6702 & 0.0641 \\ 0.0241 & 0.1228 & 0.8444 \end{bmatrix} \begin{bmatrix} R \\ G \\ B \end{bmatrix} \quad (1)$$

$$\begin{bmatrix} L \\ M \\ S \end{bmatrix} = \begin{bmatrix} 0.3897 & 0.6890 & -0.0787 \\ -0.2298 & 1.1834 & 0.0464 \\ 0.0000 & 0.0000 & 1.0000 \end{bmatrix} \begin{bmatrix} X \\ Y \\ Z \end{bmatrix} \quad (2)$$

$$\begin{bmatrix} l \\ \alpha \\ \beta \end{bmatrix} = \begin{bmatrix} \frac{1}{\sqrt{3}} & 0 & 0 \\ 0 & \frac{1}{\sqrt{6}} & 0 \\ 0 & 0 & \frac{1}{\sqrt{2}} \end{bmatrix} \begin{bmatrix} 1 & 1 & 1 \\ 1 & 1 & -2 \\ 1 & -1 & 0 \end{bmatrix} \begin{bmatrix} L \\ M \\ S \end{bmatrix} \quad (3)$$

Inverse conversion from Lab to RGB color space is possible using the following equations [8]:

$$\begin{bmatrix} L \\ M \\ S \end{bmatrix} = \begin{bmatrix} 1 & 1 & 1 \\ 1 & 1 & -2 \\ 1 & -1 & 0 \end{bmatrix} \begin{bmatrix} \frac{\sqrt{3}}{3} & 0 & 0 \\ 0 & \frac{\sqrt{6}}{6} & 0 \\ 0 & 0 & \frac{\sqrt{2}}{2} \end{bmatrix} \begin{bmatrix} l \\ \alpha \\ \beta \end{bmatrix} \quad (4)$$

$$\begin{bmatrix} R \\ G \\ B \end{bmatrix} = \begin{bmatrix} 0.4679 & -3.5873 & 0.1193 \\ -1.2186 & 2.3809 & -0.1624 \\ 0.0497 & -0.2439 & 1.2045 \end{bmatrix} \begin{bmatrix} L \\ M \\ S \end{bmatrix} \quad (5)$$

2.2 The Dataset

A total of 553 square images of 512 × 512 pixels in a 24-bit RBG (red, green, blue) color space with an area of 22 square microns were selected by pathologists from the WSI, having only homogeny patterns of cancer according to Gleason grading system [9].

2.3 Color Transfer Between Images

A simplified color transfer between images was implemented (Reinhard [8]):

$$\begin{aligned} l^* &= l - \langle l \rangle \\ \alpha^* &= \alpha - \langle \alpha \rangle \\ \beta^* &= \beta - \langle \beta \rangle \end{aligned} \quad (6)$$

$$\begin{aligned} l' &= \frac{\sigma_t^l}{\sigma_s^l} l^* \\ \alpha' &= \frac{\sigma_t^\alpha}{\sigma_s^\alpha} \alpha^* \\ \beta' &= \frac{\sigma_t^\beta}{\sigma_s^\beta} \beta^* \end{aligned} \quad (7)$$

where (i) l, α, β are the initial pixel values for each color channel in the source image, (ii) <l>, <α>, <β> are the average values for each color channel in the source image, (iii) σ_t^l, σ_s^l, σ_t^α, σ_s^α, σ_t^β, σ_s^β are the standard deviations of each color channel in the source and target image. Next, the target averages are added to each color channel.

A short description of the method would be: transferring the average and variation proportion of colors from one image to another.

Using the described algorithm, each image receives the color proportions of a unique, empirically selected, and perceptually good stained sample chosen by the two pathologists.

2.4 K-means Clustering

K-means clustering is an algorithm that aims to partitioning n observations into k ($\leq$n) sets, to minimize the within-cluster variance, originally designed for signal processing [10, 11]. In our specific application each pixel is an observation. A short description of the method would be: splitting the image into sub-images each of these having smaller color variance.

2.5 External Validation

Each image and collagen segmentation, were assessed by two pathologists. For each image each pathologist gave two scores.

Image score: refers to the image itself "suitable for collagen assessment" with two options: reject or accept.

Segmentation score (applied only to the previous accepted images): refers to the quality of the algorithm output: and its performance was quantified with four classes:

- (−2)—strong reject
- (−1)—week reject
- (+1)—week accept
- (+2)—strong accept

2.6 Hardware and Software

Images were acquired with a Leica Aperio AT2 slide scanner and the proprietary software, using a 20x objective lens. All algorithms were implemented in MATLAB (MathWorks, USA).

3 Results

84 images were marked as inappropriate (rejected) for collagen assessment by the pathologists (Table 1).

For the remaining images the collagen mask was computed. Segmentation score results are presented in Table 2.

Figures 1, 2, 3 and 4 show examples of collagen segmentation, for each evaluation mark from the segmentation score.

4 Discussion

Both pathologists marked as inappropriate (rejected) for collagen assessment, the same 59 images. In addition one of the pathologist rejected 18 other images while the other only 7. Computed Cohen's kappa was 0.8063 (strong agreement) showing relative uniform perception on image score (quality and composition) between them.

Table 1 Image score

	Pathologist 1	
Pathologist 2	Reject	Accept
Reject	59	7
Accept	18	469

Table 2 Segmentation score

	Pathologist 1			
Pathologist 2	−2 strong reject	−1 weak reject	+1 weak accept	+2 strong accept
−2 strong reject	115	2	0	0
−1 weak reject	22	28	72	44
+1 weak accept	3	22	72	44
+2 strong accept	0	0	11	143

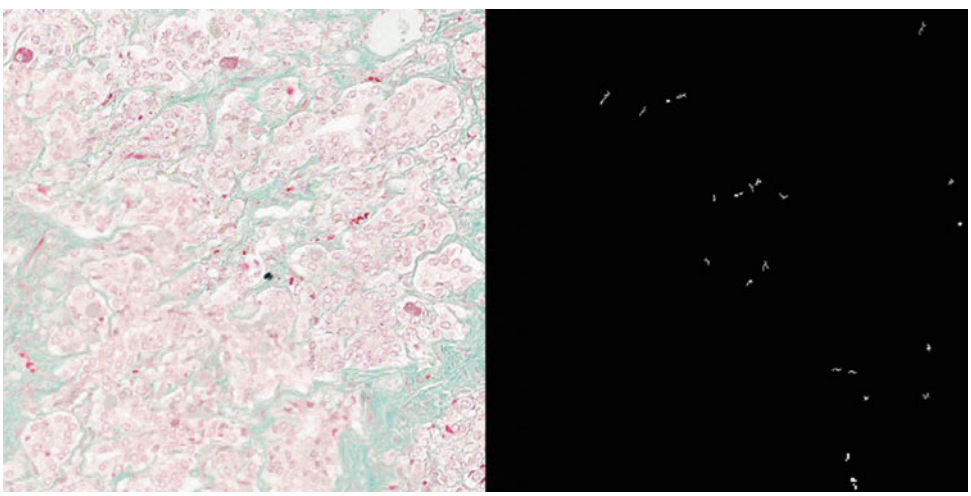

Fig. 1 Collagen segmentation (−2)—strong reject

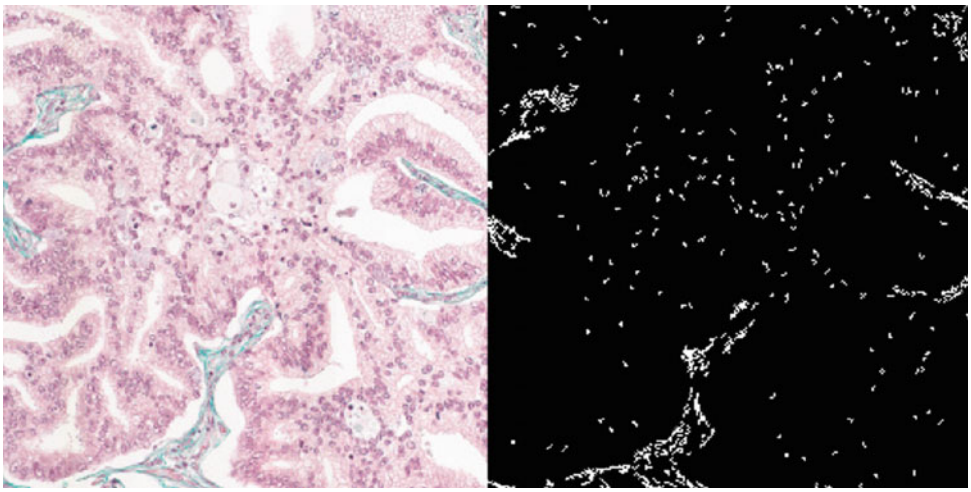

Fig. 2 Collagen segmentation (+1)—weak accept

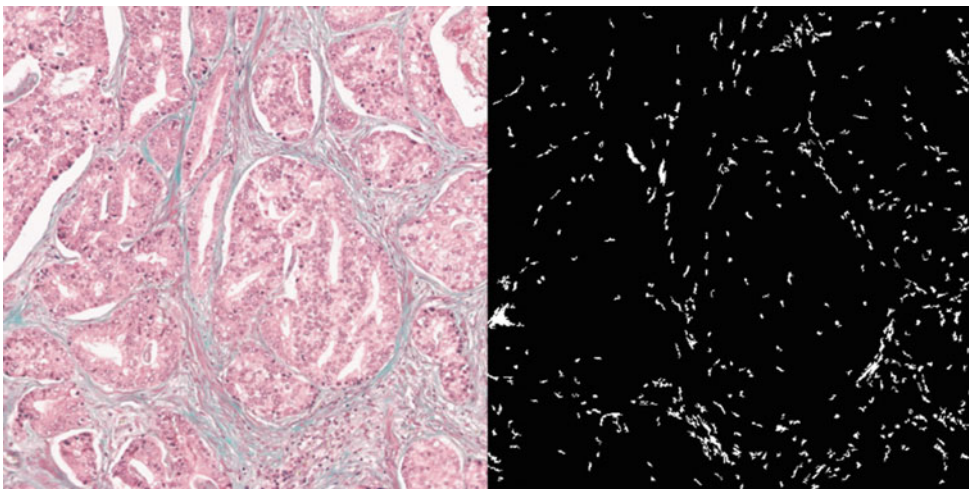

Fig. 3 Collagen segmentation (−1)—weak reject

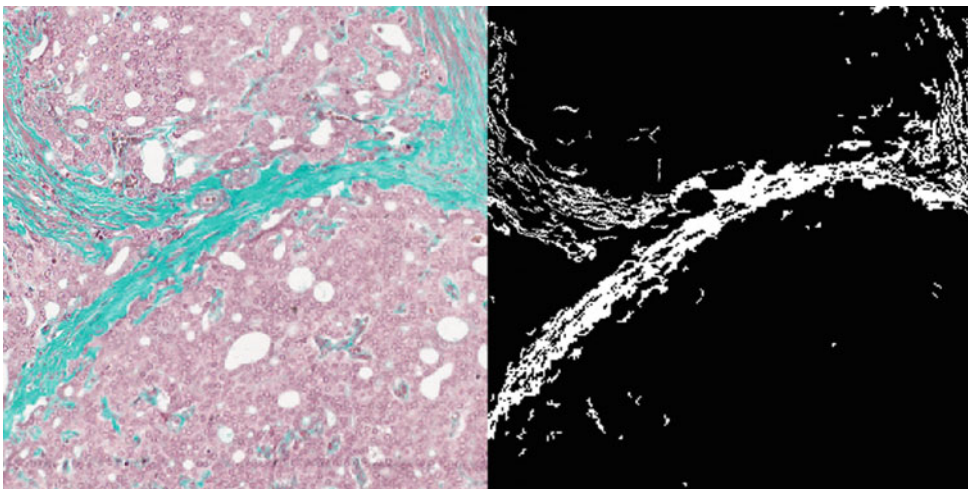

Fig. 4 Collagen segmentation (+2)—strong accept

Regarding the segmentation score (Cohen's kappa result 0.6729) shows moderate agreement. We observed that there were differences in the segmentation perception. As expected, most differences were between weak accept and strong accept, pathologist No. 1 tended to be more radical with accepting or rejecting the segmentation result, while pathologist No. 2 tended to be more flexible in accepting the segmentation result.

57.57% of the segmentation results were accepted by both pathologists, while 63.75% were accepted by at least one. 24.52% of the segmentation results were strongly rejected by both pathologists.

Since there was one empirically selected image used as model in the process of color transfer between images the algorithm output shows good performance. Having only one image as model we neglect the inner image real variation and consider it as a technical error, this somehow being wrong, as we shown in previews work [12]. Having no hardware stain marker this is the only solution for a controlled image enhancement.

The average collagen mask computational speed on a Intel (R) Core (TM) I7-7700HQ processor at 2.800 GHz was below 1 s, though containing 4 color space changes, making it available for real-time applications.

5 Conclusions

We have developed a competitive, unsupervised algorithm for collagen segmentation from Masson's trichrome special staining based on a k-means segmentation algorithm applied on pre-processed images with color transfer from an optimum-stained perceptual image model.

The research proved that there is no perceptual uniformity among pathologists on collagen assessment: Cohen's kappa was 0.6729 on the segmentation score.

From the medical (research) point of view the algorithm is a step forward, reducing the human-time for the assessment of the collagen mask and in the same time being an objective measurement.

Conflict of Interest The authors declare that they have no conflict of interest.

References

1. Pernar, C.H., Ebot, E.M., Wilson, K.M., et al.: The epidemiology of prostate cancer. Cold Spring Harb. Perspect. Med. a030361 (2018). https://doi.org/10.1101/cshperspect.a030361
2. Stoiculescu, A., Plesea, I.E., Pop, O.T., et al.: Correlations between intratumoral interstitial fibrillary network and tumoral architecture in prostatic adenocarcinoma. Rom. J. Morphol. Embryol. **53**(4), 941–950 (2012)
3. Mitroi, G., Plesea, R.M., Pop, O.T., et al.: Correlations between intratumoral interstitial fibrillary network and vascular network in Srigley patterns of prostate adenocarcinoma. Rom. J. Morphol. Embryol. **56**(4), 1319–1328 (2015)
4. Plesea, I.E., Stoiculescu, A., Serbanescu, M.: Correlations between intratumoral vascular network and tumoral architecture in prostatic adenocarcinoma. Rom. J. Morphol. Embryol. **54**(2), 299–308 (2013)
5. Plesea, R.M., Serbanescu, M.S., Alexandru, D.O., et al.: Correlations between intratumoral interstitial fibrillary network and vascular network in Gleason patterns of prostate adenocarcinoma. Curr. Health Sci. J. **41**(4), 345–354 (2015)
6. Wulff, S., Hafer, L., Cheles, M., et al.: Guide to Special Stains. Fort Collins, Colorado, USA, pp. 41–42 (2004)
7. Masson's trichrome stain at https://en.wikipedia.org/wiki/Masson%27s_trichrome_stain
8. Reinhard, E., Adhikhmin, M., Gooch, B., et al.: Color transfer between images. IEEE Comput. Graph. Appl. **21**(5), 34–41 (2001)
9. Gleason, D.F.: Histologic grading and staging of prostatic carcinoma. In: Tannenbaum, M. (ed.) Urologic Pathology: The prostate. Lea & Febiger, Philadelphia, pp. 171–197 (1977)
10. MacQueen, J.: Some methods for classification and analysis of multivariate observations. In: Proceedings of the Fifth Berkeley Symposium on Mathematical Statistics and Probability, vol. 1, California, USA, pp. 281–297 (1976)
11. Steinhaus, H.: Sur la division des corps materiels en parties. Bulletin de l'Academie Polonaise des Sciences Classe III **IV**(12), 801–804 (1956)
12. Serbanescu, M.S., Plesea, I.E.: A hardware approach for histological and histopathological digital image stain normalization. Rom. J. Morphol. Embryol. **56**(2S), 735–741 (2015)

The Role of Convolutional Neural Networks in the Automatic Recognition of the Hepatocellular Carcinoma, Based on Ultrasound Images

D. Mitrea, R. Brehar, P. Mitrea, S. Nedevschi, M. Platon(Lupşor), and R. Badea

Abstract

Hepatocellular carcinoma (HCC) represents the most frequent form of liver cancer. It evolves from cirrhosis, as the result of a restructuring phase at the end of which dysplastic nodules appear. HCC is the main cause of death in people affected by cirrhosis. The most reliable method for HCC diagnosis, the golden standard, is the needle biopsy, but this is an invasive technique, dangerous for the human body. We develop computerized methods, based on ultrasound images, in order to perform automatic diagnosis of HCC in a noninvasive manner. In our previous research, we elaborated the textural model of HCC, based on classical and advanced texture analysis methods, in combination with traditional classification techniques, which led to a satisfying accuracy. We aim to improve this performance in our current and further research. In this article, we analyzed the role of specific deep learning techniques concerning the automatic recognition of HCC from ultrasound images. We chose the Convolutional Neural Networks (CNN), this method being well known for its performance in the field of image recognition. Thus, CNN are based on artificial neural networks, they also performing image processing operations, such as inner convolutions. In order to evaluate the newly adopted technique, we assessed the classification accuracy achieved in the cases of distinguishing HCC from the cirrhotic parenchyma on which it had evolved, respectively when differentiating HCC from the hemangioma benign liver tumor. We compared the accuracy of CNN with our previous results, based on texture analysis methods and it resulted that CNN yielded better recognition rates than the classical texture analysis techniques, respectively comparable with those provided by the advanced texture analysis methods. However, further improvements will be necessary, which we mention within the last section of this article.

Keywords

Hepatocellular Carcinoma (HCC) •
Ultrasound images •
Convolutional Neural Networks (CNN) •
Noninvasive diagnosis •
Classification performance

1 Introduction

The Hepatocellular Carcinoma (HCC) is one of the most frequently met malignant liver tumors, representing the main form of liver cancer (75% of the liver cancer cases), besides cystadenocarcinoma, hepatoblastoma and cholangiocarcinoma [1]. HCC usually evolves from cirrhosis, after a restructuring phase at the end of which dysplastic nodules (future malignant tumors) result, being the primary cause of death for patients affected by cirrhosis. It has been concluded by the specialists that the liver aggressions have a specific evolution pattern in most of the cases, the following phases being highlighted: firstly inflammation, followed by necrosis, fibrosis, regeneration (cirrhosis), dysplasia, and, finally, the HCC tumor. The most reliable method for the diagnosis of HCC, nowadays, is the needle biopsy, this being an invasive investigation method, dangerous for the human body. This method can lead to infections, respectively to the spreading of the malignant tumor inside the body [1]. In our research, we elaborate computerized, non-invasive techniques for the automatic and computer aided diagnosis of HCC, based on ultrasound images, aiming to overcome the above mentioned problem. Ultrasonography represents a non-invasive investigation technique which is inexpensive,

D. Mitrea (✉) · R. Brehar · P. Mitrea · S. Nedevschi
Computer Science Department, Faculty of Automation and Computer Science, Technical University of Cluj-Napoca, Cluj-Napoca, Romania
e-mail: Delia.Mitrea@cs.utcluj.ro

M. Platon(Lupşor) · R. Badea
Department of Medical Imaging, I. Hatieganu University of Medicine and Pharmacy of Cluj-Napoca, Cluj-Napoca, Romania

S. Vlad and N. M. Roman (eds.), *6th International Conference on Advancements of Medicine and Health Care through Technology; 17–20 October 2018, Cluj-Napoca, Romania*, IFMBE Proceedings 71,
https://doi.org/10.1007/978-981-13-6207-1_27

safe and thus repeatable, useful in the case of chronic and malignant disease monitoring. In the current research, we target the diagnosis of the inoperable HCC in advanced evolution phases, which has to undergo a specific surgical treatment, based on robot-assisted injection of a damaging substance. Concerning the aspect of HCC within ultrasound images, in advanced evolution phases, it is usually characterized through a hyperechogenic and inhomogeneous aspect, due to the coexistence of various tissue types, such as necrosis, fibrosis, fat cells, and active growth regions. In our experiments, HCC was compared with the hemangioma benign liver tumor. This tumor structure is constituted by a conglomerate of blood vessels and visually resembles HCC is many situations [1]. Cancer detection based on medical images has been widely performed within the state of the art [2–4]. Deep learning methods have been applied recently [5–9]. The technique of CNN was employed both for the recognition [9] and segmentation [6–8] of the potentially dangerous structures. In our previous research, we elaborated the textural model of HCC, consisting of the relevant textural features, able to distinguish HCC from other visually similar structures, respectively of the specific values for the relevant textural features (arithmetic mean, standard deviation and probability distribution) [10]. Corresponding to the image analysis phase, we applied both classical texture analysis techniques [11], as well as advanced texture analysis methods, originally elaborated, such as the superior order Gray Level Cooccurrence Matrix (GLCM) [10], the superior order Edge Orientation Cooccurrence Matrix (EOCM) [10], the Complex Textural Microstructure Cooccurrence Matrices (CTMCM) [12]. We validated the textural model by employing traditional classification methods, the best results being provided by Support Vector Machines (SVM), Multilayer Perceptron (MLP), Random Forest (RF), respectively Adaboost combined with the C4.5 decision trees classifier [12]. In this work, we performed a preliminary study, concerning the possibility to employ the technique of CNN in order to perform the automatic recognition of HCC, based on ultrasound images. This is a deep learning method, based on Artificial Neural Networks, which eliminates the need of a separate feature computation phase, by performing additional image processing operations. This method aims to embed, within a single technique, image analysis, dimensionality reduction and recognition [13, 14]. Multiple architectures were experimented and the one leading to the best accuracy results was chosen. The performance of the newly adopted method was comparable with that obtained during the previous research and also with other state of the art methods. Considering the state of the art in the domain, methods based on the CNN technique were not applied previously with the purpose of HCC recognition within ultrasound images. Also, no systematic comparison has been done between the performance provided by CNN and the performances due to the texture-based methods. The rest of this paper is organized as follows: the state of the art is described in Sect. 2; in Sect. 3, the adopted solution, based on the CNN technique is described and also the methods employed during the former research are mentioned; the experimental results and the discussions are integrated within Sect. 4; then, the conclusions and further development possibilities are presented in Sect. 5.

2 The State of the Art

Initially, texture based methods in combination with classifiers have been employed for the automatic recognition of the pathologies, particularly of the tumor structures, within medical images [2–4]. Deep learning methods such as Stacked Denoising Autoencoders (SAE), Recurrent Neural Networks (RNN), Deep Belief Networks (DBN) and CNN have been recently applied [5–9, 15, 16]. CNN have shown in the last decade extremely good results for tasks such as image recognition, image segmentation, localization, detection, or relevant feature extraction. Their good performance has led to their adoption in numerous fields among which medical image processing and even medical image diagnosis. Relevant surveys identify the wide application of CNN for different types of medical images and for different pathologies. The work of [5] and [6] provide a summary of different image types and CNN suitable for 2D or 3D image structures. They emphasize the importance of CNN in the learning task and motivate their good performance due to their characteristic of keeping local image relations. They also revise state of the art CNN architectures used for classification, detection or segmentation of medical images such as X-ray images, CT and MRI images, digital images capturing the fundus of the eye, histopathology images. The study also identifies the challenges and limitations of CNN when applied to medical images due to the lack of labelled data. All the methods presented by the study imply datasets collected from less than 100 patients. Hence, there are numerous domains for applying CNN for medical images. As our work focuses on the recognition of malignant tumors, we revise relevant work in the field, but we take into account other severe affections, as well. A method that performs patch based classification of liver lesions within CT images is presented by Li et al. [7]. Here, the authors train CNN using image patches centered at each pixel. These patches were divided into tumor and normal liver tissue. A given patch is labelled as a positive sample if it contains at least 50% or more of liver tumor pixels, otherwise it is labelled as a negative sample. The authors found that CNN still have limitations on segmenting tumors with inhomogeneous density and unclear boundary, especially the under-segmentation of the tumor adjacent to structures with

similar densities. Liver tumor segmentation within CT images, taking baseline CT as input, using 2D CNN, is performed by Vivanti et al. [8]. The proposed algorithm defines a region of interest (ROI) using a deformable registration of the baseline scan, as well as tumor delineations to the follow-up CT scan and automatic liver segmentation. A voxel classifier is built by means of a CNN. A number of 67 tumors, belonging to 21 patients, were employed for the experiments. An average overlap error of 16.26% resulted. A high diagnostic performance in the staging of five liver fibrosis is obtained by Yasaka et al. [15], where the authors employ a Deep Convolutional Neural Network (DCNN) model using gadoxetic, acid-enhanced, hepatobiliary phase magnetic resonance (MR) imaging. Here, the area under the ROC curve was 85%. A complex approach is presented by Byra et al. [16]. The authors employ the Inception-ResNet-v2 deep CNN pre-trained on the ImageNet dataset [16] in order to extract high-level features in liver B-mode ultrasound image sequences. A Support Vector Machines (SVM) classifier is then trained on the high level features in order to recognize images containing fatty liver. The technique of DCNN was also employed in [9] in order to detect pulmonary malignant nodules in incipient phase, within CT images. DCNNs were trained using 62492 ROIs belonging to 40772 nodules, respectively 21720 non-nodules from the Lung Image Database Consortium (LIDC) database. A maximum classification accuracy of 86.4% resulted in this case.

We can conclude that there are no relevant studies which aim to perform the automatic recognition of advanced, inoperable HCC within ultrasound images by employing the CNN technique. Also, no systematic comparison with the texture analysis methods has been previously performed concerning this subject.

3 The Proposed Solution

3.1 Our Previous Research: The Textural Model of HCC

The textural model of HCC consists of the relevant textural features, able to perform the distinction between HCC and the visually similar tissues, respectively of the specific values of the relevant textural features: arithmetic mean, standard deviation, probability distribution [10]. During the image analysis phase, both classical and newly developed texture analysis methods were applied. Among the originally developed methods, we mention the Gray Level Cooccurrence Matrix (GLCM) of superior order [10], the superior order Edge Orientation Cooccurrence Matrix (EOCM) [10], the Complex Textural Microstructure Cooccurrence Matrix (CTMCM) [12], respectively the Complex Extended Textural Microstructure Cooccurrence Matrix (CETMCM) [12]. In the last two cases, co-occurrence matrices of order two and three were computed, after applying the Laws' convolution filters, and/or edge detection filters, followed by an improved k-means clustering technique. During the learning phase, methods such as Confidence Intervals, respectively the Bayesian Belief Networks [12] were applied in order to determine the mean, standard deviation, respectively the probability distributions. The model was validated by applying powerful classifiers [12], the best results being provided by Support Vector Machines (SVM), Multilayer Perceptron (MLP), Random Forest (RF), Adaboost combined with C4.5 [10, 12].

3.2 The Current Solution, Based on Convolutional Neural Networks (CNN)

3.2.1 Convolutional Neural Networks (CNN)

Convolutional Neural Networks (CNN) represent a class of deep, feed-forward, artificial neural networks, appropriate for the image recognition context. They were inspired from biology, so the organization of the connections between the neurons resembles the structure of the animal visual cortex [13]. CNN have started to be extensively used with the emergence of powerful parallel computing resources such as graphics processing units (GPU), their great value being highlighted to the computer vision field by means of the ImageNet competition in 2012. As stated by the work described in [17], CNN have been acknowledged as one of the top 10 breakthroughs of 2013, having various applications ranging from natural language processing to hyperspectral image processing and to medical image analysis. CNN are different from neural networks through the fact that they are a combination of multiple layered perceptron structures, which activate when they recognize a certain input. They contain convolutional layers that are used to compress the input data into recognized data patterns, thus reducing the data size and focusing on patterns of interest. CNN enforce a local connectivity pattern between neurons belonging to adjacent layers. Thus, the inputs of hidden units within layer m are provided by a subset of units in layer $m-1$, these units having spatially contiguous receptive fields, as illustrated in Fig. 1. If we imagine that layer $m-1$

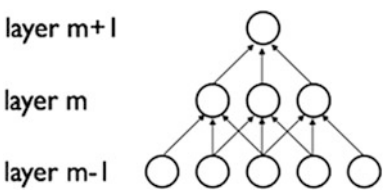

Fig. 1 The local connectivity pattern with an CNN [17]

is the input retina, in Fig. 1, it results that the units within layer m have receptive fields of width three. Within CNN, each convolution filter is replicated across the entire visual field (layer within the CNN). The replicated units (convolution filters) share the same parameterization: weight vector and bias. As presented by [17], at each layer, the input image is convolved with a set of K kernels, with the corresponding weights $W = \{W_1, W_2, ..., W_K\}$ and added biases $B = \{b_1, ..., b_K\}$, each generating a new feature map $X_k, k \in \{1, \ldots, K\}$. These features are subjected to an element-wise non-linear transform $\sigma(\cdot)$ and the same process is repeated for every convolutional layer m. The corresponding formula is provided in (1).

$$X_k^m = \sigma\left(W_k^{m-1} * X^{m-1} + b_k^{m-1}\right). \quad (1)$$

In (1), $W_k^m, k \in \{1, \ldots, k\}$ is a vector containing weights, w_{ij}, which connect the pixels at level m, having the coordinates (i, j), with the corresponding pixels at the layer $m - 1$, having the same coordinates. Eloquent examples of the $\sigma(\cdot)$ transform are the hyperbolic tangent ($\tan h$), respectively the sigmoid function [17].

CNN also incorporate *pooling layers* [13] where pixel values of image neighborhoods are aggregated using a permutation invariant function, typically the maximum or average operation. This operation aims to reduce the computational complexity at superior layers within the CNN, and also induces an amount of translation invariance [17]. Pooling is a form of a non-linear down-sampling operation. *Rectified Linear Unit (ReLU)* layers can also be present within a CNN. They apply non-saturating activation functions of low computational cost in order to enhance the non-linear properties of the CNN and of the decision function [13]. The last part of a CNN is represented by fully connected layers (i.e. regular neural network layers) and a distribution over classes is generated by feeding the activations in the final layer through a *softmax* function [13]. The network is trained using the maximum likelihood or gradient descent techniques [13, 17]. As denoted by Tajbakhsh et al. [14], the main power of a CNN lies in its deep architecture, which allows to extract a set of discriminating features at multiple levels of abstraction. Training a CNN from scratch requires a large amount of labeled training data—a requirement that may be difficult to meet in the medical domain where expert annotation is expensive and some diseases (e.g., lesions) are scarce in the datasets [14]. Typical examples of CNN architectures are ResNet or LeNet [13].

3.2.2 Our Methodology

We perform the comparison between the classification performance provided by CNN, respectively that provided by classical and advanced textural features in combination with powerful classification methods, or classifier combination techniques. For this purpose, we employ the following parameters: accuracy (recognition rate), TP Rate (sensitivity), TN Rate (specificity), Area under the ROC (AUC) [12].

4 Experiments and Discussions

Our experimental dataset contained the following classes: HCC, cirrhotic parenchyma on which HCC had evolved and the hemangioma benign liver tumor. For HCC and cirrhotic parenchyma, 200 cases (patients) suffering from HCC were considered and also 100 cases of hemangioma were taken into account. All the patients were subjected to biopsy, for diagnostic confirmation. The classes were combined in equal proportions within the dataset. For these patients, B-mode ultrasound images were taken into account, acquired by the medical specialists using a Logiq 7 (General Electrics, USA) ultrasound machine, under the same settings: frequency of 5.5 MHz, the gain of 78 and the depth of 16 cm. For each patient, 3 images were considered, corresponding to various orientations of the transducer. Regions of Interest (ROIs), of about 50 × 50 pixels in size, were selected inside the tissue of interest (HCC, cirrhotic parenchyma, hemangioma). These ROIs represented the entries for the CNN, respectively the areas on which the textural features were computed, independently on orientation, illumination and ROI size. A number of 822 ROIs (patch images) per class were included in the dataset for HCC/cirrhotic parenchyma comparison, respectively 260 ROIs were considered in the case of HCC/hemangioma differentiation. The CNN technique was implemented in Matlab 2018 using the Neural Network toolbox [14], on a computer with an Intel Core i_7—3770K CPU, of 3.5 GHz frequency and 16 GB of RAM, without GPU. The textural features were computed using our Visual C++ software modules [10, 12], the feature selection techniques and the traditional classifiers being employed using the Weka 3.6 library [18], as described in [12]. The strategy of 5-folds cross-validation was adopted for classification performance assessment, in all cases.

4.1 The Adopted Architecture for CNN

Multiple architectures (e.g. a ResNet architecture, the resulting features being also provided to a CNN classifier) were experimented in our work and the one providing the best results was chosen. We propose a CNN architecture that is trained from scratch. The structure of our architecture is shown in Fig. 2 and it contains 18 different layers. Each ROI, selected on HCC, cirrhotic parenchyma or hemangioma tissues, constitutes the input of the CNN. Due to this image dimension (48 × 48 pixels) in the proposed architecture we use convolutional layers of dimension

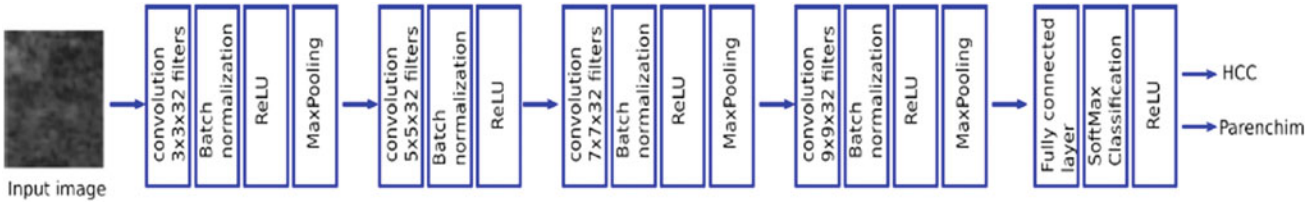

Fig. 2 The adopted CNN architecture

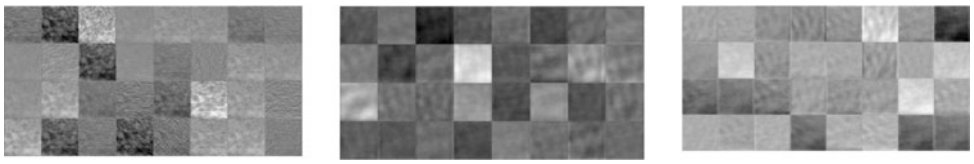

Fig. 3 Activations

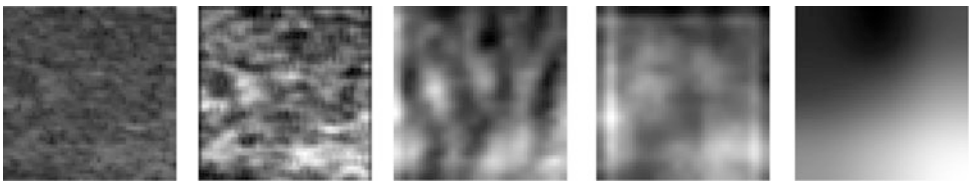

Fig. 4 HCC strongest activations

3 × 3, 5 × 5, 7 × 7 and 9 × 9. The convolutional layer consists of neurons that connect sub-regions of the input or the outputs of the layers before. These layers learn significant features while scanning the image. We can investigate the relevant features by observing which areas in the convolutional layers activate on an image. For example, the activations for a HCC patch image for the convolutional layers are shown in Fig. 3. Different texture patterns can be identified as being learnt by the CNN.

The channels with largest activations for each convolutional layer are shown in Fig. 4 for HCC image patches and in Fig. 5 for a sample parenchyma image patch. Figures 4 and 5 highlight the variability of textural patterns within HCC, the heterogeneity and complexity of the HCC tissue structure. We can notice that the first activations show large granular textural features while the last activations focus on detailed textural features.

4.2 Classification Performance Assessment for the CNN

For training the CNN network described in Fig. 2 we have used the stochastic gradient with momentum algorithm, a batch size of 64 and 20 training epochs, the learning rate being 0.02. The duration of the training process was less than 1 h. The classification performance parameters resulted in this case are depicted in Table 1. Thus, satisfying classification accuracies resulted in both considered cases. Based on this table, we observe the increased values for the specificity (TN Rate) in both cases, so the false diagnosis will be avoided with a high probability, fact that is very important in our practical case, involving surgical treatment for advanced phase HCC. We also observe the increased values of AUC, around 90%, obtained in both cases. The fact that the classification accuracy is more decreased in the

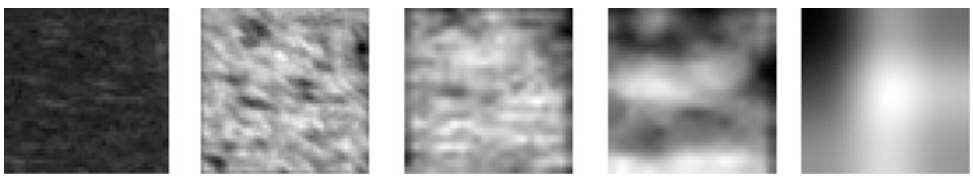

Fig. 5 Parenchyma strongest activations

Table 1 The classification performance parameters in the case of CNN

Classes	Recogn. rate (%)	TP rate (%)	TN rate (%)	AuC (%)
HCC/Cirrhotic parenchima	81.70	78.66	84.76	88
HCC/Hemangioma	78.03	63.62	92.46	90

case of HCC/hemangioma comparison is due to the smaller number of hemangioma cases within our dataset, which influences the performances of the CNN. The classification time was 5.6 ms in both cases, which was also satisfying.

4.3 Comparison with Our Previous Approach, Based on the Imagistic Textural Model of HCC

The comparison of the classification accuracies achieved in the case when our previously computed textural features were employed, in combination with traditional classifiers, against the classification accuracies resulted in the case when the CNN technique was applied, is illustrated in Fig. 6 and explained below.

- *The case of differentiation between HCC and the cirrhotic parenchyma on which HCC had evolved*

When comparing the classification accuracy provided by the CNN technique with the classification accuracies provided by the texture analysis methods, followed by feature selection, in combination with classifiers, in the case of HCC/cirrhotic parenchyma comparison, the following conclusions were drawn, according to Fig. 6 (the left hand side):

- CNN led to a recognition rate of 81.70%, which was higher than that resulted in the case of the classical textural features, when the maximum accuracy was 69% (resulted for the RF classifier);
- CNN led to a classification accuracy of 81.70%, which was higher than that resulted in the case when the classical textural features, combined with superior order GLCM and superior order EOCM features were employed, when the maximum recognition rate was 79.38%, achieved in the case of the SVM classifier;
- the classification accuracy (81.70%) obtained for the CNN was smaller than the maximum accuracy, of 84.3%, obtained in the case of Adaboost combined with the C4.5, when the CTMCM features were taken into account, together with the other textural features, but it was higher than the average recognition rate, of 79.68%, resulted in this case for all the considered classifiers.

- *The case of differentiation between HCC/hemangioma*

In the case when comparing HCC with hemangioma, the following conclusions resulted, according to the right hand side of Fig. 6:

- CNN provided a classification accuracy of 78.03%, higher than the maximum accuracy, of 71.5% resulted in the case when the classical textural features were employed, obtained for Adaboost combined with C4.5;
- the classification accuracy provided by the CNN (78.03%) was almost the same as the maximum accuracy, of 80.2%, achieved for the Adaboost combined with C4.5, in the case when the superior order GLCM features, respectively the superior order EOCM features were used together with the classical textural features;
- the classification accuracy provided by the CNN (78.03%) was smaller than the maximum recognition rate, of 88%, obtained, for the SVM classifier, in the case when the CTMCM textural features were used in combination with the other textural features. Also, it was more decreased than the average recognition rate, of 84.3%, achieved in the case when the CTMCM features were employed together with the old textural features.

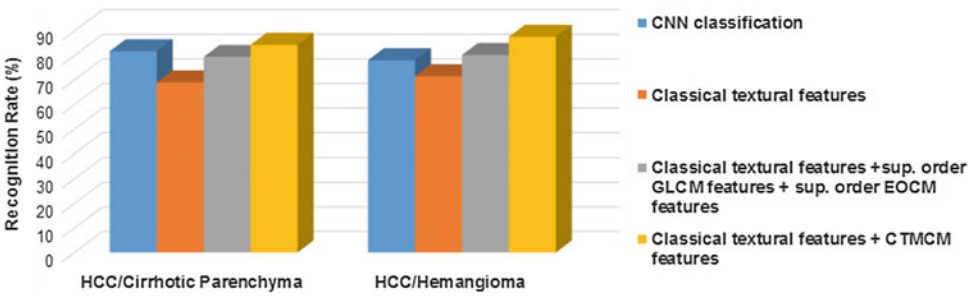

Fig. 6 Comparison between CNN and the texture-based methods from the maximum classification accuracy point of view

5 Conclusions

The CNN method proved to be efficient in the case of HCC recognition, providing classification accuracies around 80%, when differentiating HCC from the cirrhotic parenchyma, respectively from hemangioma. The lower accuracy resulted in the case of differentiation between HCC and hemangioma is due to the small number of available hemangioma cases, which influenced the performances of the CNN. When compared with our previous approaches, based on classical and advanced texture analysis methods, the accuracy of the CNNs overpassed that of the classical texture analysis methods and it was comparable with that of to the advanced texture analysis methods. The obtained accuracy was also comparable with that of other state of the art methods. In our future research, we aim to extend our dataset by including ultrasound images corresponding to new HCC cases, acquired with the aid of new generation ultrasound machines and through more evolved technologies, such as Contrast Enhanced Ultrasound Images (CEUS), as well as by the fusion with other relevant medical data. Preprocessing operations upon the initial image could also be performed, such as the computation of the textural microstructure map [12]. We will also continue our experiments for performing multiclass classification using the CNN technique, in order to further enhance the automatic diagnosis accuracy. Providing the textural features at the entries of other deep learning classifiers, such as SAE, respectively DBN, trained in supervised manner, could also lead to classification performance improvements.

Acknowledgements This work was founded by the Romanian National Authority for Scientific Research and Innovation under Grant number PN-III-P1-1.2-PCCDI2017-0221 Nr. 59/1st March 2018.

Conflict of Interest The authors declare that they have no conflict of interest.

References

1. Sherman, M.: Approaches to the diagnosis of hepatocellular carcinoma. Curr. Gastroenterol. Rep. **7**(1), 11–18 (2005)
2. Yoshida, H., Casalino, D.: Wavelet packet based texture analysis for differentiation between benign and malignant liver tumors in ultrasound images. Phys. Med. Biol. **48**, 3735–3753 (2003)
3. Madabhushi, A., et al.: Automated detection of prostatic adenocarcinoma from high-resolution ex vivo MRI. IEEE Trans. Med. Imaging **24**(12), 1611–1626 (2005)
4. Chikui, T., et al.: Sonographic texture characterization of salivary gland tumors. Ultrasound Med. Biol. **31**(10), 1297–1304 (2005)
5. Ker, J., Wang, L., et al.: Deep learning applications in medical image analysis. IEEE Access **6**, 9375–9389 (2018)
6. Jiang, J., et al.: Medical image analysis with artificial neural networks. Comput. Med. Imaging Graph. **34**(8), 617–631 (2010)
7. Li, W., Jia, F., Hu, Q.: Automatic segmentation of liver tumor in CT images with deep convolutional neural networks. Comput. Commun. **3**, 146–151 (2015). https://doi.org/10.4236/jcc.2015.311023
8. Vivanti, R., Ephrat, A., et al.: Automatic liver tumor segmentation in follow-up CT studies using convolutional neural networks. In: Patch-Based Methods in Medical Image Processing Workshop, pp. 54–61 (2015)
9. Li, W., Cao, P., et al.: Pulmonary nodule classification with deep convolutional neural networks on computed tomography images. Comput. Math. Methods Med. 7 pages (2016). https://www.hindawi.com/journals/cmmm/2016/6215085/
10. Mitrea, D., Mitrea, P., Nedevschi, S., Badea, R., et al.: Abdominal tumor characterization and recognition using superior order co-occurrence matrices, based on ultrasound images. Comput. Math Methods Med. 17 pages (2012)
11. Materka, A., Strzelecki, M.: Texture Analysis Methods—A Review. COST B11 Report (1998). http://citeseer.ist.psu.edu/viewdoc/summary?doi=10.1.1.97.4968
12. Mitrea, D., Nedevschi, S., Badea, R.: Automatic recognition of the hepatocellular carcinoma from ultrasound images using complex textural microstructure co-occurrence matrices (CTMCM). In: Proceedings of the 7th International Conference on Pattern Recognition Applications and Methods (ICPRAM), Jan 2018, pp. 178–189 (2018)
13. Deep Learning Tutorial, Release 0.1, LISA lab, University of Montreal, Copyright Theano Development Team (2015)
14. Tajbakhsh, N., et al.: Convolutional neural networks for medical image analysis: full training or fine tuning? IEEE Trans. Med. Imaging **35**(5), 299–1312 (2016). https://doi.org/10.1109/tmi.2016.2535302
15. Yasaka, K., Akai, H., et al.: Liver fibrosis: deep convolutional neural network for staging by using gadoxetic acid-enhanced hepatobiliary phase MR images. Radiology **287**(1), 146–155 (2018)
16. Byra, M., Styczynski, G., et al.: Transfer learning with deep convolutional neural network for liver steatosis assessment in ultrasound images. Int. J. Comput. Assist. Radiol. Surg. **13**(12), 1895–1903 (2018)
17. Litjens, G., Kooi, T., et al.: A survey on deep learning in medical image analysis. Med. Image Anal. **42**, 60–88 (2017)
18. Weka 3 (2018). http://www.cs.waikato.ac.nz/ml/weka/
19. Neural Network Toolbox for Matlab (2018). https://www.mathworks.com/products/neural-network.html

An Augmented Reality Platform for Preoperative Surgical Planning

S. Teodoro Vite, C. F. Domínguez Velasco, S. Muscatello, M. Á. Padilla Castañeda, and L. T. De Paolis

Abstract

Researching in new technologies for diagnosis, planning and medical treatment have allowed the development of computer tools that provide new ways of representing data obtained from patient's medical images such as computed tomography (CT) and magnetic resonance imaging (MRI). In this sense, augmented reality (AR) technologies provide a new form of data representation by combining the common analysis using images and the ability to superimpose virtual 3D representations of the organs of the human body in the real environment. In this paper we describe the development of a generic computer platform based on augmented reality technology for surgical preoperative planning. In particular, the surgeon can navigate in the 3D models of the patient's organs in order to have the possibility to perfectly understand the anatomy and plan in the best way the surgical procedure. In addition, a touchless interaction with the virtual organs is available thanks to the use of an armband provided of electromyographic muscle sensors. To validate the system, we focused in two cases of study: navigation through aorta artery for mitral valve repair surgery and navigation through vascular structures in the brain for the treatment of cerebral aneurysms.

Keywords

Augmented reality • Surgical planning • Touchless interaction

S. Teodoro Vite · C. F. Domínguez Velasco · M. Á. Padilla Castañeda
Applied Sciences and Technology Institute, National Autonomous University of Mexico, Mexico City, Mexico

S. Muscatello · L. T. De Paolis (✉)
Department of Engineering for Innovation, University of Salento, Lecce, Italy
e-mail: lucio.depaolis@unisalento.it

1 Introduction

Advances in computer technologies applied to medicine are offering new tools for diagnosis, preoperative planning, image-guided surgery, training and even the formulation of new treatments that help the surgeon to taking decisions before, during and after performing a surgical procedure. These advances are conferring considerable advantages on the patient, but they are also imposing an additional difficulty on the surgeon, who needs to develop new skills in order to adapt to newer systems [1].

In this sense, the technology of augmented reality begins to be a novel alternative because it supposes in a single space a transition that combines common elements in the real world with virtual elements. In medicine, the use of the AR technology makes possible to overlay virtual models of the organs on the real patient; this allows the surgeon to have a sort of 'X-ray vision' of the patient's internal anatomy. AR 'augments' the surgeon's perception with a better spatial perception and a reduction of the duration of the surgical procedure [2].

Thus, surgeons have at their disposal a mixture of techniques, between traditional and digital methods that involve new forms of representation, interaction and analysis of medical data.

Currently more and more research teams are approaching the world of augmented reality applied to medicine due to the necessity to refine surgical practices and reduce the human error factor alongside the specialist's experience with advanced techniques [3].

One of the first publications in this sense, presented by Wagner et al. [4], consists of a visualization system for image-guided stereotactic navigation in tumour surgery that sought to provide an innovative tool using augmented reality instead of fully virtual environments. Some years later a research group from the University of Auvergne, began the development of a guided laparoscopy system in gynaecology [5]. Subsequently, the original system was improved [6]

S. Vlad and N. M. Roman (eds.), *6th International Conference on Advancements of Medicine and Health Care through Technology; 17–20 October 2018, Cluj-Napoca, Romania*, IFMBE Proceedings 71,
https://doi.org/10.1007/978-981-13-6207-1_28

involving a framework for the semi-automatic registering of MRI images with the video of the laparoscopic procedure.

Another interesting works comprise specializations such as dental surgery [7], maxillo-facial surgery [8, 9], liver surgery [2, 10] and neurosurgery [11, 12].

In this work we propose a generic augmented reality platform for the manipulation of medical images (CT or MRI) and the visualization of anatomical structures in three dimensions, extendible to any type of surgical planning. The general concept of the system is to show the user an augmented scene (view of the real world and virtual elements) so that it can have a better spatial and shape understanding of the anatomical structures that will be involved in a surgical procedure. Also, the system provides the surgeon with a way to plan trajectories or movements that can be executed during minimally invasive procedures.

The platform has been designed in order to permit surgeon to navigate in the 3D models of the patient's organs in order to have the possibility to perfectly understand the anatomy and plan in the best way the surgical procedure. During the navigation it is possible to visualize the virtual environment in the helmet and also in a computer screen in order to provide the surgeon the possibility to discuss with other colleagues on the specific clinical case. A touchless interaction with the virtual organs is available thanks to the use of an armband provided of electromyographic muscle sensors.

In the current version, the system is capable to manage two clinical cases, which correspond to two different applications, one in heart surgery and the other in neurosurgery that served as a basis for testing the proposed platform.

2 Methodology

The system proposed in this paper consists of a set of blocks that execute tasks in real time to create an augmented scene. The architecture shown in Fig. 1 consists of three types of devices (sensors) that permit the user (a surgeon) to visualize the 3D models of the organs and interact with these.

- a Myo armband is used to recognize some user's gestures and provide the system with commands used to manipulate transformations of the virtual models [13];
- a set of stereo cameras used to obtain the view of the real environment where the subject is located;
- an Oculus Rift helmet used to define a reference between the space of virtual models and the position of the user's head.

Additionally, the graphics device is responsible for duplicating the user's view of the RV helmet on a standard screen. From a functional point of view, AR application can be divided into three processing steps: tracking, alignment and rendering.

In the tracking step, Oculus OVRPlugin analyses the IR video data flow coming from the Oculus camera and

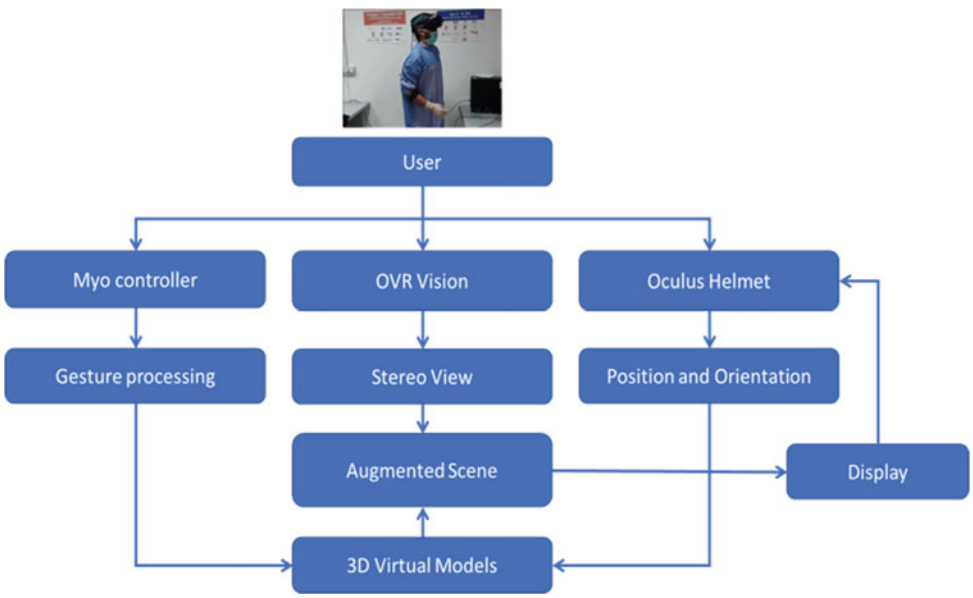

Fig. 1 Architecture of the AR system

Fig. 2 Navigation and interaction system

processes the detected tracking system. Oculus's positional tracking system, used to track the position of the user's head, consisting of external infrared tracking sensors that optically track the headset. The Oculus is fitted with a series of infrared LEDs that permit to determine with sub-millimetre accuracy and near-zero latency the precise position of the device and, consequently, of the user's head.

During the alignment phase, some algorithms are used to align the virtual camera with the real one. This aims to make the portion of the augmented scene to appear perfectly coincident with the user's point of view that changes in real time. In every frame, the camera transformation matrix is calculated to consequently update the virtual objects parameters of position, rotation and scale and make them proportional to the user's real movements.

In addition to this phase, it's necessary to consider a sub-phase that can be called "augmentation" of the Oculus point of view. This step consists into a second alignment phase to match the Oculus virtual camera with the OVR-Vision virtual image plane, in which there is the video stream captured by the lenses of the stereo camera system attached on Oculus front cover. In this way, it's possible to convert a VR viewer, such as the Oculus Rift, into an immersive AR see-through system.

Finally, in the last phase of rendering, digital information is displayed in the augmented scene in such a way that the user hardly can distinguish the virtual objects from the real ones. For this purpose, some efficient graphics libraries and three-dimensional rendering engines are used to create the virtual elements, and moreover, to render the appropriate texture based on the virtual object.

Figure 2 shows the navigation and interaction system with all the involved devices:

(1) Oculus tracking for virtual object positioning;
(2) reference display of the model;
(3) Myo armband for gestures detection;
(4) Oculus Rift with the OVRVision Pro stereo camera.

3 Virtual Models

The reconstruction of virtual models has been made from CT images; two patient-specific cases were selected, a case of study for mitral valve surgery and a case of cerebral aneurysm in a non-haemorrhagic state (Fig. 3).

In the case of heart surgery the focus was the representation of the aorta, from the level of the groin to the heart, passing through the aortic valve to reach the mitral valve that empties into the left atrium. In the case of cerebral vascularity, the region of the cerebral arteries was considered, including the carotid arteries and their bifurcation in the region of the middle cerebral, anterior cerebral and posterior communicating arteries.

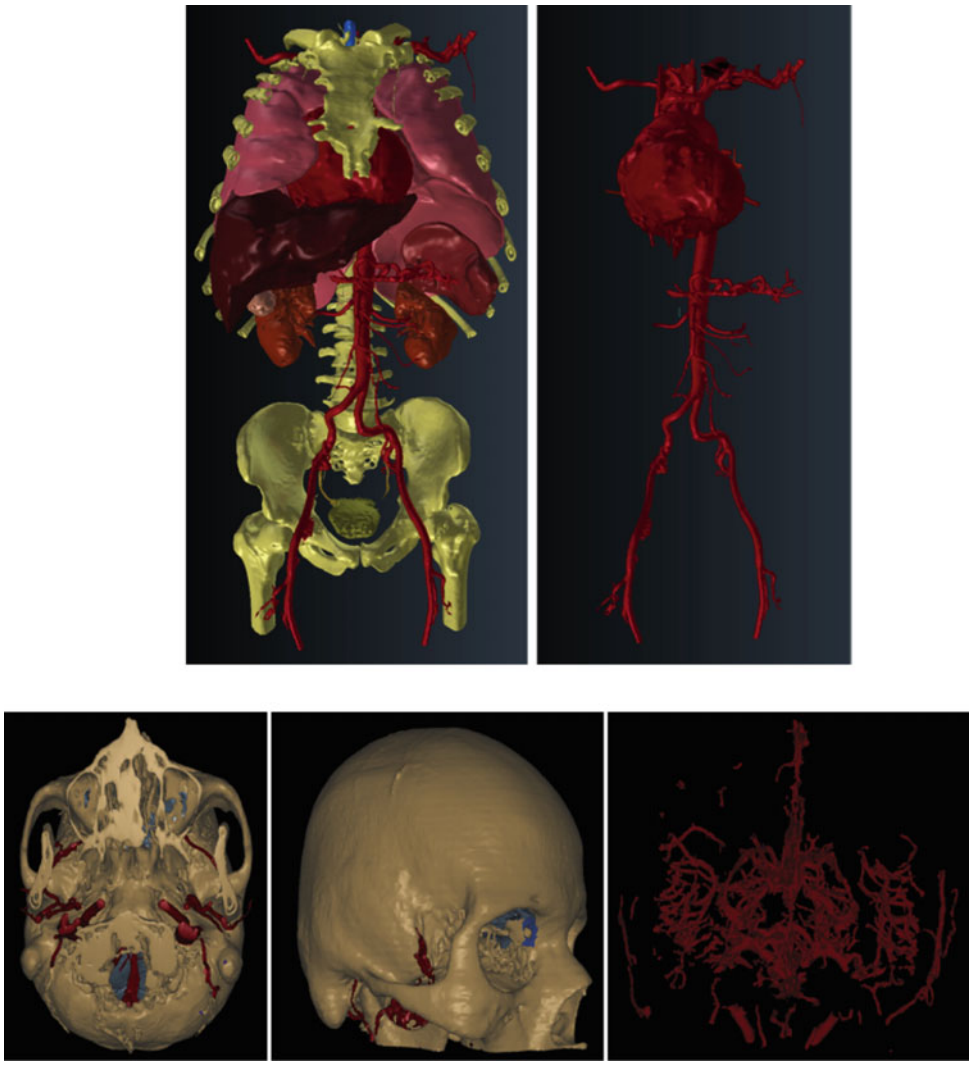

Fig. 3 3D Reconstructions of organs from CT images

The segmentation of the images was performed using semi-automatic algorithms based on thresholds, morphological operations (erosion and dilation) for noise reduction, elimination of islands and smoothing. Using the software 3D Slicer [14], marching cubes algorithm was applied for the reconstruction of the surface of the segmented anatomical structures.

The resulting surfaces were submitted to post-processing using the MeshLab [15] software, to iteratively apply a quadric edge collapse decimation algorithm. Later the models were refined and placed in their final position using Blender [16] framework, where the experimental setup was built and later exported to Unity3D [17] engine.

4 Gesture Recognition

The interaction with the virtual contents implements a touchless method through hand gestures and forearm movements. Myo armband uses electromyographic muscle sensors that, in contact with the skin, are able to read the electrical activity of the forearm muscles and to translate in real-time them into digital commands [13, 18].

The association between the gestures and the tasks to be performed on the 3D models has been realized in such a way to implement a form of interaction as natural as possible as shown in Fig. 4.

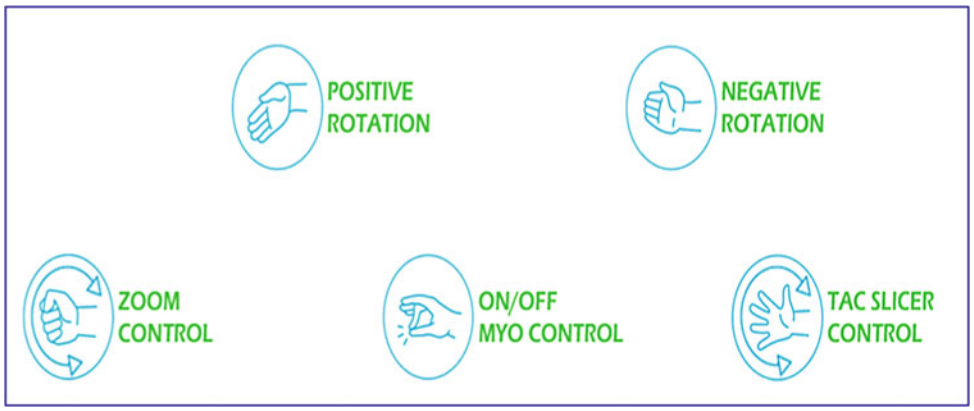

Fig. 4 Recognised gestures and performed task

Two kinds of user feedback have been introduced to inform that the gesture has been detected and recognized: the first consists in a haptic feedback through a small vibration pattern inside Myo's hardware and the second one provides a graphic user interface on the top of the display device that allows to see if the Myo control is activated or deactivated. This is important because the surgeon can decide if the Myo controller must remain deactivated in order prevent incorrect or unwanted gestures.

5 Visualization System

Unity3D and Oculus Rift DK2 were used for the development of the visualization system.

The tracking system allows 6 degrees of freedom that are divided into rotational and positional tracking. The rotational tracking (with 1000 Hz refresh rate) is embedded inside the lenses using a gyroscope, an accelerometer and a magnetometer. For the positional tracking (with 60 Hz refresh rate) there is a camera with a near-infrared CMOS sensor that continually perceives the infrared points emitted by the HMD.

Fig. 5 Oculus Rift and OVRVision Pro

OVRVision Pro VR stereo camera were used to enable the augmented vision capability with the Oculus DK2, as shown in Fig. 5. The cameras were configured on full mode according to the manufacturer's description that adds a more realistic interaction. By means of the incorporation of the cameras on the scene of Unity it is possible to regulate the distance of each one of the cameras, as well as their vertical movement with respect to each other.

6 Conclusions

The surgeons showed great interest in the application of augmented reality and made suggestions for improvements and adaptations in other specialities. This is possible thanks to the general architecture of the system that allows the adaptation of new cases of study following the described methodology.

About the devices used, most of the users did not present problems to adapt to its use and managed to become familiar with the interface in short periods of time.

A variant of the system, that incorporates tracking using infrared technology, could be used to guide the surgeon during a procedure by superimposing the virtual models of the organs on the real patient; in this way the surgeon could have an increased view of the patient's anatomy and know in real time the position of the instrument inside the patient's body. That allows him to take more accurate decisions taking into account the anatomical structure of interest. However, this last task introduces some complications, such as the correct alignment of the virtual models with respect to the position of the patient in the operating room. Algorithms based on fiducial points are used in order to have a correct registration phase [10]. However, the use of pre-acquired CT

images in order to obtain the 3D model of the organs is not possible if the surgery involves tissues that are deformed during the procedure; in that case is required the adoption of other algorithms able to adapt with precision the geometry obtained in the process of segmentation and reconstruction to the new situation in the patient's body.

Acknowledgements The platform described in this paper is part of the project No. UNAM-DGAPA_PAPIME-PE109018.

Conflict of Interest The authors declare that they have no conflict of interest.

References

1. Lamata, P., Ali, W., Cano, A., Cornella, J., Declerck, J., Elle, O.J., Freudenthal, A., Furtado, H., Kalkofen, D., Naerum, E.: Augmented reality for minimally invasive surgery: overview and some recent advances. In: Augmented Reality. InTech, Croatia (2010)
2. De Paolis, L.T., Ricciardi, F.: Augmented visualisation in the treatment of the liver tumours with radiofrequency ablation. Comput. Methods Biomech. Biomed. Eng. Imaging Vis. **6**(4), 396–404 (2018)
3. De Paolis, L.T., Aloisio, G.: Augmented reality in minimally invasive surgery. In: Advances in Biomedical Sensing, Measurements, Instrumentation and Systems, pp. 305–320. Springer, Berlin (2010)
4. Wagner, A., Ploder, O., Enislidis, G., Truppe, M., Ewers, R.: Virtual image guided navigation in tumor surgery technical innovation. J. Craniomaxillofac. Surg. **23**(5), 271–273 (1995)
5. Collins, T., Pizarro, D., Bartoli, A., Canis, M., Bourdel, N.: Computer-assisted laparoscopic myomectomy by augmenting the uterus with pre-operative MRI data. In: IEEE International Symposium on Mixed and Augmented Reality, pp. 243–248 (2014)
6. Collins, T., Chauvet, P., Debize, C., Pizarro, D., Bartoli, A., Canis, M., Bourdel, N.: A system for augmented reality guided laparoscopic tumour resection with quantitative ex-vivo user evaluation. In: International Workshop on Computer-Assisted and Robotic Endoscopy, pp. 114–126. Springer, Berlin (2016)
7. Wang, J., Suenaga, H., Hoshi, K., Yang, L., Kobayashi, E., Sakuma, I., Liao, H.: Augmented reality navigation with automatic marker-free image registration using 3-D image overlay for dental surgery. IEEE Trans. Biomed. Eng. **61**(4), 1295–1304 (2014)
8. Ricciardi, F., Copelli, C., De Paolis, L.T.: An augmented reality system for maxillo-facial surgery. In: Fourth International Conference Augmented and Virtual Reality and Computer Graphics (AVR 2017), pp. 53–62. Springer, Berlin (2017)
9. Ricciardi, F., Copelli, C., De Paolis, L.T.: A pre-operative planning module for an augmented reality application in maxillo-facial surgery. In: International Conference on Augmented and Virtual Reality, pp. 244–254. Springer, Berlin (2015)
10. De Paolis, L.T.: Augmented visualization as surgical support in the treatment of tumors. In: International Conference on Bioinformatics and Biomedical Engineering, pp. 432–443. Springer, Berlin (2017)
11. Kersten-Oertel, M., Chen, S.J., Drouin, S., Sinclair, D.S., Collins, D.L.: Augmented reality visualization for guidance in neurovascular surgery. Stud. Health Technol. Inform. **173**, 225–229 (2012)
12. Kersten-Oertel, M., Gerard, I., Drouin, S., Mok, K., Sirhan, D., Sinclair, D.S., Collins, D.L.: Augmented reality in neurovascular surgery: feasibility and first uses in the operating room. Int. J. Comput. Assist. Radiol. Surg. **10**(11), 1823–1836 (2015)
13. Indraccolo, C., De Paolis, L.T.: Augmented reality and myo for a touchless interaction with virtual organs. In: International Conference on Augmented Reality, Virtual Reality and Computer Graphics, pp. 63–73. Springer, Berlin (2017)
14. D Slicer at http://www.slicer.org
15. Cignoni, P., Callieri, M., Corsini, M., Dellepiane, M., Ganovelli, F., Ranzuglia, G.: MeshLab: an open-source mesh processing tool. In: Scarano, V., Chiara, R.D., Erra, U. (eds.) Eurographics Italian Chapter Conference (2008)
16. Hess, R.: Chapter 1—an introduction to 3D: recreating the world inside your computer, or not. In: Hess, R. (ed.) Blender Foundations, pp. 1–11. Focal Press, Boston (2010)
17. Unity at http://docs.unity3d.com/Manual/index.html
18. Myo at http://www.myo.com

Part IV
Telemedicine and Health Care Information Systems

Multi-agent Healthcare Information System on Hadoop

Gabriel Cristian Dragomir-Loga, A. Lacatus, L. Loga, and L. Dican

Abstract

The healthcare industry generates a large amount of data by keeping patients' medical history and due to the diversity of clinical medical equipment. In this paper we address problems that exist in the organ transplantation medical field. Some matching algorithms (based on centralized data) were already presented but expanding the system when it comes to Big Data was not considered before. Problems that may occur in the context of Hadoop are related to uneven data distribution and MapReduce processing. The question that arise is whether a centralized graph algorithm can be adapted to MapReduce in order that the results to be equivalent to centralized processing and efficiency to grow through parallel processing. Our solution uses intelligent agents to collect and process medical data. In case of the matching algorithm, the distributed version can approximate a solution obtained by using the centralized application, but it is more effective as a response time in the Big Data context.

Keywords

Multi-agent system • Hadoop • MapReduce • Healthcare information system • Data warehouse

1 Introduction

Institute for Health Technology Transformation estimates that in 2011 the US Healthcare industry generated 150 Exabytes of data [1].

In the above article it is said that Big Data, seen as a concept, has become a necessity in healthcare not only because of the large data volume but also because of the diversity of the data type and the pace with which the data volume increases.

According to the statistics published by Eurotransplant international collaborative framework [2] which refers to the following countries: Austria, Belgium, Croatia, Germany, Hungary, Luxembourg, Netherlands and Slovenia, the average number of donors per year was around 1800 and the average number of recipients on waiting list per year was around 11,000 since 2008.

For each patient there are performed several medical tests like blood type, Human Leukocyte Antigens, panel reactive antibodies and lymphocytotoxic cross-match between each donor and each recipient.

In a previous paper [3] we have presented a matching algorithm for kidney transplantation, but we have not considered the volume of data. The study carried out in the current paper addresses the issues of heterogeneous data collection and a large amount of data processed.

2 Hadoop and Mapreduce

2.1 Hadoop

Distributed databases or distribution of processing have been the subject of research for over 40 years. Once the modern technology evolved, ideas could be put into practice.

At the beginning of the new millennium (2003), Google published works where it described the GFS system (Google

G. C. Dragomir-Loga (✉) · A. Lacatus
Computer Science Department, Technical University of Cluj-Napoca, Baritiu St. 26-28, Cluj-Napoca, Romania
e-mail: gabriel.dragomir@cs.utcluj.ro

L. Loga
Clinical Institute of Urology and Renal Transplantation, Cluj-Napoca, Romania

L. Dican
Biochemistry Department, "Iuliu Hatieganu" University of Medicine and Pharmacy, Cluj-Napoca, Romania

S. Vlad and N. M. Roman (eds.), *6th International Conference on Advancements of Medicine and Health Care through Technology; 17–20 October 2018, Cluj-Napoca, Romania*, IFMBE Proceedings 71,
https://doi.org/10.1007/978-981-13-6207-1_29

File System) and MapReduce [4]. GFS moved to the Hadoop project in 2006.

Apache Hadoop is an open-source system that allows data sharing through the HDFS file management system and parallel processing of large datasets using the MapReduce programming model.

Hadoop Ecosystem [5] includes the following: Flume, Sqoop, HDFS, MapReduce, HBase, Pig, Hive, Apache Oozie.

2.2 MapReduce

The MapReduce programming model [6] which stands above HDFS works in batch mode. The MapReduce processing unit is the job. A job has input data, the MapReduce program and the configuration parameters. When executed, the job is divided into map and reduce tasks. The user application is transmitted through a client to NameNode (master node), and NameNode sends the algorithm to be executed with local data to each DataNode (slave node) in the cluster. The result of processing is written again in HDFS.

The study [7] concluded that MapReduce model outperform in scalability and fault tolerance a Relational Database Management System (RDBMS) and also underlined the performance limitations of the MapReduce model, in terms of computation time, attributed mainly to the fact that the model was not originally designed to perform structured data analysis and lacks many of the basic features that the relational databases routinely provide.

2.3 Join Implementations in MapReduce

MapReduce has two main join implementations: the map side join and the reduce side join. Map side join requires the data inputs to be partitioned and sorted in the same way. The preprocessing needed is expected to degrade its performance assuming that each dataset is partitioned in the same number of partitions and using the same Partitioner, records that have the same value of the join key will reside in the same partition for each dataset.

Reduce side join is the most general join approach implemented in the context of the standard map/reduce framework. However, its biggest drawback is its I/O cost. The basic idea behind the reduce side join is that the mapper tags each record with its source and uses the join key as the map output key so that the records with the same key are grouped for the reducer. When each reducer receives a set of records (likely from multiple map tasks) they are being sorted and grouped before entering the reduce function.

The records are primarily sorted on join key and secondarily on tag. First, the join key of each record is compared and in case of ties, sorting is done based on the tag. On the other hand, grouping depends only on the value of the join key (types of joins and optimization of joins were studied among other research papers in [8–10]).

Suppose we are joining R(A, B) ⋈ S(B, C), and the sizes of relations R and S are r and s, respectively. Each chunk of the files holding R and S is fed to one Map task, so the sum of the communication costs for all the Map tasks is r + s [10]. Communication from Map tasks to Reduce tasks is O(r + s), so the communication cost of a join algorithm is O(r + s).

An efficient method to mitigate the cost related to the reduce side join is to minimize the redundant transfers between map and reduce. A Bloom filter [11] could be created for the smallest of the two relations (R or S) in the mapper and distributed cache sent to reducer.

In a star schema where multi way join is a common operation between one fact table and many dimensions, the number of Bloom filters is proportional with the number of foreign keys in the fact table.

A Bloom filter consists of two components: a bit vector of m bits and a set of k hash functions. Every hash function h_1, h_2, …, h_k returns values in the range 1 … m, so $h_i : X \rightarrow 1 \ldots m$. In a join operation X is the value of the fact table foreign key. If we want to construct a Bloom filter for a set $A = \{a_1, a_2, \ldots, a_n\}$ of n elements, we compute k hashes of each element and turn on those bits in the bit array. To check whether a value is present, we compute k hashes, and check all those bits in the array to see if they are turned on. If those bits are set to 1, the filter returns true, otherwise false. There were other works that uses bloom filters on MapReduce as in [12].

3 Proposed System

3.1 Architecture

Usage of multi-agent is a method to integrating and developing information systems, supporting intelligent and distributed data storage, enabling an optimized environment, improving reusability, flexibility and reliability [13, 14]. Each agent has a knowledge base and a set of rules.

The responsibilities of the agents are as follows:

- The Medical Agent—the agent's basic tasks are: receiving a test report for laboratory results, receiving alerts of the exceptions in laboratory results, receiving notifications with available results according to the searching criteria established by a doctor, receiving donor-recipient compatibility suggestions. The artefacts received by medical agent will be distributed to involved medical staff.

- The Coordinating Agent—the basic function of this agent is to find and transmit information that another agent may need (Fig. 1).
- The Laboratory Agent—this agent should have the ability to interfere with laboratory instruments (medical devices). He is responsible for the acquisition, management and transfer of data in the patient's electronic system. The agent provides real-time delivery of the examination reports that have been requested by the physician. Other tasks of the agent would be: prioritization of tests based on patient conditions and to notify the medical agent (via coordinator or directly) that results are available. In the architectural version of Fig. 2, the laboratory agent validates the data, alerts for exceptions that cannot be automatically corrected, and uploads data directly to Hadoop. According to Fig. 1, the role of the laboratory agent is reduced. He can only collect from the medical device and transmit to the coordinating agent the laboratory results. The validation task belongs to the coordinating agent, as well as the loading in Hadoop is made by the coordinating agent.

3.2 Discussion About the Two Kinds of Architecture

In Fig. 1, laboratory agents collaborate with the coordinating agent in an Extract-Transform-Load (ETL) manner [15]. The first part of an ETL process involves extracting data from multiple sources.

Each laboratory agent can use a different data/format organization. Frequent formats are tab-delimited text files.

Variants for communication between the laboratory agent and the coordinating agent may be PUSH or PULL [16]. In the PULL variant, the coordinating agent should bind to the laboratory data sources and should collect data in MapReduce mode. We suppose that in the architectural version of Fig. 1, the Coordinating Agent has access to a DataBase (DB) of medical device templates (each medical device typically has a distinct structure for the resulting data).

Upon the emergence of a new medical device, a new template will be defined and inserted into templates DB. A template describes the form of data and processing features needed when data from medical device will be loaded

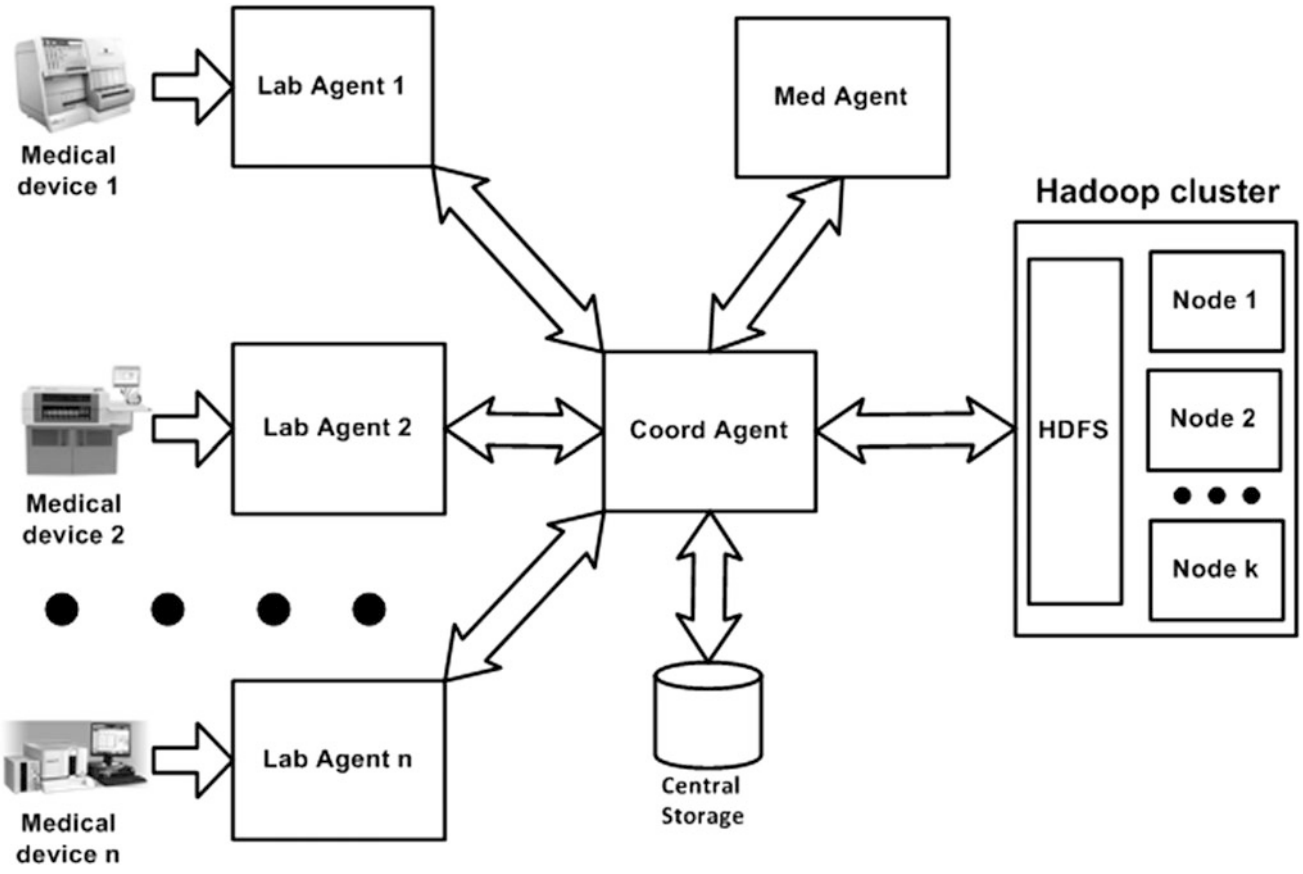

Fig. 1 Architecture with coordinator agent

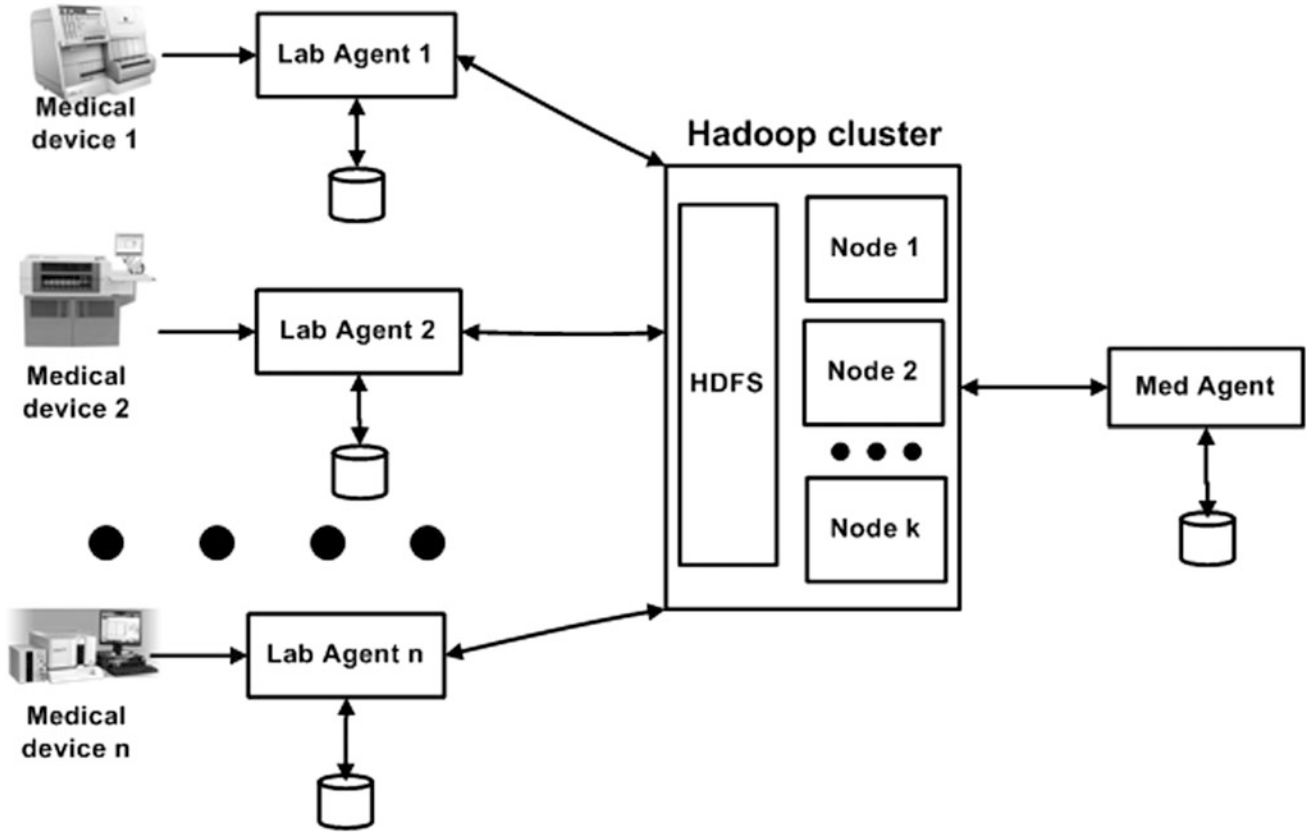

Fig. 2 Autonomous agents architecture

into Hadoop. There is a dedicated hierarchical directory structure where data from each Laboratory Agent is stored. The structure includes the following: INPUT_FILES directory, OUTPUT_FILES directory and EXCEPTION_FILES directory. Since Hadoop is batch-oriented, data loading is done using the files in the OUTPUT folder.

Also, when introducing a new medical device into the system, the Laboratory Agent needs to be configured to collect data from it.

The approach with templates DB ensures the flexibility and scalability of the system.

The Coordinating Agent will apply different forms of data validation. If validation fails, it can lead to full or partial data rejection. In the transformation stage of the ETL process, a set of rules is applied on the data extracted from the source to obtain new data to load it into Hadoop. One or more of the following types of transformation may be required:

- Select only certain columns to load.
- Select missing values (NULL) to not load.
- Translation of encoded values (for example, if the source system stores 1 for male and 2 for female, but the Data Warehouse (DW) stores M for the male and F for the female).
- Automatic data cleaning.
- Reconciliation of identifiers (for example, the input file has a person's name, or an identification code assigned by the On-Line Transaction Processing (OLTP) system, and in DW fact table must contain the identifier from the global electronic system).

If exceptions occur, the Coordinating Agent tries to mitigate issues and will save unsolved cases in a file in the exceptions folder. After the changes which will be done manually by an authorized person, the new file will be moved to the folder containing the input data.

Current DW approaches exclude the intermediate data transformation process by postponing the various changes and validations to be performed in a MapReduce job (in the Map task). The architecture in Fig. 2 tends to address this approach. DW (the data stored in Hadoop) is composed of multiple data marts, each data mart having a star-schema. There is a data mart for crossmatch (Fig. 3) and a data mart for laboratory results (Fig. 4). Fact tables are updated like we described above.

We suppose that Kerberos will be used for authenticating distributed agents. The laboratory agents will obtain tickets from the Kerberos Key Distribution Center (KDC), and they

Fig. 3 Cross-match data mart

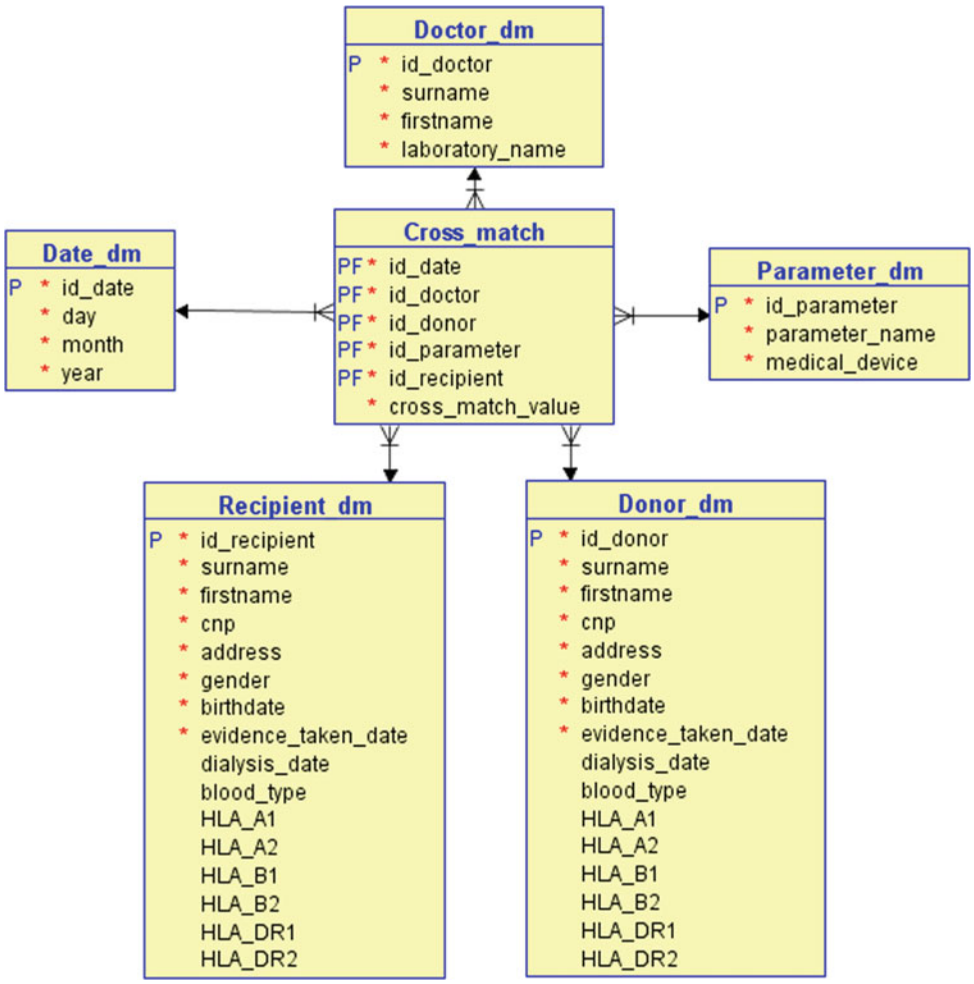

present these tickets to coordinating agent when connections are established.

3.3 Matching Algorithm on MapReduce

We consider in the implementation of data marts [17] from Figs. 3 and 4 denormalization in the sense that the fact tables contain only foreign key(s) to the patient dimension. The fact tables will be flat files stored in HDFS (partitioned on different nodes of the Hadoop cluster) and laboratory results will be continuously added to them. We do not consider how patient information is added from the global electronic system.

We assume that we use Hbase table as data format for Patient dimension (also for Receiver and Donor dimensions). The considerations are that Patient dimension should be updated.

In the first job we started from Cross-match data mart. We use some knowledge about the donor group's period (date_1 and date_2). The intention is narrowing the amount of data to that of interest. We do not need to implement a custom partitioner. In the mapper, the line number from CROSS_-MATCH.TXT will represent the key and the text will represent the value. In the job configuration filtering parameters (date_1 and date_2) will be read. When parsing the value, filter on date will be applied. In the reducer we prepare the output file, CROSS_MATCH1.TXT, only with that combinations (FK_donor, FK_recipient) for which ALL cross_-match_value = 0, so it could be used in a multiway join with the Patient Hbase table in the next job.

The second job has only the mapper. In the proposed solution, Hbase table permits an implementation of the join in the mapper. By not using reducer (no partitioning, no shuffle, no sorting) we bring a significant improvement to the performance. The combination (FK_donor, FK_ recipient) will be the key and (donor_details, recipient_details) will be the value. In the configuration of the job has been read the filtering parameter ϵ. The mapper writes directly to the output file named CROSS-MATCH_2.TXT all the records which pass the test donor_details − recipient_details $< \epsilon$. We also create and serialize a Bloom filter on FK_recipient.

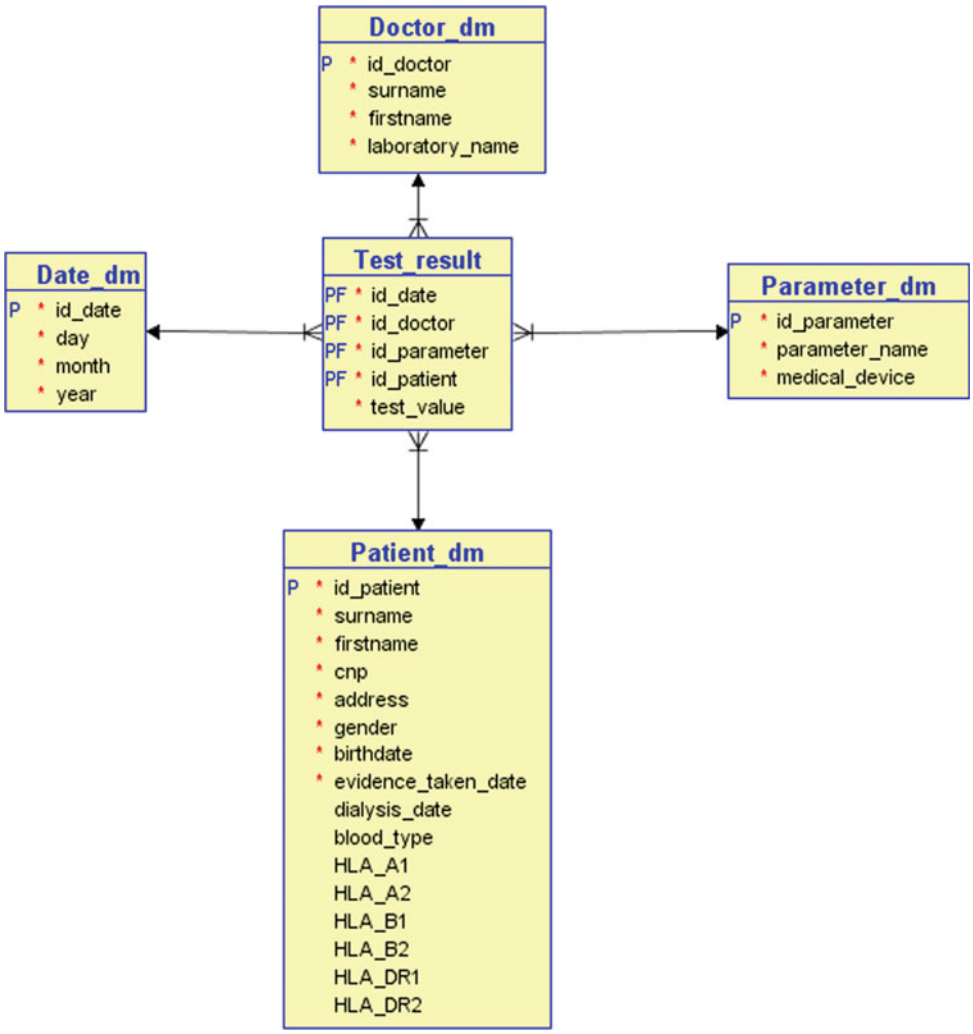

Fig. 4 Laboratory test results (antibody HLA) data mart

The last job of phase one of the Matching Algorithm joins CROSS_MATCH_2.TXT with Test_Results fact table (Fig. 4) in reducer-side manner. In the job configuration score parameters and percentage threshold will be read and the Bloom filter on FK_recipient will be deserialized. In the mapper, when parsing the value of TEST_RESULTS.TXT we filter FK_recipient using the Bloom filter, parameter_-name on 'antibody_HLA' and test_value on percentage_threshold. The output is COST_RECIPIENT_LIST.TXT file. Each line of the output file contains FK_recipient, Donors_count and a list of (FK_donor, cost). The output file is ordered descending by the maximum cost of each recipient's list. The inner lists are also ordered descending by cost.

In parallel a similar job is executed. This job has the output a file COST_DONOR_LIST.TXT with FK_donor, Recipients_count and a list of (FK_recipient, cost).

The second phase starts from the cost lists and calculates the matching list. It consists of an initial job (Job_4) and several repeatable jobs, determined by conflicts discovered in the reducer task of the previous job. The order in which jobs of phase two are executed is as follows:

1. Job_4
2. Job_5, if count_conflicts > 0 continue with Job_6 else RECIPIENT_MATCHING.TXT contains the solution
3. Job_6, if count_conflicts > 0 continue with Job_5 else DONOR_MATCHING.TXT contains the solution.

The mapper of Job_4 scans the list of recipients and selects the first unallocated donor (we use a HashMap for this). The reducer performs join with the list of donors to prevent a particular donor from remaining unallocated and we maintain a HashMap of allocated recipients to prevent

conflicts between recipients. However, when more reducers are used, conflicts may arise. To resolve conflicts, we use Job_5/Job_6, where we switch between lists (donors list and recipients list). We perform join between the previously founded list and the original opposite list in order to continue in descending order from the donor/recipient which generated conflict (in Job_5 COST_RECIPIENT_LIST.TXT - DONOR_MATCHING.TXT and in Job_6 COST_DONOR_LIST.TXT - RECIPIENT_MATCHING.TXT).

3.4 Discussion

We suppose data from Fig. 5 and a configuration with 3 Mappers and 2 Reducers. Figures 6 and 7 show the results of Job_4.

We can observe in Fig. 7 that there is a conflict between don_5 at node_1 and don_2 at node_2. The conflict should not appear if we use only one reducer, in which case don_2 will be paired with rec_5, cost_5.

		Recipient									
		1	2	3	4	5	6	7	8	9	10
Donor	1	0	9	6	0	0	0	7	5	8	1
	2	0	0	0	0	5	0	1	6	4	0
	3	5	10	10	0	0	4	0	1	3	2
	4	0	8	5	0	0	0	8	6	7	2
	5	6	0	0	0	5	6	0	7	3	1
	6	1	0	7	2	6	2	3	0	0	4

Fig. 5 Case study with six donors and ten recipients

Mapper

node_1	rec_2	don_3, cost_10, I	don_1, cost_9, E	don_4, cost_8, E		
	rec_3	don_3, cost_10, D	don_6, cost_7,I	don_1, cost_6, E	don_4, cost_5, E	
	rec_9	don_1, cost_8, I	don_4, cost_7, E	don_2, cost_4, E	don_3, cost_3, E	don_5, cost_3, E
node_2	rec_7	don_4, cost_8, I	don_1, cost_7, E	don_6, cost_3, E	don_2, cost_1, E	
	rec_8	don_5, cost_6, I	don_2, cost_6, E	don_4, cost_6, E	don_3, cost_1, E	
	rec_1	don_5, cost_6, D	don_3, cost_5, I	don_6, cost_1, E		
node_3	rec_6	don_5, cost_6, I	don_3, cost_4, E	don_6, cost_2, E		
	rec_5	don_6, cost_5, I	don_2, cost_5, E	don_5, cost_5, E		
	rec_10	don_6, cost_4, D	don_3, cost_2, I	don_4, cost_2, E	don_1, cost_1, E	don_5, cost_1, E
	rec_4	don_6, cost_2, D				

Fig. 6 Case study, results of mapper task, Job_4. E—normal edge, I—included in the solution edge, D—deleted edge

Fig. 7 Case study, results of reducer task, Job_4

Reducer

node_1	don_1	rec_9, cost_8		
	don_3	rec_2, cost_10	rec_1, cost_5	rec_10, cost_2
	don_5	rec_8, cost_6	rec_6, cost_6	
node_2	don_2	? rec_8, cost_6 ?		
	don_4	rec_7, cost_8		
	don_6	rec_3, cost_7	rec_5, cost_5	

4 Experimental Results

4.1 Experimental Data

For testing the algorithm and the system, we used specific characteristics of donor-recipient as: blood type, tissue type compatibility, organ size, waiting time, age, if patient is receiving dialysis or not, distance to transplant center, emergency level. To generate the volume of data needed in testing the implementation of the algorithm, we implemented a script, which generated values randomly.

For example, people in Romania have only certain types of HLA antigens, we generated 100,000 patients having only those types, age between 18 and 60 years old, weight between 50 and 95 kg, the interval of time when the patients where registered in the system we supposed to be between Jan 01 2015 and May 01 2018. Also, we considered how to generate some values to obtain specific cases.

4.2 Configuration of Experiments

We evaluated the MapReduce jobs on a commodity computer with 1.36 GHz CPU four cores, 8 GB RAM, 1 TB, 5400 rpm SATA 3 HDD.

4.3 Experimental Results

For measuring the performance of the Matching Algorithm on MapReduce we used different thresholds for different combinations of age and weight (range 15, 30; 5 by 5) with 50 donors and 100,000 recipients.

A relational DB with Java implementation of the algorithm lasted 5 min and 17 s for 100,000 recipients and 50 donors. On the other hand, the duration of execution of the implementation on MapReduce of the first phase of the Matching Algorithm was 2 min and 10 s and the duration of the second phase was 5 s (unpartitioned data).

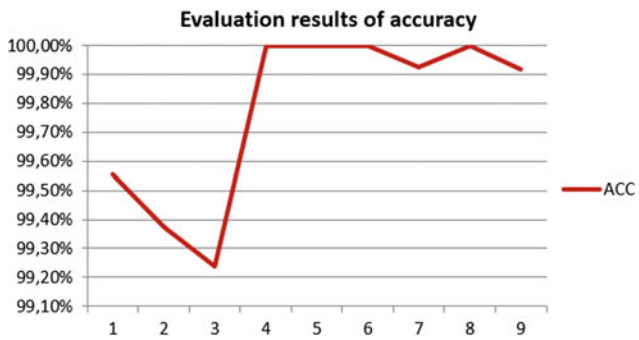

Fig. 8 ACC = (TP + TN)/(TP + FP + TN + FN)

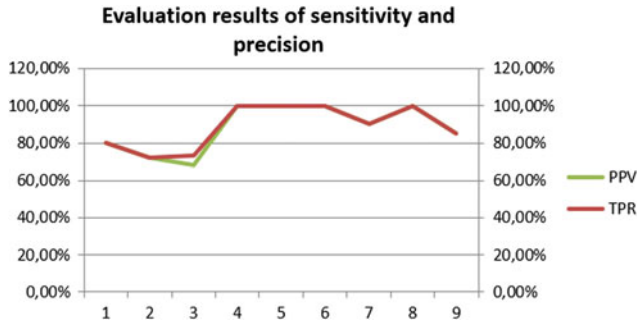

Fig. 9 Sensitivity TPR = TP/(TP + FN), average TPR ≈ 100% and precision PPV = TP/(TP + FP), average PPV ≈ 100%

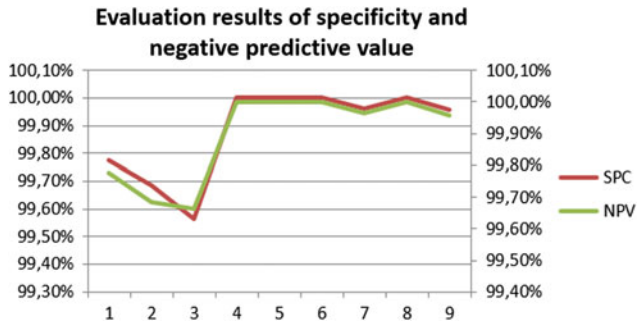

Fig. 10 Specificity SPC = TN/(TN + FP), average SPC ≈ 100% and Negative Predictive Value NPV = TN(TN + FN), average NPV ≈ 100%

We can see in Fig. 8 that best accuracy (100%) was obtained for age threshold 20 years and weight threshold 25 kg (point 4 on X axis) or age threshold 25 years and weight threshold 25 kg (points 5 and 6 on X axis) (Figs. 9 and 10).

5 Conclusions

For collecting large volumes of heterogeneous data, the chosen solution with agents and Hadoop we consider behaves well. For complex processing, on graphs, where more pipeline jobs are needed, we consider that will be bad for performance.

Current RDBMSs have parallelization, in-memory and columnar facilities. With MapReduce, optimization strategy at implementation level must be considered. For example, an RDBMS optimizer decides the execution plan, the order in which the basic operations for an SQL statement (table-scan or access with hash or B-tree indices) are executed.

With MapReduce, starting from an SQL statement, the equivalent relational algebra (RA) operator tree can be built and then the optimal implementation is found. First filtering is done versus the RA selection operator in order to reduce

the amount of data for the next steps; next, the RA join operator is applied where choice between join type (nested loop join, hash join, sort-merge join, respectively map-side join or reducer-side join) is made and finally the RA union operator is applied.

As further development, we aim to implement the agents and deploy the implementation of the Hadoop jobs on a cluster having a significant number of nodes. More tests will be made by varying the volume of data.

Conflict of Interest The authors declare that they have no conflict of interest.

References

1. Healthcare applications of Hadoop and Big data, at https://www.dezyre.com/article/5-healthcare-applications-of-hadoop-and-big-data/85 (2015)
2. Statistics Eurotransplant at http://statistics.eurotransplant.org
3. Luscalov, S., Loga, L., Luscalov, D., Lăcătuş, A., Dragomir, G., Dican, L.: Algorithm with heuristics for kidney allocation in transplant information system. In: International Conference on Advancements of Medicine and Health Care through Technology; 12th–15th Oct 2016, Cluj-Napoca, Romania, pp. 213–218
4. Cafarella, M., Lorica, B., Cutting, D.: https://www.oreilly.com/ideas/the-next-10-years-of-apache-hadoop. March 30, 2016
5. White, T.: Hadoop: The Definitive Guide, 4th edn. O'Reilly Media, USA (2015)
6. Dean, J., Ghemawat, S.: MapReduce: simplified data processing on large clusters. Commun. ACM **51**(1), 107–113 (2008)
7. Pavlo, A., Rasin, A., Madden, S., Stonebraker, M., DeWitt, D., Paulson, E., Shrinivas, L., Abadi, D.J.: A comparison of approaches to large scale data analysis. In: SIGMOD '09, pp. 165–178 (2009)
8. Palla, K.: A comparative analysis of join algorithms using the hadoop map/reduce framework. Master's thesis, School of Informatics, University of Edinburgh (2009)
9. Przyjaciel-Zablocki, M., Schätzle, A., Hornung, T., et al.: Cascading map-side joins over HBase for scalable join processing, CoRR, abs/1206.6293 (2012)
10. Afrati, F.N., Ullman, J.D.: Optimizing joins in a map-reduce environment. In: EDBT '10 Proceedings of the 13th International Conference on Extending Database Technology, pp. 99–110
11. Bloom, B.H.: Space/time trade-offs in hash coding with allowable errors. Commun. ACM **13**(7), 422–426 (1970). https://doi.org/10.1145/362686.362692
12. Lee, T., Im, D.-H., Kim, H., Kim, H.-J.: Application of filters to multiway joins in MapReduce. Math. Prob. Eng. **2014**, Article ID 249418, 11 pages (2014). https://doi.org/10.1155/2014/249418
13. Russell, S., Norvig, P.: Artificial Intelligence: A Modern Approach, 3rd edn. Prentice Hall, USA (2010)
14. Kifor, T., Varga, L.Z., Vázquez-Salceda, J., Álvarez, S., Willmott, S., Miles, S., Moreau, L.: Provenance in agent-mediated healthcare systems. IEEE Intell. Syst. **21**(6), 38–46 (2006)
15. Kimball, R., Caserta, J.: The Data Warehouse ETL Toolkit: Practical Techniques for Extracting, Cleaning, Conforming, and Delivering Data. Wiley, USA (2004)
16. Ozsu, M.T., Valduriez, P.: Principles of Distributed Database Systems, 3rd edn. Prentice Hall Press, Upper Saddle River, NJ, USA (2007)
17. Kimball, R., Ross, M.: The Data Warehouse Toolkit: The Definitive Guide to Dimensional Modeling, 3rd edn. Wiley Publishing, USA (2013)

PAC Bayesian Classifier with Finite Mixture Model for Oral Cancer Classification

S. K. Prabhakar and H. Rajaguru

Abstract

One of the most commonly reported malignancy with serious health hazards in the world is oral cancer. In developing countries, the estimated cases of oral cancer are much higher when compared to the developed countries. The easiest way to detect and classify the oral cancer is by means of visual inspection and it is followed by the biopsy procedure. The inspection of oral cancer in a visual manner is not always reliable and it is based mainly on the analysis of clinical features and sometimes during its initial stage it may go unnoticed by highly trained specialists too. Therefore, there is an absolute necessity to screen and classify the oral cancer that should be quite accurate, reliable and with less human manual intervention. Here, in this paper, classification of oral cancer is given prior importance and so Probably Approximate Correct (PAC) Bayesian Classifier is used a first level classifier and then it is further optimized with the Finite Mixture Model (FMM) which is used as a second level classifier. Results show that when PAC Bayesian is used, an average classification accuracy of 96.23% is obtained for all the stages and when it is further optimized with FMM, it gives a classification accuracy of 100%.

Keywords

Oral cancer • PAC Bayesian • FMM

1 Introduction

One of the primary threats to human life is oral cancer [1]. Oral cancer occurs when cells on the lips or in the mouth starts to develop mutations in the DNA. These mutations exhibit the cancer cells to immensely grow and divide while the healthy cells would die simultaneously. The accumulated oral cancer cells grown in an abnormal fashion forms a tumour. With time, they easily spread inside the entire mouth and to other regions of head, neck and body. Oral cancers mostly originate in the flat squamous cells that are present inside the mouth and so most oral cancers are squamous cell carcinomas [2]. There is a steady increase in the death rate related to the oral cancer. The occurrence of cancer may be in specific areas such as cheeks, lips, sinuses, tongue, palates, pharynx and floor of the mouth. The primary risk factors associated with oral cancer are smoking, use of tobacco, heavy exposure to certain chemicals, heavy exposure to sunlight, poor diet and hereditary change [3]. Oral cancer patient's survival ranges from a few months to a few years depending on the risk of the tumor. The diagnosis is usually done with the help of biopsy if the patient reports to the clinician with the following symptoms; occurrence of red spots in the mouth, loose teeth, a sore on the lip and mouth with blood, pain or difficulty swallowing, stinging pain in cheeks and ears, sore throat, chronic neck pain, corrosion in the gums, lips and coarse spots on inner parts of the mouth [4]. Weight loss and bleeding in nose and mouth are also noticed in most of the cases. Surgery is an option to eradicate the growth of cancer and then chemotherapy can be used to eliminate or kill the remaining cancerous cells. The clinician uses X-rays to check whether the cancer cells have spread to the lungs, chest and jaw, uses a PET scan to test if the cancer has travelled to the lymph nodes, uses a CT scan to determine the presence of tumours in mouth, neck, throat and lungs, uses a MRI scan to show a much clear image of the neck and head to determine the extent of the cancer and uses an endoscopy procedure to deeply investigate the nasal passages, inner throat, windpipe, sinuses and trachea [5]. There are four stages in oral cancer. In stage 1, the tumour is about 2 cm or even much smaller than that and the cancer has not been spread to the lymph nodes. In stage 2, the tumor size ranges from 2 to 4 cm and still the cancer cells have not spread to the lymph nodes. In stage 3, the tumour size is larger than 4 cm and has spread to one lymph node but not to other regions of the body. In stage 4, the

S. K. Prabhakar (✉) · H. Rajaguru
Department of ECE, Bannari Amman Institute of Technology, Alathukombai, Sathyamangalam, India
e-mail: sunilprabhakar22@gmail.com

S. Vlad and N. M. Roman (eds.), *6th International Conference on Advancements of Medicine and Health Care through Technology; 17–20 October 2018, Cluj-Napoca, Romania*, IFMBE Proceedings 71,
https://doi.org/10.1007/978-981-13-6207-1_30

tumours may be of any size and the dangerous cancer cells might have spread to other neighboring tissues, lymph nodes and to the other parts of the body.

In this work classification of oral cancer has been given prior importance and some of the significant and most relevant works discussed in literature are explained as follows. Principal Component Analysis (PCA) and K means nearest neighbor analysis was used for classifying the oral tissue fluorescence spectra by Kamath and Mahato [6]. A Hybrid ABC-PSO along with Bayesian Linear Discriminant Analysis (BLDA) classifiers were used for oral cancer classification by Rajaguru and Prabhakar [7]. The computer aided analysis and detection of oral lesions on Computed Tomography images was performed by Galib et al. [8]. Multilayer Perceptrons (MLP) and Gaussian Mixture Models (GMM) were used for oral cancer classification by Rajaguru and Prabhakar [9]. A hybrid fuzzy C-means and neutrosophic logic for jaw lesions segmentation was proposed by Alsmadi [10]. The predictive data mining techniques for oral cancer classification was utilized by Sharma and Om [11]. With the help of fuzzy linear regression, the deduction of oral cancer was done by Arulchinnappan et al. [12]. Softmax Discriminant Classifier (SDC) was also used for oral cancer classification by Rajaguru and Prabhakar [13]. Artificial Intelligence techniques were utilized to identify the people at risk for oral cancer by Rosmai et al. [14]. Hybriding the feature selection along with machine learning methods, the prognosis of oral cancer was done based on the genomic and clinic pathology makers by Chang et al. [15]. In this work, the oral cancer classification is done with the help of two level classification process. The block diagram of the work is shown in Fig. 1.

Initially all the clinical values are obtained from the hospital from analyzing various reports of the oral cancer patients. The reports are thoroughly analyzed and the numerical values or parameters for the different indices are tabulated for mathematical convenience. Then it is classified with the help of PAC Bayesian Classifier. To improve the classification accuracy further, the output of PAC Bayesian Classifier is fed to the FMM Classifier and the performance metrics are analyzed.

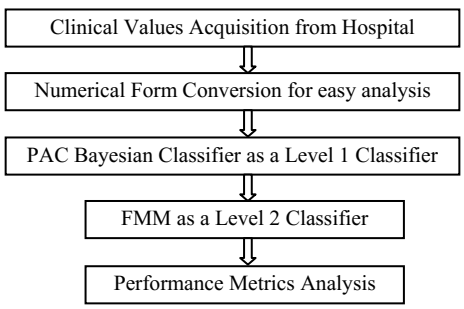

Fig. 1 Block diagram of the work

Table 1 Risk level of the cancer patients

Stages	Risk level	Number of patients
T1	Severity level is low	16
T2	Severity level is moderate	22
T3	Severity level is high	26
T4	Severity level is very high	11

2 Materials and Methods

For this study, a total number of 75 patients who are suffering from oral cancer are considered. With the help of oncologists from Department of Oncology of G Kuppuswamy Naidu Hospital (GKNM), Coimbatore, India, the dataset was obtained. The consolidated report was analyzed from operative reports, radiation and chemotherapy reports, pathological reports, hospital charts, radiological reports, referral charts and so on. The main indices considered for oral cancer are the size of the tumor and its particular location, usage of tobacco and smoking habits, gender, age, food habits, history of other diseases, immunity levels, exercise levels, life style etc. According to the International Union Against Cancer (UICC), the oral cancer tumor was differentiated into 4 stages as shown in Table 1. The 75 patients were categorized according to the various risk stages of the oral cancer.

3 Classification Using Two Level Classifiers

In this work, a two level classification procedure is utilized. Initially, the oral cancer classification is done with the help of PAC Bayesian Classifier and to achieve much higher classification accuracy, it is further classified with the help of FMM Classifier.

3.1 PAC Bayesian Classifier

It is considered as the first level classifier in this work. This classifier focuses on the establishment of a data-dependent upper bound on a true risk factor [16]. It also establishes the risk of misclassification of unseen data which has a primary association with a probabilistic classifier. This approach is quite Bayesian in nature as these distributions can be learnt easily from a finite data sample. If the divergence is greater then it indicates that there is a huge risk for the classifier. The divergence and training error are the main things associated with the PAC Bayesian Classifier.

The primary goal of this classifier is to upper bound the main risk related with a probabilistic classifier q [16]. The

closely associated Gibb's classifier selects a particular model randomly from this distribution in order to assess the input feature vectors. Assume a binary classification problem with a particular input space $Z \subset \Re^n$ and the output space $W = \{1, -1\}$. It is assumed that the input data $(z, w) \in Z \times W$ are drawn mainly according to a specific distribution F. Now the true risk is defined as

$$R(q) = E_{(z,w)\sim F}[I(q(z) \neq w)] \tag{1}$$

where the indicator function is denoted by I. The empirical risk of 'q' which is related to the training set V is defined as

$$R_v(q) = \frac{1}{\|V\|} \sum_{z,w \in V} I(h(z) \neq w) \tag{2}$$

Assuming $\Psi : [0,1] \times [0,1] \to \Re$ be a convex function and let J_P be the Gibbs classifier with a prior 'A' and a posterior distribution P defined on a space Q of the classifiers. Now the true and empirical risks of a Gibbs J_P classifier is defined as

$$R(J_P) = \underset{q\sim P}{E}[R(q)]; \quad R_v(J_p) = \underset{q\sim P}{E}[R_v(q)] \tag{3}$$

Thus the PAC Bayesian boundary limits for Gibbs classifier holds good for the majority vote classifiers.

3.2 FMM Classifier

It is considered as the second level classifier for further optimization and accurate classification. Initially consider the following two sets; $K = \{1, 2, \ldots, P\}$ and $M = \{1, 2, \ldots, F\}$. The finite index set is denoted as Q and is observed as $Q = \{1, 2, \ldots, Z\}$. The finite index set Q refers to the location or sites. Assuming 'A' and 'B' to be the two random fields, their respective spaces are indexed by respective set of sites expressed as $A_i = \{a_i : a_i \in K\}$ and $B_i = \{b_i : b_i \in M\}$. Their product space $A = \prod_{i=1}^{Z} a_i$ and $B = \prod_{i=1}^{Z} b_i$ is expressed as the configuration space of the state values of the site locations $a = (a_i)$ and $b = (b_i)$ [17]. For signal segmentation application, a signal comprising of Z parts is segmented into P classes, b_i expresses the observation value and a_i expresses the corresponding class label of the ith part. For every $f \in K$ and $i \in Q$, the probability is expressed as

$$p(a_i = f) = \pi_f \tag{4}$$

is the prior distribution of the part b_i which belongs to the class $a_i.b_i$ and which follows a conditional probability $p(b_i|\theta_f)$ is expressed as a Gaussian distribution [17]. If the independent assumption is taken into context, then FMM is computed as

$$p(b_i|\pi, \theta) = \sum_{f=1}^{P} \pi_f p(b_i|\theta_f) \tag{5}$$

Thus FMM is used widely for its effectiveness and simplicity and so it's used here a second level classification technique.

4 Results and Discussion

For the analysis of the two level classification process, the parameters taken for the consideration are Rate of False Alarm, Rate of Perfect Classification, Rate of Missed Classification Measures, sensitivity and specificity measures and accuracy measures are given by the following mathematical formulae as

$$PI = \left(\frac{PC - MC - FA}{PC}\right) \times 100 \tag{6}$$

PC = Perfect Classification, MC = Missed Classification and FA = False Alarm. The Sensitivity, Specificity and Accuracy measures are mathematically given by the following formulae

$$Sensitivity = \frac{PC}{PC + FA} \times 100 \tag{7}$$

$$Specificity = \frac{PC}{PC + MC} \times 100 \tag{8}$$

$$Accuracy = \frac{Sensitivity + Specificity}{2} \tag{9}$$

Table 2 explains the results obtained when PAC Bayesian Classifier is utilized for oral cancer classification for all the stages. Table 3 explains the results obtained when FMM Classifier is utilized for oral cancer classification for all the stages. Table 4 explains the consolidated accuracy measures comparison for both the PAC Bayesian classifier and FMM classifier.

The results from Table 2 report an average performance index of 91.07% for all the four stages of oral cancer classification if employed with PAC Bayesian classifier. On the second level classification with FMM, an average classification accuracy of 100% is obtained as seen from Table 3. However, we had even checked for the cases of overfitting and no such cases were reported in our work. After level 1, the results showed an average classification accuracy of 96.23%. Only after the second level classification, after a careful fine tuning, we had obtained 100% employing FMM Classifier.

Table 2 Performance analysis of PAC Bayesian Classifier for the different stages of oral cancer

	T-1	T-2	T-3	T-4	Average
PC (%)	100	100	73.68	100	93.42
MC (%)	0	0	15.78	0	3.94
FA (%)	0	0	10.52	0	2.63
PI (%)	100	100	64.30	100	91.07
Sensitivity (%)	100	100	87.50	100	96.87
Specificity (%)	100	100	82.36	100	95.59
Accuracy (%)	100	100	84.93	100	96.23

Table 3 Performance analysis FMM Classifier for the different stages of oral cancer

	T-1	T-2	T-3	T-4	Average
PC (%)	100	100	100	100	100
MC (%)	0	0	0	0	0
FA (%)	0	0	0	0	0
PI (%)	100	100	100	100	100
Sensitivity (%)	100	100	100	100	100
Specificity (%)	100	100	100	100	100
Accuracy (%)	100	100	100	100	100

Table 4 Consolidated accuracy measures comparison

S. No.	Oral cancer stages	Classification by clinical means (%)	Classification by PAC Bayesian (%)	Classification by FMM (%)
1	T1	98	100	100
2	T2	100	100	100
3	T3	97	84.93	100
4	T4	100	100	100

5 Conclusion

Thus oral cancer also named as mouth cancer is where a tumour starts to develop in the inner lining of the mouth. It may occur on the inside of cheeks, lips, gum, roof of the palate or on the surface of the tongue. Tumors can easily develop in the glands which secrete saliva, at the windpipe and even in the tonsils at the back of the mouth. Thus oral cancer and its treatment can cause a variety of problems and complications. It can easily make swallowing and speaking difficult and also it affects the appearance of the mouth. In this paper, oral cancer classification has been dealt with two level classification procedures. Initially after first level classification with the help of PAC Bayesian classifier, the T1, T2 and T4 stages gave a classification accuracy of 100% while T3 stage gave a classification accuracy of 84.93%. When further classified with Finite Mixture Model, it gave a classification accuracy of about 100% classification accuracy for all the four stages. Future works aim to classify with various other classifiers for oral cancer classification.

Conflict of Interest The authors declare that they have no conflict of interest.

References

1. Hanahan, D., Weinberg, R.A.: Hallmarks of cancer: the next generation. Cell **144**, 646–674 (2011)
2. Exarchos, K.P., Goletsis, Y., Fotiadis, D.I.: Multiparametric decision support system for the prediction of oral cancer reoccurrence. IEEE Trans. Inf. Technol. Biomed. **16**, 1127–1134 (2012)
3. Chuang, L.-Y., Wu, K.-C., Chang, H.-W., Yang, C.-H.: Support vector machine-based prediction for oral cancer using four snps in DNA repair genes, pp. 16–18 (2011)
4. Exarchos, K.P., Goletsis, Y., Fotiadis, D.I.: A multiscale and multiparametric approach for modeling the progression of oral cancer. BMC Med. Inform. Decis. Mak. **12**, 136 (2012)
5. Rosado, P., Lequerica-Fernández, P., Villallaín, L., Peña, I., Sanchez-Lasheras, F., de Vicente, J.C.: Survival model in oral

squamous cell carcinoma based on clinicopathological parameters, molecular markers and support vector machines. Expert Syst. Appl. **40**(4770), 4776 (2013)
6. Kamath, S.D., Mahato, K.K.: Optical pathology using oral tissue fluorescence spectra: classification by principal component analysis and k-means nearest neighbor analysis. J. Biomed. Opt. **12**(1), 014028 (2007)
7. Rajaguru, H., Prabhakar, S.K.: Oral cancer classification from hybrid ABC-PSO and Bayesian LDA. In: 2nd IEEE ICCES, IEEE Xplore, Coimbatore, India, 19–20 Oct (2017)
8. Galib, S., Islam, F., Abir, M., Lee, H.-K.: Computer aided detection of oral lesions on CT images. J. Instrum. **10**(12) (2015)
9. Rajaguru, H., Prabhakar, S.K.: Performance comparison of oral cancer classification with Gaussian mixture measures and multi layer Perceptron. In: 16th International Conference on Biomedical Engineering (ICBME), pp. 123–129 (2016)
10. Alsmadi, M.K.: A hybrid Fuzzy C-Means and Neutrosophic for jaw lesions segmentation (2016)
11. Sharma, N., Om, H.: Predictive data mining for oral cancer (Chap. 15). In: Case Studies in Intelligent Computing—Achievements and Trends, pp. 303–328. CRC Press, Taylor and Francis Group (2014)
12. Arulchinnappan, S., Karunakaran, K., Rajendran, G.: Deduction of oral cancer using fuzzy linear regression. J. Comput. Sci. **7**(8), 1141–1145 (2011)
13. Rajaguru, H., Prabhakar, S.K.: An approach to classification of oral cancer using Softmax discriminant classifier. In: 2nd ICCES, IEEE Xplore, Coimbatore, India (2017)
14. Rosmai, M.D., Sameemii, A.K., Basir, A., Mazlipahiv, I.S., Norzaidi, M.D.: The use of artificial intelligence to identify people at risk of oral cancer: empirical evidence in Malaysian University. Int. J. Sci. Res. Educ. **3**(1), 10–20 (2010)
15. Chang, S.W., Abdul-Kareem, S., Merican, A.F., Zainv, R.B.: Oral cancer prognosis based on clinicopathologic and genomic markers using a hybrid of feature selection and machine learning methods. BMC Bioinform. **14**(1) (2013)
16. Shawe-Taylor, J., Williamson, R.C.: A PAC analysis of a Bayesian estimator. Technical report, Royal Holloway, University of London, NC2-TR-1997-013 (1997)
17. McLachlan, G., Peel, D.: Finite Mixture Models. Wiley, New York (2000)

Health Information Exchange for Management of Disaster Victims Using FANET

Adrian Crețu, Camelia Avram, Dan Radu, Benoît Parrein, Adina Aștilean, and Claudiu Domuța

Abstract

The main objective of this paper is to introduce a public system architecture and application for emergency situations that could improve the medical services by efficiently distributing resources between a FANET (Flying Ad Hoc Network) and MANET (Mobile Ad Hoc Network) hybrid network and nearby hospitals. The proposed solution has a Fog edge node that collects medical care data from the mobile network and forwards it to the medical centers. Data transmission efficiency in a high mobility scenario is ensured by the multiple paths provided by MP-OLSR routing protocol. Furthermore, MP-OLSR is evaluated in comparison to OLSR.

Keywords

MANET • FANET • Fog computing • Public safety

1 Introduction

The unforeseen circumstances requiring extensive actions of emergency medical services systems can be grouped in several main categories. Natural disasters (earthquakes, fires, floods, hurricanes), human errors (nuclear, chemical, biological, radiological exposures or railway and chain reaction car accidents) and criminal actions (terrorist attacks) are the most common incidents resulting in the significant increasing of volume of medical cases during a short time interval [1].

Over recent years, influenced by climate changes, natural disasters are more and more frequently and their effects have grave consequences on large areas. Besides their direct consequences on the physical integrity and health status of residents, their effect is amplified by an extensive damage to physical infrastructure, limiting the access and even isolating the respective zones.

Successful actions are in close connections with the possibility to activate, in the shortest possible time, the emergency care system and to continue with a corresponding triage and treatment of victims. A professional and prompt intervention [2] is needed not only at the site but also during the transportation of patients with appropriate vehicles and finally at the hospitals delivering specialized care.

The nature and level of incidence, the level of exposure and vulnerability of individuals are the main factors determining the characteristic on-site operations—the first goal is the stabilization of patients having life threatening injuries and illness—and the amount of resources needed to respond to this unexpected events. Specialized field training of medical personnel is needed for status assessment of injured persons and the initiating of a basic medical treatment.

Another important step of rescue operations following the on-site assessment is the transfer of patients to the appropriate care units taking into account their particular medical condition. The distance, the offered medical services and procedures and their existing availability are the main factors which can be considered to avoid a poor distribution of the patients. It must be mentioned that generally, even on more extended areas, there are few medical centers offering comprehensive services and having the medical personnel and capacities needed for the treatment of serious injuries and different categories of illnesses, the majority having only limited emergency facilities. On the other side, even if patients are directed to an adequate emergency department there are many others management problems that remain to be solved, such as a considerable higher number of patients and the need of supplementary special treatment areas [3].

The implementation of complex rescue operations, beginning with the search and on-site triage phases and ending with appropriate hospital treatments, cannot succeed without pre-established actions and coordination plans which become operational during the corresponding events.

A. Crețu (✉) · C. Avram · D. Radu · A. Aștilean · C. Domuța
Technical University of Cluj-Napoca, Cluj-Napoca, Romania
e-mail: adriancr.ro@gmail.com

B. Parrein
LS2N, Polytech' Nantes, Nantes, France

S. Vlad and N. M. Roman (eds.), *6th International Conference on Advancements of Medicine and Health Care through Technology; 17–20 October 2018, Cluj-Napoca, Romania*, IFMBE Proceedings 71,
https://doi.org/10.1007/978-981-13-6207-1_31

All of them need performing information and communication systems. Collaborations between interventional structures (health care personnel, fire departments, police, volunteers) across the disaster area and continuous information exchange with urgent care centers are of vital importance in such circumstances.

Unfortunately, most of catastrophic events have as immediate result the destruction of important components and parts of the telecommunication infrastructure. Moreover, even valid, the communication lines become overloaded. In these situations, any attempt to transmit vital information and to create communication networks needed for actualized decision making becomes much more difficult or impossible.

During the last decades, the development of many technologies and devices offered viable alternative based on wireless communication solutions to connect areas where the existing networks were destroyed or are not available yet. Communication systems implying the implementation of ad hoc networks demonstrated some of their capabilities for applications in military field, sensor networks, cooperative work, rescue operations, vehicular communications and others [4, 5].

Having incontestable and proven advantages, autonomous unmanned aerial vehicles (UAVs) Ad Hoc Networks can offer support for rescue operations, surveying inaccessible areas and transmitting cost effective video information.

Multi-UAV cooperation can lead to an improved operation performance of the as-hoc network and to an extension of monitored areas [6].

Fog computing is a scalable infrastructure that allows the collected data from multiple sources to be efficient and to be processed at the edge of the network before it gets forwarded to cloud services. It aims to efficiently distribute the resources (computation power, network bandwidth) between different types of devices (Internet of Things) and the cloud.

2 State of the ART

Small and lightweight UAVs are being used in disaster response to capture high-resolution imagery and for micro-transportation too. To cover large areas several UAVs can be launched. The usage of networked aerial vehicles for rescue operations and information transmission across the disaster areas raises specific issues which were intensively studied.

Appropriate navigation and data fusion algorithms were developed to provide autonomy. Important advantages and disadvantages of UAVs usage in disaster-affected zones are discussed in [7]. The authors highlight the necessity to solve some aspects regarding a corresponding autonomy or the needed safety and security levels of these types of vehicles.

In [8, 9], the author presents multiple possibilities of drones' utilizations in applications related to disasters prevention and monitoring and for the damage assessment. Many aspects are analyzed in an attempt to demonstrate the advantages of UAVs' usage and to respond to questions related to their effectiveness during this kind of operations. Their capabilities to elaborate high-resolution maps of the affected zones is only a representative example in that sense.

Various UAVs movements have been simulated and analysed in order to evaluate the performance of the system under several network conditions. A comparative study has been conducted between FANET based optimized link state routing (OLSR) and predictive optimized link state routing (P-OLSR) using an experimental test platform and it proves that P-OLSR out performs on OLSR significantly [10–12].

Erdelj et al. [13] identify and classify the results of research on leveraging the latest advances in unmanned aerial vehicles (UAVs) for network-assisted first response to disaster management, and points out the open issues that need to be solved.

In a comprehensive study dedicated to drone networks [14], their implementations and possible applications, the authors analyze existent solutions and implement methods aiming to improve the performances of the communication channels.

Even if a significant progress was registered in this field, a lot of research and experiments are still needed to find reliable solutions.

3 System Design

The main objective of this work is to design and develop a smart system architecture, based on FANET and MANET networks and Fog Computing infrastructure that can improve the quality of public safety in different emergency scenarios (e.g.: fire, flooding, earthquakes).

The overview of the proposed FANET Public Safety Application network topology is presented in Fig. 1 and it is composed of three main components:

- MANET composed of WiFi capable devices;
- FANET of WiFi capable drones responsible for data forwarding from the affected area to the edge node;
- Fog infrastructure that manages data forwarding to the nearby hospitals and medical facilities.

FANET and MANET nodes are responsible, in the proposed system, for sensitive medical care information forwarding to the Fog Central Administration Module located at the edge of the network. This module ensures an Internet connection to the medical facilities that can support the

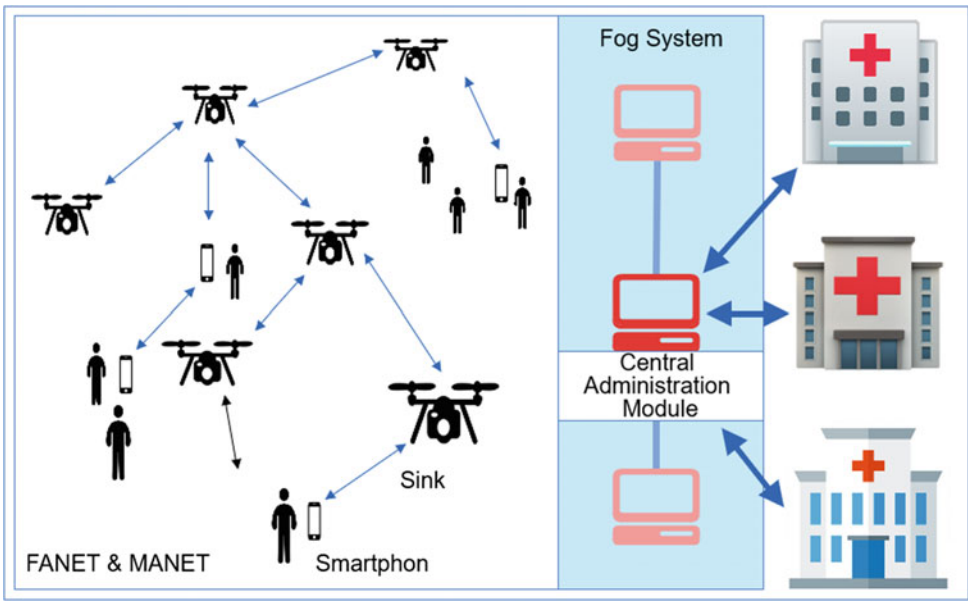

Fig. 1 System overview

urgent treatment of disaster affected victims. Some of the main advantages of the proposed system are:

- Improved Quality of Service (QoS) for data transmission using MP-OLSR routing protocol to manage data forwarding inside the MANET and FANET network;
- Inexpensive and widely available technologies and components;
- Ease of deployment in a different range of emergency scenarios;
- Efficient medical resource planning for emergency scenarios.

The presented architecture, specific for high mobility scenarios, has the following characteristics:

- Extensibility;
- Reliability;
- Resilience.

4 Performance Evaluation

4.1 Simulation Scenario

For the simulations we configured a 64 nodes FANET and MANET hybrid network placed in a 1480 m^2 grid topology. Qualnet 5 was used as a discrete event network simulator. For the high mobility of drones we used the Random Waypoint Model mobility pattern with different maximal speeds 1–15 m/s (3.6–53.6 km/h) suitable to this types of devices. We make the assumption that only a subset of nodes need to communicate with the Fog edge node through the mesh network so the data traffic is provided by 6 Constant Bit Rate (CBR) sources. The parameters used for the Qualnet network scenario and routing protocols configuration parameters are listed in Table 1. The simulations are performed to evaluate MP-OLSR in the proposed FANET and MANET scenario. The Quality of Service performance parameters are compared between OLSR and MP-OLSR. For each routing protocol a number of 1000 simulations were executed. To compare the performances of the protocols, the following metrics are used:

- **Packet delivery ratio (PDR)**: the ratio of the data packets successfully delivered to all destinations.
- **Average end-to-end delay**: averaged over all received data packets from sources to destinations. Qualnet uses the following formula to compute CBR average end-to-end delay:

$$Delay(s) = \frac{End\ to\ end\ delay}{Number\ of\ packets\ received} \quad (1)$$

- **Jitter**: average jitter is computed as the variation in the time between packets received at the destination caused by network congestions and topology changes. Qualnet CBR server average jitter formula is:

$$Jitter(s) = Abs(Jitter(1)) + \cdots + \frac{Abs(Jitter(n-2))}{n-2} \quad (2)$$

- **Throughput**: describes how many units of information a system can process in a given amount of time

Table 1 Parameters for the Qualnet network scenario

Simulation parameter	Value
Simulator	Qualnet 5
Routing protocols	OLSRv2 and MP-OLSR
Simulation area	1480 × 1480 × 34.85 m^2
Number of nodes	64
Initial nodes placement	Random
Mobility	Random Waypoint
Speeds	0–53, 6 km/h
Number of seeds	20
Transport protocol	UDP
IP	IPv4
IP fragmentation unit	2048 bytes
Physical layer model	PHY 802.11b
Link layer data rate	11 Mbit/s
Number of CBR sources	6
Simulation duration	100 s
CBR start-end	15–95 s
Transmission interval	0.05 s
Application packet size	512 bytes
Mobility	Random Waypoint

$$Throughput\left(\frac{bits}{s}\right) = \frac{Bits\ receiced}{Bits\ sent} \quad (3)$$

The packets data for the simulation was provided by a constant bitrate (CBR) source that operates at 491 Kbits/s.

4.2 Results

Figures 2, 3, 4 and 5 show the QoS performance of MP-OLSR and OLSR in terms of PDR, throughput, end-to-end delay and jitter results. The multiple paths provided by MP-OLSR are mainly used for load balancing and they bring an overall better Quality of Service in comparison to OLSR. From the obtained results it can be seen that PDR decreases slightly with the mobility as expected. For the proposed system scenario MP-OLSR delivers an average of 15% higher PDR than OLSR protocol. Overall, MP-OLSR performs better than OLSR in terms of Delay and Jitter. This aspect is important for the proposed public safety application in the medical domain where the data transmission quality must be reliable in order to allow the forwarding

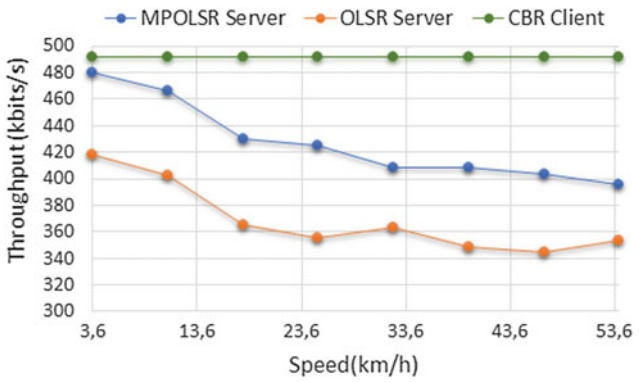

Fig. 2 Throughput

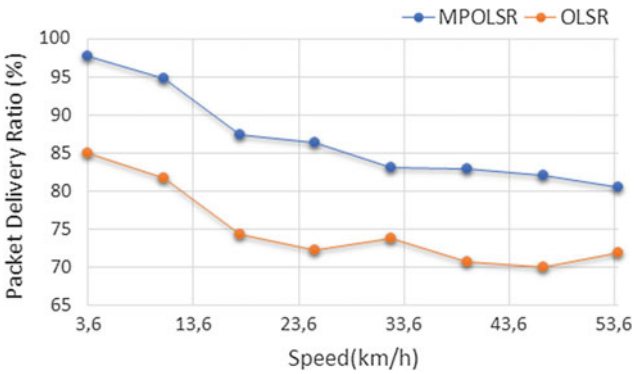

Fig. 3 Packet delivery ratio

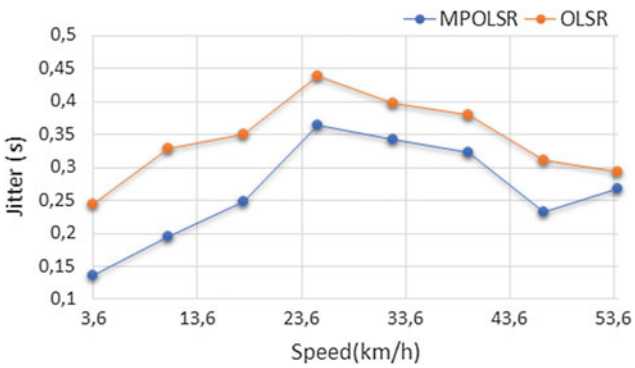

Fig. 4 Jitter

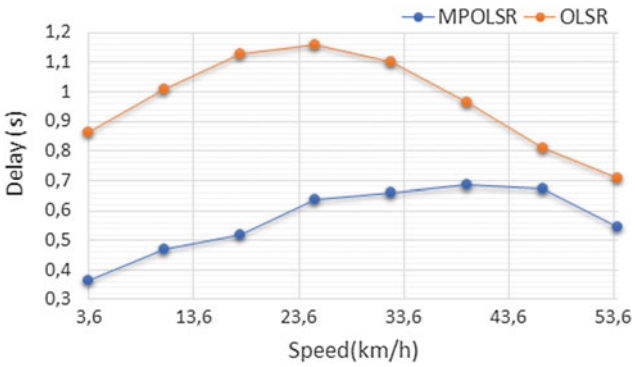

Fig. 5 Delay

of urgent/important health information to the nearby medical centers through the fog computing edge coordinator.

5 Conclusions

We described a system architecture that could be used as a possible emergency application for MP-OLSR routing protocol which employs a hybrid FANET and MANET network to forward data packets from drones, through a central management system, to the nearby aiding centers in case of emergency. The presented system could be used as an alternative for fixed network infrastructure that could connect users and emergency teams to a central administration module that processes medical information and forwards it to the local hospitals and helping centers.

The performance evaluation results show that MP-OLSR is suitable for the proposed scenario. The data transmission performance, especially Speed and Delivery Ratio, is essential for public safety services.

Our future work include the development of a real testbed for the system in question that contains real drones connected to a fog module that employs the mentioned public safety services.

Conflict of Interest The authors declare that they have no conflict of interest.

References

1. Ejeta, L.T., Ardalan, A., Paton, T.: Application of Behavioral Theories to Disaster and Emergency Health Preparedness: A Systematic Review. Public Library of Science (2015)
2. Tang, J., Zhu, K., Guo, H., Liao, C., Zhang, S.: Simulation optimization of search and rescue in disaster relief based on distributed auction mechanism. Algorithms **10**(12), 1–17 (2017)
3. Hick, J.L., Hanfling, D., Cantrill, S.V.: Allocating scarce resources in disasters: emergency department principles. Disaster Medicine/Concepts **59**(3) (2012)
4. Hiwale, M.S., Kinariwala, S.A., Ghode, S.D.: Literature survey on mobile adhoc networks and routing protocols. Int. J. Innov. Res. Comput. Commun. Eng. **5**, 10 (2017)
5. Al-Omari, S.A.K., Sumari, P.: An overview of mobile ad hoc networks for the existing protocols and applications. Int. J. Appl. Graph Theory Wirel. Ad Hoc Netw. Sens. Netw. **2**(1), 87–110 (2010)
6. Bupe, P., Haddad, R., Rios-Gutierrez, F.: Relief and emergency communication network based on an autonomous decentralized UAV clustering network. In: SoutheastCon, pp. 1–8 (2015)
7. Tanzi, T.J., Chandra, M., Isnard, J., Camara, D., Sebastien, O., Harivelo, F.: Towards "drone-borne" disaster management: future application scenarios. ISPRS Annals of the Photogrammetry, Remote Sensing and Spatial Information Sciences III-8 (2016)
8. Restas, A.: Drone applications for supporting disaster management. World J. Eng. Technol. (2015). http://dx.doi.org/10.4236/wjet.2015.33C047
9. Restas, A.: Water related disaster management supported by drone applications. World J. Eng. Technol. **6**, 116–126 (2018). http://www.scirp.org/journal/wjet
10. Rosati, S., Kruzelecki, K., Heitz, G., Floreano, D., Rimoldi, B.: Dynamic routing for flying ad hoc networks. IEEE Trans. Veh. Technol.
11. Bekmezci, I., Ermis, M., Kaplan, S.: Connected multi UAV task planning for flying ad hoc networks. In: Proceedings of the 2014 IEEE International Black Sea Conference on Communications and Networking (BlackSeaCom), pp. 28–32 (2014)
12. Mukherjee, A., Dey, N., Kausar, K., et al.: A disaster management specific mobility model for flying ad-hoc network. Int. J. Rough Sets Data Anal. **3**(3) (2016). https://doi.org/10.4018/ijrsda.2016070106
13. Erdelj, M., Natalizio, E., Chowdhury, K.R., Akyildiz, I.F.: Help from the sky: leveraging UAVs for disaster management. IEEE Pervasive Comput. **16**, 24–32 (2017). http://doi.ieeecomputersociety.org/10.1109/MPRV.2017.11
14. Yanmaza, E., Yahyanejad, S., Rinnerc, B., Hellwagnerd, H., Bettstettera, C.: Drone networks: communications, coordination, and sensing. Ad Hoc Netw. (2017)

Random Forest and Sequential Model for Anomalies Detection in the Activities of the People with Dementia

D. Moldovan, A. Visovan, M. Bologa, C. Pop, V. R. Chifu, I. Anghel, T. Cioara, and I. Salomie

Abstract

Dementia is a very complex disease that affects the ability to think and remember. The thinking ability affects the daily living activities (DLAs) pattern of the people with dementia (PwD) and thus the caregivers and the healthcare professionals that are responsible for assisting PwD can take preventive actions when anomalies in DLAs are identified to improve the health condition of PwD. The main contributions of the article are: (1) the development of an approach for the anomalies detection (AD) in the DLAs of the PwD, (2) the description of the preprocessing of the DLAs data, (3) the presentation of an approach for the detection of the baseline of PwD using Random Forest (RF), (4) the presentation of an approach based on a Sequential Model (SM) for the detection of the baseline of PwD and (5) the AD in DLAs of PwD using the predicted baseline and the data monitored in a day.

Keywords

Big data • Deep learning • Daily living activities • Dementia • Anomalies detection

1 Introduction

Dementia is a disease that consists of a very broad category of brain related diseases that affect the ability to think and consequently the daily functioning of the people that suffer from this condition. In [1] are presented a selection of statistics that highlight the high costs that are necessary for treating the PwD: in 2017 over 16 million unpaid caregivers and family members provided approximately 18.4 billion hours for the caring of the PwD, the payments for healthcare in 2018 for PwD is estimated to be $277 and the early accurate diagnosis for the PwD can save more than $7.9 trillion.

The approach that we propose for reducing the costs associated with dementia is based on the AD in the DLAs of the PwD using big data (BD) and deep learning (DL) that otherwise would require the continuous monitoring and assistance of the healthcare professionals and caregivers. In our approach we consider that anomalies occur in the cases in which the PwD must perform different DLAs with respect to the DLAs predicted by the BD and DL techniques. The input is represented by a set of time series data that describe the DLAs performed by a PwD during a monitoring period and the output is represented by the description of the anomalies for a specific day.

The article is organized as follows: Sect. 2 presents related work, Sect. 3 presents the problem definition, Sect. 4 presents the research methodology, Sect. 5 presents the prediction of the baseline for a day using big data and deep learning approaches, Sect. 6 presents the experimental results and Sect. 7 presents the conclusions.

2 Related Work

The first part presents approaches used in literature for AD in the DLAs of the PwD and the second part presents BD and DL approaches for AD.

The authors of [2] describe the results obtained using a system that is based on motion, bed and latch sensors that detects the wandering behavior of the PwD. In [3] is proposed a shoe-based tracking and rescue system for PwD that can perform a set of functionalities such as: real time location tracking and detection of abnormal behavior. The authors of [4] describe a system for early detection of dementia that is based on home behaviors in which they consider the following behaviors predictive for dementia: the number of times the monitored person goes to toilet, the wandering in the middle of the night and the forgetting to

D. Moldovan (✉) · A. Visovan · M. Bologa · C. Pop · V. R. Chifu · I. Anghel · T. Cioara · I. Salomie
Department of Computer Science, Technical University of Cluj-Napoca, 26 Baritiu, Cluj-Napoca, Romania
e-mail: dorin.moldovan@cs.utcluj.ro

S. Vlad and N. M. Roman (eds.), *6th International Conference on Advancements of Medicine and Health Care through Technology; 17–20 October 2018, Cluj-Napoca, Romania*, IFMBE Proceedings 71,
https://doi.org/10.1007/978-981-13-6207-1_32

turn off the electronic devices. In [5] is presented an Android application for PwD. The application can detect the position of the PwD using GPS Navigation and can also detect falls of the PwD using the Rotation Matrix sensor.

In [6] a method based on Hidden Markov Model is used for detecting anomaly behavior of PwD. The model detects two types of symptoms: memory loss and wandering using a set of monitoring sensors. The behaviors that are detected are the wandering in the middle of the night, the going to the resting room too often, the forgetting to take a bath or taking baths too many times and the forgetting to turn off the TV. The authors of [7] propose a method for detecting dementia using AD on stroke data. The method divides the input data into units, extracts the features, samples to prevent bias and uses Variational Autoencoder (VAE) for AD. The VAE is a type of generative model which is based on the variational Bayesian and is built using neural networks.

3 Problem Definition

The research problem that we want to approach in this article is presented next. For a PwD for whom data that is generated by the monitoring sensors is known we want to determine the distribution of anomalies in that day so that the associate healthcare professional or caregiver can take the appropriate actions. In our approach we suppose that a PwD is monitored using three types of sensors. Figure 1 presents an example of house in which sensors that monitor DLAs of a PwD are installed.

The three types of sensors used in our approach are:

- ***Presence sensors***—are used for identifying if a PwD is in a room or not and the data generated by them is used for computing the total duration of time the monitored person spends in each room of the house;
- ***Motion sensors***—are installed on doors and other devices that require the movement of the PwD and for each motion sensor we consider the number of times it was triggered;
- ***Medication sensors***—are installed on the pillboxes or other similar boxes in which the medication of the PwD is stored and for each sensor we count the number of times the PwD interacts with the pillbox;

The input data for our approach is represented by a set of days for which the following information is known: the total duration the PwD spends in each room, the number of times each door or device that has a motion sensor on it is opened or closed and the number of times the PwD interacts with the pillboxes that contain the medication that must be taken. From this data we extract a baseline that describes the behavior of the PwD. Then we compare the baseline with the data that was monitored in a day and we identify the possible types of anomalies. As output we provide the distribution of the anomalies for that day.

The three types of anomalies that we identify in our approach are correlated with the three types of monitoring sensors:

- presence anomalies
- motion anomalies
- medication anomalies.

4 Research Methodology for AD in DLAs of PwD

Figure 2 presents the research methodology used in our approach for detecting anomalies in DLAs of PwD. The following subsections detail each step of the proposed methodology.

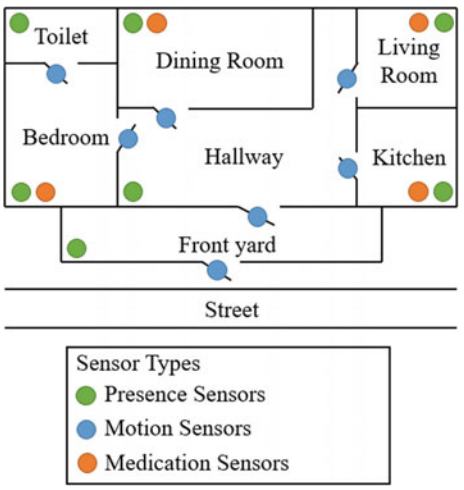

Fig. 1 Example of house with sensors that monitor DLAs of PwD

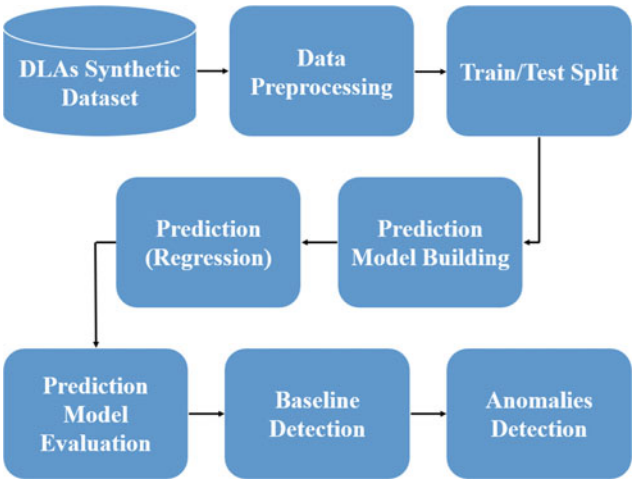

Fig. 2 Research methodology steps for AD in DLAs of PwD

4.1 DLAs Synthetic Dataset

The data used in our research methodology as experimental support is a synthetic dataset from the context of the MedGUIDE project [9]. We suppose that there are three types of monitoring sensors: presence sensors, motion sensors and medication sensors.

4.2 Data Preprocessing

In this phase the data is normalized to take values from the interval [0, 1]. The data is preprocessed in KNIME (Konstanz Information Miner) [8].

4.3 Train/Test Split

The data is split in two parts: 80% of the data is used for training and 20% of the data is used for testing the proposed prediction model.

4.4 Prediction Model Building

In this step the model that is used for the prediction of the baseline of the PwD is built. We compare two approaches: a big data approach based on RF algorithm using Apache Spark framework and a deep learning approach based on a SM created with Keras and TensorFlow.

4.5 Prediction (Regression)

This is the step in which the actual prediction is made. The data that is predicted by the prediction model is then evaluated using the testing data.

4.6 Prediction Model Evaluation

The prediction model is evaluated using the Root Mean Square Error (RMSE). The objective of this step is to identify the prediction model that gives the best results.

4.7 Baseline Detection

In this step using the best prediction model based on the RMSE evaluation metric, the baseline of the PwD is predicted.

4.8 Anomalies Detection

The anomalies are detected by comparing the predicted baseline with the data monitored in a day for a PwD by the monitoring sensors. The output is represented by the distribution of the three types of anomalies for the monitored day.

5 Baseline Prediction Using Big Data and Deep Learning Approaches

In this section are presented the preprocessing of the data that describes DLAs in KNIME, the prediction of the baseline for a day using a big data approach based on RF and the prediction of the baseline for a day using a deep learning approach based on SM.

5.1 DLAs Data Preprocessing in KNIME

In this section are presented the steps that are followed for preprocessing the DLAs data in KNIME. The approach is applied on a DLAs synthetic dataset, a dataset that was developed in-house and that simulates the data that is generated by the monitoring sensors. We suppose that for each day the following information is monitored: total sleeping duration, total feeding duration, total hygiene duration, total mobility duration, how many times the doors were opened or closed, how many times the TV was turned on or off, how many times the fridge door was opened or closed, how many times the switches were turned on or off, how many times the Donepezil box was opened or closed, how many times the Galantamine box was opened or closed, how many times the Rivastigmine box was opened or closed and how many times the Memantine box was opened or closed.

We suppose that the data also contains missing values and that in some days the monitored PwD presents unusual behavior such as repeating the same action too many times or forgetting to perform some actions.

The KNIME workflow that is used for data preprocessing is presented in Fig. 3.

The DLAs synthetic dataset is loaded in the KNIME workflow by the **Excel Reader (XLS)** node and the missing values are replaced using the mean heuristic by the **Missing Value** node. The **Normalizer** node normalizes the data so that it takes values from the interval [0, 1] and the **Number to String** node preprocesses the data prior to oversampling. The **SMOTE** node oversamples the data by a factor of 10 and the **Shuffle** node shuffles the rows. After the transformations are performed, the data is written on the disk by the

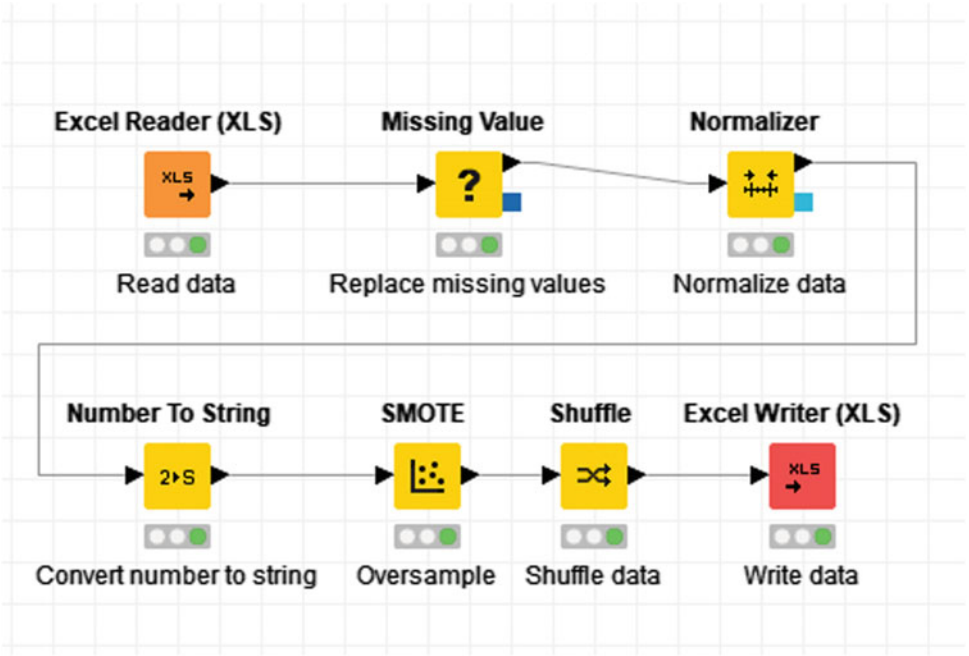

Fig. 3 KNIME workflow for DLAs synthetic dataset preprocessing

Excel Writer (XLS) node. In the next sections 80% of the data is used for training the prediction model and 20% of the data is used for testing the prediction model.

5.2 Big Data Random Forest Approach for Detection of Baselines of PwD

The RF regression algorithm that is used in our approach is the classical one.

Algorithm 1: Random Forest

Input: *k, depth, noOfTrees, trainingData, K,* day_i
Output: *predictedValue*
begin
  $F = \{f_1, \ldots, f_{12}\} - \{f_k\}$
  select randomly K features from F
  calculate the best split based on the *trainingData* and from
    the set of K features obtain the d node
  using the best split calculate the daughter nodes
  repeat 5.6,7,8 until a specific number of nodes is reached
  repeat 5,6,7,8,9 until the forest has the size *noOfTrees*
  obtain RF_k which is the RF prediction model for feature k
  $predictedValue = RF_k(day_i)$
  return $predictedValue$
end

In our approach we use 12 RF regression models for predicting the values for each feature of the baseline. The training data of the predictors is represented by the monitored data. When predicting the baseline for a day, for each dimension of the activities baseline we use a different RF predictor that takes as input the values of the other dimensions that are monitored for the day for which the baseline is predicted and returns as output the predicted value for that dimension.

The input parameters that are used for the creation of the RF regression model are detailed next: k is the feature for which the prediction is made, *depth* is the depth of the forest, *noOfTrees* is the number of trees, *trainingData* is a set that contains monitored data for a specific number of days, K is a parameter used for computing the best split and day_i is the day for which the prediction is made. The output is represented by the *predictedValue* for day_i.

5.3 Deep Learning Sequential Model Approach for Baseline Detection of PwD

The Sequential Model is created in Keras and TensorFlow.

Algorithm 2: Sequential Model

Input: *k, noOfEpochs, trainingData, layer1, layer2,* day_i
Output: *predictedValue*
begin
  model - initialize a sequential model
  add a layer with *layer1* number of nodes and *relu* activation function
  add a layer with *layer2* number of nodes and *relu* activation function
  add a layer with *linear* activation function
  SM_k = *model.fit(trainingData, k, noOfEpochs)*
  $predictedValue = SM_k(day_i)$
  return $predictedValue$
end

We apply 12 sequential models (SM) for predicting the values of the baseline. As in the case of the RF regression approach, the training data is represented by the entire monitored data and when we predict the baseline for a day for each dimension we use a different SM. For each dimension of the baseline, the corresponding SM predictor takes as input data the values of the other dimensions that are monitored and returns as output the predicted value for that dimension.

The sequential model has four layers: the first one has 11 nodes, the second one has *layer1* number of nodes, the third one has *layer2* number of nodes and the fourth one has a single node. The other input parameters are the following: *k* is the dimension for which the prediction is made, *noOfEpochs* is the number of epochs, *trainingData* is the data that is used for training the sequential model and day_i is the day for which the prediction is made. The output is the *predictedValue*.

6 Experimental Results

In this section are presented the DLAs data preprocessing results, the results obtained using the big data RF approach, the results obtained using the deep learning SM approach and the anomalies detection experimental results.

6.1 DLAs Data Preprocessing

Table 1 presents the characteristics of the DLAs Synthetic Dataset before the application of the preprocessing steps in KNIME and after the application of the preprocessing steps in KNIME.

6.2 Random Forest Experimental Results

For each dimension of the baseline we determine the optimal depth and number of trees of the RF regressor model that returns the best RMSE value. Figure 4 illustrates the variation of RMSE for sleeping duration when the depth is varied.

Table 1 Characteristics of the DLAs synthetic dataset before and after data preprocessing in KNIME

Characteristics	Before data preprocessing	After data preprocessing
Number of samples	100	1000
Missing values	Yes	No
Normalized values	No	Yes

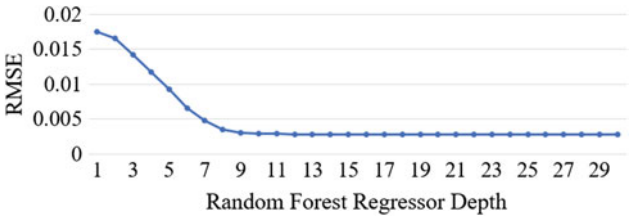

Fig. 4 RMSE for sleeping duration when depth is varied

Table 2 Best RMSE values when maximum depth and number of trees are varied

Feature	Depth	Number of trees	RMSE
Sleeping duration	7	28	0.00251
Feeding duration	12	29	0.00062
Hygiene duration	12	30	0.00059
Mobility duration	13	29	0.00070
Doors interactions count	10	30	0.00136
TV interactions count	11	28	0.00097
Fridge interactions count	10	27	0.00133
Switches interactions count	9	28	0.00207
Donepezil box interactions count	12	26	0.00158
Galantamine box interactions count	13	29	0.00075
Rivastigmine box interactions count	15	30	0.00042
Memantine box interactions count	12	27	0.00082

We consider that 7 is the best value because the value of the RMSE metric does not change much when the value of the depth is bigger.

Then using the best depth value for each dimension, we vary the number of trees in the interval [10, 30]. Table 2 presents the best configurations for each dimension.

The 12 different RF regression models are tuned using the parameters from Table 2.

6.3 Sequential Model Experimental Results

Figure 5 presents the variation of the RMSE when the number of epochs is varied for the feeding activity.

We consider that 70 is an optimal value for the number of epochs because for values that are bigger than 70 the values of the RMSE metric do not change much.

Table 3 presents the best RMSE values when the number of nodes of the neural network is varied and the number of epochs is set to 70.

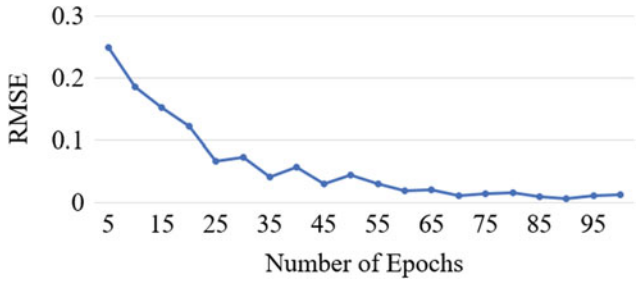

Fig. 5 RMSE for feeding duration when number of epochs is varied

Table 3 Best RMSE values when number of nodes are varied

Feature	Layer#1	Layer#2	RMSE
Sleeping duration	50	100	0.03073
Feeding duration	40	110	0.00973
Hygiene duration	60	90	0.00996
Mobility duration	50	110	0.01178
Doors interactions count	70	100	0.01424
TV interactions count	80	110	0.00700
Fridge interactions count	90	100	0.01527
Switches interactions count	100	50	0.00522
Donepezil box interactions count	110	40	0.00671
Galantamine box interactions count	90	110	0.01280
Rivastigmine box interactions count	80	70	0.00752
Memantine box interactions count	60	110	0.00823

The 12 different SM predictors are tuned using the parameters from Table 3.

6.4 Anomalies Detection Experimental Results

In our approach we compute the anomalies using the predicted baseline and the monitored data for a day. Suppose that the predicted baseline has the following data:

$$baseline = \left(\mathrm{f}_{1,\mathrm{predicted}}, \ldots, \mathrm{f}_{12,\mathrm{predicted}}\right) \quad (1)$$

where $f_{i,predicted}$ with $i = \overline{1,12}$ are the predicted values for the dimensions that are monitored for a PwD. We suppose that a monitored day has the structure:

$$day = \left(\mathrm{f}_{1,\mathrm{monitored}}, \ldots, \mathrm{f}_{12,\mathrm{monitored}}\right) \quad (2)$$

where $f_{i,monitored}$ with $i = \overline{1,12}$ are the monitored values.

Prior to the computation of the distribution of the anomalies using the approach proposed by us, we compute the following values:

$$d_{presence} = \sqrt{\sum_{\mathrm{i}=1}^{4} \left(\mathrm{f}_{\mathrm{i,predicted}} - \mathrm{f}_{\mathrm{i,monitored}}\right)^2} \quad (3)$$

$$d_{motion} = \sqrt{\sum_{\mathrm{i}=5}^{8} \left(\mathrm{f}_{\mathrm{i,predicted}} - \mathrm{f}_{\mathrm{i,monitored}}\right)^2} \quad (4)$$

$$d_{medication} = \sqrt{\sum_{\mathrm{i}=9}^{12} \left(\mathrm{f}_{\mathrm{i,predicted}} - \mathrm{f}_{\mathrm{i,monitored}}\right)^2} \quad (5)$$

The distribution of the anomalies is given by the following equations:

$$a_{presence} = \frac{d_{presence}}{d_{presence} + d_{motion} + d_{medication}} \quad (6)$$

$$a_{motion} = \frac{d_{motion}}{d_{presence} + d_{motion} + d_{medication}} \quad (7)$$

$$a_{medication} = \frac{d_{medication}}{d_{presence} + d_{motion} + d_{medication}} \quad (8)$$

Figure 6 presents the normalized values for the data monitored in a day, for the baseline detected using the RF approach and for the baseline detected using the SM approach.

As can be seen in Fig. 6, for some features the RF gives better results while for the other features the best results are given by SM. Figure 7 presents the distribution of the anomalies predicted using the two compared approaches.

In the RF approach the medication anomalies have the highest ratio while in the SM approach the highest ratio is given by the presence anomalies.

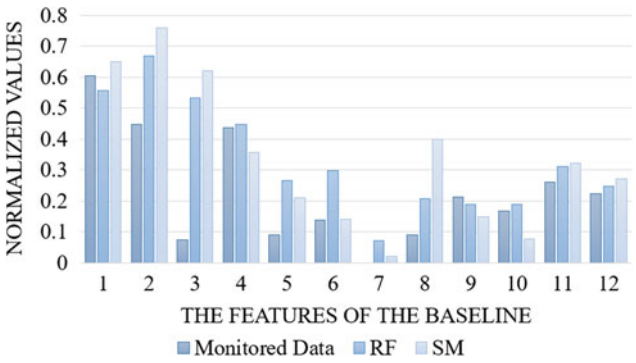

Fig. 6 RMSE for feeding duration when number of epochs is varied

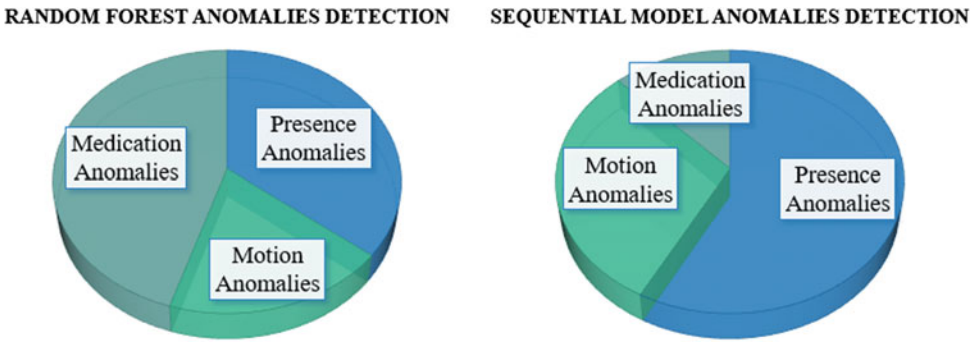

Fig. 7 Comparison of DLAs anomalies detection using RF and SM

7 Conclusions

The main contributions are: (1) the development of an approach for AD in DLAs of PwD, (2) the preprocessing of the DLAs data, (3) the detection of the activities baseline of PwD using RF, (4) the detection of the activities baseline of PwD using SM and (5) the comparison of the two approaches. As future perspectives we plan: (1) to use more features for the description of the activities baseline, (2) to compare the results with the results given by other algorithms and (3) to adapt the proposed approach for other datasets that describe the DLAs of PwD.

Acknowledgements This work was supported by a grant of the Romanian National Authority for Scientific Research and Innovation, CCCDI UEFISCDI and of the AAL Programme with cofunding from the European Union's Horizon 2020 research and innovation programme project number AAL 44/2017 within PNCDI III [9].

Conflict of Interest The authors declare that they have no conflict of interest.

References

1. Alzheimer's Association: 2018 Alzheimer's disease facts and figures. Alzheimer's Dement. **14**, 367–429 (2018). https://doi.org/10.1016/j.jalz.2018.02.001
2. Wallace, B., Harake, T.N.E., Goubran, R., Valech, N.: Preliminary results for measurement and classification of overnight wandering by dementia patient using multisensors. In: 2018 IEEE International Instrumentation and Measurement Technology Conference (I2MTC) (2018). https://doi.org/10.1109/i2mtc.2018.8409727
3. Wu, H.-K., Hung, T.-W., Wang, S.-H., Wang, J.-W.: Development of shoe-based dementia patient tracking and rescue system. In: Proceedings of IEEE International Conference on Applied System Innovation, 2018, pp. 885–887 (2018). https://doi.org/10.1109/icasi.2018.8394407
4. Kimino, K., Ishii, H., Aljehani, M., Inoue, M.: Early detection system of dementia based on home behaviors and lifestyles backgrounds. In: 2018 IEEE International Conference on Consumer Electronics (ICCE), 2018, pp. 1–2 (2018). https://doi.org/10.1109/icce.2018.8326192
5. Acharya, M.H., Gokani, T.B., Chauhan, K.N., Pandya, B.P.: Android application for dementia patient. In: 2016 International Conference on Inventive Computation Technologies (ICICT), Coimbatore, India, 2016 (2016). https://doi.org/10.1109/inventive.2016.7823231
6. Ishii, H., Kimino, K., Inoue, M., Arahira, M., Suzuki, Y.: Method of behavior modeling for detection of anomaly behavior using hidden markov model. In: 2018 International Conference on Electronics, Information, and Communication (ICEIC), 2018 (2018). https://doi.org/10.23919/elinfocom.2018.8330718
7. Kawanishi, K., Kawanaka, H., Takase, H., Tsuruoka, S.: A study on dementia detection method with stroke data using anomaly detection. In: 2017 6th International Conference on Informatics, Electronics and Vision & 2017 7th International Symposium in Computational Medical and Health Technology (ICIEV-ISCMHT), Himeji, Japan, 2017 (2017). https://doi.org/10.1109/iciev.2017.8338566
8. Dwivedi, S., Kasliwal, P., Soni, S.: Comprehensive study of data analytics tools (RapidMiner, Weka, R tool, Knime). In: 2016 Symposium on Colossal Data Analysis and Networking (CDAN), Indore, India, 2016 (2016). https://doi.org/10.1109/cdan.2016.7570894
9. MedGUIDE AAL Project at www.medguide-aal.eu

Sequence Labeling for Extracting Relevant Pieces of Information from Raw Text Medicine Descriptions

Radu Razvan Slavescu, Constantin Masca, and Kinga Cristina Slavescu

Abstract

In Natural Language Processing, Named Entity Recognition aims to delimit and appropriately label the chunks of text containing a specific information. The paper presents the preliminary results we obtained by using a Conditional Random Fields approach for extracting information of interest from drug prescriptions. So far, our model was trained to extract the amount of medicine, measuring unit, frequency of administration, treatment duration and the treatment beneficiary condition. The model was trained using a corpus of drug prescriptions constructed and annotated by hand. The results obtained so far indicate the CRF model we developed performs well, scoring a 91% F1 score on the test set.

Keywords

Named entity recognition • Conditional random fields • Drug prescriptions • Information extraction

1 Introduction

The task of prescribing medicines to patients becomes more and more cumbersome for doctors. This is because of the increasing quantity of specific information about the available drugs they need to possess in order to make the best decision when elaborating a prescription. Therefore, doctors must either memorize or repeatedly look for the connection between the medical problems and the medications required to treat them, as well as for the details of medicine administration such as quantity, frequency, route or patient condition. Since the number of products keeps increasing, keeping up with the whole amount of associated information becomes more and more time consuming. At the same time, simply ignoring the newly introduced medicines is not an option as it could make the practitioner miss the best cure for a disease.

The proposed solution is to build a system able to learn, then automatically extract the previously mentioned elements from raw text description of medicines. It relies on Conditional Random Fields (CRF), a general solution proposed by the researchers in the field of Natural Language Processing (NLP) for the task of Named Entity Recognition (NER). This kind of solution is used for labeling sequences of words, based on contextual information modeled as a set of features. As an example, one can consider the following sentence which specifies the way a given drug must be administered, together with its respective labeling: "The/O dosage/O recommendation/O for/O adult/B-WHO is/O 30/B-DOS mg/B-UNIT per/B-FREQ day/I-FREQ and/O 20/B-DOS mg/B-UNIT per/B-FREQ day/I-FREQ for/O children/B-WHO given/O a/O total/O of/O two/B-DUR weeks/I-DUR".

The meaning of that "per day" represents the frequency of drug administration. B-FREQ marks the beginning of the word sequence describing the frequency, while I-FREQ means the labeled words is inside the sequence. An O stands for "out of interest area".

Thus, NER actually tries to label words or groups of words from a sentence into a specific predefined class, for example dosage, frequency, unit of measure etc. The semantic value of a word is context dependent and many variables have to be taken into consideration when assigning meaning to a particular word, such as the position of the word in the sentence, the neighboring words, it's part of speech etc. NER is a non-trivial NLP task that has to be approached with an appropriate model that can handle the complexity of natural language.

R. R. Slavescu (✉) · C. Masca
Department of Computer Science, Technical University of Cluj-Napoca, Baritiu, no. 28, 400027 Cluj-Napoca, Romania
e-mail: radu.razvan.slavescu@cs.utcluj.ro

K. C. Slavescu
Department Mother and Child, "Iuliu Hatieganu" University of Medicine and Pharmacy, Cluj-Napoca, Romania

S. Vlad and N. M. Roman (eds.), *6th International Conference on Advancements of Medicine and Health Care through Technology; 17–20 October 2018, Cluj-Napoca, Romania*, IFMBE Proceedings 71,
https://doi.org/10.1007/978-981-13-6207-1_33

Besides building this system, we created a dataset of over 1200 labeled sentences. The sentences were selected from larger pieces of texts in English, harvested from various online sources containing drug prescriptions. These descriptions contained much information, such as a general drug description, dosage indications, side effects, warnings etc. Sentences that contained relevant information i.e. contained one or more of the wanted entities were extracted from the full description. Part of speech (POS) tags for each word are also included in the dataset and are used as a feature.

The paper's main contribution is the creation of the CRF model for drug information extraction based on a set of features we proposed and on a manually labeled corpus we prepared for model training. The CRF-based solution was assessed in order to see how appropriate this if for the task of extracting the information of interest for a medical practitioner. The specific features and implementation of our system are described in Sect. 3. Measuring the performance of our system is done using different metrics commonly used for NER systems i.e. precision, recall and F1-measure. K-fold cross-validation was employed for measuring the performance during the training process. Overall, the system's ability to identify the named entities is good.

The paper's structure is as follows. Section 2 gives an overview of the CRFs for named entity extraction. Section 3 details our implementation. Section 4 shows the obtained results. Section 5 presents the related work. The last section gives the conclusions and the future developments we intend.

2 Conditional Random Fields for Entity Extraction

2.1 Conditional Random Fields

CRFs are a probabilistic method for performing structured predictions [1]. They have various applications, such as natural language processing, computer vision and bioinformatics. CRFs combine the predictive power of classification on large input feature vectors and the ability of graphical models to describe dependencies between multiple variables. Unlike simple classification models that predict single labels, CRFs are sequence predicting models. Thus, the previously assigned labels are used when predicting others, therefore increasing the contextual information for every input variable. The most likely sequence of labels is chosen when performing prediction.

CRF is a conditional or discriminative type of model which means that they learn the conditional probability distribution $P(y/x)$. In other words, the separating hyperplane that is the boundary between different classes is computed and then used to perform classification. Discriminative models are considered better than the generative ones for classification. Their main advantage is they do not model the dependencies between the input variables, so they have a simpler structure, hence an increased efficiency [2].

The formal definition of general linear chain conditional random fields, taken from [1], is presented next. Let Y, X be random vectors, $\theta = \{\theta_k\} \in \mathbb{R}^k$ be a parameter vector, and $F = \{f_k(y, y, x_t)\}, k = 1, \ldots, K$, be a set of real-valued feature functions. Then a linear-chain conditional random field is a distribution $p(y|x)$ that takes the form:

$$p(y|x) = \frac{1}{Z(x)} \prod_{t=1}^{T} \exp\left\{ \sum_{k=1}^{K} \theta_k f_k(y_t, y_{t-1}, \mathbf{x}_t) \right\}$$

where $Z(x)$ is an input-dependent normalization function

$$Z(x) = \sum_{y} \prod_{t=1}^{T} \exp\left\{ \sum_{k=1}^{K} \theta_k f_k(y_t, y_{t-1}, \mathbf{x}_t) \right\}$$

The set of input variables, that is the features of the words in a sentence is X and Y is the set of output variables, the labels. Factors are functions of the form $\psi_a(\mathbf{y}_a)$ where a is an integer indexing the factors. Each factor ψ_a depends only on a subset $Y_a \subseteq Y$ of the variables. The value $\psi_a(\mathbf{y}_a)$ is a non-negative scalar that indicates how compatible the values $\mathbf{y}_a$ are with each other. The parameter vector θ is learned from data using maximum likelihood. This algorithm computes the parameters such that the training data has highest probability under the model.

2.2 Named Entity Recognition

The NER task requires identifying and classifying segments of text into predefined entities or classes, even if they are rare in the training set [1]. So, the classification must be based on the words' context, consisting of the neighboring words and their respective features. Knowing where a sentence starts and ends is important for the word context information it may provide. Therefore, the first step for NER is tokenizing or segmenting a large text into individual sentences, then words. Unfortunately, relying on regular expression for separating words or sentences does not scale well due to the large number of exceptions that can occur (e.g., Mr. Johnson, 3.14 g etc.).

Usually, the label assigned to a word depends on its neighbors, suffixes and prefixes, capitalization or position in the sentence. Besides these, the part of speech tags provides significant information for word labeling. A POS (e.g., noun, verb, adjective) is basically a class of words which share similar grammatical properties and behave in like manner in terms of syntax and function.

3 Implementation Details

3.1 Labeling the Data Set

To label the data set, a simple iterative process was developed. An initial manual labeling resulted in a small but varied corpus. It was used to train a model that had good performance on that particular data set. This model was then used to annotate an unlabeled set of sentences that were then manually checked for bad labels or unlabeled entities. These sentences were then added to the initial data set and the process of training, labeling and checking was repeated. A final check was manually performed at the end of this iterative process to check for inconsistencies and other entities that the process might have missed on labeling.

The named entities that were labeled and their respective symbols are the following:

- dosage (DOS) e.g. 1, two, 3 or 4 etc.
- measuring unit (UNIT) e.g. grams, spoons, ml. etc.
- who is the beneficiary of the treatment (WHO) e.g. infants, adults above 40 etc.
- frequency (FREQ) e.g. 5 times a day, twice a week etc.
- duration (DUR) e.g. tree days, one week etc.

Highlighting these entities in a text would be sufficient to help identify the main information when prescribing medication. The name of the drug was out of our objectives, since it is already known.

3.2 Model Features

The input feature vector associated with a word uses various types of information describing different aspects of the word. The feature vector is composed of the following: POS tag; POS 2 letters prefix; lowercase word; suffix (the last 2 and 3 letters); is it an uppercase word; the word is a title; the word contains digits. When generating a feature vector for a word, these features are extracted from the current word and from the three neighboring words as well.

The part of speech tag offers much information on the semantics of the word. A number of 36 different POS tags can be obtained with the system we used, some being derivatives of others, such as the adjective (with the symbol JJ) and the superlative adjective (JJS). Since these to POS's behave similarly—they describe nouns or pronouns—useful information could be extracted from just the prefix, the first two letters.

In our data set, we observed many cases in which the medication name was present, shortly followed by dosage and unit of measure information. Often, the drug's name was written in uppercase or had the first letter uppercased i.e. was a title. We chose two separate features for this information.

Information on digits being present in the word is based on the POS tags describing if the word contains only digits or is a number written with letters e.g. "two", "thirty".

3.3 CRF Model Implementation

For the system implementation, we used a Python wrapper for the CRFsuite library [3], along with the Natural Language Toolkit (NLTK) [4]. When training the CRF, the gradient descent is done via the "Limited memory Broyden Fletcher Goldfarb Shanno" (L-BFGS) algorithm. The regularization parameters are determined using randomized search and 3-fold cross-validation. The process of labeling a text begins by first tokenizing it into sentences and then into individual words. A POS tag is then attached to each word. These operations are done using the NLTK API.

4 Results

To measure the performance we used precision, recall and F1-measure. The final row in each table shows the average for all the entities weighted by the number of true labels for each entity. The performance of the system on the training set is described in Table 1. To assess it, we used the 10-fold cross validation method, with a different fold held for test at each iteration. The 10 results were then averaged to obtain the results in Table 1.

Table 1 Results on train set using 10-fold

	Precision	Recall	F1
B-DOS	0.973	0.969	0.970
O-DOS	0.833	0.780	0.804
B-DUR	0.857	0.799	0.820
I-DUR	1.000	0.614	0.727
O-DUR	0.888	0.908	0.886
B-FREQ	0.986	0.961	0.973
I-FREQ	0.977	0.985	0.981
O-FREQ	0.986	0.961	0.973
B-UNIT	0.980	0.975	0.978
I-UNIT	1.000	0.774	0.820
O-UNIT	0.988	0.896	0.938
B-WHO	0.909	0.914	0.912
I-WHO	0.904	0.907	0.900
O-WHO	0.825	0.842	0.832
Avg./total	0.956	0.936	0.945

Table 2 Results on test set

	Precision	Recall	F1
B-DOS	0.979	0.955	0.967
O-DOS	1.000	0.933	0.966
B-DUR	0.558	0.784	0.652
I-DUR	1.000	0.167	0.286
O-DUR	0.532	0.962	0.685
B-FREQ	0.955	0.894	0.924
I-FREQ	0.914	0.955	0.934
O-FREQ	0.973	0.900	0.935
B-UNIT	0.978	0.961	0.970
I-UNIT	1.000	0.143	0.250
O-UNIT	0.930	0.784	0.851
B-WHO	0.815	0.871	0.842
I-WHO	0.658	0.945	0.776
O-WHO	0.574	0.738	0.646
Avg./total	0.922	0.919	0.915

Table 2 shows the results obtained on a separate test set of sentences. This set was labeled manually without using the iterative method described in the implementation section. The size of the test set is one quarter of the size of the training data set. The error distribution for the 10-fold method approaches the normal distribution.

Figure 1 shows the system's output for a text to be labeled. Different types of relevant information are highlighted in different colors (e.g. orange for dosage, red for unit measure etc.). The system permits loading an already trained model, a new training (i.e., creating a new model) or loading a piece of text and labeling it based on the existing model.

5 Related Work

Various solutions to the NER problem have been tried, and among them, hand-crafted rules, grammar-based techniques or statistical methods. In the Message Understanding Conference the NER challenge, most models were rule-based. The best system entering the contest scored a 93.69% F1-measure, while human annotators scored 97.60%.

However, while certain rules might work well on a specific data set, they most likely fail when presented with completely new styles of texts. New rules must be added to accommodate the texts, and this takes significant efforts. The main advantage of statistical models over hand-crafted rule-based systems is their domain independence. Paper [5] describes a rule-based approach for named entity identification. Adding a CRF-based solution does not improve the performance due the limited amount of training data available; with more data at hand the CRF-based approach resulted in performance improvement.

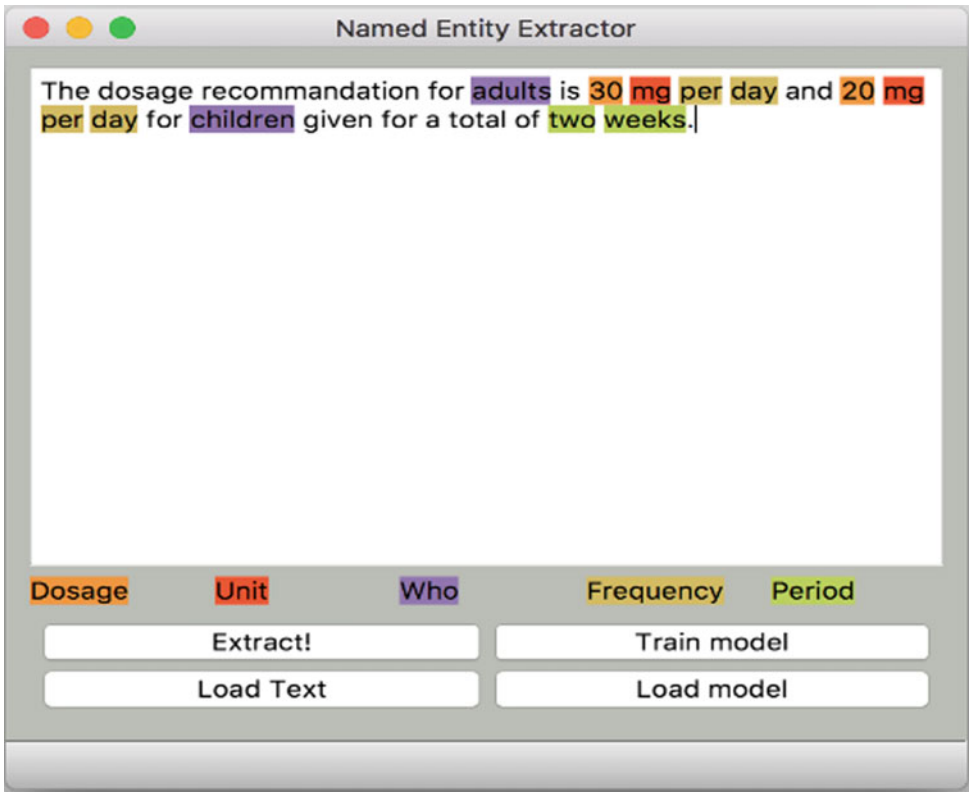

Fig. 1 System output with information highlight

The differences between most CRF based NER models come from the set of features used. POS tags are used in most models. Word-based features like suffixes, length etc. are usually present as well. Other features can be extracted using gazetteers, a type of dictionary that includes certain words with labels. This may dramatically improve performance on a fixed set but is prone to bad generalization.

6 Conclusion and Future Work

We have shown that a CRF approach to extracting the relevant information from drug prescriptions can offer good results. The implemented system may provide help to the medical staff by highlighting the words of interest into large texts written in natural language in English. Using the system for other languages could be done by first translating the text into English, the performance being limited only by the accuracy of the translator. While prescribing medicine to a patient, this would increase the efficiency by decreasing the time it takes to find information on specific drug.

Based on the order in which groups of entities appeared in the sentences, a set of structures was generated to provide insight into how many ways of phrasing the details of a prescription one can meet. Most sentences of our data set fell into few distinct groups, that all shared a similar way of describing the prescription. This suggests the possibility for additional information extraction, e.g., relationships between the entities. Identifying the relationship between duration, dosage and weight of patient could be used to automatically calculate the needed quantity of a certain drug with the associated duration and frequency. A system with detailed relations description could mine the texts and extract a database or an ontology, thus further increasing the efficiency of the prescription task. New drugs on the market would be easily integrated into the database and be accessible instantly.

Conflict of Interest The authors declare that they have no conflict of interest.

References

1. Sutton, C., McCallum, A.: An introduction to conditional random fields. Found. Trends Mach. Learn. **4**(4), 267–373 (2012)
2. Ng, A.Y., Jordan, M.I.: On discriminative vs. generative classifiers: a comparison of logistic regression and naive bayes. In: Advances in Neural Information Processing Systems, pp. 841–848. MIT Press (2002)
3. Wijffels, J., Okazaki, N.: CRFsuite: conditional random fields for labelling sequential data in natural language processing based on CRFsuite: a fast implementation of conditional random fields (crfs). [Online] Available: https://github.com/bnosac/crfsuite
4. Bird, S., Klein, E., Loper, E.: Natural Language Processing with Python. O'Reilly Media (2009)
5. Tikk, D., Solt, I.: Improving textual medication extraction using combined conditional random fields and rule-based systems. J. Am. Med. Inform. Assoc. **17**(5), 540–544 (2010)

Development of Bluetooth Enabled Pediatric Temperature Monitoring Device

Ciprian Mugurel Fort, N. M. Roman, and S. Gergely

Abstract

Accurate body temperature measurement is imperative in pediatric assessment and can signal symptoms such as fever onset. This paper presents the development of a Bluetooth enabled pediatric temperature monitoring device, envisaged for home usage. The temperature monitoring device consist of a skin temperature sensor, OLED display, PIC microcontroller, Bluetooth module and a power supply unit. The measured temperature data are wirelessly transmitted via Bluetooth protocol to a PC. Data storage and visualization is provided by a LabView interface. The results are presented and discussed.

Keywords

Bluetooth data transmission • Biomedical data • Real time monitoring • Temperature sensor

1 Introduction

The increase of body temperature is a complex fighting mechanism against the majority of pathogenic agents. On one hand, these pathogenic agents stop multiplying at temperatures above 37 °C and on the other hand, at temperatures above 38.5 °C, the production of the endogenous interferon, T lymphocyte, B lymphocyte, and NK (Natural-Killer) cells is triggered [1]. However, an increase in body temperature above 41.5 °C represents a serious threat for the human brain due to protein denaturation. Such high fever occurs particularly in infants that do not yet have a well developed thermoregulation system. For such cases, constant body temperature monitoring and prevention of body temperature rise above 40 °C become imperative.

Rapid advances in wireless systems communications give rise to new possibilities for body temperature data acquisition and transmission. However, such systems must be characterized by ease of use, ease of implementation and a high degree of precision and reliability.

The main goal of this paper is to present the development and investigation of a system capable of body temperature data transmission and real time monitoring based on the Bluetooth wireless communication protocol. As a secondary contribution to the presented work, a new method that improves Bluetooth connection reliability is presented and discussed.

This study is divided into three main sections, as follows: a general description of the hardware and software implementation, containing a detailed description of the Bluetooth protocol reconnect improvement; results and discussions based on temperature measurement data and post processing using LabView GUI (Graphical User Interface); conclusions and future related work.

2 General Description of the Temperature Monitoring Device and Tools

2.1 General System Description

A simplified schematic of the system described in this paper is presented in Fig. 1. The main component of the system is the PIC 18F2520 microcontroller produced by Microchip. The microcontroller receives temperature data from the TSic 306 sensor unit. The TSic sensor is produced by IST (Innovative Sensor Technology). The body

C. M. Fort (✉) · N. M. Roman
Department of Electrotechnics and Measurements, Biomedical Engineering, Technical University of Cluj-Napoca, 26-28 G. Baritiu, Cluj-Napoca, Romania
e-mail: fortciprian@yahoo.com

S. Gergely
National Institute for Research and Development of Isotopic and Molecular Technologies, Cluj-Napoca, Romania

S. Vlad and N. M. Roman (eds.), *6th International Conference on Advancements of Medicine and Health Care through Technology; 17–20 October 2018, Cluj-Napoca, Romania*, IFMBE Proceedings 71,
https://doi.org/10.1007/978-981-13-6207-1_34

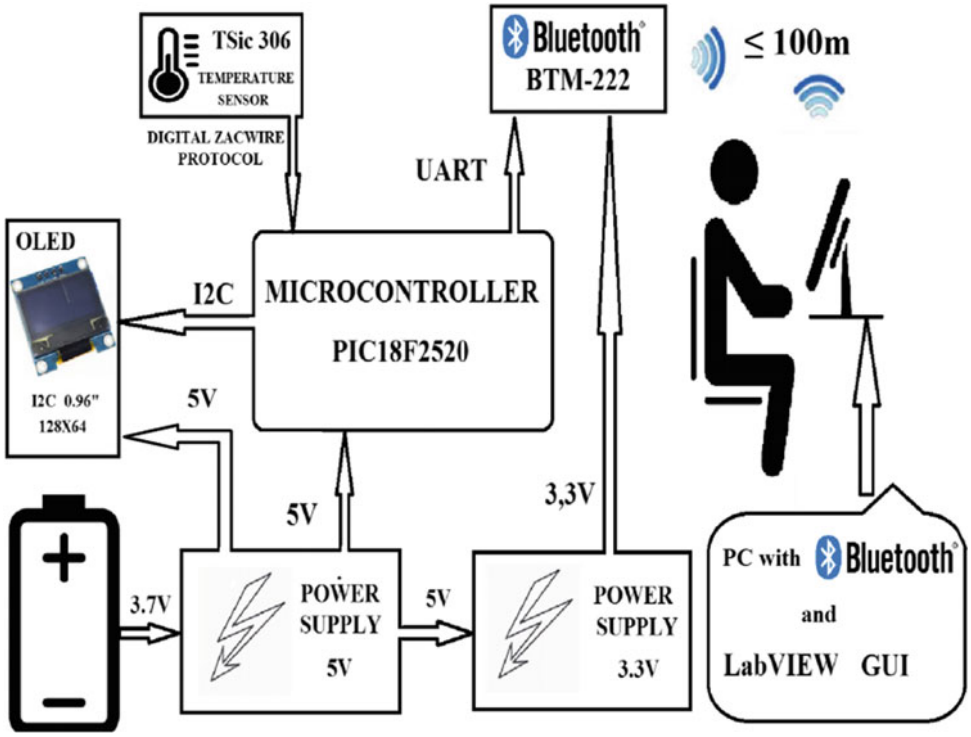

Fig. 1 General system schematic

temperature is both displayed on the OLED (Organic Light Emitting Diode) module (SSD1306) and sent to a PC computer using the BTM-222 Bluetooth module. The wireless connection range can reach up to 100 m. The data is stored on local hard drive and displayed using the developed LabView GUI. At this point data post processing and analyses can be performed.

2.2 Skin Temperature Sensor

The TSic 306 is a digital temperature sensor that provides high accuracy of ±0.1 °C and a resolution of 0.1 °C on the 30–45 °C temperature measurement interval. This sensor communicates with the Microcontroller using the 1-Wire interface using digital ZACwire protocol [2].

The TSic 306 high accuracy is provided by the on-chip reference with a PTAT (proportional-to-absolute-temperature) output, a high-precision ADC (Analog to Digital Converter) and a DSP (Digital Signal Processor) EEPROM (Electrically Erasable Programmable Read-Only Memory) core [2].

Equation (1) provides an example of digital output on 11 bits, provided by the TSic 306 datasheet [2]:

$$T = \frac{DIGITAL\,VALUES}{2047} \times (HT - LT) + LT[C] \quad (1)$$

where:

- HT is the higher temperature limit (+150 °C)
- LT is the lower temperature limit (−50 °C)
- 2047-11 bit resolution (internal sensor configuration)
- DIGITAL VALUES—sensor digital output

The sensor transmits the temperature data to the Microcontroller using the ZACwire protocol over a 1-Wire interface. The data transmission starts with the Tstrobe, for microcontroller timer synchronization. The Tstrobe determination is presented in the following routine (Fig. 2).

When the falling edge of the start bit occurs, the time until the rising edge of the start bit is measured, and the value represents the strobe time. After the acquisition of the Tstrobe, the Intrerupt Service Routine then waits for the following 9 falling edges, that consists of 8 data bits and 1 parity bit.

For reasons concerning compatibility issues regarding the TSic interrupting the PIC microcontroller, the PIC must initiate the temperature read process. This issue is resolved by supplying power to the TSic306 through a digital port on the PIC microcontroller. 65–85 ms after powering up, the TSic will transmit its first temperature data. Powering the TSic306 through the microcontroller also provides the possibility to power down the TSic306, thus reducing the quiescent current from 45 to 0 µA. [2]

Fig. 2 Determination of Tstrobe

```
while(input(senzor));   // expected falling edge
set_timer0(0x00);       // timer initialization
while(!input(senzor)); // waiting for the rising edge
STR= get_timer0();      // save value STROBE
```

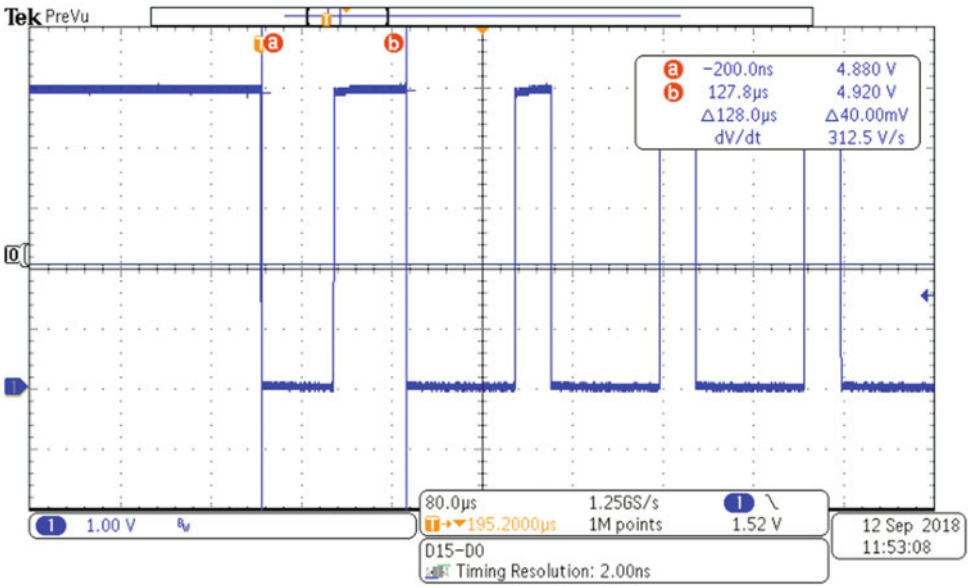

The bit format is encoded by duty cycle:

Start bit—50% duty cycle used to set up strobe time
Logic 1—75% duty cycle
Logic 0—25% duty cycle.

2.3 PIC18F2520 Microcontroller

The PIC18F2520 microcontroller is the main component of the device and provides connection between the rest of the components [3].

In order for the microcontroller to communicate with the Bluetooth module, a hardware level translator (TTL-5 V to TTL-3.3 V) is required.

2.4 OLED Display Module

The OLED Display module is built around a OLED single-chip driver/controller for a dot-matrix display system consisting of 128 segments and 64 commons. The data/commands are being sent between the OLED Display Module and Microcontroller using the I^2C interface [4].

2.5 Bluetooth Data Communication

The data communication based on Bluetooth protocol is implemented using the BTM222 module. The communication between the BT222 and the microcontroller is provided through UART (Universal asynchronous receiver-transmitter).

2.6 Power Supply Unit

The power section of the system consists of a 3.7 V Li-Ion battery powering two switching voltage convertors to 5 and 3.3 V respectively. The 5 V power is necessary for powering the temperature sensor, OLED display module and PIC microcontroller. The 3.3 V power is required for the Bluetooth module.

2.7 LabView GUI

The developed LabView GUI general window is presented in Fig. 3. In the upper side of the GUI window the local measurement time is presented along with the patient name field (it can be modified by the user, and is recorded in the data-base). The resulting file is automatically generated in D:\Data. Alongside this data fields the GUI presents a ON/OFF toggle switch for the OLED display, a write data notification indicator as well as a database path field and a Bluetooth connection status indicator. In the lower side of the GUI window, the measured body temperature data is presented in a data field and also in a plot mode as a function of time.

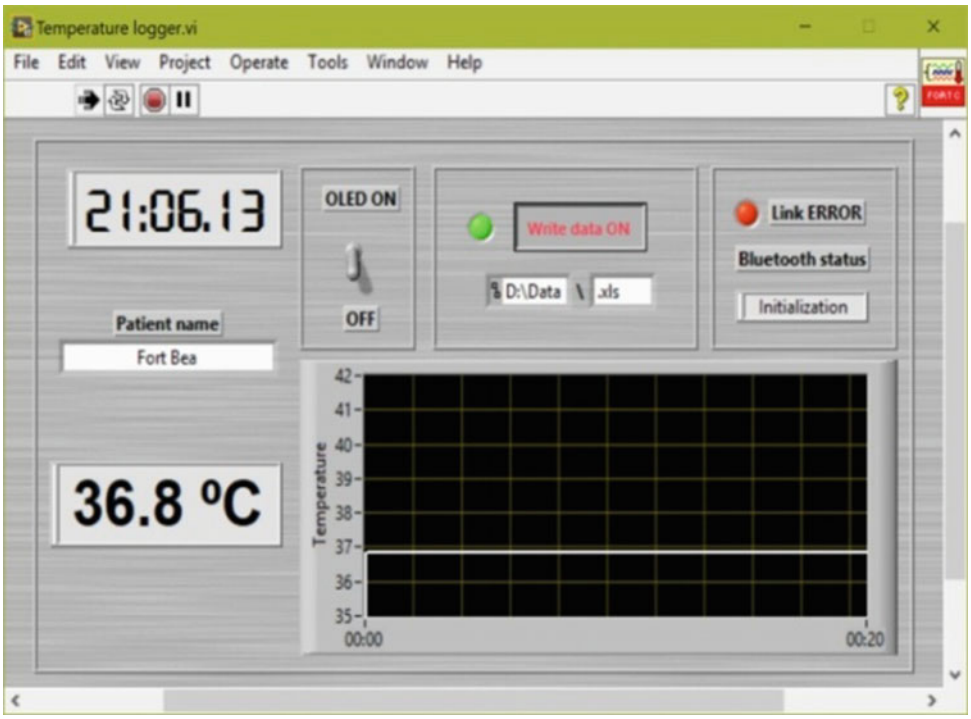

Fig. 3 LabView GUI

The Bluetooth communication protocol is using a specific address of the Bluetooth SSP (Secure Simple Paring) module rather than a virtual communication port.

The physical address of the BTM 222 module is set in the VI (Virtual Interface). If connection initialization is successful, and the routine detects data being transferred, then the received data processing starts. If after 1 s of connection initialization no data is received, then an error code is generated in the Bluetooth connection loop. Contrary, if the error code is activated, the connection is automatically closed, even if previously open, following the Bluetooth connection loop. The Bluetooth reconnection is done automatically, without the need of confirmation or manual reconnect.

Figure 4 presents the LabView GUI Main SubVI.

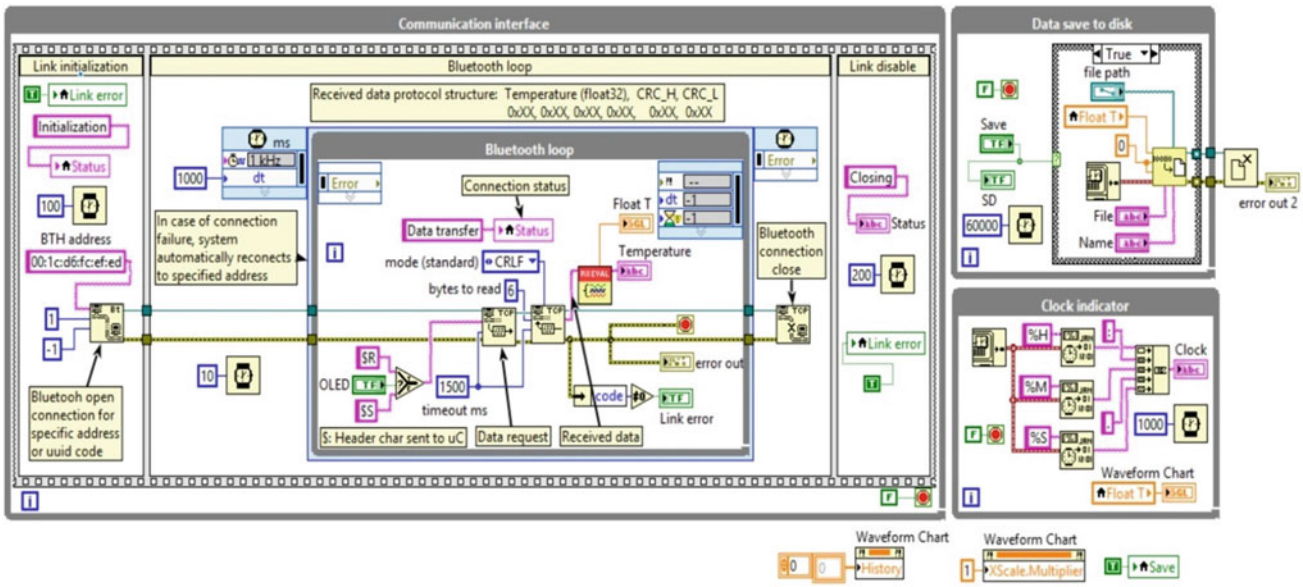

Fig. 4 LabView main SubVI

2.8 Electronic Device Implementation

For construction purposes double sided PCB (Printed Circuit Board) with SMD (Surface Mount Device) components were used, giving the benefit of miniaturization and lightweight. This further benefits the portability of the device. Also, the board dimensions (58 × 38 mm) are closely related to the battery dimensions.

The general electronic schematic of the device is presented in Fig. 5.

3 Results and Discussion

This newly developed device described in the present paper provides body temperature data transmission and real time monitoring based on Bluetooth wireless communication protocol. The benefits of this approach are given by the device portability (lightweight and small physical dimensions), long range data transmission, and the possibility for data aquisition and remote body temperature monitoring. During the development of this device it was observed that

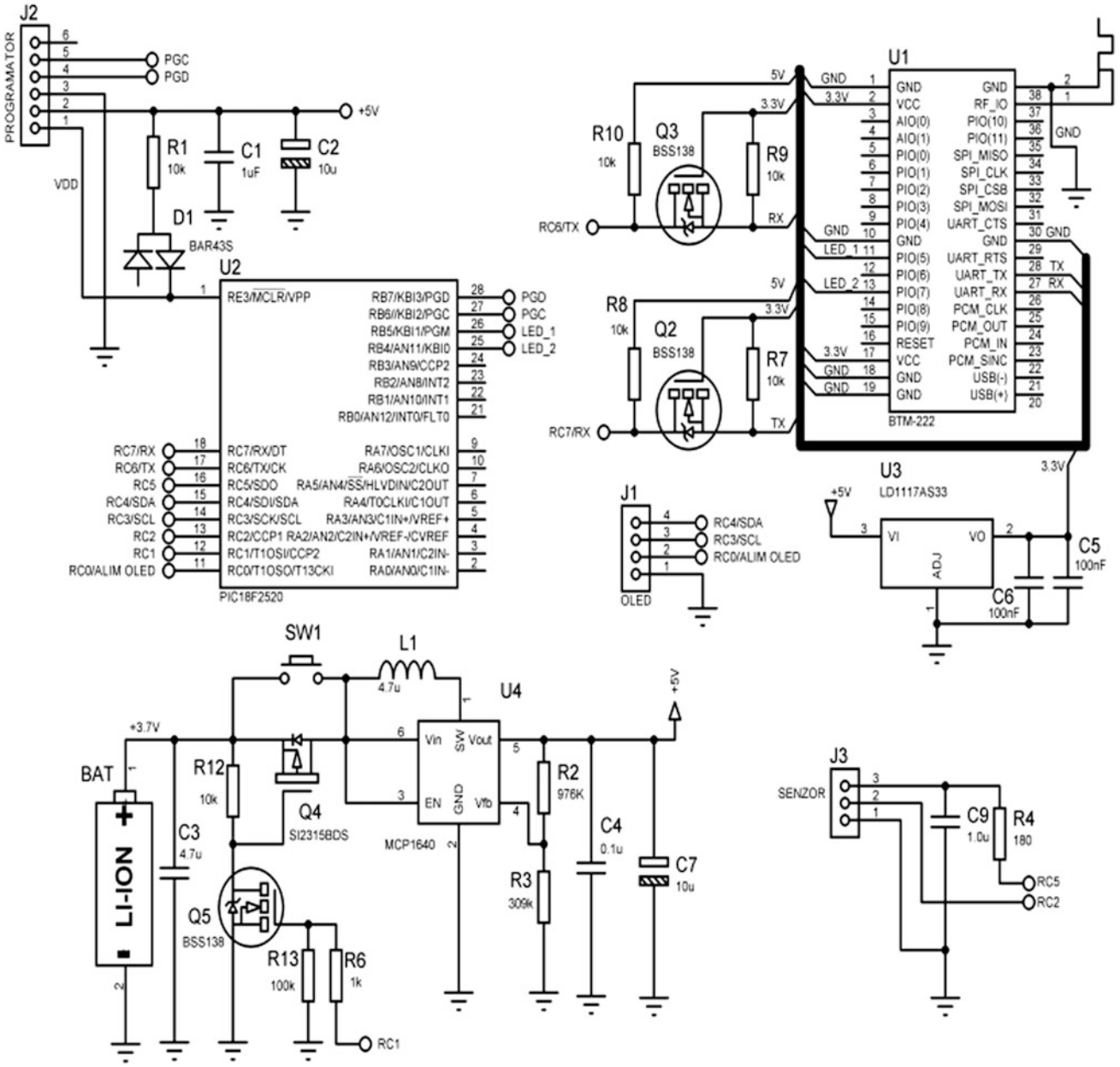

Fig. 5 Electrical system schematic

the Bluetooth connection to the PC is very stabile and the autoconnect feature is reliable. At the time of this study few technical documentation was available for the TSic 306 and a data read algorithm, based on ZACwire protocol, was developed and implemented by the authors.

A LabView GUI was developed that provides data processing, storage and visualization. This represents an original contribution, providing higher versatility when compared with other body temperature monitoring devices. Using the LabView GUI new features can be developed such as networking multiple devices for real time monitoring of multiple patients, or data visualization on portable devices.

4 Conclusions

The present work presents the development and investigation of a system capable of body temperature data transmission and real time monitoring based on Bluetooth wireless communication protocol. The Bluetooth reconnect feature that was also developed during this study shows promising results.

5 Future Work

The possibility of using a fitting function for body temperature prediction will be investigated. Also, we will include in the mathematical model algorithms for calculating the amount of administered anti-pyretic substance. This calculations will take in account different factors such as age, body weight, etc. Statistical clinical data will be acquired for the purpose of determining a suitable correlation for the mathematical model.

Acknowledgements We acknowledge the Technical University of Cluj-Napoca for granting us access to the Medical Engineering Laboratory.

Conflict of Interest The authors declare that they have no conflict of interest.

References

1. Todar, K.: Immune defense against bacterial pathogens: adaptive or acquire immunity. In: Todar's Online Textbook of Bacteriology. http://www.textbookofbacteriology.net/adaptive
2. Inovative Sensor Technology 1-Wire Digital Thermometer (datasheet) at http://www.istag.com/sites/default/files/ATTSic_E.pdf
3. Microchip Technology Inc. PIC18F2520 (datasheet) at http://ww1.microchip.com/downloads/en/devicedoc/39631e.pdf
4. Solomon Systech Semiconductor Technical Data (datasheet) at http://www.adafruit.com/datasheet/SSD1306.pdf

Part V
Biomechanics, Robotics and Rehabilitation

The Analysis of Bio-Signals and Sensors for Robotic Assisted Rehabilitation

Nicoleta Pop, Calin Vaida, Giuseppe Carbone, Florin Craciun, Kinga Major, Cristian Abrudan, Ferenc Puskas, and Doina Pisla

Abstract

The paper presents some considerations on the development of an external system of sensors for post-stroke robotic assisted rehabilitation. A conceptual integrated system which places the patient as an active component is proposed. A set of bio-signals and the corresponding sensors are described to use the data as real-time information during rehabilitation exercises. A novel robotic system is presented for bed confined patients with its kinematic structure and workspace generation for medically relevant motions along with the positioning of the system of external sensors.

Keywords

Robotic post-stroke rehabilitation • Bio-signals • External sensors • Mechanism analysis

1 Introduction

Latest statistical data show that cardiovascular diseases, including stroke, remain the most frequent cause of incapacity in developed countries [1]. It is also expected an increase in the number of people that will develop a form of cardiovascular disease which will reach 43.9% of the US population by 2030. Moreover, by 2050 the number of stroke patients will raise to more than double, with a higher rate among the elderly people (>75 years). In Europe, according to the data provided by the World Health Organization cardiovascular diseases are responsible for 42% of male deaths (out of which 10% are strokes) and 51% of women deaths (15% attributed to strokes). In Romania, cardiovascular diseases are responsible of 58% of the annual deaths affecting males at an earlier age compared to women. In order to prevent and to reduce deaths attributable to cardiovascular diseases and stroke by the year 2020 (American Heart Association announced its 2020 Impact Goals) it is important to focus on both (1) improvement of healthcare systems approaches including direct/active implication of patient in the rehabilitation process and (2) prevention through treatment and control of health behaviors and risk factors. It is extremely important to increase the patient self-efficacy, to use electronic systems for monitoring and tracking specific health factors (blood pressure etc.), to use electronic medical devices for providing immediate feedback to users [2].

All this data point out that the number of stroke patients will increase dramatically and even though this disease has an excellent one year survivability rate, for about 75% of the subjects, over 80% of them suffer long term impairment. The most common motor impairment is hemiparesis which affects, with different levels of severity, the movement control on one half of the body which can be restored (up to a certain point) through extensive rehabilitation.

All these mentioned aspects lead towards a critical conclusion: the number of impaired stroke survivors will increase dramatically up to a point when the medical system will be unable to manage them. As the rehabilitation specialists cannot be increased at the same rate, a paradigm change must be applied in this field: the role of the therapist must shift from performing exercises with the patients to the development and monitoring of personalized treatment plans performed with efficient autonomous devices. Research

N. Pop · C. Vaida · F. Craciun · K. Major
CESTER, Technical University of Cluj-Napoca, Cluj-Napoca, Romania

G. Carbone
LARM, University of Cassino and South Latium, Cassino, Italy

C. Abrudan
"Iuliu Hatieganu" University of Medicine and Pharmacy Cluj-Napoca, Cluj-Napoca, Romania

F. Puskas
S.C. Electronic APRIL Ltd, Cluj-Napoca, Romania

D. Pisla (✉)
CESTER, Technical University of Cluj-Napoca, 28 Memorandumului Str, Cluj-Napoca, Romania
e-mail: doina.pisla@mep.utcluj.ro

S. Vlad and N. M. Roman (eds.), *6th International Conference on Advancements of Medicine and Health Care through Technology; 17–20 October 2018, Cluj-Napoca, Romania*, IFMBE Proceedings 71,
https://doi.org/10.1007/978-981-13-6207-1_35

centers all over the world are developing such devices in the form of robotic rehabilitation systems for the different body segments. Even though at the moment the kinematic capability of these systems trail behind the human therapist, continuous progress is made.

The loss of motion control at the level of the lower limb affects about one third of the stroke survivors which lose their independent walking ability [3]. The rehabilitation process for the lower limb is divided into three phases [3]: (1) the bedridden patient is mobilized into the chair, (2) restoration of gait and (3) improvement of gait.

Up to the present day most of the existing robotic systems used for lower limb rehabilitation focus on the second and third stage, using a treadmill and body weight support for the patient and are focused on gait recovery in vertical position. Even though they have proven medical efficiency they share a common drawback as the initial patient setup is very difficult especially for the more severe cases as the patient has to be strapped to the machine in a special harness and afterwards the leg actuation system must be carefully aligned to the body joints. Several such systems are presented below:

Lokomat is based on gait orthosis and a body weight support used in combination with a treadmill. The computer-controlled drives incorporated in each hip and knee joint assure the synchronization between the velocity of treadmill and the orthosis;

LokoHelp consist of an electromechanical system positioned on a treadmill with body weight support;

ReoAmbulator is similar to the Lokomat and LokoHelp systems, but in this case, the patient will perform the stepping exercises based on predefined patterns;

ARTHuR is used for control and measurement of patient stepping on a treadmill;

POGO and PAM form a robotic system which uses three pneumatic cylinders attached in the pelvic area to support the body weight and two additional ones used to manipulate the hip and the knee;

ALEX provides an active leg exoskeleton with linear actuators placed on hip and knee joints;

GTI is based on two separate foot plates, assuring only harness security for the patient, not body weight support in order to stimulate various gait patterns;

HapticWalker contains foot plates entirely programmable which allow high challenging foot motion [3];

Rutgers ankle is a six degrees of freedom mechanism consisting of two platforms, a fixed one and a mobile one which has connected six chains. Moreover, this system presents also a virtual reality interface [4].

A critical analysis of the state of the art emphasis a *white spot* in the rehabilitation process for the bed confined patients, which refers to the first phase of the therapy.

As a solution for this problem, the authors propose the development of RAISE, a robotic rehabilitation device attachable to the hospital bed able to perform exercises with the patient in horizontal position. The system includes a set of external biosensors that are used for real time patient data measurements that are used as inputs in the robot controller.

The paper is organized as follows: Sect. 2 proposes a description of the main components of a typical robotic assisted rehabilitation system and the bio-signals of interest. Section 3 focuses on a detailed description of the robotic system and the proposed external sensors, followed by conclusions and future development plans for the system.

2 A Systematic Overview of the Critical Elements of a Robotic Assisted Rehabilitation System

One drawback of the early rehabilitation systems refer to their closed and independent loop control. In order to achieve better results the patient must become an integral, active part of the system supplying real-time data that can be used to adapt the robot behavior to the particular needs of each patient. Thus, a generalized overview of the main components of an efficient rehabilitation system is proposed.

2.1 The Main Components of the Rehabilitation System

Figure 1 illustrates the main system components: Patient, Sensors, Medical Personnel, Integrated interface, Robot controller and the Robotic system itself.

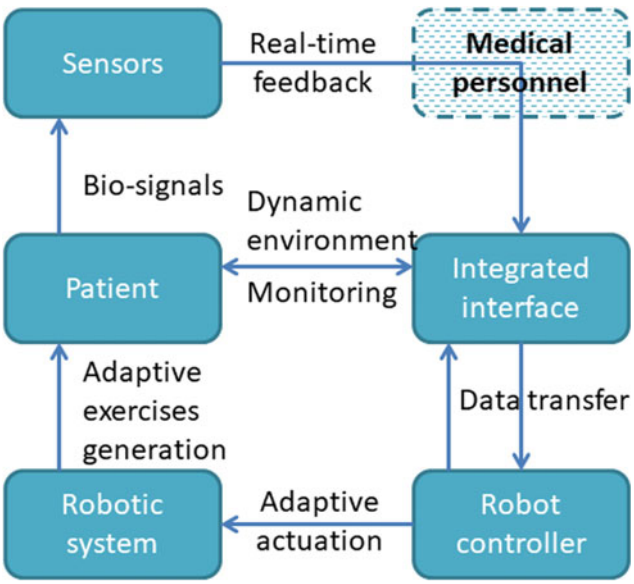

Fig. 1 The conceptual overview of the robotic assisted rehabilitation system

Patient: The patient becomes an active component of the rehabilitation system supplying real-time data through the system of sensors. It also receives continuous information from the integrated interface as additional stimuli and motivation.

Sensors: The sensors are grouped in two main categories: **the external ones** which monitor in real-time multiple relevant parameters, namely multiple bio-signals measured directly on the patient; **the internal ones** which belong directly to the robotic system: encoders, inductive sensors for homing and so on.

Integrated interface: represents the decision maker or the "brain" of the system. Designed on multiple access levels (patient, physician, and engineer) the interface allows the definition of personalized exercise plans combined with different audio-visual virtual reality environments to stimulate the patient neural activity on multiple levels. Within the interface patient data must be stored (securely) enabling the continuous monitoring of the patient progress on the overall and on specific exercises. This allows physicians to personalize the rehabilitation process aiming to achieve maximum results. Another important aspect is that such systems are to be used in hospitals in the first weeks after the incident followed by a period when the patient is treated in specialized centers or at home. In such cases the patient must be able to exercise daily while being monitored from distance.

Robot controller: contains the control architecture of the robotic system, incorporating a real-time PLC, input output ports and drivers for the actuation system. The controller communicates directly with the Integrated interface to load the desired motion parameters. The system must support multiple working modes which range from the performing of simple motions to assistive ones when the patient will partially perform a motion with the robot being just an aid.

Robotic system: represents the mechanical structure of the robot and the actuation system. Using the data supplied by the controller the robotic system will perform the actual motions upon the targeted patient limb.

Medical personnel: the rehabilitation process includes continuous patient assessment from kineto-therapists and neurologists. However the system can perform exercises based on predefined protocols without their direct involvement sending relevant recorded patient data at regular intervals or warnings whenever a medical parameter exceeds its preset limits.

2.2 The Bio-Signals of Interest in Robotic Assisted Rehabilitation

To have an objective quantification of the efficiency of the robot-assisted rehabilitation in stroke patients, several physiological parameters might offer reliable guidance.

First, by using **real-time heart-rate monitoring**, one can fine-tune the intensity of the applied forces and frequency of motion. If the paretic limb is passively moved, venous return is enhanced, a higher volume of blood is sent to the heart, increasing slightly the heart-rate. If the assistance is not entirely passive, but requires also the patient to participate with his residual power during the exercise, the heart-rate might show a further increase, and this should be monitored for example in the condition of heart-failure and consecutive tachyarrhythmia, frequently a preexisting condition in stroke. If the applied forces are higher than tolerated or required, the patient might experience a sympathetic overflow, producing a further increase in heart-rate, this being potentially a dangerous condition.

Along with the mobilization of venous blood, **better oxygenation** of the peripheral tissue might occur, which can be easily monitored using pulsoxymetry. This is beneficial for the paretic tissue, mostly from the point of view of maintaining a good trophicity. Awareness should be imposed, if the preload increases significantly, a degree of failure might be triggered by the exercise itself, which in turn decreases the peripheral blood and oxygen supply.

By applying repetitive exercises, on one hand the mobility increases by passive enhancement of the joint range of motion, on the other hand this can be increased by the gradual return of the **active movements** of the patient. This effect is objectively assessed by goniometry.

The residual forces are usually increased by exercises. A motor unit is composed of the nerve terminal and the muscle fibers innervated by it. **Motor unit action potential recording**, an EMG technique, monitors volitional muscle activity. Individual fiber contractions are summed in a single potential and recorded as a potential change either by using a needle electrode, or on the surface of the muscle. The second method is not as precise, but is less invasive. By exercising, the amplitude of the MUAPs show a gradual increase, a good measure for the efficiency of the rehabilitation method.

Besides the valuable information that is provided during the exercise times, as rehabilitation is a very long time process the recording of the bio-signals data is of critical importance to assess the patient progress, evaluate his active involvement in the exercises and as the authors intent, also to assess its mood. It has been shown in numerous studies and synthetized in [5] that better results are obtained during exercises when multiple stimuli are applied. However, each individual has different perceptions about these stimuli and it is very hard to develop a solution that would comfort everyone. **Visual aids**, like virtual reality or augmented reality can be useful but depending on the patient background what can be very entertaining for a person might have the opposite effect on another one. Also, it is well-known that most stroke patients which suffer mild to severe limb control loss have a certain level of depression.

Why is this relevant? It has been shown [6] that an uninvolved, bored, uninterested patient will benefit extremely less from the physical exercises. This is why a long term analysis of the bio-signals, their variation during exercises and their comparison with normal data will reveal critical information also about the patient mental involvement in the process. Furthermore, referring to the monitoring of the motion amplitudes a faster progress can be achieved by gradually increasing the dynamic parameters (angles, velocities, number of repetitions) while monitoring the other data to evaluate the patient response to the changes. As severe affected patients might not experience any pain when a certain articulation is stretched to its limits, the authors will attempt to detect it based on the combined variation of the bio-signals and robot sensors information.

2.3 The External System of Sensors

As presented in Sects. 2.1 and 2.2, the authors propose a set of 4 biological parameters that will be monitored in real time during the rehabilitation exercises.

Heart rate and oxygen saturation of a person's blood: can be measured and monitored utilizing a pulse oximeter device. It will be applied to a patient's finger and it will be integrated in a monitoring system during rehabilitation process Fig. 2 [7].

Myoelectric activity: Electrical activity resulted after muscular contraction could be recorded using biopotential electrodes attached to the surface of the skin on desired muscle [8, 9]. EMG sensors contain small integral electrodes placed at 20 mm distance [9]. Those will cover the leg muscles in order to measure and monitor the muscle activity in the rehabilitation process for the lower limb, in both static and dynamic applications Fig. 3. In order to obtain a high quality EMG signal, the final number and position of

Fig. 2 Pulse oximeter

Fig. 3 Surface EMG sensors [9]

electrodes on the lower limb muscle will be identified by a kinetotherapist. Therefore, the sensors will be positioned parallel to the muscle fibers. They will be connected to a computer which allows to collect and display EMG data in real time using a software program and to correlate it with data from other types of sensors [9].

Motion amplitudes: can be measured using twin-axis electrogoniometers which allow the angle measurement in up to two planes of movement. These sensors will be placed for each joints in such a way that the ends blocks will reach across the joint. For minimal errors, these end blocks should be positioned where least movement occurs between the skin and skeletal structure, e.g. for the knee motion, the end blocks are mounted on the lateral sides of the leg. The length of the cable connecting the two end blocks will be selected according to the joint size Fig. 4 [9].

3 Raise – an Innovative Parallel Robotic System for Lower Limb Rehabilitation

RAISE is a parallel robotic structure developed for the rehabilitation of the lower limb, which aims to help patients lying on the bed in the acute post stroke phase [10]. The robot has a modular structure consisting of a module for the hip and knee rehabilitation with two degrees of freedom (DoF) and an ankle module with an additional two DoF. Table 1 illustrates the targeted motions for each joint and their corresponding amplitudes.

Figure 5 presents the kinematic structure of the robotic system. The hip and knee rehabilitation module is a planar robot working in the plane parallel with the mid-sagittal one. It consists out of three kinematic chains with the following structure, defined with respect to a fixed coordinate system, OXYZ:

– the first two are of PPR type (Prismatic—Prismatic—Rotational) consists of a passive linear DoF along the OY axis, an active linear DoF that moves parallel with the

Fig. 4 Electrogoniometers [9]

Table 1 Motion amplitudes for each joint

	Hip [°]	Knee [°]	Ankle [°]
Flexion/Extension	5 ÷ 80	5 ÷ 80	−20 ÷ 35
Abduction/Adduction	–	–	−20 ÷ 20

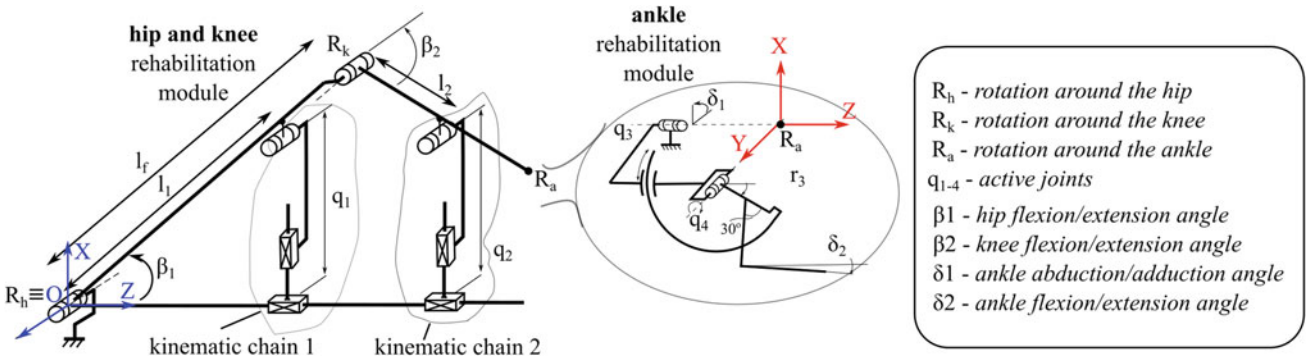

Fig. 5 The kinematic scheme of the RAISE robotic system

OY axis and a passive rotation around an axis parallel with OY;

– the third chain is of RR type having two passive rotational joints around axes parallel with OY.

The actuated joints, q_1 and q_2 perform translational motions that generate the independent rotation of the R_h and R_k joints enabling the flexion—extension motion for the hip and the knee.

The ankle rehabilitation module kinematic scheme Fig. 5 has the R_aXYZ coordinate system positioned in the ankle center of rotation. The module is RR type, performing pure rotational motions around the R_aZ axis (q_3) and R_aY axis (q_4).

Figure 6 presents a schematic view of the robotic device mounted at the end of the patient bed. The fixed rail provides support for the healthy leg and two anchor points for the affected one. The first anchor point is located in the lower third of the thigh and the second one close to the ankle. On the fixed rail there are mounted, following the kinematic scheme the mobile segments that will move the limb. Each segment has a variable length to fit patients with heights between 140 and 190 cm. The ankle module is connected to the first module to provide also support when the other segments are exercised. The four active joints have simple kinematic equations which enable efficient control of the motion of each leg segment or any possible combinations of it. The equations for the four active joints are presented next:

$$\begin{cases} q_1 = l_1 \cdot \sin(\beta_1) \\ q_2 = l_f \cdot \cos(\beta_1) + l_2 \cdot \cos(\beta_1 - \beta_2) \\ q_3 = \delta_1 \\ q_4 = \delta_2 \end{cases} \quad (1)$$

Because a rehabilitation device is capable of moving the limbs beyond their natural operating ranges leading to unwanted damage it is important to determine the workspace of the system as a safety measure [11, 12]. For this reason the motion amplitudes for the workspace have been defined with lower values than those of healthy patients keeping in mind that the flexibility of a post stroke patient cannot be achieved equally with a healthy patient. This is one of the safety measures so that the patient's joints are not overstretched.

With the above considerations taken into account, the workspace of the system for the leg module can be seen in Fig. 7, respectively the ankle module in Fig. 8.

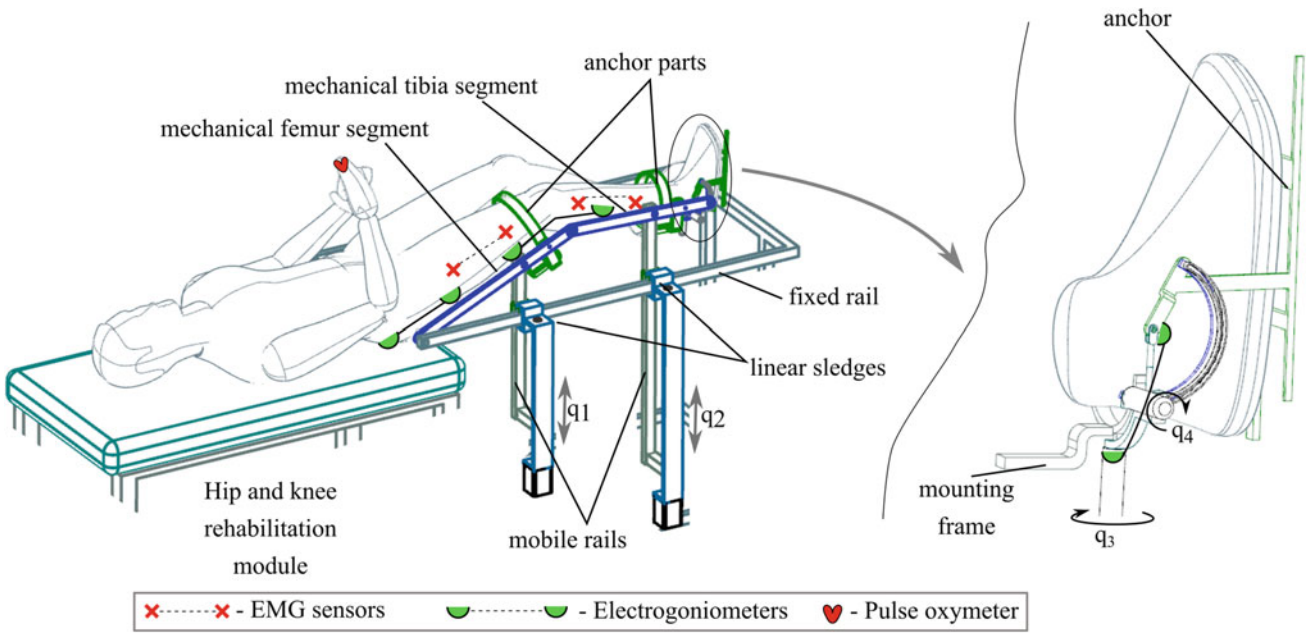

Fig. 6 A schematic view of the robotic device attached to the patient with the external system of sensors

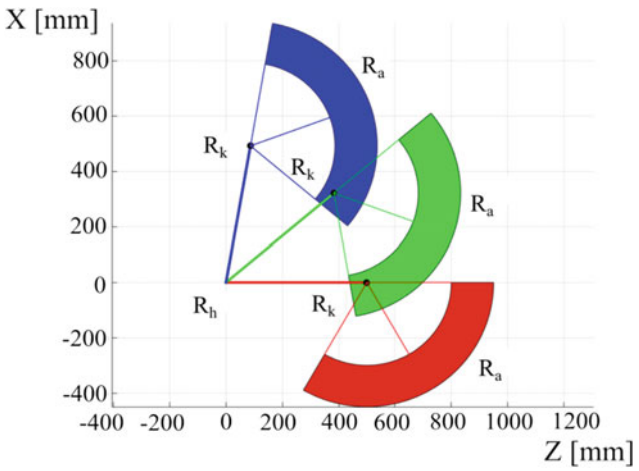

Fig. 7 Workspace of the leg module

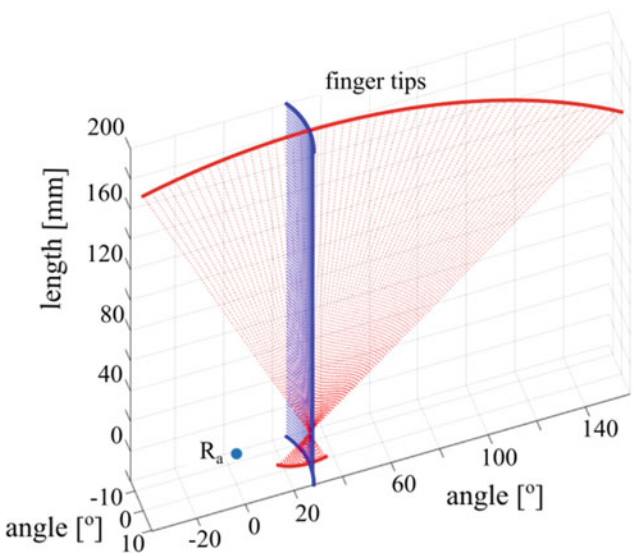

Fig. 8 Workspace of the ankle module

The workspace of the leg module has been defined considering 3 cases of the upper leg (R_h–R_k) position in the following angles: red color (intermediate gray) = horizontal position of the upper leg, green color (light gray) = 40° angle of the upper leg, and in blue color (dark grey) = 80° of the upper leg whereas R_k–R_a is the lower leg segment represented by the flexion extension of the lower leg from the knee joint.

The workspace of the ankle module is represented as 3D plot due to the existence of two rotational motions from the q_3 and q_4 active joints of the system in two different geometrical planes. The motions represent rotations around the R_aZ and R_aY axes. The red hatch represents the plantar flexion-dorsiflexion motion and the blue hatch represents the abduction-adduction one.

4 Conclusions

Robotic rehabilitation is a growing field of research out of a need of paradigm shift in the management of post-stroke patients. An overview of the main components of a rehabilitation system has been presented with a detailed

description of several biosignals proposed by the authors to be used as patient data real-time feedback. A novel robotic system for lower limb has been introduced as a solution for the bed confined patients. Its structure and workspace have been illustrated. Future work will focus on the detailed design of the system and the experimental study of the biosignals to develop a comprehensive real-time data strategy.

Acknowledgements The paper presents results from the research activities of the project ID P_37_215, MySMIS code 103415 "Innovative approaches regarding the rehabilitation and assistive robotics for healthy ageing" cofinanced by the European Regional Development Fund through the Competitiveness Operational Programme 2014–2020, Priority Axis 1, Action 1.1.4, through the financing contract 20/01.09.2016, between the Technical University of Cluj-Napoca and ANCSI as Intermediary Organism in the name and for the Ministry of the European Funds.

Conflict of Interest The authors declare that they have no conflict of interest.

References

1. Truelsen, T., et al.: Stroke incidence and prevalence in Europe: a review of available data. Eur. J. Neurol. **13**(6), 581–598 (2006). https://doi.org/10.1111/j.1468-1331.2006.01138.x
2. Benjamin, et al.: Hearth Disease and Stroke Statistics—2017 Update. A.H.A., Circulation **135**(10), (2017). https://doi.org/10.1161/CIR.0000000000000485
3. Diaz, I., Gil, J., Sanchez, E: Lower-limb rehabilitation: literature review and challenges. J. Rob. vol. **2011** (2011)
4. Yoon, J., et al.: A 6-DOF gait rehabilitation robot with upper and lower limb connections that allows walking velocity updates on various terrains. IEEE/ASME Trans. Mechatron. **1599**(2), 201–215 (2010)
5. Vaida, C., et al.: On human robot interaction modalities in the upper limb rehabilitation after stroke patients. Acta Tehnica Napocensis, Series AMMM **60**(1), 91–102 (2017)
6. Basteris, A., et al.: Error augmentation enhancing arm recovery in individuals with chronic stroke: a randomized crossover design. Neurorehabil Neural Repair **28**(2), 120–128 (2014)
7. Jubran, A.: Pulse oximetry. BioMed. Central **19**, 272 (2015). https://doi.org/10.1186/s13054-015-0984-8
8. Devasahayam, S.: Signals and Systems in Biomedical Engineering, pp. 267–294. Kluwer Academic, New York (2000)
9. http://www.biometricsltd.com. Last accessed 6 July 2018
10. Vaida, C., et al.: Raise—an innovative parallel robotic system for lower limb rehabilitation. In: New Trends in Medical and Service Practice, pp. 293–302, Springer, 2019
11. Carbone, G., et al.: Design issues for an inherently safe robotic rehabilitation device. Advances in Service and Industrial Robotics, MMS, vol **49**, Springer, Cham (2018)
12. Major, K.A, Major, Z.Z., Carbone, G., Pisla, A., Vaida, C., Gherman, B., Pisla, D.L.: Ranges of motion as basis for robot-assisted post-stroke rehabilitation. HVM Bioflux 2016 **8** (4), 192–196 (2016)

Experimental Study Regarding the Performance of a Motor-Imagery Brain-Computer Interface Across Different Electrodes Placement

A. Ianoşi-Andreeva-Dimitrova and Dan S. Mândru

Abstract

This paper present an experimental study that evaluates the performance of a Motor-Imagery (MI) Brain-Computer Interface (BCI) using different electrodes configuration in order to determine the most efficient usage of an 8-channels limited biosignal acquisition device. It is well known the fact that biosignal acquisition devices tend to be very expensive, especially if they have more than 8 electrodes: if in a research context this cost is manageable, for care giving institutions this cost is often prohibitive, which drastically limits the research transfer to practical applications Therefore, it is important to determine the most efficient way in which a more affordable device might be used. A total of 19 configuration were tested, and the results compared against each other. Recommendation for further testing are made.

Keywords

Brain-computer interface • Motor imagery • Biosignal amplifier • Rehabilitation engineering

1 Introduction

Disability is one of the issues that has a very profound impact on individuals and society; long-term suffering changes radically one style of life, forcing the affected individual to find ways to compensate for function loss. The recurring issue about finding options to compensate for disability is related to cost: despite remarkable progress in science and technology, many cutting-edge technologies are prohibitive expensive for many individuals and even for state funded medical insurance. Brain-Computer Interface (BCI), a technology born more than 40 years ago, is an eloquent example: until recently it was too costly even for research centers, which had led to small progress toward the science needed for the development of a market-ready rehabilitation equipment, but this is about to change [1]. Therefore, research done determining an efficient use of limited existent technologies, is relevant.

This paper investigates 19 electroencephalography (EEG) electrodes placement configurations in order to determine an arrangement that provide adequate performance for a Motor Imagery (MI) BCI. Motor Imagery is a BCI paradigm that uses the detection of changes in rhythmic activity recorded over motor cortex elicited by imagination of limb movement [2]; as such, it provides a fairly natural, relatively easy to learn way of interaction between an individual and a rehabilitation equipment [3]. The downside is given by the fact that there are a limited set of brain electrical signals easily accessible to a noninvasive BCI as well as other challenges detailed by [4].

The present paper presents and discusses the results, draw conclusions from them and make recommendation for future research as well as for the usage of the most efficient configuration found by our experiments.

2 State of the Art

The placement of electrodes in order to efficiently collect brain signals is a problem of interest especially in the case of electrocorticographic measurements: several methods were elaborated, in an attempt to register magnetic resonance imaging (MRI) data with computed tomography (CT) scan for correct association between brain structures and function [5]. For non-invasive approaches, the flexibility provided by easy reconfiguration of the electrodes placement make such studies rare: the scientific literature provided only a few articles, which are discussed below.

The open source movement has influenced even the field of BCI, and [6] evaluates if an OpenBCI headgear is suitable for MI tasks. They used a full open-source tool chain

A. Ianoşi-Andreeva-Dimitrova (✉) · D. S. Mândru
Technical University of Cluj-Napoca, Blvd. Muncii, 103-105, Cluj-Napoca, Romania
e-mail: Alexandru.Ianosi@mdm.utlcuj.ro

S. Vlad and N. M. Roman (eds.), *6th International Conference on Advancements of Medicine and Health Care through Technology; 17–20 October 2018, Cluj-Napoca, Romania*, IFMBE Proceedings 71,
https://doi.org/10.1007/978-981-13-6207-1_36

(OpenViBE, OpenBCI) and concluded that the headgear design was lacking; no relevant recommendation were made.

A method for optimizing number of electrodes and their placement is given by [7]; the solution involves the usage of the non-dominated sorting genetic algorithm II, and they back up their method with empirical results. Overall, the method makes use of heavy mathematics, which bears the risk to veer any clinical practitioner.

Another method is presented by [8], which formulate the problem of simultaneous selection of significant electrodes and features in terms of optimization problem with the aim of simultaneously satisfying four criteria: maximization of correlation between EEG features, minimization of mutual information between them, electrode selection and maximization of classification accuracy. As with the previous example, the heavy use of mathematics does not cope well with a real-life usage scenario.

Not directly optimizing the location of electrodes, [9] presents a method for localization of brain electrical activity even with suboptimal number of them. They describe their experiment as successfully, being able to obtain with 8 electrodes results not significantly different than those obtained with 32 electrodes.

One final example is the study done by [10] for optimizing electrode number and configuration for a P300 BCI paradigm; they found that a reduced set of four electrodes provided similar performance than a 32 array, which simplifies the setup, reduces the overall cost and improve computation time.

3 Methodology

A number of 14 electrodes placement configuration was tested on a consenting, clinically healthy 27 year old male subject. By removing some recorded channels, an additional 5 configurations with reduced number of electrodes were tested (#15–#19 on Fig. 1). For each configuration a session of 80 trials was recorded, the subject being asked to imagine left/right hand movement at random. Each trial consisted of the following sequence: a green central cross is shown on a

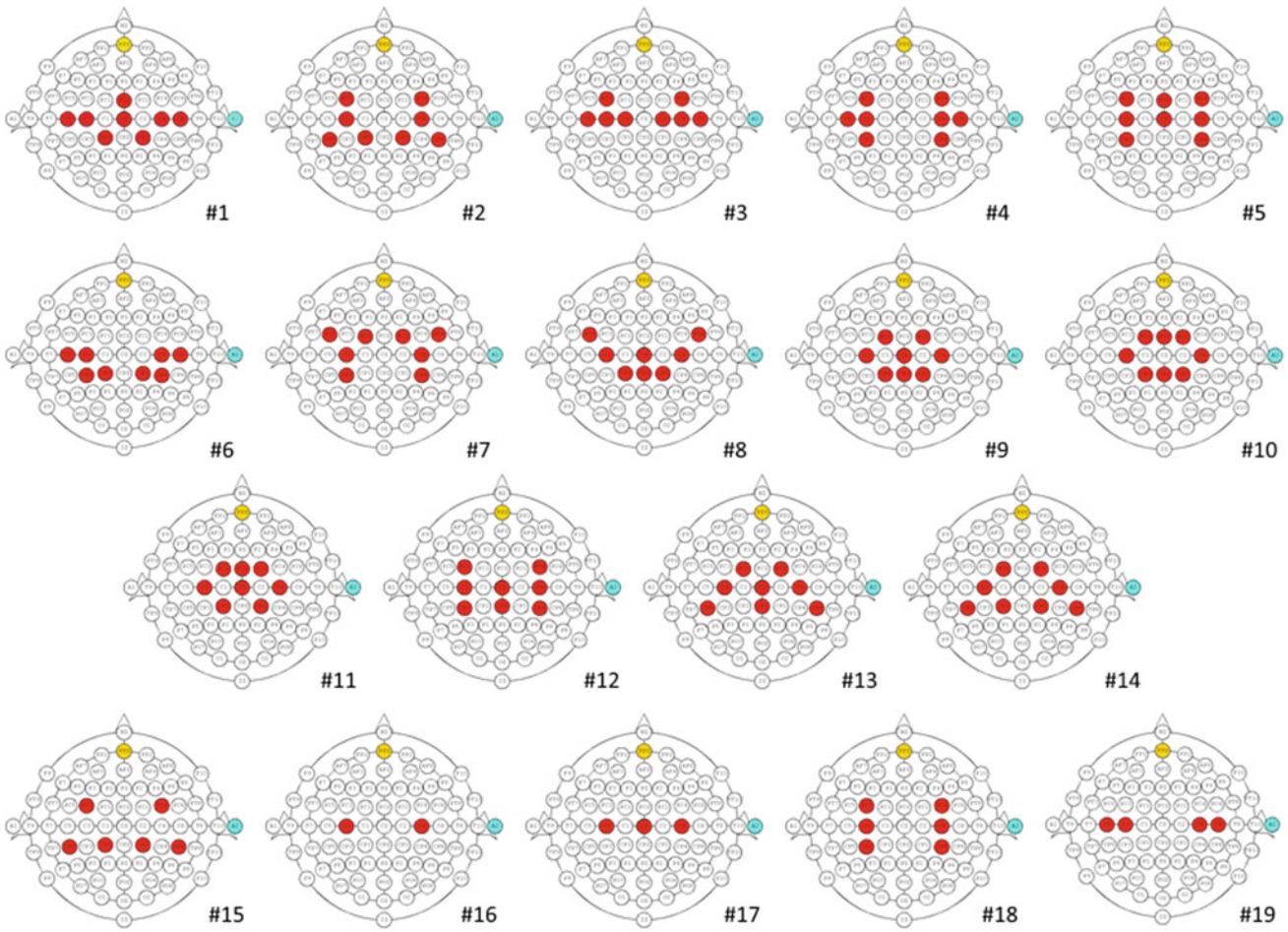

Fig. 1 Electrode placement configuration for each session: red—active electrode, yellow—ground electrode, blue—reference electrode (for B&W images: FPz-ground electrode, A2-reference electrode)

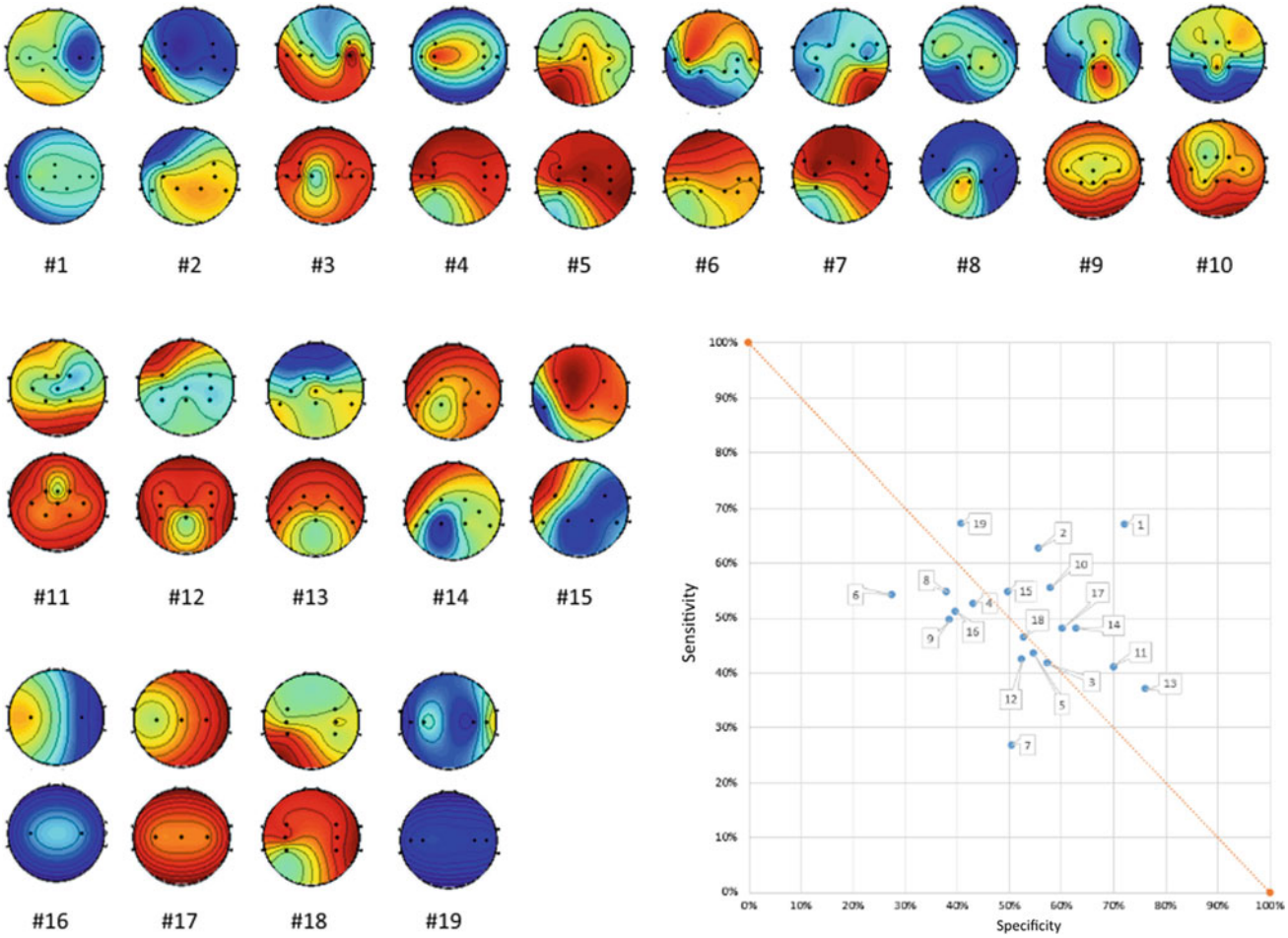

Fig. 2 Results: spectrally-weighted common spatial pattern and performance comparison by mean of sensitivity versus specificity

black screen for 1 s (attention grabbing stimulus), the cue for left/right hand movement imagination (in form of an red arrow) is displayed for 1.25 s, letting 3.75 s time for the actual imagination act (a green central cross on screen is shown again) and finally a resting period of 4 s in which the screen remains black; afterwards, the cycle repeats itself.

The signal was recorded using 8 dry g.Sahara active electrodes connected at g.MobiLab^{+} biosignal amplifier. On the software side, the data was processed using OpenViBE package and BCILAB toolbox for MATLAB. Only the signal acquired in the 3.75 s of active movement imagination is relevant, therefore, a windowing algorithm is applied which extracts only these periods (80 per session), and discards the rest.

The following electrode location were investigated (designation according to 10-10 international system, see Fig. 1): FCz, Cz, CP1, CP2, C3, C4, C5 and C6 (#1); FC3, FC4, C3, C4, CP1, CP2, CP5 and CP6 (#2); FC3, FC4, C3, C4, C5, C6, C1 and C2 (#3); FC3, FC4, C3, C4, C5, C6, CP3 and CP4 (#4); FC3, FC4, C3, C4, FCz, Cz, CP3 and CP4 (#5); CP1, CP2, C3, C4, C5, C6, CP3 and CP4 (#6); FC1, FC2, C3, C4, FC5, FC6, CP3 and CP4 (#7); CP1, CP2, C3, C4, FC5, FC6, Cz and CPz (#8); CP1, CP2, C3, C4, FC1, FC2, Cz and CPz (#9); CP1, CP2, C3, C4, FC1, FC2, FCz and CPz (#10); CP1, CP2, C3, C4, FC1, FC2, FCz and Cz (#11); FC3, FC4, C3, C4, CP3, CP4, CPz and Cz (#12); FC1, FC2, C3, C4, CP5, CP6, PCz and Cz (#13); FC1, FC2, C3, C4, CP5, CP6, CP1 and CP2 (#14).

As stated earlier, additional 5 electrodes configuration were tested by removing the following channels: for #15 the channels C3 and C4 were removed from #2 data set, for #16 only C3 and C4 were used from #2 data set, for #17 only C3, C4 and Cz were used from #5 data set, for #18 FCz and Cz were removed from #5 data set and for #19 only C3, C4, C5 and C6 were used from #6 data set.

The electrodes locations was chosen as such to cover the motor area responsible for hand movement as best as possible from different positions; these positions are mirrored left/right in order to have the same coverage for the regions responsible for each hand. It was hypothesized that some configurations will perform better than others, our aim being to identify which one and by how much. On Fig. 2, the electrodes positions detailed in Fig. 1 are marked with black dots. Results are briefly discussed in the next section.

4 Results

For each configuration a spectrally weighted common spatial pattern filter (SW-CSP) was computed (refer to Fig. 2—the spectral weights are not shown due to space constraints). In order to assess the performance, the quadratic discriminant analysis (QDA) algorithm was used as a machine learning function for left versus right hand prediction. Also, Fig. 2 reveals how much each electrodes placement configuration distort the constructed picture of the brain activity based on the signal acquired.

The results between each configuration are compared by means of two parameters: sensitivity (ratio between true-positive and sum of true-positive and false-negative) and specificity (ratio between true-negative and sum of true-negative and false-positive).

As seen on Fig. 2, the first configuration had the best performance (72.28% sensitivity and 66.98% specificity). Similar sensitivity was achieved by configuration #2 and #19, but with poorer specificity (62%, respectively 40.7%). Most of the placements configuration were barely over statistical significance (result near or on the diagonal line are not distinguishable from random chance).

Surprising results were obtained for configuration #6 and #7, where the results were consistently inverse from the prediction algorithm; being far from the red line, these results could be seen as good, with the quirk that they are mathematically opposite from the prediction.

5 Conclusion

The aim of this paper was to study how electrodes placement influence the performance of a MI BCI, in order to empirically determine an optimal configuration. Our results showed that the configuration designated with #1 provided the best balance between sensitivity and specificity. It is worth to note that over the motor area, according to 10-10 international system, with 8 channels, 87 electrodes configuration are possible; out of them, the present study was focused only on 19 which were considered more relevant. Further investigation is needed in order to empirically determine the optimal 8-channel electrode placement.

Another limitation of our study was the lack of test subjects: the experiments are time intensive. Further study is needed in order to determine whether if the individual variations significantly influence the results.

Acknowledgements Work presented in this paper was partially supported by project ID 37_215, MySMIS code 103415 "Innovative approaches regarding the rehabilitation and assistive robotics for healthy ageing" co-financed by the European Regional Development Fund through the Competitiveness Operational Programme 2014–2020, and also by PCCA Project 180/2012, titled "A Hybrid FES-Exoskeleton System to Rehabilitate the Upper Limb in Disabled People (EXOSLIM)".

Conflict of Interest The authors declare that they are full time University of Cluj-Napoca employees and have no conflict of interest with any entity that produce/commercialize the devices used for the presented research.

References

1. Leebl, R., et al.: Transferring brain-computer interfaces beyond the laboratory: successful application control for motor-disabled users. Artif. Intell. Med. **59**, 121–132 (2013). https://doi.org/10.1016/j.artmed.2013.08.004
2. Pfurtscheller, G., McFarland, D.J.: BCIs that use sensorimotor rhythms. In: Wolpaw, J.R., Wolpaw, E.W. (eds.) Brain-Computer Interfaces: Principes and Practice, p. 227. Oxford University Press, New-York (2012)
3. Alonso-Valerdi, L.M., Salido-Ruiz, R.A., Ramirez-Mendoza, R.A.: Motor imagery based brain-computer interfaces: an emerging technology to rehabilitate motor deficits. Neuropsychologia **79**, 354–363 (2015). https://doi.org/10.1016/j.neuropsychologia.2015.09.012
4. Pattnaik, P.K., Sarraf, J.: Brain computer interface issues on hand movement. J. K.S.U.-Comput. Inf. Sci. **30**, 18–24 (2016). https://doi.org/10.1016/j.jksuci.2016.09.006
5. Brancol, M.P., et al.: ALICE: A tool for automatic localization of intra-cranial electrodes for clinical and high-density grids. J. Neurosci. Methods **301**, 43–51 (2017). https://doi.org/10.1016/j.jneumeth.2017.10.022
6. Suryotrisongko, H., Samopa, F.: Evaluating OpenBCI Spiderclaw VI Headwear's electrodes placements for brain-computer interface (BCI) motor imagery application. Procedia Comput. Sci. **72**(2015), 398–405 (2015). https://doi.org/10.1016/j.procs.2015.12.155
7. Aler, R., Galvan, I.M.: Optimizing the number of electrodes and spatial filters for brain-computer interfaces by means of an evolutionary multi-objective approach. Expert Syst. Appl. **42**, 6215–6223 (2015). https://doi.org/10.1016/j.eswa.2015.03.008
8. Lahiri, R., Rakshit, P., Konar, A.: Evolutionary perspective for optimal selection of EEG electrodes and features. Biomed. Signal Process. Control **36**, 113–137 (2017). https://doi.org/10.1016/j.bspc.2017.03.022
9. Majkowskil, A., et al.: An attempt to localize brain electrical activity sources using EEG with limited number of electrodes. Biocybern. Biomed. Eng. **36**, 686–696 (2016). https://doi.org/10.1016/j.bbe.2016.07.002
10. Speier, W., Deshpande, A., Pouratian, N.: A method for optimizing EEG electrode number and configuration for signal acquisition in P300 speller systems. Clin. Neurophysiol. **126**, 1171–1177 (2014). https://doi.org/10.1016/j.clinph.2014.09.021

A New Proposal for Solving Equations of Angular Contact Ball Bearing Using Evolutionary Techniques

A. Gheorghita, M. Turnea, M. Ilea, M. Rotariu, G. Constantin, and D. Arotaritei

Abstract

Heat generation in angular contact bearings, dynamic analysis and optimization of high speed spindle bearings require to know the load-displacement values in for bearing components. The equations that describe the relationship among preload, speed, and contact angle are solved usually using iterative methods. A new method that uses genetic algorithms is proposed to solve the algebraic system with multiple dependencies with a good precision in evaluation of angular contact angle.

Keywords

Angular-contact ball bearing • Analytical model • System of algebraic equations • Genetic algorithms

1 Introduction

High speed machines based on spindle bearing systems offer a high productivity in manufacturing at required cutting speed and feed rate with a high accuracy of machined workpieced. The design of high speed rotational spindles must overcome many mechanical problems.

The main approaches that deals with static or dynamic analysis of spindle bearings are: vibrational analysis, dynamic analysis and thermal analysis [1, 2]. The basic types of bearings used in these assemblies are angular contact and cylindrical roller. The main sources of heating in spindle bearing assemblies are the cutting area of workpieces, bearings and supplementary, if the spindle is driven by embedded electric motor, the heat generation by the electric motor in rotor and stator as a function of torque and speed [3]. The heat generated by angular ball bearings depends on the dynamic condition of working that is of angular contact and deflection [1].

The general accepted literature provides model to mathematical modeling of angular contact of ball bearing in the case of axial load, preload and radial load [4–7]. These models are described by a system of nonlinear equations with many dependencies, where that basic unknown are the displacements (named by some authors' deflections) or other related variables.

The analysis can be extended to micromachinery, and we refer there to medical tools, e.g. for bone or tooth grinding [8]. Lifetime (LT) of bearings is a very important criterion in spindle bearing systems. LT optimization depends mainly by mechanical factors but also working thermic regimes, that is a strong dependencies of heat generated by bearings and cooling systems [9].

System o nonlinear equation is one of the most complicated when is about a solution but applications and spread of this type of problems is an important area of research. The classic numerical solution to compute the deflection and contact angle in angular contact bearings is an iterative one based on Newton-Raphson method [10]. Due to nonlinear dependencies, an iterative solution of nonlinear system of equation that describes the dynamic equilibrium of bearing taking into account the forces and momentum that act on all the bearing components, an analytical solution is extremely difficult to be found and no notable solution can be mentioned until now.

Practically, only one paper proposed an approximate analytical solution for this problem using an iterative method in [11]. The convergence of proposed algorithm is analyzed and authors demonstrated experimentally that the goal (minim error) is achieved after a small number of steps (4–6 steps).

A. Gheorghita (✉) · G. Constantin
Polytechnic University of Bucharest, Splaiul Independentei 313, Bucharest, Romania
e-mail: andu_ghe@yahoo.com

M. Turnea · M. Ilea · M. Rotariu · D. Arotaritei
Grigore T. Popa University of Medicine and Pharmacy Iasi, Universitatii Street, No. 16, Iasi, Romania

S. Vlad and N. M. Roman (eds.), *6th International Conference on Advancements of Medicine and Health Care through Technology; 17–20 October 2018, Cluj-Napoca, Romania*, IFMBE Proceedings 71,
https://doi.org/10.1007/978-981-13-6207-1_37

Evolutionary algorithm and mimetic based algorithms proved to be a good alternative solution to complicated optimization problem. The are many applications to differential equation and system of partial differential equation, but few proposals refer also to algebraic system of equations that is our case.

In [12] the authors proposed the usage of a feed-forward neural network as a solver for a system of n nonlinear equations with n unknowns using a function of energy. The accuracy of result is high but the implementation is difficult to implement in the case of adaptive learning rate due to complicated formulas developed based on back-propagation algorithm.

Another approach proposed is to use ant colony algorithm (ACA) for nonlinear equation group adding species formation to explore new solution for the problem [13].

Particle swarm algorithm is inspired by flocking behavior of birds or fish schooling and consists of swarm of particles that moves into search space in order to optimize an objective function, the optimal position where the errors between obtained solution and real solutions is very close to zero. Because the tendency of PSO is to converge fast in the first iterations and after that the convergence becomes slow, a modified PSO was proposed in [14]. The key approach is the way of updating each particle [14].

The ABC (Artificial Bee Algorithm) is a novel global optimization algorithm which is based on swarm intelligence. This method has been successfully applied to solve numerically a differential equation, an initial-value problem (IVP) [15]. The method is promising but the extension to system of nonlinear equation is more complicated to be developed in this case.

Genetic Algorithms (GA) belong to a larger class of algorithms based on heuristic search. Based on strategies of evolution (natural selection, crossover, mutation and survival of fittest), the GA is applied to a system of nonlinear equations in [16]. The authors proposed 12 variants of GA applied to 20 variants of single variable function. The extension of a system of algebraic equation of GA solver was proposed in [17].

2 Dynamic Contact Angle with Preload, Speed and Radial Load

It is well known that Newton-Raphson (and other Newton methods) is very sensitive to initial values that are the initial guess of the solution.

In Figs. 1 and 2 it is depicted the usual approach of angular contact ball bearing schema and the relationship among center of the ball, deflections and groove curvatures [1]. The relationship from these figures stands for angular position ψ with and without load (preload, radial).

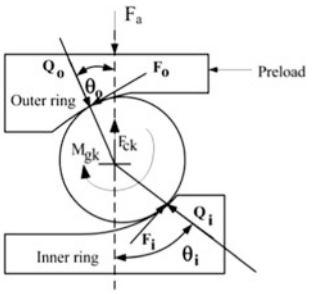

Fig. 1 Relationship between center of ball and raceway curvatures

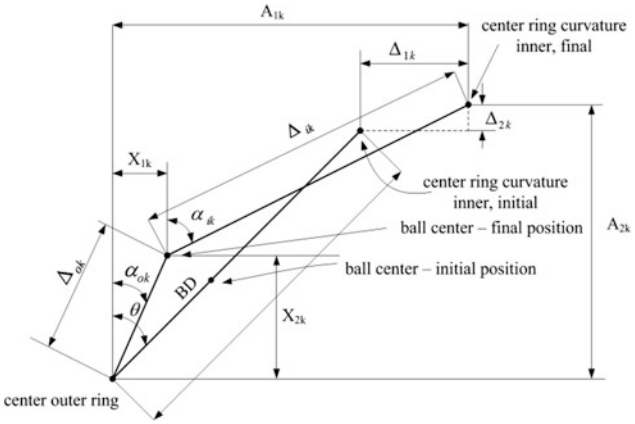

Fig. 2 Equilibrium of forces and moments on a ball

The system of equations that must be solved taking into account as unknown variables $x = \{X_{1k}, X_{2k}, \delta_{ik}, \delta_{ok}\}$ where δ is notation for ball deflection, i stands for inner ring and o stands for outer ring.

The Hertz contact theory is the most used to model the contact force between balls and the inner ring and the outer ring (we denote by δ, as symbol general of the deflection).

$$(A_{1k} - X_{1k})^2 + (A_{2k} - X_{2k})^2 - \Delta_{ik}^2 = 0 \tag{1}$$

$$X_{1k}^2 + X_{2k}^2 - \Delta_{ok}^2 = 0 \tag{2}$$

$$Q_{ok}\cos\alpha_{ok} - \frac{M_{gk}}{D}\sin\alpha_{ok} - Q_{ik}\cos\alpha_{ik} + \frac{M_{gk}}{D}\sin\alpha_{ik} - F_{ck} = 0 \tag{3}$$

$$Q_{ok}\sin\alpha_{ok} + \frac{M_{gk}}{D}\cos\alpha_{ok} - Q_{ik}\sin\alpha_{ik} - \frac{M_{gk}}{D}\cos\alpha_{ik} = 0 \tag{4}$$

Let's denote by h = D/[(di + do)/2], where D—diameter of balls, r_i—inner groove radius and r_o—outer groove radius. The notations and dependencies from Eqs. (1)–(4), depending of frequency of rotation of inner ring (or outer

ring) fixed of spindle are given shortly by (if we neglect θ—bearing misalignment angle) [1–3]:

$$\Delta_{ik} = (f_i - 0.5)D + \delta_{ik} \tag{5}$$

$$\Delta_{ok} = (f_o - 0.5)D + \delta_{ok} \tag{6}$$

$$A_{1k} = BD\sin\alpha^0 + \delta_a \tag{7}$$

$$A_{2k} = BD\sin\alpha^0 + \delta_r\cos\psi_k \tag{8}$$

$$\cos\alpha_{ok} = X_{2k}/[(f_0 - 0.5)D + \delta_{ok}] \tag{9}$$

$$\sin\alpha_{ok} = X_{1k}/[(f_0 - 0.5)D + \delta_{ok}] \tag{10}$$

$$\cos\alpha_{ik} = (A_{2k} - X_{2k})/[(f_0 - 0.5)D + \delta_{ik}] \tag{11}$$

$$\cos\alpha_{ij} = (A_{1j} - X_{1j})/[(f_0 - 0.5)D + \delta_{ij}] \tag{12}$$

$$F_{ck} = \frac{1}{2}mD\omega^2\left(\frac{\omega_E}{\omega}\right)_k^2 \tag{13}$$

$$M_{gk} = J\omega^2\left(\frac{\omega_b}{\omega}\right)_k\left(\frac{\omega_E}{\omega}\right)_k\sin\alpha_k \tag{14}$$

$$Q_{ik} = K_i\delta_{ik}^{3/2}, \quad Q_{ok} = K_o\delta_{ok}^{3/2} \tag{15}$$

$$\alpha_k = \tan^{-1}(\sin\alpha_{ik}/(\cos\alpha_{ik} - h)) \tag{16}$$

$$\left(\frac{\omega_E}{\omega}\right)_k = \frac{\cos(\alpha_{ik} - \alpha_{ok}) - h\cdot\cos\alpha_{ok}}{1 + \cos(\alpha_{ik} - \alpha_{ok})} \tag{17}$$

$$\left(\frac{\omega_B}{\omega}\right)_k = \frac{1}{h\cos\alpha_k} \times \frac{-1}{\left(\frac{\cos\alpha_{ok} + \tan\alpha_k\sin\alpha_{ok}}{1 + h\cos\alpha_{ok}} + \frac{\cos\alpha_{ik} + \tan\alpha_k\sin\alpha_{ik}}{1 - h\cos\alpha_{ik}}\right)} \tag{18}$$

The main notations in above equations are [1, 2]: $B = r_i/D + r_o/D - 1$, α^0 is the initial contact angle (before loading) or free contact angle, R_i—radius to locus of raceway groove curvature centers, θ—misalignment angle, δ_a—relative axial displacement, δ_r—relative radial displacement, *m*—the mass of ball, J—inertial moment, F_{ck}—the centrifugal forces, M_{gk}—gyroscopic moments on bearing ball, ω_m—orbital speed or rotating ball that is in position ψ_k [1], ω_R—angular speed of ball, F_{ik} and F_{ok} are forces due to gyroscopic moment, M_{gk} is the gyroscopic moment of ball in *k* position and k_i, k_o the stiffness of contact due to Hertzian theory [1]. The subscript notation *r* stands for radial and *a* stands for axial.

In Newton-Raphson method, because Eqs. (1)–(4) are derivative in any point in $x = \{X_{1k}, X_{2k}, \delta_{ik}, \delta_{ok}\}$ variable (derivative of the first order and second order), the Jacobian is used to update x at each iteration. The detailed derivatives are calculated in [2]. The right terms from Eqs. (1)–(4), denote by 0 is replaced by y_i, i = 1, …, 4. As sequel, the update at step n + 1, depending at step n is given by:

$$\{x^{n+1}\} = \{x^n\} - [a_{ij}]^{-1}\{y^n\} \tag{19}$$

$$\{y\} = \{y_1\ y_2\ y_3\ y_4\}^{-1} \tag{20}$$

We observe that no constraints are included in Newton-Raphson method even some situation can arise from Eqs. (9)–(12), where trigonometric function must take the values in range [−1.0, 1.0].

3 Genetic Algorithm with Migratory Individuals

GA has been applied successfully for many optimization problems as efficient alternative to classic methods [18, 19]. A classic GA approach is proposed with improved convergence by migratory individual as solution to avoid the saturation in local minima and step out toward to global minima (GAMI). The main schema used by GAMI is presented in Fig. 3.

Each individual chromosome is constructed by four genes that codified binary be '0' and '1' all the values scaled linear

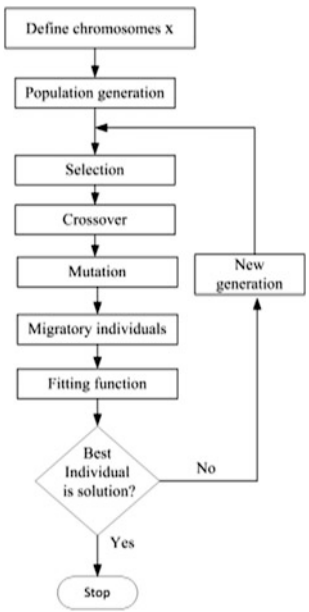

Fig. 3 Summary of GA used in solving the system on nonlinear equations with multiple dependencies

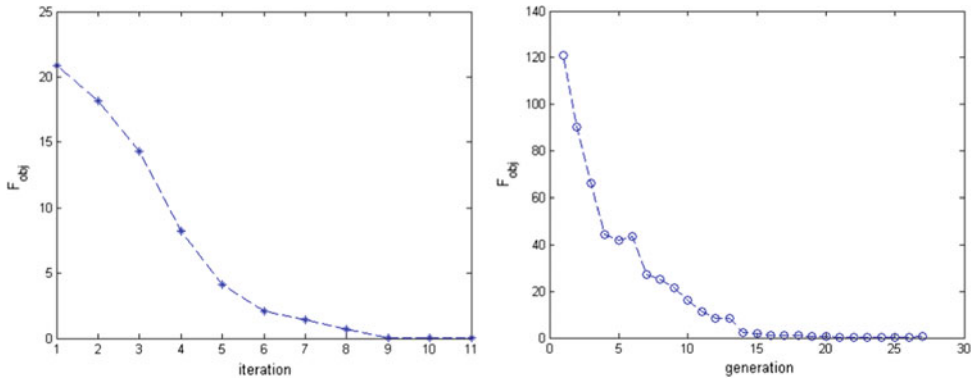

Fig. 4 Experimental results, best Newton-Raphson approach versus GAMI approach

of interval $[p_i\ q_i]$, the same for the first two variables (X_{1k}, X_{2k}) and the same but smaller with a lower order of magnitude for the last two variables (δ_{ik}, δ_{ok}). Using intervals populated with random values coded in chromosomes, the search of solution is extended from one set of initial values to an interval of values, which can improve the heuristic search for a solution of Eqs. (1)–(4).

In GA, the selection can be made by different algorithms and we have been chosen tournament selection. The two selected parents are subjects of crossover (the genetic information is combined) in order to generate new offspring (children). The four individuals are evaluated using the fitness function and the best two of them (elitist method) are selected as individuals in the next generation. The migratory individuals (p_y—percent of total population) introduces with a low probability by replacing the worst individuals in current population in order to expend the diversity of solution and avoid the local minima.

The fitness function in this case is chosen to be $F_{obj} = |y_1| + |y_2| + |y_3| + |y_4|$, and the objective of GA is to minimize F_{obj} toward zero.

4 Experimental Results

We start with an initial population of 100 individuals, $p_{crossover} = 0.35$, single point crossover, $p_{mutation} = 0.01$, $p_y = 4\%$, probability of migration $p_{mig} = 0.15$. After 27 generations and 11 iterations the results are shown in Fig. 4.

We can see that the results are similar but the iterative methods is selected as the best from 49 trials, meanwhile the GAMI give a performant solution in 18 generations from a single trial.

5 Conclusions

A usage of GA was proposed to solve a know problem from mechanics, as alternative solution to classic methods. The results are slight better in terms of computing time and iterations but clearly the results can be improved by extending the range of genes from chromosome.

The main advantage of the proposed solution is the avoiding of problem of initial value by a more relaxant one, the range of values.

Conflict of Interest The authors declare that they have no conflict of interest.

References

1. Harris, T.A.: Rolling Bearing Analysis, 4th edn. Wiley, New York (2001)
2. Cao, Y., Altintas, Y.: A general method for the modeling of spindle-bearing systems. J. Mech. Des. **126**, 1089–1104 (2005)
3. Bossmanns, B., Tu, J.F.: A power flow model for high speed motorized spindles-heat generation characterization. J. Manuf. Sci. Eng. **123**, 494–505 (2001)
4. Brecher, C., Shneor, Y., Neus, S., Bakarinow, K., Fey, M.: Thermal behavior of externally driven spindle: experimental study and modelling. Engineering **7**, 73–92 (2015)
5. Than, V.-T., Huang, J.H.: Nonlinear thermal effects on high-speed spindle bearings subjected to preload. Tribol. Int. **96**, 361–372 (2016)
6. Bossmanns, B., Tu, J.F.: A thermal model for high speed motorized spindles. Int. J. Mach. Tools Manuf. **39**, 1345–1366 (1999)
7. Bossmanns, B.: Thermo-mechanical modeling of motorized spindle systems for high speed milling. Ph.D. thesis, Purdue University (1997)

8. Samadli, V.: Rotor-bearing system dynamics of a high speed micro end mill spindle. Ph.D. thesis, University of Florida (2006)
9. Yanfang, D., Zude, Z., Mingyao, L.: A new model based machine tool spindle bearing preload optimization method. Int. J. Eng. Technol. **6**(11), 416–423 (2016)
10. Ben-Israel, A.: A Newton-Raphson method for the solution of systems of equations. J. Math. Anal. Appl. **15**(2), 243–252 (1996)
11. Antoine, J.-F., Abba, G., Molinari, A.: A new proposal for explicit angle calculation in angular contact ball bearing. J. Mech. Des. **128** (2), 468–478 (2005)
12. Goulianas, K., Margaris, A., Refanidis, I., Diamantaras, K., Papadimitriou, T.: A back propagation-type neural network architecture for solving the complete n × n nonlinear algebraic system of equations. Adv. Pure Math. **6**, 455–480 (2016)
13. Min, Z., Li, Y.: A novel ant colony algorithm of solving nonlinear equations group. IERI Procedia **2**, 775–780 (2012)
14. Jaberipour, M., Khorrama, E., Karimi, B.: Particle swarm algorithm for solving systems of nonlinear equations. Comput. Math. Appl. **62**, 566–576 (2011)
15. Djerou, L., Khelil, N., Aichouche, S.: Artificial bee colony algorithm for solving initial value problems. Commun. Math. Appl. **8**(2), 119–125 (2017)
16. Pourrajabian, A., Ebrahimi, R., Mirzaei, M., Shams, M.: Applying genetic algorithms for solving nonlinear algebraic equations. Appl. Math. Comput. **219**, 11483–11494 (2013)
17. Michalewicz, Z.: Genetic Algorithms + Data Structures = Evolution Programs. Springer, Berlin (1996)
18. Goldberg, D. E.: Genetic Algorithms in Search, Optimization, and Machine Learning. Addison-Wesley Professional (1989)
19. Price, K., Storn, R.M.: Differential Evolution: A Practical Approach to Global Optimization. Springer (2005)

Modeling of the Complex Walk Assist Equipment

Adrian Abrudean and Dan S. Mândru

Abstract

This paper presents aspects of modeling an original complex assistive system designed to work in two ways; first, ensuring mobility and second, assisting and regaining the ability to walk.

Keywords

Rehabilitation system • Assistive technology • Modeling • Gait trainer

1 Introduction

The ability to maintain bipedal posture is essential in performing daily tasks, social interaction with larger communities or tend to ordinary activities at home. Any deviation from normal walking and ability to maintain biped posture reduces the individual's ability to interact with the environment.

Disability is any reduction or lack of an ability (resulting from medical condition or accident) to perform an activity in the manner or level considered normal for a human being [1].

Assisting individuals with mobility deficiencies represents a facet of rehabilitation. The equipment specifically designed for this purpose are produced in a great variety of functional and constructive forms.

Rehabilitation is the third side of current medicine, along with prophylactic and curative medicine, also called (functional) recovery or reconstruction. Rehabilitation is the form of complex medical and social assistance, but at the same time unitary in conception, which is being carried out continuously and aims at the final reintegration of people with disabilities into society and family [2].

The basic principle of rehabilitation is to assist or even replace the remaining functions of the person with disabilities [3].

Assistive Technology (AT) includes products, services, equipment, tools and software that seek to offset functional limitations, facilitate independent living, and enable people with disabilities to reach their own potential. Assistive Technology refers to products, devices and services for those needs that are specific to three groups: disabled, elderly, and chronically ill [2].

Gait rehabilitation is an important step in the process of recovering and assisting people with mobility deficiencies.

2 Designing of an Assistive Device

The starting point for modeling a complex assistive device is to define the functions to be assisted or substituted. In this regard, it is presumed a waking disabled individual, for whom an assistive system must be developed to assist the patient during lifting from the seated position (verticalization), to ensure the person's access to different positions of the environment (mobility) assisting/resuming walking, as well as relearning functions and postural stability [4]. Figure 1 shows the sequence of body positions required to be reached with the assistive system in order to achieve the proposed objectives [5].

The kinematic diagram of the assistive device that meets the required criteria is shown in Fig. 2 [4, 5].

The numbered items are as following:

1. arm support;
2. double action distance adjustment system;
3. rotation system;
4. horizontal translation module;
5. vertical translation module;
6. power wheels;

A. Abrudean (✉)
Drive Medical SRL, Subcetate Str., No. 16, Bistrita, Romania
e-mail: adrianabrudean@yahoo.com

D. S. Mândru
Faculty of Mechanical Engineering, Technical University of Cluj-Napoca, Muncii Str., No. 103-105, Cluj-Napoca, Romania

S. Vlad and N. M. Roman (eds.), *6th International Conference on Advancements of Medicine and Health Care through Technology; 17–20 October 2018, Cluj-Napoca, Romania*, IFMBE Proceedings 71,
https://doi.org/10.1007/978-981-13-6207-1_38

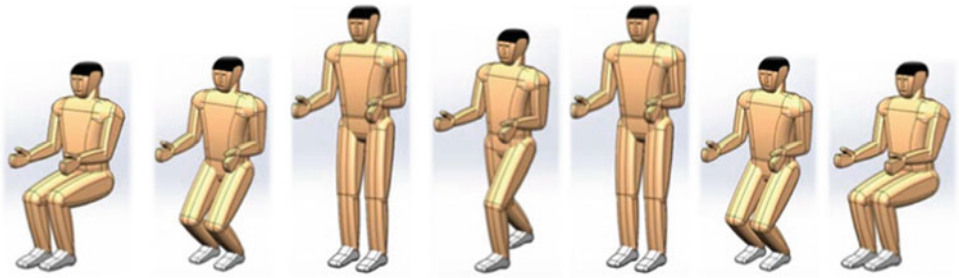

Fig. 1 Position sequence for gait assistance

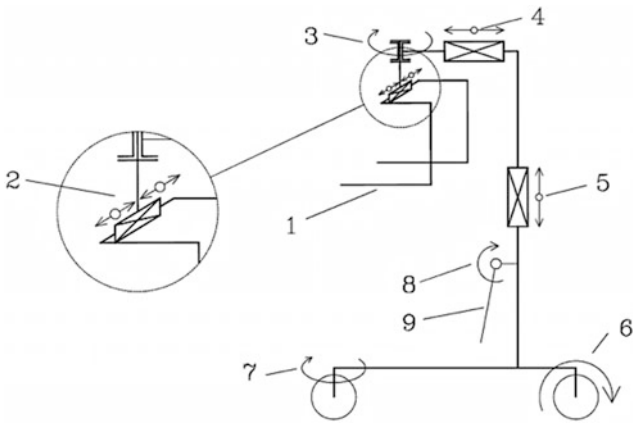

Fig. 2 Kinematic diagram of the assistive device

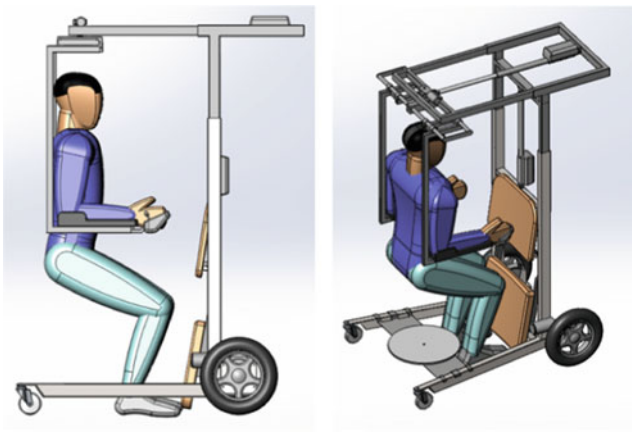

Fig. 3 Phase of positioning the system

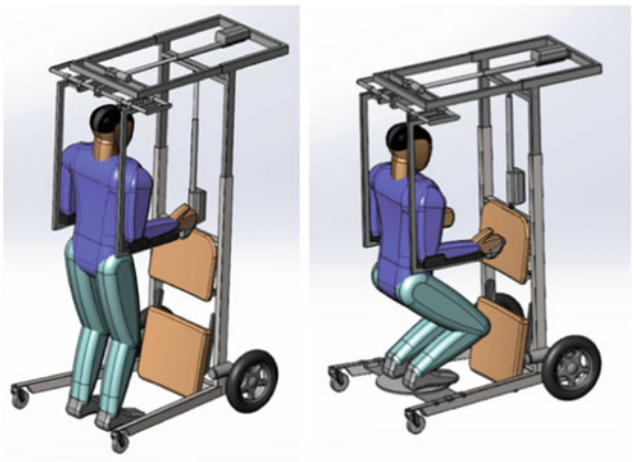

Fig. 4 Phase of standing up

7. idle turning wheels;
8. seat pivot point;
9. seat.

The assistive device is designed to work in two ways: in the mobility assistive and transfer function mode, shown by the right-hand figures, and as vertical posture and walking trainer, shown in the left-hand figures, but also providing the mobility and transfer functions [1].

The sequence of operations for device usage is shown below, being presented in parallel for the two modes of operation:

- the device is positioned in front of the seated subject. For the first mode, the subject places its feet on the rotatable support;
- the armrests are brought in place, a safety corset is put on, and the distance between the arm supports is adjusted so that the arms are rested on the supports as shown in Fig. 3;
- the body is lifted in upright position, as shown in Fig. 4;
- the patient is 180° rotated, as seen in Fig. 5;
- the patient is now facing the front, in upright position, as in Fig. 6;
- from here the patient uses the device either as a gait trainer (left-hand in Fig. 7) or is seated and can use the device as a mobility aid or as a patient transfer system (right-hand Fig. 7).

The device performs the movement and the user follows suit. The device works in closed feedback loop in two modes: the device moves by helping the subject to step, but monitoring the steps: if the subject stops the device stops. In the second mode the device starts the movement, but the travel velocity is defined by the subject's cadence. In this

Fig. 5 Phase of rotation

Fig. 6 Phase of stand up

Fig. 7 Phase of use

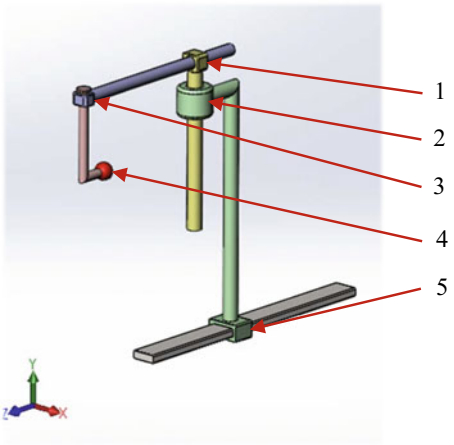

Fig. 8 Simplified kinematic diagram of the assistive device

way the subject is the generating signal of the movement. This second mode is used for subjects advanced enough [4].

In order to obtain information on the movement of the user in the transfer phase, a study of the movement of the user's mass center using a simplified system shown in Fig. 8 is carried out.

The following notations were used:

1. sliding horizontal joint;
2. sliding vertical joint;
3. cylindrical joint;
4. pacient center of mass;
5. sliding horizontal joint;

The motion sequence of the assistive device required for the patient transfer from seating to upright position is shown in Fig. 9.

On the Fig. 10 shows the anthropometric dimensions of the model used to simulate the movement, the anatomical dimensions resulting in the necessary displacement on the axes to make the transfer from the sitting position on the standing position.

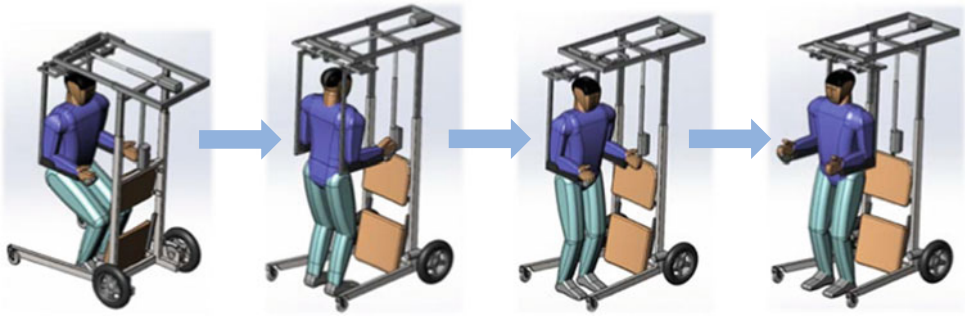

Fig. 9 Patient transfer from seating to upright position

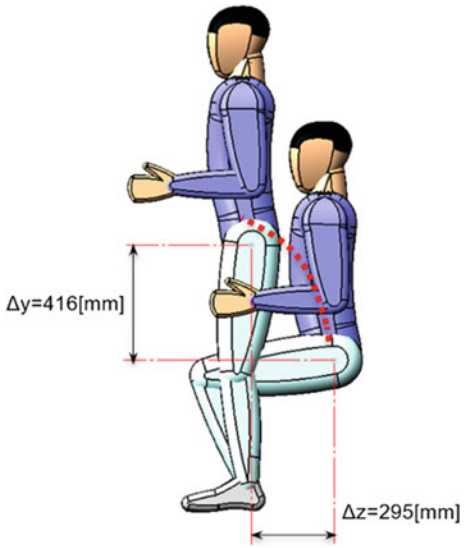

Fig. 10 Simulated patient transfer from seating to upright position with the simplified kinematic model

Using the simplified kinematic diagram, the same sequence is illustrated in Fig. 11.

Two translational movements and a rotational motion are required to effect the transfer. Using the Oxyz coordinate system with the orientation shown in Fig. 8, a translation on the Y and Z axes and a rotation around the Y axis is required to make the transfer between the two positions. The mass of the patient is considered 90 kg. The calculation time required for the transfer is considered 1 min, the timetable of the movements is shown in Fig. 12. The axle displacements considered for the analysis are: $\Delta Y = 416$ [mm]; $\Delta Z = 295$ [mm]; $\Theta y = 180°$.

The simulation of the transfer motion provides insight on the trajectory, velocity and mass center acceleration [4].

Figure 13 shows the projection of the trajectory on the Ox, Oy and Oz axes, and Fig. 14 shows the space curve described by the center of mass during the transfer phase.

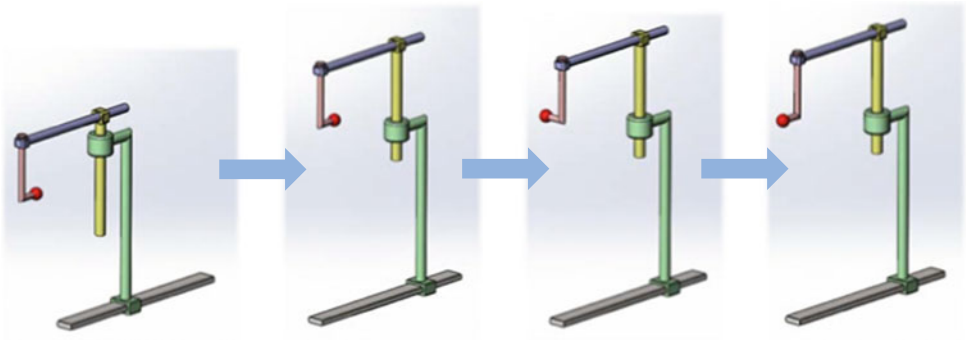

Fig. 11 Simulated patient transfer from seating to upright position with the simplified kinematic model

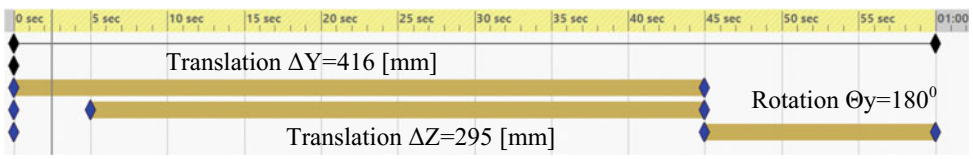

Fig. 12 Timetable for the motion sequence

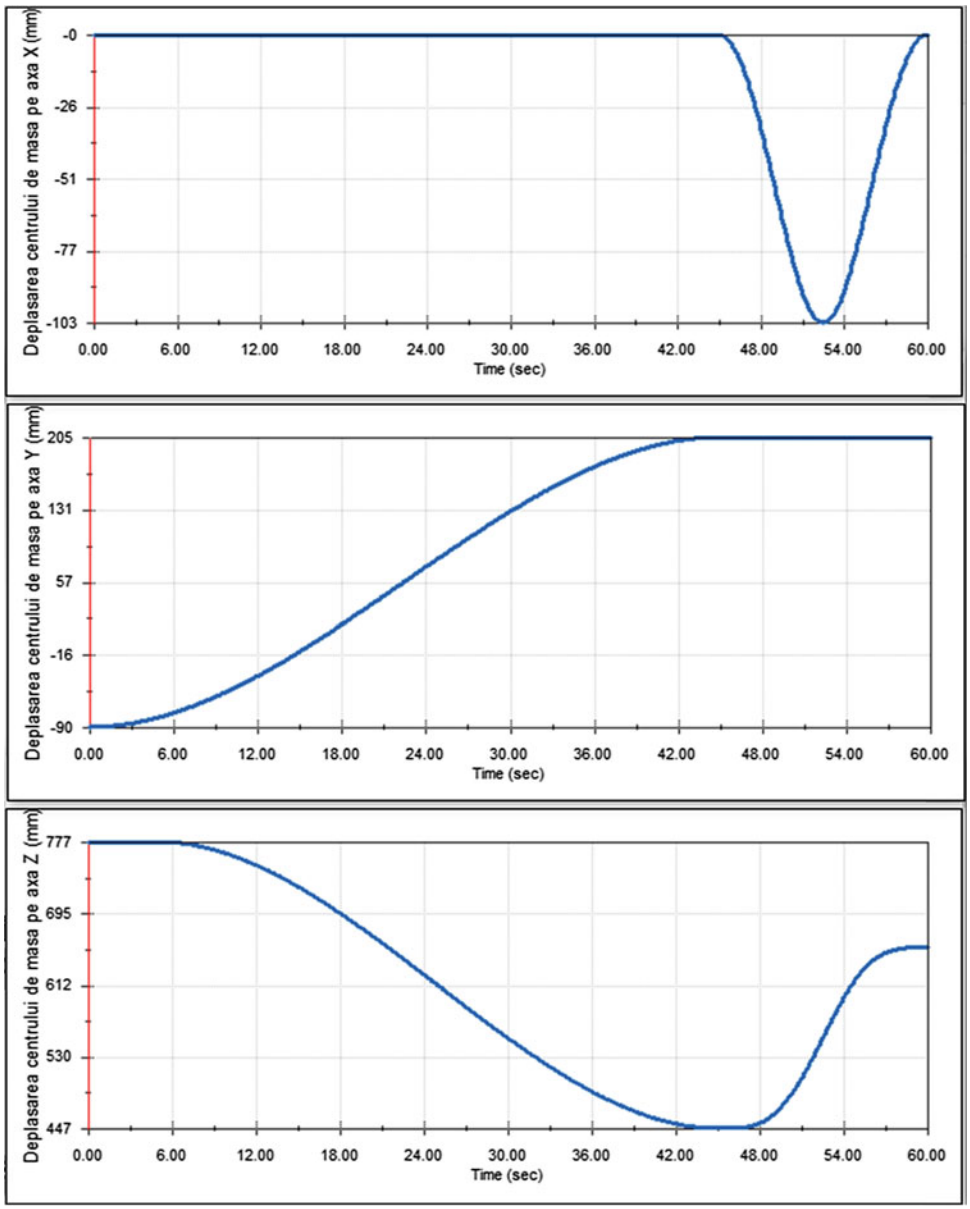

Fig. 13 Center of mass trajectory projected on Ox, Oy and Oz axes

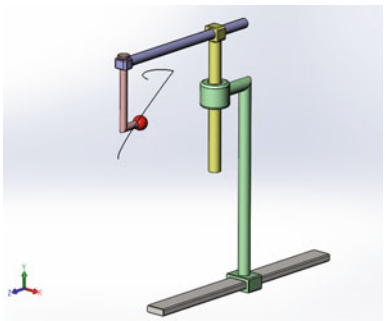

Fig. 14 Center of mass space curve trajectory

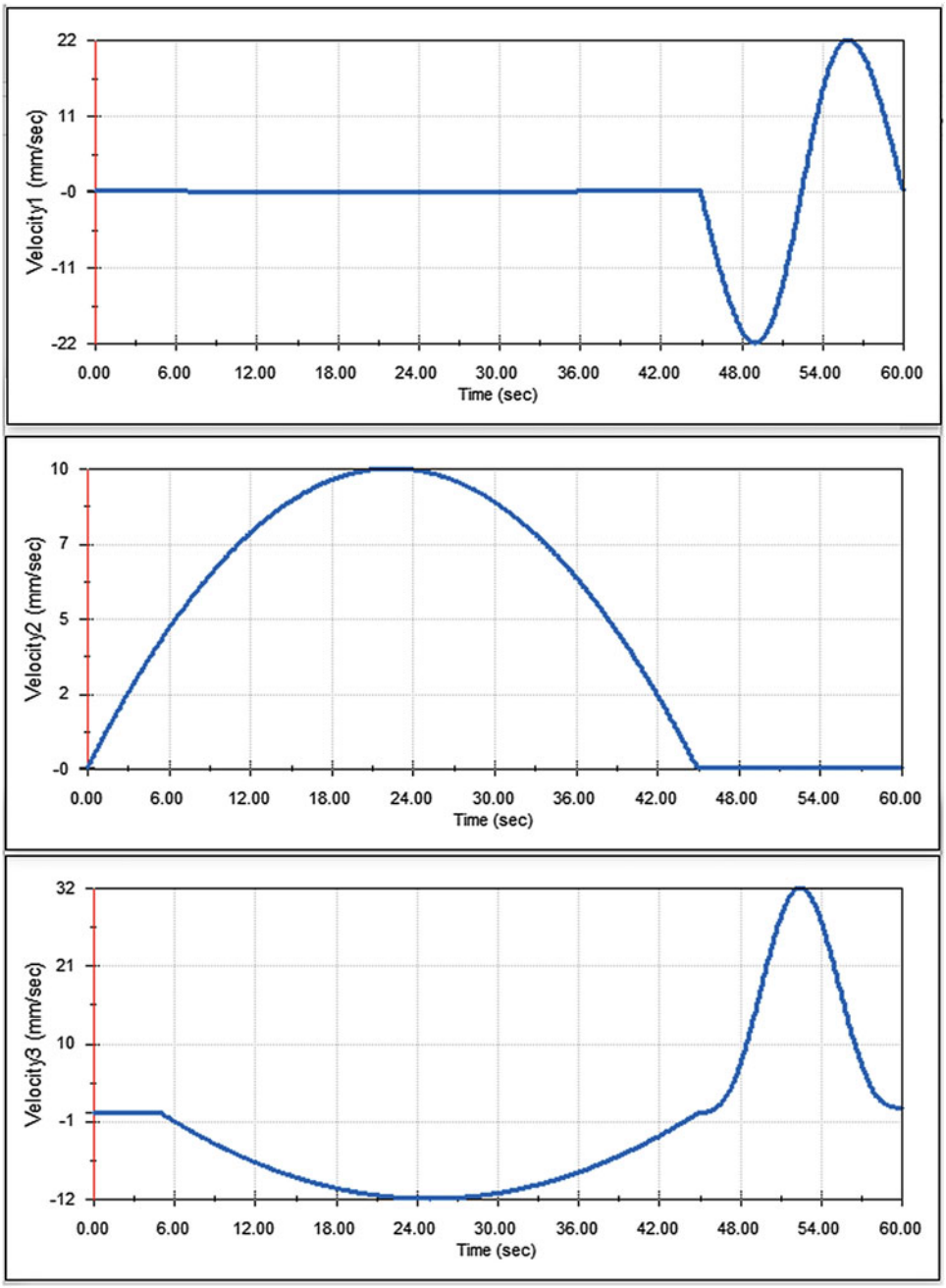

Fig. 15 Center of mass velocity projection on Ox, Oy and Oz axes

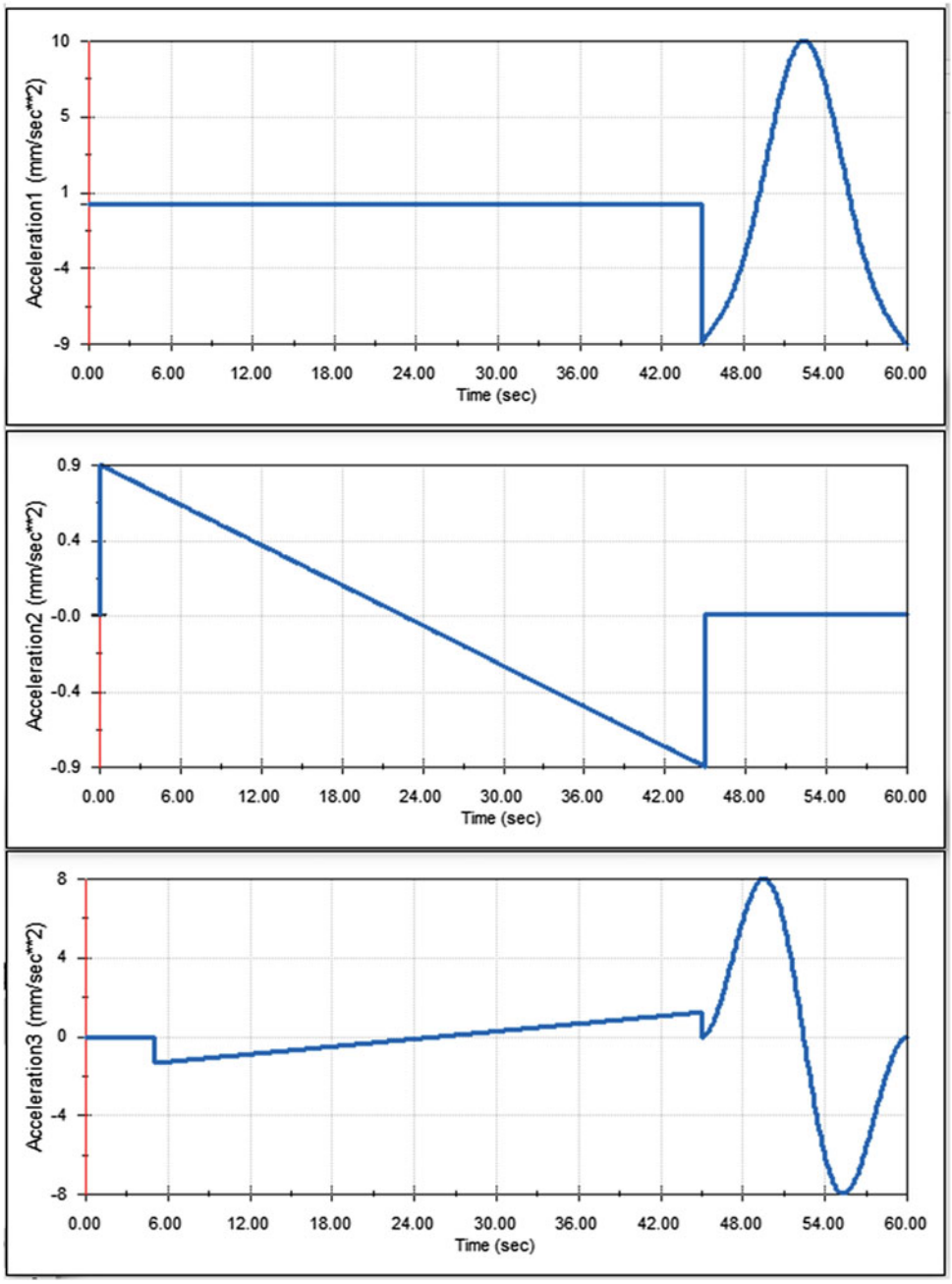

Fig. 16 Center of mass acceleration projections on the Ox, Oy and Oz axes

Figure 15 shows the velocity projection on the Ox, Oy and Oz axes, and Fig. 16 shows the acceleration projections on the Ox, Oy, Oz axes.

3 Conclusions

In general, assistive devices are complex systems that assist or substitute one or several functions.

The structure of the assistive device presented here is determined by the functions it must assist or substitute. These functions is the action of holding the body in a certain position and moving from one position to the other. This assistive device combines the functions offered by various assistive systems such as autonomous wheelchair, transfer lift, rollator and gait trainer.

The modeling and simulation of the device movements is a necessity for obtaining information about the requirements

to which the user may be subjected while using the assistive system.

Conflict of Interest The authors declare that they have no conflict of interest.

References

1. Bouri, M., et al.: The walk-trainer: a robotic system for walking rehabilitation. In: Proceedings of the 2008 IEEE International Conference on Robotics and Biomimetics, Kunming, pp. 1616–1621
2. Mândru, D., Crişan, N., Stan, S.: Echipament pentru asistarea mersului. Rom. Rev. Precis. Mech. Opt. Mechatron. **1**(20a), 391–396. ISSN 1220-6830 (2002)
3. Mândru, D., Ianosi-Andreeva-Dimitrova, A., Abrudean, A., Noveanu, S., Tătar, O.: Innovative assistive and rehabilitation robotic systems. J. Plus Educ. **XII A**(Special Issue), 30–34 (2015)
4. Abrudean, A.: Teză de doctorat „Dezvoltarea sistemelor specifice ingineriei de reabilitare", Iunie 2018
5. Abrudean, A., Stephen, S., Mândru, D.: Assistive and rehabilitation robotic system. Robotica Manage. **20**(1), 7–12 (2015)

Voice Controlled Wheelchair for People with Disabilities

P. Pop-Coman, N. M. Roman, M. Steopan, V. Ispas, S. Bugnar, and M. Olea

Abstract

Almost 15% of the planet's population (approximately 785 million people) suffer from mental or physical disabilities, with 5% of children in this segment, according to a report issued by the World Health Organization. In the whole world, the estimated number of wheelchair users is over 130 million people. It is estimated that only 5–15% of people in need of wheelchairs own and hold one. In countries with a life expectancy of over 70 years, people spend an average of about 8 years or 11.5% of their life, living with a disability [1]. To help people with movement disabilities who suffer from Tetraplegia (complete loss of lower and upper limb movements), we have made a voice-driven mobile platform for movement. The voice recognition system was adapted to a wheelchair and programmed to perform basic movements for patient movement. At the wheelchair used by us has been attached a sensor system to avoid impact with certain objects. For Voice Recognition we used the EasyVR voice recognition module and an Arduino Mega 2560 module. The power side for controlling the two engines was made with IGBT transistors.

Keywords

Voice control • Mobile platform • People with disabilities

1 Introduction

Disability should not be an obstacle to success [2].

Results of international studies show that there is a continuing increase in the number of elderly people with physical disabilities worldwide. With the aggravation of physical disabilities, these people are increasingly losing their autonomy and becoming dependent on the help of the caretaker and nursing staff in solving daily tasks. This situation can lead to the financial overload of the social system in question.

Thus, in the SMC, the user can intervene correctively in a self-executed action if an erroneous situation is detected.

As an example, the point-to-point bringing can be recalled to a selected final position. In the event of a collision hazard, the user can influence the trajectory by direct command.

One way to prevent this situation is to implement new technologies in the health assistance process. Moreover, the way people with a disability are related to society could be improved if we consider that the majority are fit for certain types of work and the only thing that prevents them is a detail related to the degree of access to a given environment or space, for example. The main application and the greatest impact is to promote the mobility of people with disabilities by solving the problem of limb movement and improving their lives by allowing access to buildings and urban space designed for people without disabilities. The European Commission has adopted a strategy to remove these obstacles.

The main objective of the project was to develop an integrated hardware and software platform for people with movement disabilities. By implementing this project, we are giving hope to persons with disabilities who are in special situations.

Robots are one of the promises of the future. Although the robot has not yet emerged to know and make it all, robotic mechanisms already know to perform a certain task very well.

Robotics, from the application point of view, can be divided into industrial robotics and service robotics.

If industrial robotics is already a well-saturated domain. Industrial robot applications generally have found a clear usage between industrial applications and in the near future there are no spectacular developments expected, while

P. Pop-Coman (✉) · N. M. Roman · M. Steopan · V. Ispas · S. Bugnar · M. Olea
Technical University of Cluj Napoca, Cluj Napoca, Romania
e-mail: popcomanp@yahoo.com

S. Vlad and N. M. Roman (eds.), *6th International Conference on Advancements of Medicine and Health Care through Technology; 17–20 October 2018, Cluj-Napoca, Romania*, IFMBE Proceedings 71,
https://doi.org/10.1007/978-981-13-6207-1_39

service robotics are in full swing and identification of new applications.

Following the introduction of simple commands, the system must be able to independently plan and execute a series of actions necessary to accomplish a particular task.

In the literature there is a unitary name for human-machine cooperation, known as shared-mode-control (SMC). Within SMC there is a continuous switch between the autonomous actions of the system and the direct command of the user [6, 7].

2 Development of the Project

The block diagram for voice control used in the project is shown in Fig. 1.

Microphone: It has a condenser type with the ready-made power system on the EasyVR module.

EasyVR Voice Recognition Module: Takes the analog audio signal from the microphone to our capacitor type, amplifies it, and sends it for analysis to an ADC converter. The signal is sampled, quantised, filtered and encoded in a digital sequence.

The voice recognition program is structured with two priority levels. In the first level, a single "ROBOT" command is introduced. This command prepares the robot for the following instructions (Fig. 2).

After the command "ROBOT" disconnects the electromagnetic braking system, a new instruction from the set of commands can be activated. The commands are recorded in the internal library of the EasyVR module. We have tried commands in Romanian, English and combinations to get a clear distinction between commands.

In the current library we loaded the voice tag that was assigned an identification number.

ÎNAPOI/BACKWARDS ====== 0,
DREAPTA/RIGHT ==== 1,
STÂNGA/LEFT ===== 2,

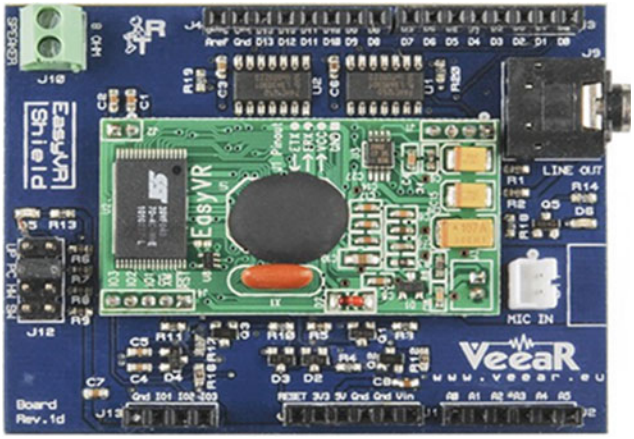

Fig. 2 EasyVR module [3]

ÎNAINTE/FORWARDS ===== 3,
STOP ======= 4,
ROBOTSTOP = 5,

None of the second level orders will be accepted before the first level passes.

The command, ROBOTSTOP will reset the robot to the first level of commands.

The ARDUINO MEGA2560 module: It is based on a microcontroller developed by Atmel "ATMEGA 2560" (Fig. 3).

Connecting the Arduino to the EasyVR module is simple. It consists in overlaying the two modules with pins already prepared in a father-mother configuration. Connecting to a PC is done through the USB plug and the Arduino programming software requires no cost. Because our mobile platform uses two electrical motors, through their combined control, you can get forward, reverse, left, right, swivel. For safety concerns there is an electromagnetic braking system.

The brake system is released in our case at the "ROBOT" main command and brakes the "ROBOT STOP" command. The program loaded on the Arduino module is presented later in the paper.

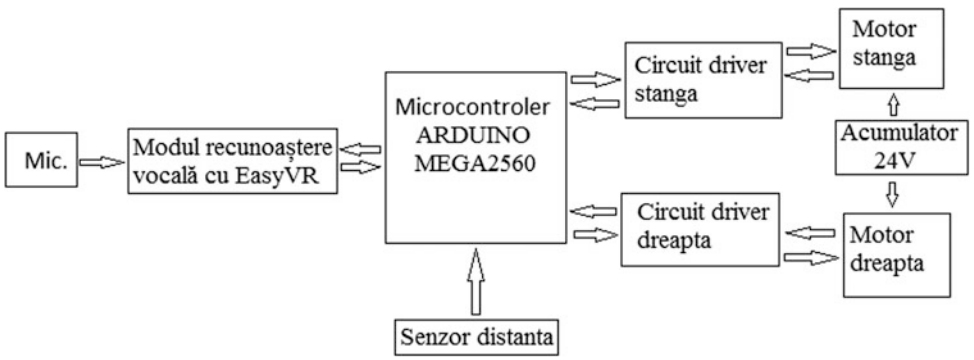

Fig. 1 Block diagram for voice control

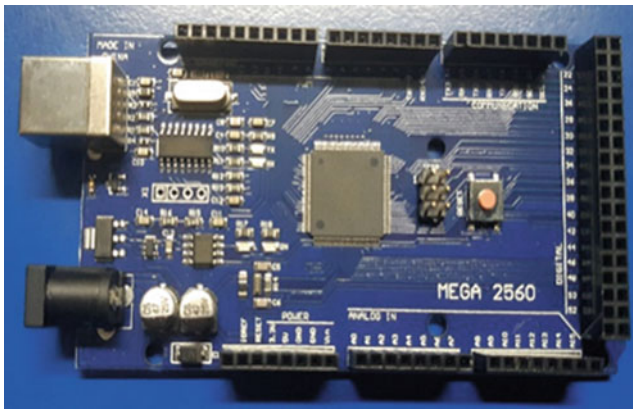

Fig. 3 ARDUINO MEGA2560 [3]

In the program we took into account the command history of the drive motors. If in the last command both engines were "on" and if the left command (right) was activated, after executing the new command the engines were set again on "on". We used the same procedure when the engines were "off".

In the case of the turn, we opted to stop one of the engines if the platform was in motion. If the platform was "off" the corresponding engine was turned counterclockwise.

Engine driver mode: The engine driver module required for supplying power to the motors was built using transistors. The diagram is presented in Fig. 4.

MOSFET transistors have the advantage of very low power consumption in the control circuit, but because of the high source drag–drain resistance, the losses are high.

On an IRFP360PBF mosfet transistor (N-Ch 400 V 23 A 280 W 0.2 R) which carries a 23 A current in the drain, the catalog gives a value of 0.2 Ω source drain-ON.

$$P = R^{*}I\hat{}2 = 105\,W \quad (1)$$

105 W is loss that dissipates in the form of thermal energy.

For a bipolar transistor like TYPE 35, the E-C voltage in the ON position is 1.8 V.

$$P = U^{*}I = 41\,W \quad (2)$$

For these reasons, I used a hybrid transistor that is voltage-controlled as a MOS transistor and the execution is done by a bipolar transistor, IGBT.

The IGBT is a semiconductor three-terminal power device mainly used as an electronic switch, and in new devices it has been noted for high efficiency and switching speed.

The IGBT transistor for engine speed control was commanded with a PWM signal generated by the Arduino module and for reversing the sense of the wheel motion we used a relay.

The printed wiring was photographed and designed with the Pad2Pad program (Fig. 5).

The coated circuit was prepared by coating the board with a photosensitive paint (POSITIV20) after its preliminary cleaning.

For clearing we used a low NAOH solution until the ultraviolet sensitive paint was removed. Corrosion was done using a $FeCl_3$ solution. After making the wiring, we went on to mounting and gluing electronic components (Fig. 6).

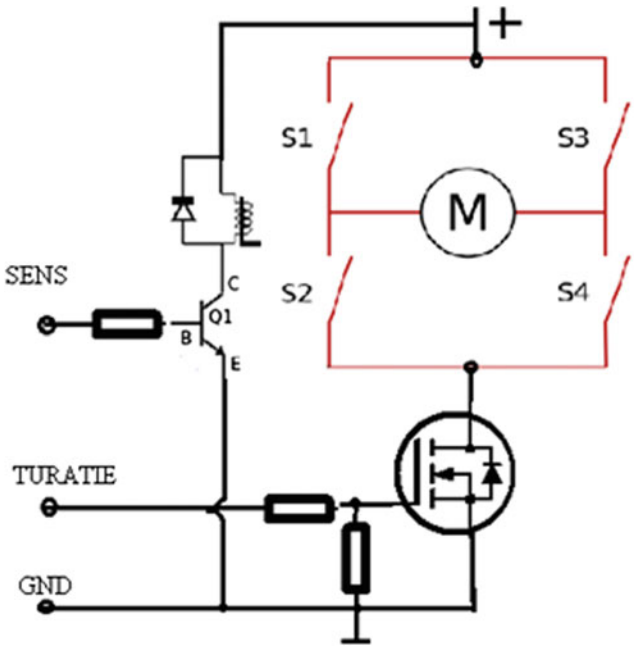

Fig. 4 MOS-FET transistor control

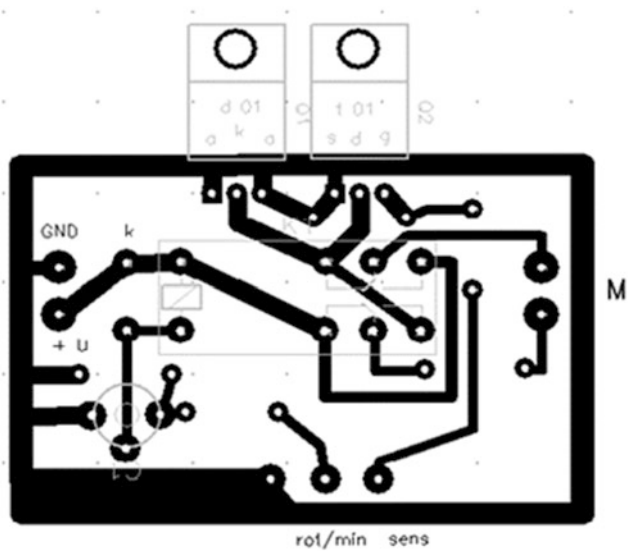

Fig. 5 Printed cable design

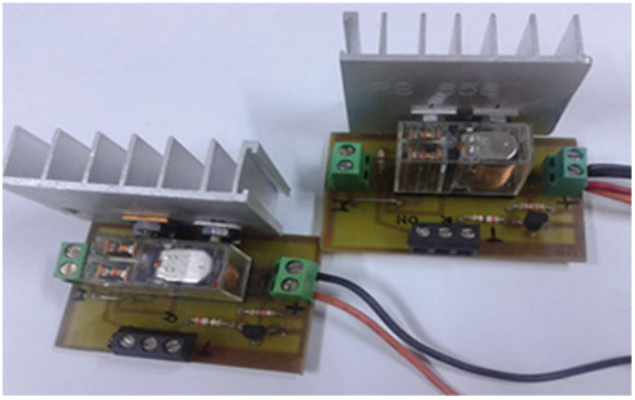

Fig. 6 Motor drivers

The output pins on the Arduino Mega2560 board used by us are:

1. 31 right engine speed control
2. 33 right direction control
3. 35 left engine speed control
4. 37 Left sense control
5. 41 pin electromagnetic brake control.

Since the signals generated by the microcontroller have values between 0 and 5 V and the mos transistor requires a high voltage in the grid, it was necessary to introduce into the circuit an optocoupler which also ensures the galvanic separation between the high voltage applied to the motors and the Arduino module (Fig. 7).

The electronic installation was first tested in the laboratory and subsequently mounted on a wheelchair (Fig. 8).

For our project we used a wheelchair powered by two DC motors with a power of 250 W each and power supply at 24 V (Fig. 9).

Remote sensor: we used in this project a Sharp GP2Y0A21YK infrared sensor for object detection (Fig. 10).

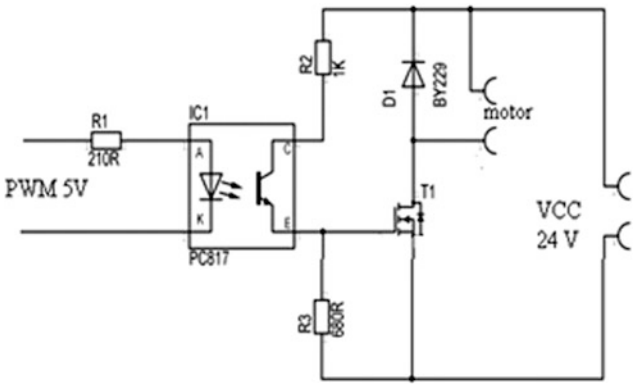

Fig. 7 Optical command diagram [5]

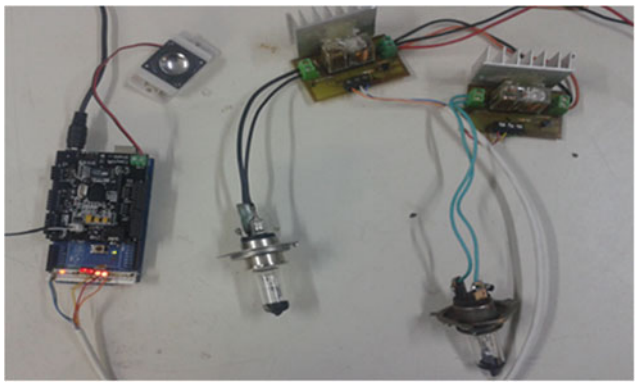

Fig. 8 Testing in laboratory conditions

Fig. 9 Test wheelchair

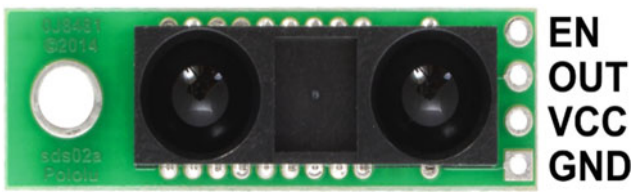

Fig. 10 Optical distance sensor [3]

The Sharp distance sensor can be used with Arduino to measure distance to various surrounding objects.

From the Sharp GP range there are 3 types of sensors with maximum efficacy on a particular area in terms of measured distance: proximity sensor, effective for measurements between 3 and 40 cm, average distance sensor, effective between 10 and 80 cm, and a 15–150 cm effective distance sensor.

The sensor we use is efficient between 10 and 80 cm, the distance that we are interested into avoid collision with various objects, considering that the speed of travel is low.

Because it is an analog sensor that generates variable voltage with the distance, connecting to Arduino is made on one of the analog inputs.

The device has 3 pins, two of which are supply pins (GND and VCC), and the third one is the pin that indicates the distance through the potential difference present on it.

The voltage/distance feature is illustrated in Fig. 11.

The sensor code given by the manufacturer is a simple one, does not use much of the CPU resources and does not affect the voice recognition program. An example of how to calculate the distance:

Arduino Program

```
void setup() {
  Serial.begin(9600);
}
void loop() {
  int valoareSenzor = readDistanceMediata(10, 0);
  Serial.print("Valoare senzor:");
  Serial.println(valoareSenzor);
  delay(100);
}
int readDistanceMediata(int count, int pin) {
  int sum = 0;
  for (int i = 0; i<count; i++) {
  float volts = analogRead(pin) * ((float) 5/1024);
  float distance = 65 * pow(volts, -1.10);
  sum = sum + distance;
  delay(5);
  }
  return (int) (sum/count);
}          [3]
```

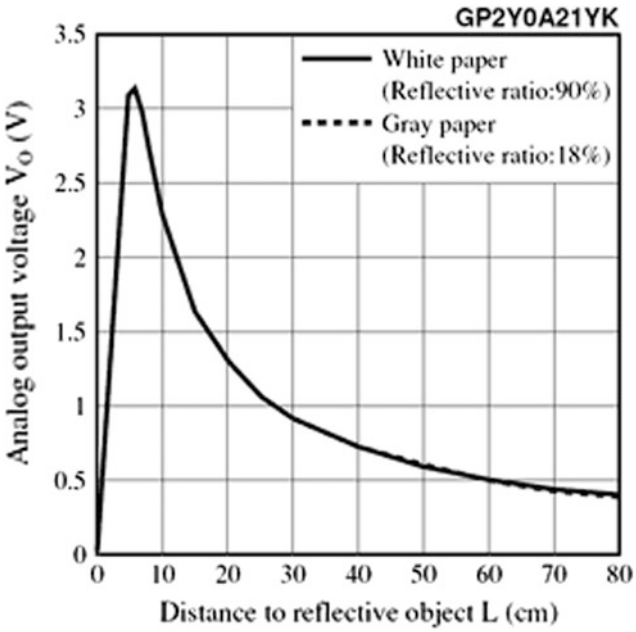

Fig. 11 Characteristic curve for Sharp GP2Y0A21YK sensor [3]

3 Experimental Results

Following tests, we made a voice-controlled robot for basic commands.

The main difficulty faced by voice recognition programs is that the voices of two people are not at all similar, and even the voice of the same person may vary in certain situations. Another problem is the rate OF speech recognition.

In all voice recognition programs, mistakes can sometimes be made. Microsoft claims that 95% of the words are recognized correctly, that is, just one word out of twenty is wrong. There are some apps with better performance, but none exceeds the 97% rate [4].

The design is designed in such a way that it can be mounted on any wheelchair that uses C.C. and can also be adapted to wheelchairs or other platforms that use special motors with small changes to microprocessor-based software.

4 Conclusions

By implementing this project, we are giving hope to persons with disabilities who are in special situations.

The proposed solution is accessible especially because these people do not have high incomes to invest in sophisticated platforms.

In the proposed project, we have not rebutted the rules of security and protection, especially since the people using such a device cannot take care of themselves.

The novelty in the project consists in the fact that a good result was achieved by programming a microcontroller that has been used for a long time in the industrial robots' market.

Voice control also has drawbacks such as:

- Sensitivity to environmental noise
- Inability to use in cases of diseases that degrade the voice.

Connecting the microcontroller with the power side was done with minimal effort, resulting in a low price.

It is very important that other extensions are developed in the future such as:

– Foot control if only upper limbs are affected,
– Tongue or eye control if there are more serious conditions that can be implemented on the same microcontroller (which has open gates).

It is also necessary to monitor heart rate, breathing, blood pressure, etc. for people with these conditions, applications that can be further deployed on the same module that controls voice commands.

Conflict of Interest The authors declare that they have no conflict of interest.

References

1. http://2013.incluziune.org.ro/biroul-de-presa/informatii-si-statistici
2. Organizația Mondială a Sănătății, Raport mondial privind dizabilitatea 2011. ISBN 978-973-0-13597-8
3. Arduino pentru incepatori. www.robofun.ro
4. https://www.news.ro/economic/sistemul-de-recunoastere-vocala-dezvoltat-de-microsoft-a-ajuns-la-fel-de-eficient-ca-omul-19224018190020161009156023 42
5. Hurgoi, D.: Modernizarea si Controlul Proceselor de Fabricatie. Casa Cartii de Stiinta, Cluj-Napoca (2013)
6. Toderean, G., Căruntu, A.: Metode de Recunoaștere a Vorbirii. Risoprint, Cluj-Napoca (2005)
7. Giurgiu, M., Peev, L.: Sinteza din Text a Semnalului Vocal. Risoprint, Cluj-Napoca (2006)

Rehabilitation of Orthopedic and Neuropsychological Complications After Hip Arthroplasty

A. M. Culai, P. Mihancea, and I. Onac

Abstract

After hip arthroplasty can occur morphological, functional and psychological complications, as a result of a complex of determinants. Preserving a good quality of life must be our first aim. Rehabilitation is one of the major key in preventing and treating. From a health perspective, the existence of one or more limitations due to physical or mental impairment, has a major impact over the quality of life is strictly related and reduced well-being during illness.

Keywords

Hip arthroplasty • Pain • Rehabilitation • Dysfunctional attitudes

1 Introduction

After total/partial hip arthroplasty, the quality of life is an essential component in postoperative rehabilitation. Each person's quality of life [1] is strictly related to their ability to influence the environment, to influence daily life. Whatever definition we accept, complication after hip arthroplasty certainly is a factor contributing to the reduction of the quality of life by limiting the mobility of the patient, thus limiting social contact, by pain that often occurs [2].

The main complication from orthopedic and neuropsychological perspective are pain and the adaptative mechanisms of emotive reaction for chronical patients which suffered a hip arthroplasty [3] according to Hip Society [4]. The goals are achieved through the emergence of mechanisms that ensure optimal functionality of the hip joint, in terms of mobility, decreasing pain and functional walking [5–7].

On the other hand to analyse in terms of disease response neuropsihologic is a useful method in quantifying the level of health and quality of life after Hip Arthroplasty behavior is adaptive. So emotions are dependent variable with which we describe a series of changes at many levels. Consequences of stress appear as after-effects of long-term chronic reactions [8]. Investigating the physiological mechanisms and consequences of stress, [9] demonstrates that stress involves both adaptation and stimulation and body wear. in this context, distress is generated by limiting the information processing capacity owing to either inadequate cognitive skills, either an excess or deficiency of the informational self esteem as part of cognitive patterns represents an overall assessment of yourself [10] and it's the combination of the resultant value evaluation and the ability to achieve a goal. Having a tendency to assess negatively, by anticipating actually terminates, this kind of negative affects patients will live, through anger, depression or anxiety. Mental health contains as a feature and the level of self-esteem, this may be interpreted as a good predictor of well being.

Research ethics the study was approved by the Council of Ethics of Recovery Hospital Cluj-Napoca, respecting the integrity, confidentiality and personal data protection of the persons included in the study. Also, all the patients who participated in the study signed the informal consent to use and publication of the results obtained during their assessment for research purposes.

2 Objectives

In our approach we've gone from need to interpret the condition of chronic patient, by a plurifactorial model which integrates the analysis of changes of functional and neuropsychological parameters. We have taken into account the effect biomechanical and psychological factors, namely pain

A. M. Culai (✉) · I. Onac
"Iuliu Haţieganu" University of Medicine and Pharmacy Cluj-Napoca, str Aleea Negoiu nr 8D, Cluj-Napoca, Romania
e-mail: anamaria.culai@yahoo.com

P. Mihancea
Faculty of Medicine Oradea, Oradea, Romania

S. Vlad and N. M. Roman (eds.), *6th International Conference on Advancements of Medicine and Health Care through Technology; 17–20 October 2018, Cluj-Napoca, Romania*, IFMBE Proceedings 71,
https://doi.org/10.1007/978-981-13-6207-1_40

and psychosocial parameters as measurement units of psychological response [11], and for the second study we intend to investigate the quality of life of patients after hip arthroplasty at different time intervals, by analyzing variables such as: distress, perceived self-efficacy, self-esteem, dysfunctional attitudes and automatic cognition depending on the time elapsed time from measurements (immediately after the surgery, more than a year after the surgery). The aim was to establish these differences in impairment of quality of life [12]. Settling this frameworks we thing we set out to demonstrate that physical therapy programs (before and after surgery) are effective by decreasing clinical complaint (failure and pain) Active rehabilitation leads to optimize the results and quality of life after hip arthroplasty. The approach from the perspective of medical psychology of the patient with a hip prosthesis is not only useful but also necessary, in the context of primary and tertiary prevention of the complications that may occur.

3 Materials and Methods

Participation in the study was voluntary, based on established inclusion and exclusion criteria. The assessment tools were used before surgery (day hospital patient) and after surgery (one month, respectively on and a half month). The questionnaires were done in pencil-paper format, complying with the standard procedures provided.

A. For the first study, a number of 55 patients admitted to the Rehabilitation Hospital Cluj-Napoca, between January 2016 and January 2018. Evaluation was made in different period of time (before surgery, 30 and 90 days after).
   The inclusion criteria were: patients programmed for hip arthroplasty without other major pathology, with the diagnosis of primary coxarthrosis unilateral surgical stage (Sect. 4). Exclusion criteria were: acute phase of the disease, intens pain, lack of cooperation. Assessment tools were: score the balance function assessment Harris Score. Criteria: pain (maximum 44 score), (lamenes, with support, walking distance, max score 33), activity (max 13), biomechanical parameters (changes in flexion, internal rotation, Member: adductive, inequality score 4), mobility (flexion, abduction, adductive, internal rotation, external rotation-6). Points accumulate a maximum total of 100.
   VAS scale: on a scale of 0–10, where 0 represents the absence of pain and the 10 most intense pain is felt, a horizontal line which included painful perception level, with high level of reliability and validity. Scales are variants of Physiotherapeutic predictor programs carried out pre surgical, 30 day and 90 days after, pain, functional impotence, results of measurements. With this instruments functionality was analyzed by determining the control statistics, the predictive value of the independent variables [4].
B. The research has been in the form of a controlled clinical trial with two-sample design compared between pairs. In setting the volume of the sample taken into account methodological criteria relating to the power of the test. The criterion for inclusion, (to participate in the study) was represented by the situation of a prosthetic hip with any psychiatric problems.
   Survey participants are 40 subjects who fulfilled the conditions for inclusion, at different intervals of time operator (0–1 year more than 1 year). Customer results in parallel has conducted a study of control, comparison was made with the applied standards of clinical scales. 20 of subjects were patients that were admitted for total hip arthroplasty, the other lot of 20 subjects were admitted on the Balneology section of Rehabilitation Hospital Cluj Napoca. Interval-was March 2016 to April 2017. The tools of the method were PDA (Distress Affective Profile), SS (Self Esteem Scalar), SES (Self Esteem Scale), DAS (Scale of Dysfunctional Attitude) and ATQ (Automatic Thinking Questionaire) from SEC (System of Clinical Evaluation) [4]. Those were the instruments applied to analyzed: the affective distress profile, self-esteem scale [8, 13]. Self esteem coping attitude must be for certain evaluated in order to make a holistic image over the status of an patient with hip arthroplasty.

4 Results

4.1 Results for the First Study

Descriptive statistical results obtained for evaluation before surgery VAS scales, 30 days after and 90 days after the surgery, between batches of patients who performed kinetic programs and those programs haven't. The results reveal that physical therapy programs explain 33.5% of the variation of VAS Score Harris, 29.6% variation. F values were obtained (2.49) = 12.46 (p = 0.001) and F (2.49) = 9.00 (p = 0.001). Application of individualized programmes leading with an average of 7.22 points to Score Harris, decreasing by an average of 17.87 estimated pain within the VAS Scale Table 1.

Table 2 shows the results obtained for the variable mobility and gait. To score Harris, mobility variable predicts 15.8% of variation F (2.49) = 4.56 (p = 0.016). For VAS, 7.6% predict the mobility variable from variation, F (2.49) = 2.05 (p = 0.14).

Table 1 Regression coefficients for Medical variables (Score Harris Scale VAS)

Parameters	Score Harris	VAS
Predictor	Kinetoprograms	
Non-standardized		
Coefficients B	7.259	−17.927
Standard error	1.508	4.345
t	4.815	−4.126
P	0.001	0.001
95.0% confidence		
Interval B		
Inferior limit	4.229	−26.658
Interval B		
Superior limit	10.288	−9.195

Table 2 Regression coefficients for walking (Score Harris)

Parameters	Score Harris
Predictor	Kinetoterapeutical programs
Non-standardized	
Coefficients B	−15.560
Standard error	6.173
t	−2.511
P	0.016
95.0% confidence	
Interval B	
Inferior limit	−28.000
95.0% confidence	
Interval B	
Superior limit	−3.098

Table 3 Regression coefficients for medical variables 90 days after surgery (Score Harris Scale VAS)

Parameters	Score Harris	VAS
Predictor	Kinetoprograms	
Non-standardized		
Coefficients B	−683	1.288
Standard error	0.109	0.401
t	−6.002	3.099
P	0.001	0.003
95.0% confidence		
Interval B		
Inferior limit	−0.911	0.448
Interval B		
Superior limit	−489	1.888

Table 3 shows the regression analysis in which the variables are physical therapy programs. Both scores are predicted if the patients continue standardized programs of physical therapy. Describe F (3.48) = 16.38 (p = 0.001). For variable pain we have obtain (t = 3.18, p = 0.003).

The only significant variable remains kinetic programs, according to this statistical model. Preoperative physical kinetic programs, added to a postoperative rapid mobilization of the patient, will provide a better hip functionality recovery.

4.2 Results for the Second Study

Regression testing was performed by introducing the SPSS for Windows software (version 16): initial testing of the most common predictors, and then by statistical testing of all predictors. We obtained a predictive model in which the variables were significantly altered, a statistically significant difference, $p < 0.03$ for functional emotions. At the threshold $p < 0.01$ a statistically significant difference for self-esteem, perceived self-efficacy, dysfunctional attitudes.

The two averages obtained were compared by t Test.

There is also a statistically significant difference between the level of functional negative emotions recorded by subjects and the general population.

There are differences between the two groups of patients (immediately after surgery and after a period of time—more than 1 year) in terms of quality of life. The t test was calculated to compare the average of the patients who were admitted for total/partial hip arthroplasty and those who were more than one year ago. Table 4 shows the mean values and the standard deviations for dependent variables in the study.

Although the differences between the dysfunctional emotions recorded immediately after surgery and those at least one year apart are not statistically significant, there is a tendency to decrease them after one year, while the functional emotions tend to increase (Table 5).

In other words, the meaning is the regaining of the quality of life, to distinct the level of self-confession only as a tendency to reduce the distress.

This study has indicated that from the point of view of self-esteem, distress, and dysfunctional attitudes, endo-prosthetic patients that suffered also complications, have a lower quality of life than the general population. Even more than a year after surgery, there are differences in perceived self-efficacy, but fortunately negative emotions are decreasing. Also after one year, self-esteem and dysfunctional attitudes again show some stability [4].

Table 4 Descriptive statistics for life quality variables

Parameters	No	Average	Average	df degree test	t	Predictability of standard	
ATQ	40	29.4250	28	HB9	858	0.396	
SS	40	23.9000	31	39	−20.051	0.000	
SES	40	27.3750	30	39	−3.757	0.001	
DAS	40	160.9500	142	39	6.216	0.000	
PDA	40						
Disfunctional	26.9750	25	39	1	0.057	0.0297	
PDA							
Functional	40	28.2000	23	39	3	0.295	0.002

Table 5 Variable of life quality

Variable	Groups	N	Average	Standard deviation
SS_Total	Recent	20	23.8000	22.2504
	Over 1 year	20	23.9000	24.0394
SES_Total	Recent	20	25.8500	42.2222
	Over 1 year	20	28.6000	41.3612
Saddnes_Functional	Recent	20	13.5000	56.8331
	Over 1 year	20	14.8500	4.86976
Sadness_Disfunctional	Recent	20	15.0000	8.08927
	Over 1 year	20	13.8700	6.76462
Fear_Functional	Recent	20	14.7000	5.15446
	Over 1 year	20	15.6000	4.86115
Fear_Disfunctional	Recent	20	12.0000	5.00325
	Over 1 year	20	13.4500	5.09789
Positive-emotions	Recent	20	40.5500	8.87620
	Over 1 year	20	39.8000	6.09418
DAS_Total	Recent	20	15.7500	15.44239
	Over 1 year	20	16.1500	22.83182
ATQ_Total	Recent	20	30.9000	11.99956
	Over 1 year	20	27.9500	8.82863
Total_Functional	Recent	20	27.9500	10.70403
	Over 1 year	20	28.4500	9.47281
Total_Disfunctional	Recent	20	27.6000	12.61328
	Over 1 year	20	26.3500	11.25903

5 Discussions

The rate of success in this type of surgery is demonstrated in all analyses of literature. However about 15% of cases are reported with complications, pain and functionality are on top [14]. The aim of this study was to develop a predictive model of the functional parameters. In this sense, we have achieved an exploratory regression analysis. The following variables were selected: pain, kinetic programs, mobility, testing of measurements obtained. Regression analyses were also carried out for the different time periods (before surgery, at 30, 90 days after surgery), and was achieved through statistical control. The results of the study are similar to the literature data, and physical therapy programs shows effective rehabilitation after hip arthroplasty. Increased physical activity has a good therapeutic efficacy, facilitate recovery. Predictive model takes in consideration as criterion of Scale

VAS-pain-34.6% this explains the variable. In this model, though programs have significant benefits and increased recovery. Patients have to cope not only with the physiological and psychological stresses that precede surgery [15], but also with the requirements of the recovery process [16]. The degree of pain and joint mobility after surgery, they both influence independent functioning and are influenced by patient expectations [11]. Chronic pain is the most common complication of any major surgery. It is the major cause of dysfunction and maladaptative reactions..

6 Conclusions

All this predictive factors must be evaluated in the moment of taking the decision of hip arthroplasty. The type of surgery and the preparation of the joint by kinetic programs are very important.

A limit of the studies is related to their application to independent, not longitudinal samples, the inter-individual differences may influence the results.

Another limit of the study is related to the control group. These subjects were not selected by randomization, but only after meeting inclusion criteria.

In the post-surgery phases, quality of life was positively influenced by changes in VAS parameters, inducing an increase of physical functioning. Walking patients after Hip Arthroplasty can be corrected by means of the application of the programs, though kinetic.

The implication of the second study can aim to improve the relationship between those patients taking into account dysfunctional attitudes.

The first study was a follow up between results with those obtained in the same clinic, regarding quality of life after hip arthroplasty [17]. The particularity in our case refers to a model of prediction for avoiding, as much as is possible complications such as pain and functional.

The conclusion of those studies are similar and lead us to the necessity of treating our patients from a holistic and interdisciplinary perspective, in the benefit of our patient, his life expectancy and quality of life.

Conflict of Interest The authors declare that they have no conflict of interest.

References

1. Hollon, S., Kendal, P. (2007)
2. Carver, C.S., Scheier, M.F., Weintraub, J.K.: Assessing coping strategies: a theoretically based approach. J. Person. Soc. Psych. **56** (2), 267–283 (1989)
3. Garellick, G., Malchau, H., Herberts, P.: Specific or general health outcome measures in the evaluation of total hip replacement: a comparison between the Harris Hip Score and the Nottingham Health Profile. J. Bone Joint Surg. Br. **80**, 600–606 (1998)
4. https://doi.org/10.1007/s11999-015-4341-7: Complications of total hip arthroplasty: standardized list, definitions, and stratification developed
5. King, L.: Case study: physical therapy management of hip osteoarthritis prior to total hip arthroplasty. J. Orthop. Phys. Therapy. (1997)
6. Steinberg, M.E., Lotke, P.A.: Postoperative management of total joint replacement. Orthop. Clinic. Norh. Am. (1988)
7. Antonescu, D.M.: Patologia Aparatului Locode recuperare, Edit. Medicală, Bucureşti, 1987. motor vol. II, Edit. Medicală, Bucureşti, p. 847 (2010)
8. Elliot (1982)
9. Selye (1968, 1980)
10. Rosenberg, 1965
11. Filip, N., Balazsi, R., Ciulei, R., et al.: Studiu comparativ al evoluţiei pacienţilor cu artroplastie totală de şold practicată pe abord chirugical minim invaziv vs. clasic: date preliminarii. Clujul Med. **85**, 476–482 (2012)
12. David, Holdevici, Szamoskozi, Băban (2000)
13. Macavei, B.: Dysfunctional attitudes scale, form a; norms for the romanian population. J. Cogn. Behav. Psychother. **6**(2) (2006)
14. Pablo et all; Vilardo and Shah, 2011
15. Filip, N., Ciulei, R., Pocol, P., Georgescu, A.: Palestrica Mileniului III—Civilizaţie şi Sport, vol. 13, no. 3, pp. 234–240. Iulie-Septembrie 2012 (2012)
16. 19:3, 307–320, https://doi.org/10.1080/0887044042000193460
17. Wiklund, I., Romanus, B.: A comparison of quality of life before and after arthroplasty in patients who had arthrosis of the hip joint. J. Bone Joint Surg. **73A**, 765–769 (1991)

Robotics in Minimally Invasive Procedures: History, Current Trends and Future Challenges

C. Vaida, N. Al Hajjar, V. Lazar, F. Graur, A. Burz, R. Elisei, E. Mois, and D. Pisla

Abstract

Cancer is considered as the disease of the XXI century being still one of the deadliest afflictions even though continuous advancement is achieved in the treatment of different malignances. In parallel with the technological progress minimally invasive therapies like radiofrequency, ablation, and targeted drug delivery attempted to provide methods that minimize the side effects while maximizing the therapeutic impact. Taking into consideration the number of elderly people that is expected to increase over the years to come, cancer therapies must progress to ensure a real improvement of the quality of life. This paper is an overview of the evolution and challenges of robotic systems for minimally invasive procedures (MIP) that covers both surgical and non-surgical therapies for cancer diagnosis and treatment. A benefit of using robotic assisted MIP in cancer treatment is the high precision/low adjacent damage to neighboring tissues which supervised by different real-time monitoring solutions represent the cornerstone in the future advancement of cancer treatment technologies.

Keywords

Robotic assisted minimal invasive procedures • Cancer diagnosis and treatment • Needle guided procedures

C. Vaida · V. Lazar · A. Burz · D. Pisla (✉)
CESTER, Technical University of Cluj-Napoca, Memorandumului 28, Cluj-Napoca, Romania
e-mail: doina.pisla@mep.utcluj.ro

N. Al Hajjar · F. Graur · R. Elisei
University of Medicine and Pharmacy "Iuliu Hatieganu" Cluj-Napoca, Cluj-Napoca, Romania

E. Mois
Regional Institute of Gastroenterology and Hepatology "Octavian Fodor", Cluj-Napoca, Romania

1 Introduction

Robotics has slowly entered every domain where progress-imposed activities/actions that were beyond the natural capabilities of humans. The most relevant example in this sense is the industry with all its branches where the higher and higher level of quality and output capacity have imposed the use of specialized devices that could perform faster and more reliable.

However, there are other fields of work, where classical industrial robots cannot be integrated, imposing the development of personalized, dedicated solution which would fit perfectly a certain task. Such case is the medical field where, especially when talking about direct interaction between the robot and the patient, the robot will never act based on pre-defined programs but rather as an advanced, highly capable, accurate and safe human controlled device.

In medicine, notable achievements which refer to the use of robotics for different tasks date from the early 80s whereas today there are multiple situations where robotic assisted procedures represent the gold standard for a continuous increasing number of medical treatments.

Making a generic comparison between an industrial manufacturing process where robots have been introduced to increase the productivity and thus the financial efficiency, in medicine the main purpose of a robotic device is to improve the quality of life for the patient. One of the most difficult tasks is to properly identify the medical areas where the need of robotics is most dire and then, to find development solutions that will lead towards efficient medical outcomes.

One of the major changes with multiple implications in the field of healthcare is represented by the demographic changes of the population. More specifically, Europe is facing an increase of the life expectancy whereas, if in 2008 the population aged over 65 represented something around 17% this will increase to over 30% by 2060 while the population aged over 80 will shift from 4.4% to over 12% (EUROSTAT projections). Even on national level, a

S. Vlad and N. M. Roman (eds.), *6th International Conference on Advancements of Medicine and Health Care through Technology; 17–20 October 2018, Cluj-Napoca, Romania*, IFMBE Proceedings 71,
https://doi.org/10.1007/978-981-13-6207-1_41

comparison between the last two demographic evaluations there is a reported increase of over 20% of the elderly population (aged over 60).

While it is clear that the elderly population has a greater tendency towards different medical conditions, the healthcare system will slowly become incapable of providing proper care for all the patients, while aiming towards a continuous increase of the life quality. On the positive side, some of the existing studies have already raised these issues and solutions are thought to prepare the society for the future [1].

The European Commission [2] through the Eurobotics AIBSL forum has identified three major areas of interest where robotics would play an important role:

Clinical robotics: robotic systems that interact directly with the patient supporting the "care" and "cure" processes.

Rehabilitation: robotic system that would interact with the patient in order to enhance a recovery process or act as a replacement for a lost function.

Assistive robotics: refer to secondary aspects related to the medical process, providing assistance to the healthcare givers of the patients.

This paper is organized as follows: Sect. 2 presents a brief description of the evolution of surgical robots, the most important milestones, challenges and some considerations regarding the RCM concept (remote center of motion), followed by a classification of minimally invasive procedures. Section 3 describes a short overview of the challenges in the non-surgical approaches for cancer diagnosis and treatment and robotic needle guided procedures with furthermore developments in Sect. 4 on medical robotic structures developed within CESTER. Future challenges in minimally invasive robotic assisted procedures are presented in Sect. 5.

2 Surgical Robots-Evolution and Challenges

2.1 Brief Description of Milestones, Concept of RCM

Clinical robotics covers three major areas of intervention: surgery, diagnosis and therapy. The overall potential for clinical robotics is huge because their development would bring benefits in virtually all areas medical specialties aiming to boost the overall outcome of the procedures.

The main area of intervention where surgical robots fit is minimally invasive surgery (MIS); the first documented minimally invasive procedure dates back from 1901 when Kelling [3] reported the results of a procedure performed on a dog model where he attempted to control the blood loss in the abdomen by insufflation of high pressure air in the abdominal area.

Following this pioneering age, the 20th century was the birth of minimally invasive surgery with a continuous development of surgical tools, vision systems and along with them techniques that would gradually change the way surgery is performed.

Like many other pioneering technique, it took some time for MIS to be widely accepted in the operating room, but slowly it became the gold standard for most procedures performed in the abdominal area.

The evolution of robotic surgery is somehow similar, with its major milestones and share of criticism during the early stages of development. One of the first documents which describes the idea of robotic surgery and also defines the particularity of the motion of such devices was published by Russel Taylor in 1995 [4]. In his paper Taylor introduces the concept of Remote Center of Motion (RCM), defining the entrance point in the abdomen as a fixed point within the workspace of a surgical robot, through which the instruments are introduced inside the human body (Fig. 1). Based on Fig. 1, it can be stated that with respect to point B (the entry point in the patient body) the instrument can achieve 4 independent motions:

- In spherical coordinates: two rotations that would position the point E on a surface of a "sphere" with radius BE, one translation along the A-B-E segment or the longitudinal axis of the instrument and one rotation around the same axis;
- In Cartesian coordinates: three translations which enable the positioning of the point E in space with respect to the point B and one rotation around the longitudinal axis of the instrument.

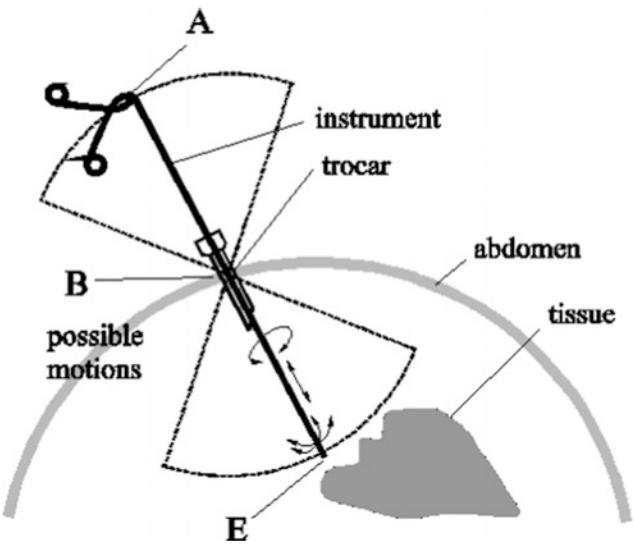

Fig. 1 The motion of a surgical instrument inside the human body in MIS [5]

Furthermore, the instruments used in the MIS can be grouped in two categories:

- The endoscopic camera (the laparoscope, Fig. 2): which is basically a device which has a set of lenses and a camera on top which with the help of a light source provides intra-operatory images during the procedure—this device will not enter into physical contact with the internal organs;
- Surgical instruments (Fig. 3): surgical tools of different complexity, which have at the distal head a special configuration that allows the performing of a certain procedure and a special handle at the opposite end from which the surgeon operates the instrument.

1985 was the first year in which a robot, a modified PUMA 560, was used for medical purposes and later used as a prototype for the FDA approved Neuromate in 1999.

In 1992 was developed at the University of California and IBM a robot for hip surgery. The robot has five joints and integrated sensors which check the robot's position and the forces of the cutting head.

Da Vinci surgical robot got FDA approval in 2000. It is able to perform complex minimally invasive surgery being controlled by a surgeon from a console.

A modified Zeus robotic system was used for the first telesurgery in 2001. This means that a surgeon can perform a procedure from a different location than the one of the patient's.

University of Calgary physicians, nurses and scientists in collaboration with Canadian space engineering developed a system designed to take advantage of the MRI so that real-time images and robotic technologies could be coupled. This system, NeuroArm, launched in 2007, is able to give the surgeon image guidance, precision, dexterity and it was used for the first time in 2008.

Fig. 2 Laparoscopic camera (left—viewing angles, right—proximal head) [6]

Fig. 3 Different types of laparoscopic instruments [7]

2.2 Classification of Minimally Invasive Procedures

Advancing hand in hand with technology, minimally invasive robotic assisted procedures have evolved in the last years towards multiple new approaches that can be classified into two main categories:

- Pure minimally invasive surgical procedures that aimed a continuous reduction of scaring and collateral damage while maximizing the surgical outcome;
- Minimally invasive non-surgical techniques that provide specific treatments for patients where surgery is not an option, with emphasis on targeted cancer treatment.

3 Non-surgical Minimally Invasive Robotic Assisted Procedures for Cancer

3.1 A Short Overview of the Challenges: Early Detection Is Better but Harder

Cancer, considered the disease of the XXI century, is one open problem in which every progress means a step forward in the fight between life and death. The fight against cancer has two main components strongly interconnected: diagnosis and treatment. An early, accurate diagnosis can provide the means for local targeted treatment of the tumors with excellent life expectancy. Thus, the proper diagnosis and staging of cancer [8, 9] is the first step towards a positive prognosis for a cancer patient.

The current standard has high percentages of false negative results in early stages supporting the worldwide efforts in finding new, accurate ways of diagnosis for this disease.

3.2 The Two Main Areas of Robotic Usability: Diagnosis and Treatment

Cancer Diagnosis. Described in a very roughly way, it refers to the identification of malignant tumors that grow inside the body. There are several imagistic, non-invasive methods, (CT and MRI and their derivate) which provide high contrast and high-resolution images of the internal structure of the body, but they have certain limitations [10] (identifying the nature of the tumor, the correct indication of the cancer stage, etc.) whereas the most conclusive investigation remains the biopsy of the tissue.

Cancer treatment. Considering the deadly character of cancer, therapies aim to optimize the treatment in such a way that its toxicity is eclipsed by the benefits of the procedure. The curative treatment involves multiple procedures for the same cancer such as: surgery, radiation, chemotherapy, each with its drawbacks. The palliative treatment for patients with advanced cancer stages might be considered too invasive or too costly to be justified. Nowadays cancer treatment can be divided in two main categories: local targeted treatment, (brachytherapy [11, 12], radiofrequency ablation [13–16] and wide spread treatments (external radiation, chemotherapy).

A reasonable conclusion for the enhancement of cancer treatment would be to perform accurate early diagnosis to identify potential malignant tumors in early stages and to perform local targeted treatment to destroy the tumors in both curative and palliative approaches.

3.3 Needle Guided Procedures

To provide a clear overview of the targeted treatments, the procedures are shortly presented:

- Biopsy: the prelevation of tissue from inside an organ by using a special needle [17] (core biopsy needle or aspiration needle)—schematic view (Fig. 4a);
- Brachytherapy: the positioning of radioactive seeds (with high but locally distributed radiation) directly in the tumor with minimal damage to the proximal healthy tissues (Fig. 4b);
- Radiofrequency ablation: the ablation of a tumor using the heat generated from a high frequency alternating current [18], (Fig. 4c).

Brachytherapy, also known as internal radiation, enables the delivery of higher doses of radiation to more-specific areas of the body, compared with the conventional form of radiation therapy (external beam radiation) that projects radiation from a machine outside the body. A very high dose can be delivered to a well-defined area, without damaging the healthy tissue in the immediate vicinity (Fig. 5).

However, the precision of the radioactive placement is crucial, as a geographical miss of a part of the tumor might cause a recurrence, whereas inserting the catheters outside the tumor will profoundly and uselessly irradiate healthy tissue, inducing necrosis and severe complications.

4 Medical Robotic Structures Developed Within Cester

Within the Research Center for Industrial Robots Simulation and Testing (CESTER), one of the main fields of research is represented by medical robotics, whereas in the last 10 years, multiple national premieres were achieved:

- PARAMIS is a parallel robot with 3 degrees of freedom (DOF), which has been developed for laparoscopic camera positioning. The control input allows the user to give commands in a large are of the laparoscope using different interfaces such as: joystick, microphone, keyboard and mouse, haptic device [22];
- PARASURG-5M is a hybrid parallel robot used to guide either a laparoscope or an active surgical instrument. The control input allows the user to give commands in a large

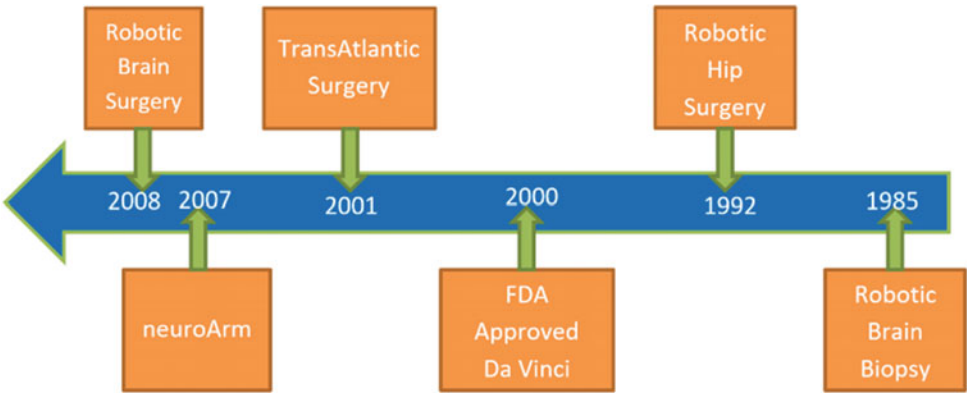

Fig. 4 Timeline of milestones in medical robotics

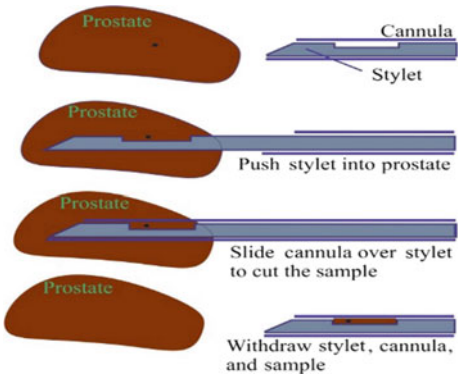

(a) Core needle biopsy[19]

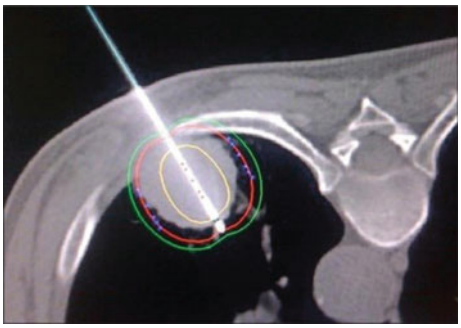

(b) Brachytherapy needle [20]

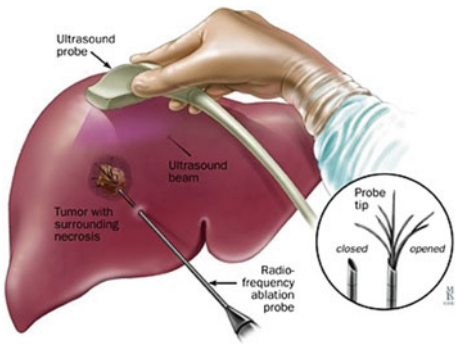

(c) Radiofrequency ablation [21]

Fig. 5 Needle guided procedures in the diagnosis and treatment of cancer. **a** Core needle biopsy [19], **b** brachytherapy needle [20], **c** radiofrequency ablation [21]

area for the positioning of the laparoscope using different interfaces: Joystick; Microphone (laparoscope only); keyboard & mouse; haptic device (active instruments) [23];

- PARASURG-9M is a versatile robot, being composed of a positioning and orientation module, PARASURG-5M having the possibility of attaching at its end either a laparoscope or an active surgical instrument for cutting/grasping, PARASIM, with four DOF robot [23];
- PARA-BRACHYROB is a parallel robot with 5 DOF developed for needle positioning and orientation towards the insertion point of the patient body in MIS procedures [24];
- BIO-PROS-1 is a parallel robot for transperineal biopsy of the prostate. Each module has 5 DOF and two redundant DOF for the simultaneous control of the biopsy needle and the ultrasound probe [19].

5 Future Challenges in Minimally Invasive Robotic Assisted Procedures

Hepatocellular carcinoma (HCC) is the most common primary malignant tumor of the liver. HCC represents more than 5% of all cancers localizations on a world scale, the number of newly diagnosed cases exceeding 782,000 (2012), being the fifth malignant localization in the male and the ninth in the female. Although diagnostic and therapeutic options have made substantial progress in recent years, HCC is the second leading cause of death by neoplasia, producing about 746,000 deaths annually in the world. The number of HCC deaths per year is almost equal to the incidence, confirming a high lethality index (0.93/1). Surgical resection of HCC is a curative therapeutic option but only applicable to 20% of patients with HCC for various reasons related to the disease (location, size, multicenter form, residual functional reserve, etc.) or patient (other associated diseases, acceptance, general state etc.).

Other therapeutic options for the remaining 80% of the tumors refer to techniques which aim to destroy the malignant cells without removing them from the body:

- Brachytherapy;
- Radiofrequency ablation;
- Delivery of chemotherapeutic drugs which target only the malignant cells.

All these approaches, which have proven their medical efficiency, share a common white spot which prevents their use in the treatment of HCC: a device capable of positioning the instruments inside the tumors, in a safe way.

To answer this challenge a consortium which integrates engineers, surgeons and chemists has been setup in a joint effort to develop a robotic device capable of positioning specialized tools (needles) inside the hepatic tumors with high accuracy and real-time ultrasound (US) monitoring.

The overall procedure has three main stages:

Preoperative: procedure pre-planning based on imaging-molecular diagnosis (by associating techniques and image processing algorithms with medical data) which defines the therapeutic approach and the optimal needle trajectory (ies);

Intraoperative: the minimally invasive treatment of the tumor;
Postoperative: efficient, non-invasive monitoring of the procedure results and patient evolution.

Due to the procedure complexity the therapy has to be performed inside the operating room, using a total of three independent medical instrument:

- a manually guided endoscopic camera used to enable the fast transfer of the US probe in the area of interest of the liver and the visual evaluation of the surgical field;
- a robotic guided US probe that would be used to locate the tumor (based on preoperative data) and to monitor the needle insertion;
- a robotic guided arm capable of positioning the therapeutic needle on the liver parenchyma and then insert it inside the tumor under US guidance.

Without any loss of generalization several characteristics for the robotic system can be defined as critical requirements for a successful procedure, reuniting most of the achievements in robotic assisted MI therapies:

1. The use of independent, reconfigurable RCMs for each robotic arm;
2. Efficient force feedback for both instruments, where in case of the US probe a contract pressure too high would lead to tissue deformation while for the needle this would induce deflection [20];
3. Independent user—interface options for each arm: the US probe imposes highly dexterous free motions to locate the tumor and align the probe in the desired plane, while the needle must be inserted based on pre-defined sets of coordinates, on linear (safe) trajectories;
4. Efficient alignment between the US head and the needle (in order to visualize the needle, it must be inserted in the incident plane of the US probe);
5. The robot must drive both instruments through holes of 3, 5 or 10 mm (while this is straight forward for the US probe, imposing only that all the actuation elements must be positioned outside the body, the needle driving module must be designed to comply to these constraints);
6. A supplementary guiding element in the liver proximity for the needle—due to the use of the US probe and the endoscopic camera, the patient will be inflated with CO_2 to create a virtual volume for the instruments; however, as compared to classical needle guided procedures where the entire length of the needle inside the body is maintained firmly by surrounding tissues, here the needle will pass through an empty volume that will lower its stiffness in the most critical point (the penetration of liver parenchyma);
7. Compliance with other equipment in the operating room and fast removal in case of patient decompensation.

6 Conclusions

The paper provides an overview that emphasizes the need for robotics in the healthcare field dedicated to new developments in the MIS. Furthermore, the history and evolution of medical robotics is presented with the highlight of important milestones achieved in healthcare robotics, as well as medical robotic structures developed within CESTER. The current challenges, such as the requirement for high precision instrument manipulation inside the patient body during surgery is an important requirement for any robotic MIS device. Another interesting topic presented in this paper includes the development of a robotic device capable of positioning specialized drugs inside the hepatic tumors with high accuracy and real-time ultrasound monitoring described in the last section of the paper which represents the focus of the IMPROVE project.

Acknowledgements This work was supported by a grant of the Romanian Ministry of Research and Innovation, PCCCDI—UEFISCDI, project number PN-III-P1-1.2-PCCDI-2017-0221/59PCCDI/2018 (IMPROVE), within PNCDI III.

Conflict of Interest The authors declare that they have no conflict of interest.

References

1. Shrivastava, S.R.B.L., Shrivastava, P.S., Ramasamy, J.: Health-care of elderly: determinants, needs and services. Int. J. Prevent. Med. **4**(10), 1224–1225 (2013)
2. Multi-Annual Roadmap: https://www.eu-robotics.net/sparc/upload/about/files/H2020-Robotics-Multi-Annual-Roadmap-ICT-2016.pdf. Accessed on September 2018
3. Kelling, G.: Die Tamponade der Speiseroehre und des magens mit beigsamen instrumenten. Verdhandlungen der Gesellschaft Deutscher Naturtorscher und Aerzte. Vogel verlag (1901), Leipzig 73, pp. 117–119
4. Taylor, R.H., et al.: A telerobotic assistant for laparoscopic surgery. IEEE Eng. Med. Biol. **14**, 279–287 (1995)
5. Vaida, C., Gherman, B., Pisla, D., Plitea, N.: A spherical robotic arm for instruments positioning in minimally invasive medical applications. In: The 2nd IFToMM Asian Conference on Mechanism and Machine Science November 7–10, Tokyo, Japan (2012)
6. http://www.neomed.com.uy/portfolio/image1-hd/. Accessed Sep 2018
7. Hpnonline.com: [online] Available at: https://www.hpnonline.com/ce/pdfs/1409cetest.pdf. Accessed Sep 2018 (2018)

8. Filson, P.C.: Improvement in clinical TNM staging documentation within a prostate cancer quality improvement collaborative. Urology **83** http://dx.doi.org/, https://doi.org/10.1016/j.urology.2013.11.040 (2014)
9. Meerbeeck, J.P., Janssens, A.: The seventh tumour–node–metastasis staging system for lung cancer: sequel or prequel? Eur. J. Cancer Suppl. **11**(2) (2013)
10. Verma, S., et al.: Overview of dynamic contrast—enhanced MRI in prostate cancer diagnosis and management. AJR Am. J. Roentgenol. **198**(6). https://doi.org/10.2214/ajr.12.8510 (2012)
11. Shah, C., et al.: The American brachytherapy society consensus statement for accelerated partial breast irradiation. Brachytherapy **12**(4). https://doi.org/10.1016/j.brachy (2013)
12. Kharofa, J., et al.: 3-T MRI-based adaptive brachytherapy for cervix cancer: treatment technique and initial clinical outcomes. Brachytherapy **13**(4). https://doi.org/10.1016/j.brachy (2014)
13. Van Tilborg, M., et al.: Long-term results of radiofrequency ablation for unresectable colorectal liver metastases: a potentially curative intervention. Brit. J. Radiol. **84**(1002), http://dx.doi.org/10.1259/bjr/78268814 (2014)
14. Kennedy, T., et al.: Laparoscopic radiofrequency ablation for the management of colorectal liver metastases: 10-year experience. J. Surg. Oncol. **107**(4). https://doi.org/10.1002/jso.23268 (2013)
15. Birsen, O., et al.: A critical analysis of postoperative morbidity and mortality after laparoscopic radiofrequency ablation of liver tumors. Ann. Surg. Oncol. **21**(6). https://doi.org/10.1245/s10434-014-3526-8 (2014)
16. Vogl, T., et al.: Thermal ablation therapies in patients with breast cancer liver metastases: a review. Eur. Radiol. **23**(3). https://doi.org/10.1007/s00330-012-2662-4 (2013)
17. Lee, Y.N., et al.: Core biopsy needle versus standard aspiration needle for endoscopic ultrasound-guided sampling of solid pancreatic masses: a randomized parallel-group study. Endoscopy **46** (12). https://doi.org/10.1055/s-0034-1377558 (2014)
18. Neagos, H., Graur, F., et al.: The contribution of technology in cholangiocarcinoma treatment. IFMBE Proc. **36** https://doi.org/10.1007/978-3-642-22586-4_39 (2011)
19. Pisla, D., Tucan, P., Gherman, B., Crisan, N., Andras, I., Vaida, C., Plitea, N.: Development of a parallel robotic system for transperineal biopsy of the prostate. Mech. Sci. **8**(1), 195–213 (2017)
20. Sharma, D., Thulkar, S., Pandit, S., Rath, G., Bahl, A., Julka, P.: Computerized tomography-guided percutaneous high-dose-rate interstitial brachytherapy for malignant lung lesions. J. Cancer Res. Ther. **7**(2), 174 (2011)
21. South Florida Sugical Oncology: Liver Tumors & Liver Cancer. [online] Available at: https://southfloridasurgicaloncology.com/liver-tumors/. Accessed Oct 2018 (2018)
22. Pisla, D., et al.: PARAMIS parallel robot for laparoscopic surgery. Chirurgia **105**, 677–683 (2010)
23. Pisla, D., et al.: PARASURG hybrid parallel robot for minimally invasive surgery. Chirurgia **106**(5), 619–625 (2011)
24. Pisla, D., Cocorean, D., Vaida, C., Gherman, B., Pisla, A., Plitea, N.: Application oriented design and simulation of an innovative parallel robot for brachytherapy. V05BT08A012. https://doi.org/10.1115/detc2014-35047 (2014)

Part VI
Health Technology Assessment

The Influence of Socio-Demographic, Psychological and Medical Variables on Patient Satisfaction with Diabetes Care in the Hospital Setting in Romania

Anca Constantinescu-Dobra, A. Sabou, and M. C. Coțiu

Abstract

Diabetes is a chronic illness in which disease management is crucial in preventing associated complications. Patient satisfaction with medical care is closely linked to patients' treatment adherence and disease management. In the context of an increased number of patients diagnosed with diabetes each year, the research we propose analyses the influence of socio-demographic, psychological and medical variables on patient satisfaction with diabetes care in the hospital setting in Romania. The research was conducted using mailed patient satisfaction questionnaires between July 2014 and February 2015 on 339 diabetes patients in Romania. The response rate was 39.5%. Results show that the most important factors influencing patient satisfaction with diabetes care in the hospital setting are patients' age, educational and income levels, diabetes type, whether or not the patient incurs associated complications and patients' perspective on diabetes management.

Keywords

Diabetes • Patient satisfaction • Socio-demographic • Medical

1 Introduction

In the past few decades, patient satisfaction has gained an important role in discussions regarding healthcare from both a medical and a marketing perspective. Research in this field indicates that an increased level of patient satisfaction is associated with increased staff morale, a decrease in patients' intent for seeking a second opinion, stronger treatment adherence and a positive image of the medical institution in the community [1, 2]. The interest in patient satisfaction is also supported by the development of increased competition between medical care units and a shift registered in the past decades regarding patient-doctor relationships. The classical patient-doctor relationship generally regarded the physician as the one in charge of making all decisions, while the patient carefully obeyed the recommendations. At present, this balance is changing more towards a consumer-type relationship, where the patients and their physicians discuss and agree on the terms which will lead to an improvement in the patients' healthcare [3]. This means patients today require not just a treatment from their physician, but also time, information, answers to their questions, empathy and politeness [4]. Patients therefore closely approach a consumer profile [5] which means that the strategies adopted by the medical care facilities for satisfying these needs require efficient marketing plans, policies and practices adapted to the different consumer segments [6].

In spite of the increased interest for this topic, there is still no consensus in the literature regarding a definition of patient [7–9]. For the purpose of this research, we chose to use the definition offered by Hjortdahl and Laerum [10], who argue that patient satisfaction represents a set of "complex relationships between the perceived needs of the patient, their expectations and experiences of care; the particular reaction of the patient to the consultation and its result in comparison to a conscious or unconscious standard that the patient had set before or during the consultation."

A. Constantinescu-Dobra (✉) · M. C. Coțiu
Department of Electroenergetics and Management, Faculty of Electrical Engineering, Technical University of Cluj-Napoca, George Baritiu, nr. 26-28, Cluj-Napoca, Romania
e-mail: aconst@mae.utcluj.ro

A. Sabou
Department of Computer Science, Faculty of Automation and Computer Science, Technical University of Cluj-Napoca, Cluj-Napoca, Romania

S. Vlad and N. M. Roman (eds.), *6th International Conference on Advancements of Medicine and Health Care through Technology; 17–20 October 2018, Cluj-Napoca, Romania*, IFMBE Proceedings 71,
https://doi.org/10.1007/978-981-13-6207-1_42

With regards to determinants of patient satisfaction in general and in the particular case of diabetes patients, factors considered in the literature vary considerably among studies. Socio-demographic and medical variables are often analysed with sometimes contradictory results. Other factors analysed include disease management, history with the disease and associated complications [11–17].

Romanian patients tend to be quite unsatisfied regarding public healthcare services in terms of access to medication, emergency services, the information offered to them in a medical setting, or the procedures for accessing medical services [18]. This situation is further amplified by the fact that the Romanian healthcare system in focused on cost monitoring and cost reduction, which most often leads to a lower focus on patient satisfaction.

In figures, the Romanian healthcare services market is split between public and private providers. The public system accounts for 77% of hospitals and 59.8% of medical laboratories, while the private sector groups 96.1% of clinics and 89% of practices for different medical specialties [19]. The private sector market is constantly developing, being considered one of the most dynamic markets in Romania [20]. In 2012, the market was estimated at 500 mil. euro [20, 21], where the total healthcare budget in Romania was of 5.5 mld. euro [22].

It is our belief that improving the relationships with medical services beneficiaries will contribute to an increased satisfaction level with positive effects on the medical facilities by improving their image, profitability and prestige in the community, while also contributing, as shown above, to increased staff morale, treatment adherence and a lower tendency to seek a second opinion.

Diabetes represents a chronic illness with high growth rates regarding the number of diagnosed patients in recent years [23, 24]. Furthermore, the nature and particularities of this illness determine an increased number of patients' interactions with the healthcare facilities and the medical staff. The increased number of patients with diabetes also has a direct economic and social effect. From an economic point of view, an increased number of diabetes patients generates increased associated medical costs (treatment, periodic check-ups), as well as medical leaves costs, or costs arising from a decrease in these patients' productivity. From a social point of view, diabetes is often associated with reduced quality of life, isolation and depression [25]. Furthermore, diabetes management implies a number of restrictions in terms of diet, self-administration of medication, lifestyle changes and a constant monitoring of potential associated complications [16, 26], which affect both the patient and their family and friends. According to the International Diabetes Federation, in 2013, the number of diabetes patients worldwide was of 382 mil. and was estimated to rise to 592 mil. by 2035 (a 55% increase) [23]. Data available from the Ministry of Health indicates the number of diabetes patients in Romania in 2011 was of 796,803, although IDF estimated a total number of 1,506,000. The disease incidence in Romania is of 64,000 new cases every year [27]. The average cost/patient is of 1000 RON/year [28].

The purpose of the article is to contribute to expanding the knowledge regarding the formation of patient satisfaction with diabetes care, as well as supporting medical facilities in the public sector in their efforts of adopting a marketing orientation ad consolidating their market position. The added value of the article lies in the investigation of patient satisfaction determinants for patients with diabetes. The article is mostly addressed at healthcare marketing professionals, healthcare decision-makers and researchers interested in patient satisfaction determinants.

2 Methodology

The research was conducted using a questionnaire designed for the purpose of the study. Questionnaires were distributed to patients with diabetes (type I and type II) residing in Romania by mail or in the online environment. A total number of 58 messages containing the link to the electronic version of the questionnaire and 800 printed questionnaires were distributed. A total number of 339 valid questionnaires were collected, representing a 39.5% response rate. Probabilistic sampling was attempted but failed as a consequence of the unavailability of data regarding access to the databases for patients with diabetes. In this context, a non-probabilistic sampling method was used, namely sampling based on the researcher's judgement. According to this method, the researcher, selects individuals to be included in the sample based on the researcher's rationale and expertise in the field of research [29, 30]. This sampling method is considered suitable for extended research, with a difficult to access population [31]. We therefore opted to distribute the questionnaire through diabetes patients associations and in the online environment by posting the link to a dedicated platform on websites, groups and social networks dedicated to or easily accessed by patients with diabetes. This choice is supported by the fact that diabetes patients associations group diabetes patients of different age groups, from different socio-professional backgrounds. A high geographical coverage was attempted. We avoided distributing the questionnaire within medical facilities as previous research indicates patients tend to score higher when research is conducted in the medical facility where they are admitted or receiving their treatment [32]. The study was conducted between 15 July 2014 and 15 February 2015.

Data collected was analysed using IBM SPSS Statistics v. 21. The sample obtained closely follows the distribution of diabetes patients in Romania, as shown in Table 1.

Table 1 Sample structure versus official Ministry of Health data

Criterion	Category/Interval	Percentage—Ministry of Health (%)	Sample (%)
Age	0–14 yo	3	1.1
	15–64 yo	62	69
	>64 yo	35	29.9
Residence	Rural	33	28.1
	Urban	67	71.9

Socio-demographic, medical and psychological variables were analysed in relation to patients general satisfaction with the services they had benefitted from in the hospital setting. We researched the differences existing in patients' general satisfaction in the hospital setting and the following socio demographic, medical and psychological aspects: age, gender, residency, education level, marital status, monthly income, self-evaluation of their medical condition, history with the disease, history in administering insulin, diabetes associated complications, patients perspective on life and diabetes management. T-test and one-way ANOVA were used. The data were tested for adequacy for these tests with positive results.

3 Results

With regards to socio-demographic aspects (age, gender, residence, education level and monthly income), results showed no significant influence of gender, residence and marital status. The sample structure is presented in Table 2.

In terms of age, results indicated that older patients tend to be more satisfied than the young ones ($F(6,261) = 5.290$, $p = 0$ (<0.05); Welsh ANOVA, $p = 0.035$, $p < 0.05$). With regards to the educational levels, the analysis conducted indicated the existence of significant differences among the groups considered. Highest satisfaction rates were registered among primary, professional and post-high-school education graduates, while the lowest scores were registered among higher education and high-school graduates ($F(3,264) = 6.463$, $p = 0$ (<0.05), Welsch ANOVA $p = 0 < 0.05$). In terms of their monthly income, results indicated that generally patients with low income levels (<220 euro) or higher income levels (>500 euro) tend to be more satisfied than those with average income levels.

For the medical aspects investigated (self-appreciation of one's medical status, diabetes type, history with the illness history in administering insulin, diabetes complications, number of hospital admittances and average hospital admittance duration), we found no significant influence for the following variables: self-appreciation of one's medical status, history with the illness and history in administering insulin, number of hospital admittances and average hospital admittance duration. The sample structure is presented in Table 3.

Table 2 Sample socio-demographic structure

Criterion	Category/Interval	(%)
Age	0–14 years	1.1
	15–64 years	69
	>64 years	29.9
Gender	Male	45.6
	Female	54.4
Residence	Rural	28.1
	Urban	71.9
Marital Status	Married	62.6
	Single	14.4
	Divorced	4.4
	Widow/er	18.5
Studies	Primary school	5.6
	Gymnasium	14.4
	Vocational school	19.6
	High school	25.6
	Post-secondary school	10.4
	Higher education	24.4
Occupation	Public employee	3.2
	Private employee	10
	Private entrepreneur	1.3
	Freelancer	3.3
	Family worker	2.1
	Unemployed	1.7
	Pensioner	74.4
	Student	2.1
	Homemaker	0.8
Income level	<75 euro	11.7
	75–150 euro	25.2
	150–225 euro	26.3
	25–335 euro	22.9
	335–450 euro	9
	450–670 euro	3.4
	670–1000 euro	0.8
	>1000 euro	0.8

Regarding diabetes type, results indicated patients with Type II diabetes tended to be more satisfied than those with Type I. The difference is statistically significant (t-Welsh test, $t(269) = -3.112$, $p < 0.05$) and has a low intensity effect ($r = 0.2$).

Table 3 Sample structure based on medical characteristics

Criterion	Category/Interval	%
Health state self-assessment	Very good	1.5
	Good	23.6
	Acceptable	55.6
	Poor	15.4
	Very poor	3.9
Type of diabetes	Type 1	36.5
	Type 2	63.5
Type of treatment	Insulin	63.7
	Oral antidiabetic drugs	36.3
Complications associated with diabetes	Yes	66.5
	No	33.5
Affliction duration from onset	<5 years	33.3
	5–18 years	55.4
	18–40 years	7.9
	>40 years	3.4
Value of last glycated hemoglobin test	<7	33.3
	7–9	41
	>9	15.8
	I don't know	9.9
Number of hospital admissions for diabetes	1–3	53.6
	4–10	34.5
	>10	11.9

In terms of diabetes associated complications, patients with complications tended to be more satisfied than the others. The difference is statistically significant (t-Welsch test, $t(274) = 2.097$, $p = 0.04 < 0.05$) and represents a low intensity effect ($r = 0.12$).

Psychological aspects investigated included patients perspective on life and diabetes management. No significant differences were registered in terms of satisfaction for optimistic, pessimistic and realistic patients. Results though indicated significant differences in terms of patients' perspective on diabetes management. Those patients who self-evaluated themselves as very careful in respecting their treatment tended to be more satisfied than those declaring they were only some-how careful. The least satisfied were those patients who admitted being less careful with their treatment (one-way ANOVA, $F(2,270) = 5.015$, $p = 0.007$ (<0.05)).

Regarding age, results are similar to those registered in other general patient satisfaction studies [12, 13, 33] and can be explained by lower expectations levels in the case of older patients who tend to be more inclined to accept medical services as they are delivered.

Concerning the education level, results obtained are similar to those registered in other general patient satisfaction research [13], where patients with lower educational levels tend to be more satisfied. This could be once again justified by lower expectations as such patients are less inclined to research information online, and tend to more easily accept medical services as they are provided.

In terms of income influence on patients' satisfaction, results indicated a higher satisfaction level in the lower or higher income level area. Similar research indicates a positive association between patient satisfaction and income levels [33]. Regarding the higher satisfaction levels for lower income patients, given the nature of the disease, a possible explanation could be the fact that, during their hospital admittance, these patients enjoy care without being preoccupied to ensure the resources required for keeping up with the diet and medication for that respective timeframe, as well as a lower level of expectations as compared to average income patients.

Regarding medical aspects, Type II diabetes patients and patients suffering from associated complications tend to be more satisfied than Type I diabetes patients, and those with no associated complications, respectively. This is somehow surprising given the fact that Type II diabetes management and associated complications are more complex and require more time, material and emotional resources. An explanation could be the fact that these patients interact much more frequently with the medical unit and the medical personnel which, in time, determines an adjustment of their expectations to the level of the existing reality.

Concerning the psychological aspects, results indicated that patients offering increased attention to their disease management tend to be more satisfied than those who are less careful. This can be explained through the positive results they obtain following a careful disease management, which can contribute to a perception of self-efficiency in the management of this disease [16], but also to a reduction in the number of interactions they have with the medical care facility and the medical staff.

4 Conclusions

Following the analysis of the influence of socio-demographic, medical and psychological factors on general diabetes patients satisfaction in the medical sector, the aspects influencing satisfaction were related to socio-demographic variables (age, education and income levels), medical variables (diabetes type and the existence of diabetes complications) and psychological factors (patients perspective on diabetes management).

Acknowledgements This research was co-financed through the European Social Fund through Sectoral Operational Programme Human Resources Development 2007–2013, project number

POSDRU159/1.5/S/142115 "Performance and Excellence in Doctoral and Postdoctoral Research in Romanian economics science domain".

Conflict of Interest The authors declare they have no conflict of interest.

References

1. Taylor, C., şi Benger, J.R.: Patient satisfaction in emergency medicine. Emerg. Med. J. **21**, 528–532 (2004)
2. Boudreaux, E.D., O'Hea, E.L.: Patient satisfaction in the emergency department: a review of the literature and implications for practice. J. Emerg. Med. **26**, 13–26 (2003)
3. Haug, M.R., Lavin, B.: Practitioner or patient—who's in charge? J. Health Soc. Behav. **22**(3), 212–229 (1981)
4. Shendurnikar, N., Thakkar, P.A.: Communication skills to ensure patient satisfaction. Indian J. Pediatr. **80**, 938–943 (2013)
5. Bell, R., et al.: Charting patient satisfaction. Mark. Health Serv. **17** (2), 22–29 (1997)
6. Chahal, H., Mehta, S.: Developing patient satisfaction construct for public and private health care sectors. J. Serv. Res. **13**, 7–30 (2013)
7. Gill, I., şi White, L.: A critical review of patient satisfaction literature. Leadership in Health Serv. **22**(1), 8–18 (2009)
8. Crow, R., et al.: The measurement of satisfaction with healthcare: implications for practice from a systematic review of the literature, executive summary, health technology assessment, **6**, 32 (2002). Smith, J., Jones, M., Houghton, L., et al.: Future of health insurance. N. Engl. J. Med**. 965**, 325–329 (1999). https://doi.org/10.10007/s002149800025
9. Wolf, M.H., et al.: The medical interview satisfaction scale: development of a scale to measure patient perceptions of physician behavior. J. Behav. Med. **1**, 391–401 (1978)
10. Hjortdahl, P., Laerum, E.: Continuity of care in general practice: effect on patient satisfaction. British Med. J. **304**, 1287–1290 (1992)
11. Rahmqvist, M.: Patient satisfaction in relation to age, health status and other background factors: a model for comparisons of care units. Int. J. Qual. Health Care **13**(5), 385–390 (2001)
12. Jackson, J.L., et al.: Predictors of patient satisfaction. Soc. Sci. Med. **52**, 609–620 (2001)
13. Quintana, J.M., et al.: Predictors of patient satisfaction with hospital health care. BMC Health Sci. Res. **6**, 102–111 (2006)
14. Jenkinson, C., et al.: Patients' experiences and satisfaction with health care: results of a questionnaire study of specific aspects of care. Qual. Satisf. Health Care **11**, 335–339 (2002)
15. Boudreaux, E.D., et al.: Determinants of patient satisfaction in a large, municipal ed: the role of demographic variables, visit characteristics, and patient perceptions. Am. J. Emerg. Med. **18**(4), 394–400 (2000)
16. Diț, L., et al.: Impactul severității bolii asupra satisfacției cu calitatea îngrijirii medicale la pacienții cu diabet de tip 2. Clujul Med. **85**, 573–577 (2012)
17. Narayan, K.M.V., et al.: Relationship between quality of diabetes care and patient satisfaction. J. Nat. Med. Assoc. **95**, 64–70 (2003)
18. Tănăsescu, D.: Marketing public şi optimul social, editura ASAB, București (2008)
19. Institutul Național de Statistică (INSSE), Biroul de presă, Comunicat de presă: 7 aprilie—Ziua mondială a sănătății. Available at http://www.insse.ro/cms/files/statistici/comunicate/alte/2014/ziua%20mondiala%20a%20sanatatii_cu%20poza%20OMS.pdf (2014). Accessed 19 Apr 2014
20. David, I.: Piața de jumătate de miliard de euro a serviciilor medicale private, dezbătută la ZF Pharma Summit, Ziarul Financiar, 17 Sep 2013. Available at http://www.zf.ro/companii/piata-de-jumatate-de-miliard-de-euro-a-serviciilor-medicale-private-dezbatuta-la-zf-pharma-summit-11341640 (2013). Accessed 3 May 2014
21. Bănilă, N.: Ce frânează creșterea pieței serviciilor medicale private în România, Capital, 23 June 2013. Available at http://www.capital.ro/183482.html (2013b). Accessed 3 May 2014
22. Rentrop & Straton: Serviciile clinicilor medicale de stat şi private. Analiză comparativă. Market Research Division. Rentrop & Straton. Available at http://rsresearch.ro/pages/serviciile-clinicilor-medicale-de-stat-si-private-analiza-comparativa-193.html (2012). Accessed 15 Aug 2014
23. International Diabetes Federation (IDF): Diabetes: facts and figures. Available at http://www.idf.org/worlddiabetesday/toolkit/gp/facts-figures (2013). Accessed 6 Aug 2014
24. European Commission (EC): Major and chronic diseases—diabetes. Available at http://ec.europa.eu/health/major_chronic_diseases/diseases/diabetes/index_en.htm#fragment7 (2015). Accessed 20 Aug 2015
25. Saatchi, E., et al.: The well-being and treatment satisfaction of diabetic patients in primary care. Health Qual. Life Outcomes **8**, 67–75 (2010)
26. Redekop, W.K., et al.: Health-related quality of life and treatment satisfaction in dutch patients with type 2 diabetes. Diab. Care **25**, 458–463 (2002)
27. Federația Asociațiilor Diabeticilor din România (FADR): Diabetul în România. Available at http://fadr.ro/despre-diabet/diabetul-in-romania/ (2015). Accessed 7 March 2014
28. Ministerul Sănătății (MS): Programul Național de Diabet Zaharat şi alte boli de nutriție. Available at http://www.ms.gov.ro/documente/8_51_329_c.htm (2014). Accessed 15 July 2014
29. Malhotra, N.K., Birks, D.F.: Marketing research. An Appl. Appr. 3rd edn, Prentice Hall, Harlow (2008)
30. Kothari, C.R.: Research Methodology—Methods and Techniques, 2nd edn, New Age International (P) Limited, New Delhi (2004)
31. Bernard, H.R.: Research Methods in Anthropology: Qualitative and Quantitative Approaches, 4th edn. Alta Mira Press, New York (2006)
32. Mazor, K.M., et al.: A Demonstration of the impact of response bias on the results of patient satisfaction surveys. Health Serv. Res. **37**(5), 1403–1417 (2002)
33. Bleich, S.N., et al.: How does satisfaction with the health-care system relate to patient experience? Bull. World Health Org. **87**, 271–278 IFMBE at http://www.ifmbe.org (2009)

Is Internet Marketing a Useful Tool for GPs Communicating with Students? A Focus Group Exploratory Study

Anca Constantinescu-Dobra and M. C. Coțiu

Abstract

Patient satisfaction is an important indicator of medical care. Existing literature suggests patient satisfaction has a considerable influence on patient retention rates, medical outcomes, treatment adherence, as well as on medical staff satisfaction or patients' intent to seek a second opinion. Furthermore, the past couple of decades have also brought significant changes to the medical systems and practice around European countries. Such changes include the development of private medical care units, increased competition in the medical sector, the availability of considerable medical information on the internet, as well as a strong tendency to have patients positioned as partners in the patient-doctor relationships. As a consequence, patients today demand time and answers to their questions, as well as empathy, politeness and attention from their physician. Although all these changes strongly affect the medical surrounding, the literature investigating patient satisfaction from a marketing perspective remains scarce. The article takes on this challenge and aims to investigate patients' expectations and satisfaction regarding the services offered to them by their family physician (GP). A qualitative exploratory study was conducted in the form of three focus groups with undergraduate students in Romania. Results showed that attention given to patients plays an important role in satisfaction together with reduced waiting times. The added value of the article lies in its investigation regarding patients' expectations form their family physician which can represent a starting point for the latter in adapting and improving their services. Furthermore, the article brings new information regarding patients' expectations in terms of their physician's online presence, which can help the latter develop new services for their patients. The article is particularly addressed to family physicians and professionals in the medical and marketing fields involved in drafting policy, medical services or marketing strategies for family physicians practices.

Keywords

Patient satisfaction • Medical care • Online • GP

1 Introduction

Patient satisfaction, from a marketing perspective, involves the positioning of patients as clients of public or private medical care units. This implies that the doctor-patient relationship will no longer be dominated by the physician, but it will shift more towards a partnership in which the doctor identifies a solution to the patient's illness, that is then proposed to and accepted by the patient, as an informed decision [1, 2]. Mostly as a consequence of increased access to medical information over the internet, patients are nowadays much more inclined to discuss the solutions proposed by their physicians, ask for alternative treatments, or suggest they require certain tests or medical services. For patients today, the medical service is no longer limited to a diagnosis and a treatment, they require time, information, answers to their questions, as well as politeness, empathy and attention from their physician [3].

Family physicians represent the first point of contact. According to recent estimates, family physicians are generally in charge of treating 80–90% of the medical issues of the population, also ensuring primary and specific prevention activities. They are directly accessible to the population, without any intermediaries (i.e. appointments are set directly by the patients, no other referral is necessary). At the same time, the activity of family physicians in Romania takes place in a competitive market, where physicians try to attract as many patients as possible [4]. It is therefore important that family physicians are able to answer patients' expectations. On the one hand, this enables them to attract a sufficient

A. Constantinescu-Dobra (✉) · M. C. Coțiu
Department of Electroenergetics and Management, Faculty of Electrical Engineering, Technical University of Cluj-Napoca, Str. George Baritiu, nr. 26-28, Cluj-Napoca, Romania
e-mail: aconst@enm.utcluj.ro

S. Vlad and N. M. Roman (eds.), *6th International Conference on Advancements of Medicine and Health Care through Technology; 17–20 October 2018, Cluj-Napoca, Romania*, IFMBE Proceedings 71,
https://doi.org/10.1007/978-981-13-6207-1_43

number of patients to have an economically viable practice, while on the other hand, having satisfied patients also ensures higher treatment adherence and increased propensity to schedule an appointment at the onset of symptoms [5].

Given the competitive nature of the primary care services and changing patient expectations, we strongly believe an analysis of patient satisfaction in the medical setting thus becomes particularly important in order to ensure the services provided continue to answer patients' needs. For the purpose of this article, we chose to define patient satisfaction as a set of "complex relationships between patient's perceived needs, their expectations and experiences of care; the particular patient reaction to the consultation and its result confronted to a conscious or unconscious standard that the patient had set before or during the consultation" [6].

The aim of this article is therefore to explore patients' perspectives on different aspects of medical services delivery and their relation to patient satisfaction regarding medical services offered by the family physicians.

Following a careful review of the literature [6–10], factors influencing patient satisfaction were grouped in four main categories: caring and reassurance defined as the relationship established between patients and their physicians, interaction defined as the quality of the discussion between patients and their physicians and the answers provided by the latter to address patients' concerns, medical outcome understood as the degree to which the medical problem of the patient was approached and solved and facility procedures defined as the relevant procedures for scheduling a visit, time allotted per patient etc. A fifth dimension, online services, was added by the researchers, given the tendency for digitization, increased access to information and considerable use of the young generation for this medium. Students tend to often value online marketing communication, even in the medical area. They appreciate if information about the physicians is available on portals or social media. They are also inclined to use medical applications to reduce the time spent for obtaining different medical services.

The added value of this article is twofold. On the one hand, the exploratory nature of the study allowed us to obtain original, spontaneous information which could have been otherwise restricted if a questionnaire had been used. On the other hand, this is one of the very few analyses of patients satisfaction with primary medical care in Romania, thus shedding more light on what influences satisfaction with such services and how family physicians can improve their practice generating positive impacts for their patients and the medical system. Furthermore, the analysis of the online component indicates the opportunity for the development of a new service category, as detailed in the following sections of this article.

The article is mainly addressed to family physicians and professionals in the medical and marketing fields involved in drafting policy, medical services or marketing strategies for family physicians practices.

2 Materials and Methods

2.1 Rationale for the Use of Focus Groups

Focus groups represent a tool for exploratory qualitative research which allow the collection of "rich, descriptive data in a small group format, for participants who agreed to focus on a topic of mutual interest" [11]. Focus groups are particularly useful to discuss respondents' perceptions, opinions, ideas or thoughts [12], while also allowing for the generation of much more in depth thinking about a certain topic than in the case of pre-defined questionnaires [13]. It is also important to note that focus groups are based on social interaction as a critical element of this research method [13], which allows for the formation of a sense of belonging to a group of focus group participants [12]. This is beneficial to the research as the literature indicates an increased sense of participant cohesiveness which helps respondents feel safe to share information, thus "creating the opportunity for more spontaneous responses", even for the generation of solutions [12].

2.2 Focus Group Participants and Protocol

Focus group questions were grouped in five main categories according to the patient satisfaction influencing factors identified based on the patient satisfaction literature.

All questions were tested for both clarity and relevance before the focus groups were conducted. No major changes were made to the initial questions set.

A total number of 3 focus groups were conducted (n = 21). Participants in all focus groups were undergraduate students, enrolled at the Technical University of Cluj-Napoca. The demographic distribution of participants is of 13 females and 8 males, from both urban area (16) and rural area (5), ages between 21 and 23 years old. Focus groups were conducted between May and June 2018.

Focus groups were homogenous in terms of age and studies completed and were heterogeneous regarding gender, disposable income and place of residence.

The focus groups were conducted in quiet areas, appropriate for such discussions. Participants were clearly informed regarding the purpose of the focus groups and of the fact that all answers will remain anonymous, confidential and will only be used for the purpose of this research. Participants consented to taking part in the research and to their answers being audio recorded for analysis purposes. The average duration of one focus group was 30 min. A number of 6–10 participants took place in each focus group.

Information saturation was reached during the three focus groups conducted. The number of focus groups is considered sufficient for research relevance [14].

3 Results

3.1 Caring and Reassurance

According to focus group participants, satisfaction regarding interactions with their physician is especially influenced by the true involvement of the medical staff (namely the practitioner). The following attributes were identified by respondents as defining for the caring and reassurance dimensions: physicians should be devoted to their profession, care about patients, respect them, offer patients feedback, remember patients and their medical condition, ask patients questions and provide a thorough examination, identify the best solution for their medical condition. Respondents also appreciated the time allotted for each consultation. Consult times tend to be higher as practitioners are more involved in examining patients.

A third of respondents also indicated that the manner they are addressed to by the medical staff impacts their satisfaction levels. Students generally expected to be treated with respect and politeness. Furthermore, respondents tended to link the manner they were treated by their physician to the quality of the specialist they would be referred to if required. In general, students indicated that practitioners treating them with respect and politeness were more likely to make referrals to good, honest specialists to whom GPs has also spoken to about the patient's medical condition before the referral.

3.2 Interaction

Focus group participants particularly appreciated when the medical staff inspired confidence from a professional point of view, even though they sometimes found the diagnosis and medical explanations to be too technical for their understanding. Even when patients do not fully understand the name of their illness, they generally insist on understanding how the treatment is to be administered. 70% of respondents consider it essential that the medical staff clearly explain why a certain treatment or medical procedures were chosen.

Respondents tended to be somehow dissatisfied regarding the fact that GPs tended to use a trial and error approach in treatment rather than refer them for more detailed examinations with a specialist. Participants indicated GPs preferred to experiment "until they got the correct treatment".

With the exception of two participants, all focus group respondents indicated communication with the GPs nurse as very important in the medical care received. The nurse is generally regarded as the first link in solving one's medical problems, indicating that "it's important to understand if it's an emergency and you need to get started quickly."

3.3 Medical Outcome and Facilities Procedures

Regarding the medical outcome, participants generally indicated the following: receiving a diagnosis (80%), receiving treatment and an improvement in their state of health (50%). Participants also expected they were told the exact procedures for following the treatment to make sure they were safe and the treatment was not harmful. According to focus group participants, being treated well "can be nice, but is not vital".

Cleaning is very important for young patients and is closely related to GPs involvement in treating patients. "It is useful if the clinic is clean and you are treated properly when presenting in sick". Participants suggested the exam room should be impeccable, having furniture that was in good condition. They also indicated that all medical utensils should be clean and disinfected and that a nice smell, even of disinfectant, was appreciated. This element can be connected to safety expectations: patients hope all other diseases would be extinct with disinfectants considering the number of sick patients entering a GPs practice on a daily basis. One participant also mentioned that it was very important to them that the medical staff washed their hands before examining him. For most of the students it was also important that the waiting room was nice and clean, with a pleasant atmosphere, airy, not crowded, having sufficient chairs and "instructive posters to make sure you do not get bored when you wait".

Regarding administrative procedures, most respondents indicated that it was important for them that their medical appointment was made as quickly as possible (especially for an acute/urgent disorder). The amount of time spent for the examination was less important for focus group participants.

Satisfaction limit is beyond the 2-day scheduling although they are understanding with urgent cases or pregnancies. If they call a doctor, they want to see them the next day and the time until the results come to them does not really matter for their level of satisfaction.

3.4 Attention Given to Family

Participants consider that the attention given by the GP to family members depends on the severity of the problem or the age of the patients. When they were younger, they were always accompanied and now they come with family when they are extremely sick and cannot stand on their feet. Males appreciated this item to a larger extent than females.

3.5 Overall Satisfaction

Overall satisfaction for focus group respondents was determined by: physician's involvement, correct/appropriate diagnosis, information offered regarding additional examinations ("send me wherever I need", "physician's recommendations"), how soon the GP can see the patient, waiting time before the examination up to 30 min, explaining what is going on with the body and the exams to complete, cleanliness, the manner in which the patient was spoken to.

A perfect consultation implies little waiting time (max 5 min), schedule adherence, speaking nicely to the patient even if their parents are not well-known to the GP/asking how the patient feels, remembering patients' names and previous conditions, inviting patients to sit comfortably, GP washing their hands before the exam, referring the patient to a specialist the GP had previously spoken to, investments made in modern equipment. Respondents also indicated they would appreciate chronic and acute patients not mixing in the waiting room. Other expected behaviour included: medical staff issuing compensated prescription without it being especially asked for by the patient and without complaining regarding funding available, not taking a cigarette break, medical staff not taking it out on patients for a bad day. GPs should be involved, treat severely ill patients with priority and clearly explain treatments.

3.6 Online Communication

Respondents do not consider interaction with the medical staff via social media or website as important.

However, respondents would appreciate the possibility of making an appointment online, online secured access to their medical records and a reminder application for annual check-ups and exams. E-mail communication is considered valuable if respondents want to ask questions regarding concerns they might have on the treatment prescribed. Respondents would not switch GPs just to achieve more online communication.

4 Conclusions

In conclusion, patients satisfaction with their GP is related to how much the staff is involved in the medical act, how they care about their patients, the attention given to family, the time spent for an appointment, as well as the time spent waiting for the consultation.

Regarding online communication, students agree that concerning medical services, these techniques are not so important for them, but they would appreciate the possibility to make an appointment online or access their medical files online.

Conflict of Interest The authors declare that they have no conflict of interest.

References

1. Baron-Epel, O., et al.: Evaluation of the consumer model: relationship between patients' expectations, perceptions and satisfaction with care. Int. J. Qual. Health Care **13**, 317–323 (2001)
2. Mooney, G.: Beyond health outcomes: the benefits of health care. Health Care Anal. **6**, 99–105 (1998)
3. Shendurnikar, N. și Thakkar, P.A.: Communication skills to ensure patient satisfaction. Indian J. Pediatr. **80**, 938–943 (2013)
4. Consiliul Concurenței, Raport privind piața serviciilor de asistență medicală din România și a activităților conexe acestora. Available at: http://www.consiliulconcurentei.ro/uploads/docs/items/bucket12/id12155/raport_servicii_medicale.pdf. Accessed 20 Aug 2018
5. Taylor, C. și Benger, J.R.: Patient satisfaction in emergency medicine. Emerg. Med. J. **21**, 528–532 (2004)
6. Hjortdahl, P. și Laerum, E.: Continuity of care in general practice: effect on patient satisfaction. Br. Med. J. **304**, 1287–1290 (1992)
7. Boudreaux, E.D., et al.: Determinants of patient satisfaction in a large, municipal ED: the role of demographic variables, visit characteristics, and patient perceptions. Am. J. Emerg. Med. **18**(4), 394–400 (2000)
8. Rahmqvist, M.: Patient satisfaction in relation to age, health status and other background factors: a model for comparisons of care units. Int. J. Qual. Health Care **13**(5), 385–390 (2001)
9. Jenkinson, C., et al.: Patients' experiences and satisfaction with health care: results of a questionnaire study of specific aspects of care. Qual. Satisfaction Health Care **11**, 335–339 (2002)
10. Quintana, J.M., et al.: Predictors of patient satisfaction with hospital health care. BMC Health Sci. Res. **6**, 102–111 (2006)
11. Wilkinson, D., Birmingham, P.: Using Research Instruments. A Guide for Researchers. Routledge Falmer, London (2003)
12. Onwuegbuzie, A., et al.: A qualitative framework for collecting and analyzing data in focus group research. Int. J. Qual. Methods **8**(3), 1–21 (2009)
13. Sagoe, D.: Precincts and prospects in the use of focus groups in social and behavioural science research. Qual. Rep. **17**(15), 1–16 (2012)
14. Larson, C.O., et al.: The relationship between meeting patients' information needs and their satisfaction with hospital care and general health outcomes. Int. J. Qual. Health Care **8**(5), 447–456 (1996)

Utility of 3D Reconstructions for Preoperative Planning in Functional Endoscopic Sinus Surgery (FESS)

D. Radeanu, Constantin Stan, and A. A. Maniu

Abstract

Introduction: CT scanning generate tridimensional reconstructions to permit the observation of paranasal sinuses and nasal cavity, and other anatomic structures of our body. The use and application of the 3D reconstructions generated from files of CT examination. The evaluation before sinus surgery through 3D reconstructions from the CT files may help the surgeon for diagnosis, preoperative planning and to acquire more information than with the traditional two-dimensional images obtained with the three different plans: axial, coronal and sagittal. *Objective*: To investigate and demonstrate the reliability and the feasibility of the evaluation before sinus surgery through 3D reconstructions from CT examinations of patients with a free software. *Method*: The reconstructions were carried out before the surgeries in order to assess the paranasal sinuses and nasal cavity for 45 patients. After this study, the surgery was digitally stored. *Conclusion*: With simple tools and personal computer, we evaluated the possibility to generate 3D reconstructions, the preoperative knowledge of the paranasal sinuses and nasal cavity may generate benefits during the performance of surgeries.

Keywords

3D reconstruction • Endoscopic • Surgery • Paranasal sinuses • Nasal cavity

1 Introduction

CT scanning generate tridimensional reconstructions to permit the observation of the paranasal sinuses and nasal cavity, and other anatomic structures of our body. The use and application of the 3D reconstructions generated from files of CT examination [1].

The evaluation before sinus surgery through 3D reconstructions from the CT files may help the surgeon for diagnosis, preoperative planning and to acquire more information than with the traditional two-dimensional images obtained with the three different plans: axial, coronal and sagittal [1, 2].

The Joint Council of Allergy, Asthma, and Immunology (2005) [5] stated that CT is the optimal method for preoperative evaluation of the paranasal sinuses and nasal cavity [3].

An accurately objective method of measurement disease severity preoperative using DICOM files was only recently described [4]. 3D reconstruction of CT scanning probably provide the most completed objective extent of the status and volumetric surface of the sinuses available through imaging [5].

The main goal of this study was to demonstrate the reliability and the feasibility of the evaluation before sinus surgery through 3D reconstructions from CT examinations of patients with a free software.

2 Materials and Methods

This study was a prospective one and included 114 patients hospitalized between January 2018 and June 2018 in the ENT Clinic, SCJU Cluj-Napoca, Romania, with sinonasal tract pathology.

We included in study patients older than 20 years who had a paranasal sinus CT exam.

Patients with a antecedents of anterior maxillofacial trauma, congenital abnormalities, nasal or paranasal surgery were excluded from the study. Also patients with sinonasal tumors, due to various locations, aggressive and extensive character with orbital invasion and skull base involvement were excluded from our study [6].

The 3D reconstructions were carried out before the surgeries using DICOM files to assess disease severity of the

D. Radeanu · C. Stan (✉) · A. A. Maniu
Department of Otorhinolaryngology, "Iuliu Hatieganu" University of Medicine and Pharmacy, Clinicilor 4-6, Cluj-Napoca, Romania
e-mail: stan.constantin90@yahoo.com

S. Vlad and N. M. Roman (eds.), *6th International Conference on Advancements of Medicine and Health Care through Technology; 17–20 October 2018, Cluj-Napoca, Romania*, IFMBE Proceedings 71,
https://doi.org/10.1007/978-981-13-6207-1_44

paranasal sinuses and nasal cavity for 45 patients who meet the inclusion criteria.

CT files were achieved from patients taking part in the study in the preoperative approach and they were carried out in different multi-slice equipment. The CT examinations presented slices that varied between 0.5 and 2 mm of thickness.

DICOM files of the CT's were reconstructed with the free software ITK-SNAP, version 3.6.0 by using personal computer.

Statistical analyses were performed with SPSS package version 20.0. The numeric variables were presented as total numbers, percentages, and mean standard deviation (SD) values. Normally distributed volumes are represented by mean and standard deviation (SD).

Full informed consent was given by all participants and the study had the approval of the local Ethical Committee from our institution.

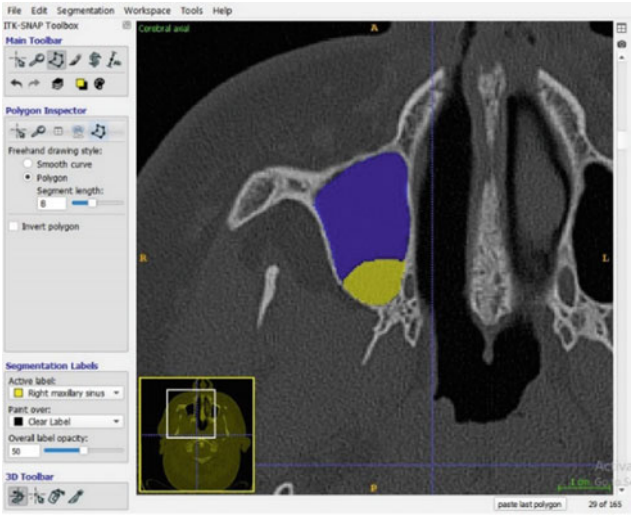

Fig. 1 Manual segmentation of the right maxillary sinus for one cut. We marked with blue the air filled maxillary part and with yellow the mucosal thickening area

3 Results

The gender distribution was predominantly male (29 [64.4%]) with values of the mean age of the patients about 39.9 ± 10.8 years.

Of the 45 patients included in this study, 26 suffer nasal polyposis, 42 patients had maxillary sinus mucosal thickening, 32 patients had frontal sinus mucosal thickening and 39 patients had sphenoid mucosal abnormalities.

All slices that determine a distinct sinus are segmented by determine perimeter of the borders starting at the lowest level of the sinus and advancing upward to the most higher cut. Segmentation was done manually, but tools to increase the speed of this method exist.

Once the whole sinus is segmented, it is possible to calculate the complete volume, free air volume and volume of mucosal thickening. Each individual sinus total percentage of

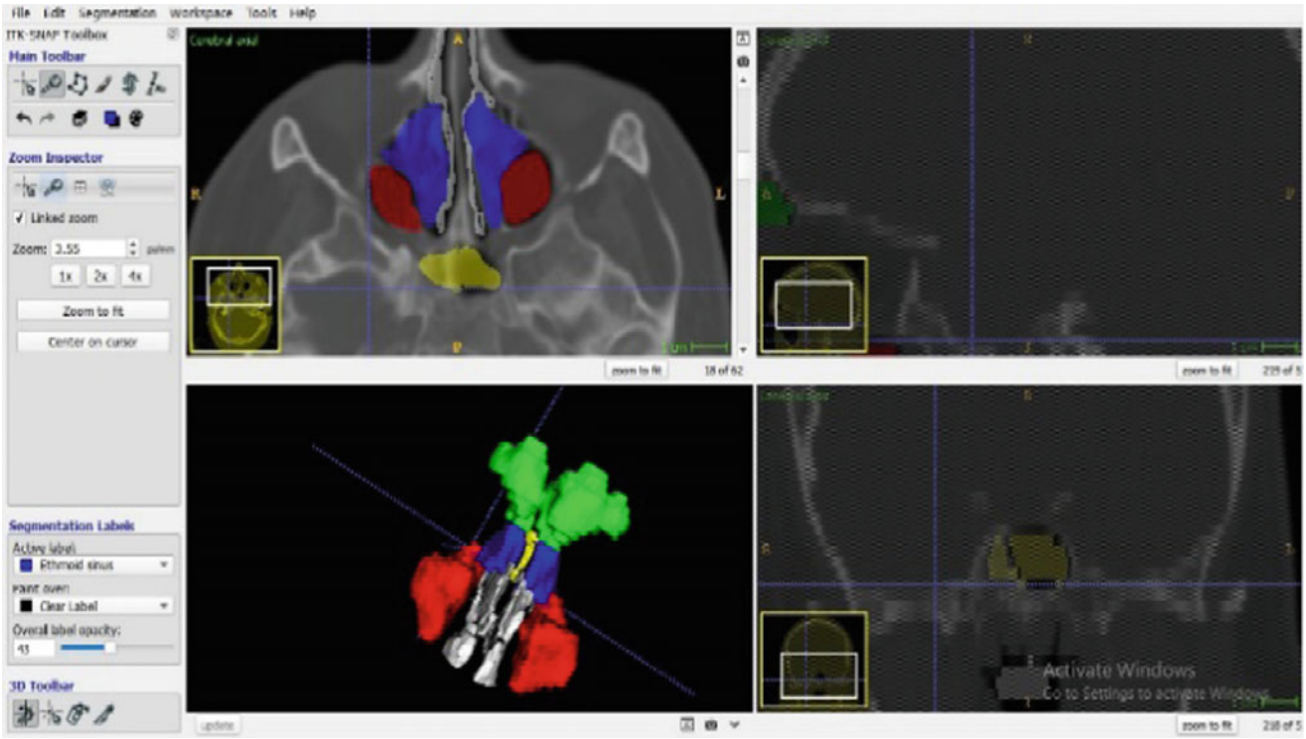

Fig. 2 Three-dimensional (3D) volumetric reconstruction

Table 1 The volume quantification for the maxillary, sphenoid and frontal sinuses and mucosal thickening (mm^3)

	Maxillary sinus	Maxillary sinus mucosal thickening	Sphenoid sinus	Sphenoid sinus mucosal thickening	Frontal sinus	Frontal sinus mucosal thickening	P value
Right (cc ± SD	14.54 (±3.78)	7.42 (±4.32)	4.52 (±4.21)	3.54 (±2.30)	2.89 (±2.64)	2.06 (±1.54)	<0.001
Left (cc ± SD)	14.78 (±4.56)	6.14 (±3.71)	4.30 (±3.23)	3.24 (±2.83)	3.24 (±2.17)	1.98 (±1.44)	<0.001
Mean (cc ± SD)	14.66 (±3.92)	6.78 (±4.19)	4.41 (±3.89)	3.39 (±2.94)	3.06 (±2.82)	2.02 (±1.76)	<0.001
Sum (cc ± SD)	29.32 (±7.72)	13.56 (±4.48)	8.82 (±4.48)	6.78 (±3.11)	6.13 (±4.67)	4.04 (±2.14)	<0.001

mucosal thickening was then determined by the following calculation: mucosal thickening volume/(volume of mucosal thickening + free air volume) = opacity percentage.

Each sinus was determined manually by marking the lumen of the sinus in each of the axial plane cuts. The lumen of a sinus was defined as space within the bony walls of the sinus in all three planes (axial, coronal and sagittal). After execution of the marking action, a 3D picture of the sinus was automatically made by the software (Figs 1 and 2).

After each slice of the sinus is segmented, the free air volume, volume of mucosal thickening and the total volume of sinus are calculated (Table 1).

The manual volume calculation process that was developed and manual segmentation system were based on the 45 patients examinations, for maxillary, sphenoid and frontal sinus. An average total maxillary sinus volume of 14.66 ± 3.9 cm^3 was establish in the evaluated patients. The average volume for the sphenoid sinus was 4.41 ± 3.89 cm^3 and for frontal sinus was 3.06 ± 2.82 cm^3.

Also we calculated the volume of mucosal thickening, the mean volume for mucosal thickening of the maxillary sinus was 6.78 ± 4.19 cm^3, 3.39 ± 2.94 cm^3 for mucosal thickening of the sphenoid sinus and 2.02 ± 1.76 cm^3 the mean volume for mucosal thickening of the frontal sinus.

4 Discussions

With simple tools and personal computer, we evaluated the possibility to generate 3D reconstructions, the preoperative knowledge of the paranasal sinuses and nasal cavity may generate benefits during the performance of surgeries [1].

The dimensions of the human paranasal sinuses was initially determined by taking morphometric measurements or performing plain radiography [7–9]. The introduction of CT and magnetic resonance imaging has allowed more precise assessments of these structures [7, 10, 11]. Computer tomography is widely used for measuring the size of the paranasal sinuses [12, 13]. While magnetic resonance imaging is better in rendering soft tissue, its application is restricted by its relatively high cost and limited accessibility [11]. The big benefit of computer tomography examination is the superior osseous anatomic detail that it afford, highlighting the circumferences of the paranasal sinuses. Consequently, CT is the gold-standard imaging exam for inflammatory diseases of the paranasal sinuses [13].

Pirner et al. related no important differences between male and female maxillary sinus volumes [14]. Some studies have shown that maxillary sinus volume is significantly less in patients with chronic rhinosinusitis compared with controls [16]. However, Fernandez et al. indicated that maxillary sinus volumes in chronic rhinosinusitis patients were larger than in the reference group [7].

In clinical application, CT-based sinus volumetry has been declared to be an helpful tool for objectively rating sinus opacity [15, 16]. Pallanch et al. rated the entire rate volume of sinus disease based on CT examinations in patients who were being medically treated for chronic diseases of paranasal sinuses. This outcome show that sinus preoperative volumetry can contribute to the clinical management of chronic rinosinusitis [4].

Therefore, CT-based volume determinations can frequently be performed exactly and effectively, but a fully automated system may have better applicability in clinical practice [17].

Our volumetric findings for the maxillary sinus are similar to the outcome that were reported by Park et al. (14.8 ± 1.5 cm^3) [18]. Though, Kawarai et al. rated patients with a mean age of 29.5 years and related volumes of 21.3 ± 6.5 cm^3 and 23.1 ± 6.7 cm^3 for the left and right maxillary sinuses, and these volumes were greater than those found in our study [19].

Also, Cohen et al. [22] reported mean volumes of 4.50 cm^3 (±1.97) and 2.95 cm^3 (±2.30) which are similar with our results.

5 Conclusions

Reconstructed 3-D data enhances viewing of pathology and enhances service to referring surgeons, since selected 3-D images can be annexed to the radiology report. These images exemplify the diagnosis and may even be shown to patients while talking about the pathology [20].

This method allows surgeons to do noninvasive visualization, simulation, and precise quantitative measurements of paranasal sinuses. It was developed as a complementary tool for endoscopic surgery. It could be mostly preferable for the patients who could not tolerate rigid endoscopy [21].

Our outcome of this study may contribute in the future to preoperative 3D evaluation of sinuses and may even be used for scoring of sinus disease.

Conflict of Interest The authors declare that they have no conflict of interests.

References

1. Martins, M.J.B., Aguiar, C.V., Júnior, J.F.N., Abreu, J.P.S., Feijão, M.X., Jataí, I.O., et al.: Preoperative planning using 3D reconstructions and virtual endoscopy for location of the frontal sinus. Int. Arch. Otorhinolaryngol. **15**(1), 48–53 (2011)
2. Minni, A., Messineo, D., Attanasio, G., Pianura, E., D'ambrosio, F.: 3D cone beam (CBCT) in evaluation of frontal recess: findings in youth population. Eur. Rev. Med. Pharmacol. Sci **16**, 912–918 (2012)
3. Slavin, R.G., Spector, S.L., Bernstein, I.L., et al.: The diagnosis and management of sinusitis: a practice parameter update. J. Allergy Clin. Immunol. **116**(6 suppl), S13–S47 (2005). (PubMed: 16416688)
4. Pallanch, J., Yu, L., Delone, D., et al.: 3-D volumetric computed tomographic scoring as an objective outcome measure for chronic rhinosinusitis: clinical correlations and comparison to Lund-Mackay scoring. Int. Forum Allergy Rhinol. (Published online 17 Sept 2013)
5. Micah, M., Pallanch, J.F., Sherris, D.A., Kita, H., et al.: Computed tomography scans as an objective measure of disease severity in chronic rhinosinusitis. Otolaryngol. Head Neck Surg. **150**(2), 305–311 (2014). https://doi.org/10.1177/0194599813513881
6. Tuşaliu, M., Zainea, V., Mogoantă, C.A., Dragu, A.A., Goanţă, C. M., Niţescu, M., Oţelea, M.R., Budu, V.A.: Diagnostic and therapeutic aspects in malignant sinonasal lymphoma. Rom. J. Morphol. Embryol. **57**(1), 233–236 (2016)
7. Sanchez Fernandez, J.M., Anta Escuredo, J.A., Sanchez Del Rey, A., Santaolalla, Montoya F.: Morphometric study of the paranasal sinuses in normal and pathological conditions. Acta Otolaryngol. **120**(2), 273–278 (2000). PMID: 11603789
8. Selcuk, O.T., Erol, B., Renda, L., Osma, U., Eyigor, H., Gunsoy, B., et al.: Do altitude and climate affect paranasal sinus volume? J. Cranio-Maxillo-Facial Surg. Official Publi. Eur. Assoc. Cranio-Maxillo-Facial Surg. **43**(7), 1059–1064 (2015). https://doi.org/10.1016/j.jcms.2015.05.013
9. Ikeda, A., Ikeda, M., Komatsuzaki, A.: A CT study of the course of growth of the maxillary sinus: normal subjects and subjects with chronic sinusitis. ORL; J. Oto-Rhino-Laryngology Relat. Spec. **60** (3), 147–152 (1998). (PMID: 9579359)
10. Sahlstrand-Johnson, P., Jannert, M., Strombeck, A., Abul-Kasim, K.: Computed tomography measurements of different dimensions of maxillary and frontal sinuses. BMC Med. Imaging **11**, 8 (2011). https://doi.org/10.1186/1471-2342-11-8. (PMID: 21466703; PubMed Central PMCID: PMC3080316)
11. Tikku, T., Khanna, R., Sachan, K., Srivastava, K., Munjal, N.: Dimensional changes in maxillary sinus of mouth breathers. Journal of oral biology and craniofacial research. **3**(1), 9–14 (2013). https://doi.org/10.1016/j.jobcr.2012.11.005. (PMID: 25737873; PubMed Central PMCID: PMC3941914)
12. Aksoy, E.A., Ozden, S.U., Karaarslan, E., Unal, O.F., Tanyeri, H.: Reliability of high-pitch ultra-low-dose paranasal sinus computed tomography for evaluating paranasal sinus anatomy and sinus disease. J Craniofac Surg. **25**(5), 1801–1804 (2014). https://doi.org/10.1097/SCS.0000000000000966. (PMID: 25203576)
13. Deutschmann, M.W., Yeung, J., Bosch, M., Lysack, J.T., Kingstone, M., Kilty, S.J., et al.: Radiologic reporting for paranasal sinus computed tomography: a multi-institutional review of content and consistency. Laryngoscope **123**(5), 1100–1105 (2013). https://doi.org/10.1002/lary.23906. PMID: 23619621
14. Pirner, S., Tingelhoff, K., Wagner, I., Westphal, R., Rilk, M., Wahl, F.M., et al.: CT-based manual segmentation and evaluation of paranasal sinuses. Eur. Arch. Oto-Rhino-Laryngology: Official J. Eur. Fed. Oto-Rhino-Laryngological Soc. **266**(4), 507–518 (2009). https://doi.org/10.1007/s00405-008-0777-7. (PMID: 18716789)
15. Coronado, C., Arriadaga, O., Galdames, I.V.: Easy and unbiased determination of the maxillary sinus volume. Int. J. Morphol. **19** (4), 1375–1378 (2011)
16. Barboni, B., Mangano, C., Valbonetti, L., Marruchella, G., Berardinelli, P., Martelli, A., et al.: Synthetic bone substitute engineered with amniotic epithelial cells enhances bone regeneration after maxillary sinus
17. Apuhan, T., Yildirim, Y.S., Ozaslan, H.: The developmental relation between adenoid tissue and paranasal sinus volumes in 3-dimensional computed tomography assessment. Otolaryngol. Head Neck Surg. Official J. Am. Acad. Otolaryngol. Head Neck Surg. **144**(6), 964–971 (2011). https://doi.org/10.1177/0194599811399712
18. Park, I.H., Song, J.S., Choi, H., Kim, T.H., Hoon, S., Lee, S.H., et al.: Volumetric study in the development of paranasal sinuses by CT imaging in Asian: a pilot study. Int. J. Pediatr. Otorhinolaryngol. **74**(12), 1347–1350 (2010). https://doi.org/10.1016/j.ijporl.2010.08.018. PMID: 20863577
19. Jun, B.C., Song, S.W., Park, C.S., Lee, D.H., Cho, K.J., Cho, J.H.: The analysis of maxillary sinus aeration according to aging process; volume assessment by 3-dimensional reconstruction by high-resolutional CT scanning. Otolaryngol. Head Neck Surg. Official J. Am. Acad. Otolaryngol. Head Neck Surg. **132**(3), 429–434 (2005). https://doi.org/10.1016/j.otohns.2004.11.012. (PMID: 15746857)
20. Flohr, T.G., Schaller, S., et al.: Multi-detector row CT systems and image reconstruction techniques. Radiology **235**, 756–773 (2005)
21. Kapakin, S.: The paranasal sinuses: three-dimensional reconstruction, photo-realistic imaging, and virtual endoscopy. Folia Morphol. (Warsz) **75**(3), 326–333 (2016). https://doi.org/10.5603/FM.a2016.0006. (Epub 26 Feb 2016)
22. Cohen, O., et al.: Volumetric analysis of the maxillary, sphenoid and frontal sinuses: a comparative computerized tomography based study. Auris Nasus Larynx **45**(1), 96–102 (2018)

Quantifiable Risk Factors in Medical Equipment Management Program

Călin Corciovă, D. Andriţoi, C. Luca, and R. Ciorap

Abstract

The provision of today's health services depends on a steady increase in the evolution of medical technology. There is no hospital department that has not felt the impact of electronic, mechanical, hydraulic equipment in daily routine. The development of medical technology, the complexity of medical equipment has been rapid, producing a proliferation of growing medical devices. This paper was conducted to provide a comprehensive study evaluating the maintenance and repair program for medical equipment to determine the optimal method for a cost-effective management system and to identify risk factors. When a risk assessment tool is being developed, quantified and implemented, many applications are possible to generate procedure risk monitoring presentations across the institution to implement a technical competence program for biomedical/clinical engineers, technicians and clinicians.

Keywords

Risk factors • Medical equipment assessment • Management program • Quality guidelines

1 Introduction

Nowadays expect competence and efficiency to guide the development, implementation and support of medical technology. By agreement, biomedical/clinical engineers who work in hospitals face the challenge of managing appropriate health technologies with limited resources every day. To capitalize as much resources and to provide health care quality in the most cost effective, Department of Medical Bioengineering or Engineering Department Clinical must develop a system for measuring risk and integrate it into its program management of medical technology. An early stage of any technology management program requires an assessment of existing technology [1, 2].

Medical evaluation of technology has been proposed as a way to improve the care and health of patients by providing adequate environmental health technologies. In addition to providing technical evaluation and clinical trials of equipment, technology assessment attempts to control negative legal and economic consequences through risk assessment through the life cycle of medical equipment [3]. From a historical perspective, the risk assessment was twofold: perceived and quantitative.

The perceived style of risk assessment is usually qualitative, informal, intuitive, and generally not documented. This style is reactive and involves on-site response to risk events or hospital situations [4]. On the other hand, the quantitative risk assessment of style is formal, clear, disciplined, and rigorous, generally revised and documented (Fig. 1).

The importance of developing a dynamic risk assessment tool that can quantify the risk environment of its medical equipment and include as many measurable elements from this environment as possible has led to the following objectives being defined:

1. to create a method of classifying medical equipment to ensure the effective deployment of available resources;
2. provide a comprehensive and accurate tool to identify the technical and clinical training needs of the equipment;
3. replacement of distribution, preventive maintenance (PM) and other service requirements based on their effectiveness in reducing the risks associated with the equipment;
4. to develop the Biomedical Engineering Program beyond the traditional, reactive risk assessment, normally based on a failure analysis, on a more quantitative and proactive approach;

C. Corciovă (✉) · D. Andriţoi · C. Luca · R. Ciorap
Biomedical Sciences Department, University of Medicine and Pharmacy "Grigore T. Popa", Universitatii, No. 16, Iasi, Romania
e-mail: calin.corciova@bioinginerie.ro

S. Vlad and N. M. Roman (eds.), *6th International Conference on Advancements of Medicine and Health Care through Technology; 17–20 October 2018, Cluj-Napoca, Romania*, IFMBE Proceedings 71,
https://doi.org/10.1007/978-981-13-6207-1_45

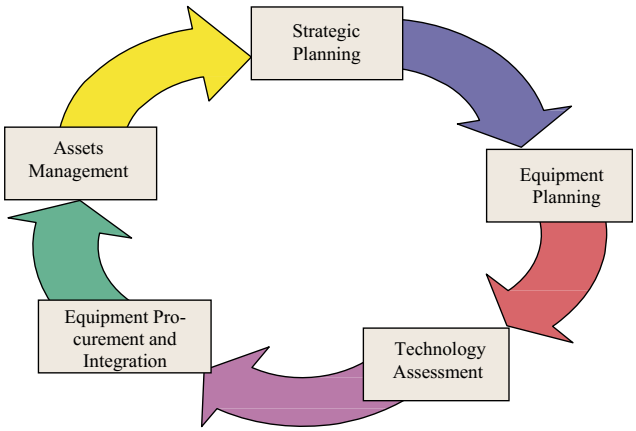

Fig. 1 The technology management process in biomedical engineering department

5. to develop and implement methods to easily make large amounts of data without losing the ability to identify details of equipment and incidents greater than acceptable failures of the operator, failure of equipment without it. Biomedical/clinical engineers can adapt these guidelines to the development of technical skills. Technical skills should measure the technician's competence with regard to maintenance equipment as well as the clinical effectiveness of the equipment, compatibility with other equipment, cost-effectiveness and risk-related properties [4, 5].

2 Risk Assessments—Risk Equipment

Dynamic risk assessment tool analyzed (Table 1) contains four modules, with the associated risk characteristics of static and dynamic. The two static components, the function of the equipment and the physical risk are attributed when the medical equipment is introduced into the Biomedical Engineering Management System Database, and this category provides the basic risk level of the equipment. Measure tool equipment assigns a risk level for the purpose equipment, the highest survival equipment as his defect potential should be accompanied by the highest level of risk [6, 7].

Measuring physical risk is an estimate of the worst case if the equipment does not function as expected, and the death of the patient receives the highest rating. These two modes are classified as static, as their values are usually the same throughout the lifecycle of medical equipment. Physical measurement of risk is an estimate of the effect of the worst if the equipment does not function as expected, and the patient's death becomes the highest rating. These two modules are classified as static because their values are usually the same throughout the life of medical equipment.

The two modules are dynamic risk factors maintenance requirements and risk points. The measures necessary maintenance is based on the assumption that an increased number of interventions technician indicates cause risks. For example, if the defibrillator requires high maintenance, this indicates an incident waiting to happen. In addition, repeated equipment testing shortens the life of relays, capacitors and high voltage cables and moves the equipment closer to the defect. Measure risk point combines different risk factors, such as real defects, reasons for failure or poor performance in terms of criteria such as MTBF [8].

The result of each of the four modules is the summed algebra, averaged over a six-month period and rated from 1 (low) to 5 (high) (Table 1). As there are no standard criteria for risk assessment, the tool uses practical practices to establish a baseline. Then, a feedback loop allows the clinical engineer to review the equipment that shows an increase in risk over a predetermined period of time. If the engineer confirms an increase in the risk factor, action is required to

Table 1 Baseline risk level for medical equipment

Dynamic risk factors		Static risk factors	
Maintenance	Risk points	Equipment function	Physical risk
– Equipment type and hours per maintenance occurrence [25]	– Employee/patient injury [25] – Equipment failure [5] – Exceeds MTBF [8] – Equipment back again [10] – PM inspection failure [15] – Physical damage [20] – PM overdue [5] – Operator error [8]	– No patient [0] – Patient related and other [5] – Computer and related [8] – Laboratory accessories [10] – Analytical laboratory [15] – Additional monitoring [18] – Surgical and IC monitoring [20] – Life support [25]	– No significant risks [5] – Patient discomfort [10] – Improper therapy or misdiagnosis [15] – Patient or operator injury [20] – Patient death [25]

RISK GROUP G1—[1–20]; **G2**—[21–40]**; G3**—[41–60]; **G4**—[61–80]**; G5**—[81–100]

reduce this risk. However, if the system learns to judge the appropriate level of risk and over-responds, a scaling factor empirically reduces the sensitivity of the system to that equipment by 5%. This scaling factor keeps biomedical resources as it automatically reduces the intensity of the inspection, unless an engineer manually overwrites it.

3 Monitoring Risk Equipment

Due to the evolution of medical technology, at present, hospitals can hold inventories of dozens or even hundreds of thousands of equipment. Managing this volume of items can be overwhelming for safety, education or technology assessment groups. At present, high risk equipment categories have been created from the risk assessment module modules (Fig. 2). Using these assignments, the technical staff can focus their attention on the equipment with the highest potential for injury or damage. The selection is based, in part, on repairing the repair service completed by technicians [9, 10].

In view of the above, an item is included in the high risk category if the technical staff considered it and labeled with the "Equipment Error" code. In addition, for validation, each of the static modules should have a minimum value of 15. Equipment with these ratings would include, for example, monitoring equipment, defibrillators, dialysis equipment and electrosurgical equipment. The critical risk decision can be identified by "Failed PM" error code. If this occurs and the equipment is found to be out of tolerance or defective during PM, identified by technical staff during PM, not a clinician trying to use the equipment. This is called a high risk software failure and is not as serious as when "failed PM" is not present. If the problem was detected by the clinician during a clinical procedure, it becomes a serious risk and is considered the most dangerous condition.

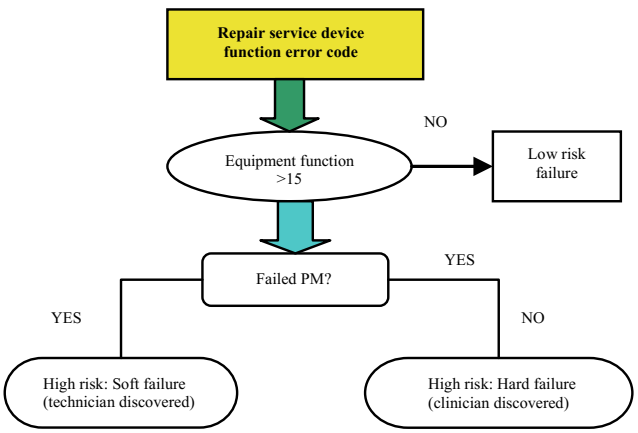

Fig. 2 High risk medical equipment—most potential for causing injury or damage

Identified strategy is to improve procedures to reduce the number of failures heavy (clinician found) by technical staff found the equipment problem during PM and, ultimately, to reduce the total number of failures for high-risk equipment. As we move toward this goal, we monitor the ratio of heavy failures and software failures and compare reports for different categories of equipment, identifying strengths and weaknesses in our procedures along the road PM.

To achieve our goals, however, we must also look at the PM program in a more creative light. For example, PM outlined by the manufacturer is geared for the hospital, average usage, and average technical support, with a safety margin factored into the equation. Depending on where a particular institution fits in this definition, PM frequency and content should be reviewed. It may be possible to modify the current PM program to conserve resources in some areas, apply them more effectively in others, and keep equipment failures out of the hands of the clinician. The goal of this process is to reduce risk to the patient, clinician, and hospital [11].

The risk assessment data and reports should be formatted so that both the biomedical/clinical engineer and the clinician can understand and each report should only provide the necessary information to a particular department. With these PM records, repairs, failure codes, and high risk equipment information help engineers manage the risks for their areas of responsibility. A similar report, which includes statistical thresholds, is ready for the review of the safety committee. Finally, Biomedical Engineering Management receives a report showing trends for each category of information [12].

In turn, the risk factors for the equipment are managed by the clinical engineer. It could be compared with risk factors for the same type of equipment managed by all technicians in the department. Performance would become partly a function of the risk management skills of the technician and clinical engineer and technical follow-up testing techniques would become a component of risk management. Ideally, clinical engineers and technicians could become creative partners in risk management for medical equipment and clinical areas under their responsibility [13, 14].

4 Technical Competencies—Risk Assessment

Technical personnel in hospitals should pass proficiency testing clinic. Clinical competence means that it possesses the necessary knowledge and skills for adequate clinical performance, and competence based assessment aims at facilitating the individual development of each individual, increasing accountability and autonomy, benefiting the consumer and promoting care high quality [15]. Clinical engineers and technicians can adapt this concept to the development of technical skills. Technical skills should

Table 2 Technical competency checklist

Technical competency checklist		
Equipment Type: MONITOR PATIENT Manufacturer/Model Number: XXX Competency Title: PREVENTIVE MAINTENANCE AND REPAIR Job Titles to Perform: Biomedical engineer, clinical engineer, technician		
CRITICAL ELEMENTS	YES	NO
1. Is able to diagnose problems specific to this device		
2. Is able to distinguish operator error from equipment malfunction		
3. Performs preventive maintenance on this device in accordance with Procedure No. XXX		
4. Is able to perform repairs on this device to the component level		
5. Identifies the physiologic applications for this device		
6. Identities the hazards of blood and chemical contaminants as related to this device		
7. Identifies the interaction of this device with other equipment in the clinical environment		
8. Identifies potential hazards related to the interaction of this device with other equipment in the clinical environment		
9. Is able to provide in-service training for clinicians on the operation of this device		
10. Is able to cross-train other biomedical engineering staff in the operation and repair of this service		
Employee Name……. Qualified Observer……. Validation Date……		

measure skills in terms of maintenance equipment, as well as evaluating the clinical effectiveness of the equipment, compatibility with other equipment, profitability and risk related projects (Table 2).

Currently, however, in a time when health care resources are controlled overtime management is not practical technical skills. However, if skills training and testing could be administered at a frequency and depth that corresponds to the assessed risk level, the benefits would exceed the resources spent. In other words, the risk associated equipment is higher, the more frequent testing.

5 Conclusions

When developing, quantifying and implementing a risk assessment tool, many applications are possible, from generating reports/presentations to monitor the risk of equipment across the institution, to implementing a technical competence program for engineers and clinical technicians. An essential ingredient involves accurately formatting information so that it is relevant to the professionals it addresses (Table 3).

Table 3 Technical competency should be tested according to equipment risk

Risk group	Testing interval	Equipment to be selected
1	Upon completion of training only	All equipment for which training has been received
2	Upon completion of training and every 2 years	Equipment that is randomly selected or that has specific problem areas
3	Upon completion of training and every 2 years	Equipment selected according to frequency of service
4	Upon completion of training and annually	Equipment selected according to free-Quincy service. Exception: all items in Life Support category should be competency tested
5	Upon completion of training and annually	All equipment items within this class

Medical staff does not have time for complex tables or diagrams but will use relevant information and can easily apply them to improve their daily patient delivery protocol. And since the precision of any risk assessment scheme can not be measured against any known standards, clinical engineers must permanently update the reference or reference references for validating and improving the results of their assessment tools.

Biomedical Engineering Department can provide technical expertise for both, technical staff and for the medical to ensure safe and effective clinical interventions. A strategy is to develop, track and make changes based on performance indices that measure the transparency of the medical equipment management program for the clinician and the patient. In other words, if the program works well, it should complement the work of doctors and improve the patient's comfort and expectations regarding his medical condition.

Conflict of Interest The authors declare that they have no conflict of interest.

References

1. Atles, L.R.: A Practicum for Biomedical Technology & Management Issues. Kendall-Hunt Publishing, Dubuque, IA (2008)
2. Bagadia, K.: Computerized Maintenance Management Systems Made Easy: How to Evaluate, Select, and Manage CMMS. McGraw-Hill, New York (2006)
3. Corciovă, C., Andriţoi, D., Luca, C., Ciorap, R.: Prioritization of medical devices for maintenance decisions. In: Vlad, S., Roman, N. (eds.) International Conference on Advancements of Medicine and Health Care through Technology; 12–15 Oct 2016, Cluj-Napoca, Romania. IFMBE Proceedings, vol. 59. Springer, Berlin (2017)
4. Baretich, M.: Equipment control and asset management. In: Dyro, J. (ed.) Clinical Engineering Handbook, pp. 122–123. Elsevier, San Diego (2004)
5. Chien, Y.H., Sheu, S.H.: Extended optimal age-replacement policy with minimal repair of a system subject to shocks. Eur. J. Oper. Res. **174**(1), 169–181 (2006)
6. Cockburn, A.: Agile Software Development. Addison Wesley Longman, Reading, Massachusetts (2001)
7. Gluch, D.P.: A Construct for Describing Software Development Risks. Software Engineering Institute, Pittsburgh, PA CMU/SEI-94-TR-14
8. Backhouse, M., Wonder, M., Hornby, E., Kilburg, A., Drummond, M.F., Mayer, F.K.: Early dialogue between the developers of new technologies and pricing and reimbursement agencies. Value Health **14**(4), 608–615 (2011)
9. Busse, F.R., Orvain, J., Velasco, M., Perleth, M., et al.: Best practice in undertaking and reporting health technology assessments. Int. J. Technol. Assess. Health Care **18**, 361–422 (2002)
10. Emanuel, E.J., Fuchs, V.R., Garber, A.M.: Essential elements of a technology and outcomes assessment initiative. JAMA **298**, 1323–1325 (2007)
11. Drummond, M.F., Schwartz, J.S., Jönsson, B., Luce, B.R., Neumann, P.J.: Key principles for the improved conduct of health technology assessments for resource allocation decisions. Int. J. Technol. Assess. Health Care **24**(3), 244–258 (2008)
12. Neumann, P.J., Drummond, M.F., Jönsson, B., Luce, B.R., Schwartz, J.S., Siebert, U., Sullivan, S.: Are key principles for improved health technology assessment supported and used by health technology assessment organizations? Int. J. Technol. Assess. Health Care **26**(1), 71–78 (2010)
13. Drummond, M.F., Neumann, P.J., Jönsson, B., Luce, B.R., Schwartz, J.S., Siebert, U., Sullivan, S.: Can we reliably benchmark health technology assessment organizations? Int. J. Technol. Assess. Health Care **28**(2), 159–165 (2012)
14. Stamatis, D.H.: Failure Mode and Effect Analysis. FMEA from Theory to Execution, 2nd edn. American Society for Quality, Quality Press, Milwaukee (2003)
15. Guidelines for Failure Modes and Effects Analysis (FMEA) for Medical Devices. Dyadem Press, Ontario, Canada (2003)

Oncological Outcome After Robotic Surgery for Rectal Cancer

Bogdan Vasile Micu, C. M. Micu, D. Chirila, H. Silaghi, R. A. Iusan, M. S. Muresan, T. R. Pop, C. Ionescu, and N. Constantea

Abstract

The aim of the study was to assess and analyse the oncologic postoperative outcome of patients after robotic surgery for rectal cancer We conducted a study on patients with rectal cancer undergoing robotic surgery at the 5th Surgery Clinic of the Municipal Clinical Hospital in Cluj-Napoca between January 2010 and December 2013 and evaluated postoperative survival after 5 year follow-up. There were 10 patients, median age was 62 ± 11 years. Five anterior rectal resections, three lower rectal resections and two abdominoperineal resections were performed. Most tumors were stage III (6 cases). Of the patients included in the study, 7 patients survived and 3 patients died during the 5-year follow-up period. Survival at 5 years after robotic surgery was similar to open or laparoscopic surgery. Robotic surgery may be an alternative to laparoscopic surgery in the treatment of rectal cancer, especially with regard to the identification and preservation of nerve plexuses and dissection in a narrow pelvis with similar oncologic outcome.

Keywords

Rectal cancer • Robotics • Surgery • Minimally invasive • Survival

B. V. Micu (✉) · C. M. Micu · D. Chirila · H. Silaghi · M. S. Muresan · T. R. Pop · C. Ionescu · N. Constantea
5th Surgical Department, "Iuliu Hateganu" University of Medicine and Pharmacy, Tabacarilor no. 11, Cluj-Napoca, Romania
e-mail: micubogdan@yahoo.com

C. M. Micu
Department of Anatomy and Embryology, "Iuliu Hateganu" University of Medicine and Pharmacy, Cluj-Napoca, Romania

R. A. Iusan
Faculty of Electrical Engineering, Technical University of Cluj Napoca, Cluj-Napoca, Romania

1 Introduction

The da Vinci surgical system has been specifically developed to compensate the technical limitations of laparoscopic instruments. The system offers a three-dimensional image, an ergonomic position, a steady camera, improved movement dexterity, the elimination of physiological tremor, the endowrist—a seven degrees of freedom instrument, with 180° of articulation and 540° of rotation, the ability to safely perform intracorporeal suturing, the ability to perform precise finite movements, thorough dissection of the mesorectum in the narrow pelvic space with the preservation of the pelvic nerve plexuses [1].

Nevertheless, the da Vinci surgical system has some technical disadvantages. First of all, there is a lack of tactile sensation. As a result, tissue damage can easily occur during robotic arm traction and during the movement of robotic instruments. Moreover, the suture material can be cut because there is no stretching feedback while performing the suture. But, with the fine image of the optical system this technical disadvantages can be overcome [2]. Laparoscopic surgery is now accepted as an approach for the treatment of colorectal cancer with superior results in terms of immediate postoperative recovery but with survival rates that are comparable to open surgery. Many authors have demonstrated that total mesorectal excision can be performed laparoscopically, with patients benefiting from the advantages of minimally invasive techniques.

The aim of our study is to assess and analyse the oncologic postoperative outcome of patients after robotic surgery for rectal cancer in 5th Surgery Clinic in Cluj-Napoca.

2 Material and Methods

We carried out a retrospective study on patients undergoing robotic surgery for rectal cancer at the 5th Surgery Clinic of the Municipal Clinical Hospital in Cluj-Napoca between

S. Vlad and N. M. Roman (eds.), *6th International Conference on Advancements of Medicine and Health Care through Technology; 17–20 October 2018, Cluj-Napoca, Romania*, IFMBE Proceedings 71,
https://doi.org/10.1007/978-981-13-6207-1_46

January 2010 and December 2013. A database was created including patient characteristics, diagnosis, tumor location, type of surgery, operating time, hospitalization period, intraoperative and postoperative complications and postoperative progression, conversion rate, morphopathological features: tumor macroscopic size, appearance, T stage—degree of bowel wall invasion, type of histology, grade of the tumor (well-differentiated, undifferentiated), number of lymph nodes excised, N stage, number of examined lymph nodes, the ratio between the number of metastatic involved lymph nodes and the number of examined lymph nodes (defined as lymph node ratio—LNR), TNM stage.

In patients with stage III (N+), was calculated the lymph node ratio (LNR) obtained by dividing the number of lymph nodes invaded by tumor to the total number of lymph nodes resected. Using this criterion, patients were divided into five groups, with the cut-off values: <0.10, 0.11–0.21, 0.22–0.36, 0.37–0.6, and >0.61. These cut off values have also proven important in other studies [3].

The study was approved by the Ethics Committee of the Cluj-Napoca Municipal Clinical Hospital and all patients signed the informed consent form. We follow-up the patients for a period of 5 years, in the first year at 3 and 6 months and after that annually with clinical examination, complete laboratory tests, abdominal ultrasound, chest X-ray and screening colonoscopy and whole CT scan. We identified distant recurrences by local and general exam, laboratory tests, general ultrasound, computed tomography, chest X-ray, scintigraphy (when was necessary) and local recurrences with lower gastrointestinal endoscopy with anastomotic biopsy and abdominal ultrasound. In the study we calculated and defined as relapse-free survival the period (number of months) following surgery until the appearance of the recurrences (local-regional or distant).

3 Results

During the study, a total of 10 patients underwent surgery for rectal cancer using the da Vinci surgical system. Of these, 6 were men and 4 women, and median age was 62 ± 11 years. The body mass index was 28.20 ± 3.92 kg/m^2. Tumor localization was in the upper rectum in 5 cases (>11 cm), in the middle rectum in 3 cases (6–11 cm) and in the lower rectum in 2 cases (<6 cm). None of the patients had history of surgery and 2 patients received preoperative radiotherapy. The following procedures were performed: 5 anterior rectal resections, 3 lower rectal resections with mechanical coloanal anastomosis and two abdominoperineal resections. Total operating time including connecting time was 270 ± 50.73, decreasing once the learning curve is traversed. Most tumors were stage III (6 cases), 2 cases were stage II and 2 cases were stage I. The main intraoperative complications were significant hemorrhage that determined the conversion to open surgery and 1 case of technical difficulty during mesorectal excision. Postoperative complications were represented by 1 case of anastomotic fistula. The main characteristics of the study group are presented in Table 1.

Table 1 The main characteristics of the study group

Characteristics		
Gender		
Men	6	Cases
Women	4	Cases
Age	62 ± 11	Years
BMI	28.20 ± 3.92	
Stage		
Stage I	2	Cases
Stage II	2	Cases
Stage III	6	Cases
Type of surgery		
Anterior rectal resection	5	Cases
Lower rectal resection	3	Cases
Abdominoperineal resection	2	Cases
Total operative time	270 ± 50.73	min
Intraoperative complication	1	Cases
Postoperative complication	1	Cases
Conversion	1	Cases

Of the 10 patients in the study, 7 survived and 3 died and 4 developed recurrences. Three patients developed distant recurrences and one patient local relapse. All 3 patients who developed distant recurrences died. The patients who died had higher T stage and the patient who developed local relapse was stage T4a. The number of lymph nodes excised through robotic surgery varied between 16 and 18. It was observed that LNR was higher in deceased patients. The tumor size did not differ significantly between the two groups. Most patients had G2 tumor grade, one patient with G3 grading developed distance recurrences and died. The main morphopathological characteristics of the study group are presented in Table 2.

Table 2 The main morphopathological characteristics of the study group

Characteristics	Survivors	Deceased	Recurrences
TNM			
Stage I (T2N0)	2		
Stage II A (T3N0)	1		
Stage II B (T4aN0)	1		1 (local)
Stage III A (T2N1b)	2		
Stage III B	2		
T2N2a		1	1 (distant)
T3N2a	1		
Stage III C		2	
T3N2b		1	1 (distant)
T4aN2a		1	1 (distant)
LNR 1	1		
LNR 2	2		
LNR 3		1	
LNR 4		2	
LNR 5			
Tumor size			
<4 cm	2	2	1
>4 cm	2	2	1
Tumor grade			
G1			
G2	6	2	1
G3		1	

4 Discussions

Total mesorectal excision for rectal cancer can be safely done using the da Vinci surgery system. The method is safe and feasible, as confirmed by other studies in the literature [4, 5].

Total mesorectal excision (TME) is a standard technique in rectal surgery. The correct dissection of the mesorectum is an important prognostic factor affecting the postoperative outcome. The da Vinci surgical system is best suited for mesorectal dissection, both due to the three-dimensional image and the possibility of a precise dissection in the narrow space of the pelvis enabled by the robotic surgical instruments. Several studies that compared the results of robotic rectal surgery versus laparoscopic surgery showed the obvious utility of robotic dissection, especially when performed under difficult conditions (narrow pelvis) [6, 7].

Studies have shown that there are no significant differences between robotic and laparoscopic surgery of the rectum in terms of: operating time, blood loss, postoperative recovery. However, the dexterity and flexibility of the da Vinci robotic system have proven useful in certain situations and especially in the mobilization of the splenic flexure, the dissection of the lower mesenteric artery, the identification and preservation of nerve plexuses, the dissection in a narrow pelvis (especially in men).

In the study we showed that there are no statistical differences between deceased patients and robotic survivors. Local or distant relapse still depends on staging, especially on stage T and N. In robotic patients, the number of excised lymph nodes was between 16 and 18, higher than the average of 12 lymph nodes in laparoscopic or open surgery. Patients with advanced T and N stages experienced relapse more frequently. Patients with higher LNR experienced more frequent relapse at a distance.

Robotic-assisted rectal surgery using the da Vinci platform is technically achievable and safe, and total mesorectal excision (TME) can be performed via robotic surgery [8], resulting in excellent outcomes, even under difficult conditions (narrow spaces, post-radiotherapy), being an alternative to laparoscopic surgery, especially in what concerns nerve-sparing surgery [9]. Survival and recurrence at 5 years after robotic surgery was similar to open or laparoscopic surgery for rectal cancer. Local recurrence occurred in patients with higher T status and distant recurrences in patients with advanced N-stage rectal cancer and with higher LNR, similar results obtained in laparoscopic or open surgery. Although in terms of survival and relapse robotic surgery has no major advantages [10, 11]. The possibility of careful dissection in narrow spaces with preservation of nervous plexuses, better lymph node dissection and better mesorectal excision make robotic surgery a feasible and particularly useful technique in rectal cancer surgery [12].

5 Conclusions

Regarding survival and postoperative recurrences, there are no significant differences between robotic and laparoscopic or open surgery. The main advantages of robotic surgery are the possibility of careful dissection in narrow spaces with the nerve plexuses preservation, which will lead to an increase the quality of life of these patients. However, the method should be evaluated over long-term on large number of patients through randomized trials before being generally accepted as surgical technique in rectal cancer.

Conflict of Interest The authors declare that they have no conflict of interest.

References

1. Baik, S.H., Ko, Y.T., Kang, C.M., Lee, W.J., Kim, N.K., Sohn, S.K., et al.: Robotic tumor-specific mesorectal excision of rectal cancer: short-term outcome of a pilot randomized trial. Surg. Endosc. **22**, 1601–1608 (2008)
2. Baik, S.H.: Robotic colorectal surgery. Yonsei Med. J. **49**, 891–896 (2008)
3. Micu, B., Micu, C., Leucuta, D.C., Crivii, C., Constantea, N.: The role and prognostic impact of lymph node ratio on stage III colorectal cancer. Clujul Med. **86**(3), 245–249 (2013)
4. Kim, C.N., Bae, S.U., Lee, S.G., Yang, S.H., Hyun, I.G., Jang, J.H., et al.: Clinical and oncologic outcomes of totally robotic total mesorectal excision for rectal cancer: initial results in a center for minimally invasive surgery. Int. J. Colorectal Dis. **31**(4), 843–852 (2016)
5. Hellan, M., Ouellette, J., Lagares-Garcia, J.A., Rauh, S.M., Kennedy, H.L., Nicholson, J.D., et al.: Robotic rectal cancer resection: a retrospective multicenter analysis. Ann. Surg. Oncol. **22**(7), 2151–2158 (2015)
6. Park, S., Kim, N.K.: The role of robotic surgery for rectal cancer: overcoming technical challenges in laparoscopic surgery by advanced techniques. Korean Med. Sci. **30**(7), 837–846 (2015)
7. Araujo, S.E., Seid, V.E., Klajner, S.: Robotic surgery for rectal cancer: current immediate clinical and oncological outcomes. World J. Gastroenterol. **20**(39), 14359–14370 (2014)
8. Feroci, F., Vannucchi, A., Bianchi, P.P., Cantafio, S., Garzi, A., Formisano, G., Scatizzi, M.: Total mesorectal excision for mid and low rectal cancer: laparoscopic vs robotic surgery. World J. Gastroenterol. **22**(13), 3602–3610 (2016). https://doi.org/10.3748/wjg.v22.i13.3602
9. Crolla, R.M.P.H., Tersteeg, J.J.C., van der Schelling, G.P., Wijsman, J.H., Schreinemakers, J.M.J.: Robot-assisted laparoscopic resection of clinical T4b tumours of distal sigmoid and rectum: initial results. Surg. Endosc., 16 May 2018. https://doi.org/10.1007/s00464-018-6210-4
10. Pinar, I., Fransgaard, T., Thygesen, L.C., Gögenur, I.: Long-term outcomes of robot-assisted surgery in patients with colorectal cancer. Ann. Surg. Oncol. (2018). https://doi.org/10.1245/s10434-018-6862-2
11. Fransgaard, T., Pinar, I., Thygesen, L.C., Gögenur, I.: Association between robot-assisted surgery and resection quality in patients with colorectal cancer. Surg. Oncol. **27**(2), 177–184 (2018). https://doi.org/10.1016/j.suronc.2018.03.003
12. de Jesus, J.P., Valadão, M., de Castro Araujo, R.O., Cesar, D., Linhares, E., Iglesias, A.C.: The circumferential resection margins status: a comparison of robotic, laparoscopic and open total mesorectal excision for mid and low rectal cancer. Eur. J. Surg. Oncol. **42**(6), 808–812 (2016). https://doi.org/10.1016/j.ejso.2016.03

Prognostic Implications of Sentinel Lymph Node Mapping in Stage I and II Colorectal Cancer Patients

Bogdan Vasile Micu, C. M. Micu, D. Chirila, H. Silaghi, D. R. Miclaus, M. S. Muresan, T. R. Pop, N. Constantea, and C. Ionescu

Abstract

The aim of the study was to identify lymph node micrometastases in order to demonstrate the prognosis of colorectal cancer patients staged I and II undergoing curative surgery. We conducted a prospective study on a total of 44 patients with stage I–III colorectal cancer, undergoing radical surgery at the Fifth Department of Surgery of Cluj-Napoca Municipal Clinical Hospital between September 2012 and January 2015. For the identification of micrometastases we used the sentinel lymph node mapping by two techniques, in vivo and ex vivo. In N0 patients we conducted an immunohistochemical study to identify micrometastases. Patients were followed 3 years after surgery to identify possible relapses. The mean age was 63 years, 24 patients were males and 20 (45.5%) women. Ten patients (12.8%) had stage I cancer, 12 patients (27.3%) had stage II cancer, and 22 had stage III cancer. Sentinel lymph node detection rate was similar for the in vivo technique and for the ex vivo technique. The percentage for the detection of micrometastases was 25% in vivo and 33.3% ex vivo. The 3-year postoperative recurrence rate was 25% in overstaged patients. The presence of micrometastases should be considered as a negative prognostic factor in patients with stage I and II colorectal cancer.

Keywords

Micrometastases • Colorectal cancer • Prognosis • Sentinel lymph node

B. V. Micu (✉) · C. M. Micu · D. Chirila · H. Silaghi · D. R. Miclaus · M. S. Muresan · T. R. Pop · N. Constantea · C. Ionescu
5th Surgical Department, "Iuliu Hateganu" University of Medicine and Pharmacy, Tabacarilor no. 11, Cluj-Napoca, Romania
e-mail: micubogdan@yahoo.com

C. M. Micu
Department of Anatomy and Embryology, "Iuliu Hateganu" University of Medicine and Pharmacy, Cluj-Napoca, Romania

1 Introduction

The most important prognostic factor in colorectal cancer is the stage of the tumor determined by the identification of T and N stage [1]. N0 stage in which the histopathological examination did not identify any regional lymph node metastasis requires no adjuvant treatment. N+ with positive lymph nodes requires adjuvant therapy.

Cancer recurrence occurs in approximately 20–30% of NO cases [2]. One reason could be the presence of lymph node micrometastases at the time of surgery. All excised lymph nodes should be evaluated for the presence of micrometastases, objective achieved by immunohistochemistry and chain-growth polymerization, techniques that are extremely costly and they are not part of the current practice. the sentinel lymph node is the first lymph node receiving drainage from the primary tumor, and once identified, it may be more easily subjected to tests to identify macro or micro metastases. If micrometastases are detected, overstaging may occur, which means that a patient that was initially identified with N0 stage becomes N+, with the possibility of being at a more advanced stage and receiving adjuvant treatment [3]. In colorectal cancer, the method for the detection of the sentinel lymph node has the role of determining lymphatic staging more precisely in order to identify patients at high risk of developing tumor progression or recurrence [4–6].

The aim of our study is to identify lymph node micrometastases using the sentinel lymph node (in vivo and in vitro) in order to demonstrate the prognosis of colorectal cancer patients undergoing curative surgery.

2 Materials and Methods

We conducted a prospective study consisting of 44 patients with stage I–III colorectal cancer, admitted and undergoing radical surgery at the Fifth Department of Surgery of the

S. Vlad and N. M. Roman (eds.), *6th International Conference on Advancements of Medicine and Health Care through Technology; 17–20 October 2018, Cluj-Napoca, Romania*, IFMBE Proceedings 71,
https://doi.org/10.1007/978-981-13-6207-1_47

Municipal Clinical Hospital in Cluj-Napoca between September 2012 and January 2015. Exclusion criteria in the study were the presence of distant metastases, synchronous primary tumors, locally advanced tumors (T4a, T4b), emergency surgery, palliative surgery, patients with preoperative chemotherapy, patients with tumors located in the lower or medial rectum, patients with BMI > 30, with incomplete data and those who did not. All the patients sign the informed consent form and the study was approved by the Ethics Committee of Cluj-Napoca Municipal Clinical Hospital.

To identify the sentinel lymph node we used two different techniques—in vivo and ex vivo—using 1% methylene blue vital stain. The in vivo technique for the detection of the sentinel lymph node was performed as indicated by Saha et al. [7]. After the peritoneal cavity was opened, loco-regional exploration was performed to identify the tumor, to check tumor topography, features, mobility, penetration in neighboring organs, general examination regarding the presence of synchronous tumors and remote metastases. The tumor mass moved to gain access to the tumor site without interrupting the lymphatic drainage pathways. The injection of 1–5 ml dye was made at circumferential peritumoral level using a 26–28 gauge needle. The injected area was gently massaged for about 5 min. The first colored lymph nodes (between 1 and 4) within the first 10 min after injection were considered the sentinel lymph nodes and they were stained intraoperatively. Surgery continued in the proposed standard manner. After surgery, the stained sentinel lymph nodes were excised and separately sent to the Department of Pathological Anatomy together with the resection piece.

The ex vivo technique for the detection of the sentinel lymph node was performed as described by Wong et al. [8]. Within 30 min after colorectal resection, the specimen was longitudinally incised on the anti-mesostenic edge. Submucosal injection of 0.5–1 ml methylene blue dye was performed into each of the four quadrants around the tumor. The injection sites were gently massaged for 2–5 min. The lymph nodes stained with blue dye in the first 10 min are considered the sentinel lymph nodes and are dissected and presented separately for pathological analysis.

The resections and the lymph nodes were examined histopathologically using the standard method. In case of patients with negative lymph-nodes and sentinel lymph nodes (N0) we performed an immunohistochemistry examination in order to identify micrometastases in sentinel or in other lymph node. For the immunohistochemical examination we used anti-cytokeratin 20 antibodies (K20.8 clone, CK20, dilution 1:400, DAKO, Carpinteria, CA).

The aim was to study the detection rate, accuracy, sensitivity, and overstaging, defined as the number of patients with micrometastasis in sentinel lymph nodes in relation to the number of patients staged N0 in routine histopathological examination. Our intention was to identify micrometastases in patients with colorectal cancer undergoing surgery in order to identify the recurrence rate (local or distant) in overstaged patients and to compare it with the recurrence rate of stage I and II patients. We follow-up the patients for a period of 3 years, in the first year at 3 and 6 months and after that annually through clinical examination, complete laboratory tests, abdominal ultrasound, chest X-ray and screening colonoscopy and whole CT scan. We identified distant recurrences by local and general exam, laboratory tests, general ultrasound, computed tomography, chest X-ray, scintigraphy (when was necessary) and local recurrences with lower gastrointestinal endoscopy with anastomotic biopsy and abdominal ultrasound.

We also calculated the survival rate after 3 years postoperatively.

The statistical analysis was performed using SPSS version 20. The data was considered to be nominal, ordinal or quantitative. Quantitative data were tested for normal distribution by the Kolmogorov-Smirnov test. Quantitative variables were scored by median and percentiles 25 and 75 (non-normal distribution). The nominal and ordinal variables were characterized by frequency and percentage.

3 Results

A total of 44 patients were enrolled in the study. The in vivo technique for the detection of the sentinel lymph node was performed in 22 patients and the ex vivo technique for the detection of the sentinel lymph node in the other 22 patients. The age in the study group was 63 (mean) years ranging between 46 and 84 years. 24 patients (54.5%) were men and 20 patients (45.5%) were women. The tumor was located in the cecum in 6 (13.6%) patients, in the ascending colon in six patients, in the transverse colon in 6 patients, in the left colic flexure in two patients, in the descending colon in two patients, in the sigmoid colon in 16 (36.6%) patients, and in the rectum in six patients.

From the 44 patients, stage T1 were classified two, stage T2 were 10 and the other 32 were stage T3. In 17 cases, the tumor was moderately differentiated. According to the TNM staging system, ten patients were classified as stage I, 12 patients as stage IIA, two patients as stage IIIA, 18 patients as stage IIIB and two patients as stage IIIC. In the study group patients with more than 12 resected lymph nodes were 72.3%. The main clinical and histopathological characteristics of the patients in the group are presented in Table 1.

Sentinel lymph node detection was performed in 16 out of 22 patients using in vivo technique and in 18 out of 22 patients using the ex vivo technique. In all cases where the sentinel lymph node could not be detected, the failure was due to technical mistakes.

Table 1 The main clinical and morphopathological characteristics of the patients in the study group

Variables	Ex vivo (no./%)	In vivo (no./%)
Men	14 (63.6)	10 (45.5)
Women	8 (36.4)	12 (54.5)
Right colon	6 (27.3)	6 (27.3)
Transverse colon	4 (9.1)	8 (18.2)
Left colon	14 (63.3)	6 (27.3)
Rectum	–	6 (27.3)
Stage I	4 (18.2)	6 (27.3)
Stage IIA	6 (27.3)	6 (27.3)
Stage IIB	–	–
Stage IIIA	–	2 (9.1)
Stage IIIB	10 (45.5)	8 (36.3)
Stage IIIC	2 (9.1)	–
Number of excised lymph nodes		
>12	18 (81.2)	16 (72.7)

Ex vivo technique was characterised by 88.8% accuracy rate, a false negative rate of 16.7 and 83.3% sensitivity. In vivo technique was characterised by 75% accuracy, a false negative rate of 25 and 75% rate of sensitivity. Between the two techniques there were no statistically significant differences in the detection rate, accuracy, false negative rate, sensitivity, and overstaging. In patients where standard examination of lymph nodes using hematoxylin and eosin staining did not detect any invasion (N0), immunohistochemical examination was performed to identify possible micrometastasis, using cytokeratin, in both sentinel lymph nodes and other lymph node.

We identified 14 cases of N0 where we were able to apply the immunohistochemical method and the result was 4 positive cases. In vivo technique, two cases of micrometastases in sentinel lymph nodes were identified in a number of 8 N0 cases, while in ex vivo technique, two cases of micrometastases in sentinel lymph nodes were identified out of 6 N0 cases. Resulting the overstaging phenomenon was 33.3% in ex vivo and 25% in in vivo, which increased sensitivity in the two cases. Overstaging occurred in 28.6% of N0 patients and in 9% of the entire study group. Overstaging was superior when using the ex vivo technique compared to the in vivo technique, but there were no statistically significant differences. Of the two patients overstaged using the ex vivo technique, one was stage I and the other stage IIA, and both patients overstaged using the in vivo technique were stage IIA. The four patients were followed for 3 years postoperatively and none followed adjuvant therapy. In the postoperative follow-up period, a single patient, stage IIA and overstaged using the ex vivo technique, showed recurrence, respectively secondary hepatic tumors. The result was a recurrence rate of 25% in overstaged patients.

4 Discussions

In our study, the number of locally advanced tumors (T3) accounted for 72.7% of all cases. This explains the reduced sensitivity rate and the increased false negative rate [6, 9].

As in other studies in the literature [10], there were no statistically significant differences between the two techniques in terms of detection rate, accuracy, sensitivity, false negative rate and overstaging.

Overstaging, one of the reasons for the detection of the sentinel lymph node, was 33.3% for the ex vivo technique and 25% for the in vivo technique, using immunohistochemistry to identify micrometastases in sentinel lymph nodes, while the rest of the lymph nodes remained negative. These values correlated with data in the literature, ranging between 0 and 50%. Overstaging was 28.6% in N0 patients and 9% in the entire study group, results slightly lower than other data in the literature [11] due to the fact that almost half of the patients in the study group were diagnosed in stage III (N+).

Recurrence rate was 25% in overstaged patients, compared with N0 patients, which was a statistically significant difference. Data on recurrence and survival in overstaged patients are contradictory in the literature, some studies showing similar results [4, 12], while others do not confirm the results [13], therefore further studies on larger and more homogeneous groups of patients with colorectal cancer are necessary, in which the technique used for the detection of the sentinel lymph node and of micrometastases should have higher detection rate and specificity.

5 Conclusions

The two techniques used for sentinel lymph node detection in colorectal cancer patients is a feasible, safe and inexpensive method both in vivo and ex vivo. In overstaged patients the recurrence rate is significantly higher when apply this technique and the presence of micrometastases should be considered in patients with colorectal cancer stage I and II. The presence of micrometastases should be considered in N0 patients with colorectal cancer a negative prognostic factor.

Conflict of Interest The authors declare that they have no conflict of interest.

References

1. Stephen, B.E., Byrd, D.R., Compton, C.C., et al.: Part III Digestive system: colon and rectum. In: Anonymous AJCC Cancer Staging Manual, 2017, 8th edn. Springer, New York (2017)
2. Figueredo, A., Coombes, M.E., Mukherjee, S.: Adjuvant therapy for completely resected stage II colon cancer. Cochrane Database Syst. Rev. 3 (2008)
3. Micu, B., Micu, C., Gherman, A., Sava, M., Pop, T.R., Constantea, N.: The role of sentinel lymph node analysis in patients with colorectal cancer undergoing surgery. HVM Bioflux **7**(2), 114–117 (2015)
4. Sloothaak, D.A., Sahami, S., van der Zaag-Loonen, H.J., van der Zaag, E.S., Tanis, P.J., Bemelman, W.A., et al.: The prognostic value of micrometastases and isolated tumour cells in histologically negative lymph nodes of patients with colorectal cancer: a systematic review and meta-analysis. Eur. J. Surg. Oncol. **40**(3), 263–269 (2014)
5. Märkl, B., Herbst, C., Cacchi, C., et al.: Prognostic significance of histologically detected lymph node micrometastases of sizes between 0.2 and 2 mm in colorectal cancer. Int. J. Colorectal Dis. **28**(7), 977–983 (2013)
6. van der Zaag, E.S., Bouma, W.H., Tanis, P.J., et al.: Systematic review of sentinel lymph node mapping procedure in colorectal cancer. Ann. Surg. Oncol. **19**(11), 3449–3459 (2012)
7. Saha, S., Wiese, D., Badin, J., et al.: Technical details of sentinel lymph node mapping in colorectal cancer and its impact on staging. Ann. Surg. Oncol. **7**(2), 120–124 (2000)
8. Wong, J.H., Steineman, S., Calderia, C., et al.: Ex vivo sentinel node mapping in carcinoma of the colon and rectum. Ann. Surg. **233**(5), 155–221 (2001)
9. Iddings, D., Ahmad, A., Elashoff, D., Bilchik, A.: The prognostic effect of micrometastases in previously staged lymph node negative (N0) colorectal carcinoma: a meta-analysis. Ann. Surg. Oncol. **13**, 1386 (2006)
10. Viehl, C.T., Guller, U., Langer, I., et al.: Factors influencing the success of in vivo sentinel lymph node procedure in colon cancer patients: Swiss prospective, multicenter study sentinel lymph node procedure in colon cancer **37**(4), 873–877 (2013)
11. Wang, F.L., Shen, F., Wan, D.S., Lu, Z.H., Li, L.R., Chen, G., et al.: Ex vivo localization and immunohistochemical detection of sentinel lymph node micrometastasis in patients with colorectal cancer can upgrade tumor staging. Diagn Pathol. **22**(7), 71 (2012)
12. Sloothaak, D.A.M., van der Linden, R.L.A., van de Velde, C.J.H., Bemelman, W.A., Lips, D.J., van der Linden, J.C., et al.: Prognostic implications of occult nodal tumour cells in stage I and II colon cancer: the correlation between micrometastasis and disease recurrence. Eur. J. Surg. Oncol. **43**(8), 1456–1462 (2017)
13. Estrada, O., Pulido, L., Admella, C., Hidalgo, L.A., Clavé, P., Suñol, X.: Sentinel lymph node biopsy as a prognostic factor in non-metastatic colon cancer: a prospective study. Clin. Transl. Oncol. **19**(4), 432–439 (2017)

Metallic Nanoparticles in Otology

A. A. Maniu, M. Perde-Schrepler, E. Fischer-Fodor, A. Florea, George Sebastian Chis, and A. I. Roman

Abstract

Introduction. Nanomedicine is the medical application of nanotechnology and concerns the use of precisely engineered materials at nano length scale, to early detection and prevention, improved diagnosis, proper treatment and follow-up of diseases. This new and exciting specialty finds more and more applications in all medical fields, the otology being part of them. This review considers current developments and future prospects for metallic nanomaterials used in otology. Materials and Methods. The online medical reference databases PubMed, Google Scholar, ISI Web of Science and Science Direct were searched with search terms "Nanotechnology, Nanomedicine, Metallic Nanoparticles" in combination with "Otology, ENT, middle ear, inner ear diseases" in turn. Furthermore, we are giving an overview of the work of the Department of Otorhinolaryngology, Head and Neck Surgery, "Iuliu Haţieganu" University of Medicine and Pharmacy, Cluj-Napoca and Tumor Biology Department, The Institute of Oncology "Prof. Dr. I. Chiricuta", Cluj-Napoca Results. Metallic Nanoparticles proved to have strong anti-bacterial, anti-viral, and anti-fungal activities by the inhibition of biofilm formation, destruction of viruses and fungi and stimulation of the host's immune response. These properties make metallic nanoparticles such as silver nanoparticles extremely attractive to be used to treat middle ear infectious diseases such as otitis media. For the inner ear diseases many studies have used metallic nanoparticles to deliver drugs, genes, and growth factors. The current limitations for the clinical application are related to their possible cytotoxic effect. Conclusions. The future treatment of otological diseases could be revolutionized by advances in nanomedicine. The current review suggest that further studies are required to be able to confirm the safety of metallic nanoparticle derived application to use in life.

Keywords

Nanomedicine • Metallic nanoparticle • Middle ear diseases • Inner ear diseases

1 Introduction

The nanotechnology is a new field in science based on combining the ultrafine size dimensions of nanometers with technology [1]. Nanomedicine is the medical application of nanotechnology [2], and concerns the use of precisely engineered materials at nano length scale (10–9 m), to early detection and prevention, improved diagnosis, proper treatment and follow-up of diseases [3]. The domain has grown exponentially in past 30 years with the participation of chemists, biologists, biotechnologists, biomedical scientists, doctors, clinicians, and is focus particularly on spreading the research to find treatment of difficult diseases [4]. Nano-otology is the application of nanomedicine to diseases and disorders of the ear. In ear diseases, as in other medical fields, nanomaterials can be useful for both in vivo and in vitro biomedical research and applications [5]. The list includes fluorescent biologic labels, drug and gene delivery, biodetection of pathogens, detection of proteins, probing of

A. A. Maniu
Department of Otolaryngology, University of Medicine and Pharmacy "Iuliu Hatieganu", Cluj-Napoca, Romania

M. Perde-Schrepler · E. Fischer-Fodor
Tumor Biology Department, The Institute of Oncology "Prof. Dr. I. Chiricuta", 400015 Cluj-Napoca, Romania

A. Florea
Department of Molecular Biology, University of Medicine and Pharmacy "Iuliu Hatieganu", Cluj-Napoca, Romania

G. S. Chis (✉)
Department of Economics Informatics, Faculty of Economics and Business Administration, Babeş Bolyai University, Teodor Mihali no. 58-60, Cluj-Napoca, Romania
e-mail: George.chis@econ.ubbcluj.ro

A. I. Roman
Department of Regional Gastroenterology Institute, Cluj-Napoca, Romania

S. Vlad and N. M. Roman (eds.), *6th International Conference on Advancements of Medicine and Health Care through Technology; 17–20 October 2018, Cluj-Napoca, Romania*, IFMBE Proceedings 71,
https://doi.org/10.1007/978-981-13-6207-1_48

DNA structures, tissue engineering, thermal ablation of tumors, separation and purification of molecules and cells, and MRI contrast enhancement. There are many types of nanomaterials, and a variety of others are expected to appear in the future. These can be grouped in: carbon based materials, metal based materials, dendrimers and composites. From all of them, metallic nanoparticles (MNPs) have become very attractive for otology due to theirs specific chemical properties such as: large surface energies, plasmon excitation, quantum confinement, and short range ordering [6]. A number of metals have been reported to yield nanoparticle (NPs) structures, some of them being gold, silver, zinc, iron, titanium, magnesium and copper. While gold and silver form NPs as pure metals, others yield NPs in their oxidized form. The antibacterial effect of metallic NPs is of interest for middle ear inflammatory diseases, while for the inner ear the first wide-scale concern is in drug delivery. The current limitations for the clinical application are related to their possible cytotoxic effect. This review considers current developments and future prospects for MNPs, particularly for silver nanoparticles (AgNPs), used in otology.

2 Materials and Methods

The online medical reference databases PubMed, Google Scholar, ISI Web of Science and Science Direct were searched with search terms "Nanotechnology, Nanomedicine, Metallic Nanoparticles" in combination with "Otology, ENT, middle ear, inner ear diseases" in turn.

3 Results

3.1 MNPs and Middle Ear Diseases

Middle ear inflammatory diseases are termed as otitis. Acute otitis media (AOM) caused by either bacteria or virus, is one of the most common illnesses in childhood. Up to 80% of children under the age of six will experience at least one ear infection, and while most resolve spontaneously, 30–40% will persist, leading to chronic disease [7]. It is known that in acute otitis media the germs involved are those Gram positive: *Streptococcus pneumoniae* and *pyogenes*, *Haemophilus influenzae* and *Moraxella catarrhalis* [8], while in chronic otitis media (COM) prevails Gram negative forms such as: *Pseudomonas aeruginosa*, *Staphylococcus aureus*, Proteus, Klebsiella and Escherichia species [9]. COM, characterized by recurrent infections is a significant public health issue having high morbidity and complications: hearing loss, dizziness, due to vestibular impairment and even though intracranial fatal complications as meningitis and cerebral abscesses [10]. Despite a lot of research regarding the pathogenesis of COM, many aspects still need to be clarified, that is: what are the factors that allow the acute infection within the middle ear and mastoid to develop into chronic disease, and why in some children the disease heals while others turn into chronic illness. Besides varied factors involved in the evolution, of COM (immunological, and genetically determined factors, as well as Eustachian tube characteristics,) biofilms microbial infection are supposed to have a significant role [11]. A biofilm is a population of bacterial cells growing on a surface, enclosed in an exopolysaccharide matrix; being difficult to eradicate, they may attach to damaged tissue, such as exposed osteitic bone and ulcerated middle-ear mucosa, or to otologic implants such as tympanostomy tubes and could be the source of persistent infections. Many bacterial species relevant to otologic infections are known to form biofilms, including: *Pseudomonas aeruginosa*, *Haemophilus influenzae*, *Streptococcus pneumoniae*, and *Staphyloccocus aureus* [12, 13]. Furthermore the presence of antibiotic-resistant bacterial biofilms in particular forms of COM such as cholesteatoma may elaborate lipopolysaccharide and other bacterial products that stimulate osteoclastogenesis with bone erosion, this being able to explain their aggressiveness, which leads to bone erosion and complications [13].

Despite the advances recorded in the drug industry, and the appearance of new classes of antibiotics, medical professionals all over the world face one major cause of concern, that is, the development, of multiple drug-resistant bacteria [14]. In otology as in other medical field, multi-drug resistance still represents an increasing problem in the treatment of infections, and the widespread use of broad-spectrum antibiotics has produced antibiotic resistance for many human bacterial pathogens. NPs possess antimicrobial activity which makes them a proper alternative for antibiotics. In recent years, there has been growing interest in the synthesis and study of the antibacterial effect of NPs. In all the NPs with antibacterial properties, MNPs are the best and of these most studied are AgNPs [15].

Among the metallic nanoparticles (MNPs) those based on Copper, Zinc, Gold, Iron oxide and Silver have been studied for their antibacterial properties. There are several mechanisms of action by which they produce growth inhibition of microbes [16–18]. The main mechanism refers to cell wall and cell membrane damage, causing cell lysis. MNPs adhere to the bacterial membranes via electrostatic interactions, thereby disrupting their integrity [19]. AgNPs was found to degrade the lipopolysaccharide molecules of the cell wall and to adhere to the bacterial membranes via electrostatic interactions altering the membrane permeability [20, 21]. Copper NPs and ZnO NPs were analyzed for their interference with cell growth by hamper the cellular membranes [22, 23].

Another mechanism considered to be the most important for their cytotoxicity, is their capacity to dissolute into toxic

ions that cause inactivation of cellular proteins and enzymes penetrate the cell surface, and induce DNA damage [24]. This phenomenon happens especially for Silver NPs but also Gold NPs and Zinc oxide NPs are also known to react in this way [25, 26].

Other mechanisms of action studies, no less important, are generation of reactive oxygen species, DNA damage and interaction with vital proteins [26–28]. Among all of MNPs, AgNPS is the most used due to their unique physical and chemical properties. AgNPs with different sizes and shapes exhibit distinct antimicrobial activity. Smaller particles are more efficient to kill bacteria than the larger ones, probably due to the higher surface areas, which make it easier for them to attach to cell membranes and enter the cells [29]. AgNPs acts by killing bacteria rather than bacteriostatic mechanism and has a vast spectrum of antimicrobial activity both Gram-positive and Gram-negative bacteria (including *Escherichia coli*, *Staphylococcus aureus*, *Pseudomonas aeruginosa*, *Staphylococcus aureus*, and *Streptococcus mutans*) [30]. Furthermore it action extends to multidrug-resistant *Pseudomonas aeruginosa*, ampicillin-resistant *E. coli* O157:H7 and erythromycin-resistant *Streptococcus pyogenes* [31, 32]. AgNPs antifungal and antiviral activity has also been reported [33, 34]. The potential application of nanoparticles for the prevention of acute ear infections was investigated in a recent study in which AgNPs was obtained by, using cerumen microflora [35]. The antibacterial assays were performed by standard disc diffusion method against cultures of inoculums (50 μl) of *Streptococcus pneumonia* which is a prevalent bacterium in acute ear infections [35]. The same therapeutic strategy was encouraged by a clinical study on treatment of relapses of chronic suppurative otitis media using a preparation containing AgNPs. The study showed that AgNPs eliminated clinical symptoms and positive dynamics of the objective signs of the disease, such as reduction or termination of pathological exudation and stimulation of the epidermization processes, which was stable during the observation time of 6 months [36]. In COM surgical treatment allow to reconstruct hearing mechanism when the medical therapy falls, damaged middle ear ossicles are replaced by various prosthesis (metals, ceramics, plastics and composites). In the surgery of ossicular replacement prosthesis none of implants possess bactericidal properties. Therefore, antimicrobial polymers are highly demanded as a strategy to avoid otitis media infections [37]. Some studies that tested the biological properties of a new composite prosthesis containing AgNPs 45T, have shown encouraging results regarding the elimination of bacteria during inflammation in the middle ear [38].

Despite the fact that a large number of publications have studied the potential beneficial effects of AgNPs in treating infectious diseases, due to its antimicrobial activity, there are very few studies exclusively focusing on ear. Even though germs such as *Streptococcus pneumonia* or *Pseudomonas aeruginosa* are also involved in the pathogenesis of otitis media, it is of the utmost importance that research is done on the best modality to use and dose the silver nanoparticles to treat inflammatory middle ear diseases, therefore avoiding toxicity.

3.2 MNPs and Inner Ear Diseases

Hearing loss is a common feature of many inner ear diseases, including presbycusis, sudden sensorineural hearing loss, genetic diseases, noise-induced hearing loss, ototoxic hearing loss, and autoimmune inner ear disease [39, 40]. Once the sensory-neural transducer epithelial cells and nerve cells of the inner ear have been destroyed, they never recover, and hearing loss is definitive [40]. One of several reason for this condition, is that the drug does not readily reach the inner ear. When a drug is administered systemically, it must cross the blood labyrinth barrier to reach the inner ear. Therefore, high doses of medication must be administered to achieve the appropriate drug concentration in the inner ear and have a therapeutic effect. Intratympanic drug injection has been used to address these problems [41]. Several methods have been proposed to improve the efficiency of intratympanic drug injection, such as use of microcatheter implantation, hydrogels, and nanoparticles [42]. Direct observation of drugs or nanoparticles in the inner ear with micro-CT or MRI can be used for quantitative analysis of the amount or distribution of a drug delivered to the cochlea. Zou et al. [44] recently injected AgNPs intratympanically and observed the distribution of AgNPs in the middle and inner ear using micro-CT, showing a gradient concentration from the middle ear to the inner ear. Another modality to help drugs to get access to the inner ear passing round window membrane is through magnetic assistance using Iron oxide NPs [43].

Silica nanoparticles have a number of attractive properties, including commercial availability, narrow particle size distribution from 20 to 200 nm, and biodegradability under physiological conditions, therefore can be used as medicines carrier [45].

Of the prospective applications in nanomedicine, targeted delivery of therapeutics and enhanced MRI imaging, both utilizing NPs Fe_3O_4, may have the greatest clinical impact [46]. Delivering therapeutics only to target tissues may reduce both side effects and cost while improving treatment. Substances with limited access to the inner ear may traverse the round window carrying a payload of drugs or genes to the inner ear [47].

The cochlear implant, the first device to restore a human sense, is an electronic substitute for lost mechanosensory hair cells. Users of cochlear implants however, suffer from in processing complex sounds such as music and in discriminating sounds in noisy environments [48]. Recent advances in

regenerative biology and medicine are opening new avenues for enhancing the efficacy of cochlear implants by improving the neural interface in the future and offer the possibility of an entirely biological solution for hearing loss.

There is a compelling need for the development of new sensory and neural prosthetic devices which are capable of more precise point stimulation. Metal nanoparticles like Au have strong surface interactions with electromagnetic fields —light, due to availability of free electrons in their conduction bands [49]. For small size particles (<20 nm) nearly all energy is absorbed and converted into heat presented a visible light stimulation method for modulating the firing patterns of electrically-excitable cells using surface plasmon resonance phenomena. In in vitro studies using gold (Au) NPs-coated nanoelectrodes, showed that this method (substrate coated with NPs) has the potential for incorporating this new technology into neural stimulation prosthetics, such as cochlear implants for the deaf, with very high spatial resolution [50].

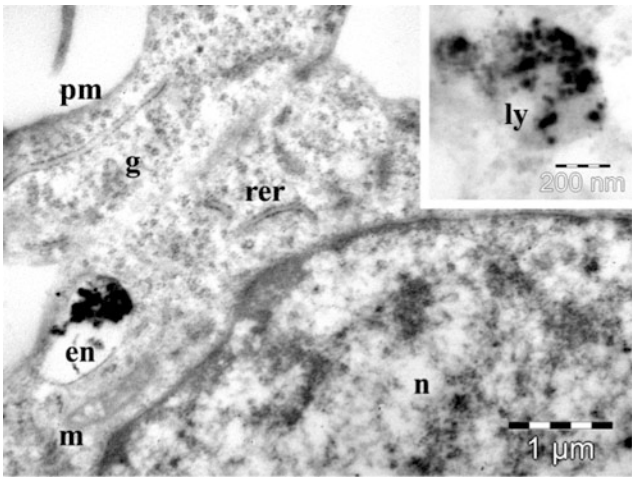

Fig. 1 Ultrastructure of a HEI-OC1 cell incubated for 24 h with the AgNPs with diameter of 110 µm. The NPs are present in an endosome (en) and in a lysosome (ly) (inset). g-glycogen granules; m-mitochondrion; pm-plasma membrane; rer-rough endoplasmic reticulum

3.3 Toxicity of the AgNPs

MNPs have been found to have different toxic effects on the environment and human health [51, 52]. Silver is found to have adverse toxic effects in the environment; its toxicity is largely believed to be due to free silver ions present in the aqueous phase. Free silver ions can cause adverse effects on all living beings which include permanent bluish gray discoloration of the skin or the eyes [53, 54]. However, the precise toxicological mechanisms are not known in detail for AgNPs. According to numerous reports, the overproduction of free radicals, which leads to oxidative stress, is caused by ions being released from AgNPs, including by a Trojan horse–type mechanism [55]. Size-dependent internalization of nanoparticles was demonstrated in a large number of studies being, in general, the highest for 40–50 nm particles. The size of nanoparticles is considered to be one of the most important factors influencing their toxicity [56]. In one of our unpublished study, in which we investigated the toxicity of AgNPs in vivo we found out that the intracellular silver concentration was not correlated with the cytotoxicity but the size was (Fig. 1).

Although AgNPs may directly damage the sensorineural cells in the inner ear, complete recovery of hearing loss induced by 200 µg/ml AgNPs (in vivo studies) suggested that most of the inner and outer hair cells and spiral ganglion cells are preserved, and hearing loss is mainly due to destabilized ion homeostasis [57]. One comparative study investigated the toxicity of silver nanoparticle in vivo and in vitro (rat ear and BALB/c 3T3 cell line). In in vitro studies, the IC50 for AgNPs in neutral red uptake assay was lower than that in NAD(P)H-dependent cellular oxidoreductase enzyme assay (WST-1) and higher than that in total cellular ATP and nuclear membrane integrity (propidium iodide) assessments [57]. In vivo experiments, magnetic resonance imaging (MRI) showed that significant changes in the permeability of biological barriers occurred in the middle ear mucosa, the skin of the external ear canal, and the inner ear at 5 h post-transtympanic injection of AgNPs at concentrations ranging from 20 to 4000 µg/ml. The alterations in permeability showed a dosage-response relationship, and were reversible. Their results showed that individual cells in vitro are more sensitive to AgNPs than the inner ear cells in vivo. The main mechanism of toxicity of AgNPs was the impairment of the mitochondrial function [58]. Another recent study hypothesized that AgNPs induced glycosaminoglycan accumulation in the basement membrane that associated with the up-regulation of its component hyaluronic acid, known as a hydrophilic molecule of binding and retaining water, and caused toxicities in the kidney and cochlea. The study was carried out on rats that received a single injection of AgNPs either in the tail vein or middle ear cavity and induced hearing loss (a reduction of threshold shifts in the AgNP-ear group was observed at all tested frequencies). The explanation could be that the up-regulation of hyaluronic acid in the basilar membrane might disorganize the tuned resonant frequency map, as mass, thickness, and stiffness of the basilar membrane that are essential to create response to sound wave [59]. However, before formal application in the clinic practice, sophisticated toxicological study on AgNPs in the inner ear to evaluate any potential risk of the new agent is necessary and the concentration of

AgNPs should be tightly controlled in clinic application in treating ear disease. The rat ear model might be expended to other engineered nanomaterials in nanotoxicology study.

4 Conclusions

This article has attempted to provide a useful overview of the new and exciting world of nanootology. In the future MNPs may solve the problems for infectious middle ear diseases. For the inner ear the first wide-scale application of MNPs will probably be in drug delivery. Anyway the toxicity of this materials still need to be investigated.

Conflict of Interest The authors declare that they have no conflict of interest.

References

1. Taniguchi, N.: On the basic concept of nanotechnology. In: Proceedings of the International Conference Production Engineering, Tokyo, Part II, Japan Society of Precision Engineering, pp. 18–23 (1974)
2. Freitas, R.A. (1999). Nanomedicine: Basic Capabilities, 1. Landes Bioscience, Austin, TX. ISBN 978-1-57059-645-2
3. Farokhzad, O.C., Langer, R.: Nanomedicine: developing smarter therapeutic and diagnostic modalities. Adv. Drug Deliv. Rev. **58**, 1456–1459 (2006)
4. Chhikara, B.S.: Current trends in nanomedicine and nanobiotechnology research. Appl. Nanomed. **2**(1), 1–6 (2017)
5. Curtis, A., Wilkinson, C.: Nantotechniques and approaches in biotechnology. Trends Biotechnol. **19**, 97 (2001)
6. Appenzeller, T.: The man who dared to think small. Science **254**, 1300 (1991)
7. Verhoeff, M., van der Veen, E.L., Rovers, M.M., Sanders, E.A.M., Schilder, A.G.M.: Chronic suppurative otitis media: a review. Int. J. Pediatr. Otorhinolaryngol. **70**, 1–12 (2006)
8. Rosenblüt, A., Santolaya, M.E., González, P., Corbalán, V., Avendanõ, L.F., Martínez, M.A., Hormazabal, J.C.: Bacterial and viral etiology of acute otitis media in Chilean children. Pediatr. Infect Dis. J. **20**(5), 501–507
9. Indudharan, R., Haq, J.A., Aiyar, S.: Antibiotics in chronic suppurative otitis media: a bacteriologic study. Ann. Otol. Rhinol. Laryngol. **108**(5), 440–445 (1999)
10. Verhoeff, M., van der Veen, E.L., Rovers, M.M., Elisabeth A.M. Sanders, Schilder, A.G.M.: Chronic suppurative otitis media: a review. Int. J. Pediatr. Otorhinolaryngol. **70**, 1–12 (2006)
11. Post, J.C., Hiller, N.L., Nistico, L., Stoodley, P., Ehrlich, G.D.: The role of biofilms in otolaryngologic infections: update 2007. Curr. Opin. Otolaryngol. Head Neck Surg. **15**, 347–351 (2007). https://doi.org/10.1097/MOO.0b013e3282b97327
12. Bjarnsholt, T.: The role of bacterial biofilms in chronic infections, APMIS Suppl **136**, 1–51 (2013)
13. Georgescu, M., Vranceanu, D., Radulescu, L., Martu, C., Tusaliu, M., Curutiu, C., Dhya, M., Budu, V.: Microbial biofilms and implantable hearing aids—Rom. Biotechnol. Lett. **22**(4), 12681–12686 (2017) IF 0.381
14. Preciado, D., Caicedo, E., Jhanjee, R., Silver, R., Harris, G., Juhn, S.K., Choo, D.I., Ondrey, F.: *Pseudomonas aeruginosa* lipopolysaccharide induction of keratinocyte proliferation, NF-kappa B, and cyclin D1 is inhibited by indomethacin. J. Immunol. **174**(5), 2964–2973 (2005)
15. Rwrew Walker, B., Barrett, S., Polasky, S., Galaz, V., Folke, C., Engström, G., Ackerman, F., Arrow, K., Carpenter, S., Chopra, K., Daily, G., Ehrlich, P., Hughes, T., Kautsky, N., Levin, S., Mäler, K.G., Shogren, J., Vincent, J., Xepapadeas, T., de Zeeuw, A.: Environment. Looming global-scale failures and missing institutions. Science **325**, 1345–1346 (2009)
16. Halawani, R.E.M.: Nanomedicine opened new horizons for metal nanoparticles to treat multi-drug resistant organisms. Int. J. Curr. Microbiol. Appl. Sci. **5**(2), 397–414 (2016)
17. Rerwe Kaur, P., Thakur, R., Kumar, S., Dilbaghi, N.: Interaction of ZnO nanoparticles with food borne pathogens *Escherichia coli* DH5α and *Staphylococcus aureus* 5021 & their bactericidal efficacy. AIP Conf. Proc. **1393**, 153–154 (2011)
18. Li, Q., Mahendra, S., Lyon, D.Y., Brunet, L., Liga, M.V., Li, D., Alvarez, P.J.: Antimicrobial nanomaterials for water disinfection and microbial control: potential applications and implications. Water Res. **42**(18), 4591–4602 (2008)
19. Thill, A., Zeyons, O., Spalla, O., Chauvat, F., Rose, J., Auffan, M., Flank, A.M.: Cytotoxicity of CeO_2 nanoparticles for *Escherichia coli*. Physico-chemical insight of the cytotoxicity mechanism. Environ. Sci. Technol. **40**, 6151–6156
20. Iavicoli, I., Fontana, L., Leso, V., Bergamaschi, A.: The effects of nanomaterials as endocrine disruptors. Int. J. Mol. Sci. **14**, 16732–16801 (2013)
21. Salomonl, R., Léo, P., Montemor, A.F., Rinaldi, B.G., Rodrigues, M.F.A.: Antibacterial effect of silver nanoparticles in *Pseudomonas aeruginosa*. Science and Applications **10**, 115–121 (2017)
22. Sinha, R., Karan, R., Sinha, A., Khare, S.K.: Interaction and nanotoxic effect of ZnO and Ag nanoparticles on mesophilic and halophilic bacterial cells. Bioresour. Technol. **102**, 1516–1520 (2011)
23. Midander, K., Cronholm, P., Karlsson, H.L., Elihn, K., Moller, L., Leygraf, C., Wallinder, I.O.: Surface characteristics, copper release, and toxicity of nano and micrometer-sized copper and copper (II) oxide particles: a cross-disciplinary study. Small **5**, 389–399 (2009)
24. Kaur, P., Chaudhury, A., Thakur, R.: Synthesis of chitosan-silver nanocomposites and their antibacterial activity. Int. J. Sci. Eng. Res. **4**(4), 869 (2013)
25. Kaur, P., Thakur, R., Kumar, S., Dilbaghi, N.: Interaction of ZnO nanoparticles with food borne pathogens *Escherichia coli* DH5α and *Staphylococcus aureus* 5021 & their bactericidal efficacy. AIP Conf. Proc. **1393**, 153–154 (2011)
26. Kasemets, K., Ivask, A., Dubourguier, H.C., Kahru, A.: Toxicity of nanoparticles of ZnO, CuO and TiO_2 to yeast Saccharomyces cerevisiae. Toxicol. in Vitro **23**(6), 1116–1122 (2009)
27. Hanagata, N., Zhuang, F., Connolly, S., Li, J., Ogawa, N., Xu, M.: Molecular responses of human lung epithelial cells to the toxicity of copper oxide nanoparticles inferred from whole genome expression analysis. ASC Nano **5**(12), 9326–9338 (2011)
28. Feng, Q.L., Wu, J., Chen, G.Q., Cui, F.Z., Kim, T.N., Kim, J.O.: A mechanistic study of the antibacterial effect of silver ions on Escherichia coli and Staphylococcus aureus. J. Biomed. Mater. Res. **52**(4), 662–668 (2000)
29. Pal, S., Tak, Y.K., Song, J.M.: Does the antibacterial activity of silver nanoparticles depend on the shape of the nanoparticle? A study of the gram-negative bacterium *Escherichia coli*. Appl. Environ. Microbiol. **73**(6), 1712–1720 (2007). https://doi.org/10.1128/aem.02218-06
30. Lara, H.H., Ayala-Nunez, N.V., Turrent, L.D.I., Padilla, C.R.: Bactericidal effect of silver nanoparticles against multidrug-resistant bacteria. World J. Microbiol. Biotechnol. **26**(4), 615–621 (2010). https://doi.org/10.1007/s11274-009-0211-3

31. Li, W.R., Xie, X.B., Shi, Q.S., Duan, S.S., Ouyang, Y.S., Chen, Y. B.: Antibacterial effect of silver nanoparticles on *Staphylococcus aureus*. Biometals **24**(1), 135–141 (2011). https://doi.org/10.1007/s10534-010-9381-6
32. Shahverdi, A.R., Fakhimi, A., Shahverdi, H.R., Minaian, S.: Synthesis and effect of silver nanoparticles on the antibacterial activity of different antibiotics against *Staphylococcus aureus* and *Escherichia coli*. Nanomedicine **3**(2), 168–171 (2007). https://doi.org/10.1016/j.nano.2007.02.001
33. Wright, J.B., Lam, K., Hansen, D., Burrell, R.E.: Efficacy of topical silver against fungal burn wound pathogens. Am. J. Infect. Control **27**(4), 344–350 (1999). https://doi.org/10.1016/S0196-6553(99)70055-6
34. Butler, K.S., Peeler, D.J., Casey, B.J., Dair, B.J., Elespuru, R.K.: Silver nanoparticles: correlating nanoparticle size and cellular uptake with genotoxicity. Mutagenesis **30**(4), 577–591 (2015)
35. Dixit, A., Das, S., Jyoti, A., Kaushik, S.: Biogenic synthesis of silver nanoparticles and its potential application in prevention of acute ear infections. J. Pharm. Sci. Res. **9**(1), 14–17 (2017)
36. Ray, M., Yadav, A., Gade, A.: Silver nanoparticles as new generation of antimicrobials. Biotechnol Adv 27:76–83 (2009)
37. Semenov, F.V., Fidarova, K.M.: The treatment of the patients presenting with chronic inflammation of the trepanation cavity with a preparation containing silver nanoparticles following sanitation surgery of the open type. Vestn. Otorinolaringol. **6**, 117–119 (2012)
38. Ziąbka, M., Dziadek, M., Menaszek, E., Banasiuk, R., Królicka, A.: Middle ear prosthesis with bactericidal efficacy—in vitro investigation. Molecules **22**, 1681 (2017). https://doi.org/10.3390/molecules22101681
39. Ziąbka, M., Menaszek, E., Tarasiuk, J., Wroński, S.: Biocompatible nanocomposite implant with silver nanoparticles for otology—in vivo evaluation. Nanomaterials **8**, 764 (2018). https://doi.org/10.3390/nano8100764
40. Cavaleriu, B.D., Martu, D.V., Hritcu, L., et al.: Idiopathic sudden hearing loss: oxidative status before and after corticoid treatment. Arch. Biol. Sci. **67**(4), 1297–1302 (2015)
41. Juhn, S.K., Rybak, L.P., Fowlks, W.L.: Transport characteristics of the blood-Perilymph barrier. Am. J. Otolaryngol. Head Neck Med. Surg. **3**(6), 392–396 (1982)
42. Sajjadi, H., Paparella, M.M.: Meniere's disease. Lancet **372**(9636), 406–414 (2008)
43. McCall, A.A., Swan, E.E.L., Borenstein, J.T., Sewell, W.F., Kujawa, S.G., McKenna, M.J.: Drug delivery for treatment of inner ear disease: current state of knowledge. Ear Hear. **31**(2), 156–165 (2010)
44. Zou, J., Hannula, M., Misra, S., et al.: Micro CT visualization of silver nanoparticles in the middle and inner ear of rat and transportation pathway after transtympanic injection. J. Nanobiotechnol. **13**(1) (Article no. 5) (2015)
45. Ge, X., Jackson, R.L., Liu, J., Harper, E.A., Hoffer, M.E., Wassel, R.A., Dormer, K.J., Kopke, R.D., Balough, B.J.: Distribution of PLGA nanoparticles in chinchilla cochleae. Otolaryngol. Head Neck Surg. **137**, 619–623 (2007)
46. Hsiao, J.K., Tsai, C.P., Chung, T.H., Hung, Y., Yao, M., Liu, H. M., Mou, C.Y., Yang, C.S., Chen, Y.C., Huang, D.M.: Mesoporous silica nanoparticles as a delivery system of gadolinium for effective human stem cell tracking. Small **4**, 1445–1452 (2008)
47. Shinkai, M., Ito, A.: Functional magnetic particles for medical application. Adv. Biochem. Eng. Biotechnol. **91**, 191–220 (2004)
48. Kopke, R.D., Wassel, R.A., Mondalek, F., Grady, B., Chen, K., Liu, J., Gibson, D., Dormer, K.J.: Magnetic nanoparticles: inner ear targeted molecule delivery and middle ear implant. Audiol. Neurotol. **11**, 123–133 (2006). https://doi.org/10.1159/000090685
49. Dabdoub, A., Fritzsch, B., Popper, A.N., et al.: The Primary Auditory Neurons of the Mammalian Cochlea. Springer, New York (2016)
50. Vohr, B.: Overview: infants and children with hearing loss-part I. Ment. Retard. Dev. Disabil. Res. Rev. **9**, 62–64 (2003)
51. Coronado, E.A., Encina, E.R., Stefani, F.D.: Optical properties of metallic nanoparticles: manipulating light, heat and forces at the nanoscale. Nanoscale **3**, 4042–4059 (2011)
52. Bazard, P., Frisina, R.D., Walton, J.P., Bhethanabotla, V.R.: Nanoparticle-based plasmonic transduction for modulation of electrically excitable cells. Sci. Rep. **7**, 7803. https://doi.org/10.1038/s41598-017-08141-4
53. Moreno-Garrido, I., Pérez, S., Blasco, J.: Toxicity of silver and gold nanoparticles on marine microalga. Mar. Environ. Res. **111**, 60–73 (2015)
54. Panyala, N.R., Pena-Mendez, E.M., Havel, J.: Silver or silver nanoparticles: a hazardous threat to the environment and human health? J. Appl. Biomed. **6**, 117–129 (2008)
55. Kahru, A., Savolainen, K.: Potential hazard of nanoparticles: from properties to biological and environmental effects. Toxicology **269** (2–3), 89–91 (2010)
56. Wijnhoven, S.W.P., Peijnenburg, W.J.G.M., Herberts, C.A., Hagens, W.I., Oomen, A.G., Heugens, E.H.W., Roszek, B., Bisschops, J., Gosens, I., van de Meent, D., Dekkers, S., de Jong, W.H., van Zijverden, M., Sips, A.J.A.M., Geertsma, R.E.: Nano-silver—a review of available data and knowledge gaps in human and environmental risk assessment. Nanotoxicology **3**(2), 109–138 (2009)
57. Zapór, L.: Effects of silver nanoparticles of different sizes on cytotoxicity and oxygen metabolism disorders in both reproductive and respiratory system cells. Arch. Environ. Prot. **42**(4), 32–47 (2016)
58. Zou, J., Zhang, Y., Yin, S., Wu, H., Pyykko, I.: Mitochondrial dysfunction disrupts trafficking of Kir 4.1 in spiral ganglion satellite cells. J. Neurosci. Res. **87**(1), 141–149 (2009)
59. Zou, J., Feng, H., Mannerström, M., Heinonen, T., Pyykkö, I.: Toxicity of silver nanoparticle in rat ear and BALB/c 3T3 cell line. J. Nanobiotechnol. **12**, 52 (2014)

New Era for Technology in Healthcare Powered by GDPR and Blockchain

O. P. Stan and L. Miclea

Abstract

The development of patients' electronic healthcare records has been hampered by bureaucracy and by heavy regulation within the medical field. Medical data recorded in a patient health records is a valuable source of information that can be used by doctors and researchers to improve the quality of healthcare and the quality of life. Medical data should be owned and controlled by the patient instead of being scattered in different healthcare systems that does not support transfer and semantic interoperability between different healthcare providers. Blockchain technology has demonstrated in the financial field that it is possible to create a safe, secure and auditable mechanism by using a decentralized network along with a public ledger. But with the adoption of the newly General Data Protection Regulation, all technological advances discovered by the Blockchain are now blocked. In this paper we present the main aspect of the GDPR and Blockchain technology in healthcare and a way in which this two can work together.

Keywords

GDPR • Blockchain • Personal data • Information governance • Medical informatics system

1 Introduction

The information's stored in an electronic healthcare record are sensitive and critical data used to diagnose and to provide the best treatment a patient can have. Throughout a life time, a patient can visit several medical units or hospitals, and doctors, in order to provide the best medical services, must have access to the entire history of a patient.

If the patient has to share its clinical data for research purposes or transfer them from one hospital to another, even with his or her consent, the trial is a lengthy process. Lately, a number of methods have been tried to get the transfer of this information in a safe and secure environment, but at the same time to achieve the semantic and syntactic interoperability of data [1, 2]. Because of this, a number of medical standards have emerged, such as HL7, openEHR, EN/ISO 13606 and the newest FHIR.

Aggregation of data for research purposes also requires consent, unless data are anonymous. However, it has been demonstrated that the independent release of local anonymous medical data corresponding to the same patient and coming from different sources (e.g., several health care institutions visited by the patient) could lead to patient de-identification and, therefore, confidentiality [3].

Due to the interoperability and security characteristics of medical information system [4], when Blockchain appeared, IT professionals in the medical field breathed lightly. They realized that this new technology is an important step in creating a mechanism for transfer and anonymization of the information in different medical units as well as research centers. But as early as May 2018, the European Community launched a new regulation named General Data Protection Regulation (GDPR) [5] on a person's personal data. The medical field is no exception to this new regulation.

In this paper we will present the main aspects of GDPR in health, what is Blockchain and how could revolutionize the medical system and the breach on how this two can coexist together.

2 General Data Protection Regulation

The General Data Protection Regulation (GDPR) [5] was launched by the European Parliament on April 14, 2016 and will enter into force from May 25, 2018, in all member states

O. P. Stan (✉) · L. Miclea
Faculty of Automation and Computer Science, Department of Automation, Technical University of Cluj Napoca, Cluj Napoca, Romania
e-mail: ovidiu.stan@aut.utcluj.ro

S. Vlad and N. M. Roman (eds.), *6th International Conference on Advancements of Medicine and Health Care through Technology; 17–20 October 2018, Cluj-Napoca, Romania*, IFMBE Proceedings 71,
https://doi.org/10.1007/978-981-13-6207-1_49

of the European Union. The GDPR will replace the Directive 95/46/EC and was designed to strengthen and to harmonize the data privacy laws of all European Community citizens. Basically, the GDPR is a new data framework law that enables citizens of EU to control their personal data and sensitive personal information's [6].

The GDPR seeks to harmonize the legislation on personal data within the European Community. This regulation lists the essential rights and freedoms of individuals with regard to the safety of their individual data [4].

At the same time, GDPR requires non-EU IT&C professionals to provide greater privacy concerns due to the fact that the GDPR also has extraterritorial applications. Even though data processors and data operators from outside the EU are increasingly using the international landscape for business globalization, with this new law, their responsibilities have grown heavily. This measure of the EU comes as a response to the effects of globalization, the increasing use of cloud computing, advanced technical advances, and new ransom ware attacks [7].

2.1 Personal Data

Personal data is defined in GDPR as any complex information (physical, genetic, mental, cultural, social, etc.) that can be used to identify a person directly or indirectly. These can be names, addresses and even online identifiers. Thus, as soon as GDPR enters into force, IP address information, cookies, etc. will be considered personal data if they can be used without too much effort in order to identify a person. At the same time, there is no differentiation of personal data related to the active environment—at home or at work [5, 6].

The GDPR define the sensitive personal data as being that complex information regarding political affiliation, sexual orientation, religious beliefs, racial or ethnic origin.

2.2 Deciphering Terminology

GDPR introduces innovative provisions as data controllers and data processors. Data controllers are those who established what will happened with personal data while the data processors represent the organizations or the individual who processes this information on behalf of the controller. This fact has an important impact in software/hardware systems and even in cloud systems since IaaS, SaaS and PaaS is now considered to be data processors [8].

According GDPR [5], data controller is not necessarily an individual. Most of the time, data controller is an organization. In fact, any company that stores personal data about a European Community citizen is considered a data controller and is responsible for processing employees' data but also for its customers' data. The data controller concept also exists in the US law, but there are a few differences. In the US, the person who administratively controls a paper or paperless document is called a custodian. The difference between the two terms is that the custodian is only in possession of the information while the data controller in GDPR has the power to determine the purpose and the way of processing the personal data.

The data processor's responsibilities are strongly highlighted in the GDPR, but the most important duties of the processor are stated in Art. 28 and Art. 42. They refer to the fact that the processor must offer reasonable assurances that the data security right is attained. GDPR also makes no distinction if data processing is performed by individuals or a computer, and in defining the data process it is included the entire life cycle of the information (from the collection till the destruction). For example, within GDPR, if a person examines any document then this process is seen as a form of processing. In other words, if a person or company uses personal data in some way, then they think you have processed them [9].

2.3 Data Transfer Process in GDPR

GDPR also presents aspects of the transfer of information both within and outside the European Community. The term "cross-border" is used when data transfer is desired within European Community. The transfer of information to countries outside the European Union is called "third-country data transfers" [5]. This information exchange process may take place not only between countries but also towards an area or territory of a country or an international organization but only after the recipient's security and equipment level has been considered adequate by the European Commission. If there is no such adequate compliance document, the transfer can only be done after the adoption of a supervisory authority, in accordance with Art. 46.2 of the GDPR [5]. If the transfer of information is done within the acceptance of the subject and not by being comply with the EU Regulation, then a consensus document must be explicitly created and should contain all the necessary information in order to inform the subject of all the risks a data transfer may encounter [10, 11, 12].

2.4 GDPR and Healthcare Sector

One of the most affected areas by this new law on processing personal data is healthcare. The GDPR present and define a new concept namely "data concerning health". This concept aggregate all personal data of a patient that discloses information about their past, present or future physical and

mental health [5]. It also includes all the administrative information collected by medical units during a hospital episode or during a simple general practitioner visit such as registration number, unique identification number, all data derived from laboratory test, laboratory results, etc.

Today's medical information systems contain a lot of personal information of patients that can be used to lead to major breakthroughs in medicine. But, unfortunately, the Art. 5 in GDPR, states that keeping personal data longer than necessary and without altering the original purpose for collection is not allowed.

Therewith, taking into account the importance and the sensitivity of the data handled in a medical information system, GDPR adds a series of 5 additional regulations when it talks about processing data concerning health. Firstly, under the conditions provided in Art. 9.2, it specifies that data controllers and data processors must enquire the explicit consent of the person to process their information. The individual exposure referred to in Art. 22 does not refer to the data on the health of the individual unless the individual has been explicitly given his consent or if the processing thereof is a public interest mentioned as such. Even if they are processed because it is a public interest, it is necessary to take all the necessary measures in order to protect the rights and the confidentiality of the data subjects. If medical information is processed on a large scale, then it is necessary to add an upshot assessment on the protection of these data. The Art. 37 brings additional charge, namely that a data protection agent should be appointed for organizations where the main activities involve large-scale processing of data concerning health. The last additional ground rule added by GDPR through the Art. 30.2 specifies that data controllers must keep a written record (audit) of all processing activities performed for and on behalf of the data controllers [5, 13, 14].

3 Blockchain Technology

Originally developed to keep financial transactions, Blockchain is actually an open decentralized database. The difference between Blockchain and the traditional way used by the banks or by the governments with a centralized database, Blockchain technology uses a distributed registry on a network of nodes (peer-to-peer) as show in Fig. 1. The decentralized cryptographic model in the Blockchain allows users to rely on each other and to make peer-to-peer transactions without the need for intermediaries [15].

The openness propriety of the Blockchain is in a consequence of the fact that all transactions made on the Blockchain are public and anyone can join and create their own transactions.

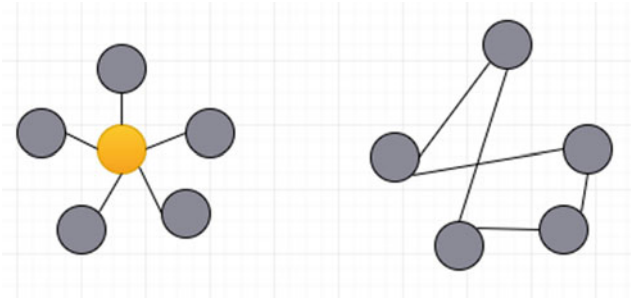

Fig. 1 Difference between centralize (left) and a P2P network (right)

P2P networks interact with each other as the human interact within people's social groups. They did not appear with the Blockchain, they have existed for a long time. Although it has a number of advantages, they also have their flaws, of which the most important are the safety and security gasp. This issue was resolved in 2008 with the emergence of the Bitcoin virtual currency. This virtual currency introduced a solution by adding a mathematical model in order to ensure the integrity of the system. Therefore, Blockchain is composed of a series of complex elements or process such as: description of the property; protecting the property of non-authorized access; storage of transaction data (ledger); preparing these ledgers in order to be distributed among an unsafe environment; creating a system with and from these ledger; adding new transactions to the already existing ledger; the process of determining what is the ledger with the most accurately truth.

A Blockchain can be represented as a stack in a vertical position where blocks are kept one over the other. The lowest block is the foundation of the entire stack. Blocks are linked together, and each block holds a reference to the previous block in the chain. These blocks use the SHA-256 hash algorithm in order to be identified. A block may have only one parent, but may have as many children as it wants (Fig. 2).

Basically, a block represents a set of transactions. If we analyze the block, it has several properties. First of all, they are safe from changes. This is because each block contains an identifier created by applying a SHA-256 function over the inside data of the block. This identifier number is named *hash* and its role is to verify the integrity of the transaction. When the hash of a block is created it is used not only the inside block data but also the hash of the previous block, making them dependent. This makes the whole blockchain free from changes, because if we change the hash of block N, then the hash of the $N + 1$ block automatically changes.

If changes are made to the existing data block, then all nodes present in the network run an algorithm to evaluate, verify and match transaction information across Blockchain's history. If most nodes approve the transaction, then a new block is added to the existing chain.

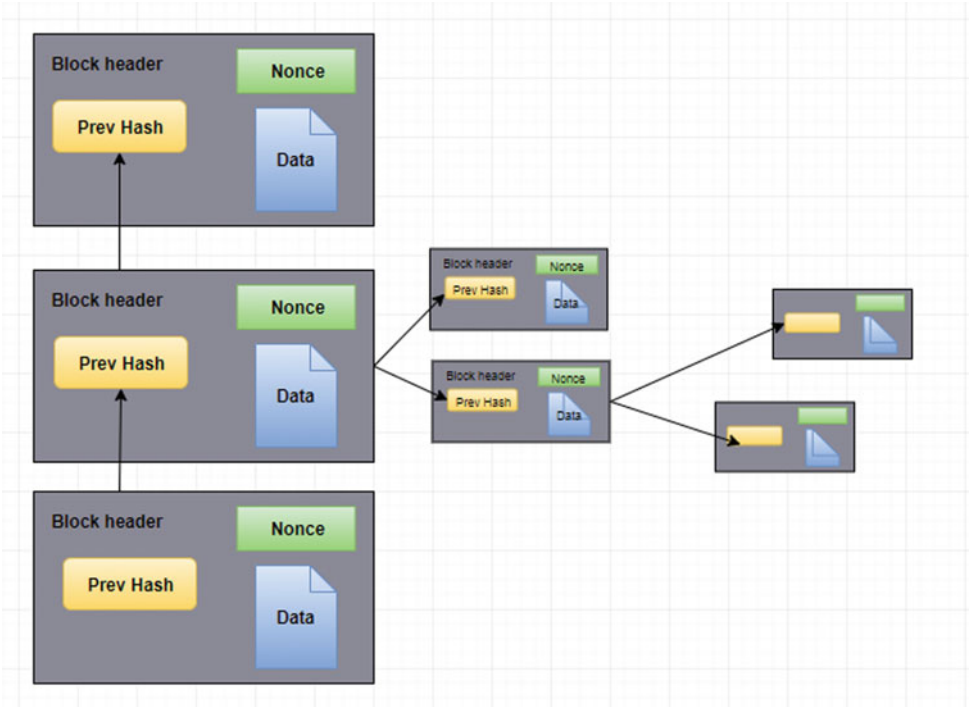

Fig. 2 Blockchain architecture

If someone wants to add a new block to the chain, then a resource-consuming operation needs to be done. In order to get rid of this problem, some techniques are used, such as Proof of Work in Bitcoin or Proof of Stake [16].

The location where the blocks are assembled and after that added to the block of blocks is called *miners*.

In order to summarize this section, the Blockchain is immutable. In nodes are kept individual copies of the ledger and in order to reach a consensus to the real register each individual copies are compared. Blocks and transactions are also validated through the nodes, and they are all looking for illegal transactions using cryptography. This leads to the emergence of a monetary stimulus in order to provide the computing power to the block. This way transparency and openness is guaranteed by using the resources needed to solve complicated mathematical algorithms.

4 Bonding Blockchain and GDPR

Comparing GDPR and Blockchain we realize that the major difference is evidenced by the fact that GDPR specify that personal data must be deleted when the need for storage expires or when a person withdraws consensus.

The main characteristic of the Blockchain is that the inside data is immutable and cannot be edited. The revolutionary feature of the Blockchain is that information is stored in a variety of distributed systems to ensure the highest level of security. Data inside a block cannot be deleted or edited but only updated by creating a mining node, therefore by adding another block to the existing chain. Thus, all the transactions within a Blockchain are transparent which contradicts GDPR.

Currently, due to the fact how GDPR is written, it is clear that is incompatible with Blockchain. Of course compromises can be made. For example, even if you cannot delete information inside of a block, you can separate the information stored on the chain. However, if block platforms begin to divide the stored information, then the security provided by Blockchain is compromised. Also, within the GDPR, the deletion term is not defined even if the terms erase and erasure appear 12 times in the entire document. Even though the data is deleted, there are many ways to recover it. A method by which the block of chains can do this is by destroying the encryption key and so the data can no longer be accessed. In this way, logical deletion is achieved, a method recommended by the medical standards in the field such as HL7, openEHR or EN/ISO13606.

Concluding, the only way the two can coexist is to convince authorities that deleting data does not necessarily mean physical deletion but also that if data is inaccessible is also a form of deletion.

The fundamental element of the Blockchain, hashing, is based on the fact that data is converted in a way that it cannot be returned to its original state. GDPR defines a person's personal data as those data through which a person can be identified. If they are completely anonymous then they are outside the sphere of influence of GDPR.

Therefore, if all of a data concerning health are stored only as a hash on a block, it could be argued that the existence of hashes in a Blockchain is not a violation of GDPR because it is sufficiently anonymous.

The GDPR specifications and regulations were principally focused on CRUD methodology (Create|Read|Update|Delete) systems. Blockchain technology does not use these principles. Since the data in a Blockchain cannot be erased/deleted, the principle behind Blockchain is CRAB (Create|Retrieve|Append|Burn). Adding information, which replaces the Update method, specifies that only new transactions can be added, and the Burn operation means that the encryption keys used for hashing the information are deleted or removed.

At the same time, according to Article 29 [8], advisory article, it is specified that data hash is in fact a pseudonymization process by which the data is disconnected from the individual. This conclusion is based on a mathematical conclusion that it still leaves a gateway to attack the information. Also, by encrypting all the data with an encryption key and then deleting this key at the request of the person leads to a result in which those data can no longer be used and accessed, and thus they may be erased.

Another measure that can be taken is that personal data is stored outside the Blockchain.

Another issue raised by the GDPR is that the personal data of a European Community citizen should be physically store only on the territory of the European Community. Here's the big problem, because in Blockchain there is no control over who and where a node is hosted. To solve this problem, a foundation or organization can be set up to secure this GDPR regulation by building a public Blockchain, but authorizations are only hosted in nodes.

One method to solve the above problems is exemplified in Fig. 3. First of all, personal data is stored outside the Blockchain and the reference to that information along with a hash of these data, as well as all necessary metadata is stored on the Blockchain. In the scenario shown in Fig. 3 there are two hospitals, Hospital A and Hospital B, each with their own databases, but both are connected to a Blockchain. If we assume that from the Hospital A we want to access the patient Bob information's from the Hospital B, in order to complete his medical history, at the moment, after the patient's consent, the informatics system in Hospital A makes a request to the informatics system from Hospital B based on the name and national number identification of Bob. Based on this request, the IT system receives the requested information.

By connecting the two hospitals to a Blockchain, the operation changes as follows. Because Hospital A does not know in which medical clinics are stored other medical information related with Bob, the informatics system from Hospital A sends a request to the Blockchain to retrieve all Bob's specific medical data. The Blockchain checks if the

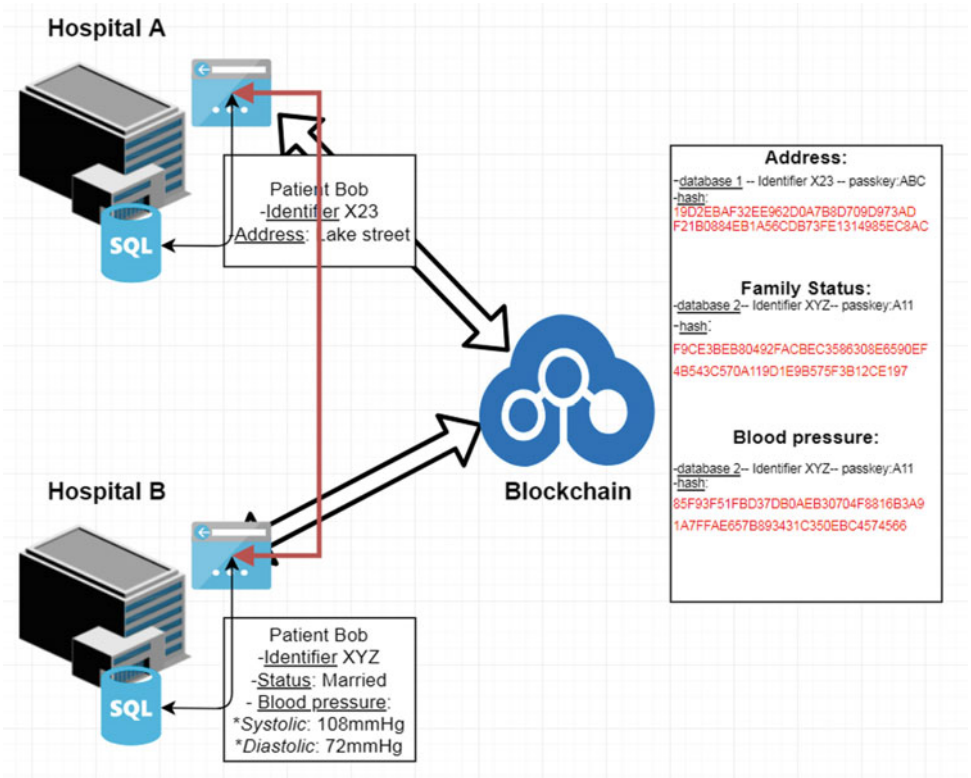

Fig. 3 Overall communication process with Blockchain

applicant, Hospital A, has all the rights to access this information. If Hospital A has the appropriate authorization, he gets the link and the hash of the required data. The link represent any kind of information such as API access address, required key, link to other databases, etc. Therefore, the Blockchain functions as a national registry that specifies who and where it holds information. On the basis of the information received from the Blockchain, Hospital A can now take and process the data directly from the Hospital B database. Once this information has been received, it is also possible to check through the Blockchain and more precisely through the hash whether the data has been altered. If the hash of the data received by Hospital A is the same as that of the Hospital B blocks, it means they keep their authenticity, and so we obtain also the syntactic and semantic interoperability.

5 Conclusions

If we look at these two concepts, GDPR and Blockchain, we can easily see that there is a vexed question. If we are referring to data portability, consent management, audibility of legal access, then Blockchain fits like a glove for GDPR. Instead, if we look at other issues, such as the right to delete information, we can see that GDPR and Blockchain want totally different things.

By those specified in the previous chapters, we believe that one can still realize such a system that complies with the GDPR rules but at the same time create a chain of blocks that can help improve the quality of the medical act and improve the patient's quality of life.

The method described in Sect. 3 is 100% compatible with GDPR specifications. This way you can physically delete data from databases from medical units. Even though Blockchain keeps hash and link to them, this link leads to nowhere and is thus useless. In the scenario presented above, the Blockchain is in fact only an access control environment, acting as a national register, the method successfully implemented in [17].

If we look at Blockchain's proposed motto, then we have to specify that the benefit of transparency disappears because if we store the data outside the Blockchain we cannot have information and control as to who and when accessed the data and why. Another problem is that once the computer system in Hospital A once has the medical records in Hospital B it does not have to go through Blockchain again. Also, once the data is stored outside Blockchain you cannot know exactly who is the owner and the data controllers of the data.

Acknowledgements The research presented in this paper was supported by the national project SeMed (2933/55/GNaC 2018).

Conflict of Interest The authors declare that they have no conflict of interest.

References

1. Gabor-Harosa, F.M., Stan, O.P., Daina, L., Mocean, F.: Proposed model for a Romanian register of chronic diseases in children. Comput. Methods Programs Biomed. **03**(130), 198–204 (2016)
2. Ovidiu, S., Miclea, L.: Local EHR management based on FHIR. In: 2018 IEEE International Conference on Automation, Quality and Testing, Robotics (AQTR), Cluj Napoca, Romania, 24–26 May 2018
3. Dubovitskaya, A., Urovi, V., Vasirani, M., Aberer, K., Schumacher, M.I.: A cloud-based ehealth architecture for privacy preserving data integration. In: IFIP Advances in Information and Communication Technology, book series (IFIPAICT), vol. 455, Springer
4. Tont, G., Vladareanu, L., Munteanu, R.A., Tont, D.: Some aspects regarding human error assessment in resilient sociotechnical systems. In: 2nd WSEAS International Conference on Sensors and Signals/2nd WSEAS Int Conf on Visualization, Imaging and Simulation/2nd WSEAS International Conference on Materials Science Location: Morgan State Univ, Baltimore, MD, 07–09 Nov 2009
5. Regulations: Regulation (EU) 2016/679 of the European Parliament and of the Council on the Protection of natural persons with regard to the processing of personal data and on the free movement of such data, and repealing Directive 95/46/EC (General Data Protection Regulation), 27 Apr 2016, Official Journal of the European Union
6. Allen & Overy: The EU General Data Protection Regulation (2017)
7. European Data Protection Supervisor: The history of the general data protection regulation. https://edps.europa.eu/data-protection_en. Accessed on Feb 2018
8. Art. 29 Working Party: Opinion 05/2012 on Cloud Computing. Adopted in 1 July 2012
9. Art. 29 Working Party: Opinion 02/2015 on C-SIG Code of Conduct on Cloud Computing. Adopted in 22 Sept 2015
10. Pyle, E., Manyé, L.B., Swerdloff, J., Sharp, L.G., Irvin, R.E., Koziol, J., Jiwnani, S., Holt, S., Goodloe, V.: Decoding GDPR—comparing terms used in GDPR with their U.S. e-discovery counterparts. Judicature **102**(1) (2018)
11. Seo, J., Kim, K., Park, M., Park, M., Lee, K.: An analysis of economic impact on IoT under GDPR. In: 2017 International Conference on Information and Communication Technology Convergence (ICTC), Jeju, South Korea, 18–20 Oct 2017
12. Dorca, V., Popescu, S., Munteanu, R., Chioreanu, A., Peleskei, C.: Agile approach with Kanban in information security risk management. In: IEEE International Conference on Automation, Quality and Testing, Robotics (AQTR), Cluj Napoca, Romania, 19–21 May 2016
13. Vojkovic, G.: Will the GDPR slow down development of smart cities. In: 2018 41st International Convention on Information and Communication Technology, Electronics and Microelectronics (MIPRO), Opatija, Croatia
14. Katulic, T., Katulic, A.: GDPR and the reuse of personal data in scientific research. In: 2018 41st International Convention on

Information and Communication Technology, Electronics and Microelectronics (MIPRO), Opatija, Croatia
15. Tapscott, D., Tapscott, A.: Blockchain revolution: how the technology behind bitcoin and other cryptocurrencies is changing the world. Portfolio, 12 June 2018, ISBN: 978-1101980149
16. King, S., Nadal, S.: PPCoin: peer-to-peer crypto-currency with proof-of-stake. Self-Published paper, Aug 2012
17. Stan, O., Sauciuc, D., Miclea, L.: Medical informatics system for Romanian healthcare system. In: 2011 E-Health and Bioengineering Conference (EHB), Iasi, Romania, 24–26 Nov 2011

Part VII
Miscellaneous Topics

Temperature Effect on Tribo-Mechanical Properties of Dental Materials

C. Birleanu, M. Pustan, V. Merie, and M. S. Pop

Abstract

The dental enamel is the hardest surface of teeth. Depending on the mechanical and tribological properties of the enamel, the sustainability of the teeth can be appreciated. These properties are influenced by the mastication conditions including humidity, temperature and abrasion effects. The aim of this work it is to consider the effect of temperature on tribological and mechanical properties of restorative dental materials using advance techniques. Nanoindentation provides information about hardness and elastic modulus. The tribological investigation in this paper is summed up to measure the friction force as a function of temperature. A temperature control system is used to monitor the temperature of investigated samples in the range of 10–60 °C. For this purpose an atomic force microscope with a nanoindentation module was used for the experimental determination of the mechanical and tribological properties of the dental materials taking into account the temperature variation. These relatively non-destructive mechanical characterization techniques can help to better understand the mechanical behavior of dental materials and thus facilitate their preparation with excellent mechanical and tribological properties.

Keywords

Dental materials • Nano-indentation • Thermal effect • Hardness • Friction

C. Birleanu (✉) · M. Pustan
Department of Mechanical Systems Engineering, Technical University of Cluj-Napoca, Cluj-Napoca, Romania
e-mail: Corina.Barleanu@omt.utcluj.ro

V. Merie
Department of Material Science, Technical University of Cluj-Napoca, Cluj-Napoca, Romania

M. S. Pop
The Emergency Military Hospital "Dr. Constatin Papilian", Cluj-Napoca, Romania

1 Introduction

Human teeth are tough they are resistant structures that appear on the jaws and around the mouth of vertebrates. The teeth are used, in principals, for masticating food, and for other proposed specialized purposes. Generally, a tooth is composed from one crown and one or more roots. The crown is the functional part of the tooth that is seen above the gum. The root is the tooth part cannot see that support and fix the tooth in the jawbone. The shape of the crown and the root varies between different teeth in the human mouth.

Generally we can define hardness as the average pressure a material can take under load. From the experimental point of view, the hardness is affected by several geometric uncertainties, such as the depth of penetration, the size and shape of the indenter.

All teeth have the same general structure and consist of three layers [1] as shown in Fig. 1. The hardest tissue in the body is an outer layer of enamel, which is completely inorganic. The enamel covers part or the entire crown of the tooth. The typical value for enamel hardness range reported in literature is from 1 to 8 GPa. Regarding enamel elastic modulus, we can say that the values range from 19.9 to 91 GPa when the measurements are perpendicular to crystal orientation, and from 93 to 113 GPa when the measurements are parallel to crystal orientation [2]. Anatomically speaking, the crowns of teeth are covered by dental enamel, which consists of 92–96% inorganic matter, 1–2% organic material and 3–4% water by its weight [3].

The hardness of the enamel is due to its high mineral content [4] and, on the other hand, its brittle property is due to the high elasticity and the reduced tensile strength [4]. Despite enamel being a very strong substrate, clinically, enamel cracks and fractures can occur. It has been shown from the literature that enamel is an anisotropic material and its mechanical properties depending on the type and direction of applied stress, as well as the prismatic orientation [5–8].

S. Vlad and N. M. Roman (eds.), *6th International Conference on Advancements of Medicine and Health Care through Technology; 17–20 October 2018, Cluj-Napoca, Romania*, IFMBE Proceedings 71,
https://doi.org/10.1007/978-981-13-6207-1_50

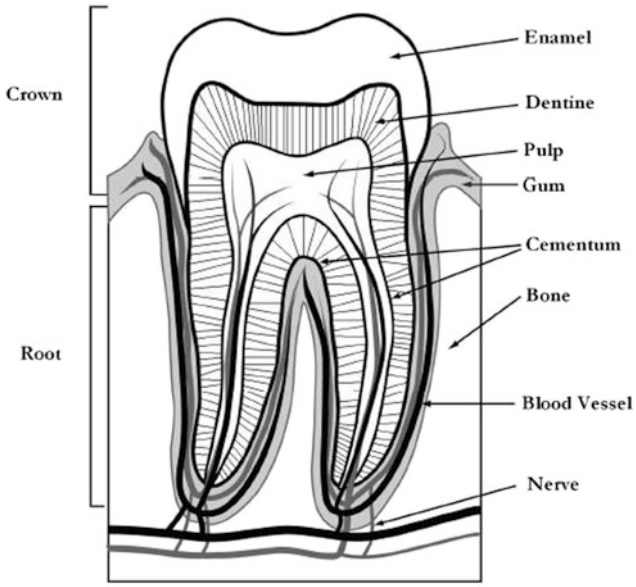

Fig. 1 Human tooth section [1]

The main reasons for placing a dental restoration are: primary caries or noncarious defects due to teeth abrasion/erosion, tooth fracture, tooth defects due to applied cosmetic treatments or those due to restoration of an endodontic tooth treated or other defects for unspecified reasons [9]. The destruction of healthy tissue has always been a big concern, and still today, the caries represent the most widespread human disease [10].

Therefore restorative materials are expected to replace and perform as natural tooth materials. The demand of achievement is so great that most of the times restorative filling materials replace enamel and dentin, which have very different mechanical properties, such as hardness and elastic modulus. Thus, the goal of research when developing these restorative materials It is to develop an ideal material for restoring the tooth to be identical to human natural tooth structure, as well as appearance and mechanical strength.

Mechanical and tribological properties of direct restorative filling materials are crucial not only to serve and allow similarity with human enamel and dentine but also to compare composites between them and determine objective criteria for their selection.

The objective of this work is to investigate the hardness and friction behavior of same commercial restorative materials using the nanoindentation and the AFM techniques.

2 Materials and Method

2.1 Investigated Samples

Four commercial dental composite resins were investigated in this work. All tested composites are one-paste systems (Fig. 2). Aspects regarding classification of tooth restoration materials, indication of use, composition of monomers, type and size of reinforced filler particles, as well as manufacturer data are presented in the following table. In Table 1 are presented the specific data regarding the analyzed samples are supplied by the manufacturer.

2.2 Nanoindentation Tests

Information on the mechanical properties of dental materials is essential to understanding how masticators strains are distributed throughout a tooth and to predict how stress and strains are altered through dental restoration procedures, age and disease [12]. It was expected that in the case of tooth restoration with sufficient and identical mechanical properties to that of the adjacent tooth structure, to the mastication loads, the restored tooth would thus have a longer lifetime [13].

Lately, the most common testing tool applied for the experimental evaluation of mechanical properties is the indentation method.

An atomic force microscope AFM-XE 70 (manufactured by the Park System Company) with a nanoindentation module enable the measurement of hardness on the surface of dental materials is used in experiment.

To monitor the sample temperature in the range of 10–60 °C a temperature control system based on the Peltier element was used. All experiments were performed in a clean room with control of humidity, temperature and air pressure.

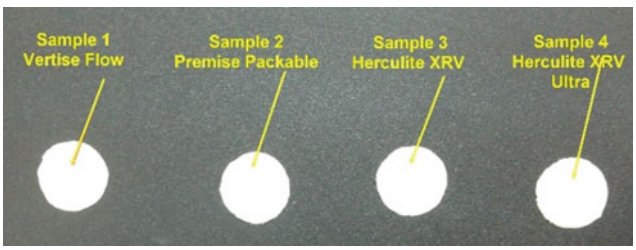

Fig. 2 Samples for experimental tests [11]

Table 1 Classification of resin composites regarding filler size and size distribution (clinical application) [12]

Type of composite resins (commercial name)	Samples dimensions (disc)	Particles size characteristics	Clinical use
XRV Herculite Ultra Nanohibride resin	Diameter —15 mm Width— 1 mm Hand made Curing time: 40 s	Enamel type, color A1, reinforcement particles which range from ∼0:5 to 3 μm	Moderate stress areas requiring optimal polishability
XRV Herculite Microhibride resin	Diameter —15 mm Width— 1 mm Hand made Curing time: 40 s	Enamel type, color A2 large filler particles, with an average size of 15–20 μm and also a small percentage in weight of colloidal silica, which has a particle size ranging from 0:01 to 0:05 μm m	High-stress areas requiring improvement polishability
Premise Packable Trimodal hybride resin,	Diameter— 15 mm Width— 1 mm Hand made Curing time: 40 s	Dentine type, color A3, Universal Trimodal Nanocomposite featuring a unique 3-filler blend (0.02; 0.4 μm and Pre-polymerised filler) and 84% filler loading, Midi/minifiller hybrid, with lower filler fraction	Situation in which improved condensability is needed
Vertise Flow Uncured methacrylate ester monomers	Diameter— 15 mm Width— 1 mm Hand made Curing time: 40 s	Midifller hybrid, with fine particle size distribution Non-hazardous inert mineral fillers, non-hazardous activators and stabilizers	Situation in which improved flow is needed and/or where access is difficult

Observation: All samples were prepared in the Laboratory of Faculty of Dental Medicine, from Cluj-Napoca, Romania

As it was shown already the indentation tests are the most used way of testing the hardness of materials. This indentation technique originates in the Mohs scale of mineral hardness and has been extended to evaluate the hardness of the material over a continuous range. Hence, the adoption of the Meyer, Knoop, Brinell, Rockwell and Vickers hardness tests were performed. Nano Indentation Technology has been established as the primary tool for micro and nano scale hardness investigations. The test is usually performed with a pyramidal or a conical indenter.

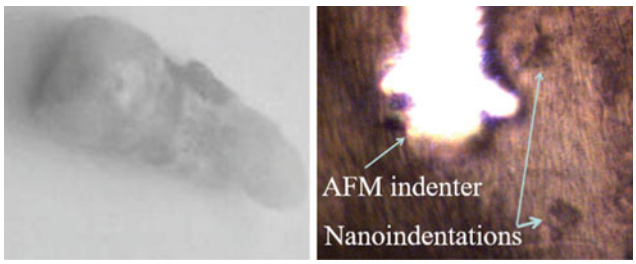

Fig. 3 Nanoindentation of human tooth

First, the indentation test was done on a human tooth. Nanoindentation places and the AFM indenter can be observed in the optical image of the human tooth enamel presented in Fig. 3. The measured hardness of human tooth is 7.24 GPa in the range reported in literature.

Then, the indentation data were obtained for all investigated dental materials using an indentation force of 250 μN. The tests were repeated five times. For all indentations a Berkovich diamond tip (three-sided pyramidal) was used. Temperature of investigated of samples material was modified during testing from 10 to 60 °C.

The analysis method used in the experimental determination of hardness is the Oliver and Pharr method. This is a standard procedure for determining the hardness and elastic modulus from the indentation load-displacement curves at micro and nano—scale. For each material the hardness was determined from the load-displacement curves during unloading process. For the mechanical characterization of soft or hard materials the Oliver-Pharr method proved to be an effective tool [13–15].

The AFM contact module was used to scan the surface before and after the indentation process at each temperature.

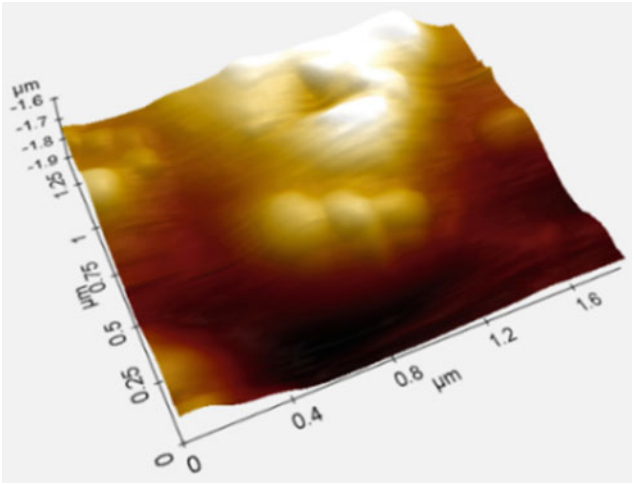

Fig. 4 Nanoindentation of Vertise Flow dental material at 20 °C with a force of 250 µN

The topography of the samples surface was then obtained by AFM scanning. Figure 4 shows the nanoindentation place of the Vertise Flow material at 20 °C with an indentation force of 250 µN.

The stamp of a series of indentation on the Vertise Flow material at different temperatures is shown in Fig. 5. The largest trace represents the indentation carried out at 60 °C while the smallest trace represents the indentation at the 10 °C. To accurately locate the regions of interest, the AFM optical microscope test was used. It was intended that the indentation stamps be spaced sufficiently apart so that the indentation behavior is not affected by the presence of adjacent indentations. The instrument's software corrected all data for thermal drift and instrument compliance.

Using the XEI Software the cross-section of the indentation places is obtained in order to measure the indentation depth. Figure 5 shows the variation of the maximum indentation depth as a function of temperature for a force equal by 250 µN. As temperature increases the indentation depth increases respectively. The same procedure is used for all the investigated samples. The results of the variation indentation depth as a function of temperature are presented in Fig. 6.

As temperature increases the indentation depth increases, respectively, under the same indentation force. As a consequence, the surface contact stiffness is changed and the hardness is modified.

The hardness was estimated by using XEI Software based on the Oliver-Pharr approach, analyzing the load-unload curves performed during experimental campaign. Hardness is directly provided by software. Figure 7a presents the hardness of Vertise Flow material at 20 °C, which is equal by 1.55 GPa for a contact depth of 21.4 nm. As temperature increases of 60 °C, the hardness decreases, respectively. For

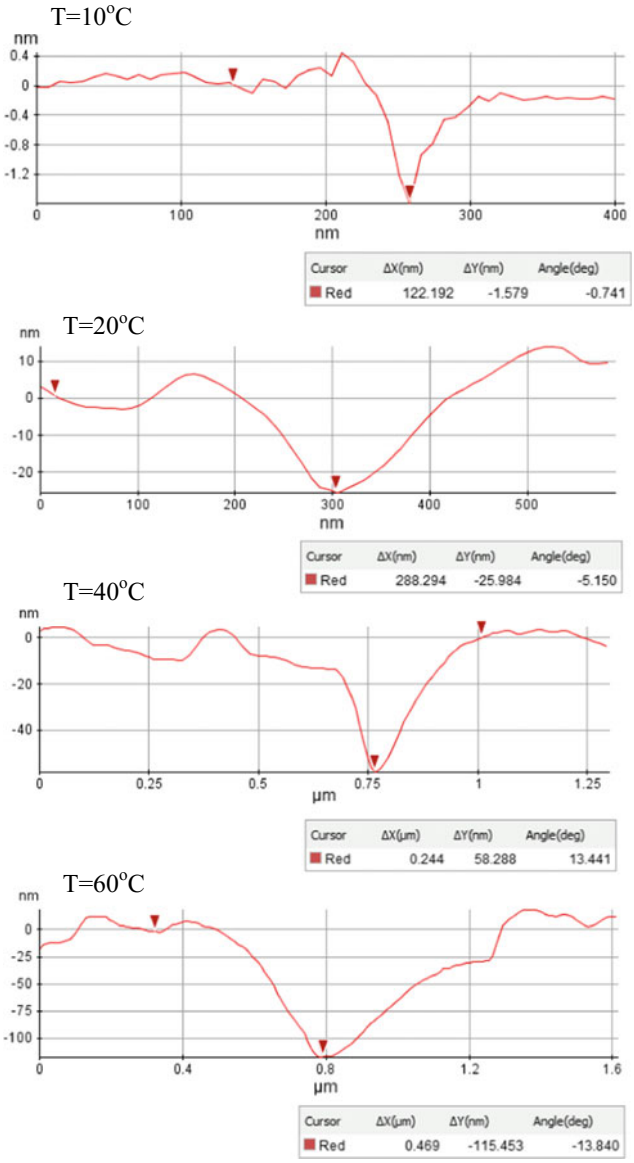

Fig. 5 Indentation depths of Vertise Flow material at different temperature for a force of 250 µN

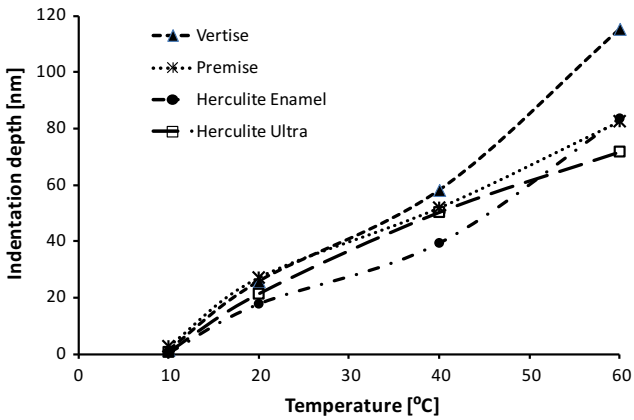

Fig. 6 The indentation depths variation as a function of temperature of investigated dental samples

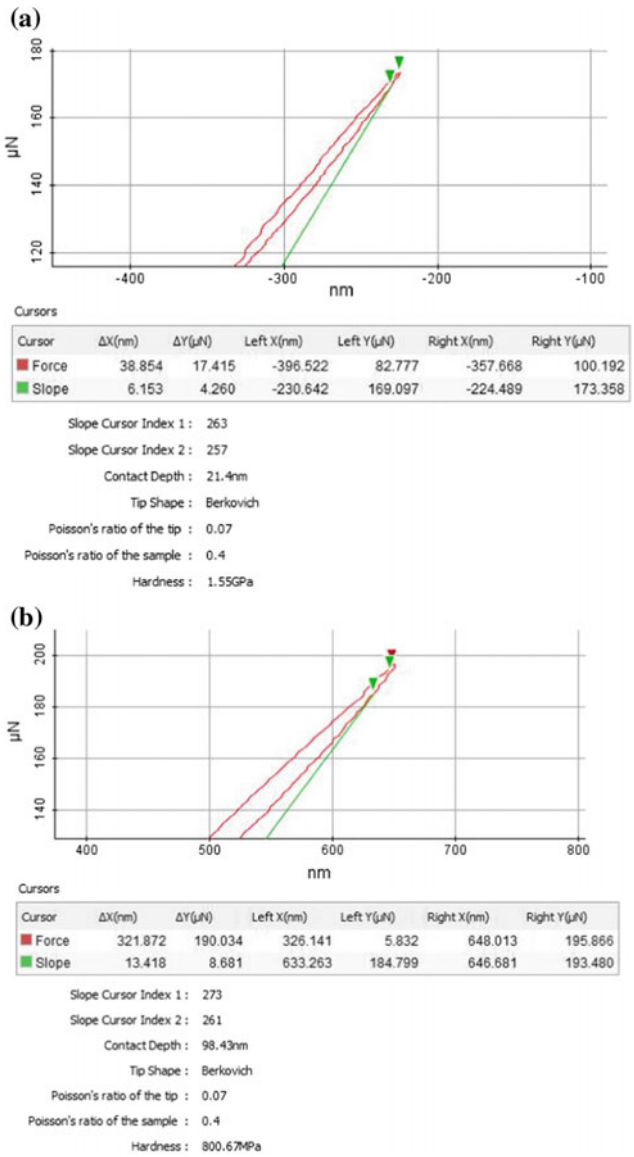

Fig. 7 The hardness variation as a function of temperature of Vertise Flow dental material at: **a** 20 °C and **b** 60 °C

Table 2 Hardness (GPa) of samples for different temperatures

Material	Temperature (°C)			
	10	20	40	60
	Hardness			
Vertise Flow	1.7	1.55	1.27	0.8
Premise Packable	2.82	2.6	1.91	1.15
XRV Herculite	1.87	1.62	1.38	0.95
XRV Herculite Ultra	2.59	2.2	1.81	1.24

the same material, using the same indentation force, a hardness of 0.8 GPa is experimentally obtained at 60 °C for a contact depth of 98.43 nm (Fig. 7b).

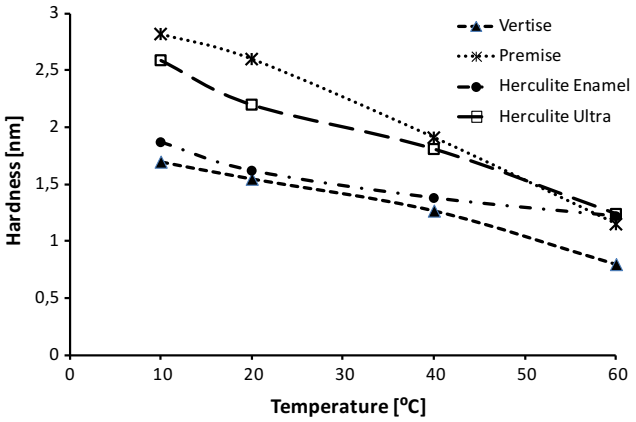

Fig. 8 The hardness variation as a function of temperature of investigated dental materials samples

The same experiment was performed for all investigated dental materials for different temperatures. The results are presented in Table 2.

The obtained results from the nanoindentation tests confirm hardness value in the range of 1–3 GPa of investigated dental material at the room temperature. The hardness decreases as temperature increases. The theoretical interpolation of the hardness variation as a function of temperature is presented in Fig. 8. The measured mechanical properties of dental resins at ambient temperatures are in the same range of those reported with other studies taken from literature [13].

3 Tribological Investigations

When the intention is to study wear behavior between dental materials that is strongly influenced by friction it is necessary to understand the environment in which they work, as well as the mechanisms involved in the processes which are the most important and finally conceive and/or use equipment adapted to the aim of the study.

The main energy source of the wear of materials in sliding contacts can be considered as the energy dissipated by friction between the bodies in contact. Coulomb's friction model determines that the frictional force is proportional to the normal load applied to the friction coupler, therefore, assuming a constant coefficient of friction, a proportional relationship between wear and friction force can be established. From the energetic approach the energy dissipation is also directly proportional to the wear volume [16, 17]. The literature has shown that during the chewing process of human beings, the magnitude of the masticatory force in the oral cavity varies from 3 to 36 N [18, 19]. In order to observed the wear of teeth in its incipient phase the micro and nano tests are needed. In our tests, the temperature

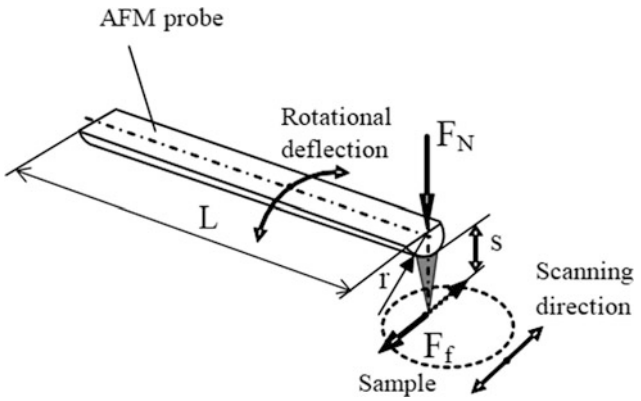

Fig. 9 The scanning principle; geometrical dimensions of an AFM probe

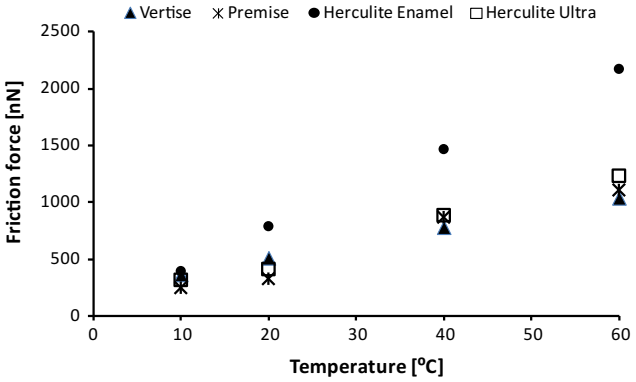

Fig. 11 The influence of temperature on friction forces between the AFM tip from diamond and investigated dental materials

influence a friction force where a normal load of 10 μN is investigated using the lateral mode of AFM.

In these investigations, the friction is determined by measuring the rotation deflection of AFM tip.

In this case, the two surfaces in contact with which friction occurs are the tip of the AFM and the sample from dental material. This experimental investigation provides an indication of the friction behavior between two materials that are in contact and in relative motion. Thus in this case the relative movement between the tip and the surface is made of a compound of the piezoelectric scanner which moves in a horizontal plane the material surface perpendicular to the AFM probe tip with a certain frequency, as shown in Fig. 9.

The scanner can also be extended or retracted in order to modify the normal force applied to the surface. This force will give us data about rotational deflection *dz* of AFM probe (Fig. 10). Thus friction will influence the relative movement between the tip of the AFM probe that comes into contact with the upper surface of the investigated materials. The lateral force, which acts in the opposite direction of the scan

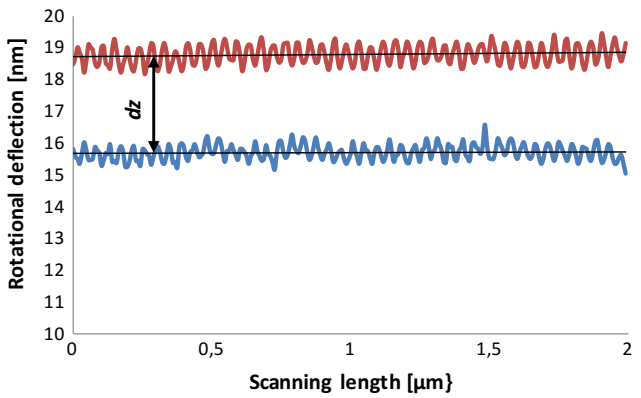

Fig. 10 The rotational deflection of AFM tip during sliding (the contact couple is between diamonds AFM tip on Premise Packable material)

velocity, causes torsion of the AFM probe. The lateral AFM probe movements during scanning are determined using a photo detector.

In order to avoid the influence of temperature on the AFM console during the scanning process, a high stiffness probe (144 N/m) and a diamond tip will be used. The geometrical dimensions of the AFM probe has the following (Fig. 9): height of the tip s = 109 μm; radius r = 24 μm; length L = 782 μm.

Measure the rotational deflection *dz* of the AFM probe (Fig. 10), and then the frictional force is determined based on the torsional beam theory with the following formula:

$$F_f = \frac{0,3 \cdot r^4 \cdot G}{L^2 \cdot s} \cdot dz \tag{1}$$

where *dz* is the calibrated deflection of AFM probe (nm); G is the shear modulus of the cantilever material and L, s, r are the dimensions of AFM probe.

Starting from the same normal load 10 μN for all investigated samples will be determined according to the temperature variation of the friction forces. The results are presented in Fig. 11. The rotational deflection of AFM cantilever increases if the temperature increases, respectively. If the friction forces of all investigated dental materials are in the same range at the room temperature, as temperature increases, the materials have different behaviors, especially for XRV Herculite Enamel.

4 Conclusions

The mechanical and tribological properties at micro and nano-scale investigations using the atomic force microscope can give us clear insights into the failure mechanism of dental materials. In this paper, is investigated the temperature influence on hardness and friction. One of the attractive methods for measuring the mechanical behavior of small

specimen volumes in dental hard materials is nanoindentation. Using this technique, the mechanical properties of nano composite resins were investigated. Experimental study has been carried out at different temperatures representing several steps of severity conditions for materials in test. This study has allowed concluding that, the hardness of dental materials decreases as temperature increases. At room temperature, Premise Packable and XRV Herculite Ultra materials have high hardness.

Tribological investigations consider friction force measurement that is evaluated based on the rotational deflection of AFM probe. A high value of friction force is determined for XRV Herculite Enamel. As temperature increases the friction force increases because the surface contact stiffness decreases which caused the AFM probe to slip harder on the investigated materials.

Conflict of Interest The authors declare that they have no conflict of interest.

References

1. Lewis, R., Dwyer-Joyce, R.: Wear of human teeth: a tribological perspective. Proc. Inst. Mech. Eng. J **219**(1), 1–18 (2005)
2. Srivicharnkul, P., et al.: Physical properties of root cementum: part 3. hardness and elastic modulus after application of light and heavy forces. Am J Orthod Dentofacial Orthop **127**(2), 68–176 (2005)
3. Eick, J., et al.: Current concepts on adhesion to dentin. Crit. Rev. Oral Biol. Med. **8**(3), 306–335 (1997)
4. Caldwell, R.C., et al.: Microhardness studies of intact surface enamel. J. Dent. Res. **36**(5), 732–738 (1957)
5. Meckel, A., Griebstein, W., Neal, R.: Structure of mature human dental enamel as observed by electron microscopy. Arch. Oral Biol. **10**(5), 775–783 (1965)
6. Urabe, I., et al.: Physical properties of the dentin-enamel junction region. Am. J. Dent. **13**(3), 129–135 (2000)
7. Rasmussen, S.T., et al.: Fracture properties of human enamel and dentin. J. Dent. Res. **55**(1), 154–164 (1976)
8. Hassan, R., Caputo, A., Bunshah, R.: Fracture toughness of human enamel. J. Dent. Res. **60**(4), 20–827 (1981)
9. Xu, H., et al.: Indentation damage and mechanical properties of human enamel and dentin. J. Dent. Res. **77**(3), 472–480 (1998)
10. Giannini, M., Soares, C.J., De Carvalho, R.M.: Ultimate tensile strength of tooth structures. Dent. Mater. J. **20**(4), 322–329 (2004)
11. Langeland, K.: Tissue response to dental caries. Dent. Traumatol. **3**(4), 149–171 (1987)
12. Birleanu, C., et al.: Nanomechanical investigation of dental restorative materials using atomic force microscopy. Acta Tech. Napocensis Ser. Appl. Math. Mech. Eng. **56**(4) (2013)
13. Kinney, J., et al.: Hardness and Young's modulus of human peritubular and intertubular dentine. Arch. Oral Biol. **41**(1), 9–13 (1996)
14. Angker, L., Swain, M.: Nanoindentation: application to dental hard tissue investigations. J. Mater. Res. **21**(8), 1893–1905 (2006)
15. Oliver, W.C., Pharr, G.M.: An improved technique for determining hardness and elastic modulus using load and displacement sensing indentation experiments. J. Mater. Res. **7**(6), 1564–1583 (1992)
16. Al-Haik, M.S., et al.: Investigation of the nanomechanical and tribological properties of dental materials. Int J Theor Appl Multiscale Mech **1**(1), 1–15 (2009)
17. Johnson, K.: Contact Mechanics. Cambridge University Press, Cambridge (1985)
18. Hamilton, G.M.: Explicit equations for the stresses beneath a sliding spherical contact. Proc. Inst. Mech. Eng. Pt. C J. Mechan. Eng. Sci. **197**(1), 53–59 (1983)
19. Dowson, D.: A tribological day. Proc. Inst. Mech. Eng. J **223**(3), 61–273 (2009)

Magnetic Submicron Systems Loaded with Chemotherapeutic Agent (Paclitaxel) for Breast Cancer Therapy

V. Balan, S. Malihin, and L. Verestiuc

Abstract

Magnetic submicron systems based on N-palmitoyl chitosan, magnetite and chemotherapeutic agent (Paclitaxel) have been prepared via ionic gelation mechanism combined with ultrasonication technique. Dynamic light scattering results showed that magnetic particles size, measured in aqueous medium is around 300 nm and the structures have positive surface charge given by the non-substituted amino groups of chitosan. In vitro release studies have shown the ability of magnetic particles to release the chemotherapeutic drug in a controlled manner over 24 h. It has been observed a more pronounced drug release within slightly acidic media (pH = 6.8) as a result of the higher polymer swelling and degradation.

Keywords

Magnetic particles • Breast cancer • Drug delivery • N-palmitoyl chitosan • Paclitaxel

1 Introduction

Due to its complexity and higher incidence, breast cancer has received increased attention over the last few years and many studies have explored the possibility to develop an effective strategy [1–3]. Although promising, current therapies including surgery, chemotherapy and radiotherapy are still limited due to: (i) lack of selectivity, (ii) multidrug resistance and (iii) severe toxic side effects [4]. Most of the breast cancer patients undergo serious adverse toxicities such as nausea, fatigue, anorexia, menopausal problems, ovarian failure, infertility and alopecia after the administration of the chemotherapeutic agents [5]. Nano- and micro technology is an emerging field that provides the means to improve the existing therapeutic and diagnostic methods. Adequate particulate systems are characterized by very small dimensions, ranging from 10 to 500 nm and are able to be prepared in a variety of shapes and many compositional structures [6–8].

Synthetic polymers and biopolymers are commonly used to design particulate systems, especially chitosan, due to its remarkable properties, such as: biocompatibility biodegradability and mucoadhesivity [9, 10]. Also, the presence of the reactive groups $–NH_2$ and –OH is an important advantage. A particular interest for the development of controlled release systems of hydrophobic drugs such as Paclitaxel exhibits the amphiphilic N-acyl derivatives of chitosan, such as N-palmitoyl chitosan [11, 12]. Paclitaxel is a cytotoxic drug used to treat various types of cancer such as breast, ovarian, lung or cervical cancer,

In this context, this paper presents the preparation and characterization of magnetic particles based on N-palmitoyl chitosan, magnetite and Paclitaxel and evaluates the ability of these systems to be used as drug delivery systems in breast cancer therapy.

2 Materials and Methods

2.1 Materials

For the synthesis of magnetic particles the following materials have been used: N-palmitoyl chitosan (PCs), with a number-average molecular weight (Mn) of 235.2 kDa, a weight-average molecular weight (Mw) of 322.5 kDa (determined by gel permeation cromatography-GPC) and a degree of substitution of 12.35% (determined by trinitrobenzene sulphonic acid assay-TNBS), prepared according to our previous report [11], Paclitaxel (PTX) isolated from fungi (*Taxusbrevifolia* and *Taxusyannanensis*), purchased from Sigma-Aldrich, sodium tripolyphosphate (TPP)—Sigma-Aldrich and magnetite suspension (M-Fe_3O_4)

V. Balan · S. Malihin · L. Verestiuc (✉)
Faculty of Medical Bioengineering, Grigore T, Popa University of Medicine and Pharmacy, 9-13 Kogalniceanu Street, 700454 Iasi, Romania
e-mail: liliana.verestiuc@bioinginerie.ro

S. Vlad and N. M. Roman (eds.), *6th International Conference on Advancements of Medicine and Health Care through Technology; 17–20 October 2018, Cluj-Napoca, Romania*, IFMBE Proceedings 71,
https://doi.org/10.1007/978-981-13-6207-1_51

prepared in our laboratory [12]. The solvents (ethanol and acetic acid) have been purchased from Sigma-Aldrich.

2.2 Methods

2.2.1 Synthesis of Magnetic Particles

Magnetic particles based on N-palmitoyl chitosan, magnetite and chemotherapeutic agent—Paclitaxel, have been prepared via ionic gelation mechanism combined with ultrasonication. 100 ml PCs (0.1% (wt./vol.) in 1% acetic acid) were mixed with 4 ml of magnetite [2.5% (wt./vol.)] and the mixture was allowed to homogenize under mechanical agitation for 5 min. Next, 25 ml of PTX (0.01% in ethanol) was added and the system was homogenized for other 5 min. Afterwards, 1 ml of Tween 80 was added, followed by 10 min of mechanical stirring. Then, 25 ml of 0.05% (wt./vol.) TPP was added dropwise. After 2 h of stirring, the synthesis product was sonicated for 5 min using a Sonopuls HD 2200 ultrasonic homogenizer, followed by solvent evaporation, centrifugation and freeze drying. Magnetic particles obtained were encoded PCsM-PTX. Similarly, drug-free magnetic particles (PCsM), polymer-based particles (PCsNP) and drug polymer based particles (PCs-PTX) were prepared.

2.2.2 Particles Characterization

Zeta potential and hydrodynamic mean diameter of magnetic particles were determined by Dynamic Light Scattering (DLS) measurements in water, at 25 °C using a Malvern Zetasizer NanoS (Malvern Instruments, UK). A Fourier Transform Infrared (FT-IR) spectrophotometer, model Vertex 70 (Brüker) was used to record the FT-IR spectra of all samples. FT-IR spectra were recorded on 500–4000 cm^{-1} domain, with a resolution of 4 cm^{-1}. The surface morphology of magnetic particles has been studied by scanning electron microscopy (SEM TESCAN-VEGA, at 30 kV, gold sputter coated before analysis).

2.2.3 In Vitro Drug Release Studies

In vitro release studies were performed in two simulated biological media (phosphate buffer—pH 7.4 and pH 6.8) at 37 °C, for 24 h. A weighed amount of particles was redispersed in PBS and transferred into a dialysis bag (molecular weight cut-off 12,400 Da) that have been placed in preheated PBS (total volume: 25 ml). The release study was performed in an incubator shaker, at 37 °C. At selected time intervals, the solution outside of the dialysis bag was removed (n = 3) for UV–Vis analysis at 227 nm (UV-1700 PharmaSpec, Shimadzu) and replaced with fresh buffer solution.

3 Results and Discussions

3.1 Preparation and Characterization of Magnetic Particles

In Fig. 1 is presented a schematic diagram of magnetic particles (PCsM-PTX) synthesis, by ionic gelation mechanism that implies electrostatic interactions between available positive amino groups of PCs and negative groups of the TPP, combined with ultrasonication that induce self-assembly process and internalization of both hydrophobic chains and chemotherapeutic drug into the microstructure core.

Ionic gelation, developed for the first time, by Calvo et al. [13] is a relatively simple technique to prepare particles but it also need to adjust the synthesis parameters in order to modulate adjusting the particles characteristics in terms of size, polydispersity index, and Zeta potential value. Thus,

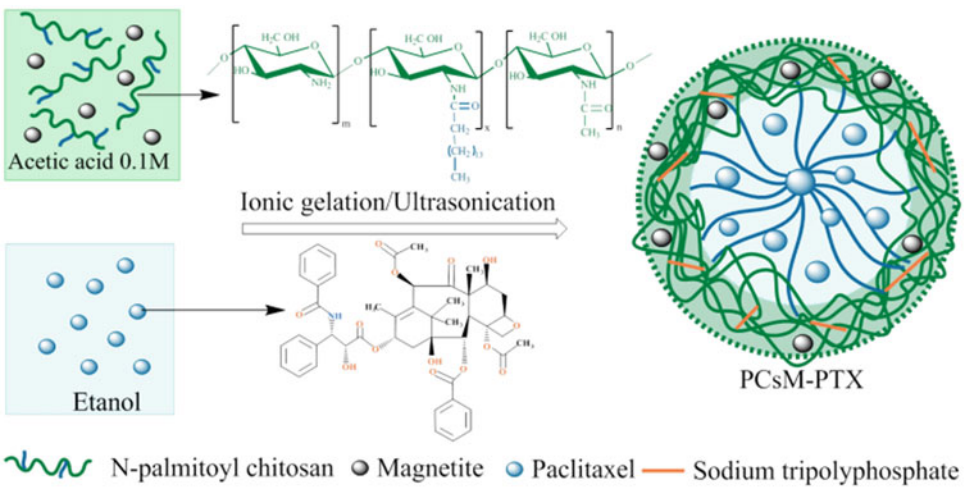

Fig. 1 Schematic diagram of magnetic particles synthesis

Table 1 Particles characteristics

Batch	Size (d-nm)/I(%)	PdI	ZP (mV)	Cond. (mS/cm)
PCsNP	304.5 (83.6)	0.922	9.58	0.353
PCs-PTX	270.76 (90.3)	1	13.6	0.855
PCsM	292.6 (75.9)	0.931	3.92	0.405
PCsM-PTX	314.7 (72.8)	0.377	8.77	0.694

I–intensity, PdI–polydispersity index, ZP—zeta potential, Cond—conductivity

several improvements such as combination with electrospraying, rotary disk processing, and addition of NaCl or ultrasonication have been proposed in the last years [14–16].

The obtained particles were analyzed in terms of size, polydispersity index, the surface charge and conductivity, the results being detailed in Table 1. Analysing the results it can be observed that particles size is around 300 nm. All batches exhibited positive surface charges given by the non-substituted amino groups of chitosan.

Surface morphology of PCsM-PTX has been investigated by SEM microscopy (Fig. 2) and it can be observed spherical particles with a diameter around 200 nm, smaller than the average size determined by Dynamic Light Scattering technique, as expected, due to the swelling of the polymer shell in the aqueous medium used in DLS measurements and the aggregation tendency as a result of magnetic material presence.

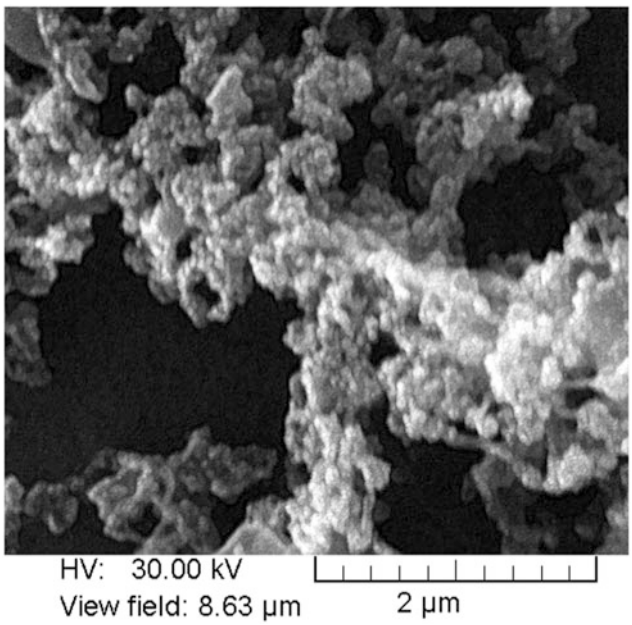

Fig. 2 SEM image of PCsM-PTX particles

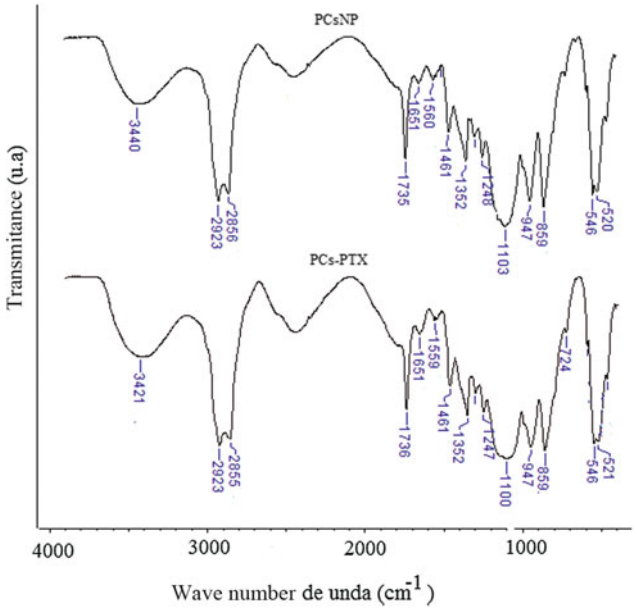

Fig. 3 FT-IR spectra of PCsNP and PCs-PTX

Magnetic particles structure was characterized by FT-IR spectroscopy (Fig. 3) and characteristic absorbance bands of the batches are detailed in Table 2, where the correlation with each functional group can be identified. Both magnetic particles spectra showed typical bands for chitosan, magnetite (at 622–627 cm^{-1} which corresponds to the vibration of oxygen-iron bonds) and palmitoyl chains. In the FT-IR spectra of PCsM-PTX it was observed that drugs bands overlap generally over those of the polymeric structure due to the fact that Paclitaxel spectra exhibited common bands at

Table 2 FT-IR bands of PCsM and PCsM-PTX

Structure	Typical FT-IR bands (cm^{-1})		Functional groups
	PCsM	PCsM-PTX	
Magnetite	622	627	Fe–O–Fe
Chitosan	3376	3339	OH, N–H
	1695	1697	C=O
	1548	1542	C–N, N–H
	1071	1070	C–O–C
Palmitoyl	1695	1697	C=O
	2913	2913	CH_2
	2855	2846	
Paclitaxel		3339	OH, N–H
		2913	CH_2
		2846	
		1697	C=O

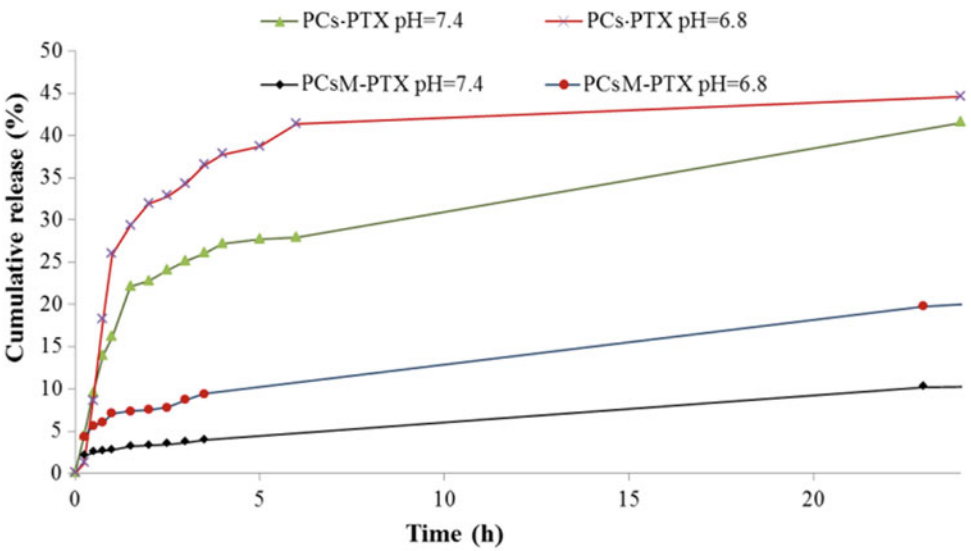

Fig. 4 In vitro drug release kinetics in buffer solutions with pH = 7.4 and pH = 6.8

the 3376 cm^{-1}, 1695 cm^{-1} (regions of the OH, N–H and C=O groups) and also in the 2913–2855 cm^{1} (area of CH_2 stretching) [17].

3.2 In Vitro Drug Release Study

In order to evaluate the potential of magnetic particles prepared to be used as drug delivery systems in breast cancer therapy, in vitro release tests were performed in PBS that mimic normal cells media (pH = 7.4) but also in PBS that simulate cancer cells media (pH = 6.8). As shown in Fig. 4, particles exhibited a biphasic drug release pattern: an initial fast release in the first 2 h, followed by a second phase corresponding to a constant release up to 24 h. It is important to note, a more pronounced drug release within slightly acidic media as a result of the higher polymer swelling and degradation. This characteristic is essential for magnetic particles prepared because tumoral tissue exhibit similar interstitial acidity values.

4 Conclusions

This study proposes a method to obtain magnetic particles based on N-palmitoyl chitosan, magnetite and a chemotherapeutic agent-Paclitaxel through ionic gelation mechanism combined with ultrasonication technique. The obtained systems exhibited submicron size and positive zeta potential. SEM images evidenced particles with spherical shape and a diameter around 200 nm, in solid state. FT-IR Spectroscopy confirmed the structure of magnetic particles. In vitro release studies have shown the ability of particles to release the drug for a period of 24 h and a more pronounced drug release within acidic media, characteristics that sustain future experiments aiming to assess the suitability of magnetic particles as drug delivery system.

Conflict of Interest The authors declare that they have no conflict of interest.

References

1. Turashvili, G., Brogi, E.: Tumor heterogeneity in breast cancer. Front. Med. **4**, 227 (2017)
2. Harris, L.N., Ismaila, N., Mcshane, L.M., Andre, F., Collyar, D.E., Gonzalez-Angulo, A.M., et al.: Use of biomarkers to guide decisions on adjuvant systemic therapy for women with early-stage invasive breast cancer: American Society of clinical oncology clinical practice guideline. J. Clin. Oncol. **34**, 1134 (2016)
3. Gingras, I., Azim Jr., H.A., Ignatiadis, M., Sotiriou, L.: Immunology and breast cancer: toward a new way of understanding breast cancer and developing novel therapeutic strategies. Clin. Adv. Hematol. Oncol. **13**(6), 372–382 (2015)
4. Chowdhury, S., et al.: An overview of drug delivery vehicles for cancer treatment: microcarriers and microparticles including photovoltaic microparticles. J. Photochem. Photobiol. B Biol. **164**, 151–159 (2016)
5. Suffredini, G., East, J.E., Levy, L.M.: New applications of microtechnology for neuroimaging. Am. J. Neuroradiol. **35**(7), 1246–1253 (2014)
6. Brigger, I., Dubernet, C., Couvreur, P.: Microparticles in cancer therapy and diagnosis. Adv. Drug Deliv. Rev. **54**, 631–651 (2002)
7. Chauhan, N., Dilbaghi, N., Gopal, M., Kumar, R., Kim, K.H., Kumar, S.: Development of chitosan microcapsules for the controlled release of hexaconazole. Int. J. Biol. Macromol. **97**, 616–624 (2017)
8. Peniche, H., Peniche, C.: Chitosan microparticles: a contribution to micromedicine. Polym. Int. **60**, 883–889 (2011)
9. Larsson, M., Huang, W.C., Hsiao, M.H., Wang, Y.J., Nydén, M., Chiou, S.H., Liu, D.M.: Biomedical applications and colloidal properties of amphiphilically modified chitosan hybrids. Prog. Polym. Sci. **38**, 1307–1328 (2013)

10. Jee, J.P., Jin, H.N., Lee, S., Sun, H.K., Choi, K., Yeo, Y., Kwon, I. C.: Cancer targeting strategies in micromedicine: design and application of chitosan microparticles. Curr. Opin. Solid State Mater. Sci. **16**, 333–342 (2012)
11. Balan, V., Dodi, G., Tudorachi, N., Ponta, O., Simon, V., Butnaru, M., Verestiuc, L.: Doxorubicin-loaded magnetic microcapsules based on N-palmitoyl chitosan and magnetite: synthesis and characterization. Chem. Eng. J. **279**, 188–197 (2015)
12. Hritcu, D., Popa, M.I., Popa, N., Badescu, V., Balan, V.: Preparation and characterization of magnetic chitosan microspheres. Turk. J. Chem. **33**, 785–796 (2009)
13. Calvo, P., Remunan Lopez, C., VilaJato, J.L., Alonso, M.J.: Novel hydrophilic chitosan-polyethylene oxide microparticles as protein carriers. J. Appl. Polym. Sci. **63**, 125–132 (1997)
14. Arya, N., Chakraborty, S., Dube, N., Katti, D.S.: Electrospraying: a facile technique for synthesis of chitosan-based micro/nanospheres for drug delivery applications. J. Biomed. Mater. Res. B Appl. Biomater. **88**(1), 17–31 (2009)
15. Huang, Y., Lapitsky, Y.: Monovalent salt enhances colloidal stability during the formation of chitosan/tripolyphosphate microgels. Langmuir **27**(17), 10392–10399 (2011)
16. Desai, K.G.: Chitosan microparticles prepared by ionotropic gelation: an overview of recent advances. Crit. Rev. Ther. Drug Carrier Syst. **33**(2), 107–158 (2016)
17. Kathiravan, G., et al.: Infra-red spectral analysis of taxol produced by different species of pestalotiopsis. J. Anal. Bioanal. Tech. **5**(4), 1–9 (2014)

Identifying Relevant Research Directions for Graduation Projects in Medical Engineering

D. Cotoros, C. Druga, I. Serban, and A. Stanciu

Abstract

The paper aims at presenting some simple and effective tools that can be used by medical engineering students in steering their research in relevant directions. This way, the results of their graduation projects may serve to address some real and urgent issues in their field of expertise. In order to achieve this goal, the students need simple and effective tools that provide reliable and fast results without involving additional skills. Therefore, the paper will present two situations of Medical Engineering and Optometry students in search for the suitable research topic for their graduation project, so that it responds to practical needs occurred from the social environment.

Keywords

Research relevance • Questionnaire survey • Graduation project

1 Introduction

Graduation project are summarizing the knowledge accumulated by the student throughout the years, being the peak of their college related activities.

Medical engineering is a relatively new study program and graduates are facing more challenges than their colleagues who attend traditional courses. Their expertise lies at the boundary between medicine and engineering and they will have to play an increasingly important role in healthcare, as technology is stepping in every day, more and more.

This is the reason why the research they perform should grow to reach enough relevance for their field of expertise even in early stages.

According to [1] relevance in research is given by the "potential in improving decision making for the practitioners" by following the right questions, hypotheses and implications. Nevertheless there are high concerns at world level about the "mismatch between the educational research and the research demanded by the practitioners" in the field or even by the future users of the research results [2].

There are also opinions concerning the fact that "since universities are publicly funded it is reasonably that the society expects something in return" [3].

High education institutions are sometimes lacking the connection to the practical aspects of the concepts they are teaching and the graduates are facing the shock of the practice challenge when they get their first job. In order to avoid this, their graduation project should be the result of some real demand on the labor market or in the social environment and come up with viable and applicable solutions.

Of course, there is to consider the fact that they don't have limitless possibilities of documenting and analyzing society needs, so the methods to be used should be simple, effective and accessible without requiring high skills in areas which are not connected to their field of expertise.

2 Materials and Methods

A major step in any practical related research is represented by data collection and one of the most used research tool, especially as far as medical research is concerned, is the questionnaire survey because it is a cheap and quick research tool and requires no special training [4].

There are several methods of conducting a survey and also several factors to be considered when designing the questions. According to [5], the following information should be relevant:

D. Cotoros (✉) · C. Druga · I. Serban · A. Stanciu
Department of Product Design, Mechatronics and Environment, University Transilvania, 29 Eroilor Av., Brasov, Romania
e-mail: dcotoros@unitbv.ro

S. Vlad and N. M. Roman (eds.), *6th International Conference on Advancements of Medicine and Health Care through Technology; 17–20 October 2018, Cluj-Napoca, Romania*, IFMBE Proceedings 71,
https://doi.org/10.1007/978-981-13-6207-1_52

- Access to potential respondents
- Literacy level of respondents
- Subject matter
- Motivation of respondents
- Resources

Questionnaire surveys, if cleverly designed, can be a very useful and effective tool in collecting data and determining major issues in certain social or economic environments.

There are many possibilities of creating questionnaire surveys, the most used being Google Forms platform and SurveyMonkey. They can be easily shared online and made available to potential respondents or printed and distributed to people with no internet access.

The intention of the paper is to present two situations of Medical Engineering and Optometry students searching for the right research topic for their graduation project, so that it responds to the needs of a certain social environment or fits in a less explored niche, being also in accordance to their own research interests.

Thus, the Medical Engineering student was preoccupied by enhancing the independence of disabled persons who wish to have an active life and even perform sportive activities, especially people confined to a wheel-chair due to various accidents or neurological diseases.

By help of a non-governmental foundation and a disabled persons association, the student devised a questionnaire in order to identify the requirements of wheel chairs users who wish to perform sportive activities. The survey consisted of 9 questions regarding the reasons they are using wheel-chairs, asking information about what kind of sports they liked to perform and which parts of the wheel-chair would require changes so that it doesn't impede on their performance.

The questions were formulated in Google forms, with both open and closed responses in order to offer the opportunity of providing accurate and honest information. The respondents were briefed on their task and remained anonymous.

The second situation concerns an Optometry student who wished to raise awareness regarding the negative effects of ultraviolet radiations upon the visual system and needed information about the degree of knowledge in various categories of persons. The student devised a questionnaire using SurveyMonkey aiming at persons wearing contact lenses or wishing to wear contact lenses, aged 18–45, all visiting optometry clinics. There were 10 questions requiring information about the knowledge concerning the effect of ultraviolet radiations upon the visual systems and the steps taken to avoid them.

3 Results and Discussions

3.1 First Situation-Results

A number of 28 answers were provided by persons using wheel chairs, members of various foundations and disabled persons associations. 60.7% of the respondents are depending on the use of a wheel chair due to various pathologies and only 39.3% due to accidents. 67.9% of the respondents consider they are active persons and are practicing various sports, according to the diagram in Fig. 1.

Physical activity is an essential part of a healthy life and it also provides therapeutical for disabled persons, either for recovery and rehabilitation or simply for recreational purposes [6].

Very often disabled persons suffer of a low self esteem and are predisposed to depression and isolation but physical activity can regain their capacity of feeling valuable and integrated in society. Therefore, any type of handicap should not be considered as some kind of disease or an obstacle for performing physical activities, but it is necessary to identify the types of sports which are beneficial for each kind of disability.

Thus, another important issue would be what kind of sports they would like to practice but are unable to, due to the wheel chair construction or due to other causes. The results are shown in Fig. 2.

Though the assistive equipment industry has developed in a very impressive manner during the last decades, there still are several issues to be optimized and the users are the most legitimate to know exactly what is wrong. So obviously one of the questions required them to indicate which part of the

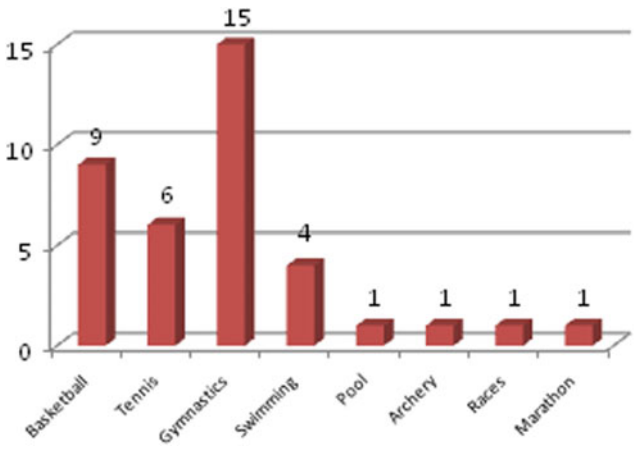

Fig. 1 Sports practiced by wheel-chair users

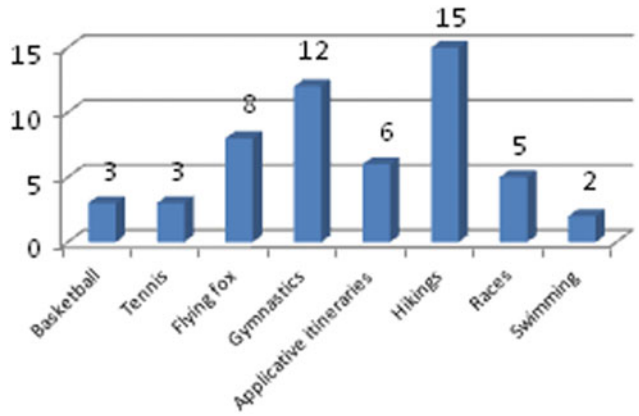

Fig. 2 Sports that are desired to be practiced

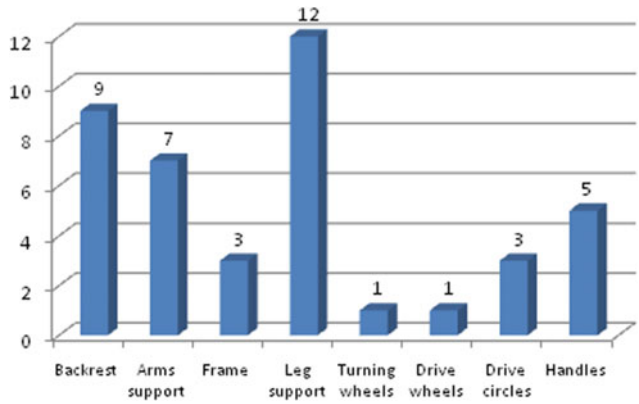

Fig. 3 Wheel chair parts that are to be optimized

wheel chair they considered that needs optimization and the results are presented in Fig. 3.

Another problem is the fact that disabled people who wish to perform a sportive activity have to acquire two or several wheel chairs, as the geometry of a wheel chair for daily normal activities is different from the one used in sportive activities. This would lead to additional spending as disabled people usually do not enjoy a flourishing economic situation. The results concerning the types of chairs they owned are presented in Fig. 4.

If we analyze the diagram in Fig. 4 it becomes obvious that there are 34 wheel chairs owned by 28 people, meaning that 6 of them possess 2 chairs in order to be able to perform sportive activities.

Based upon these results the student designed a new type of wheel chair with optimized parts and adjustable for either daily use or sports in a very easy manner, responding directly to the requirements of the users.

3.2 Second Situation-Results

The survey was performed during 3 months time among the patients of two optometry clinics in two different cities. The purpose of the investigation was to identify how much knowledge people have regarding the negative effects of ultraviolet radiations upon the visual system and what actions do they intend to initiate in order to protect themselves from these radiations.

35.5% of the respondents are wearing contact lenses, 22.2% do not wear contact lenses and are totally against trying them and 42.3% do not wear contact lenses but are willing to try.

95% of the respondents know what ultraviolet radiations are and are aware of the danger they are exposed to, but it was interesting to find out which time of the year they feel more exposed. The results are shown in Fig. 5.

Being asked about their attitude concerning the use of UV protected lenses the respondents answered as shown in Fig. 6.

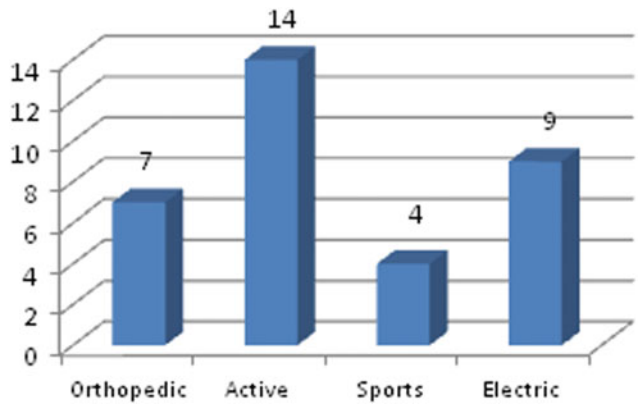

Fig. 4 Types of owned wheel-chairs

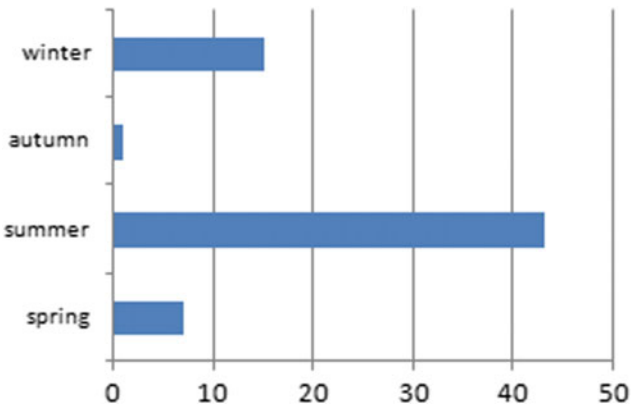

Fig. 5 Number of people feeling exposed according to seasons

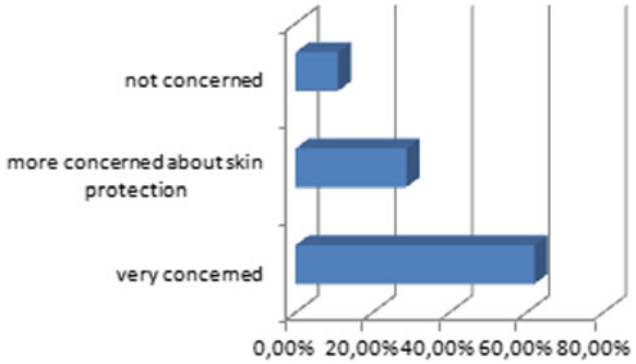

Fig. 6 People attitude regarding concern about UV protection

People are not always aware of the type of lenses they are wearing, especially if their education is not at high level. They usually wear the glasses or contact lenses because the ophthalmologist or the optometrist recommended them. One of the questions aimed at determining how well informed the people are on the lenses they are wearing.

The results of the responses are shown in Fig. 7. Around 57% of the respondents seem to know if their lenses are provided with UV protection or not, but it is a little disconcerting that the other 43% do not know or even do not care, proving that due to lack of knowledge people are more preoccupied to just "see" and neglect the negative effect of UV radiations just because they cannot see them.

An important aspect to be considered is the financial one because not all people can afford the expenses of wearing UV lenses, so a question regarding the economic implications of the matter should be asked. The responses are presented in Fig. 8.

It is a good thing that most of the users (around 80%) are willing to pay more for the lenses with UV protection.

Based upon the responses analysis, the student was able to evaluate users' attitude towards the use of lenses with UV protection and devised a strategy for informing the people

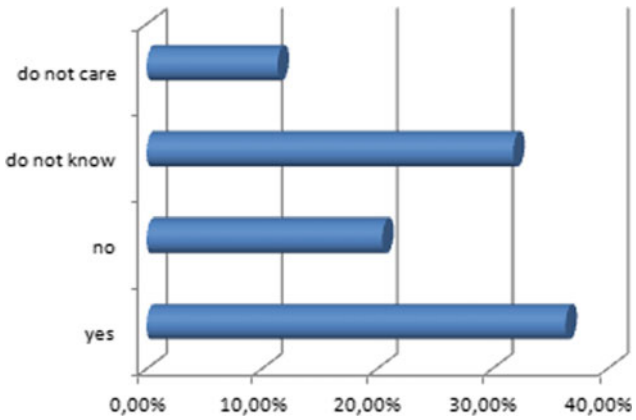

Fig. 7 Awareness on the type of lenses they wear

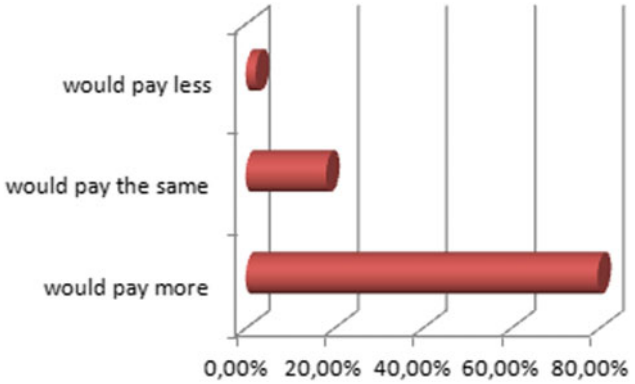

Fig. 8 Attitude of users towards costs of UV lenses

visiting the optometry clinics about the dangers posed by UV radiations and to offer them suitable alternatives for UV protection according to their preferences, age and financial possibilities.

4 Conclusions

The mission of the higher education institutions is to train experts prepared to face practical challenges in performing their future jobs and for this reason their guidance towards relevant research should start in early stages with simple and effective tools.

The two situations presented in the paper are showing that by diligent and dedicated preoccupation the students are able to steer their research results towards directions required by users and make a difference, not research just for the sake of research.

This relevance is especially important when people's health is at stake, as it becomes more and more obvious that medicine nowadays could not progress without the support of engineering.

Acknowledgements Investigations were performed within the Advanced Mechatronic Systems Laboratory from Transilvania University of Brasov.

Conflict of Interest The authors declare that they have no conflict of interest.

References

1. Toffel, M.W.: Enhancing the practical relevance of research. Production and Operations Management, Boston, USA (2016)
2. Bransford, J.D., Vye, N.J., Stipek, D.J., Gomez, L.M., Lam, D.: Equity, excellence, elephants and evidence. In: The Role of Research in Educational Improvement. Harvard Education Press (2009). ISBN 978-1-9347-4213-6

3. Bouter, L.M.: Knowledge as Public Property: The Societal Relevance of Scientific Research. Institutional Management in Higher Education (IMHE 2008), Paris, France (2008)
4. Eaden, J., Mayberry, M.K., Mayberry, J.F.: Questionnaires: the use and abuse of social survey methods in medical research. Postgrad. Med. J. **75**, 297–300 (1999)
5. Mathers, N., Fox, N., Hunn, A.: Surveys and Questionnaires. NIHR RDS for the East Midlands/Yorkshire & Humber (2009)
6. Berger, R.J.: Hoop dreams and Wheels—disability and the competitive wheelchair, [online] En.bookfi.net: http://en.bookfi.net/book/1288195

Improvement of the Fluidized Bed Tribocharging Device for Electrostatic Separation of Plastics from Electronic Medical Waste

L. Călin, M. Bilici, and A. Samuilă

Abstract

Waste of electronic medical devices contains different type of valuable plastics intermixed, generating incompatibilities and limiting the reusing potential, so that the separation of plastics is a crucial operation in recycling. The tribo-electrostatic separation, based on charging the plastic mixture in a tribocharging device then separation of charged granules in high intensity electric field is an efficient method. The paper analyses the influence of sample weight, fluidizing air flow rate, and the shape of the tribocharging chamber on the efficiency of a fluidized-bed tribocharging device with the aim to improve the plastic mixtures separation. The results highlight that the granules charging in fluidized bed has greater efficiency if the section area of the tribocharging chamber is constant, with constant fluidizing air speed. The granules charge in fluidized bed devices increases with the number of collisions but in a greater measure with the impact energy between granules.

Keywords

Plastic waste • Tribocharging • Fluidized bed • Electrostatic separation

1 Introduction

Inexpensive, durable, and lightweight, plastics have become very important materials in the economy as well in daily life. Global production of plastics has increased twice since 1960 and it is expected to double again by 2020 [1].

The use of plastics revolutionized the field of medicine making patients safer, and procedures simpler. In medical applications, plastics allow to produce economically millions of identical pieces with complex geometries and to replace metal in applications in which the high cost of metal fabrication was prohibitive. In addition, they offer many advantages such as reduced weight, better insulating properties, impact resistance, molded-in color, molded-in assembly features, easy-to-clean shapes, etc. [2].

A broad range of electronic medical devices use plastics because of reduced cost, improved ergonomics, versatility and ability to either completely replace metal, or combine with metal to create improved products with features that would otherwise not be possible.

Newer plastics in medical applications are resistant to wear, can withstand harsh disinfectants, and survive multiple sterilization environments without changing properties. Combined with 3D printing, bio-compatible plastic materials can save human lives by enabling medical innovation [3].

Once electronic medical devices reach end of life, different type of valuable plastics find themselves frequently intermixed, generating incompatibilities and limiting the reusing potential of these materials. Separation of plastics by polymer type with high purity is a crucial operation, enabling the recycled material to be used for the same array of products as its origin, i.e. product that was recycled from.

Sorting methods for plastics have made significant progress lately. Liquid density separation, infra-red light sorting, X-ray transmission sorting, color sorting, and electrostatic separation are some of technologies which can be used for plastics separation [4]. The tribo-electrostatic separation technology is useful in the selective sorting of the granular plastic mixtures having similar size, density, magnetic and electric properties [5–8].

In such a separator (Fig. 1), the granular plastic mixture is first introduced in a tribocharging device where the granules are charged with opposite polarity by contact electrification [9–11]. Then the charged material is fed into the high intensity electric field zone of a free fall separator, where the differences in the granules charge generate forces of opposite direction [12, 13]. This technology usually leads to three

L. Călin · M. Bilici · A. Samuilă (✉)
Technical University of Cluj-Napoca, Cluj-Napoca, Romania
e-mail: Adrian.Samuila@ethm.utcluj.ro

S. Vlad and N. M. Roman (eds.), *6th International Conference on Advancements of Medicine and Health Care through Technology; 17–20 October 2018, Cluj-Napoca, Romania*, IFMBE Proceedings 71,
https://doi.org/10.1007/978-981-13-6207-1_53

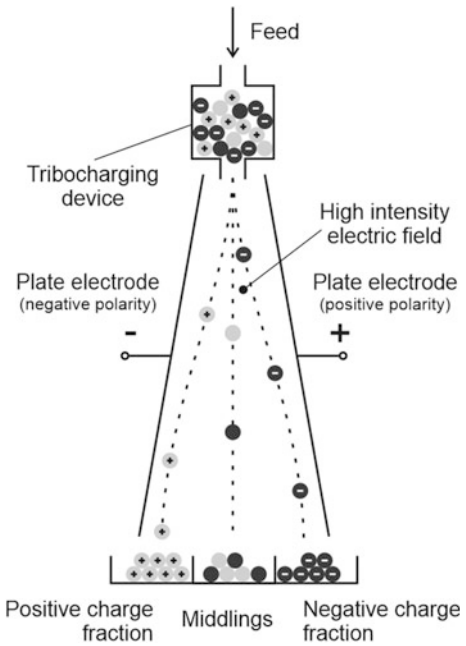

Fig. 1 Principle of tribo-electrostatic separation process of granular plastic mixtures

separation fractions: positively charged granules, neutral granules (middlings) and negatively charged granules.

The efficiency of the tribo-electrostatic separation (recovery grade and purity of the separation products) is strongly dependent on the granules charge acquired in the tribocharging device. Fluidized bed devices have already proved their efficiency in charging plastic granules [10, 14–16].

In these tribocharging devices, granule/granule collisions represent the main charging mechanism but granule/wall collisions also contribute to the granules charge.

From this point of view, the shape of the tribocharging chamber, the fluidizing air flow rate, and the mass of granular material in the tribocharging device represent key factors in increasing the granules charge and in improving the efficiency of the tribo-electrostatic separation of plastic mixtures.

The paper presents an experimental analysis of the three main factors influencing the efficiency of a fluidized-bed tribocharging device with the aim to improve the separation results of the granular plastic mixtures originating from medical electronic devices.

2 Experimental Device

In the first stage of this study, a fluidized bed tribocharging device with an air chamber of variable cross-section (Fig. 2a) was developed in the High Intensity Field Laboratory of the Technical University of Cluj-Napoca. This set-up is comprised of a fixed assembly where the air

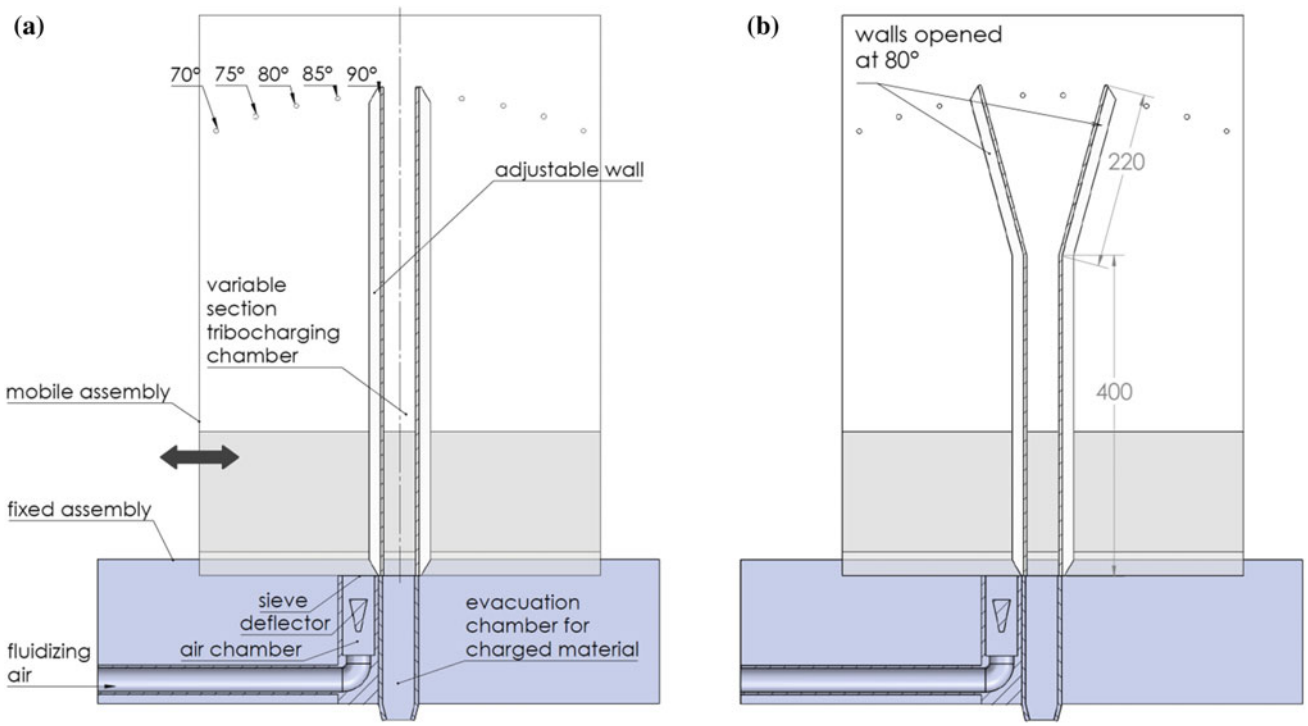

Fig. 2 Fluidized bed tribocharging devices with adjustable lateral walls (**a**) and splayed air chamber (**b**)

chamber and the evacuation chamber are situated, and a mobile assembly represented by the tribocharging chamber. The cross-section of this chamber is modified by adjusting the position of the lateral walls to one of the pre-set positions: 70°, 75°, 80°, 85°, or 90° that represents the angle α of the wall with the horizontal axis. The fluidizing air from an industrial turbo blower passes through the air chamber to the tribocharging chamber. The air chamber has a deflector that creates a quasi-uniform air flow from a round inlet to a rectangular outlet. A sieve with 2 × 2 mm openings was placed at the outlet so the granular material that will be tribo-charged can be placed on.

The tribocharging chamber is the main part of the device, as here is the place where the granular material acquires its charge through collisions in a fluidized bed. The chamber is made from 2 mm transparent PMMA walls that lets the user observe the process. The tribocharging chamber is placed above the air chamber when the material charges in the fluidized bed and can be translated over the evacuation chamber in order to transfer the charged granules to the separator.

At the base of the tribocharging chamber the section is constant—S_{min} = (4 × 6) = 24 cm^2. The adjustment of the position of the lateral walls leads to a variable section area of 24 cm^2 at its minimum value, when α = 90°, and of 304 cm^2, when α = 70°, that causes very different fluidizing air speeds for a constant air flow rate. The ratio of the section areas is S_{min}/S_{max} = 1/12 that leads to a decremental change of the fluidizing air speed with the same ratio, as shown below:

$$Q_{air} = V_1 \cdot S_{min} = V_2 \cdot S_{max} = constant \qquad (1)$$

where Q_{air}—is the fluidizing air flow generated by the turbo blower, V is the speed of the fluidizing air, and S is the cross section of the chamber.

The second set of experiments had the objective to determine the influence of the sample mass and fluidizing air speed on the tribocharging process, so the air chamber needed to be modified accordingly. The lateral walls (Fig. 2b) of the chamber are parallel over a distance of 40 cm and for another 22 cm are splayed out to α = 80°, in order to suddenly decrease the air speed and to maintain the granules in the constant section area of the tribocharging chamber.

3 Materials and Method

The tribocharging experiments were performed with virgin polyamide (PA) and polycarbonate (PC) granules, engineering thermoplastics used in medical electronic devices.

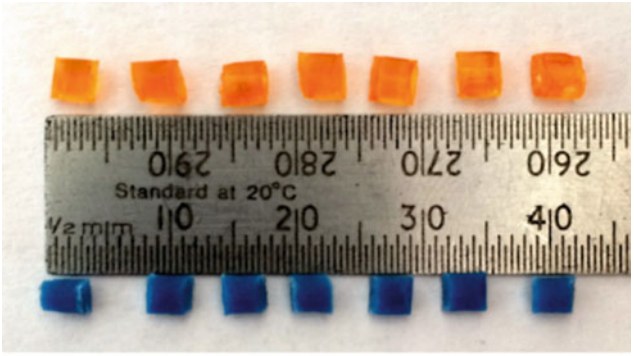

Material	Polyamide (PA)	Polycarbonate (PC)
Color	blue	orange
Shape	cylindrical	cylindrical
Size (mm)	ø 2.5 x 3.4	ø 3 x 3.6
Weight (mg)	20	22
Density (kg/m3)	1100	1200

Fig. 3 Shape, dimensions, and characteristics of PA and PC granules

The PA and PC granules (Fig. 3) have similar shape and dimensions, near similar surface areas, but different color which facilitates the evaluation of the separation results. All the granular samples used for experiments were consisted of a mixture of 50% PA and 50% PC by mass.

The first set of experiments was performed with the fluidized bed tribocharging device equipped with the variable cross-section air chamber. A total number of 50 runs, 10 for each value of the angle α, were done with granular samples of 75 g PA and 75 g PC.

Each sample was placed in the tribocharging chamber and kept in the fluidized bed for 45 s, with a constant air flow rate of Q = 115 m^3/h. Then the material was transferred in the high intensity electric field of the free fall electrostatic separator (Fig. 4), by sliding the mobile assembly on top of the evacuation chamber.

The separator is configured with 360 × 13000 mm plane electrodes supplied with 40 kV positive and negative polarity from two high voltage supplies (Gamma 100 kV, 3 mA). The distance between the electrodes is 250 mm at the top and 600 mm at the bottom. The material being separated is collected in six identical boxes of 100 mm width, covering the entire surface under the electrodes. The tests were done in ambient atmosphere, but the temperature and the relative humidity were quasi-constant at T = 27…30 °C and RH = 37…38%.

The fractions collected in the boxes nearest to the electrodes (#1 and #6) were weighed and for each fraction a recovery rate was calculated according to the formula:

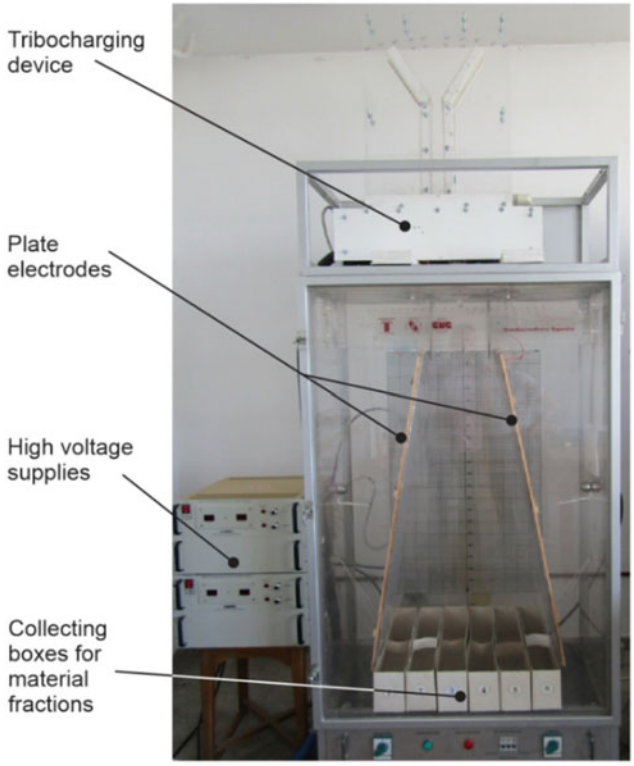

Fig. 4 The free fall electrostatic separator equipped with the fluidized bed tribocharging device

$$Recovery\ rate = \frac{\text{recovered quantity (g)}}{\text{quantity in the sample (g)}} \times 100(\%) \quad (2)$$

The tribocharging device with splayed walls (Fig. 2b) was used for the second set of experiments. In order to study the influence of the sample mass and the air flow rate over the tribocharging process, a design of experiments (DOE) quadratic response surface model was used [17], where the sample mass and air flow rate were the factors and the recovery rate of each material (fractions collected in boxes #1 and #6) were the results. Twenty-two runs were done according to a plan generated by the DOE software Modde 5.0 [18], in critical points of the factors' variation domain (Fig. 5). For each run, the tribocharging time was 45 s.

4 Results and Discussion

The results obtained for the first set of experiments show the highest recovery rate at $\alpha = 90°$ for both PA and PC (Fig. 6), putting in evidence a higher charge accumulated by the granules. This happens because the charging process takes place at constant air speed due to the fact that the

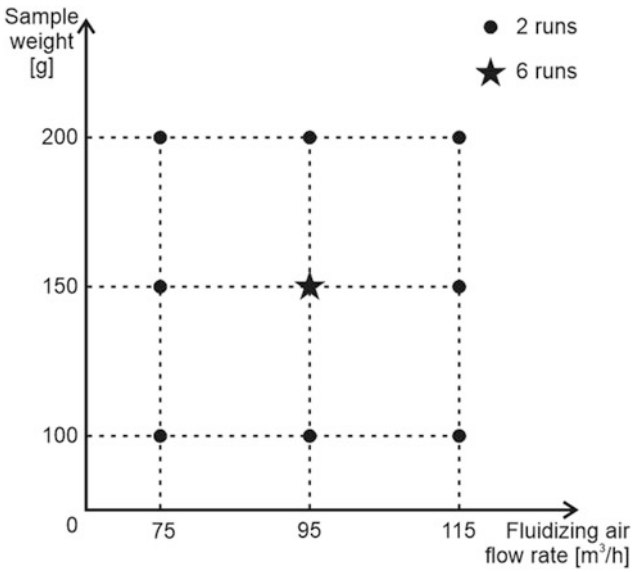

Fig. 5 Factors' variation domains of the quadratic DOE plan

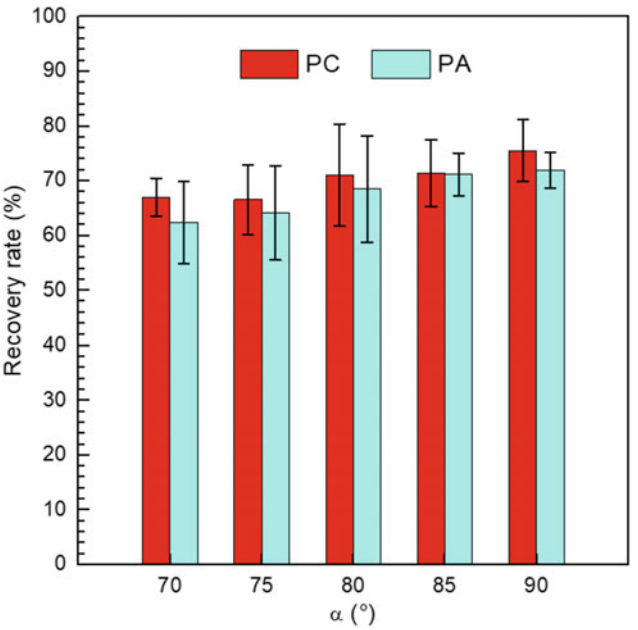

Fig. 6 Recovery rate of PC and PA as a function of angle α

section area of the tribocharging chamber is constant throughout its length.

If the walls angle α is lower the fluidizing air speed decreases towards the top, which leads to a reduction of the kinetic energy of the granules which in turn leads to fewer charge exchanges between granules. In addition, at lower angles α the volume of the triboelectrization chamber increases and the density of granules decreases, with a direct consequence being a reduction in the number of collisions between them and a lower accumulated charge per granule.

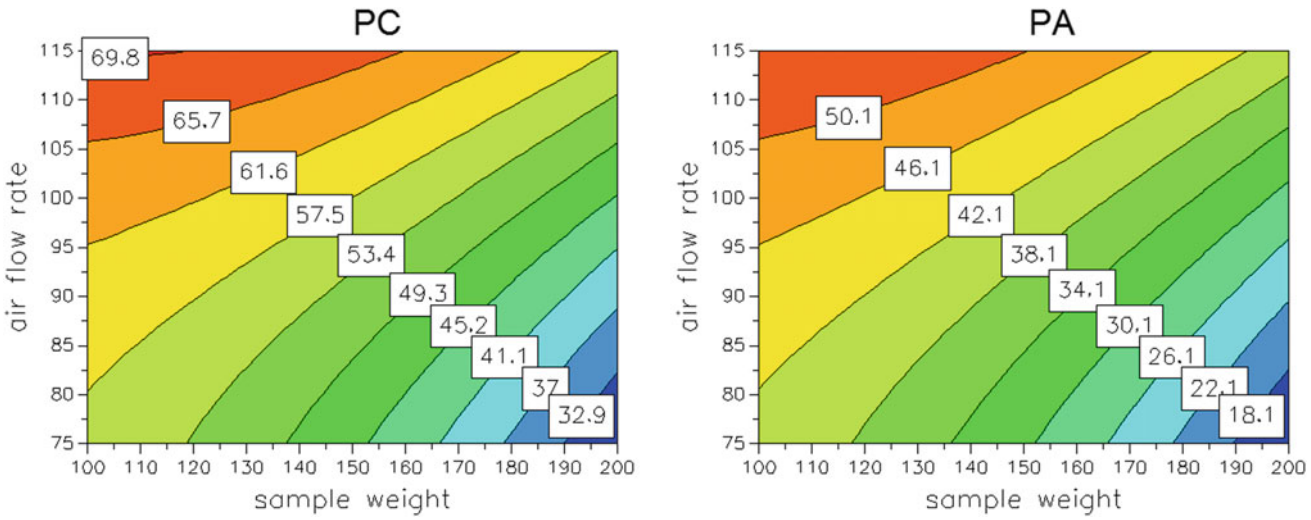

Fig. 7 Contour surfaces generated by MODDE for the recovery rate of PC and PA as a second degree polynomial function of the sample weight (g) and fluidization air flow rate (m^3/h)

The results obtained for the second set of experiments are presented as response surfaces (Fig. 7) modelled by the DOE software Modde 5.0.

A fluidizing air flow rate of 75 m^3/h represents the minimum value for which the fluidized bed can be formed, while a flow rate of 115 m^3/h corresponds to the upper limit where the granules can be maintained in the bed without exiting the zone of constant section of the tribocharging chamber.

The interpretation of these results highlights that the highest values of the granular material recovery rate are obtained for the sample weight of 100 g and the fluidizing air flow rate of 115 m^3/h. This leads to a lower granule density in the triboelectrization chamber, without a reduction of the fluidizing air speed, which allows the granules to travel greater distances between collisions, and to accumulate higher kinetic energies and implicitly higher electrical charges.

Concerning the results obtained from the first set of experiments, the increase of the triboelectrization chamber volume leads to a lower granule density, as well as a lower fluidizing air speed. The impact energy of the granules diminishes as well which conducts to lower accumulated charges per granule.

5 Conclusions

The results analysis highlights that the charging process of the granules in fluidized bed has greater efficiency if the section area of the tribocharging chamber is constant, leading to a constant fluidizing air speed.

The granules charge obtained in a fluidized bed tribocharging device increases with fluidizing air speed which conducts to greater impact energies between granules.

A lower volume density of granules in the tribocharging chamber, as well as a higher fluidizing air speed favor the charging process by increasing the kinetic energy accumulated by granules after successive collisions.

The granules charge in fluidized bed tribocharging devices increases with the number of collisions but in a greater measure with the impact energy between granules.

Acknowledgements This work was financed by The National Authority for Scientific Research and Innovation—Romania, through the TRADE-IT PN-III-P1-1.2-PCCDI-2017-0652 research grant.

Conflict of Interest The authors declare that they have no conflict of interest.

References

1. Communication from the Commission to the European Parliament, the Council, the European Economic and Social Committee and The Committee of the Regions at eur-lex.europa.eu
2. Thryft, A.: Plastics Grow as Materials of Choice for Medical Devices. Materials & Assembly at designnews.com
3. Timm, A.: Top Five Benefits of Injection Molded Parts for Electronic Medical Devices at ecnmag.com
4. Freegard, K., Tan, G., Frisch, S.: WEEE Plastics Separation Technologies. Final Report—DEFRA 2007 at https://www.gov.uk
5. Dodbiba, G., Shibayama, A., Miyazaki, T., Fujita, T.: Triboelectrostatic Separation of ABS, PS and PP Plastic Mixture. Mater. Trans., JIM, **44**, 161–166

6. Wu, G., Li, J., Xu, Z.: Triboelectrostatic separation for granular plastic waste recycling: a review. Waste Manage. **33**, 585–597. https://doi.org/10.1016/j.wasman.2012.10.014
7. Lee, J.-K., Shin, J.-H.: Triboelectrostatic separation of PVC materials from mixed plastics for waste plastic recycling. Korean J. Chem. Eng. **19**, 267–272. https://doi.org/10.1007/bf02698412
8. Calin, L., Iuga, A., Samuila, A., Dragan, C., Dascalescu, L.: Factors that Influence the Fluidized-Bed Tribo-Electrostatic Separation of Plastic Granular Mixtures, pp. 1–4. IEEE Industry Applications Society Annual Meeting, Edmonton, Canada (2008)
9. Iuga, A., Samuila, A., Morar, A., Bilici, M., Dascalescu, L.: Tribocharging techniques for the electrostatic separation of granular plastics from waste electric and electronic equipment. Part. Sci. Technol. **34**, 45–54. https://doi.org/10.1080/02726351.2015.1043675
10. Dascalescu, L., Fati, O., Bilici, M., Rahou, F., Dragan, C., Samuila, A., luga, A.: Factors that influence the efficiency of a fluidized-bed-type tribo-electrostatic separator for mixed granular plastics. JPCS **301**, 1–4. https://doi.org/10.1088/1742-6596/301/1/012066
11. Rezoug, M., Aksa, W., Miloudi, M., Medles, K., Dascalescu, L.: Triboelectrostatic separation of granular plastics mixtures from waste electric and electronic equipment. Part. Sci. Technol. **35**, 621–626. https://doi.org/10.1080/02726351.2017.1347226
12. Bendimerad, S., Tilmatine, A., Ziane, M., Dascalescu, L.: Plastic wastes recovery using free-fall triboelectric separator. Int. J. Environ. Sci. Technol. **66**, 529–538. https://doi.org/10.1080/00207230902722838
13. El-mouloud, Z., Tilmatine, A., Rizouga, M., Gouri, R., Medles, K., Dascalescu, L.: Experimental analysis of a cyclone tribocharging device for free-fall triboelectric separation of plastic particles. IEEE Trans. Dielectr. Electr. Insul. **20**, 1584–1589. https://doi.org/10.1109/tdei.2013.6633687
14. luga, A., Calin, A., Neamtu, V., Mihalcioiu, A., Dascalescu, A.: Tribocharging of plastics granulates in a fluidized bed device. J. Electrostat. **63**, 937–942. https://doi.org/10.1016/j.elstat.2005.03.064
15. Samuila, A., Bilici, M., Ilies, V., Dascalescu, L.: Design and test of a novel fluidized-bed two-insulated-rolls-type tribo-aero-electrostatic separator for granular plastics. In: Proceeding of ESA Annual Meeting on Electrostatics, Notre Dame, USA, pp. 1–9 (2014)
16. Calin, L., Mihalcioiu, A., Iuga, A., Dascalescu, L.: Fluidized bed device for plastic granules triboelectrification. Part. Sci. Technol. **25**, 205–2011. https://doi.org/10.1080/02726350701257782
17. Goupy, J., Creighton, L.: Introduction to Design of Experiments with JMP Examples, 3rd edn. SAS Institute Inc. (2007)
18. MODDE 5.0 User Guide and Tutorial, Umetrics AB, Umea, Sweden (1999)

Complex Influence of Intense Electric Fields upon Ozone and Free Radicals from Aqueous Solutions

R. E. Suărăşan, S. R. Budu, I. Suărăşan, Dumitrița Moldovan, and Radu Fechete

Abstract

Additionally to residual ozone, in processed aqueous solutions using intense electric fields, free radicals are present and determines changes of a variety of physical parameters—chemical of solutions. Ozone and free radicals remaining in the aqueous treatment processes are primarily responsible for harmful inhibiting, but also are useful for biostimulation processes of living environments (increasing the speed action of polymorphonuclear leukocytes in the healing of severe infections, changes of the pattern of collagen regeneration during ulcerations healing). This paper presents the results of a multidisciplinary research, with extensive scientific and technical aspects. Intense electric fields, especially using corona point or filiform discharge electrodes, used in specially designed treatment cells and the processes of air ionization, generates and trains a variety of electrical charge carriers, which have sufficient energy in order to brake different gas molecules, in order to produce oxygen, or to determine the generation of ozone and free radicals in retention solutions or in the present environment. The electric field parameters, the intensity, the nature and shape of high voltage, exposure time, but also the characteristics and structure of cell treatment (multipoint, filiform or brush type electrodes), gap size or the step between the discharge electrodes, all are important parameters which determines the presence and concentration of ozone and free radicals which, present in the processed aqueous solutions.

Keywords

Intense electric fields • Ozone retention • Retention of free radicals • Aqueous solutions

R. E. Suărăşan · S. R. Budu (✉) · I. Suărăşan · D. Moldovan · R. Fechete
Technical University of Cluj-Napoca, 15 C. Daicoviciu Street, 400020 Cluj-Napoca, Romania
e-mail: Sorin.BUDU@ethm.utcluj.ro

1 Introduction

Ozone is considered to be one of the strongest oxidants, having antiseptic properties, especially antibacterial, which makes it very effective in combating of microbial infections.

Depending on the user's needs, mainly in terms of quantities and concentrations, instrumentation or oxygen is used as a working agent, leading to complex installations and equipment. The main industrial or laboratory method for producing ozone in large and adjustable concentrations and quantities is corona discharge, usually through a dielectric barrier, already known from Siemens, and is in continuous refinement. Treatments that use the cumulative effects of intense electrical fields along with those of ozone can lead to some beneficial processes of inhibiting microorganisms and biostimulating useful cells from living organisms, whether human or animal, by stimulating leukocytosis locally.

The antimicrobial effect is due both to the direct action of ozone and its ability to form unsaturated fatty acids, very peroxide-active compounds that act destructively on microorganisms [1]. If at low doses and concentrations the ozone has a local destructive action on the cell membrane, at higher doses it blocks certain enzymatic systems and cellular receptors that lead to the death of pathogenic microorganisms. The bactericidal effect of ozone exceeds twice that of chlorine, is equally effective in cases resistant to antibiotic therapy and does not induce resistance. Equally good results have also been reported on viruses, fungi and protozors. The initial mechanism by which ozone acts on microorganisms is the oxidation of their membranes, a process in which glycoproteins, glycolipids, various amino acids in the cell wall are affected, resulting in the penetration of ozone molecules in the cell, enzyme control blocking, and implicitly, cell death [2].

In addition to direct action on microbial agents, ozone also exhibits an immunomodulatory action stimulating both cellular mechanisms (T-lymphocytes, monocytes) and tumor mechanisms (cytokine synthesis, and primarily interferon,

S. Vlad and N. M. Roman (eds.), *6th International Conference on Advancements of Medicine and Health Care through Technology; 17–20 October 2018, Cluj-Napoca, Romania*, IFMBE Proceedings 71,
https://doi.org/10.1007/978-981-13-6207-1_54

tumor necrosis factors). Ozone plays an important therapeutic role in various types of infections by generating free radicals of oxygen (O_2, OH, H_2O_2, NO, HOC1), radicals that are produced by granulocytes and macrophages during infectious processes.

The effect of ozone on micro-organisms is proportional to ozone concentration and exposure time. Studies have shown that ozone is effective on Gram-positive and Gram-negative bacteria, the latter requiring more ozone to neutralize than Gram-positive. On anaerobic and microaerophilic bacteria, ozone has a dramatic toxic action, given the specific energy metabolism of these bacteria, which use organic compounds as the ultimate oxygen acceptor and does not possess protective enzymes, in relation to oxygen toxicity [1].

2 Materials and Methods

Evidence of the evolution of residual ozone and free radicals from aqueous solutions processed in intense electric field of corona discharge was performed on the stand in Fig. 1.

Methodology of working with the complex installation of the aqueous solutions in ozone-generating electric fields consists in connecting the stand to the mono-phase network and verifying the connection of the equipment to the grounding grid of the electric grid, then proceeding with the introduction of the aqueous ozone solution from the container 4 in the corona cell to process the aqueous solutions of the Petri 5 vessel, the walls of which constitute a first dielectric barrier (to the desired level by actuating the valve 6), after which oxygen is introduced into the plant by actuating the valve 8 and the built-in pressure regulator (until the air is completely removed from the corona cell and replaced by oxygen); the protocol continues with the startup and adjustment of the high voltage source 17 at the required application parameters.

With the closed and 11-closed valves 6 and 8, the recirculation pump of the processed solution 12 and the ozonometer 13 are started; when the ozone concentration in the aqueous solution has reached the preset value, the entire equipment from the grid is decoupled, all the valves outside the 11 are closed, whereby the ozone aqueous solution is recovered and stored in the container 10.

The high voltage adjustable source used (pos. 18) was a source at the 50 Hz network frequency with the c.a. or cc.c. output of different polarities as a voltage level up to 25 kV.

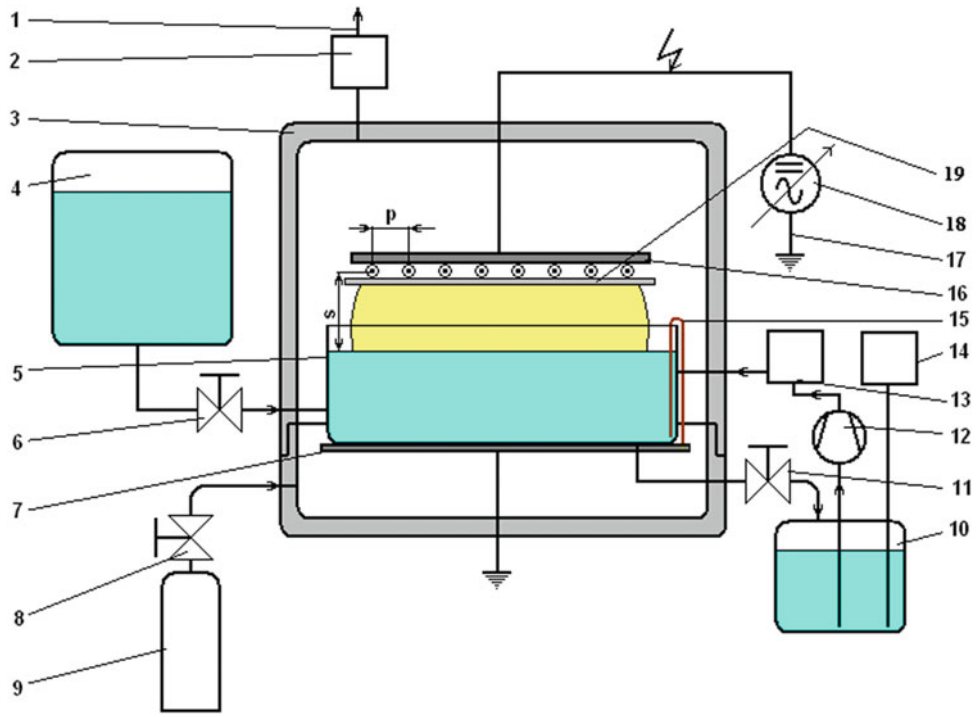

Fig. 1 The plant for direct processing in intense electric fields of aqueous solutions; 1—gas discharge; 2—residual ozone depleter (optional); 3—direct processing cell; 4—vessel for the aqueous solution to be processed; 5—petri dish for direct processing, with stationary liquid; 6—Valve (tap) for feeding Petri dish; 7—ground electrode, plate type; 8—pressure regulator valve; 9—Oxygen tube (tank or reservoir); 10—Collector of processed aqueous solution; 11—Valve (tap) for collecting the processed water; 12—recirculation pump 13—residual ozone measure in the aqueous solution; 14—pH measure or other physico-chemical parameters of processed aqueous solutions; 15—a piece for connection to the ground of the aqueous solution; 16—high-voltage corona active electrode; 17—connections to the belt and the grounding socket; 18—adjustable high voltage source; 19—dielectric barrier

Table 1 Treatment conditions and experimental results obtained before and after water treatment with ozone and intense electric field

Distilled water	Treatment hour	Decay of measurement time	T_2 (s)	pH
Witness sample	–	11^{12}–11^{16}	2.68	5.7
Treated sample d.c. (+)	10^{15}–10^{20}	11^{32}–11^{36}	2.32	6.6
Treated sample d.c. (−)	10^{25}–10^{30}	11^{45}–11^{49}	2.82	5.0
Treated sample a.c. (∼)	10^{36}–10^{41}	11^{57}–12^{01}	3.06	4.7

Corona cells were tested those with stationary aqueous solutions but in which the corona discharge was made either by a double dielectric barrier (to remove any microparticles detached from the active electrodes, with corona discharge—which led to high voltages or by far less dielectric barriers (by removing the barrier 19, while using the grounding piece 15 for the aqueous solution.

Four aqueous solutions: electrically untreated, treated at positive voltage, at negative voltage and alternatively voltage were measured by ^{1}H NMR relaxometry and vibrational infrared FT-IR spectroscopy [3].

For all samples a major peak of which position, amplitude and width is sensitive to the type of treatment was identified at T_2 values between 2 and 4 s. For untreated and treated with positive voltage the T_2 distributions presents also a minor peak associated with some impurities.

The low field NMR [3] measurements of aqueous solutions were performed using the BRUKER MINISPEC mq20 spectrometer. This instrument works at 0.5 T magnetic field and for resonance the Larmor frequency was set at 19.6712 MHz. The inter-echo time in CPMG pulse sequence was set at 2.5 ms [3]. The tipping pulse length was 9 µs and refocusing pulses with the same duration was set double in amplitude (attenuation—6 dB).

A total number of 3000 echoes were recorded. The decay of transverse magnetization during the CPMG echoes train was assumed to be influenced by transverse relaxation times, T_2 of each particular statistical sub-ensemble of protons. To this purpose the experimental data was analyzed using a Laplace inversion algorithm of which mathematically details were detailed elsewhere [1, 2]. For the vibrational spectra a Jasco FT-IR spectrometer was used.

3 Results

Experimental results obtained sequently to the carried tests on the device presented in Fig. 1, referring to the evolution of O_3, free radicals and Ph value, using three different high voltage supply configuration (positive and negative polarity of d.c. voltage and alternative pure sinus voltage) and also

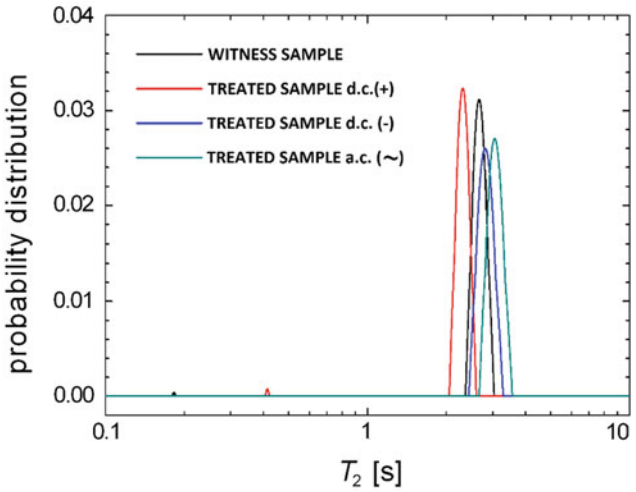

Fig. 2 Evolution of O_3, relative to the d.c. and sinus wave (a.c.) voltage

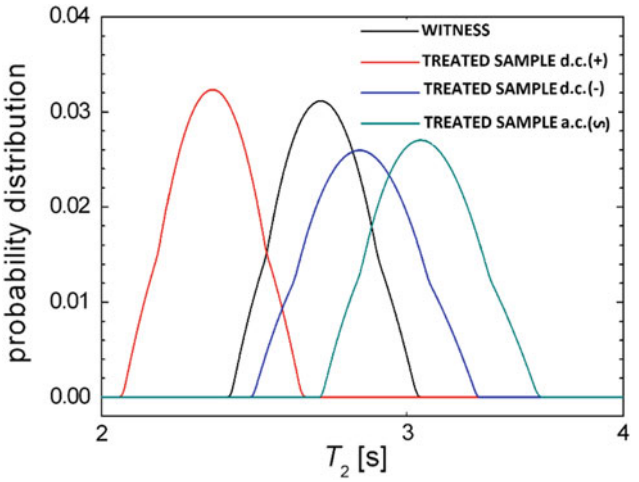

Fig. 3 Evolution of free radicals relative to the d.c. and a.c. voltage

including NMR (Magnetic Nuclear Resonance) method concerning water characteristics, are listed in Table 1 and depicted in Figs. 2, 3, 4 and 5, presents the results obtained on distillated water, processed in intense electric field (IEC).

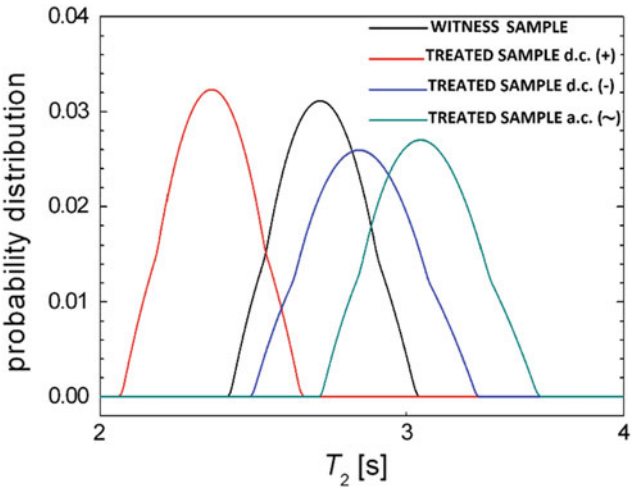

Fig. 4 Evolution of Ph, relative to the d.c. and sinus wave (a.c.) voltage

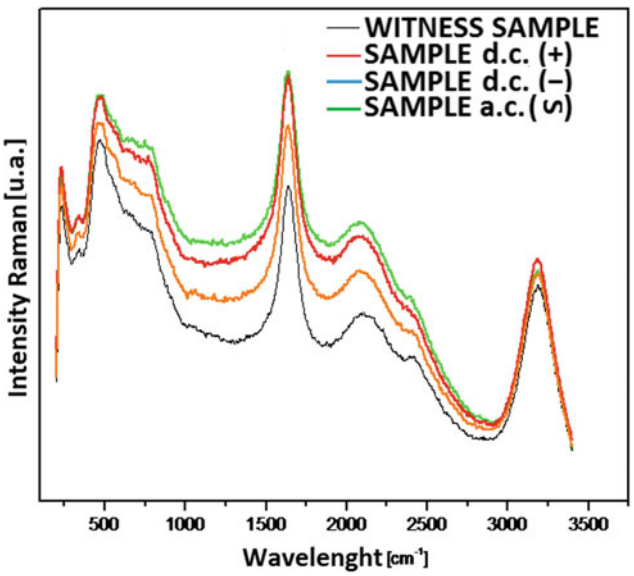

Fig. 5 Dinamic of Ramana intensity determined by NMR test

4 Conclusions

The comparative analysis of the experimental results, conducted to the following conclusions:

- increased ozone retention/time unit ("ICE footprint" type) will last significantly longer;
- the treatment method provides existence of more free radicals, resulting in their beneficial role in bio-inhibition of negative processes, or also in bio-stimulation of active processes in living environments, with an explicit reference to healing processes in the human body;
- increased pH retention and other modified parameters (O_3 generation, waveform and polarity of high voltage and electric intense field) applied on water can be very useful in treatment of traumatic and burned plagues;
- interpreting RAMAN charts can offer important indications of water behaviour in ICE;
- subsequent research using performant measurement devices will certainly bring scientific clarifications upon the presence of the clusters in aqueous solutions, as well as the cause and effects likely can conduct to extend the high frequency range to hundred of kilohertz of the applied high voltage, in order to be used in wound treatments.

Conflict of Interest The authors declare that they have no conflict of interest.

References

1. Venkataramanan, L., Song, Y., Hurlimann, M.: Solving Fredholm integrals of the first kind with tensor product structure in 2 and 2.5 dimensions. IEEE Trans. Sign. Proc. **50**, 1017–1026 (2002)
2. Song, Y., Venkataramanan, L., Hurlimann, M., et al.: T1–T2 correlation spectra obtained using a fast two-dimensional Laplace inversion. J. Magn. Reson. **154**, 261–268 (2002)
3. Chelcea, R.I., Fechete, R., Culea, E., Demco, D.E., Blümich, B.: Distributions of transverse relaxation times for soft-solids measured in strongly inhomogeneous magnetic fields. J. Magn. Reson. **196**, 178–190 (2009)

Author Index

A
Abrudan, Cristian, 229
Abrudean, Adrian, 247
Abrudean, M., 123
Albu, Corina, 157
Alexandru, D. O., 163
Al Hajjar, N., 267
Ancău, Dorina, 139
Ancău, Mircea, 139
Andrei, Lavinia, 45
Andriţoi, D., 35, 73, 103, 291
Anghel, I., 207
Arotaritei, D., 241
Arsinte, Radu, 157
Aştilean, Adina, 201
Avram, A., 109
Avram, Camelia, 201

B
Băbţan, Anida-Maria, 23
Badea, R., 169
Băldean, Doru, 45
Balan, V., 329
Balla, K., 115
Beudean, M., 17
Bilici, M., 341
Birleanu, C., 321
Bogdan, R.C., 109
Bojiţă, A., 109
Bologa, M., 207
Borzan, Adela Ioana, 45
Brehar, R., 169
Budu, S.R., 347
Bugnar, S., 255
Bunta, O., 123
Burz, A., 267

C
Călin, L., 341
Carbone, Giuseppe, 229
Chifu, V.R., 207
Chirila, D., 297, 301
Chis, George Sebastian, 305
Cioara, T., 207
Ciobanu, D.M., 3
Ciorap, Radu, 35, 73, 103, 291
Cirlugea, M., 145
Codau, C., 97
Coloşi, T., 123
Constantea, N., 297, 301
Constantin, G., 241
Constantinescu-Dobra, Anca, 277, 283
Copîndean, R., 59, 79
Corciovă, Călin, 35, 41, 65, 73, 103, 291
Coţiu, M.C., 277, 283
Cotoros, D., 29, 335
Craciun, Florin, 229
Creţu, Adrian, 201
Culai, A.M., 261

D
Datcu, M., 41
De Paolis, L.T., 177
Dican, L., 185
Dolea, P., 97
Domínguez Velasco, C.F., 177
Domuţa, Claudiu, 201
Dragan, F., 59, 79
Dragomir-Loga, Gabriel Cristian, 185
Druga, C., 29, 335
Dumitraşcu, D.L., 115

E
Elisei, R., 267

F
Farago, Paul, 23, 145
Fechete, Radu, 347
Feurdean, C. N., 23
Fischer-Fodor, E., 305
Florea, A., 305
Fort, Ciprian Mugurel, 221
Fuior, Robert, 65

G
Galatus, R., 23
Georgescu, D., 163
Gergely, S., 221

S. Vlad and N. M. Roman (eds.), *6th International Conference on Advancements of Medicine and Health Care through Technology; 17–20 October 2018, Cluj-Napoca, Romania*, IFMBE Proceedings 71,
https://doi.org/10.1007/978-981-13-6207-1

Germán-Salló, Márta, 151
Germán-Salló, Zoltán, 151
Gheorghiță, Andrei, 65, 241
Gligor, D., 17
Gligor, Elena, 17
Graur, F., 267
Grif, Horaţiu-Ştefan, 151
Grindei, L., 59
Groza, R., 23

H
Hintea, S., 145
Holonec, L., 115
Holonec, R., 59, 79, 85, 91

I
Ianoși-Andreeva-Dimitrova, A., 237
Ilea, A., 23
Ilea, M., 241
Inceu, Georgeta Victoria, 9
Ionescu, C., 297, 301
Ispas, V., 255
Iusan, R.A., 297

L
Lacatus, A., 185
Lazar, V., 267
Loga, L., 185
Luca, Catalina, 35, 41, 73, 103, 291
Lupu, Eugen, 157

M
Major, Kinga, 229
Malihin, S., 329
Mândru, D.S., 237, 247
Manea, N.C., 163
Maniu, A.A., 287, 305
Masca, Constantin, 215
Merie, V., 321
Miclaus, D.R., 301
Miclea, L., 311
Micu, Bogdan Vasile, 297, 301
Micu, C.M., 297, 301
Mihancea, P., 261
Mitrea, D., 169
Mitrea, P., 169
Mois, E., 267
Moldovan, D., 207
Moldovan, Dumitriţa, 347
Muresan, C., 79
Muresan, M.S., 297, 301
Mureşan, V., 123
Muscatello, S., 177

N
Nedelcu, L., 115
Nedevschi, S., 169
Niculescu, Manole-Stefan, 51

O
Olar, L.E., 3
Olea, M., 255
Olt, M., 17
Onac, I., 261
Ossian, V., 17

P
Padilla Castañeda, M.Á., 177
Palade, I., 97
Palade, T., 97
Papuc, I., 3
Parrein, Benoît, 201
Pastrav, A., 97
Perde-Schrepler, M., 305
Pisla, D., 229, 267
Platon(Lupşor), M., 169
Pleşea, I.E., 163
Pleşea, R.M., 163
Pop, C., 207
Pop-Coman, P., 255
Pop, Gavril-Petre, 133
Pop, M.S., 321
Pop, Nicoleta, 229
Pop, T.R., 297, 301
Prabhakar, S.K., 195
Purcar, M., 59, 109
Puschita, E., 97
Puskas, Ferenc, 229
Pustan, M., 321

R
Radeanu, D., 287
Radu, Dan, 201
Rajaguru, H., 195
Rápolti, L., 85, 91
Raza, A., 145
Roman, A.I., 17, 85, 305
Roman, G., 3, 9
Roman, Nicolae-Marius, 23, 123, 139, 221, 255
Rotariu, M., 241

S
Sabou, A., 277
Salomie, I., 207
Samuilă, A., 341
Şandor, V., 115
Şerbănescu, M.S., 163

Serban, I., 29, 335
Silaghi, H., 297, 301
Slavescu, Kinga Cristina, 215
Slavescu, Radu Razvan, 215
Stanciu, A., 29, 335
Stan, Constantin, 287
Stan, O.P., 123, 311
Ştefan, R., 3
Steopan, M., 255
Suărăşan, I., 347
Suărăşan, R.E., 347

T
Tămaş, M., 115
Tărâţă, M., 163
Teică, Rossy Vlăduţ, 163
Teodoro Vite, S., 177
Turnea, M., 241

V
Vaida, C., 229, 267
Verestiuc, L., 329
Viman, O., 115
Visovan, A., 207
Vlad, S., 85, 91
Vonica, C.L., 9

W
Wolf, W., 163